FACIES ANALYSIS AND SEISMIC GEOMORPHOLOGY OF A FLUVIAL-TIDAL DEPOSITIONAL SYSTEM FROM THE MIOCENE MALAY BASIN

NURUL ADILAH BINTI MANSHOR

FACULTY OF SCIENCE
UNIVERSITI MALAYA
KUALA LUMPUR

2021

FACIES ANALYSIS AND SEISMIC GEOMORPHOLOGY OF A FLUVIAL-TIDAL DEPOSITIONAL SYSTEM FROM THE MIOCENE MALAY BASIN

NURUL ADILAH BINTI MANSHOR

THESIS SUBMITTED IN FULFILMENT OF THE REQUIREMENTS FOR THE DEGREE OF DOCTOR OF PHILOSOPHY

DEPARTMENT OF GEOLOGY
FACULTY OF SCIENCE
UNIVERSITI MALAYA
KUALA LUMPUR

2021

UNIVERSITI MALAYA

ORIGINAL LITERARY WORK DECLARATION

Name of Candidate: **NURUL ADILAH BINTI MANSHOR**

Matric No: **17020909/2**

Name of Degree: **DOCTOR OF PHILOSOPHY**

Title of Thesis ("this Work"):

FACIES ANALYSIS AND SEISMIC GEOMORPHOLOGY OF A FLUVIAL-TIDAL DEPOSITIONAL SYSTEM FROM THE MIOCENE MALAY BASIN

Field of Study: **GEOLOGY**

I do solemnly and sincerely declare that:

(1) I am the sole author/writer of this Work;
(2) This Work is original;
(3) Any use of any work in which copyright exists was done by way of fair dealing and for permitted purposes and any excerpt or extract from, or reference to or reproduction of any copyright work has been disclosed expressly and sufficiently and the title of the Work and its authorship have been acknowledged in this Work;
(4) I do not have any actual knowledge nor do I ought reasonably to know that the making of this work constitutes an infringement of any copyright work;
(5) I hereby assign all and every rights in the copyright to this Work to the University of Malaya ("UM"), who henceforth shall be owner of the copyright in this Work and that any reproduction or use in any form or by any means whatsoever is prohibited without the written consent of UM having been first had and obtained;
(6) I am fully aware that if in the course of making this Work, I have infringed any copyright whether intentionally or otherwise, I may be subject to legal action or any other action as may be determined by UM.

Candidate's Signature Date: 22/ 09/ 2021

Subscribed and solemnly declared before,

Witness's Signature Date: 22/ 09/ 2021

Name:

Designation:

FACIES ANALYSIS AND SEISMIC GEOMORPHOLOGY OF A FLUVIAL-TIDAL DEPOSITIONAL SYSTEM FROM THE MIOCENE MALAY BASIN

ABSTRACT

Various hierarchical classification schemes for channel architectural elements have been developed based on studies of modern and ancient alluvial and paralic systems. The datasets used by different schemes are varied and include seismic, well logs, core and/or outcrops. Most studies used outcrop datasets, which provide better views of higher resolution lateral and vertical relationships of bounding scour surfaces. However, recognizing these features in 3D seismic data and well data at depths $\geq$ 1.5 km in the subsurface is very challenging. This research presents an integrated facies analysis and seismic geomorphology study of a fluvio-tidal depositional system from the Lower to Middle Miocene (within Group I and H) of the Malay Basin. The targeted interval is >1000 m below sea bottom. An integrated dataset from a selected area in the central region of the Malay Basin was used for this study, which includes a high-quality 3D seismic cube (1563km^2), 83.15 m of conventional core, and 3 well logs penetrating Group I and H. Facies analysis indicates that Group I and H strata in the study area are dominated by a mixture of fluvial and tidal facies. Identified facies associations represent paralic depositional elements such as prodelta mudstone, outer estuarine/abandoned channel deposits, and within a channel, tide-influenced barforms. The presence of a marine ichnofauna with varying degrees of diversity and bioturbation intensity is indicative of restricted marginal marine environments. Application of RMS (Root Means Square) attribute analysis and frequency decomposition in the seismic geomorphological analysis has enabled the imaging of a variety of architectural elements at different geometries, scales, and dimensions. Architectural elements of 120 channels are catalogued and evaluated. Three classes of channels are identified within the dataset, based on spatial and temporal channel geomorphology and other seismic signatures. Class-1 channel systems are the widest and characterised by high seismic amplitude, low to moderate sinuosity and are interpreted as bypass channels or estuaries. Class-2 channel systems are of high seismic amplitude, have low to moderate sinuosity, and are interpreted as fluvial/distributary channels. Class-3 channel systems contain the smallest channels with high sinuosity and are interpreted as tidal creeks and tidal channel networks. These channels show unique morphometric characteristics indicative of tidal influence, such as flaring mouths, cuspate meanders, high sinuosities, through-flow and dendritic networks. Quantitative morphometric elements have been compared to existing published datasets and modern-day tide-dominated channel systems. The characteristics of the widest channels in this study are not consistent with an incised valley interpretation and are most likely channel belts or amalgamated channel belts. The evolution of the depositional system and wide variation in channel geomorphologies is interpreted in relation to Miocene regressive-transgressive cycles and downstream autocyclic controls. A quantitative morphometric database for the Group I and H channels in the Malay Basin is presented in this project.

Keywords: Sedimentology, facies analysis, quantitative geomorphology, fluvio-tidal channel.

ANALISIS FASIES DAN SEISMIK GEOMORFOLOGI PERSEKITARAN PENGENAPAN SUNGAI-PASANG SURUT DARI MIOSEN LEMBANGAN MELAYU

ABSTRAK

Pelbagai skema pengelasan hierarki bagi unsur-unsur senibina alur telah dibangunkan berdasarkan kajian sistem aluvial dan paralik moden serta kuno. Terdapat variasi dalam set data yang digunapakai oleh skema-skema yang berlainan, termasuk data seismik, telaga log, teras dan singkapan batuan sedimen. Kebanyakan kajian sebegini menggunakan set data daripada singkapan, yang memberikan pandangan resolusi tinggi perkaitan sisi melintang dan menegak pada permukaan hakisan. Walau bagaimanapun, pengenalan ciri-ciri ini dalam data seismik 3D dan data telaga pada kedalaman ≥ 1.5 km dibawah permukaan bawah tanah adalah sangat mencabar. Kajian ini mempersembahkan satu integrasi analisis fasies bersepadu dan kajian geomorfologi seismik bagi sistem pengendapan sungai-pasang surut-delta yang berusia dari Awal Miosen hingga Pertengahan Miosen (dalam Kumpulan I dan H) di Lembangan Melayu. Sasaran kajian ini adalah unit pada kedalaman > 1000 m dibawah dasar laut. Set data yang digunakan untuk kajian ini adalah daripada bahagian tengah Lembangan Melayu, dan merangkumi satu subset seismik kubus 3D berkualiti tinggi (1563km^2), teras konvensional sepanjang 83.15 m, bacaan log dari 3 telaga berbeza yang menembusi Kumpulan I dan H. Analisis fasies menunjukkan bahawa jujukan lapisan Kumpulan I dan H di dalam kawasan kajian didominasi oleh campuran fasies fluvial dan pasang-surut. Sekutuan fasies yang dikenalpasti di dalam kajian ini mempamerkan elemen endapan paralik seperti batu lumpur prodelta, enapan muara luaran / alur yang ditinggal dan beting pasir yang dipengaruhi oleh pasang surut di dalam sungai. Kehadiran iknofauna laut dengan tahap biodiversiti dan bioturbasi yang berbeza menunjukkan persekitaran pinggiran laut yang terhad. Aplikasi analisis atribut RMS (Root Means Square) dan penguraian frekuensi dalam analisis geomorfologi seismik telah memungkinkan pengimejan pelbagai unsur senibina pada geometri, skala dan dimensi yang berbeza. Elemen seni bina daripada 120 saluran telah dikategorikan dan dinilai. Tiga kelas alur telah dikenal pasti dalam set data tersebut, berdasarkan geomorfologi spatial dan temporal alur serta data seismik yang lain. Sistem alur Kelas-1 adalah yang paling luas dan dicirikan dengan amplitud seismik yang tinggi, sinuositi rendah hingga sederhana dan ditafsirkan sebagai sungai pintasan atau muara. Sistem alur Kelas-2 mempunyai amplitud seismik yang tinggi, mempunyai sinuositi rendah hingga sederhana, ditafsirkan sebagai alur fluvial/distributari. Sistem alur Kelas-3 merangkumi alur-alur terkecil dengan sinuositi tinggi dan ditafsirkan sebagai anak alur dan alur pasang-surut. Alur-alur ini menunjukkan ciri-ciri morfometrik yang unik yang menunjukkan pengaruh pasang-surut seperti muara berbentuk corong, likuan sungai berbentuk kotak, sinuositi tinggi, jaringan alur yang bersambung dan jaringan dendritik. Unsur-unsur morfometrik kuantitatif telah dibandingkan dengan set data yang telah diterbitakan dan sistem alur moden yang didominasi pasang-surut. Ciri-ciri alur-alur terluas dalam kajian ini tidak selaras dengan tafsiran sebagai lembah terpotong, dan kemungkinan besar merupakan jalur alur atau jalur alur tergabung. Evolusi sistem pengendapan dan variasi luas dalam geomorfologi alur ditafsirkan berkaitan dengan kitaran regresif-transgresif Miosen dan kawalan-kawalan autokitaran di bahagian hilir sungai. Pangkalan data morfometrik kuantitatif untuk alur-alur Kumpulan I dan H di Lembangan Melayu ditunjukkan dalam kajian ini.

Kata kunci: Sedimentologi, analisis fasies, kuantitatif geomorfologi, sungai fluvio-pasang-surut.

DEDICATION

Alhamdulillah

This thesis is dedicated to my loved ones, for their tremendous support, encouragement, time, love, and prayers.

My lovely husband, Mohamad Hisham Romli
My sunshine, Muhammad Eusuf Uwais
My pillar of strength, Khadijah Mahamud
My mother-in-law, Wan Aison Alang Ahmad
My siblings, nieces & nephews.

Thank you!

ACKNOWLEDGEMENTS

This study was funded by the Ministry of Education of Malaysia and the University Technology Malaysia (UTM) through postgraduate scholarship programme. The utmost gratitude to PETRONAS for providing access to the precious data used in this study. Special thanks to PETRONAS Geo-Sample Centre team for helping out through the core analysis study.

I would like to thank Dr. Meor Hakif for his patience, supervision, enthusiasm, encouragement, and immense knowledge throughout the course of this study. Various people in the Department of Geology in the University of Malaya have helped me in one way or another. Special thanks to Professor Wan Hasiah Abdullah, Sapinah Salleh, and Hijaz Kamal Hasnan for their kind support and encouragement.

I would like to express my gratitude to Hafiz Baharuddin from Ellis for his technical assistance in using Paleoscan and workstation reviews.

Last but not least, I am extremely thankful to all my family for their love, prayers, understanding, and supports.

TABLE OF CONTENTS

LIST OF FIGURES

LIST OF TABLES

LIST OF APPENDICES

LIST OF SYMBOLS AND ABBREVIATIONS

3D	:	3 dimensional
CBW	:	channel belt width
CL	:	channel length
CT/h	:	channel thickness
CW/Wc	:	channel width
ENS	:	East Natuna and Sarawak embayments
GOT	:	Gulf of Thailand
LC	:	large-scale channel
LGM	:	Last Glacial Maximum
MBW/Wm	:	meander belt width
MC	:	medium-scale channel
MFS/FS	:	maximum flooding surface/ flooding surface
ML/lm	:	meander wavelength
PALEOSCAN	:	Name of software used for seismic interpretation and attributes analysis.
SC	:	small-scale channel
SCS	:	South China Sea
SI	:	sinuosity
TWT	:	two-way time
VLC	:	very-large-scale channel

CHAPTER 1: INTRODUCTION

1.1 Research Introduction

The Malay Basin is a large hydrocarbon-bearing sedimentary basin located offshore the East Coast of Peninsular Malaysia. The basin fill is up to 14 km thick and characterised by terrestrial, coastal plain and marine siliciclastics ranging in age from Oligocene to Recent. Hydrocarbon-bearing reservoirs in the Malay Basin are mainly in the form of sand bodies deposited in shallow marine and fluvial settings (Madon et al., 1999). Hydrocarbon reserves amounting to around 12 billion barrels of oil equivalent have been discovered and produced (Bishop, 2002) and the southeastern part of the basin contributes between 370,000 and 400,000 barrels of oil per day of the oil production (Madon et al., 2004)

Recently updated broadband technology in 3D seismic processing can deliver fresh insight into fluvial channel system architecture analysis, specifically in planform view geometries by employing seismic geomorphology analysis. Seismic geomorphology is a method to retrieve stratigraphic information from 3D seismic data (Posamentier et al., 2007; Posamentier, 2010). The findings will be useful in compiling quantitative and qualitative databases for deeper subsurface geobodies (> 1000 ms TWT), which helps us to better understand the hydrocarbon potential of channel systems. Databases from seismic geomorphology analysis are potentially useful in the construction of more accurate 3D reservoir geological models. The integration of seismic geomorphological analysis and borehole data is also essential for the study of subsurface channel systems. The accuracy of the interpretation can be strengthened with potential modern-day analogues.

Deltaic and estuarine channel sand bodies are the dominant reservoir types in the Lower Miocene and younger strata, which are the focus of this study. Many of the examples of channel fill deposits in the Miocene Malay Basin appear to display significant tidal influence (e.g., Carney et al., 2008; Liew et al., 2011; Brink et al., 2019; Rapi et al., 2019). Recent work using basin-scale, merged 3D seismic and seismic attribute analysis has documented the abundance of channels of numerous sizes and orientations in the Malay Basin. Despite abundant work on the relationship between relative sea-level and channel type, there is still relatively poor understanding regarding whether there is a relationship between channel fill type and geomorphology (Gibling, 2006). This research is an attempt to address such problems.

Seismic-based, geomorphological studies on the channels systems of ancient fluvial basins commonly highlight and focus on the shallower (< 500m) parts of a basin due to higher data resolution, whereby discussion of deeper (>1500m) successions are less common (e.g., Heldreich et al., 2017). This study is one of only a few other studies which look at older (in this case, targeting the deeper Miocene succession of the Malay Basin) systems. Frequently, studies on fluvial systems focus on fluvial channel sandstones, which are well-known as productive reservoirs for hydrocarbons in many basins globally such as Texas Gulf Coast Basin (Elmowafy & Marfurt, 2016), and Northern Carnarvon Basin (Heldreich et al., 2017). Sedimentological studies conducted since the 1970s have shown that the channel sand bodies in the Malay Basin display facies heterogeneities at different scales (Mazlan et al., 1999). Detailed core-based facies studies by oil and gas companies have shown that the heterogeneity in the channel bodies is mainly due to the effects of tidal reworking on fluvial deposition in such paralic environments. Modern geomorphological studies of tidal channel systems show that there are certain geomorphological features which can be used to identify tidally influenced channels (Hughes, 2012). This integrates core-based facies descriptions and 3D seismic in order to identify such features in the subsurface. This may, in future, provide predictive diagnostic criteria for the identification of tidally influenced channels in the subsurface, which can lead to improved decisions on well penetration, planning, and management.

In general, stratigraphic models have predicted changes in channel architecture as a response to a range of allocyclical processes, including sea-level fluctuation, tectonic events as well as climate change (Schumm, 2005; Miall, 2014). Typically, during base-level rise, strongly meandering channels are common, which grow through lateral accretion and development of point bars. Conversely, during sea-level fall, the channel tends to change from high to low sinuosity (Schumm, 1993, 2005; Miall, 2014). Autogenic processes are usually not considered as primary factors that lead to alterations in the locus point of channels or changes in channel geometry. Channels change their locus point and nature by continuing lateral migration, or these channels may move to the adjacent area of the floodplain by the process of avulsion (Miall, 2006).

Generally, this study will assess the spatial and temporal patterns in channel system facies and stratal architecture observed in the Early to Middle Miocene fluvial-tidal channel succession of part of the Malay Basin. A small 3D seismic subset of the Malay Basin is used to study the geomorphology of fluvio-tidal channels in the Miocene Group H and Group I stratigraphic intervals. This is then integrated with well and core data made available from the Cendor and Jambu fields by PETRONAS. The database of channel dimensions and geomorphologies in this study shall assist in the construction of a quantitative database which will provide a better understanding of the prolific Miocene fluvio-tidal reservoirs in the Malay Basin.

1.2 Aim and Objectives of the Study

This study aims to document the geometries, dimensions, orientations, and distribution of sub-surface geobodies present within the Miocene Group I and Group H of the Malay Basin. This study will employ a quantitative seismic geomorphology approach to map the spatial distribution of depositional elements in the study area and to interpret the temporal evolution of the depositional system. This study will also catalogue the geometry of fluvial depositional elements and evaluate their relationships. The specific objectives of this study are:

(1) To describe and interpret the sedimentary facies in the Middle Miocene (particularly Group H) stratigraphic interval of the Cendor and Jambu fields, offshore Malay Basin.

(2) To describe the geomorphology of the fluvio-tidal channels and other geobodies observed in the Miocene Groups I and H stratigraphic interval within the 3D seismic dataset from the Malay Basin.

(3) To compile geostatistical data of channel geometries such as channel width, channel belt width, channel length along the individual channel (thalweg distance), channel length (wavelength), meander wavelength, sinuosity, amplitude, azimuth, paleocurrent direction, and channel thickness aspect ratio from the channel bodies in the intervals of interest in Group H of the Malay Basin.

(4) To construct an integrated spatial and temporal model of channel system evolution for the Miocene Group I and H stratigraphic interval within the 3D seismic dataset from the Malay Basin.

Existing databases from previous works are often poorly constrained due to the use of variable terms that lead to confusion. Therefore, this study will minimise the confusion by using existing common terminology for the Malay Basin area. This study also highlights the range of uncertainties regarding sedimentological interpretation and the vital need for analogue data to constrain reservoir element dimensions better, rather than relying merely on well-log datasets. Seismic attribute analysis from excellent 3D seismic data can constrain facies elements and architectures more precisely and can be correlated to core and log data.

1.3 General Geology

1.3.1 Malay Basin Tectonic Framework

The Malay Basin is one of the largest Tertiary basins in the north Sunda Shelf, south-east Asia, and has an area of 83,000 km^2 (approximately 500 km long by 250 km wide) (Fig. 1.1). It is located offshore the East Coast of Peninsular Malaysia. Adjacent basins are the Pattani Basin to the north, and the Penyu and West Natuna basins to the south (Hutchison, 1989; Madon et al., 1999; Morley & Westaway, 2006; Pubellier & Morley, 2014). In total, the sedimentary fill of the Malay Basin is more than 14 km thick and comprises clastics of Oligocene to Recent age. The Oligocene strata are mainly terrestrial deposits with minor marine influence, while the Miocene to Recent strata is predominantly shallow marine and coastal to coastal plain deposits (Madon et al., 1999).

The stratigraphic succession is divided into seismic stratigraphic units, denoted as "Groups" which are labelled alphabetically (Group M to A, from oldest to youngest) (Fig 1.2). This study focused on the Early to Middle Miocene stratigraphic units of Group I and Group H. The "economic basement" is represented by pre-Oligocene rocks of the Eastern Belt (Madon, 1999; Tan, 2009; Yu & Yap, 2019). The basement rock types vary from igneous rocks such as andesites and granites in the northern region, and metasediments such as phyllites, marbles in the southwest region. The basement becomes shallower towards the southeast due to tectonic deformation and uplift, which led to the development of a series of compressional anticlines in the Middle Miocene.

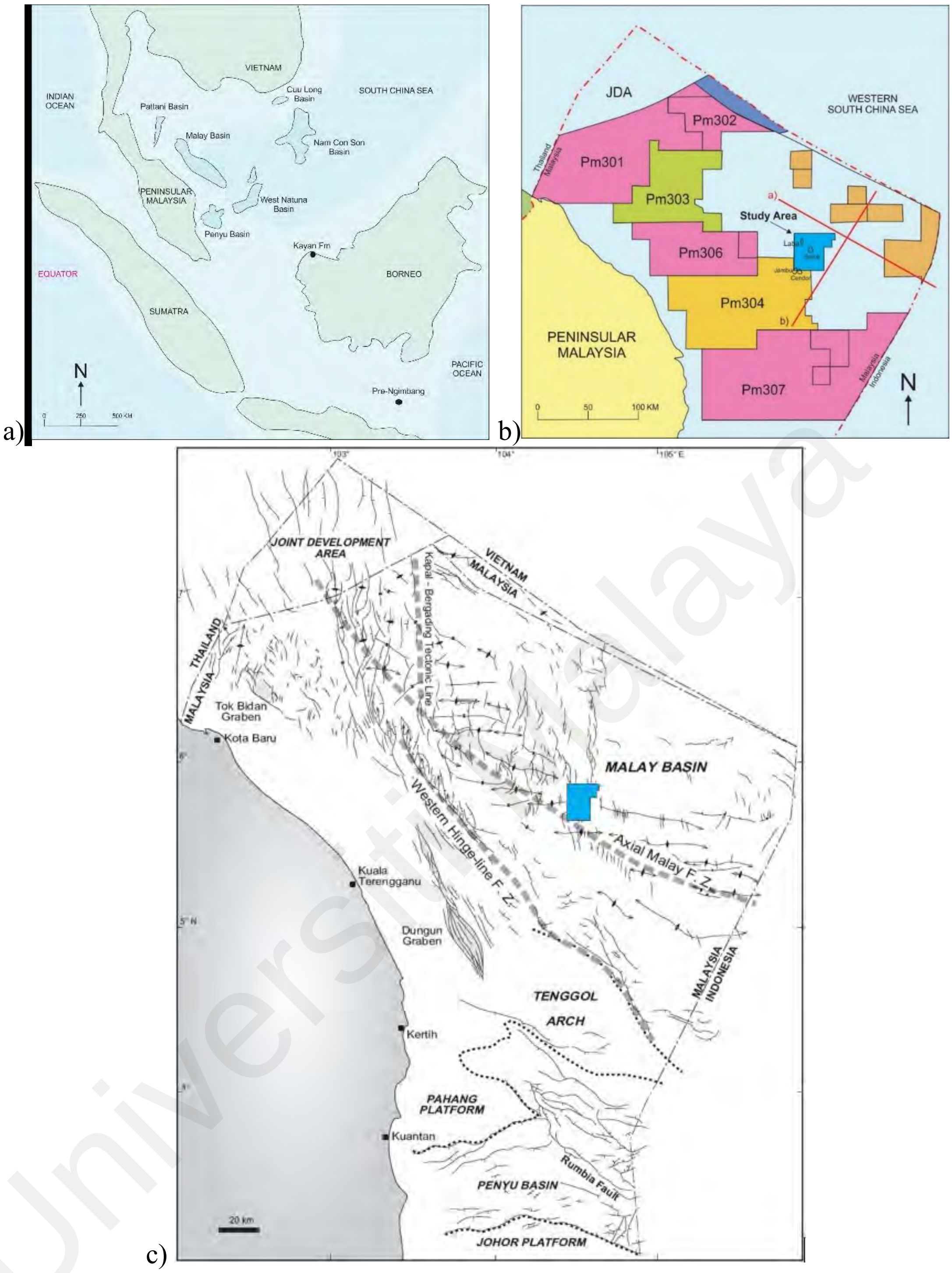

Figure 1.1: a) Location of the elongated Malay Basin trends NW-SE to NNW-SSE, and adjacent basins in Southeast Asia, b) Study area with 3D seismic data highlighted as blue box, covering the Laba, Jambu and Cendor oilfields (modified from Madon et al., 1999), c) Structural trend map of the Malay Basin. The Northern part of the Malay Basin trends NNW-SSE separated from Southern part trends NW-SE by N-S trending Kapal Bergading tectonic line. Blue box is the study area. The Malay Basin is separated from the Penyu Basin by the Tenggol Arch (after Tan, 2009).

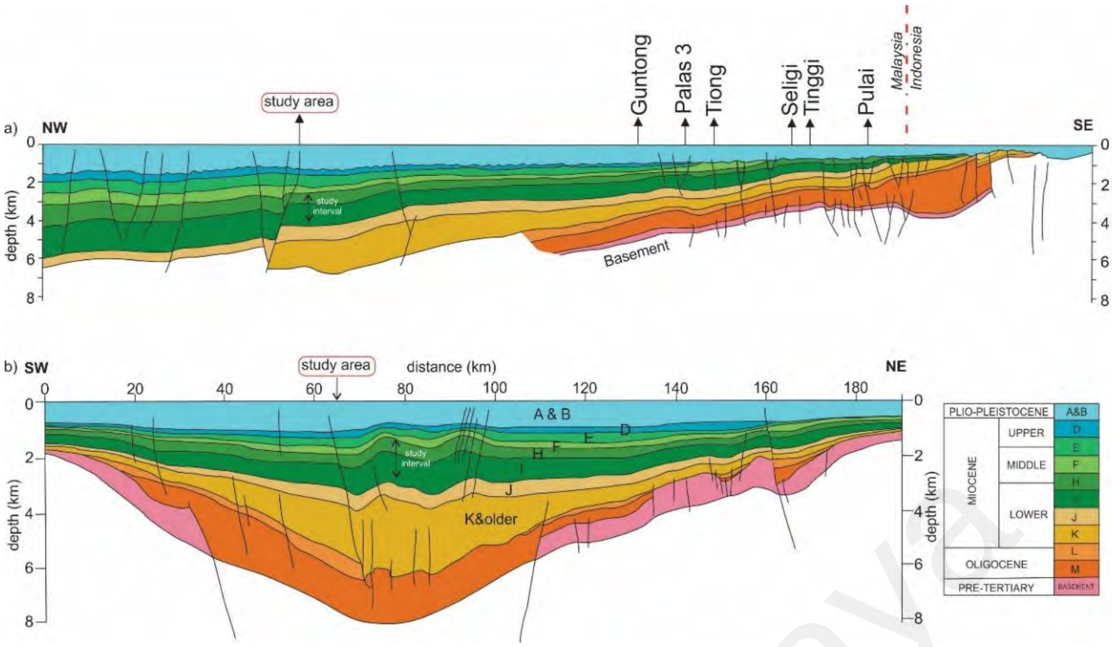

Figure 1.2: Cross-sections of the Malay Basin covering the study area (Location of Line a and b shown in Fig 1.1b). a) NW-SE section. b) SW-NE section (modified from Madon et al., 1999).

1.3.1.1 Structural Framework

The Malay Basin is an elongated, NNW-SSE to NW-SE trending asymmetric basin. The Malay Basin can be divided into a northwestern and southeastern region, which are separated by the N-S trending Kapal-Bergading Tectonic Line (Fig. 1.1c). The northwestern region is dominated by NNW-SSE trending structures, while the southeastern region is dominated by NW-SE trending structures. The axis of the Malay Basin is marked by the Axial Malay Fault Zone. Northern Malay Basin structures trend NNW-SSE to N-S, while southern region structures generally trend E-W to NW-SE (Tan, 2009).

The southwest flank of the Malay Basin is steeper and less structurally deformed, whereas the northeast flank is gentler and more structurally complex. The basement is shallow along the flanks, at a depth of less than 3 km. The Western Hinge-line fault zone marks the southwest flank. The southwest flank extends to the southeast to form the Tenggol Arch that separates the Malay Basin from the Penyu Basin in the south. A series of half-grabens marks the gentler northeast flank of the Malay Basin (Tan, 2009).

Similar to other extensive rift basins on Sundaland, the Malay Basin underwent syn-rift and post-rift periods. The Malay Basin initiated in the Late Eocene (Ngah et al., 1996; Tjia & Liew, 1996). The syn-rift period started in the Eocene and continued until the early Early Miocene. Large E–W- to NW–SE-trending normal fault systems developed during this time. The extensional stage led to the development of E–W-trending grabens and half-grabens, which were filled with thick sequences of alluvial, fluvial and lacustrine sediments. These pull-apart basins developed due to the sinistral wrenching along the Axial Malay Fault Zone (Ngah et al., 1996).

The cessation of extensional faulting in the late Early Miocene marked the beginning of the post-rift period, with the thermal subsidence of the basin continuing to the present day (Madon et al., 2006). Thermal subsidence resulted in the development of a broad sag basin. Subsidence was interrupted by a major inversion phase, which began in the Early Miocene. This inversion was due to the dextral movement along the re-activated Axial Malay fault zone and presumably continued until the Pliocene (Tjia, 1994; Madon, 1997; Madon et al., 2006). The inversion triggered a regional uplift and northwest tilting, which led to the development of a major Upper Miocene erosional unconformity at the base of Group B in the southern basin (Madon et al., 2006). Large E–W trending compressional inversion anticlines developed over pre-existing grabens and half-grabens, predominantly in the central area of the basin. The southern basin contains complex positive flower structures associated with strike-slip and wrench faults (Madon et al.,1999a; Tan, 2009). The inversion stage climaxed in the Middle to Late Miocene and is marked by an unconformity in the shallower section at top of Group D (Madon et al.,1999a; Tan, 2009), and possibly continued until Pliocene (Madon et al., 2006). Subsequently, the basin experienced subsidence without any significant tectonic activity and became a fully open marine, continuing to the present.

The Malay Basin is less than 40 million years old and is most likely still experiencing thermal subsidence. This is shown by the relatively high present-day surface heat flow, with an estimated heat flow anomaly of about 33-42 mWm^{-2} (Madon, 1997, Madon et al., 1999, Tan, 2009). The anomalous heat flow is deduced to be the result of the thinning of the lithosphere during the formation of the basin. A simple rifting model from about 35 Ma for a period of about 10 Ma (Madon, 1997) is the commonly accepted model for the heat flow in the Malay Basin. This model shown that before the trap formation, some of the hydrocarbon would have been migrated out which was suited the structure in the Malay Basin (Waples et al., 1995).

1.3.1.2 Tectonic Origin

Tectonic origin and evolution of the Malay basin have been documented by various workers such as Tjia & Liew (1996), Ngah et al. (1996), Mazlan & Watts (1998), Tjia (1998, 1999), and Mazlan et al. (1999a). There are few opinions on the tectonic model for the origin of the Malay Basin.

The Malay basin was interpreted as a pull-apart basin which developed along a major strike-slip fault zone that was reactivated by the collision between India and Asia (Tapponnier et al., 1982), a back-arc basin (Kingston et al., 1983; Mohd Tahir et al., 1994), or a basin formed by regional thinning of the continental crust (White & Wing, 1978). Other tectonic models for the basin's origin also suggest crustal extension over a hot spot, intracontinental basin (Hutchison, 1989a; Khalid et al., 1996), distributed shear deformation of a pre-existing basement fault zone (Madon, 1997a), and a broken rift in a triple junction over a hot spot (Tjia, 1998b, 1999b).

In general, three major tectonic events have occurred in the Malay Basin that contributed to the current petroleum system in the area; 1) Late Eocene to Oligocene crustal extension with left-lateral shear and significant subsidence, 2) Middle to Late

Miocene north-to-south compression with reverse or right-lateral shear, folds, and inversion, 3) Pliocene to Recent slight extension and regional thermal subsidence (Ng, 1987; Hutchison, 1996; Ngah et al., 1996).

The Malay Basin with adjacent Penyu and West Natuna Basins were initiated in the Late Cretaceous based on the failed triple-junction model (Tjia, 1998b). In the Late Cretaceous, the highest heat flow (>110 mW/m^2) in the Malay Basin was at the triple junction of the Malay, Penyu and West Natuna basins. This hotspot consisted of a mantle plume and formed a circular uplift about 500 m in radius, which is referred to as the Malay Dome (Tjia, 1998b) (Fig 1.3a). The Malay dome was likely of Late Cretaceous age due to the widespread occurrences in northern Sundaland area of Late Cretaceous granitic plutons. The failed rift arms (radiating triple junction) of the crustal dome are known as aulacogens and developed into the Malay, Penyu and West Natuna basins. These basins became the Tertiary depocentres for thick sediments.

In the Middle Eocene, hard collision between the Indian sub-plate and Eurasian plate may have caused the extrusion of crustal slabs of the Southeast Asian lithosphere towards the southeast along major NW–SE striking wrench faults (Fig 1.3b). The NW-SE-trending Axial Malay Fault inferred as an extension of the 3 Pagodas faults. The Dungun faults and Hinge-line at the west deduced as dextral strike-slip faults in comparison to the eastern area. The development of E-W trending faulted grabens and half-grabens were due to the movement of the sinistral wrench along the Axial Malay fault. The continued subsidence of the aulacogens through Late Eocene and Early Oligocene is consistent with the cooling of the mantle plume underneath the Malay Dome.

In the Late Oligocene, crustal slab extrusion from mainland SE Asia was influenced and hampered by the opening of the South China Sea basin, and subduction along NW Borneo. Asymmetric seafloor spreading indicates the discrepancies in spreading rate. The South China Sea spreading ridges split into two sections, i.e., a northern and southern section. Subsidence and extensional events of the Malay basin and adjacent basins continued throughout the Late Oligocene (Fig 1.3c).

The spreading of the South China Sea Basin stopped in the Middle Miocene, and subduction in Borneo became inactive. The termination of the South China Sea Basin's spreading allowed the westward push due to a change in the stress fields from the Pacific plate into western Southeast Asia region (Tjia, 1988). India-Australia plate proximity influenced the eastern Southeast Asia region and hindered the crustal slabs expulsion of Southeast Asia.

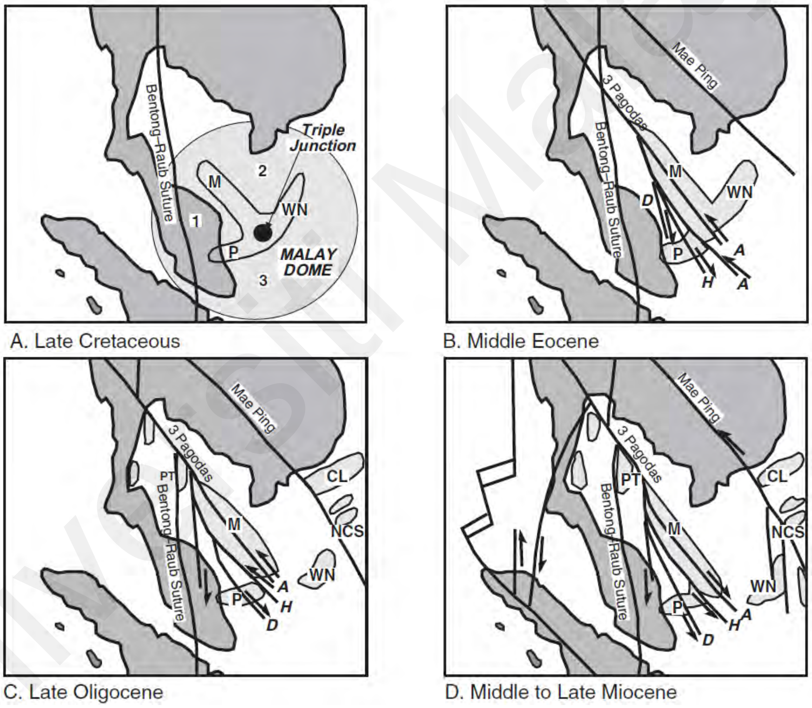

Figure 1.3: Tectonic evolution of the Malay (M), Penyu (P) and West Natuna basins (WN). (A) Late Cretaceous. Rising mantle plume formed the Malay Dome beneath a triple junction. (B) Middle Eocene. Differential extrusion of crustal slabs of SE Asia creates major strike-slip faults including the Mae Ping, Three Pagodas, Axial Malay (A), Western Hinge-line (H), and Dungun (D) faults; (C) Late Oligocene. Extrusion of SE Asian crustal slabs hindered by the opening of South China Sea Basin. (D) Middle to Late Miocene: Reversal of strike-slip movements caused structural inversion in the Malay, Penyu, and West Natuna basins. (modified after Tjia, 1998).

The westward movement of the Pacific Plate and the advancing Indian Ocean-Australia Plate resulted in the reversal of the major strike-slip faults. This encouraged development of widespread unconformities in the middle Miocene in the Tertiary stratigraphy (Fig 1.3d). The Axial Malay Fault Zone became a dextral fault zone due to a change in the regional stress field. This resulted in a structural inversion and development of E-W trending anticlines and thrust faults.

The Post-Miocene N-S striking faults on the crests of anticlines were related to tensional stress, and Post-Miocene sediments are basically horizontal although some faults are inherited from the deformed sequences underneath (Tjia, 1988).

1.3.2 Stratigraphic Record and Paleoclimate

1.3.2.1 Stratigraphic

The stratigraphy of the Malay Basin is divided into several seismo-stratigraphic units. These units are referred to as 'Groups', which are named alphabetically (from Group A to M, in descending order from youngest to oldest) in the late 1960s by ESSO (EPMI). The scheme was refined by Madon et al. (2006), constrained with biostratigraphy data, with each Group being bounded by basin-wide seismic reflectors displaying truncated, onlapping and/or downlapping surfaces (Fig 1.3 and Fig 1.4). EPMI's seismo-stratigraphic scheme was correlated with the biostratigraphic scheme, and EPMI 's seismic markers represent time planes. Two major unconformities were recognized, i.e., a Middle Miocene Unconformity (MMU), and an Upper Miocene Unconformity (UMU) (Yakzan et al., 1996).

PETRONAS (2007) has also identified older strata (Groups N, O and P) which extend the basin-fill stratigraphy into the Paleocene. The age of Groups K, L and M were also revised to be older (Oligocene) than previously thought and interpreted as mainly fluvial and lacustrine sediments. Lower to Upper Miocene Groups J to D consist of sediments deposited in a fluvial-shallow marine system with an extensive coastal plain. Lower Pliocene to Recent sediments of Group B and A were also deposited in a fluvial-shallow marine environment that developed after the Upper Miocene to Middle Miocene compressional periods.

Stratigraphic development during the Paleocene to Late Oligocene, syn-rift extensional phase, initiated with deposition in isolated grabens and half-grabens, resulting in the thick deposits of Group M, L and K. These Groups consist of alluvial and lacustrine sediments. Group M was deposited in an alluvial-lacustrine setting and estimated to be 300 m thick on average and is composed of mud and sand (Tan, 2009). Group L has similar characteristics to Group M. Group K is characterised by braided river deposits associated with alluvial and deltaic environments, has an average thickness of about 400 m of is also composed of mudstone and sandstone (Madon et al., 1999a; Tan, 2009).

The transition from Group K (lacustrine shale) to the overlying Group J (marine sandstone) signifies the beginning of marine incursion into the basin in the Early Miocene. Indication of coastal inundation is recognised from abundance of *Florschuetzia trilobata* group and regular *F. semilobata* in the Lower Miocene strata (Yakzan et al., 1996; Ismail et al., 1994). The post-rift stage commenced in the Early Miocene with basin sag due to thermal subsidence. Sediments deposited during this phase until the Late Miocene make up the subsequent units of Group J to D. Progradational to aggradational fluvial to tidal-estuarine deposits make up Group J and Group I. Group J sediments were deposited in a tidally dominated paralic to shallow marine setting, interpreted as part of a lowstand system tract, and comprises an average 250 m thick succession of mudstone, sandstone, and coal (Madon et al., 1999; Tan, 2009). Group I sediments were deposited in a fluvial deltaic environment and consist of an average 300 m thick succession of shale, sandstone, and coal (Madon et al., 1999; Tan, 2009). Group I consist of two reservoirs, i.e., a lower reservoir comprising fluvial deltaic deposits including braided fluvial channels, and an upper reservoir comprising sandy tidal estuarine sediments.

Basin inversion and compression initiated in the late Early Miocene, conformant to the top of Group I, and continued till the Late Miocene and probably into the Pliocene (Madon et al., 1999a; Tan, 2009). This led to a major uplift and erosion in the southeastern part of the Malay Basin. Groups H and F sediments were deposited during an overall relative sea-level rise and comprise marine to deltaic sediments with fluvial/estuarine channels (Madon et al., 1999a). The average thickness of Group H sediments is about 200 m. An unconformity due to the major uplift and erosion truncates folded strata of Groups H and older, with undeformed sediments of Groups A/B deposited overlying the unit. Erosion along structural crests has removed up to 1.2 km of sediment (Murphy, 1989). Meanwhile, deposition continued on their flanks during this inversion.

Group F comprises sediments deposited in low energy coastal plain, tidal environments, with marine influence, and has an average thickness of 400 m of siltstone, carbonaceous shale, sandstone, and coal. Group E sediments were deposited in a coastal plain environment with marine influence, with the sandstones interpreted as shoreface, bar, and channel deposits. Group E has an average thickness of 300 m and consists of sandstone, siltstone, carbonaceous shale, and coal. Group D sediments were deposited in a shallow marine environment and had an average thickness of 650 m of mudstone, sandstone, and coal (Tan, 2009).

The Malay Basin experienced subsidence and establishment of fully open-marine conditions during the Pliocene to Recent. Groups A and B sediments were deposited in shoreline to shallow-marine environments and mostly consist of marine silt and clay deposits. Figure 1.5 illustrates a reconstruction of the palaeogeographic evolution of the Malay Basin from Madon et al. (1999a). The basin evolved from non-marine environments (alluvial, fluvial, and lacustrine) during the Oligocene to earliest Miocene, to becoming increasingly more marine (coastal fluvio-marine to inner neritic) from the Early Miocene to the present (Madon et al., 1999). The palaeogeographic maps show that the basin was a narrow, gulf-like basin partly connected to the ancestral South China Sea via the West Natuna Basin at the southern end and received sediment from its north-eastern and south-western flanks (Nik Ramli, 1986; Madon, 1994; Madon et al., 1999).

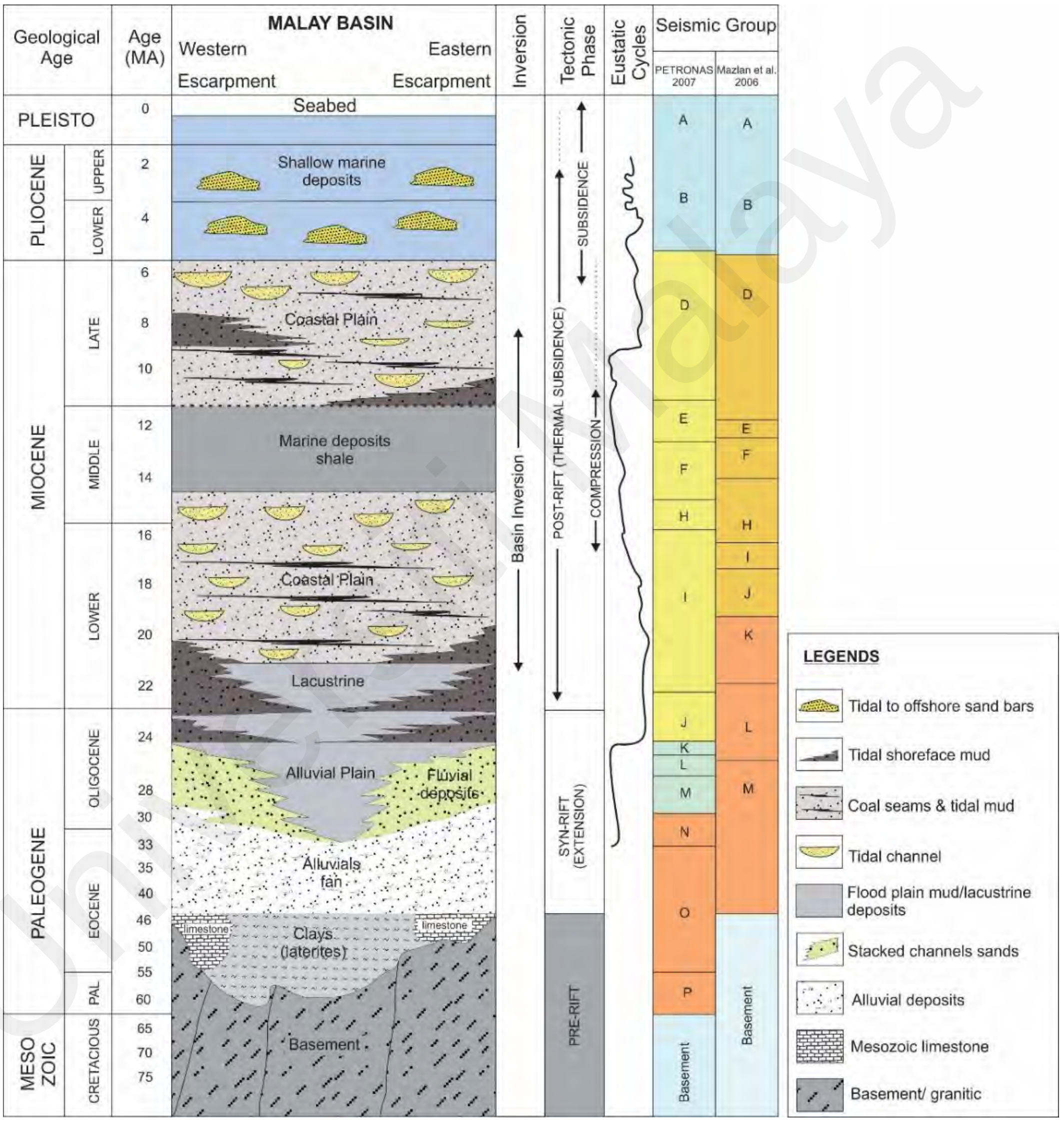

Figure 1.4: Chrono-Stratigraphic framework of the Malay Basin, including geological age, lithology and depositional settings, periods of inversion, local tectonic events, eustatic cycles and Seismic groups. Modified from Madon (1999), EPMI (1999), Madon et al. (2006), and PETRONAS (2007).

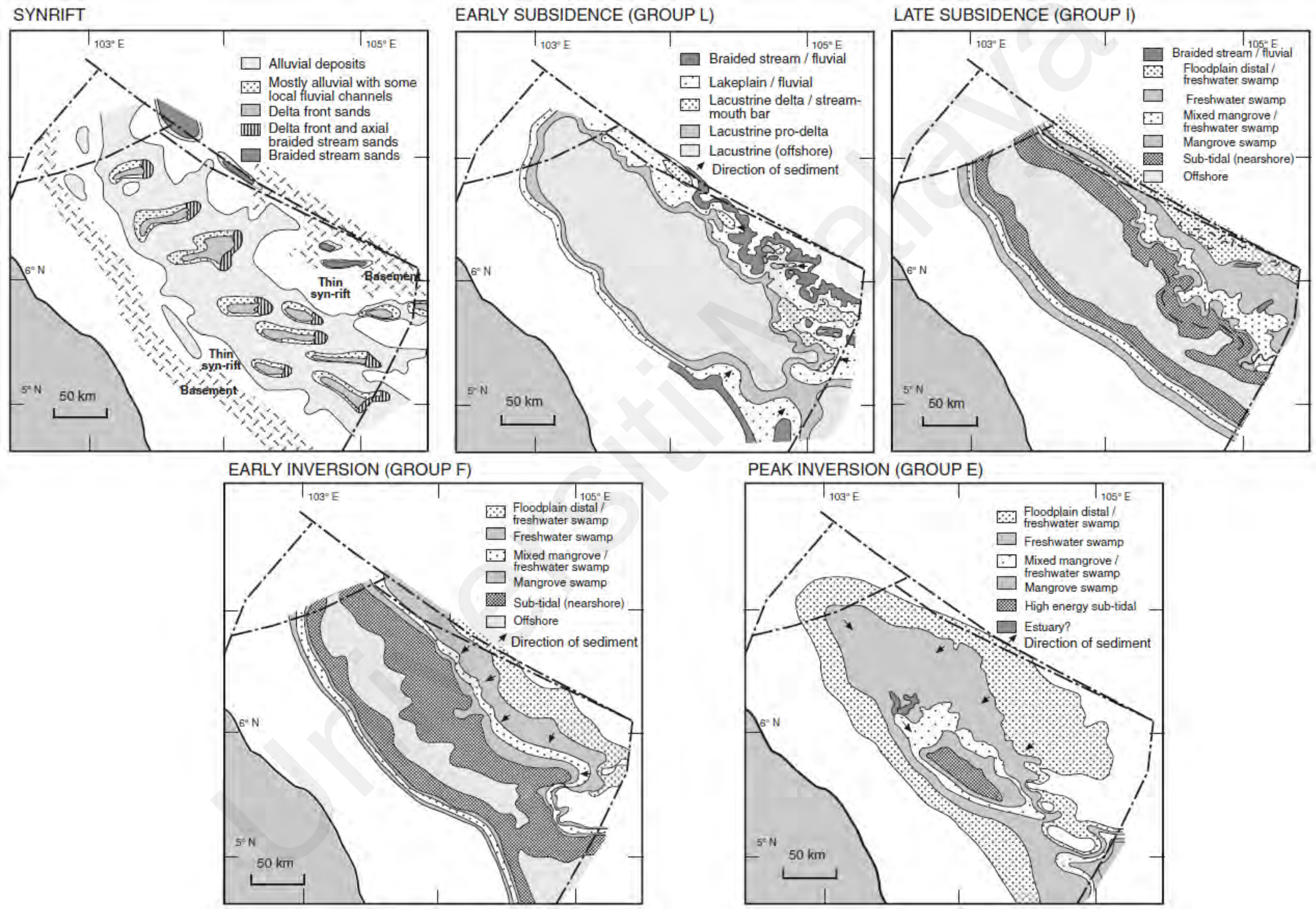

Figure 1.5: Malay Basin paleogeographic maps from EPIC (1994) study (modified from Madon et al., 1999a)

1.3.2.2 Biostratigraphy and Paleoclimate

The Sunda Shelf covers an area of approximately 125,000 km^2 and is one of the largest tropical shelves on the earth (Hanebuth & Stattegger, 2003). The complex Cenozoic geological history of Southeast Asia has influenced the climate and vegetation of the province. Yakzan et al. (1996) established fifteen (15) palynomorph assemblage zones (termed 'PR' zones) in the Malay Basin, based on the evolution of mangrove pollen. Several studies later further discussed and evaluated this scheme e.g., Boyce et al. (2006) and Morley et al. (2015). Morley et al. (2021) established a new chronostratigraphic framework to allow correlation between basins throughout Malaysia including the Malay Basin, Penyu Basin, Sarawak Basin and Sabah Basin.

Paleocene strata are poorly documented in the Malay Basin, which suggests widespread emergence during this time. The Paleocene pollen flora observed in the Kayan Formation of western Sarawak has a low diversity with many taxa not having a modern analogue but suggests a sub-humid climate in the region (Muller, 1968; Morley, 1998, 2000). Pollen from coaly sediments of the Pre-Ngimbang Formation (of possibly Paleocene and early Eocene age e.g., Phillips et al., 1991) in the East Java Sea suggest an everwet climate (Bransden & Matthews, 1992). There was a climatic gradient across Sundaland in the Paleocene, with wetter climates southeastward, due to the assemblages of a trichotomosulcate palm pollen type in coaly sediments that represents the Neotropical coccoid palms *Acrocomia* and *Ceroxylon* (Morley, 2012).

Palynological studies on subsurface and outcrops of Java and Sulawesi, which was connected to Borneo during the Middle Eocene, provide some insight into palaeoclimate conditions during the Eocene (Hall, 1998). The flora had abruptly changed in the early Middle Miocene, following the collision between Eurasia and the Indian Plate. The extinction of Paleocene pollen types was followed by the dispersal of numerous taxa of Indian origin into the Southeast Asia region. Indian elements from southern Sulawesi indicate a change in climate through the Middle Eocene. Low diversity of palynomorph assemblages dominated by Restionaceae pollen in the early Middle Miocene suggest a sub-humid climate. However, in the late Middle Miocene, the dominance of *Palmaepollenites* spp. indicates a wetter climate period in the region. Restionaceae pollen occurs following the warmest global temperatures period suggested by oxygen isotope study by Zachos et al. (2001). This may be related to the Eocene thermal maximum period, with everwet climates emerging as the global climate cooled.

The Oligocene in the Malay and West Natuna Basins is marked by climate change in association with syn-rift and post-rift basin development as well as inversion. The palynotaxon *Barringtonia* (Lecythidaceae) is common in the Oligocene (syn-rift) Benua and Lama Formations of the West Natuna Basin, which indicates a seasonal swamped freshwater setting, while the common presence of Poaceae and *Celtis* pollen without bisaccate conifer pollen, indicate an open woodland and a period of seasonally dry climate. Pollen of open woodland trees such as *Celtis* (Ulmaceae) and Combretaceae but without bisaccates and low occurrences of Poaceae pollen were seen in the younger Belut Formation, which indicates a sheltered sclerophyll woodland in a seasonally dry, slightly wet climate (Morley, 2012).

Deposits of Group M (post-rift phase) in the Malay Basin contain the same sheltered sclerophyll woodland pollen assemblage, with common *Pinus* and low frequency of Poaceae (Zones PIVB-D, and PR1–2 of Yakzan et al., 1996), which is indicative of a seasonally dry pine-dominated forest setting. Temperate taxa such as *Picea*, *Abies*, and *Tsuga* indicate intermittent cooler intervals. Later, the acme of *Shorea* type pollen, *Ephedra* pollen, and common Poaceae observed associated with Groups L and K strata in the Malay Basin suggest monsoonal dipterocarp forest development with a combination of wet and seasonal climate elements.

During the latest Oligocene (~24 Ma) (Fig 1.7), the Sunda platform was flooded, with marine incursion extending northward into the North Malay Basin (equivalent to Group K). The rise in sea-level is due to the Late Oligocene warming trend (Zachos et al., 2001) and links to palynological zones PR3–7 in the Malay Basin (Shoup et al., 2012). This event resulted in the extensive deposition of marine mud. The sudden appearance of the brackish water foraminifer *Miliammina* without any other foraminiferal elements in most lacustrine facies in this interval provides evidence of this marine incursion (Morley et al, 2007; Morley, 2012; Shoup et al., 2012). Their occurrences and distribution were seen at the same stratigraphic horizon across adjacent basins such as the Con Son Basin. This is related to a rapid rise in sea-level over a broad low gradient topography.

Deposition of the Lower to Middle Miocene succession in the Malay Basin and the adjacent basins of West Natuna, Penyu and Con Son coincided with a basin inversion phase. These basins record very similar pollen types of mostly peat swamp and rainforest pollen. TheEarly Miocene stratigraphy of the Malay Basin is mainly based on the evolution of mangrove pollen, with 2 palynological zones identified (PR9–10 of Yakzan et al., 1996). The Early Miocene stratigraphy was further refined by the integration of biostratigraphic and seismic data (Morley & Shamsuddin, 2006; Wong et al., 2006) by using benthonic foraminifera and palynology to describe depositional cycles. During sea-level rises, mangrove swamps spread widely with subsequent acme of shallow water foraminifera at the highest sea-level of the cycle.

The Early Miocene (i.e., Aquitanian ~21-23 Ma) was a period of slow, intermittent transgression, with marine influence extending to the southernmost Malay Basin at ~22 Ma (Fig 1.7) (Shoup et al., 2012). However, the earliest Early Miocene which is represented by Group J (J1000, Fig 1.6) is marked by an abundance of sands deposited during the eustatic sea-level fall associated with the M1 glaciation (see Zachos, et al., 2001) (Morley., 2012). The occurrence of herbaceous swamp elements in Lower Miocene deposits of the northern area of the Malay Basin suggests a seasonal swamp setting. The abundance spores in the northern Malay Basin associated with lower Group I suggest that terrestrial marsh ferns largely dominated the swamps. Coals are common and indicate an everwet climate, even in the lowstand deposits. Therefore, the Early Miocene is interpreted as the period of the wettest climates and the most extensive rainforest development in the region. The Malay Basin remained brackish until the Burdigalian (Shoup et al., 2012).

The highest sea-levels of the 'Middle Miocene thermal maximum' in the Middle Miocene resulted in widespread open marine conditions extending from offshore Vietnam (Mang Cau Formation) to the southern Malay Basin (Group H and F) (Shoup et al., 2012). A palynological record of widespread peat swamps during Group H deposition indicate the climate was still everwet (Yakzan et al., 1994; Shoup et al., 2012). Occasional acmes of conifer pollen indicate recurrent episodes of cooler climate during low sea-level, whereby evidence of seasonality is limited. Coals record widespread peat swamps across the Malay Basin during late Middle Miocene. The occurrence of foraminifera in the southern Malay Basin is indicative of a middle neritic setting. Hence, restricted tidally influenced marine conditions extended northward into the north Malay Basin. The occurrence of Poaceae acmes and montane conifers in the Group D succession (Late Miocene to Pliocene) indicate seasonality during low sea-level periods.

During the Late Pliocene and Pleistocene, the Sunda Shelf was tectonically stable (Madon & Watts, 1998). This suggests that the Pleistocene Last Glacial Maximum (LGM) weather was equivalent to the tropical climate of modern-day lowlands in Southeast Asia (Morley, 2000; Sun et al., 2000). However, during the Pleistocene LGM, monsoon-driven precipitation was lower than during the Holocene, suggesting that vegetation patterns in lowland areas, such as the Sunda Shelf, may have been affected by the dry winter monsoon (Wang et al., 1999). The Sunda Shelf was drowned during the

Holocene, forming one of the largest marginal seas in SE Asia, and is connected to the larger and deeper waters the South China Sea towards the east.

In the Late Oligocene, sediment input into the Pattani and Malay basins was from the western mountains in the area between Thailand and Myanmar, and the west margin in the Khorat Plateau (O'Leary & Hill, 1989; Upton, 1999; Watcharanantakul & Morley, 2000; Rigo et al., 2003)

According to Morley & Westaway (2006), the sediment source for the Pattani and Malay basins during the Miocene was from the western highlands of the Mae Ping fault zone, the Chainat Ridge and the peneplained pre-Tertiary rocks between the Suphan Buri and Ayutthaya basins.

During the Pleistocene to Recent, a major trunk river, referred to as the Paleo-Chao Phraya–Johore River, flowed southeastward across Sundaland. The river passed through the Gulf of Thailand and proceeded along the axes of the Pattani and Malay Basins and finally into the southern China Sea (Alqahtani et al., 2015). This primary trunk river is one of the most significant ancient sediment channels outspreading into the northern part of Thailand, linking the Sunda Shelf and the Malay Basin into an enormous drainage basin (ca. 1,350,000 km^2) (Alqahtani et al., 2015). The secondary source of sediment during this period was brought to the Malay Basin by eastward rivers which drained the western area of the Malay Peninsula (Leo, 1997; Morley & Westaway, 2006; Alqahtani et al., 2015).

1.3.2.3 Paleotidal Conditions

In the Late Oligocene-Miocene, the Malay Basin was situated in the western area of the South China Sea (SCS). Tides in that region were macrotidal during the late Oligocene and were able to transport gravel to coarse sand across an extended Sunda shelf (Collins et al., 2017; 2018). Three significant geomorphological characteristics were discovered in the late Oligocene – early Miocene associated with the initial closure of the proto-SCS and the marine transgression: (i) a wide shelf area of more than 400 km; (ii) partially enclosed embayment that developed from the merging of the East Natuna and Sarawak embayments (ENS); and (iii) The Gulf of Thailand (GOT), an early sinking of an elongated narrow embayment.

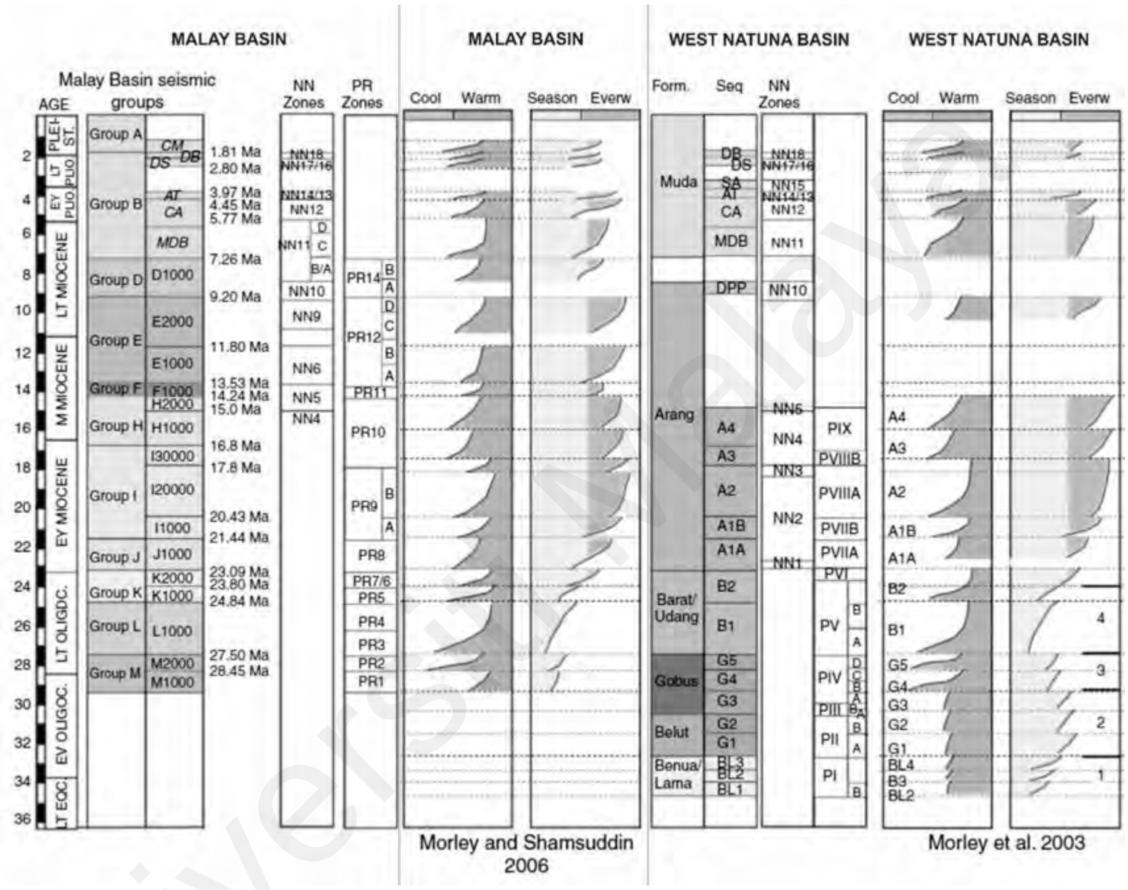

Figure 1.6: Climate trends linked to the stratigraphy in the Malay Basin (Morley & Shamsuddin, 2006) and Natuna Basin (Morley et al., 2003; Morley, 2006).

Tides at the narrow entrance at the Gulf of Thailand (GOT) and West Natuna Basin were macrotidal during the Early Miocene. However, in the narrow northwest to the southeast trending Malay Basin, tides were microtidal and only capable of carrying sand. Frictional damping rather than amplification was dominant in the Early Miocene of GOT.

There was a gradual decrease in the tidal range from macrotidal to mesotidal along the coastline of the Western SCS during the Middle Miocene, which coincided with a decline in shelf width from approximately 250 km to 200 km (Collins et al., 2018). Subsequently, the sediment grain size that was able to be carried by the tides decreased from coarse to very fine sand and mud. Convergent effects in the narrow (< 250 km wide) and shallow (< 50 m) Middle Miocene GOT resulted in greater frictional tidal damping which exceeded tidal amplification. However, tidal ranges were still mesotidal and capable of carrying coarse-grained deposits. This narrow GOT segregated greater tidal energy to the neighbouring ENS embayment.

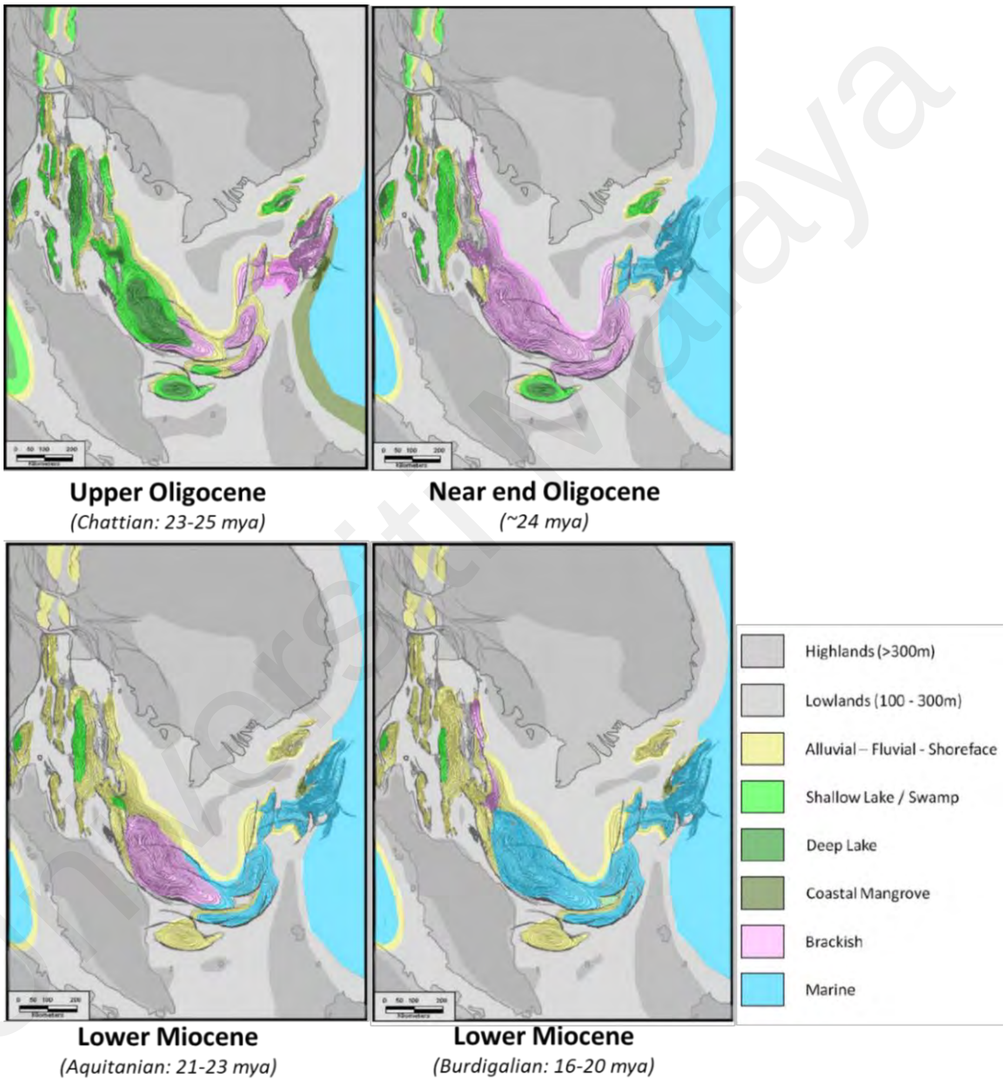

Figure 1.7: Paleogeographic maps of Late Oligocene to Early Miocene South China Sea region. Brackish –marine conditions dominated within the Malay Basin (modified from Shoup et al., 2012).

1.4 Dataset and Methodology

An integrated dataset used in this study are legally approved by Petroliam Nasional Berhad (PETRONAS). They occupy a small subset of 3D seismic from a 'mega merged' 3D seismic with a total area of 1563 km^2 (41.3 km wide by 36.7 km long). This area was chosen due to the prevalence of fluvial geobodies in the Group I and Group H succession of the Miocene Malay Basin. These geobodies can be imaged well through seismic attribute analysis to improve understanding of the fluvial reservoir distribution, stacking patterns and reservoir architecture of this type of fluvio-tidal channel depositional environment. The dataset consists of a high-quality 3D seismic volume and data from 4 exploration wells, three of which have cored intervals covering different parts of the Miocene succession. The following techniques and approaches were used: 1) Seismic facies study of the Group H and Group I succession, conducted in order to classify and separate the range of interest into seismic units; 2) production of time and iso-proportional slices for the visualisation of channel systems in planform view; 3) analysis of well data to determine lithology and lithofacies; 4) Usage of Paleoscan and Petrel tools to establish a comprehensive methodology for measuring channel morphometric parameters.

1.5 Thesis Structure

This dissertation is made up of seven chapters.

Chapter 1 is an introduction to the project, including the geological background and context of the study area, as well as the aims and the objectives of this study.

Chapter 2 reviews critical literature, concentrating on four key aspects: 1) fluvial-tidal channel systems, including channel type classification; 2) Longitudinal process, morphological and facies trends along fluvial-tidal channels. This is discussed for both estuary and deltaic settings; 3) The analysis of fluvial systems based on examples throughout the world, including the fluvial architecture elements, fluvial facies, fluvial hierarchy, the formation and identification of incised valleys and sequence boundaries, and the factors controlling fluvial deposits and morphologies, and 4) The technologies of 3D seismic geomorphology and previous studies in 3D seismic fluvial systems geomorphology.

Chapter 3 describes the approaches and techniques employed in this study, comprising the seismic attributes analysis methodology and spectral decomposition applied to evaluate 3D seismic geomorphology and to acquire and determine the geometry of the fluvial channels using developed empirical equations.

Chapter 4 provides thorough, detailed descriptions and interpretations of sedimentary facies, facies associations, and architectural elements identified within the Top of Group H of the Malay Basin. The controls on facies distribution, geobody architecture, and the spatial and temporal evolution of the depositional system are also discussed.

Chapters 5 integrates wireline and seismic data to better understand the range of fluvial architectural elements that can be imaged in a deeper section of 3D seismic data in the Malay Basin. The spatial and temporal evolution of seismic geobodies is assessed in relation to possible auto- and allocyclic controls on the regional depositional system. The architectural elements are compared to published literature in an attempt to classify and define their dimensions. The results of this study are also considered with regards to reservoir modelling implications.

Chapter 6 reviews the spatial distribution of nearly 120 channels within Group I and Group H of the Malay Basin. Integration of the parameters extracted from the 3D seismic isoslices are populated, and comparisons are made with modern-day analogue channel systems.

Chapter 7 provides conclusions of the results and key findings from research in Chapters 4 to 6. A series of potential directions for future work are recommended.

CHAPTER 2: FLUVIO-TIDAL CHANNELS IN PARALIC DEPOSITIONAL SYSTEMS; THEIR SEDIMENTOLOGY, GEOMORPHOLOGY AND GEOPHYSICAL EXPRESSION IN THE ROCK RECORD

2.1 Introduction: Fluvial Systems

There are three basic geomorphological zones which can be present in a fluvial system (Fig 2.1a), i.e., 1) an erosional zone where the rivers are deliberately cutting down into the valley floor and wall, and the eroded material is transported downhill; 2) a transfer zone, where the streams and rivers do not erode aggressively, and most sediment is bypassed downstream, and; 3) a depositional zone, where sediments are deposited within the fluvial channels and on the delta plain or floodplain areas. These three zones do not necessarily exist in all systems, as some areas are entirely erosive, while others may have mixed erosion and transfer zones. Channels can be either confined by bedrock, which is hard to erode, or un-confined, where channels are freely able to switch course and avulse (Schumm, 1977). Figure 2.1b shows the variation of fluvial types that are present in both modern and ancient systems.

Downstream fluvial morphology and evolution can be influenced by factors such as changes in river gradient, sediment load, bank material, climate, or tectonic regime (Schumm, 1969; Burnett & Schumm, 1983; Peterson 1984; Carson, 1984). Rivers may change their nature between perennial and ephemeral along its course, e.g., the Okavango River (Seely et al., 2003). Dry river channels with occasional or periodic discharge are regarded as ephemeral river systems.

Most stratigraphic and architectural studies of ancient river channel systems are limited by the nature of the data, which is typically in the form of 2-D exposures. Some good studies include work on the Miocene Siwalik Group of northern Pakistan (Willis, 1993) and the Triassic Chinle Formation of Utah (Trendell et al., 2013). Wilson et al.

(2014) used photo-panels to characterize the depositional architecture and sedimentology of the lower Permo-Triassic Beaufort Group, Karoo Basin, South Africa. However, there is still a significant level of uncertainty concerning the facies distribution and paleocurrent trend. Fluvial style may also change through a stratigraphic succession, due to temporal changes in the factors listed above.

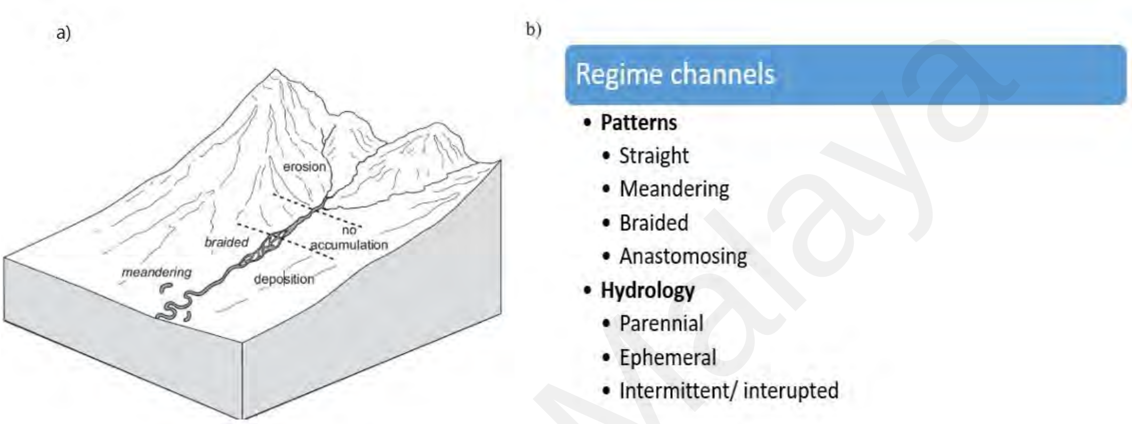

Figure 2.1: a) Adjacent regions and flowing rivers further downstream, typical braided rivers do occur (from Nichols, 2009). b) Different types of fluvial systems which exist in the world.

Channels are a common component of fluvial systems and act as the primary conduits by which sediment is transferred from the continents to the sea or lake. Channel morphology is controlled by numerous factors, including alluvial and basinal processes (fluvial, wave, and tidal control) as well as shelf gradient, climate, and tectonics. Channels are defined as "*elongate depressions in the alluvial surface, with more or less clearly defined margins or banks between which the river flow is restricted for most of the year*" by Friend (1983) (Fig 2.2). Present-day channels are runoffs and incise into the surface of the land. They are confined features and transport water and sediment (Nichols, 2009), from highland to lowland. The term channel as used in this study refers to geobodies imaged in seismic 3D data, where they are marked by a concave-up cross-section and can be described by their geometry and dimensions, i.e., channel width, depth, and sinuosity.

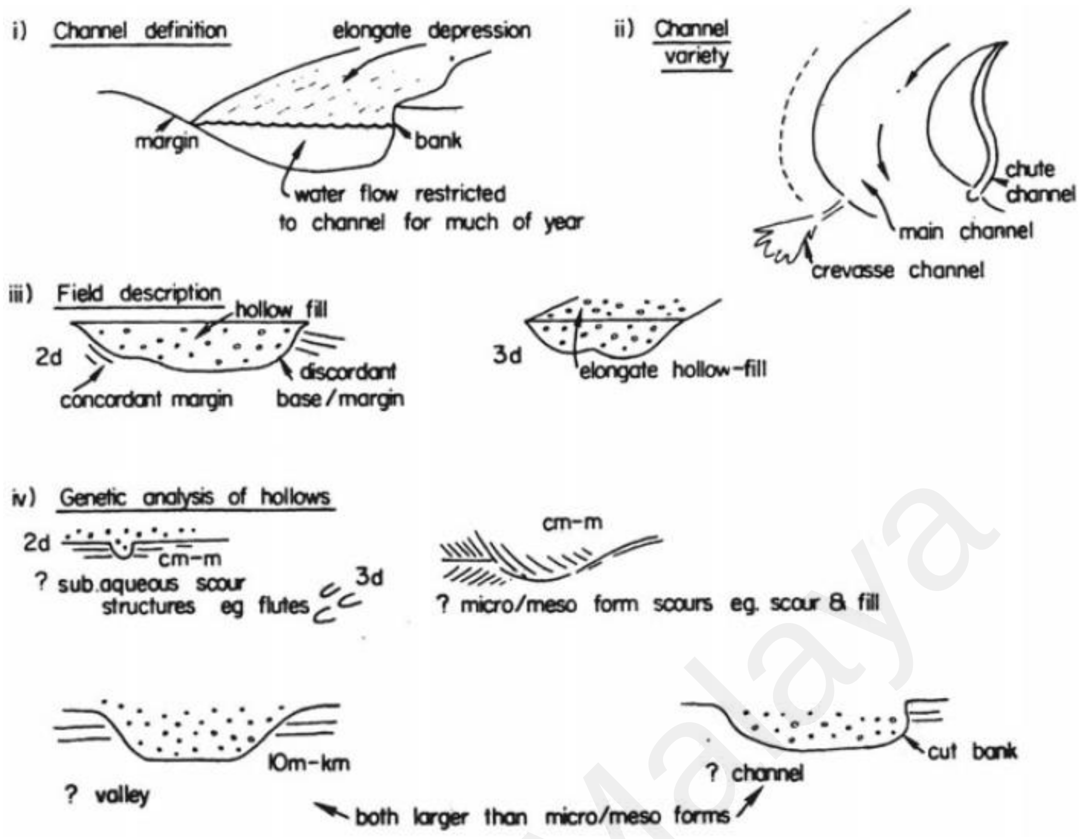

Figure 2.2: Channel description and identification by Friend (1983).

Various terminology is used to describe channels in fluvial systems, especially in the coastal paralic depositional environment, such as incised valley, fluvial channel, tidal channel, distributary, estuary, and tributary. These terms are based on the location of the channel in the depositional environment and the processes that control sediment deposition. Fluvial channels are defined by the dominance of fluvial processes in sediment transfer, erosion and deposition that occur along the river profile on the alluvial plain, while tidal channels are significantly influenced by tidal processes near the shoreline. Distributary channels are the outflowing channels which originate and branch out from fluvial channels on delta plains and supply river water and sediment to the sea. These channels can be fluvial-dominated, tide-dominated or mixed influenced. Estuaries are defined as semi-enclosed (Pritchard, 1960, 1989), and ephemeral features (Catuneanu, 2006) of transgressive coastal environments at the river mouth (Dalrymple et al., 1992, 2007), which consist of facies influenced by fluvial, wave and tide processes as it receives sediment from marine and fluvial sources. Lastly, tributary channels are defined as smaller channels which flow or drain into a larger channel, which are frequently of the tide-dominated channel type in paralic settings.

This study is mainly interested in the geometry, dimensions, facies and stratal architecture of fluvio-tidal and tidal channels in marginal marine/paralic, coastal depositional environments. Fluvio-tidal channels display signatures of both fluvial and tidal processes along the channel profile and may be found in two main paralic depositional settings, i.e., tide-dominated estuaries, tide-dominated deltas. Fluvio-tidal channels display a great diversity in their geometry, dimensions and stacking patterns.

This chapter touches on seven important topics related to fluvio-tidal channel sedimentology and geomorphology: 1) Paralic depositional setting within fluvio-tidal environments; 2) Review of channel definitions and architectural elements; 3) Fluvial channel classification and morphology; 4) Tidal channel classification and morphology; 5) Longitudinal trends along fluvio-tidal channels; 6) Review of fluvial stratigraphy, and; 7) 3D seismic geomorphology methods used in this study to determine the geometry and dimensions of fluvio-tidal channels.

2.2 Paralic Depositional Systems

Paralic environments can be defined as siliciclastic shoreline settings that exist at or above sea-level, which comprise delta plain, floodplain to shoreline-shelf organisations, and estuaries (Reynold, 2016) (Fig 2.3). Paralic coastal systems are commonly classified based on the interaction and relative dominance of river, wave, and tidal processes, which control coastal geomorphology and sediment distribution.

Galloway (1975) originally introduced a three-fold process-based classification scheme for deltas. Based on this classification, deltas are categorised into three end-member types (wave-, fluvial- and tide-dominated), with a full spectrum of delta types in between, which vary in the relative strength of the three end-member processes (Fig 2.3a). This classification was then extended by Boyd et al. (1992) to include non-deltaic paralic settings, such as estuaries, strand-plains, tidal flats, and lagoons. The scheme also recognized differences in depositional environments developing in regressive versus transgressive shorelines (Fig 2.3b).

A revised classification system was introduced by Ainsworth et al. (2011) (Fig 2.4). The new scheme recognises that the three end-member processes can interact with each other at different degrees. Thus primary, secondary, and tertiary processes affecting the coast are identified, thereby creating a semi-quantitative method of classification. If all three end-member processes interact with each other, the primary process interacting with the sediments is said to "dominate", while the secondary process "influences", and the tertiary process "affects" deposition (e.g., a tide-dominated, fluvial-influenced, wave-affected delta).

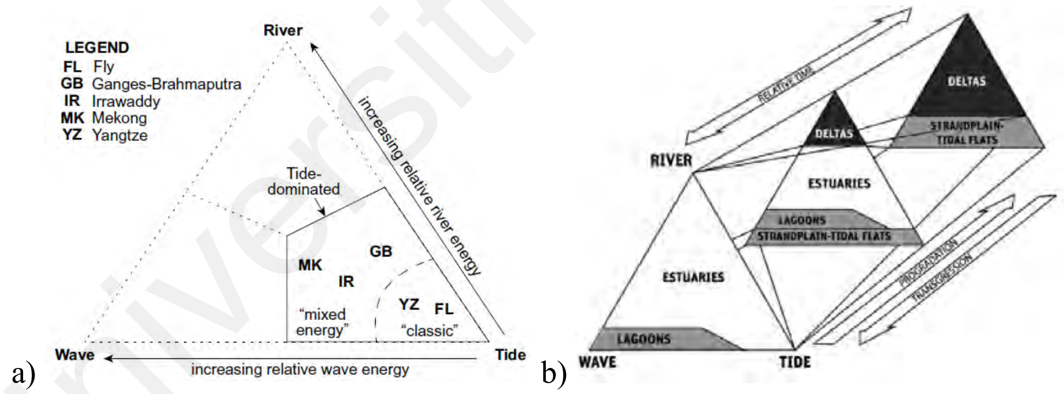

Figure 2.3: a) Classification of coastal environment based on depositional process (after Galloway, 1975), highlighting on the tide-dominated section.; b) Ternary diagram development based on the deposition process (wave, river, tide) and shoreline migration path (after Boyd et al., 1992).

The classification can then be used to predict facies geometry in ancient depositional systems buried in the subsurface. This scheme explains that every paralic system will be classified theoretically according to the magnitude of depositional processes marked by grain sizes, sand and mud ratio, and thicknesses derived from facies analysis. The process-based classification can also be applied at different hierarchical scales; thus, small depositional elements such as channels can be classified as being fluvial- or tide-dominated (Vakarelov & Ainsworth, 2013). This revised scheme has been applied to present-day paralic models (Dalrymple & Choi, 2007) and to ancient deposits (e.g., Amir Hassan et al., 2013, 2017).

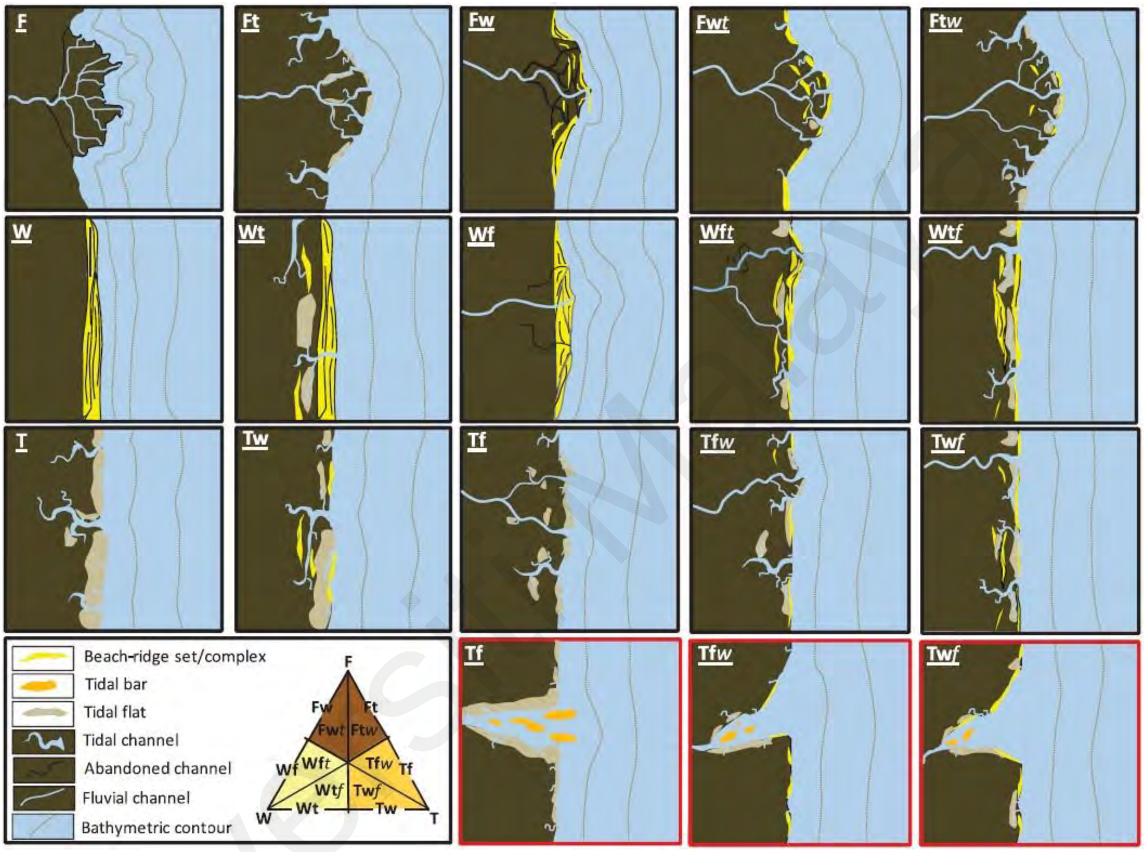

Figure 2.4: Classification of shoreline deposits as well as the interplay between fluvial, tidal and wave processes (from Ainsworth et al., 2011).

Fluvial-dominated coasts (Fig 2.5): The coast is regarded as fluvial-dominated, where river currents are the primary agent of sediment transport and deposition. Strong waves and currents do not intrude upon its protected shoreline; therefore, the sediment deposited at and near the shore zone is not reworked or dispersed laterally by marine processes. Rivers carry substantial amounts of sediment load to the coast, and over time, a delta may form and protrude from the coastline. High sediment supply from rivers also contributes significantly to deposition on the continental shelf. Fluvial-dominated sediments are deposited in three main deltas sub-environments-i.e., from landward to seaward, subaerial delta plain, delta front to prodelta. The delta plain is characterised by distributary channels and inter-distributary bays together with crevasse splays and levees. Distributary channel fill deposits typically form a scour-based, fining-upward succession. Inter-distributary bays are low energy, brackish water settings dominated by fine-grained deposition. The delta front is a gentle gradient slope, located seaward of the delta plain, and is characterized by distributary mouth bars. High flood discharge upstream can produce river-fed gravity flows or hyperpycnal flows. This flow carries a dense sediment-water mixture below seawater and deposits a normal or inverse graded bed on the delta front (e.g., Bates, 1953; Mulder et al., 2003). Further seaward, hypopycnal flows become dominant, with deposition on the prodelta mainly in the form of suspension fallout. Prodelta deposits are composed of hemipelagic mud interbedded with fine-grained sand originating from marine reworking processes. Marine trace and body fossils can be abundant.

Wave-dominated coasts: Wave reworking along the coast usually produces a laterally extensive and relatively straight to arcuate shoreline, i.e., a beach-strandplain. The beach-shoreface profile is segmented into three regions, i.e., from land to sea, foreshore (beach), shoreface (concave-up profile), offshore. The foreshore region is above water level and dominated by swash and backwash of breaking waves, and sediments deposited here are of coarse grain-sizes. The shoreface region lies consistently below water level and is characterised by daily sand transport above the fair-weather wave base. The concave-upward profile of the shoreface is the result of the wave shoaling process (Masselink & Hegge, 1995; Masselink & Hughes, 2003; Dashtgard et al., 2009; Masselink et al., 2011). Its gradient decreases seaward. The sand dominated shoreface passes into the mud dominated offshore zone. The shoreface base is marked at the intersection where interbedded sand and mud are coarsening upward into clean sandstone. A variety of bars, bedforms, and runnels occur in the shoreface. Wave processes drive sediment transport in the upper shoreface and beach, which include wave shoaling, rip and longshore currents, and storms. The wave-induced orbital water motion near to the bed is asymmetrical, leading to a net onshore movement of sand. Waves carry coarser sediment landward. Two main currents occur at the coastline, i.e., longshore currents created by oblique wave approach toward the coastline and cell circulation of rip currents. Longshore currents move parallel to the shore. When two opposite directions of longshore current flow coincide, water will flow as rip current and spread out until diminish seaward. During a storm, the frictional coupling of wind and water surface causes a strong wave towards the foreshore. Storm-weather wave base is deeper due to larger waves. Storm beds are deposited in between offshore mud and may erode and replace the rippled fair-weather shoreface deposits. Typically, in a progradational coastline, the facies succession coarsens upward, from the offshore bioturbated mudstone and interbedded hummocky cross-stratification facies to cross-bedded and laminated sandstone of the shoreface and beach.

Tide-dominated: Tide-dominated areas in paralic settings are mainly in the form of tidal flats where sediment transport and deposition is strongly controlled by tidal currents. A tidal flat is a topographically flat to gentle gradient surface, which experiences periodic flooding and exposure due to daily tides (Amos, 1995). Tidal flats are segmented into three zones based on the period of subaerial exposure and submergence, i.e., supratidal, intertidal, and subtidal. The supratidal zone is the most landward and is permanently subaerially exposed above the high tide mark. The intertidal zone is subaerially exposed during low tide and submerged during high tide. The subtidal zone is permanently submerged even during the lowest tide. Tides are characterized by alternating tidal current flow in seaward (ebb current) and landward (flood current) directions. The most significant geomorphological feature on tidal flats are tidal channels. Tidal channels have flaring mouths and narrow landward. Some tidal channels are blind-ended and have point bars along their inner banks. Progradational tidal flat facies successions tend to fine upward and are composed of tidal current-generated deposits (e.g., bedforms, heterolithic strata, rooted mud, tidal rhythmites) (e.g., Dalrymple, 2010). Tidal channel-fill deposits are typically preserved at the base of this fining upward tidal flat succession. Tide-dominated coasts are further discussed in the next section.

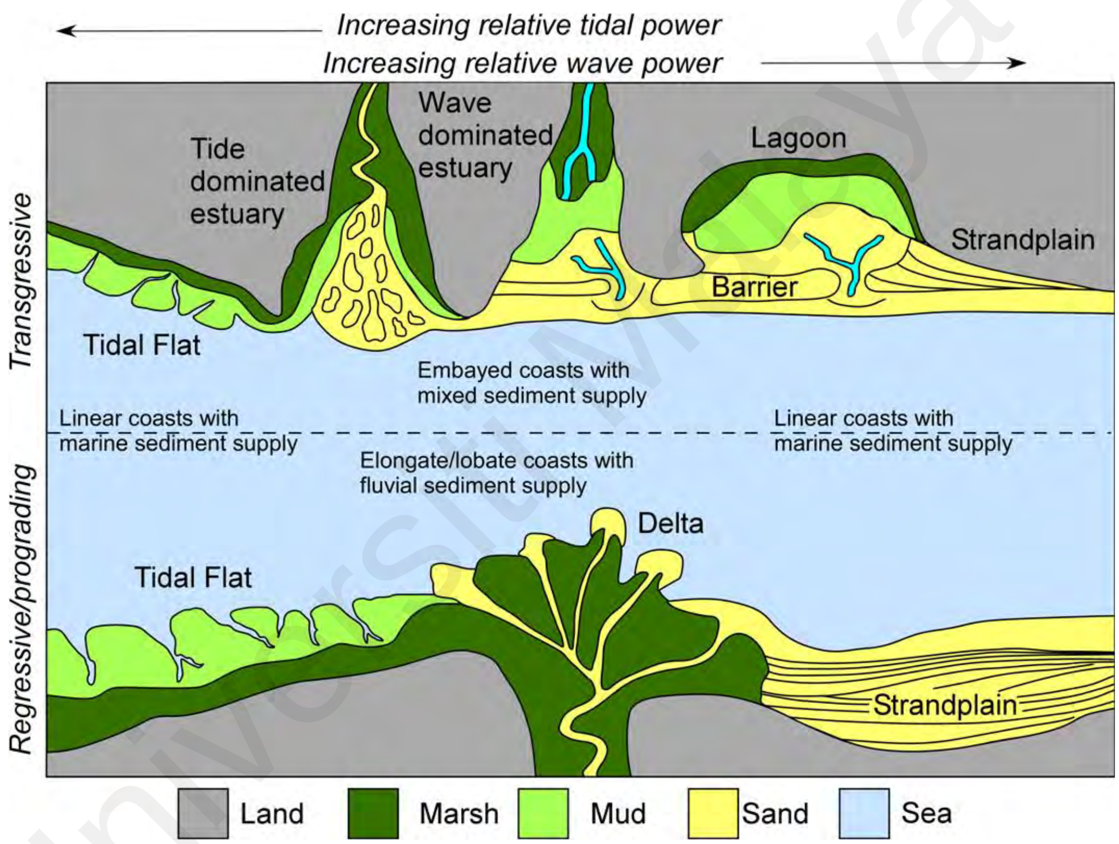

Figure 2.5: Paralic depositional environments from Boyd et al. (1992).

2.2.1 Tide-Dominated Depositional Environments and Facies

Tide-dominated paralic depositional environments are geomorphologically dominated by tidal channel networks and elongated tidal/channel bars. Physical processes and energy to transport sediment are mainly governed by tidal current processes.

Tide-dominated environments are typically hypersynchronous since the funnel-shaped geometry of channel mouths allow the incoming tide to expand its range due to the progressive decrease in cross-sectional area (Dalrymple & Choi, 2007). The funnel-shaped geometry of the distributary mouth in estuaries and deltas causes the tidal range to increase landward. However, at a certain extent landward, the tidal range and tidal-current speed decreases to zero at the tidal limit due to friction on the sides and bottom. Thus, weak tidal currents would be assumed in two areas, i.e., at the seaward mouth and at the head landward where these areas were separated by an area with stronger tidal currents. Consequently, tidal deposits would display similar characteristics in both areas leading to difficulty in reconstructing the depositional environment.

Complex tidal channel and tidal bar networks are well-known elements of tidal environments. The mapping of architectural elements in channel deposits is complicated due to rapid channel and bar migration and stacking of consecutive channel fills. Erosional surfaces of several different channel orders further complicate the stratigraphy, making recognition and placement of stratigraphic surfaces such as flooding surface more difficult (Fig 2.6). Tidal deposits may also record vertical/temporal changes in tidal current energy that replicate the changes in tidal current energy along the longitudinal channel profile (Dalrymple & Choi, 2007). However, this trend tends to be missed due to the juxtaposition of channel bodies.

Sediment transport and deposition in tide-dominated environments are characterised by slackwater suspended load, current generate bedforms, regular and rhythmic sedimentation due to tidal cycle and periodic current reversals due to ebb-flood cycles. Several typical facies observed in these environments are interlayering of rhythmic sand and mud (rhythmites), tidal bundling of sand layers bounded by mud drapes and tidal heterolithic bedding (Reineck, 1967; Reineck & Wunderlich (1968); Dalrymple, 2010; Davis, 2012).

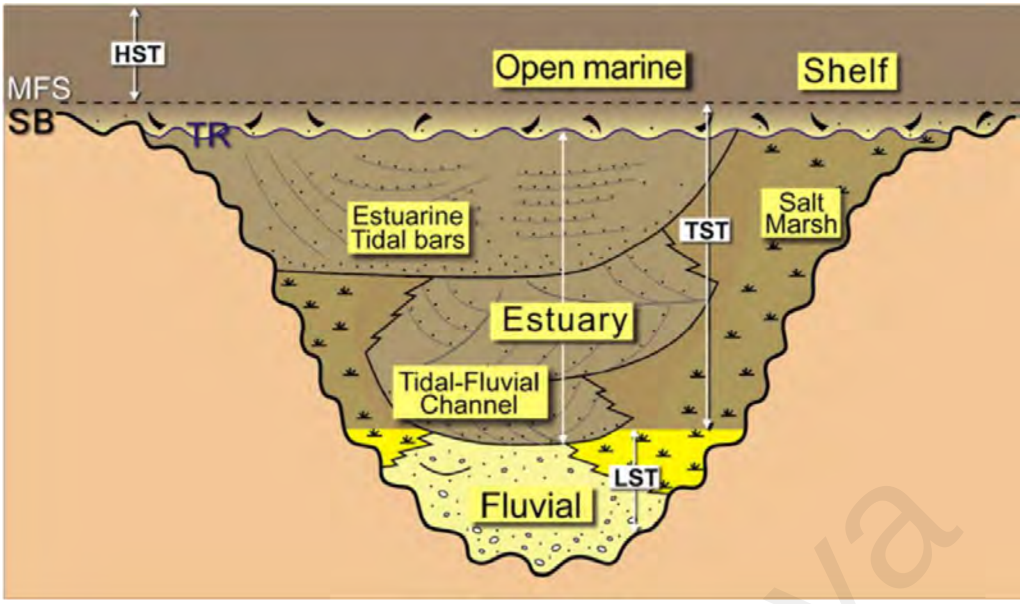

Figure 2.6: Idealized cross-section of a transgressive tide-dominated estuarine, incised valley fill. The lower part of the succession is occupied by fluvial deposits, then overlain by estuarine deposits, and topped by open-marine deposits of the succeeding progradation (from Dalrymple, 1992; Dalrymple & Choi, 2007).

Most of the well-studied modern examples of tide-dominated depositional environments are from transgressive coastlines, i.e., estuaries such as the Bay of Fundy (Dalrymple et al., 1990, 1991; Dalrymple & Zaitlin, 1994) and Gironde Estuary (Allen & Posamentier, 1993). Consequently, this bias has led to challenges in interpreting ancient tide-dominated deposits. Research on the modern and ancient regressive tide-dominated paralic settings is increasing, such as studies on sedimentology and seismic geomorphology of fluvial-tidal deposits of the modern tide-dominated Fly River Delta (Dalrymple et al., 2003), review of tide-dominated deltas (Goodbred & Saito, 2012) Ganges Brahmaputra Delta (Kuehl et al., 2005), Iron River Field, Canada (Maynard, 2006), as well as ancient tide-dominated deltas e.g., Maguregui & Tyler (1991), Willis (2005), Willis & Fitris (2012) Amir Hassan et al. (2017) and geophysical investigations of ancient meandering channels (Boaga et al., 2018).

For example, Amir Hassan et al. (2013) present a detailed facies analysis and stratigraphic study of a succession of tidal heterolithic deposits infilling deep (up to 43 m thick) incisions in the Miocene Group H (H20 and H15) of the Malay Basin. He identified six facies associations; (FA1) *offshore*, represented by bioturbated mudstone with minor interbedded micro-hummocky and graded sandstone beds; (FA 2) *tidal bar*, signified by coarsening upward successions composed of lenticular bedding, wavy bedding, and cross-bedded sandstone. These were interpreted to have formed prograding, tide-influenced, elongate, shore-normal sand bodies; (FA 3) *subtidal flat*, represented by thin fining heterolithic packages of wavy and lenticular bedding with occasional cross-bedded sandstone upward; (FA 4) *outer estuarine*, represented by lenticular bedding with moderate to strong bioturbation; (FA-5) *fluvio-tidal point bar*, represented by a sharp based succession fining upward from cross-bedded and parallel laminated sandstone into wavy and lenticular bedding, and; (FA 6) *mangrove/overbank*, represented by carbonaceous rooted mudstone and associated coal. These facies associations characterise elements of a coastal depositional system with inshore deposits being strongly modified by tides.

Furthermore, two main depositional environment morphologies will be discussed here, i.e., tide-dominated estuary and delta, together with their deposits in order to understand sedimentological facies and facies architectures of these environments. Tide-dominated deltas are actively aggrading and prograding seaward with high sediment supply, whereas tide-dominated estuaries form during transgression. Through time, estuaries can develop into deltas and *vice versa* (Ta et al., 2002; Milli et al., 2013).

2.2.1.1 Tide-dominated estuaries

Estuaries are commonly associated with drowned incised valleys (Dalrymple, 1992), but can also form where delta distributary channels are abandoned (Dalrymple, 2006). Estuaries are also known as ephemeral transgressive coastal systems (Masselink & Hughes, 2003; Masselink et al., 2011), and can be perennial due to climate variation and local dynamics of bedrock and vegetation. Typically, an estuary forms on a transgressive coastline and could be an abandoned portion of a transgressive delta plain (Dalrymple, 2006). Tide-dominated estuaries are significantly controlled by tidal current processes at the mouth.

The wide-flaring, funnel-shaped morphology of tide-dominated estuary mouths amplifies the flood tidal current strength (Fig 2.7) (Myrick & Leopold, 1963; Wright et al., 1973; Fagherazzi & Furbish, 2001; Rinaldo et al., 2004; Sulaiman et al., 2021). At the apex of the funnel-shaped mouth, where the channel shifts from channelised flow to non-channelised flow occurs (Dalrymple et al., 1992; Dalrymple and Choi, 2007), the estuary is in the form of a straight channel. Further landward, the channel becomes sinuous due to interaction between tidal and fluvial currents where the opposing flows result in a bed-load convergence. Further landward, the tidal current diminishes, and the channel becomes straighter. The point landward where tidal current energy is zero, and only fluvial processes occur, is called the tidal limit. This point is not fixed due to temporal variations of fluvial discharge and tidal cycles.

Sedimentologically, an estuary can be split into three zones, i.e., an outer zone, a middle estuary near the mouth apex, and an inner zone or fluvial-tidal transition zone (Fig 2.7). The strongest tidal currents occur in the outer zone of the estuary. The tidal current would efficiently transport and rework the mixed-load sediment from the sea into the estuary by flood current. Tidal reworking of the sediment forms elongates, laterally migrating, fining-upward sand bars in between the channels, i.e., tidal bars (Oomkens & Terwindt, 1960; Boersma, 1969; Clifton, 1983; Harris et al., 1992; Masselink et al., 2009).

Landward of the middle part of the estuary is within tide-dominated with increasing fluvial current, the channel is more sinuous here (Dalrymple & Choi, 2007; Dalrymple et al., 2012). Net sediment transport convergence occurs when tidal current energy meets the fluvial current energy in middle zone, creating an area of lowest energy which leads to deposition of the fine-grained and suspended load sediments (mud and clay).

There is a seaward trend of increasing tidal influence and decreasing fluvial influence as we transition from the river into an estuary. Daily tidal cycles would transport sediment back and forth through the estuary, where both mixed-load and suspended-load sediment is deposited in the estuary. In the tide-dominated part (seaward) the net water and sediment (both bedload and suspended load) movement may be either landward or seaward, whilst the net water and sediment migrated seaward in the river-dominated part (Dalrymple & Choi, 2007)

Point bars develop along the sinuous channels, where inclined heterolithic strata (IHS) would be formed due to the tidal fluctuations in most tide-dominated areas (Choi & Dalrymple, 2004; Choi, 2010). Fluvial currents and ebb-tidal currents would flow through the course of the channel seaward, whereby the flood tidal channel tend to flow over the inner bend of the sidebar forming a shallow flood channel (Fenies & Tastet, 1998). Gradually, this point bar would be detached and become an elongated bar such as those occurring in the outer estuary (i.e., tidal bars).

Further landward of the fluvial-tidal transition zone, channels are straighter, and tidal flow rates decline farther landward until where only fluvial processes occur (Dalrymple & Choi, 2007; Torres, 2017). Tidal influence may extend further landward because of a low gradient coastal plain and during relative sea-level rise. Variations in fluvial discharge may control the extent of landward tidal influence. Deposition always occurs on the point bars of a low sinuous fluvio-tidal channel. When the fluvial discharge rate is higher, coarser-grained sediments would be deposited, while during low fluvial discharge rate, flood currents would more efficiently transport sediment landward. During slackwater periods, fine-grained mud would be deposited forming heterolithic strata (Dalrymple & Choi, 2007).

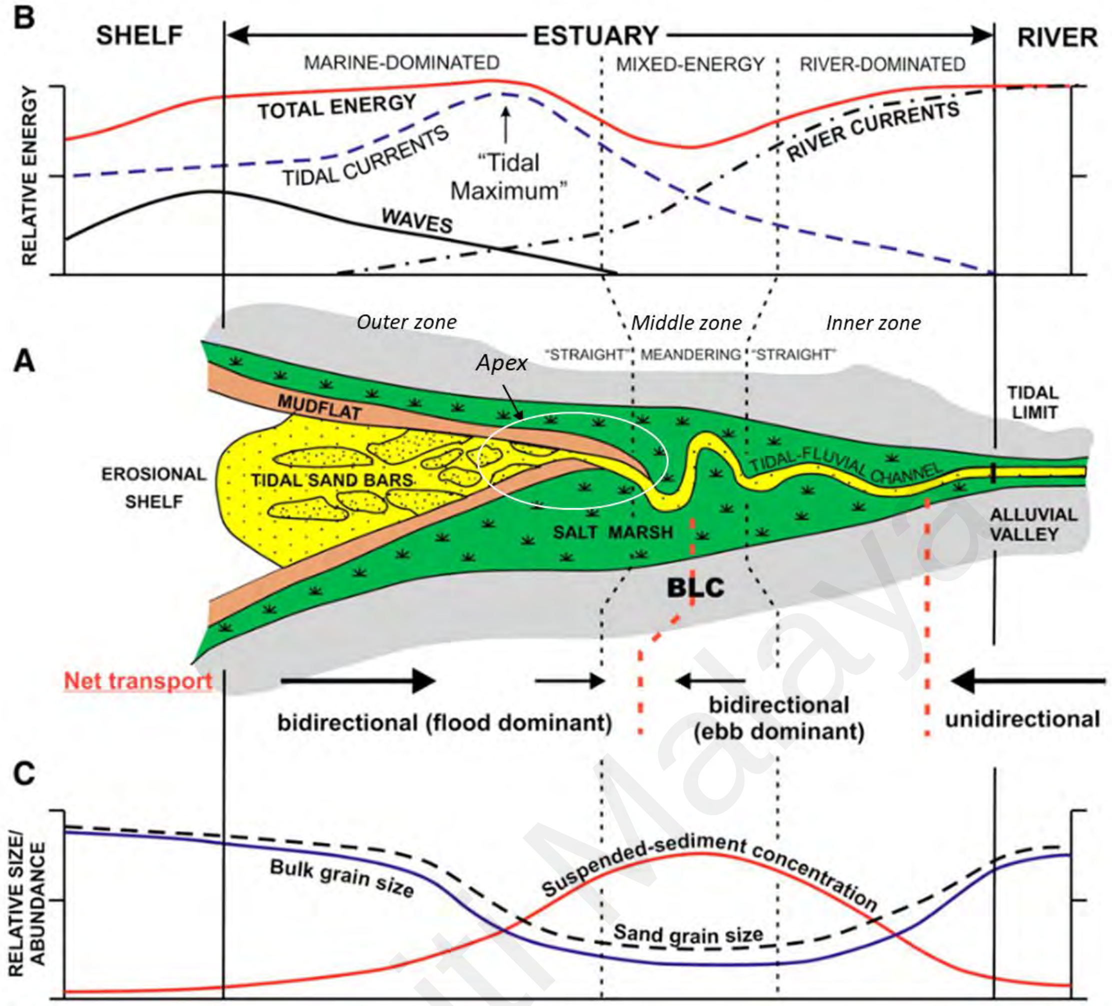

Figure 2.7: (A) Longitudinal profile of an ideal tide-dominated estuary showing the funnel-shaped mouth, elongated bars and straight-meandering-straight (SMS) fluvio-tidal channel (B) Longitudinal changes of the three main physical processes, river, tidal and waves, and the path of sediment transport. (C) Longitudinal changes of the sediment loads (taken from Dalrymple & Choi, 2007).

2.2.1.2 Tide-dominated Delta

A delta is defined as a shoreline protuberance that develops on the coast when a river flows into the ocean and where the rate of fluvial deposition exceeds the rate of reworking by basinal processes (Elliott, 1986; Bhattacharya & Walker 1992). Deposition and morphology of a tide-dominated delta is dominantly controlled by tidal processes (Galloway, 1975; Bhattacharya & Giosan, 2003). As in other deltas, tide-dominated deltas also develop clinoforms and a typically sigmoidal or S-curved topset-foreset-bottomset profile (Goodbred & Saito, 2012).

In planform view, a tide-dominated delta displays a similar funnel-shaped river mouth like the one in estuaries. However, tide-dominated deltas have fewer distributaries, which are separated by stable vegetated islands towards the apex of the funnel-shaped mouth (Fig 2.8). The fluvio-tidal channel bifurcates into distributary channels through avulsion. Tide-dominated deltas usually have a much gentler gradient than fluvial-dominated deltas (Goodbred & Saito, 2012).

The point of where the fluvial current energy begins to decrease is not fixed but travels up and down the channel together with the ebb and flood currents due to seasonal fluctuations in river discharge (Dalrymple & Choi, 2007). Tidal reworking of the fluvial deposits at the river mouth produces depositional elements resembling those observed in tide-dominated estuaries e.g., tidal bars, point bars, tidal channels and associated tidal flats, mixed with some other fluvial-dominated elements.

Coarsening up mouth bars develop on the delta front and are often composed of heterolithic strata such as flaser, wavy, and lenticular bedding combined with wave/storm and fluvial deposits, which overly prodelta deposits. The bottommost part of the succession comprises interlayering of clay and silt, with the dominance of sand further upward. Further up of the succession, mud drapes and cross-bedding become more common. The delta front succession is often overlain by fining upward delta plain deposits (Hori et al., 2002; Ta et al., 2002; Dalrymple et al., 2003; Legler et al., 2013) (Fig 2.9). The delta plain succession comprises fluvio-tidal channel, and channel bar deposits.

The area where the tidal flood currents and fluvial currents coincide, where there is a higher deposition of suspension-load sediment, is commonly located at the edge of the delta plain, further seaward than noted in tide-dominated estuaries. Sediment net convergence may even occur on the tidal shelf (Dalrymple & Choi, 2007; Goodbred & Saito, 2012). Fining upward elongated bars develop in the distributary channels (Willis, 2005; Plink-Björklund, 2012), and are similar to those observed in estuaries. However, these bars can also have a thick fluid mud deposit at their base, directly overlying the basal channel scour, as a result of the high suspended sediment concentration (Dalrymple et al., 2003).

Distributary channel avulsion can result in distributary channel abandonment, with the channel become blind-ended and receiving no fluvial sediment input. Thus, this inactive tide-dominated delta would become estuarine (Goodbred & Kuehl, 2000; Allison et al., 2003).

Further landward in the fluvial-tidal transition zone, fluvio-tidal channels on the delta plain are characterized by both fluvial and tidal influence. Flow within the channel is inconsistent due to tidal and seasonal fluctuations. Levees and crevasse splays do not commonly form along these channels. In the event of a higher flood tide surge into the channels, the water will overflow the channel to form tabular tidal flat deposits (Willis, 2005). Works on regressive tide-dominated deltas are relatively rare compared to tide-dominated estuaries. This may be due to the morphological features of modern tide-dominated deltas are more similar to river- or wave-dominated deltas, such as in the Song Hong delta in Vietnam (Hori et al., 2004) or the Mahakam delta in Indonesia (Storms et al., 2005). Few examples of prominent modern large tide-dominated deltas have been documented such as the Mahakam delta (Gastaldo et al., 1995; Allen & Chambers, 1998), Fly River delta (Dalrymple et al., 2003), Mekong (Tanabe et al., 2003), and Han River (Cummings et al., 2018). Recently, there is growing documentation on ancient tide-dominated delta deposits (Willis & Fitris 2012; Amir Hassan et al., 2017; Legler et al., 2013, 2014; Chen et al., 2014).

Legler et al. (2013) described Eocene deposits in Egypt which are represented by heterolithic channels and heterolithic coarsening upward successions. Such deposits were interpreted as prograding tide-dominated deltas developing in a protected, tide-dominated embayment. The facies associations are similar to those observed in the modern-day Fly River Delta (Dalrymple et al., 2003).

A re-assessment of the Miocene Balingian Province of Sarawak, which was initially interpreted as the fluvial-dominated delta in Balingian Province, Sarawak, has reinterpreted the deposits as being representative of a tide-dominated or tide-influenced delta (Amir Hassan et al., 2017).

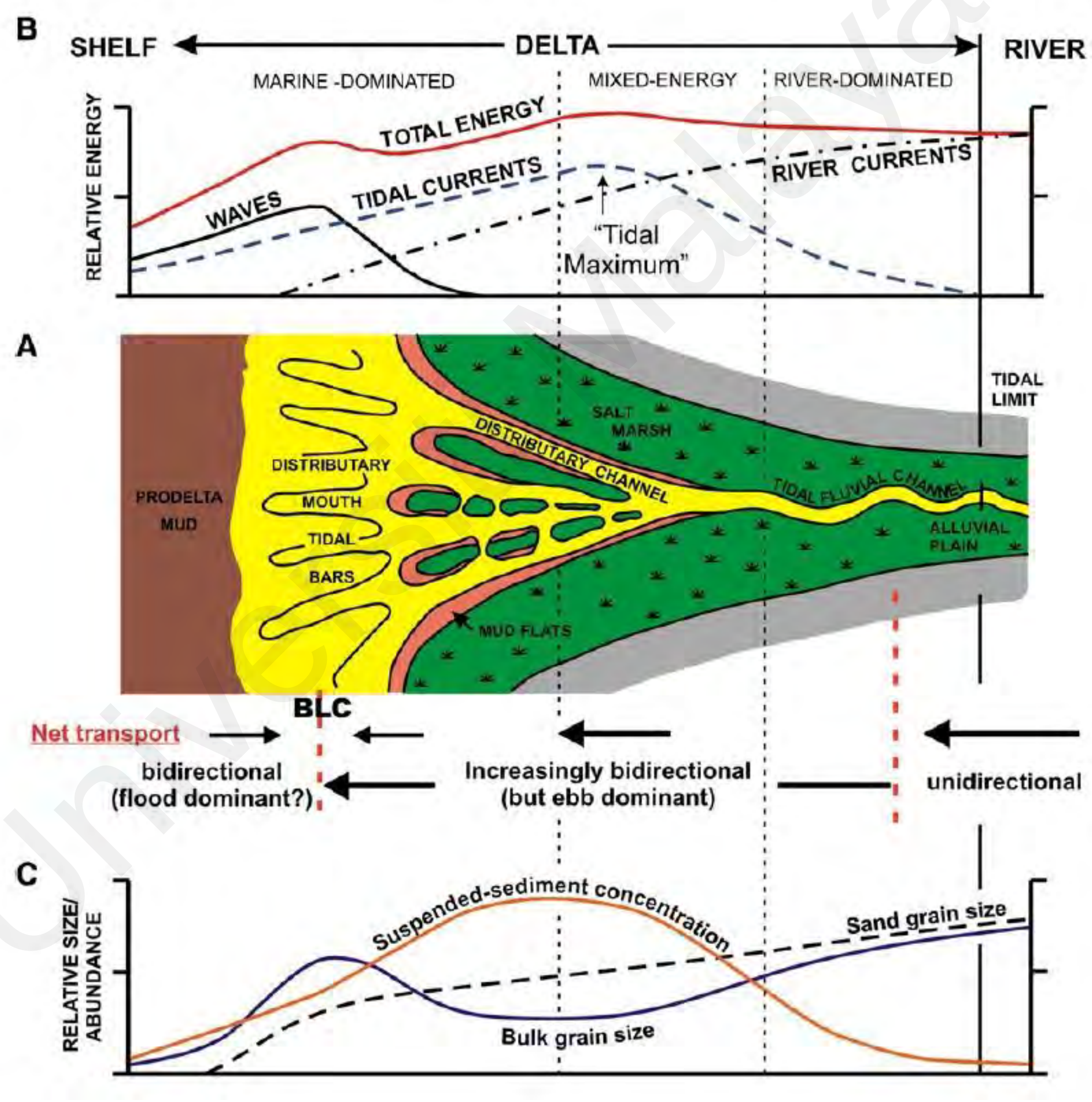

Figure 2.8: (A) Longitudinal profile of an ideal tide-dominated delta showing a funnel-shaped mouth, distributaries separated by stable vegetated islands and a trunk fluvio-tidal channel (B) Longitudinal changes of the three main physical processes, river, tidal and waves, and the path of sediment transport. (C) Longitudinal changes of the sediment loads (taken from Dalrymple & Choi, 2007).

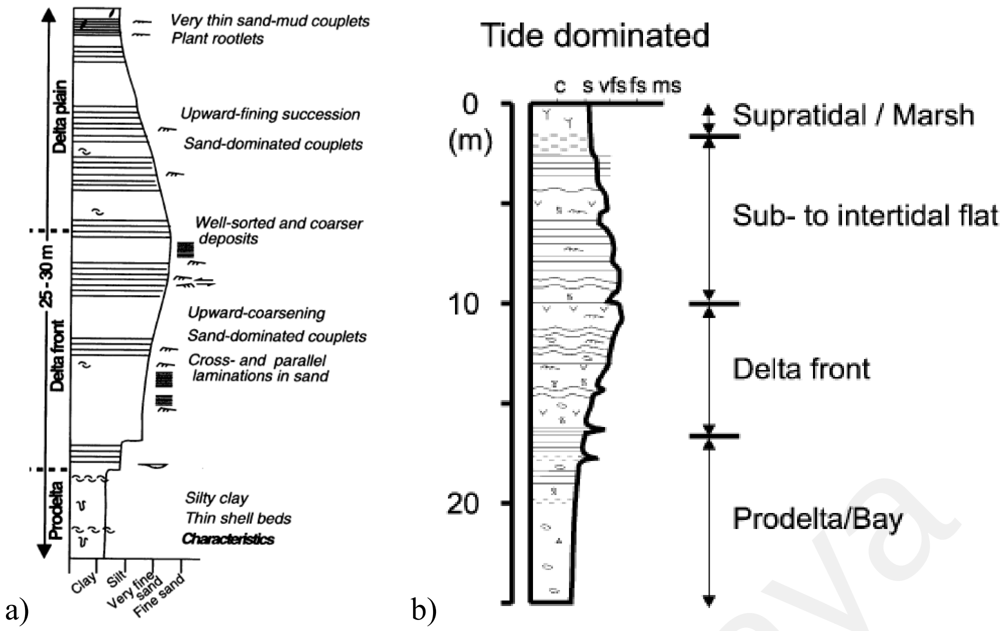

Figure 2.9: Vertical successions of modern tide-dominated deltas. a) The Yangtze delta (from Hori et al., 2002), and; b) Mekong delta (from Ta et al., 2002). Typical vertical pattern of mud overlain by coarsening upward delta front succession signifying delta progradation; then overlain by a fining upward succession representing channel fill and tidal flat deposits on the delta plain.

2.3 Channel Architectural Elements

It is best to elaborate more on the basis of the channel architectural elements before describing further on fluvial and tidal channels. Fluvial or channel architecture defined by internal arrangement and the geometry of channel and overbank deposits in a channel sequence (Allen, 1965). Channel architectural elements are well defined for alluvial plain depositional settings (Qui et al., 1987). It is relatively rare to find a description of architectural elements in paralic settings, due to the complexity of these environments (e.g., Baas et al., 2015; Gibling, 2006; Harris & Whiteway, 2011; Colombera et al., 2016;).

Channel architectural element schemes are commonly based on observations of modern river plan-view morphologies; however, these are often oversimplified and do not consider their preservation potential within the geological record (Allen, 1965). Amongst the initial attempts on the fundamental classification applying empirical record of ancient fluvial deposits was by Friend et al. (1979). He separated ‘sheets’ and ‘ribbons’ at a width-to-thickness ratio cut-off value of 15. Additionally, he describes a single/stacked succession complexity in fluvial sand bodies, where the sand bodies can comprise either single or amalgamated ‘storeys’ confined by internal bounding surfaces.

Miall (1985, 1988, 1991b) recognized nine fundamental bedding types and bounding surfaces (0^{th} – 8^{th} order) of fluvial deposits (Table 2.1) that form a hierarchy from smallest to largest scale and with increasing time and rate of sedimentation. Detailed descriptions of these units are provided in Miall (2006). Other workers (e.g., Hornung & Aigner, 1999; López-Gómez et al., 2010; Payenberg et al., 2011) have adopted these architectural elements, which display a range of dimensions over time and space.

Based on a review study in the early 1980s, Miall (1985) recognized eight basic architectural elements in fluvial deposits (Fig. 2.10). However, subsequent work (e.g., Fielding, 1993b; Cowan, 1991) have further opinions regarding this original classification. Table 2.2 lists down these architectural elements, which include channels element (CH), gravel bars and bedforms element (GB), sandy bedforms element (SB), scour hollows element (HO), laminated sand sheets element (LS), lateral and downstream accreting bar forms elements (DA, LA), sediment gravity flows element (SG), laminated sand sheets (element LS), and overbank fines element (FF) as proposed by Miall (1985).

Furthermore, overbank architectural elements have also been described, including levee (LV), crevasse channel (CR), crevasse splay (CS), floodplain fines (FF) and abandoned channel (CH(FF)) (Miall, 2006). In this review, I will restrict the discussion to the channel (CH), downstream accretion (DA) and lateral accretion elements (LA), which are frequent elements within paralic depositional environments.

Table 2.1: Architectural unit's hierarchy in fluvial deposits (after Miall, 1985, 1991b).

Grp	Time scale of process (a)	Examples of processes	Instantaneous sedimentation rate (m/ka)	Fluvial, deltaic depositional units	Rank and characteristics of bounding surfaces
1	10^{-6}	Burst-sweep cycle		Lamina	0th-order, lamination surface
2	10^{-5} -10^{-4}	Bedform migration	10^{5}	Ripple (microform)	1st-order, set bounding surface
3	10^{-3}	Bedform migration	10^{5}	Diurnal dune increment, reactivation surface	1st-order, set bounding surface
4	10^{-2} -10^{-1}	Bedform migration	10^{4}	Dune (mesoform)	2nd-order, coset bounding surface
5	10^{0} -10^{1}	Seasonal events, 10-year flood	10^{2-3}	Macroform growth increment	3rd-order, dipping 5–20° in direction of accretion
6	10^{2} -10^{3}	100-year flood, channel and bar migration	10^{2-3}	Macroform, e.g., point bar, levee, splay immature paleosol	4th-order, convex-up macroform top, minor channel scour, flat surface bounding floodplain elements
7	10^{3} -10^{4}	Long-term geomorphic processes, e.g. channel avulsion	10^{0}–10^{1}	Channel, delta lobe, mature paleosol	5th-order, flat to concave-up channel base
8	10^{4} -10^{5}	5th-order (Milankovitch) cycles, response to fault pulse	10^{-1}	Channel belt, alluvial fan, minor sequence	6th-order, flat, regionally extensive, or base of incised valley
9	10^{5} -10^{6}	4th-order (Milankovitch) cycles, response to fault pulse	10^{-1}–10^{-2}	Major dep. system, fan tract, sequence	7th-order, sequence boundary; flat, regionally extensive, or base of incised valley
10	10^{6} -10^{7}	3rd-order cycles. Tectonic and eustatic processes	10^{-1}–10^{-2}	Basin-fill complex	8th-order, regional disconformity

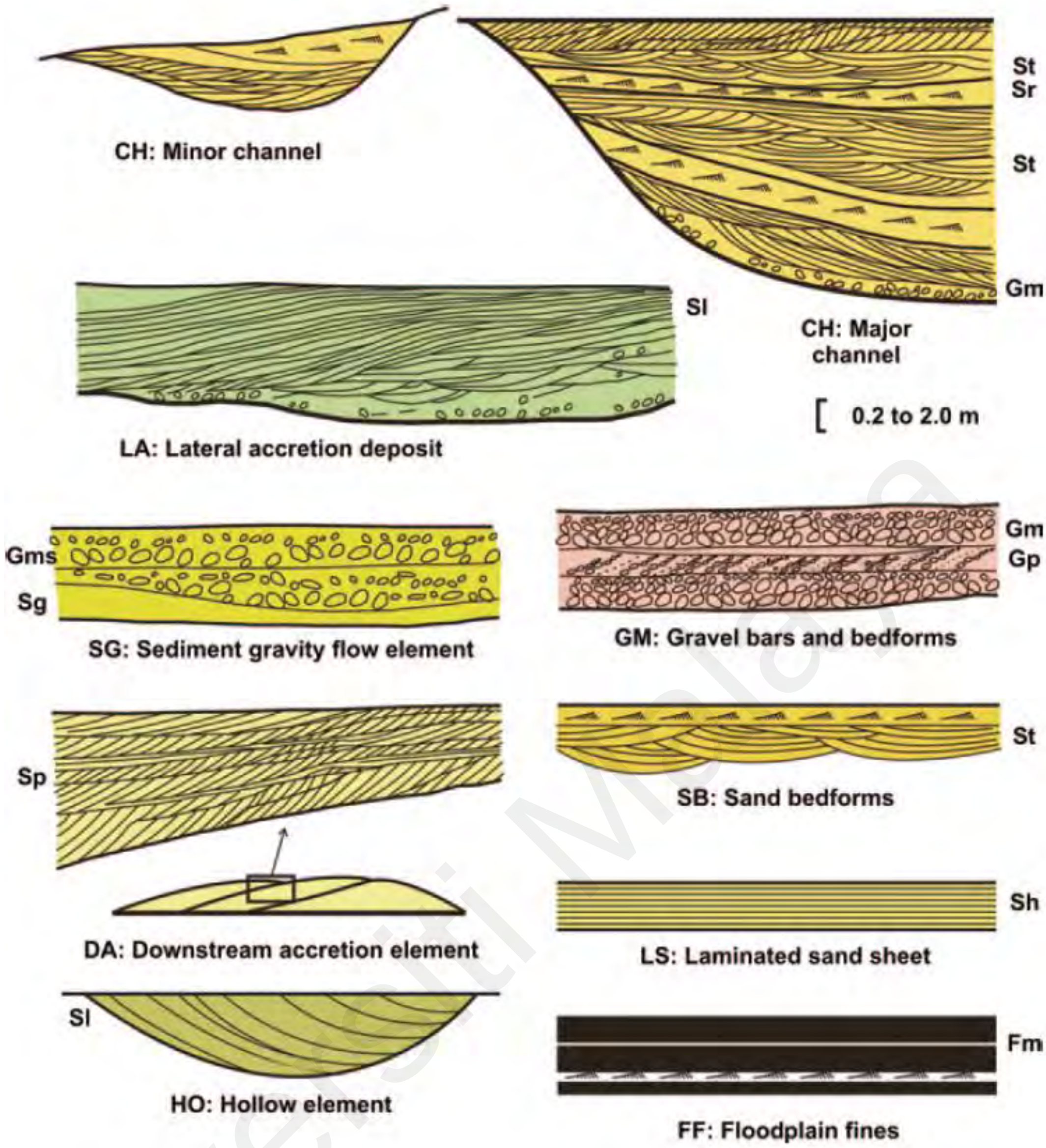

Figure 2.10: Miall 's (1985) original eight architectural elements.

Table 2.2: Architectural elements proposed by Miall (1985). Facies classification from Miall (1978b).

Element	Symbol	Principal facies assemblage	Geometry and relationships
Channels	CH	Any combination	Finger, lens or sheet; concave-up erosional base; scale and shape highly variable; internal concave-up 3rd-order erosion surfaces common
Gravel bars and bedforms	GB	Gm, Gp, Gt	Lens, blanket; usually tabular bodies; commonly interbedded with SB
Sandy bedforms	SB	St, Sp, Sh, Sl, Sr, Se, Ss	Lens, sheet, blanket, wedge, occurs as channel fills, crevasse splays, minor bars
Downstream-accretion macroform	DA	St, Sp, Sh, Sl, Sr, Se, Ss	Lens resting on flat or channeled base, with convex-up 3rd-order internal erosion surfaces and upper 4th-order bounding surface
Lateral-accretion macroform	LA	St, Sp, Sh, Sl, Se, Ss, less commonly Gm, Gt, Gp	Wedge, sheet, lobe; characterized by internal lateral-accretion 3rd-order surfaces
Scour hollows	HO	Gh, Gt, St, Sl	Scoop-shaped hollow with asymmetric fill
Sediment gravity flows	SG	Gmm, Gmg, Gci, Gcm	Lobe, sheet, typically interbedded with GB
Laminated sand sheet	LS	Sh, Sl; minor Sp, Sr	Sheet, blanket
Overbank fines	FF	Fm, Fl	Thin to thick blankets; commonly interbedded with SB; may fill abandoned channels

Jackson (1975) noted that most of the architectural elements within channels are macroform which are the results of cumulative effects of sedimentation over periods of ten to thousands of years (Group 6 deposits in Table 2.1). These architectural elements occur in various scales. In a simple aggradation fills model, minor channels and bars often seen within the larger channels. These minor channels include small-scale channel of partially to completely abandoned channels, chute channels, crevasse channels, and tidal channels. These small channels are bounded by fourth-order bounding surface. The base of these small channels rest on the surface of fifth-order bounding surface. Fifth-order surfaces are typically bounded major channels which typically have concave-up erosional bases. The geometry of the channels is described in the form of the width and depth ratio, and sinuosity. Channels fill vertical aggradation typically results in a fining upward succession.

The main products of accretion inside bar complexes of sand bed channels are downstream accretion and lateral-accretion deposits (DA and LA). A downstream accretion element includes possibly many cosets of downstream migrating bed forms related to each other by a hierarchy of inner downstream dipping boundary surfaces. These demonstrate the former presence of an active, non-periodic, probably erratic bar form, comparable in width and height to the bounding channel. Lateral accretion (LA) is the product of the lateral migration of the channel flow away from the channel bank (Miall, 1985, 1988, 1991b). Helical flow in sinuous river results in outer bank erosion and inner bank deposition, which leads to progressive lateral migration at a high angle relative to channel flow. This, combined with the increasing velocity with depth, produces a sharp-based, fining upward succession (e.g., Thomas et al., 1987).

2.3.1 Lithofacies Classification

Fluvial deposits typically consist of clastic sediments. Fluvial lithofacies models were described with regards to sediment transport mechanism and formation of bedform by Middleton (1977) and Allen (1984). Beds in fluvial deposits are characterised on the basis of bedding type, texture, and sedimentary structures. Locally relevant as additional classification attributes are biogenic structures and fossils.

Miall (1977) presented a lithofacies scheme for braided rivers, with a simple designation using a two-letter code for easy field recognition and laboratory documentation. Miall (1978c) (Table 2.3) extended the description with the identification of a variety of other subordinate lithofacies. The facies scheme is commonly used by sedimentologists up to this day. Note that the Bedforms and Bedding Structures Research Group of the Society for Sedimentary Geology (SEPM) carried out a recent review of bedforms classification (Ashley et al., 1990). Bedform development depends on the flow speed and grain size. At a constant flow depth, there is a general trend of evolution from ripples to dunes to plane beds and antidunes with increasing flow speed (Simons & Richardson, 1961).

Miall (1996) presented facies models for different types of rivers. Figure 2.11 shows examples of some of these models. They are: 1) gravel-bed braided river (Fig. 2.11A); 2) meandering river (Fig. 2.11B), and 3) anastomosing river (Fig. 2.11C). Such models were supported by the development of an extensive lithofacies classification scheme for fluvial deposits, as shown in Table 2.3. Figure 2.12 provides a comparison of facies assemblages in braided channel deposit, meander channel deposit, and stacked meander channel deposits. In general, fluvial deposits tend to form sharp-based, fining upward successions due to channel scouring, and abandonment due to lateral accretion and vertical aggradation (Miall, 1996, 2010).

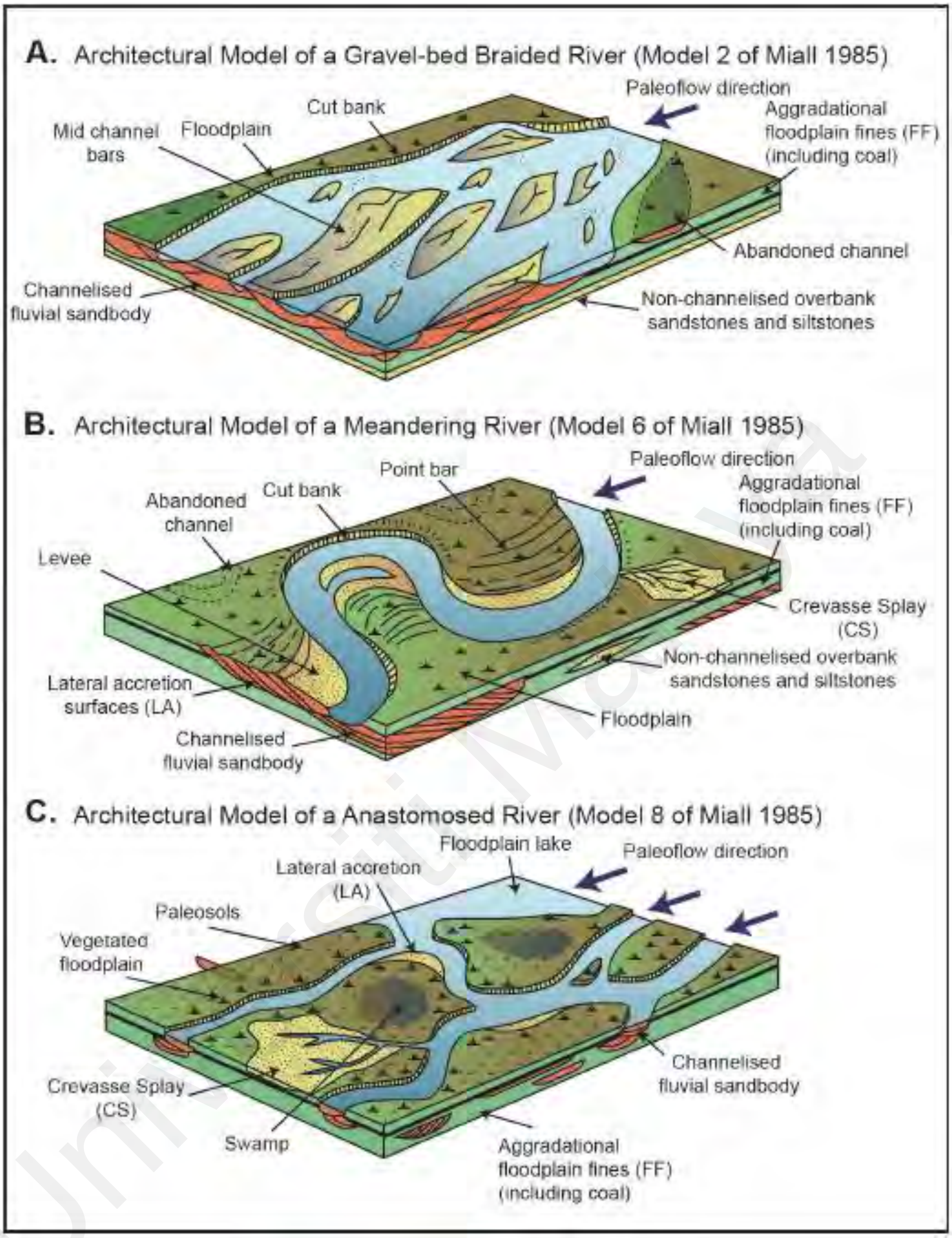

Figure 2.11: Example of fluvial facies models. A) braided river, B) meandering river. C) anastomosed river (after Miall 1985, 1996).

Table 2.3: Classification scheme of fluvial lithofacies from Miall (1978c)

Facies Code	Facies	Sedimentary Structures	Interpretation
Gmm	Matrix-supported massive gravel	Weak grading	Plastic debris flow (high-strength, viscous)
Gmg	Matrix-supported gravel	Inverse to normal grading	Pseudoplastic debris flow (low strength, viscous)
Gci	Clast-supported gravel	Inverse grading	Clast-rich debris flow (high strength), or pseudoplastic debris flow (low strength)
Gcm	Clast-supported massive gravel	-	Pseudoplastic debris flow (inertial bedload, turbulent flow)
Gh	Clast-supported crudely bedded gravel	Horizontal bedding, imbrication	Longitudinal bedforms, lag deposits, sieve deposits
Gt	Gravel stratified	Trough cross-beds	Minor channel fills
Gp	Gravel stratified	Planar cross-beds	Transverse bedforms, deltaic growths from older bar remnants
St	Sand, fine-to-very coarse may be pebbly	Solitary or grouped trough cross-beds	Sinuous-crested and linguoid (3D) dunes
Sp	Sand, fine to very coarse, may be pebbly	Solitary or grouped planar cross-beds	Transverse and linguoid bedforms (2D) dunes
Sr	Sand, very fine to coarse	Ripple cross-lamination	Ripples (lower flow regime)
Sh	Sand, very fine to coarse, may be pebbly	Horizontal lamination parting or streaming lineation	Plane-bed flow (critical flow)
Sl	Sand, very fine to coarse, may be pebbly	Low-angle (<15°) cross-beds	Scour fills, humpback or washed-out dunes, antidunes
Ss	Sand, very fine to coarse, may be pebbly	Broad, shallow scours	Scour fill
Sm	Sand, fine to coarse	Massive, or faint lamination	Sediment-gravity flow deposits
Fl	Sand, silt, mud	Fine lamination, very small ripples	Overbank, abandoned channel, or waning flood deposits
Fsm	Silt, mud	Massive	Backswamp or abandoned channel deposits
Fm	Mud, silt	Massive, desiccation cracks	Overbank, abandoned channel, or drape deposits
Fr	Mud, silt	Massive, roots, bioturbation	Root bed, incipient soil
C	Coal, carbonaceous mud	Plant, mud films	Vegetated swamp deposits
P	Palaeosol carbonate (calcite, siderite)	Pedogenic features: nodules, filaments	Soil with chemical precipitation

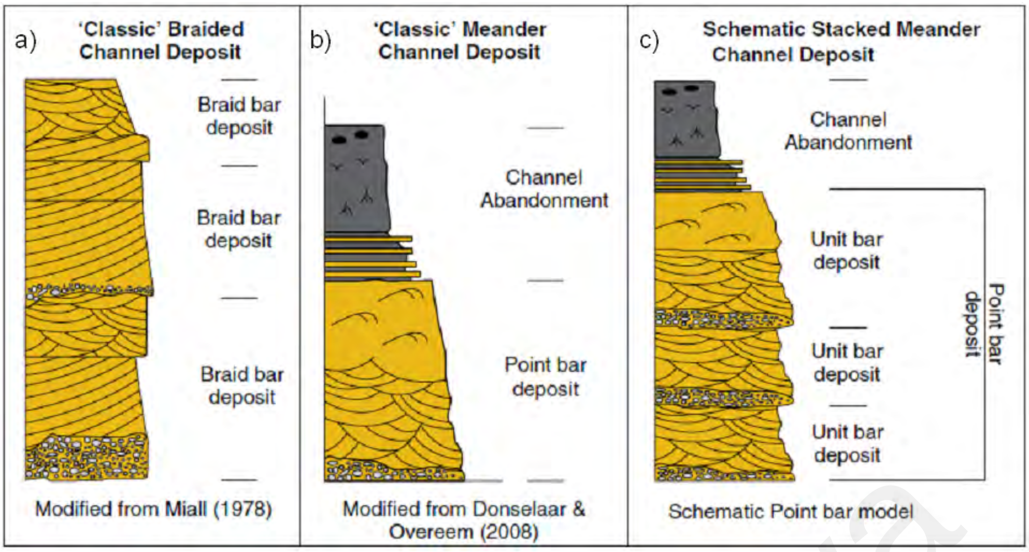

Figure 2.12: Typical vertical facies patterns for; a) braided channels (Modified from Miall, 1978); b) meandering channels (Modified from Donselaar and Overeem, 2008); c) stacked meandering channel deposits comparable to A (Swan et al., 2018).

2.3.2 Depositional Scales and Hierarchical Channel Elements

The rates of sedimentation in modern and ancient environments vary according to the time scale, control mechanisms such as tectonic events, climate change and fluctuation of base-level, and available space (Leeder, 1993) (Fig 2.13). Historical breaks cover incidents such as non-deposition or degradation in front of developing bedforms (seconds to minutes), non-deposition due to ebb tide dry up, up to significant regional unconformity arising from orogeny (millions of years) (Miall, 2006).

A number of different hierarchical schemes have been developed for fluvial deposits (e.g., Fisk, 1944; Allen, 1983; Miall, 1988, 1991). Figure 2.14 shows a hierarchy of depositional units developed for fluvial deposits of different physical scales (Miall, 1988, 1991b), and this scheme is also applicable for tidal deposits (Nio & Yang, 1990). Sedimentation rates and time for deposition vary in each depositional unit. Each depositional unit is ranked accordingly to their bounding surfaces order (number 1-6) (Table 2.1).

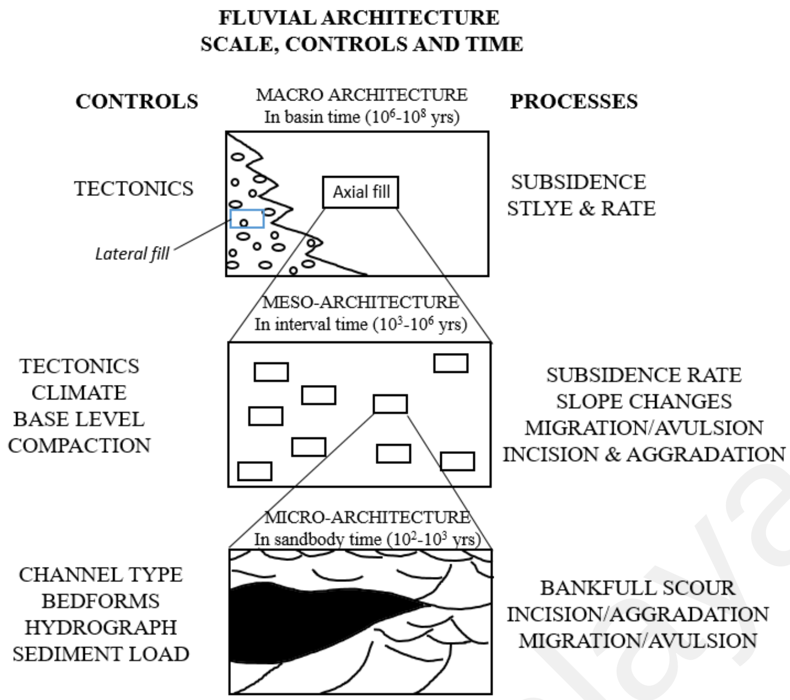

Figure 2.13: Hierarchy of scale and time in fluvial deposits (From Leeder, 1993).

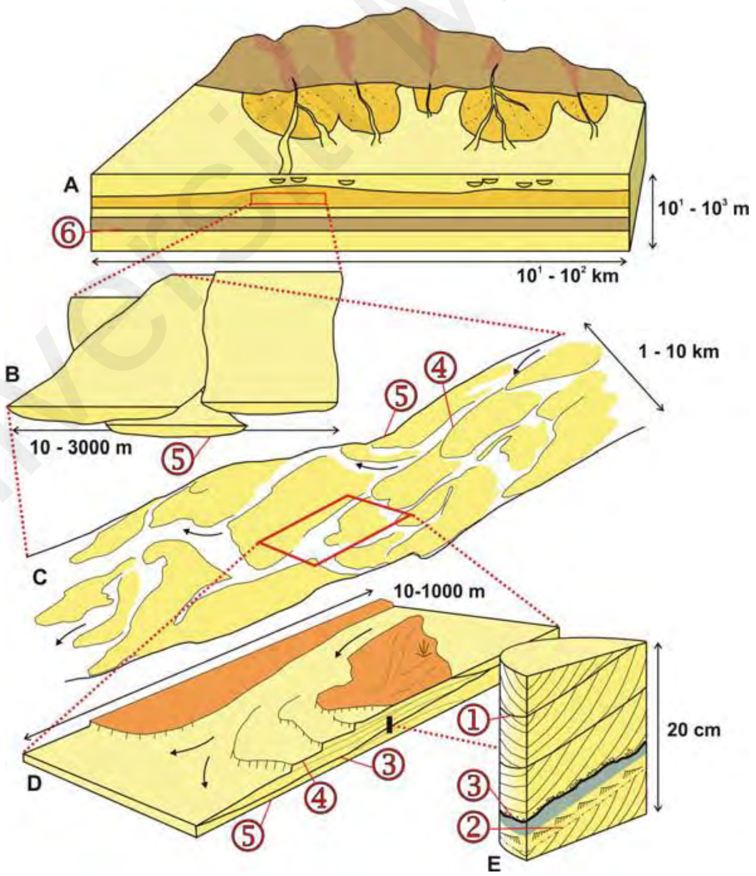

Figure 2.14: Illustration of hierarchy of depositional units developed for fluvial deposits (Miall, 1988, 1991b). Circled numbers indicate the order of the bounding surfaces (Miall, 1996, 2010).

Studies by Payenberg et al. (2011) and Gulliford et al. (2014) adopted the fluvial deposits classification scheme developed by Chevron Corporation. They used internal relationships of facies types and grain-size between different architectural units to develop the hierarchy. Beds reflect individual flood events. Vertically stacked beds form a bed-set. Higher-order hierarchies include a storey, multi-storey, and channel belt complexes (Fig 2.15., Willis, 1993; Sprague et al., 2002; Payenberg et al., 2011).

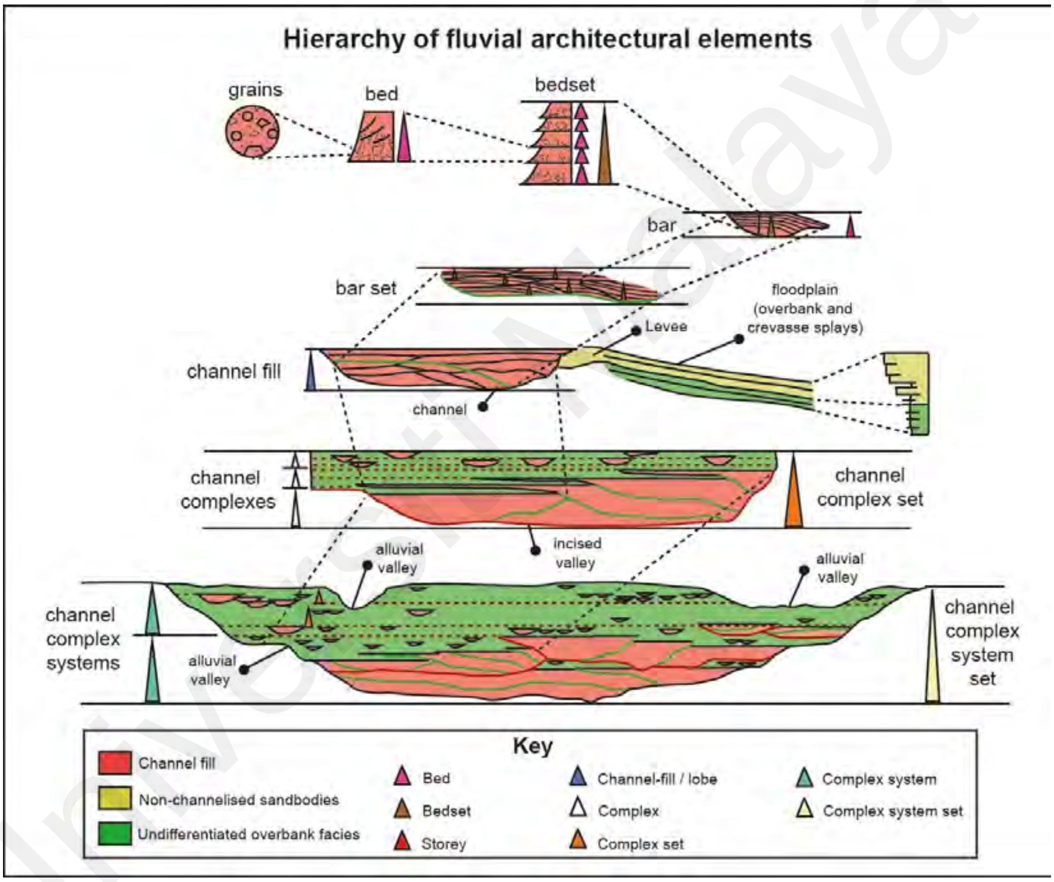

Figure 2.15: Chevron hierarchical scheme forthe fluvial depositional units (after Sprague et al., 2002).

Another hierarchy scheme, which ranges from individual channel scours through to high order valley-form sequences is used by Holbrook (2001), and Holbrook & Bhattacharya (2012). A single-storey channel is usually made up of elements such as channels, lateral accretion of channel bars, downstream accretion, and laminated sheet element with a channel abandonment fill, such as a mud plug and point bar deposits

(Labourdette, 2010; Fustic et al., 2012). Thin mud and siltstone layers usually drape overly single-storey channel fills, forming boundaries within a multi-storey channel. The mud drapes signify a break in fluvial bed-load deposition. Typically, this mudstone is almost to wholly eroded, and the base of next channel is a storey marked by an intraformational conglomerate (Gulliford, 2014), or coarser deposits.

River avulsion will produce a channel-belt (e.g., Payenberg et al., 2011). Channel-belts are described as genetically associated if they have a mutual principal paleocurrent path and show similar geometry and dimensions, or else they would form a random cluster (Wilson et al., 2014). A channel-belt fill includes the fluvial sediments deposited in a coastal plain such as lateral accretion deposits, crevasse splays, floodplain, and levees. Channel-belts can be made up of single-storey or multi-storey channels. Channel belts can form large channel-belt complexes (Payenberg et al., 2011) when they are vertically and laterally stacked. Channel-belt complexes are usually linked with a broad basin and may develop variable spatial distribution patterns.

On the other hand, Ford & Pyles (2014) have developed a new method for describing the fluvial hierarchical architecture from outcrop data. They propose models which are made up of channel belt and floodplain elements. Elements are further composed of storey units that represent the smallest component in their hierarchy classification.

2.3.3 Stratigraphy of Channel Deposits

Wright & Marriott (1993) and Shanley & McCabe (1994) designed fluvial sequence models in order to understand the relationship between fluvial architecture and accommodation. Bridge & Leeder (1979) developed computational simulation models where the magnitudes, rates, and scales of sedimentation are specified. Many of the parameters are designed as variable input for subsequent analysis, to enable the research of the dynamic interplay among variables of the quantitative model of alluvial stratigraphy.

These models of sediment stratigraphy were autogenic because the allogenic variables that govern the river system's long-term conduct are fixed to a constant value.

The sequence boundary in the Wright & Marriott (1993) model (Fig 2.16) is in the form of a subaerial erosional surface, representing valley incision that developed during a falling stage period. Paleosol maturity is used to assist in sequence stratigraphic interpretation. Marginal terraces can develop in incised valleys that preserve remnant fluvial deposits. Amalgamated, coarse grained channel elements accumulated during lowstand. During the transgressive stage, the ratio of the channel to floodplain deposits depends on the rate of relative sea-level rise. More accommodation space is created as sea-level rises quickly, which may potentially lead to thick floodplain deposits. During highstand stage, as relative sea-level rises slowly, channels develop and migrate predominantly by lateral accretion, resulting in the amalgamation of channels laterally with low finer grain ratio. Mature soils would be extensively developed as the rate of accommodation generation declines. Coarser grained braided systems will develop in the following sea-level fall stage. During this stage, the erosional process is more significant as the rivers cut down to a new lowstand.

The Shanley & McCabe (1994) model emphasizes the vertical changes in stratigraphic architecture, which are governed by the rate of accommodation space as well as the inherent processes in the depositional system (Fig 2.17). Their model is somewhat similar to Wright & Marriott (1993), where sedimentary architecture with the rate of accommodation space defines the systems tracts. However, the Shanley & McCabe (1994) model discusses the evidence that could be preserved in a fluvial system equivalent to the maximum flooding surface. In the Shanley & McCabe (1994) model, the degree of channel amalgamation is higher in the transgressive system tract (TST) relative to the highstand system tract (HST) (Fig 2.17c). During transgression, accommodation creation rate is low in the inland regime, and will increase as transgression brings the coastline farther inland. Therefore, the rate of generation of accommodation is lower during the transgression than the highstand stage and results in low net-to-gross sandstone ratios.

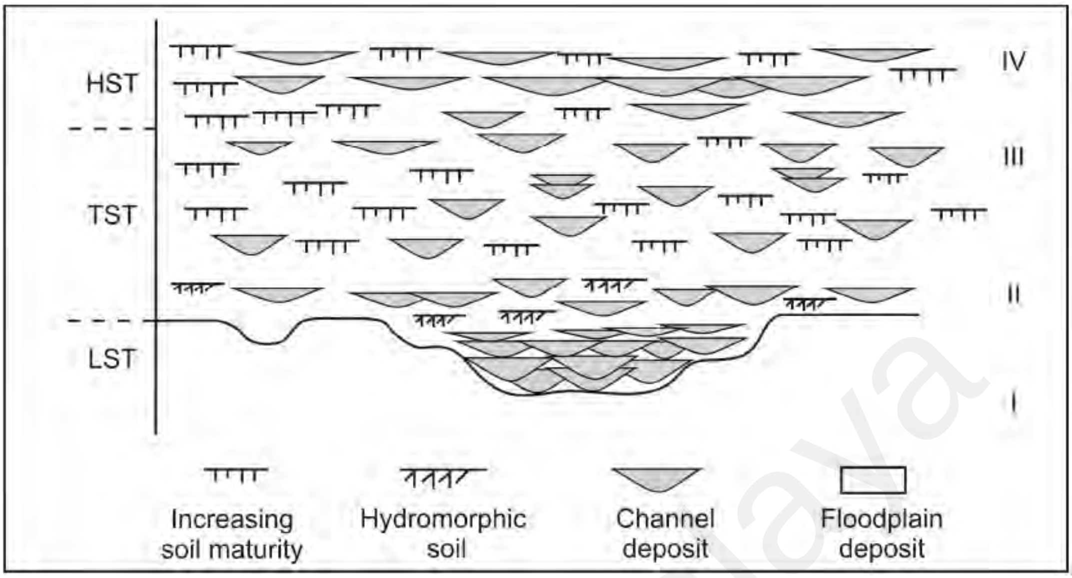

Figure 2.16: Wright & Marriott (1993) fluvial sequence model. The model incorporates the concept of the incised valley as defining the sequence boundaries.This comprises a subaerial erosion surface formed during the preceding falling stage. The Lowstand (LST) period has limited accomodation space and sedimentation is dominated by amalgamated-channel facies. During transgression (TST), rapid sea-level rise results in thicker deposition of floodplain deposits, with isolated channel bodies. Highstand (HST) period of slow sea-level rise decrease the accomodation space and channels evolve by accretion of pointbar and lateral migration.

Both of these models explain the importance and complex interplay of climate variability, tectonics, and sea-level fluctuation. These models have been used in many studies of modern and ancient fluvial systems, yet there is still an incomplete understanding of the stratigraphic development of fluvial deposits (Bridge & Tye, 2000). Seismic-based stratigraphic sequence models were also developed and commonly used as a predictive tool (e.g., van Wagoner et al., 1990; Catuneanu, 2006) in outcrop and subsurface studies.

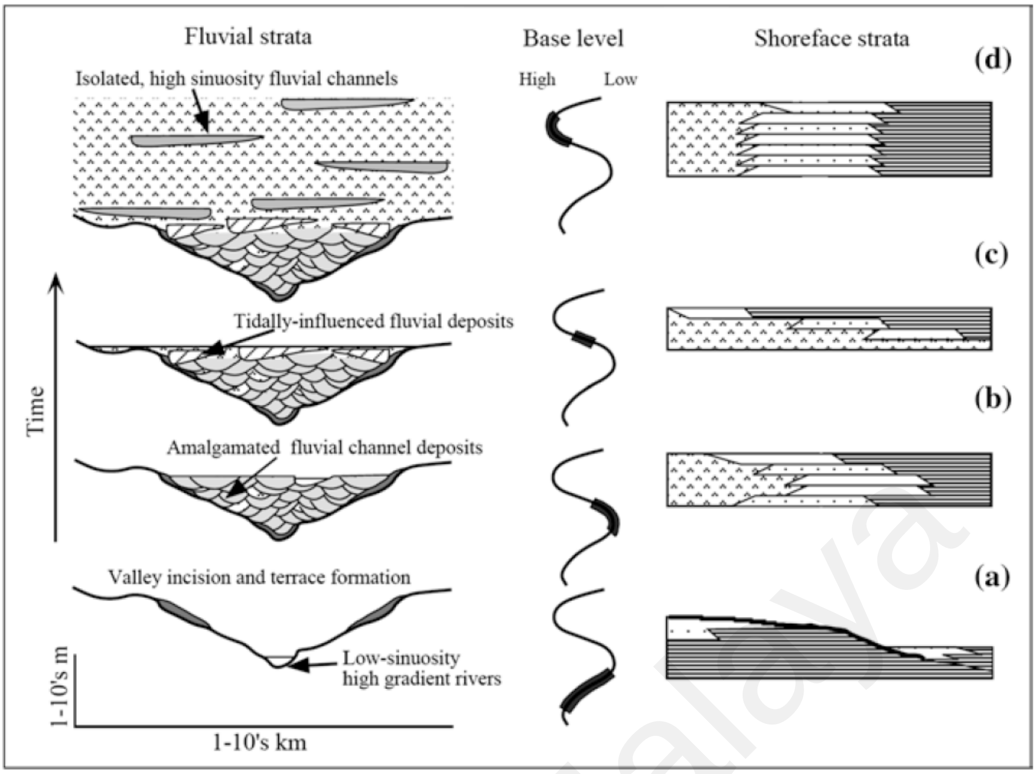

Figure 2.17: Shanley & McCabe's (1994) fluvial sequence model explains the link between fluvial architecture and shoreline with the base-level changes. a) Falling systems tract, developing fluvial terraces and incised valley, b) Low-stand systems tract, slow deposition resulted in amalgamated fluvial channel deposits c) Transgressive systems tract, prominent tidal influence, d) High-stand systems tract, deposit isolated, high sinuosity fluvial channels.

2.3.3.1 Incised valleys

Incised valley looks like a canyon feature that develop near the highstand coastline and erode into coastal plains extended landward to preserve their equilibrium-gradient profiles in response to sea-level fall. Incised valley form when sea-level fall exposes a continental shelf that has a steeper slope than the equilibrium profile of the river and typically wider than a single channel form (Schumm & Brackenridge, 1987; Schumm, 1993; Wood et al., 1993; Zaitlin et al., 1994; Schumm & Ethridge, 1994; Talling, 1998; Posamentier & Allen, 1999; Blum & Törnqvist, 2000; Ethridge et al., 2005; Gibling, 2006). When sea-level rise, marine incursion into this valley and form estuaries.

Posamentier (2001) stated that the river must have sufficiently cut into the floodplain, so when at flood stage, flow does not overwhelm the riverbanks. He described three primary mechanisms for incised valley formation: (1) product of sea-level fall; (2) tectonic tilting of alluvial settings, or (3) a substantial reduction in sedimentary discharge leading to an underfit stream. The erosional base of incised valleys commonly marks subaerial unconformities and sequence boundaries. Incised valley fills follow the pattern of relative sea level change (Fig 2.18). A basal lowstand fluvial deposit is typically preserved above the valley incision, which is overlain by a transgressive succession of fluvial-estuarine deposits. Highstand deposits tend to overlie the incised valley fill. The presence of small tributary channels draining into the main trunk valley is considered the most unambiguous evidence for incised valleys (Posamentier & Allen, 1999). These features could be easily detected within 3D seismic plan-view data.

There has been extensive research conducted on the sequence stratigraphy of incised valleys in relation to sea-level changes (Van Wagoner et al., 1990; Posamentier & Vail, 1988; Posamentier et al., 1988). However, these concepts are difficult to implement in paralic settings, which experience a complex interplay between climatic, tectonic, and autogenic controls on fluvial incision and architectures (Schumm, 1993; Shanley & McCabe, 1994). A vast array of terminology and inconsistency of nomenclature has arisen due to the various approaches to the stratigraphic analysis of fluvial systems. This makes comparisons and understanding between different studies challenging.

The area of fluvial incision associated with a sea-level fall is not always an incised valley and sea-level fall need not necessarily create a fluvial incision (Donovan & Jones, 1979). Unincised fluvial lowstand systems can also develop when a relative base-level fall does not reveal the entire shelf (Posamentier, 2001). The magnitude of the sea-level fall may reflect the geometry of fluvial incisions, including channel width and channel depth (Posamentier, 2001). Posamentier (2001) addressed possible scenarios for both unincised lowstand fluvial systems and incised valleys. These fluvial types differ in their morphologies (Fig 2.19).

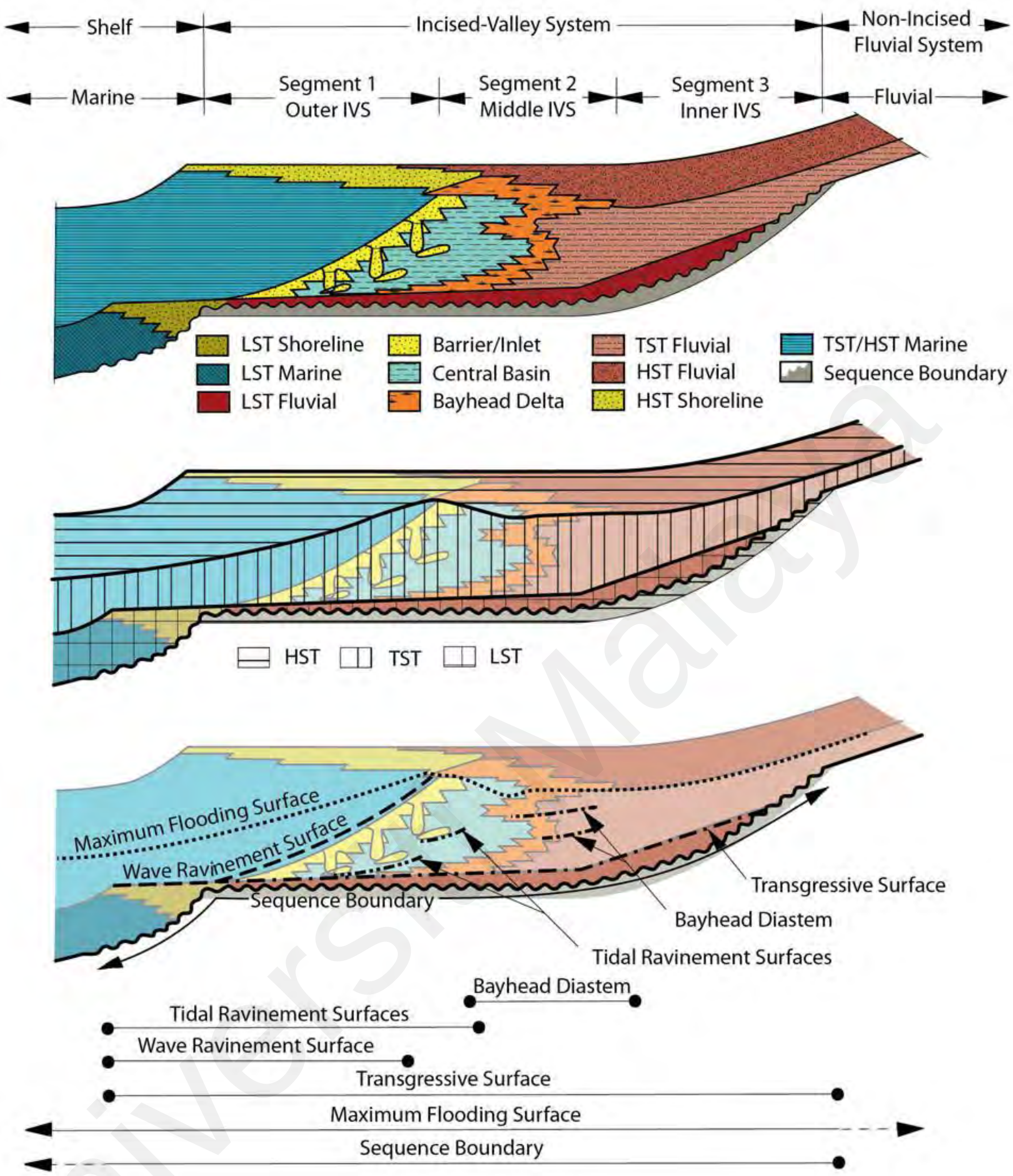

Figure 2.18: Schematic idealised longitudinal section of a simple incised valley system. A) showing the distribution of depositional environments, B) system tracts, and C) stratigraphic surfaces. (From Zaitlin et al., 1994).

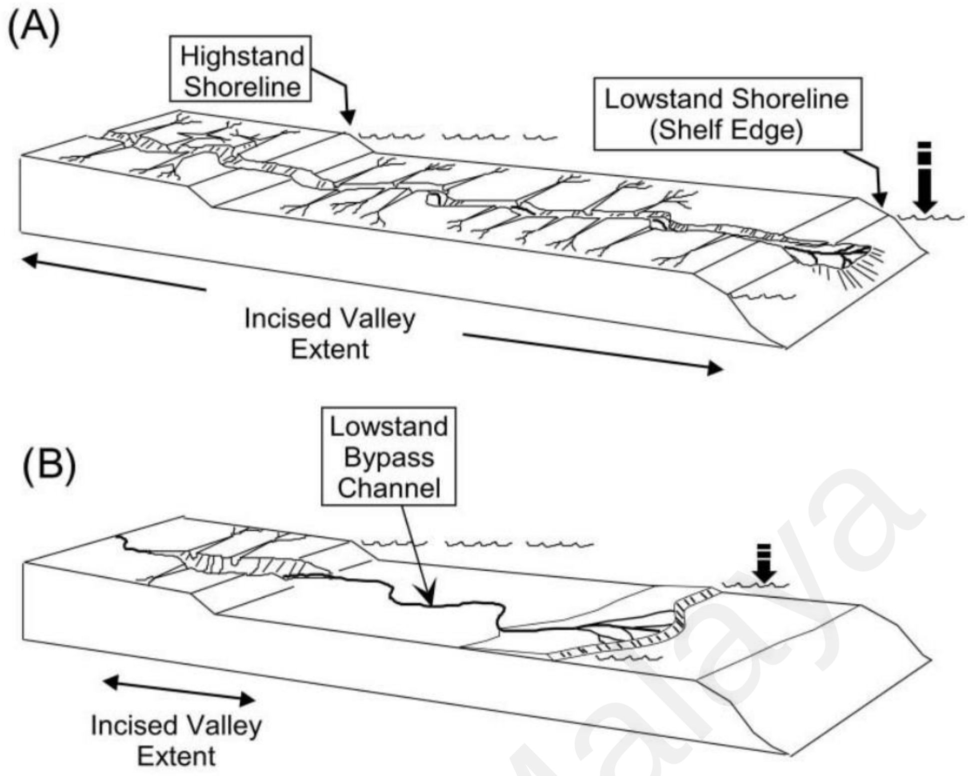

Figure 2.19: Illustration of, A) incised valley developed as sea-level fall. B) where sea-level fall did not expose the entire shelf, low-stand alluvial bypass channel system and shelf delta were developed, with or without the short extent of incised valley. (from Posamentier, 2001).

Incised valleys have been identified or interpreted in the Tertiary succession of the Malay Basin (Carney et al., 2008; Rees et al., 2008; Amir Hassan et al., 2013). As an example, Amir Hassan et al. (2013) identified incised valley fill complexes within the Miocene Group H. The valley fills were interpreted to mainly consist of progradational tide-dominated delta deposits and transgressive embayment deposits. The deep valley incisions were suggested to be formed by a combination of fluvial incision in the period of relative sea-level fall and tidal ravinement. Individual incised valleys were suggested to be lowstand incised delta distributaries. My study in here will further evaluate these interpretations by incorporating seismic imaging geomorphology to better understand the depositional environments.

2.4 Fluvial Channel Classification and Geomorphology

Much of the early work on channel characterization and geomorphology was done on fluvial channels, so here I will discuss fluvial channel concepts, including the relationship between sediment supply and channel type. This relationship was identified in modern-day fluvial channels which can be extended to ancient fluvial depositional channel systems (Galloway & Hobday, 1996).

Fluvial networks have been classified by numerous workers based on different criteria, including 1) erosion process (e.g., Davis, 1898, 1899); 2) consequential or superimposed structural control (e.g., Powell, 1875; Davis, 1898, 1899; Johnson, 1932); 3) Plan-view morphology (e.g., Davis, 1898; Miall, 1977) and; 4) classification of the process controls relating channel morphology to sediment type and discharge rate (e.g., Griffith, 1927; Leopold & Wolman, 1957,1960; Schumm, 1963, 1977).

Some of the earliest classification schemes observed the relationship between the evolution of topography, river erosion and transport strength, and erosional processes (Dana, 1850; Davis, 1899). Morphological studies have resulted in recognition of the well-established straight, braided, meandering, and anastomosing channel types (Leopold & Wolman, 1957; Miall, 1977; Brice, 1982, 1984). Straight channels are single channels with low sinuosity, and sidebars may be preserved along the channel. Meandering channels are high sinuosity single channels with point bars on the inner channel bends. Braided channels represent rapidly migrating low sinuosity channels separated by alternate and migrating channel bars in the middle and sides of the channel profile. Anastomosing channels represent multiple interconnected channels that are separated by stable islands.

These variations of fluvial channel styles develop due to the relationship between fluid and sediment discharge to the channel’s longitudinal gradient profile and bank stability. At a certain gradient, with increasing discharge, a meandering channel may change into a braided channel. This change may also occur when the discharge is constant, but with steepening channel gradient profile. Bank stability is influenced by sediment load and vegetation. Non-cohesive bed-load quickly erodes the channel path to create a low sinuous channel and possible braided channel, while high suspended-load results in meandering channel. Vegetation enhances bank stability through rooting, and the channel tends to meander with greater bank stability. In absent or sparsely vegetated areas, bank stability is low, thus forming straight and braided channels.

Many studies mostly have focused on the fourth criteria of fluvial classification, i.e., the relationship of plan-view morphology and fluvial cross-sections to sediment type and discharge (e.g., Griffith, 1927; Melton, 1936; Leopold & Wolman, 1957, 1960; Schumm, 1963; Galloway, 1981).

Leopold & Wolman (1957, 1960) demonstrated that the type of channel morphology that develops is controlled by variations in discharge, load, and slope. Later, Schumm (1963) classified rivers into three types based on sediment load; bed-load, suspended-load, and mixed-load. Channel type varies due to the relationship between sediment load, current velocity, channel sinuosity, vertical channel profile, and the inclination towards either lateral or vertical erosion and within channel sedimentation. Subsequently, based on the relationships between channel morphology and sediment load, Figure 2.20 shows the relationship between slope, load, and sinuosity of five bed-load channel models with a high width-depth ratio of >40 with sinuosity from 1.0 to 1.3, five mixed-load channel models with the width-depth ratio of >10 - 40 with sinuosity from 1.4 to 2.0, and three suspended-load channel models with the width-depth ratio of <10 with sinuosity >2.0.

The mixed-load channels of pattern 6-10 (Fig 2.20b) are relatively narrower and deeper, and the stability of the bank is higher compared to bed-load channel patterns. Higher bank stability retained the shallow, deep straight pattern 6 channels and a sinuous pattern 7 channel due to an increase in sediment load and slope. Pattern 8 is a meandering stream, and pattern 9 shows decrease in sinuosity, with increase in sediment load. With higher transport of sediments, the inclusion of bars gives it a drifting sinuous-braided appearance. Pattern 10 is a more stable island channel than the bed - load channel pattern 5. Pattern 11 suspended-load channels is a straight, short, deep channel. Finally, patterns 12 and 13 have the greatest sinuosity, and such patterns can be very consistent in both fluvial and tidal system networks.

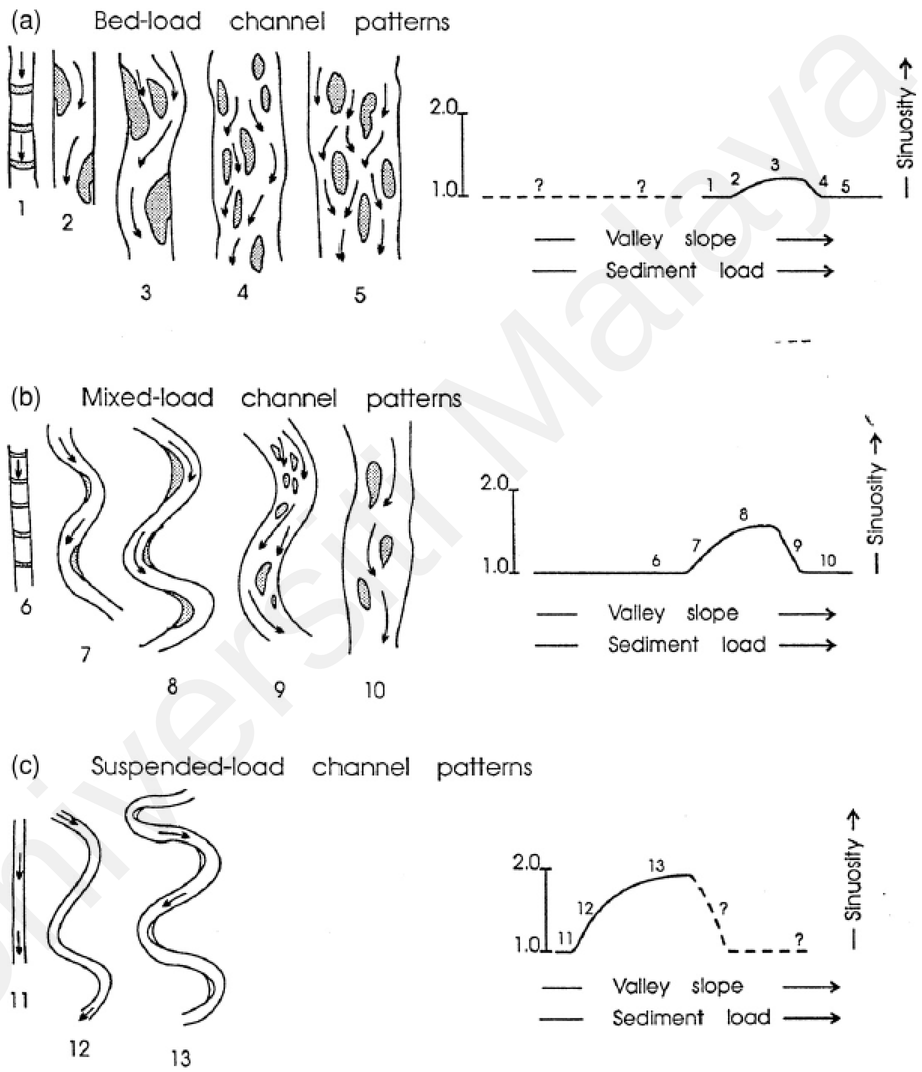

Figure 2.20: This figure shows the main three channel groups of sediment load and their relationship with slope, and sinuosity. a) five bed-load channel models with a high width-depth ratio of >40 with sinuosity from 1.0 to 1.3, b) five mixed-load channel models with the width-depth ratio of >10 - 40 with sinuosity from 1.4 to 2.0, and c) three suspended-load channel models with the width-depth ratio of <10 with sinuosity >2.0 (from Schumm (1977).

Galloway (1981) later adopted this description from Schumm (1977) as the foundation for a more detailed subdivision of fluvial types (Fig 2.21). This classification is based on the empirical relationships between geomorphology, lithology, and internal architecture of channel fill to the sediment loads. Vertical analysis of core and wireline logs showing irregular and poorly fining-upward profile is of the straight to slightly sinuous bed-load channel dominated by sand. Well-developed fining-up log profile could be of a sinuous mixed-load channel filled with mixed sand, mud, and silt. Whereby, chaotic log profile may suggest a highly sinuous suspended-load channel dominated by mud and silt.

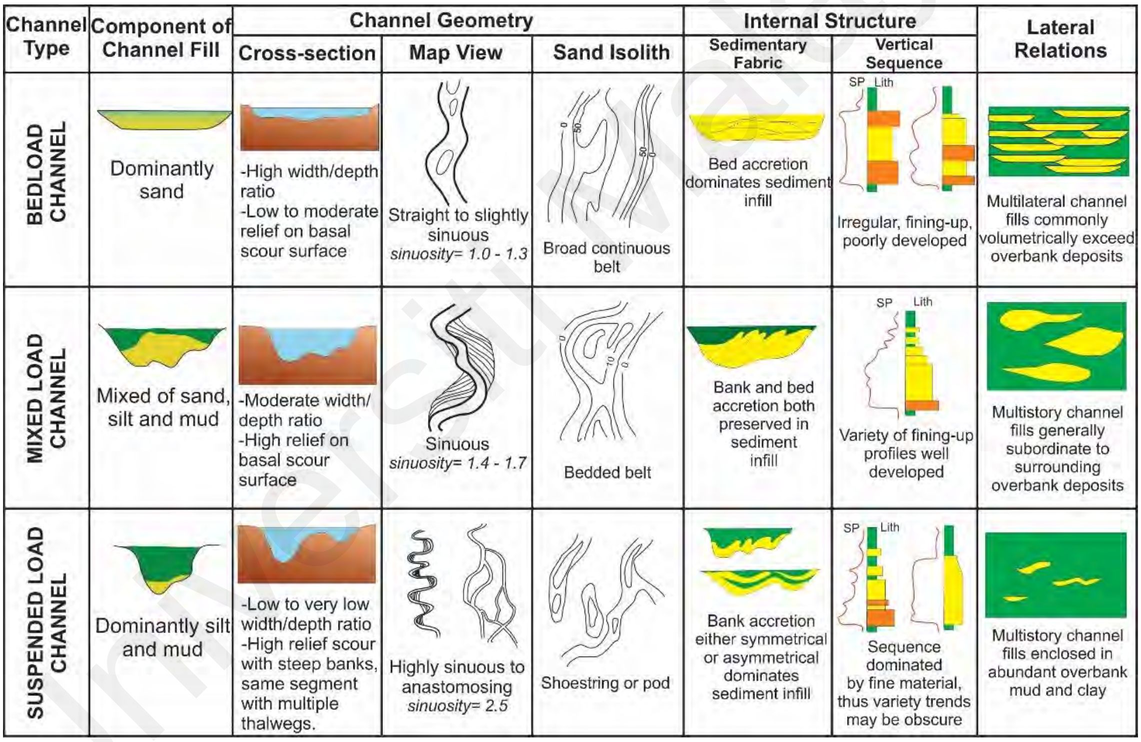

Figure 2.21: Schematic illustration of channel classes following Schumm's fluvial-geomorphological classification (1963) in the left column with geomorphic (from Galloway, 1981).

2.5 Tidal Channel Classification and Geomorphology

Tidal channels as discussed in this dissertation, refer to both tide-dominated channels and tide-influenced channels. A tidal channel is any elongated indentation or valley in a wetland originated either by tidal processes or another origin, through which water flows and deposition is primarily driven by tidal currents (Perillo, 2019). Tidal channels can be in the form of distributary, tributary, estuarine channels, or small creeks. These channels can be found in i) tide-dominated estuaries (e.g., Dalrymple et al., 1992); (ii) tide-dominated deltas (e.g., Plink- Björklund, 2012; Goodbred & Saito, 2012); (iii) tidal inlets (e.g., Hayes & Fitzgerald, 2013); and (iv) tide-dominated shelves (e.g., Levell et al., 2020). Many of these channels are closely related to tidal flats which form elements within these depositional environments.

2.5.1 Classification and Morphology

Given the extensive literature in tidal channels and creeks associated with tidal flats, I first discuss the geomorphological characteristics of tidal channels and creeks developed in such settings. There are three major morphological components in shallow, intertidal landscapes: (1) tidal flats or un-vegetated bars; (2) mangroves or marshes, or vegetated shelters; and (3) channels that interconnect and incise into the flats, bars and vegetated shelters (D'Alpaos et al., 2005; Fagherazzi et al., 2006; Hughes, 2012). These areas of marsh and channel can be intertidal (drying out or allowing standing water at low water in only the very deepest parts) or peri-subtidal (in which the wetted extent of the channel is large compared to the tidal range). Tidal channels develop at numerous scales. Perillo (2019) describes tidal channels as having widths of more than 200 m, and channel depths of more than 100 m, while channels which are less than 200 m wide and less than 100 m deep are referred to as tidal creeks. Estuarine river mouths can also be considered as large tidal channels (Dalrymple et al., 1992). Tidal channels are abundant and prevalent in macrotidal, mesotidal, and microtidal settings.

As mentioned by Marani et al. (2002) fluvial versus tidal morphologies have distinct characters. The primary feature of channel systems in tidal systems is the heterogeneity in channel architecture and floodplain morphologies. Tidal channels tend to share the following characteristics: (1) a sinuous channel plan-view morphology; (2) deposits comprising current-generated bedforms (ripples, dunes, etc.) and barforms; (3) low gradient channel beds; and (4) width to thickness ratios above 5 (Steers, 1969; D'Alpaos et al., 2005; Hughes, 2012).

From a planform view, the sinuous tidal channels also tend to have a down-current flaring, funnel-shaped geometry, with the channel width tapering landward. This tapering is caused by the decrease in tidal prism upstream (the rate of decrease may also be controlled by tidal resonance; see Wright et al. (1973) and van der Wegen et al. (2008) for further explanation). A wider funnel-shaped river mouth would amplify tidal flood currents into the channel, extending the tidal range landward. A high channel width gradient, which is present in all shallow tidal channels, and the associated presence of abundant parallel creeks and ridges in the area, distinguishes tidal from fluvial systems (Fagherazzi et al., 1999; Fagherazzi & Mariotti, 2012). Thus, tidal channels and creeks occupy a larger area on the tidal flats. This variation in channel width of the drainage area means that the tidal channels look closely spaced compared to those of similar width in fluvial systems (Hughes, 2012).

At the larger scale, tidal channels form dendritic networks, with smaller, low order channels merging into larger, higher-order channels (Ashley & Zeff, 1988) (Fig 2.22a). The lowest order of channels are the smallest streams at the end of a network which are blind-ended (Fig. 2.22a, Horton, 1945). In contrast to fluvial channels, tidal channel frameworks and morphologies are dynamic (Fagherazzi et al., 1999; Fagherazzi & Mariotti, 2012).

Zeff (1988) and Ashley & Zeff (1988), in their study within salt marshes of New Jersey, describe two types of tidal channels, i.e., through-flow (TF) and dead-end (DE) channels. Through-flow (TF) channels form connected networks separated by islands, while dead-end channels form smaller channel networks and end within a marsh or lake. These two types of tidal channels are distinguishable by their width-to-depth ratio, channel dimensions, deposits, and hydraulic mechanism. Zeff (1988) suggests that through-flow channels develop during the infilling of the back-barrier areas when vegetation protects the flood-tidal delta. Dead-end channels likely erode in a landward direction during ebb current flows and will continue to erode landward until it reaches the zero tidal limit.

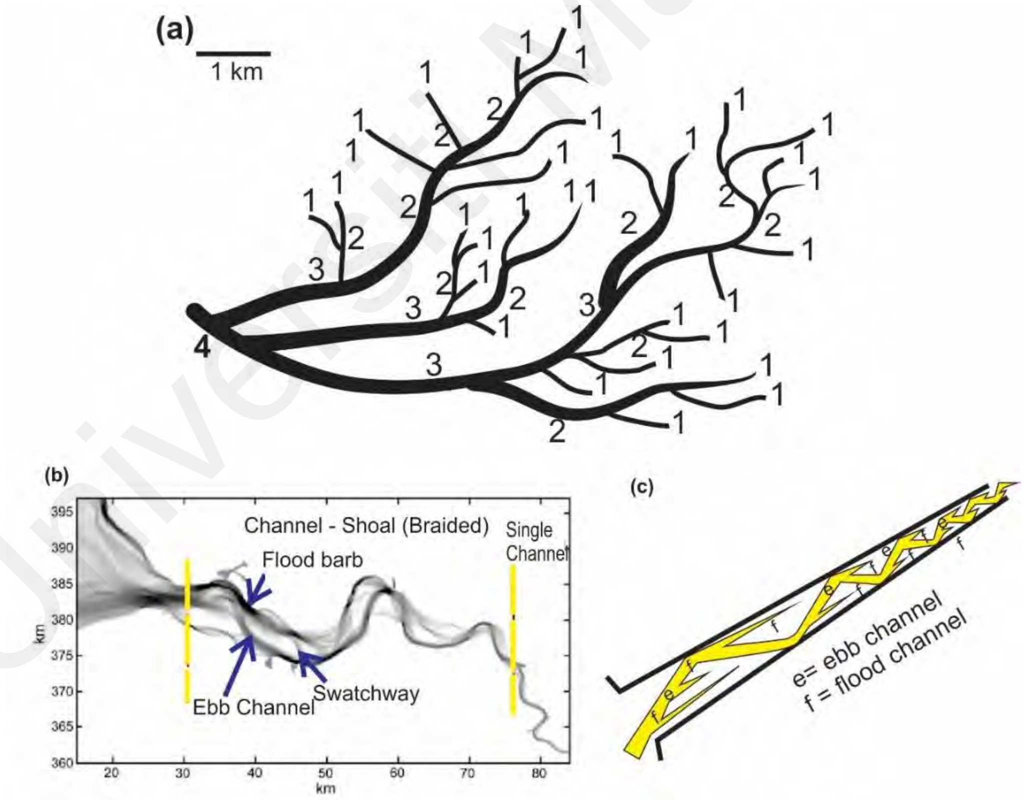

Figure 2.22: (a) Flow orders labeled according to Horton's law in a dendritic or fractal network in the Dutch Wadden Sea (Cleveringa & Oost 1999), (b) example of braided/ interconnected channeling in an estuary, and (c) ebb and flood channels in a braided network (van Veen, 1950); modified from Hibma et al., 2004a).

At the macro as well as mesoscale of large tidal channel networks along tide-dominated shorelines, networks of multiples channels generally form two distinct patterns: (1) fractal patterns and (2) braided patterns (van Veen, 1950 and the English translation in van Veen et al., 2005; Hibma et al., 2004). Fractal channel (also known as "low apple tree-like") patterns form dendritic networks, where larger channels branch into progressively smaller channels (e.g., Cleveringa & Oost, 1999). On the other hand, braided channel patterns form networks with the meandering, mutually evasive ebb, and food-dominated channels being separated by shoals in between (Fig 2.22b). Van Veen (1950) observed braided channel patterns displaying a 'poplar tree-like' network along the tidal coast of the Netherlands, with sinuous 'trunk' ebb dominant channels connected to short, blind-ended 'flood barbs'.

Such intricate emergent patterns develop due to many factors including interaction between mutually evasive ebb and flood tidal currents, the tidal prism, autocyclic channel meandering, sand transport, wind action, and near-bank turbulence. Fractal channel forms appear to be closely associated with shallow intertidal settings, while the braided channel form appears to be more characteristic of deeper, subtidal channels (Hibma et al., 2004).

Some studies on the morphological classification of tide-dominated channels have focused on the intertidal setting. Some classification schemes for intertidal, tide-dominated channels use the level of channel morphologies and the existence of one or multiple channels as defining characteristics. Eisma (1998) recognises ten types of channels within three categories occurring at a variety of scales on the intertidal zone, i.e.: (1) few or no channels which are relatively rare (infrequent tidal inundation within arid conditions); (2) single channels (sinuosity ratio > 1.5) which are linear and meandering, and (3) channel network systems which can be dendritic and elongate dendritic, parallel channels, distributary, braided, or interconnecting. Pye & French (1993) expanded on this classification scheme based on their work on channel networks in marshes. They recognise seven channel network types (Fig 2.23 and Fig 2.24): linear single, dendritic and linear dendritic, meandering dendritic; reticulate, complex, and superimposed.

Subsequently, Eaton et al. (2010) attempted to describe the morphodynamics of the river system based on a mathematical study of the flow and sediment transport parameters. The classification system is, however, basically limited to channels in which flow resistance is primarily determined by grain size distribution, which moves as bed load.

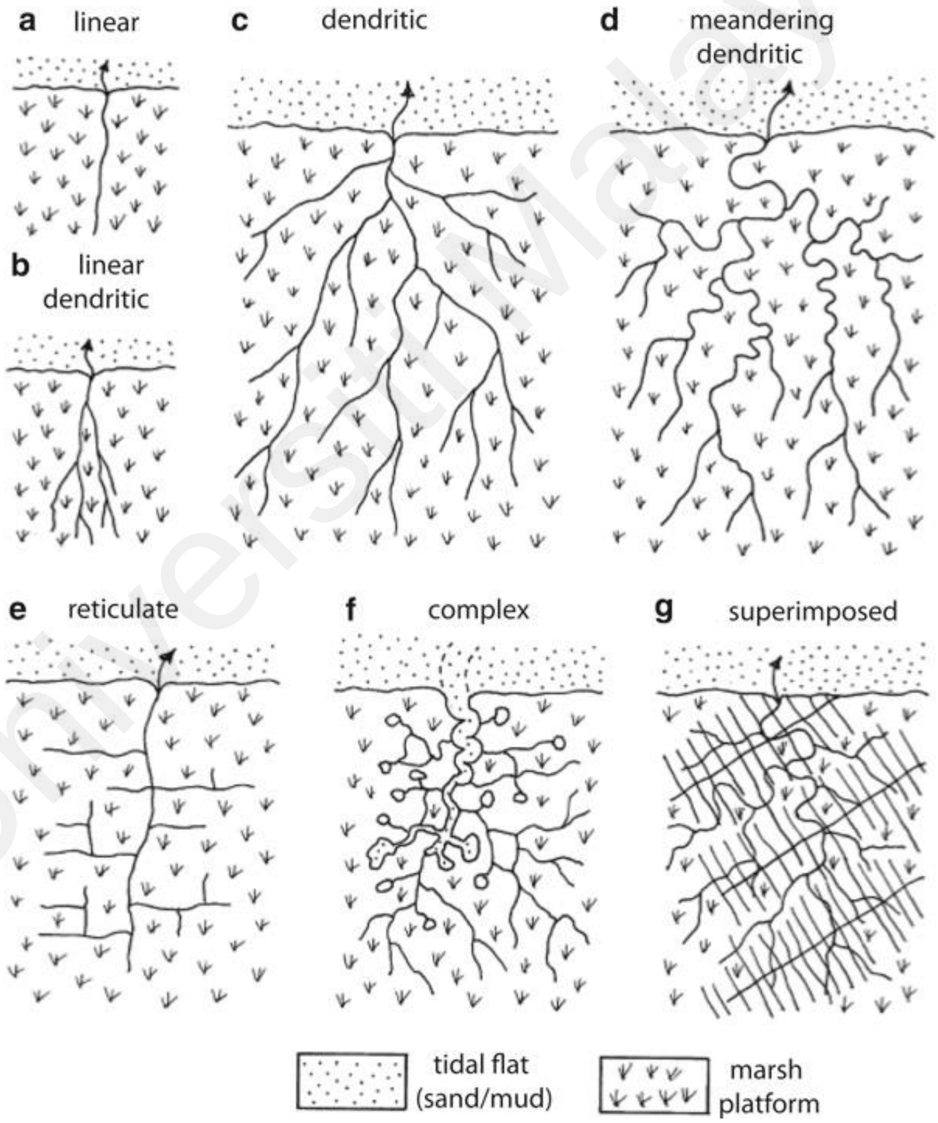

Figure 2.23: Tidal channel network classification in salt marshes (from Pye & French, 1993)

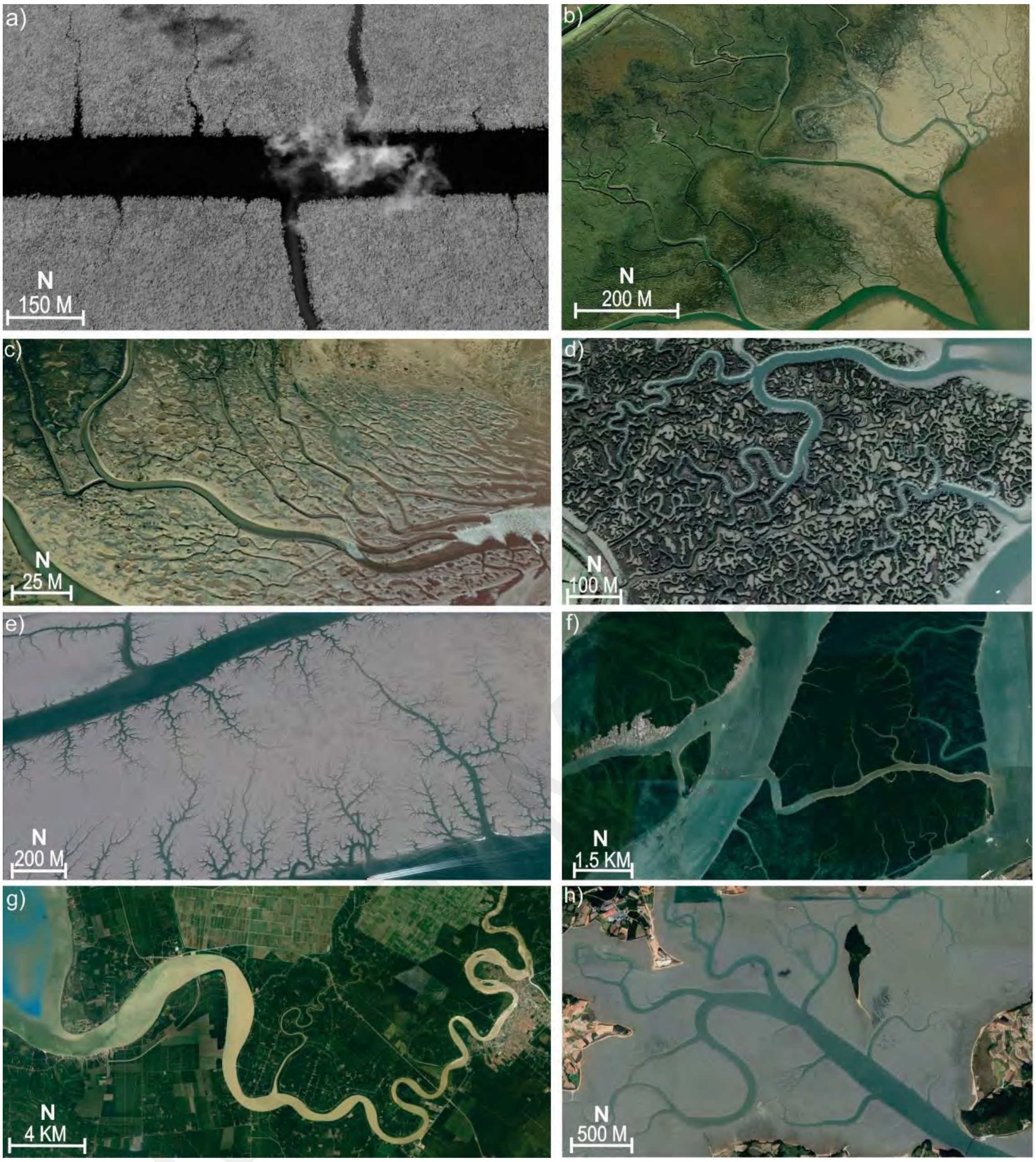

Figure 2.24: Variety of modern-day tidal channel morphologies. a) straight, small tidal channels drain into larger channel in Pulau Rangsang, Indonesia; b) dendritic network of channels in marsh area of the Wash, UK; c) Paralel dendritic network on tidal flat extend across vegetated area in the Wash, UK; d) complex morphology of tidal channel, Tollesbury Marsh, UK; e) dendritic network of West coast of Korea; f) interconnected through-flowing and dead-end channels of Kelang Delta, Malaysia; g) highly meandering channel of Lupar Estuary, Sarawak; h) meandering-dendritic network on tidal flats, in the west coast of Korea.

2.5.2 Tidal Channel Planform Geometry

2.5.2.1 Tidal channel meanders and sinuosity

Tidal channels tend to display a sinuous thalweg (Fig 2.25). The channel sinuosity is defined by the ratio of the thalweg channel length to the channel 'straight-line' distance downstream (see Chapter 3). A channel is referred to as meandering when its sinuosity ratio exceeds 1.5 (Leopold et al., 1964). The ratio of meander wavelength to channel width in fluvial channels is 2 - 3 for young channels, and 6.5-11 for very mature systems (Leopold & Wolman, 1960). It is thus reasonable to assume that shorter and younger channels are prone to be more sinuous. Generally, wider channels are inclined to display a straighter morphology compared to smaller and narrower channels, which are frequently more sinuous (Hughes, 2012). It has also been noted that straighter channels tend to develop where the substrate is non-cohesive, easily eroded and unvegetated, whereas channels which are flanked by vegetated banks, such as mangroves or salt marshes, tend to display increased sinuosities (e.g., Garofalo, 1980; Eisma, 1998).

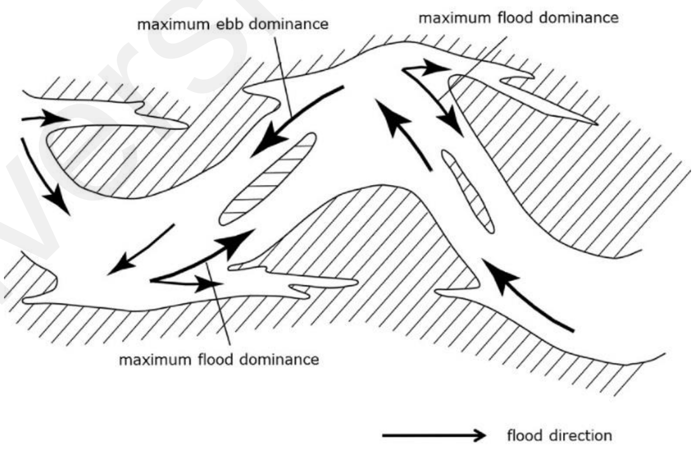

Figure 2.25: Schematic view of the ebb and flood flow in a meandering tidal channel system (from Dronkers, 1975).

Channel meanders are emergent features, and their formation is still poorly understood. Three mechanisms have been proposed to explain meander development (Eisma, 1998): 1) mechanical, where development is from minor irregularities along the channel; 2) stochastic (channel instability), where slight perturbations disrupt the channel flow, and 3) hydraulic, where meanders would lengthen a channel. However, Seminara (2006) acknowledges that any such concepts are hard to test in the field or through laboratory experiments.

Certain features of tidal meandering channels appear to be unique and not shared with their fluvial equivalent. For example, meandering tidal channels tend to display a straight-meandering-straight longitudinal trend in channel sinuosity (Solari et al., 2002). The same pattern is also observed in large-scale estuaries (see Section 2.2 and Dalrymple et al., 1992; Dalrymple & Choi, 2007). Observation have been made that the inland region of a narrow tidal channel has a greater curvature than the wider seaward region of the tidal channel (Marani et al., 2002, 2004). Tide and fluvial current interaction can distort the meander bend pattern of tidal and fluvio-tidal channels, which usually produces an asymmetry in the meanders observable in planform view, termed as bend skewing which produces a 'goose-neck' loop geometry (Fagherazzi et al., 2004; Seminara, 2006). This goose-neck loop geometry is the product of bank erosion due to the time interval between the water velocity maximum and the maximum channel curvature at the bank (Parker et al., 1983). The highest velocity flow does not necessarily overlap with the axis of the channel. Hence, the maximum erosion on the outer edge of a meander, therefore, cannot coincide with the meander curve's highest point. The feature can migrate toward skewness if erosion is sufficient (Seminara, 2006). Meandering may be distorted or symmetrical according to the relative strength of the ebb and flood currents (Fagherazzi et al., 2004).

Figure 2.26 shows the evolution of a typical channel experiencing unidirectional flow (Fig 2.26a). Initial sinusoidal condition (Fig 2.26a) will progress into asymmetric goose-neck loops because of the unidirectional flow (Fig 2.26b). A meander evolves differently under the influence of bidirectional flow. Within ebb-dominated tidal channels, bend skewing is still recognisable, even though reasonably subdued (Fig 2.26c). In the event of the ebb and flood currents having similar speeds, it will produce a symmetrical meander (Fig 2.26d),

Erosion at two points due to opposing ebb and flood tidal currents in a meander curve may also contribute to the development of a ‘cuspate’ meander bend, also known as' pinch and swale'. Such cuspate meander bends are a reliable indicator of tidal influence in channels (Fig 2.27a). The reverse flow induces the upstream or downstream meander alternately to deposition and erosion.

Additionally, a small channel that cuts across the inner meander bend may create chutes but may be elevated due to the variability of tide currents. This may also create a tidal barb in the direction of the subordinate and opposing tidal current, whereby the dominant tidal current runs in the outer meander bend. If the meander is totally cut off, the next tide cycle can create a secondary channel, which carries the residual tide.

Due to the complexity of erosional processes, hydraulic mechanisms, and dynamic forcing, some mid-channel islands can be formed within the tidal environment (e.g., in the Rajang Delta, Sarawak, Fig 2.27b). These islands often display a certain degree of detachment from the bank on the wide meandering channels (Barwis, 1978). Naturally, stream flow consistency will affect channel morphologies from straight to complex meander tidal channel systems over time (Hibma et al., 2003, 2004a, b; Seminara, 2006).

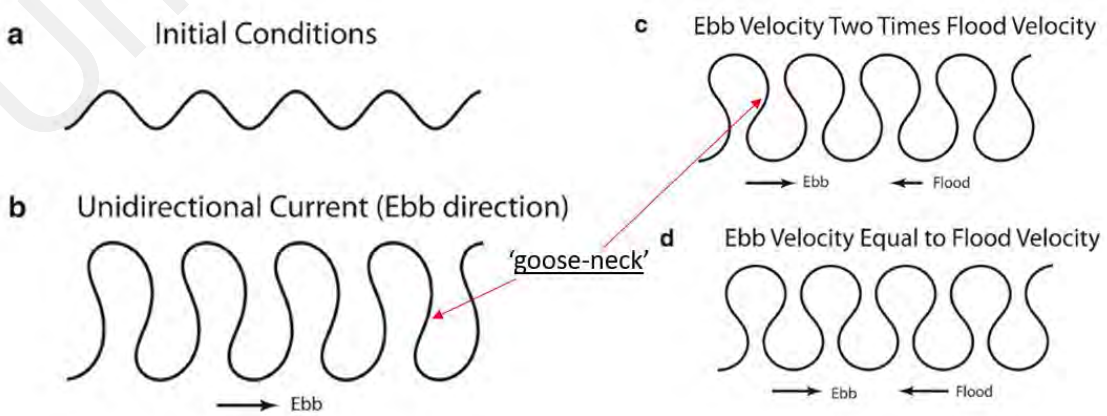

Figure 2.26: Meander morphology emerging from (a) initial irregular channel, under conditions of (b) unidirectional flow; (c) ebb-dominance of bidirectional flow; and (d) equal flood and ebb flows. (from Fagherazzi et al., 2004).

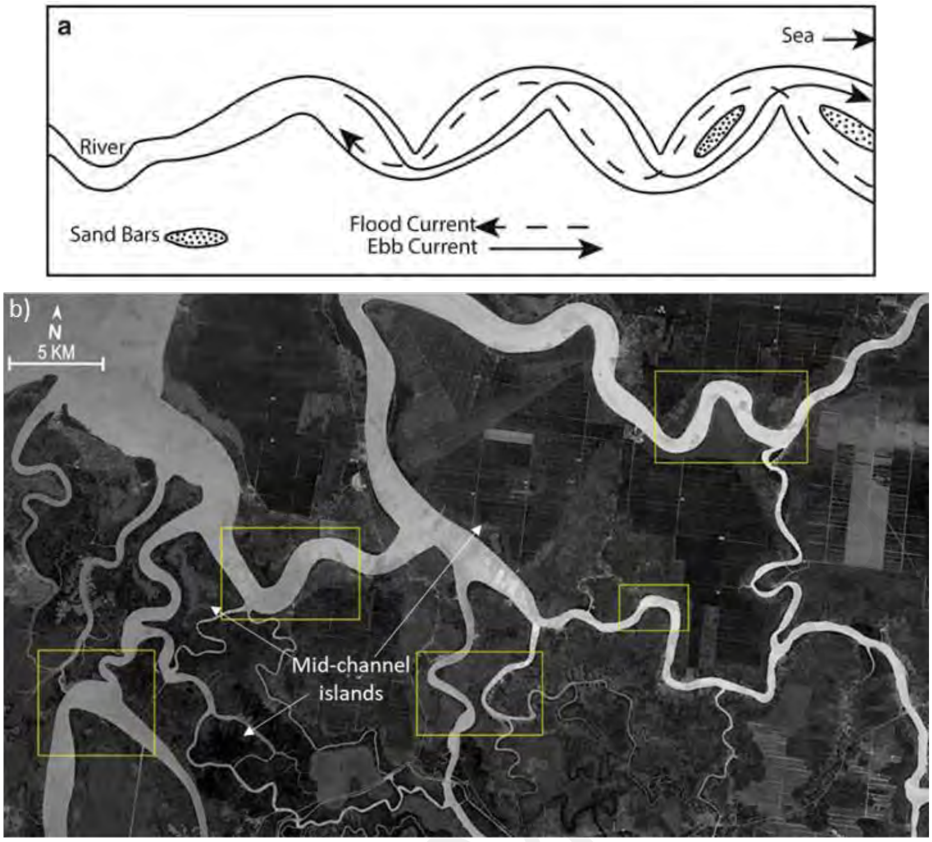

Figure 2.27: (a) Illustration of the tidal meander well-known of cuspate feature as in the yellow-lined boxes, (b) Various morphologies in the Rajang Delta, Sarawak (Malaysia), include mid-channel islands.

2.5.2.2 Dendritic networks

One of the most common features observed in tidal channel systems are dendritic networks (Fig 2.23c), especially on tidal flats and salt marshes. Based on Horton's law, two first-order channels would meet up and join to form a second-order channel (Fig 2.22a). These low order channels are the tributaries in the channel system. All the channels in tidal systems experience bidirectional flows, with both high-order and low order streams receiving and feeding flow from each other (Hughes, 2012). The bifurcation ratio (i.e., the ratio between the number of stream branches of an order to the number of stream branches of the next-higher order in a drainage network, Giusti & Schneider, 1965) in tidal channels is high (around 4) (Knighton et al., 1992; Novakowski et al., 2004). Another prevailing morphology in dendritic networks are reticulate channels (Fig 2.23e). The angle at which low - order channels connect to higher-order channels is 90° in reticulate channels (Zeff, 1988; Eisma, 1998; Ginsberg & Perillo, 2004; Hughes, 2012), even though the bed gradient angle is low. In Pestrong (1965), the low-order tidal channels bed gradients were frequently steeper than those of higher-order channels such as in the San Francisco Bay. Nonetheless, it is a nature of the tidal flow that contributes to the 90° connection angles in tidal systems, when tidal asymmetry is higher in small channels compared to the larger channels where the flow of ebb and flood are equally balanced (Zeff, 1988; Eisma, 1998; Hughes, 2012).

2.5.2.3 Distributary, braided and connected channels

Distributary channels are channels which branch off from a trunk alluvial river and transport river water and sediment to the sea. They are common elements of deltas. The distributary channels of tide-dominated deltas tend to be fluvial-dominated but with strong tidal influence. Such channels are wider in a flat landscape with a low bed gradient angle in the peak of the tidal energy area, signifying during lower water levels, that ebb flow is active (Dalrymple & Choi, 2007). In a distal location, some of distributary channels may be flood dominant due to mutual channel evasion. The main morphological features of distributary channels are channel bifurcations and confluences. In many cases, these features are morphologically linked, and their dynamics and interaction regulate many aspects of the morphology and processes of channels (Ashmore, 2013).

Braided channel networks can also be observed in tide-dominated estuaries. The formation of such networks is not fully understood in tidal environments. The mechanism is probably different from braided rivers because of the presence of opposing currents and importance of hydraulic mechanism in controlling the flow, versus bed gradient in fluvial settings (Hughes, 2012).

Interconnected or through-flowing channels (Ashley & Zeff, 1988) are commonly seen alongside dendritic channels. However, several other channel morphologies and dimensions are actually present at the same time. These channels are common within tidal range and tend to exhibit meandering, sinuous and straight morphologies. A study in the Niger Delta (Allen, 1965) indicates that interconnecting channels develop when tidal flats (due to the sediment of the river supply) accrete vertically and horizontally, when bars stabilize into vegetated islands or when blind channels merge.

2.5.3 Unique Tidal Features

The interaction between tidal processes and sediment can produce a variety of sedimentary features (Allen, 1980, 1984; Dalrymple, 1984; Kvale & Archer, 1991; Nio & Yang, 1991; Tessier, 1998). Sedimentary facies consisting of unique tidal features are known generally as 'tidalites' (Klein, 1971, 1998). Tidalites can be observed at different scales, ranging from very thin mud lamination to muddy and sandy heterolithic strata (lenticular, wavy or flaser bedding) to sand-dominated unidirectional, bidirectional (herring-bone) or tidal bundled cross-stratification (Fig. 2.27) (see reviews by Klein, 1998; Coughenour et al., 2009; Davis, 2012; Steel et al., 2012; Longhitano et al., 2012). Tidalites have been described and documented in siliciclastic (e.g., Gastaldo et al., 1995; Dalrymple et al., 2003), carbonate (e.g., Yang & Yang, 1984; Lasemi et al., 2012), and mixed siliciclastic-carbonate (e.g., Longhitano et al., 2010; Longhitano, 2011; Zand-Moghadam et al., 2013) deposits. Tidalites may develop in various depositional environments such as within coastal, fluvial, or lacustrine area. Tidalites may not be well preserved at some locations such as estuaries and tidal flats area due to variable tidal energy conditions with insufficient sediment transport or due to the influence of fluvial or wave energy that superimposes or rework any tidal signal (Dalrymple & Choi, 2007; Davis, 2012).

Tidalites are deposited under a variety of tidal strengths and various duration of tidal cycles, including periods of days, months, or years (e.g., Visser, 1980; Boersma &

Terwindt, 1981; Allen, 1981). Daily tidal cycles are represented by diurnal (one tidal cycle) or semi-diurnal (two tidal cycles) tides, depending on the basin. Monthly cycles represent fortnightly periods related to the phases of the moon. The tidal energy cyclically increases and decreases following these cycles. Alternating coarser and finer layers and/or thicker and thinner layers of sediment will be deposited due to the tidal cycles. When the sediment supply is sufficient with no erosion, sedimentary succession may record distinct tidalite features.

Good examples of ancient tidalites documented in the Carboniferous of the mid-western USA (e.g., Brown et al., 1990; Kuecher et al., 1990; Archer, 1991; Kvale & Archer, 1991). Tidalites in these examples record evidence of semi-diurnal through yearly tidal cycles. Some of the common types of tidalites are described below:

1- Tidal rhythmites

The periodic alternations of ebb and flood tidal currents with intervening low energy slackwater intervals produce cyclical stacking of mud and sand layers of varying thickness, known as tidal rhythmites (Reineck & Singh, 1973; Kvale et al., 1989; Dalrymple et al., 1991; Archer, 1996; Friedman & Chakraborty, 2006) (Fig 2.28a). Tidal rhythmites are commonly associated with protected settings in tidal environments (Choi & Park, 2000; Greb & Archer, 2007).

Tidal rhythmites may comprise sets of mud-draped sandy ripples that, as cosets, are known as heterolithic strata. Heterolithic strata are the result of periodic alternation of tidal currents and are made up of interlayered rippled sand and mud, which are expressed. Variations in the sand and mud ratio produce a spectrum of heterolithic bedding types, e.g., flaser, wavy and lenticular bedding (Reineck & Wunderlich, 1968) (Fig 2.28d). Wavy bedding comprises laterally continuous layers of rippled sand interbedded with laterally continuous mud drapes of sub-equal thickness. Flaser bedding is sand-dominated, with mud drapes occurring as discontinuous thin lenses (flasers) (Reineck & Wunderlich, 1968). Lenticular bedding is composed of isolated ripple lenses encapsulated within a thicker, muddy interval (Reineck & Singh, 1980; Collinson et al., 2006). Heterolithic strata are also observed in fluvial systems (ephemeral rivers) when the river flow regime changes over time (Picard and High, 1973). These features are very common in intertidal and subtidal environments such as estuaries and the inter-distributaries of deltas.

Tidal rhythmites can also consist of alternating mm- to cm-thick sandstone, claystone, and siltstone laminae (Kvale et al., 1997, 1999). Each set of alternating coarse-fine sediments is the result of sand deposition from traction and/or suspension fallout (high-velocity stage of the flow) during ebb or flood tide. This is followed by suspension fall out of mud during slackwater periods between tides, which produces a mud drape (Visser, 1980; Nio & Yang, 1991; Dalrymple, 1992, 2010; Flemming & Bartholomä, 1995). These tidal rhythmites may preserve a single or two sets, depending on whether the ebb- and flood tides are of equal strength or are symmetrical, resulting from a diurnal or semidiurnal system (Greb & Archer, 1995).

Tidal bundles are a type of rhythmite and are best defined as vertical or inclined rhythmites successions displaying cyclical variation of laminae of foreset laminae thickness, which formed by stronger sets of currents in an asymmetric tidal cycle (Visser, 1980; de Boer et al., 1988; Nio & Yang, 1991; Smith et al., 1991; Dalrymple, 1992; Friedman et al., 1992; Flemming & Bartholomä, 1995; Reading & Collinson, 1996; Alexander et al., 1998) (Fig 2.28b). These were originally identified in dune cross-beds, where the cross-bed foresets display rhythmic tidal bundling. Each bundle is in the form of heterolithic cross-strata which termed as couplet, that developed by dune migration. Variation in bundle thickness is due to cyclical variation in tidal current strength and speed, associated with neap-spring cycles (de Boer et al., 1988; Nio & Yang, 1991;

Dalrymple, 1992; Flemming & Bartholomä, 1995). Stronger tidal currents during spring tides resulting in deposition of thicker foreset laminae and thinner or non-existent slackwater mud drapes. During neap tides, the laminae are thinner, but with thicker mud drapes. Alternating periods of spring and neap tides results in an alternating thick-thin-thick pattern of tidal bundling in the cross-beds.

2- Reactivation surfaces

A reactivation surface is a minor erosion surface that forms between successive migrating bedforms (Klein, 1970). A current reversal can disrupt the migration of a dune in the opposite direction, which results in the removal of the dune's crest. Migration of a new dune can then commence above the erosional surface, thus preserving a reactivation surface (Dalrymple, 1992; Collinson et al., 2006) (Fig 2.28c). Reactivation surfaces are also associated with ebb-modulated fluctuations in the flow velocity (Nio & Yang, 1991; Brettle et al., 2002). These surfaces are usually gently dipping and slightly convex-up within a single cross-bed set in landward direction (Bhattacharya et al., 2012). In tidal deposits, sometimes reactivation surfaces have a common spacing and are draped by mud within cross-strata because of variation in both the ebb and flood flow velocity.

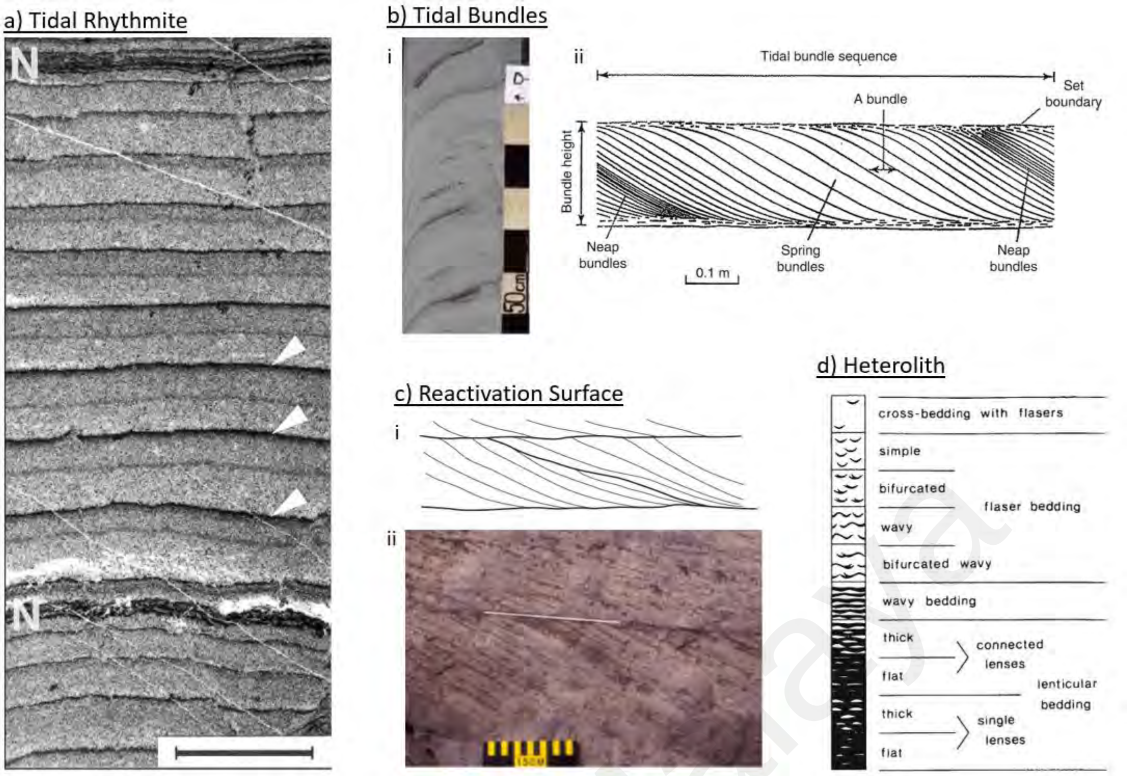

Figure 2.28: a) Tidal rhythmites of the Reynella Siltstone Member (Williams, 2004); b) i- Neap-spring tidal bundles from a tidal channel, Martens Plate, German Wadden Sea, ii- Diagram of the spring-neap cycles in tidal bundles (From Visser, 1980); c) i and ii both showing reactivation surfaces separating dune cross-beds; d) Illustration of the full spectrum of heterolithic stratification with different sand and mud proportions.

3- Bidirectional flow

Tidal deposits commonly display bipolar (two opposite flow direction) and bimodal (two main flow direction) patterns, representing the opposing ebb and flood tidal currents. These important features are not necessarily seen in all the tidal deposits due to the dominance of either the ebb or flood current in mutually evasive channels (Dalrymple & Choi, 2007). In certain cases, bipolar cross-stratification (herring-bone cross-stratification) may be observed in a single vertical section formed by alternating migration directions of ripples or dunes. This herring-bone cross-stratification is the product of frequent current reversals, which are commonly tidal in origin.

4- Desiccation and synaeresis cracks

Desiccation features are common in intertidal deposits. Subaerial exposure of less cohesive sediments during low tide results in desiccation, which leads to mud crack formation. Desiccation mud cracks tend to have a concave-upward cross-section. This crack does not strictly act as a tidal indicator, as they formed as the result of a cycle of dry and wet conditions. Desiccation features are also common in other settings with no influence of tidal currents. Desiccation cracks are often mistaken for synaeresis cracks and *vice versa*. Synaeresis cracks are attributed to sub-aqueous shrinkage of the deflocculation of clays caused by changes in salinity (Pratt, 1998). Syneresis cracks are not polygonal but are flat, smooth, or slightly curved tapering cracks, as opposed to desiccation cracks.

5- Ichnology

Tidal settings tend to develop in marginal marine environments at the intersection between fluvial and marine waters, thus salinity fluctuations and brackish water conditions are typical (Gingras & MacEachern, 2012; Gingras et al., 2012). Brackish water trace fossil assemblages are typically low diversity and composed of simple, small-sized marine taxa. The assemblage is usually a mixture of ichnotaxa taxa of the marine *Cruziana* and *Skolithos* ichnofacies (Bromley, 1996; Gingras et al., 2012) such as *Arenicolites, Chondrites, Conichnus, Gryolithes, Monocraterion, Ophiomorpha, Palaeophycus, Planolites, Scolicia, Skolithos, Teichichnus, Teredolites,* and *Thalassinoides*, and crypto-bioturbation. Monospecific assemblages are also characteristic of brackish water settings (Pemberton & Wightman, 1992; Buatois et al., 2005; MacEachern & Gingras, 2007). The trace fossil assemblage is not strictly indicative of tidal processes but indicates a stressed depositional environment.

2.6 Longitudinal Trends of Fluvio-Tidal Channels

The morphology and facies of fluvio-tidal channels change along its course due to changes in relative influence of fluvial and marine processes as well as changes in salinity. Fluvio-tidal channels may transition seaward from fluvial-dominated to tide-influenced, to tide-dominated (Dalrymple & Choi, 2007; Gugliotta et al., 2016). At the river mouth, they may form either tide-dominated estuaries or tide-dominated deltas, depending on whether the coastline is transgressive or regressive (Boyd et al., 2006).

Many works on the longitudinal profile of fluvio-tidal channels frequently use modern-day examples such as studies of sedimentology and stratigraphy in the Fly River Delta (Dalrymple et al., 2003), morphological and facies patterns in tide-dominated depositional environments through the fluvial-marine transition (Dalrymple & Choi, 2007), distributary channels in the fluvial to the tidal transition zone (Kästner et al., 2017), dimensions of fluvial-tidal meanders (Leuven et al., 2018), and geometry trends along the transition zone from fluvial to marine (Gugliotta & Saito, 2019) (Refer to Figure 2.7 in section 2.2.1.1 and figure 2.8 in section 2.2.1.2 of this Chapter, for illustration of fluvio-tidal channel transition in tide-dominated estuary and delta).

2.6.1 Fluvial-dominated zone

In the absence of waves and tides, only fluvial depositional processes are recorded in coastal settings. The facies will reflect fluvial sediment transport and deposition, i.e., unidirectional currents and episodic pulses of high energy sediment transport and rapid deposition during alluvial floods (Allen & Chambers, 1998).

The sedimentary structures formed by flood processes reflect high energy unidirectional flow of sediment transport, followed by rapid deposition from a decreasing current. Sedimentary structures which are typical of fluvial-dominated channel deposits include unidirectional cross stratification, traction and climbing ripples, upper flow regime parallel stratification, graded bedding, water escape structures, load casts and convolute bedding (Harms & Fahnestock, 1965; Allen, 1984; Langford & Bracken, 1987). Although some of these structures, such as cross- and parallel stratification can also be formed by tides and waves, the combined presence of all these structures in coastal deposits strongly suggests the presence of alluvial floods. Nevertheless, as the fluvial discharge decreases downstream, tidal processes will become more pronounced.

Nevertheless, the fluvial-dominated zone may experience weak modulation by tides. However, no tidal characters are formed. Some of the characters may mimic tidal features such as pseudo-reactivation surfaces formed by dune erosion or river stage fluctuations (Collinson, 1970; Jones & McCabe, 1980). Pseudo-tidal bundles of alternating coarse- and fine-grained laminae within cross-bed can also develop due to periodic arrival of ripples at the dune brink (de Boer et al., 1989; van den Berg et al., 2007). Mud drapes are likely to be thicker and amalgamated than mud-drapes in the tidal slackwater deposits. Inclined heterolithic deposits have also been reported, but they are not as common as in the tidal settings (Smith et al., 2009, 2011). Bioturbation may be absent or sparse in the fluvial-dominated zone.

2.6.2 Fluvial-Tidal Transitional Zone

The fluvial–tidal transition zone (FTTZ) begins upstream from the point of where the tidal current is at zero energy which is called the tidal limit. The downstream limit of this zone is very difficult to determine due to the relative influence of both fluvial and tidal currents (Dalrymple & Choi, 2007; van den Berg et al., 2007). The FTTZ is described as: '*that part of the river which lies between the landward limit of observable effects of tidally induced flow deceleration on fluvial cross-bedding at low river discharge, and the most seaward occurrence of a textural or structural fluvial signature at high river stage'* (from van den Berg et al., 2007). The fluid flow and sedimentary processes along the river continuum relate to each dominant process in the upstream (fluvial dominant) and downstream (tidal dominant) parts (Dalrymple & Choi, 2007; Torres, 2017; Sulaiman et al., 2021) (Fig 2.29). This transition zone is a mixed-energy region of fluvial and tidal processes where the conditions gradually change from fluvial-dominated with tide-influence until tide-dominated with fluvial-influence seaward (Ainsworth et al., 2011). The FTTZ is commonly discussed in terms of transgressive estuarine settings along embayed shorelines but is also present in delta distributaries (e.g., Ainsworth et al., 2008, 2011; Gugliotta et al., 2016).

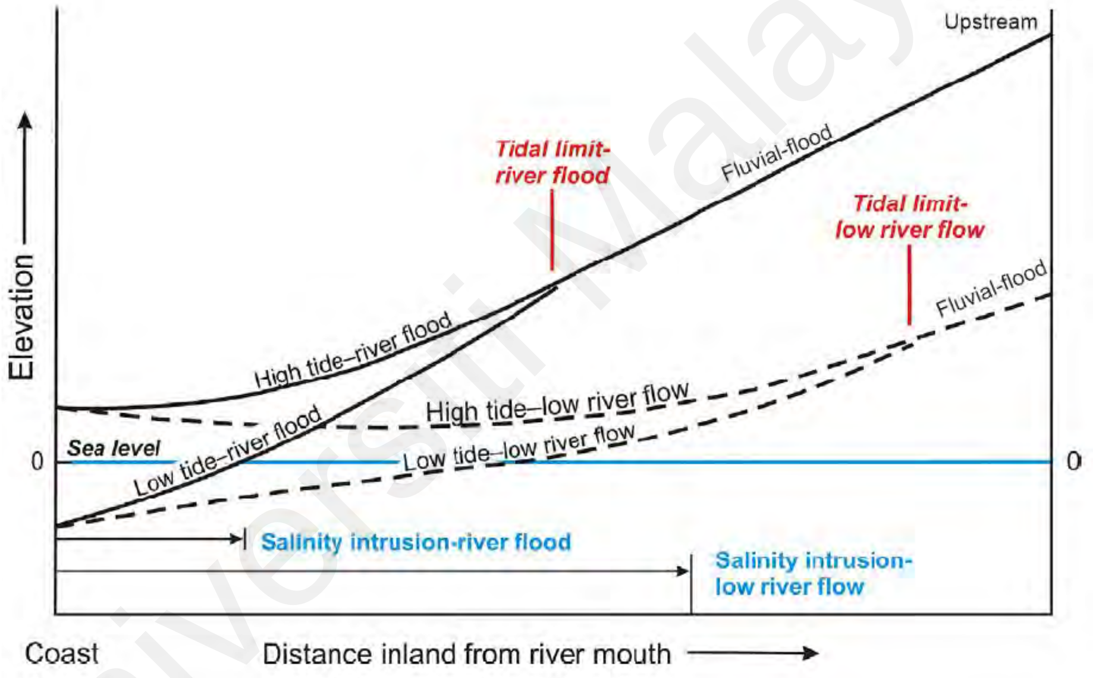

Figure 2.29: Diagram showing the entire range of depositional conditions along a fluvial-tidal channel, from fluvial-dominated to tide-dominated seaward (Dalrymple et al., 2015).

The FTTZ is similar to the ‘fluvial to marine transition zone’ (FMTZ) described by Gugliotta et al. (2016), which is characterised by concurrent occurrence of marine and fluvial processes (Dalrymple & Choi, 2007; van den Berg et al., 2007; Dashtgard et al., 2012; Freitas et al., 2012; Dashtgard & La Croix, 2015; Torres, 2017). The FTTZ may be located at number of locations within deltaic distributary systems (e.g., Kastner et al., 2017; Hoitink et al., 2017; Sassi et al., 2012) or within single-thread rivers (e.g., Torres, 2017; Sulaiman et al., 2021). In the FMTZ, deposition is governed by the interplay of physical (river, tides and waves), chemical (salinity) and biological (bioturbation) processes (Dalrymple & Choi, 2007; Jablonski & Dalrymple, 2016; Torres, 2017). However, to avoid misunderstanding of various marine processes and for consistency, I will use the term FTTZ in my study.

Fluvial currents decrease in strength downstream (seaward), whereas tidal currents and tidal range increase upstream (landward) up to an area denoted as the 'tidal maximum' (Dalrymple & Choi, 2007). Beyond the tidal maximum, bottom friction and superposition of river currents cause tidal currents at the tidal limit to be reduced to zero (Godin, 1999; Dalrymple & Choi, 2007). Tidal effects vary along the channel as upstream erosion, tidal frequency, and amplification and storm surges fluctuate with time (Wright et al., 1973; Dalrymple & Choi, 2007). For example, seasonal variations, including storms, control the fluvial flow and discharge and will, therefore, affect the downstream flow, in which the fluvial flow dominates over tidal currents (Dalrymple & Choi, 2007). The extent of the fluvial-tidal transition zone upstream will differ due to the topography gradient of the channel system and tidal penetration range (Dalrymple, 2010; Torres, 2017).

Tidal current encroachment extends further landward on a low gradient coastal plan (Savenije, 2012) compared to small channels with steeper gradients. The longest distance of tidal penetration into a modern-day river is in the Amazon River which shows tidal influence up to 800 km upstream (Dalrymple, 2015). Tidal influence has also been observed up to hundreds of kilometres in medium-sized rivers associated with a low gradient coastal setting (e.g., van den Berg et al., 2007; Savenije, 2012; Dalrymple et al., 2015; Torres, 2017).

Based on a recent analysis of five tide-dominated modern river deltas in the fluvial to marine transition region, Gugliotta & Saito (2019) observed that upstream, and downstream variations in sinuosity, channel width, and depth are interrelated. Upstream tract channel morphologies are controlled by the fluvial dynamics with little influence of tidal dynamics and show high sinuosity with consistent channel width, with increasing channel depth seaward. In contrast, downstream tract channel morphologies are controlled by tidal dynamics, with the subordinate influence of fluvial dynamics, seaward-increasing channel width, significantly broader river mouths, and low sinuosity and shallower depths.

The classification of FTTZ deposits requires the recognition of the sedimentary facies assemblages that record the presence of both fluvial and tidal current processes. Because of the fluctuation and the relative balance of tidal and fluvial currents, variation in the distribution of the sedimentary facies is expected. The vertical facies succession of FTTZ deposits may or may not consist of tidally influenced facies (van den Berg, 2007; Dalrymple et al., 2015) (Fig 2.29). Therefore, it is crucial to recognise even subtle tidal influence in fluvial deposits to limit the error in paleogeographic reconstructions (Van den Berg et al., 2007). Distribution of sedimentary facies in this zone is related to the type of channel morphological elements present and the fluvial-tidal hydrodynamics (Gugliotta et al., 2017, 2018, 2019). Such research indicates significant differences in sedimentary deposits in the upstream and downstream tract of the fluvial-tidal transitional zone. Upstream tracts, which are mainly controlled by fluvial processes, are dominantly composed of fine- to medium-grained sand and fine-grained sand-mud heteroliths. The downstream tract, which is mainly controlled by tidal processes, dominantly contains fine grained sand-mud heteroliths with slightly coarser reworked sediments. Due to the interaction between fluvial-tidal processes in the downstream tract, the distribution of sand-dominated and mud-dominated rhythmites may vary (Gugliotta et al., 2018, 2019). The variations in fluvial and tidal interactions thus largely reflects the region of morphological change and are consistent throughout the year (Gugliotta et al., 2017, 2018, 2019).

Morphologically, the channel sinuosity tends to develop a straight-meandering-straight seaward trend. However, sinuosity decreases seaward in deltaic systems. Common features of deposits in this zone include abundant inclined heterolithic strata which increase in abundance seaward, a wide range of grain sizes due to the seasonal changes, with coarser sediments supplied by the fluvial currents and finer sediments transported landward by tidal currents. Sediment grain sizes transported by fluvial currents become finer seaward. Tidal rhythmites may also develop, and in this zone, they are well-developed within fine-grained deposits during low fluvial flow periods. Additionally, heterolithic deposits (flaser, wavy, and lenticular bedding) are found in the upper section of the inclined heterolithic strata. Cross-beds and herring-bone cross-beds are also possible in this zone, while reactivation surfaces are more common further seaward. Individual thin mud-drapes may occur within cross-beds, especially in low river stage period deposits. In estuarine settings, slackwater mud drapes usually show a greater silt fraction (van den Berg et al., 2007). Overall, bioturbation in this zone is minimal and dominated by fresh-water ichnofacies.

2.6.3 Tide-dominated zone

The downstream tract becomes increasingly governed by tidal currents and processes towards the river mouth (Dalrymple & Choi, 2007; van den Berg et al., 2007; Gugliotta et al., 2016, 2019). This zone may include distributary channels and mouths up to delta front and prodelta, middle and outer parts of estuaries and tide-dominated shelves.

In an active distributary channel, the tide-dominated zone experiences both substantially significant fluvial flow and strong tidal currents. The net sediment transport direction is seaward, since these channels are the route by which sediment is exported to the distributary mouth bars (Dalrymple & Choi, 2007; van den Berg et al., 2007; Lentsch et al., 2018; Nienhuis et al., 2018). Morphologically, channel sinuosity decreases in a seaward direction and is relatively straight across this zone. Sediment sizes transported by fluvial becomes finer seaward. Paleocurrent patterns may be unidirectional at any spot. However, ebb-dominant bidirectional patterns comprising oppositely oriented cross-bedding may also be observed in other parts of the channel (Dalrymple & Choi, 2007; van den Berg et al., 2007; Dashtgard et al., 2012; Gugliotta et al., 2016). Other features of tidal processes such as reactivation surfaces, tidal bundles, and heterolithic strata are abundant in this zone. Tidal rhythmites should be developed in this zone. However, tidal cyclicity may not be completely recorded due to spring tide erosion. Other than that, mud drapes should be well developed. Single-tide mud drapes should be thicker here because of the high suspended sediment concentrations. Fluid-mud deposits (more than 0.5–1 cm thick single-tide mud drapes) may occur here, and channel-bar successions may show an overall coarsening upward trend because fluid mud would preferably be developed at the bottom of the channel (Ichaso & Dalrymple, 2009; MacKay & Dalrymple, 2011). However, channel successions still tend to fine upward. Intra-formational mud-pebble conglomerates, composed of clasts ripped up from the fluid mud layers, may accumulate at the base of channels. An upward fining overbank/tidal flat succession overlies the channel bar succession. This zone has a high rate of sedimentation with high concentrations of suspended sediments and low salinity. The degree of bioturbation would be low in this zone because the trace fossils will be scarce, low in diversity, small in size due to brackish waters (MacEachern & Bann, 2008; Gingras & MacEachern, 2012; Gingras et al., 2012). However, intensely bioturbated intervals can develop due to seasonal fluctuations in river discharge.

Active bidirectional flow of ebb and flood currents produces a series of straight tidal channels disconnected by elongated bars which lie further seaward. Deposited mud may be re-suspended in this exposed area, except for mud deposited in protected spots or during seasonally low tide. Thus, the zone is characterized by the sandiest deposits on the delta (cf. Dalrymple et al., 2003).

In various documentation, 'tidal bar 'is broadly used to describe all sorts of tide-influenced bars, including mid-channel bars, elongated bars and point bars. Tidal bars can be fining upward channel-fill deposits overlaying a sharp erosional base and coarsening upward succession overlaying prodelta mudstones. The type of tidal bars would be strongly influenced by longitudinal changes in channel curvature and width. Type of tidal bars include bank-attached point bars (landward part in a narrower and sinuous channel, (see Barwis, 1978), and elongate tidal bars/ mid-channel bars (seaward part where channel is relatively straight and wider. These bars appear to migrate laterally (i.e., oblique to the overcoming tides; Houbolt, 1968; Harris, 1988; Dalrymple & Zaitlin, 1994; Dalrymple et al., 2003). Lateral migration of these bars follows channel's lateral migration as the deposition take place inside the channel bend, and the oblique position of elongated bars to the predominant currents causing the deposition (lee-side) and erosion (stoss-side, stronger current) occur concurrently. Movement of the current parallel to the bars produce lateral accretion deposits (Dalrymple & Choi, 2007). Basal of the lateral accretion deposits is erosive due to due to the migration of the thalweg to the adjacent channel, and typically thinning and fining upward (Dalrymple & Choi, 2007). Hence, to avoid misunderstanding, the deposits of all tidal bars term as channel bars in this thesis to refer to laterally migrating, within channel barforms including bank-attached point bars and lateral bars as well as bank detached tidal bars, overlying sharp-based erosional surface. Whilst mouth bar is referred to coarsening upward tidal bars.

The delta front and prodelta area seaward of the distributary channels and bars generally preserve a coarsening upward succession of heterolithic interlayering of fine-grained sand and mud deposits, or laminated to bioturbated muds (Harris et al., 1993; Goodbred & Saito, 2012). Dune cross-bedding would develop in the medium grained size sands, together with associated reactivation surfaces that formed due to current reversals and abundant mud-drapes. Paleocurrents in this area should be bidirectional, although it may be unidirectional in some areas due to the nature of the residual transport route. Generally, bioturbation in this area is low. However, the diversity of traces is higher than in the distributary channels due to higher salinity and stronger tidal currents. Further offshore of prodelta area, mud layers are not bioturbated attributed to the rapid accumulation of suspension/fluid mud deposition (Dalrymple et al., 2003). Tidal signatures may not be well-preserved due to tidal currents not well-developed at this far offshore.

2.6.4 Case study of facies trends in fluvio-tidal channels

Amir Hassan et al. (2013, 2017) presented a study of Miocene tide-influenced deltaic deposits of the Tinjar and Balingian Provinces of Sarawak, Malaysia. The deposits include channel fill deposits displaying variations in the facies composition and ichnology, indicating different degrees of fluvial and tidal influence. Up to 30 m thick, multistorey fluvio – tidal channel facies successions were observed in these deposits and interpreted as representing vertical transitions from fluvial-dominated into tide-influenced and tide-dominated channel fill deposits (Fig 2.30). In some areas where the fluvio-tidal channel facies are not considerably thick, it is represented only by single-storey channel fill deposits. Variations of the fluvio-tidal channel facies successions may reflect longitudinal differences in fluvial and tidal energy along the channel belt continuum. Proximally (landward), channel successions are dominated by fluvial-dominated channel deposits, whereas tide-influenced or tide-dominated channel deposits were more common distally (seaward). The single-storey channels were likely located away from the channel belt axis.

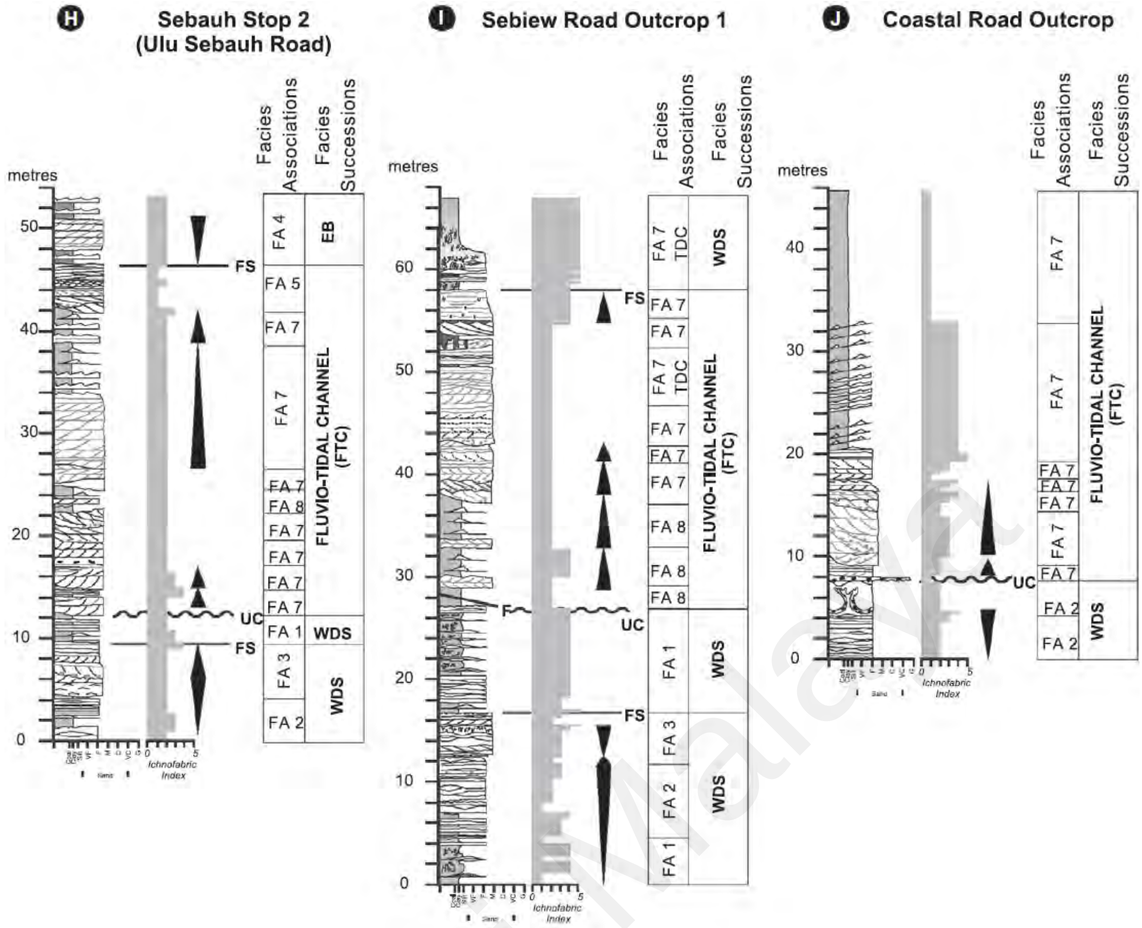

Figure 2.30: Sedimentary logs of Nyalau Formation showing multistorey fluvio-tidal channel facies successions and wave-dominated shoreface facies succession. These study areas were interpreted as a mixed wave and tide-influenced estuary (From Amir Hassan et al., 2013). Abbreviations: WDS = wave-dominated shoreface facies succession; FTC = fluvio-tidal channel facies succession; EB = estuarine bay facies succession.

2.7 Control Mechanisms

2.7.1 Controls on channel variability and evolution

Various factors control vertical and lateral changes in channel architecture, style, and size. Schumm (2005) classifies the controls into three categories (Fig. 2.31): 1) upstream controls of climate, tectonics, sediment types; 2) local internal controls, either fixed or variable, and 3) downstream controls of channel length and base-level variations. Previously, researchers related the evolution of stratigraphic units mainly to external (allogenic) forcing such as sea-level, climate, and tectonic controls. Recently, there is a focus on the internal (autogenic) mechanisms driving the evolution of fluvial stratigraphy (e.g., Hajek & Straub, 2017; Feng et al., 2019).

Paralic depositional systems respond to both allocyclic (sea-level/ base-level, climate, and tectonism) and autocyclic processes (channel avulsion). However, differentiating autogenic and allogenic signatures in the fluvial rock record is complicated (Hampson et al., 2012). Allogenic forcing results in relatively large-scale changes, especially if they are frequent or cyclic. In contrast, autogenic dynamics result in an un-mannered depositional pattern operating on shorter time spans, smaller-scale variations, and un-correlatable deposition. However, the result of physical and numerical experiments by Hajek & Straub (2017) demonstrate autogenic dynamics can be of substantial - scale and systematic. Even so, there are still many unanswered questions with regards to the equilibrium between autogenic and allogenic processes.

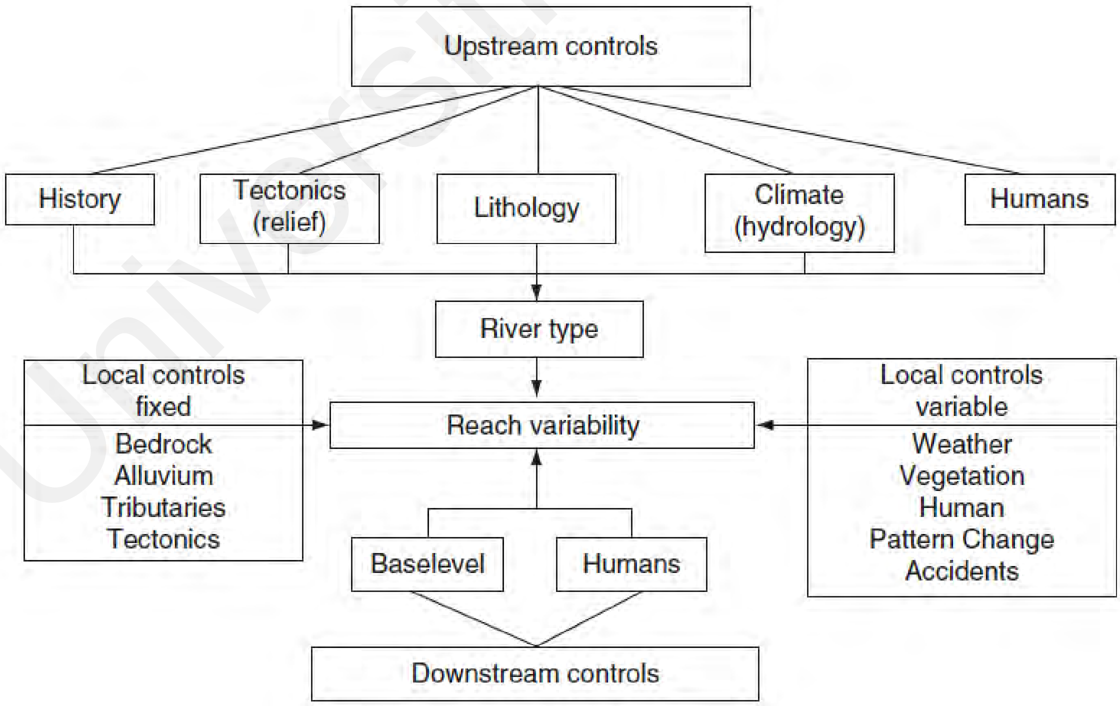

Figure 2.31: Chart showing various controls of river morphology and behaviour (after Piégay & Schumm, 2003).

2.7.1.1 Autogenic dynamics

Internal or autogenic sediment-transport dynamics may lead to depositional patterns similar to changes in climatic, tectonic, or sea-level variations. It is very challenging to accurately interpret the ancient sedimentary stratigraphy of tide-dominated/influenced deltas as autogenic control is reflected by variation of scales and types of deposits. Additionally, the variation of allogenic factors and topography gradient dampened the autogenic processes from modern and ancient records.

Hajek & Straub (2017) highlighted the role of topography in influencing autogenic processes. Sediment is transported from upstream to downstream as a natural consequence of the topographic gradient. The volume of sediments transported downstream is controlled by climate, which affects erosion and water volume to transport the sediments (e.g., Dixon et al., 2009; Perron, 2017); climate often affects vegetation and land cover, which affect weathering substantially (e.g., Chen et al., 2000). The Earth's topography can be imagined as a conveyor belt for the transport of material available in highlands through terrestrial and marine environments before ultimately reaching the ocean (Hajek & Straub, 2017). Water and sediment transported within this route are contained within a network of channels. Higher volume of water and sediment discharge leads to inherent instability and can be topographically positioned as the river channels continue to accrete laterally and downstream. Eventually, fluvial systems or channel networks include those on the floodplain, will migrate, relocate, or avulse to a more suitable lower area in the basin (e.g., Törnqvist & Bridge, 2002; Slingerland & Smith, 2004; Hajek & Straub, 2017). The cycle will repeat as a new channel is developed. The autogenic processes that occur randomly in a sediment transport network result in channel avulsion and channel migration.

It is also essential to highlight the scenario called 'signal shredding' introduced by Jerolmack & Paola (2010), where autogenic processes, such as channel migration and switching, delta-lobe switching, channel avulsion, may possibly eradicate all indication of low degree, high-frequency climate or tectonic fluctuations from the sedimentary record. This signal shredding process behaves like morphodynamics turbulence, in that a force applied at the upstream is smeared longitudinally along the channel down to downstream area (Jerolmack & Paola, 2010; Wang et al., 2011; Ganti et al., 2014; Lazarus et al., 2019). Therefore, it is assumed that autogenic dynamics control stratigraphic patterns over small spatial and temporal scales, whereas allogenic processes will govern larger scale stratigraphic patterns. However, both of these processes rely on their particular behaviour, where allogenic processes influence the autogenic processes (Jerolmack & Paola, 2010; Wang et al., 2011; Ganti et al., 2014; Hajek & Straub, 2017).

Miall (2014) discussed in detail the autogenic processes controlling avulsion and architectural elements of fluvial systems. He reviewed both classic and current opinions and interpretations of autogenic processes, their product, and their impact on sandbody connectivity. The extensive upward fining pattern of fluvial systems and the upward coarsening of deltas are characteristic of the autogenic depositional process (Hajek & Straub, 2017). Although autogenic processes occur at a shorter time scale, the fining upward deposits produced during an autogenic phase are also documented in the stratigraphic structure established by an allogenic process (Hamilton et al., 2013; Miall et al., 2014).

Another highlighted concept is what is termed the 'backwater' effect of non-uniform hydrodynamic flow conditions as defined by Paola & Mohrig (1996); Chatanantavet et al. (2012), and Nittrouer et al. (2012). This effect may influence the fluvial architecture temporally and spatially, without a change in base-level (Fig. 2.32). The impact of the backwater in low gradient river systems can stretch up to 100's km upstream (Nittrouer et al., 2012). Such effects occur when a river approaches a standing body of water, e.g., the sea. The cross-sectional flow area increases as the river flow reach the sea as the water surface profile asymptotically approaches mean sea-level. During low water discharge, the flow decelerates toward the river mouth leading to net deposition; and during floods, the flow accelerates toward the river mouth resulting in net erosion (Lane, 1957; Lamb et al., 2012; Nittrouer et al., 2012). Net sedimentation in the backwater zone can result in the preferential location of channel avulsions near the onset of backwater (Jerolmack & Swenson, 2007; Chatanantavet et al., 2012; Ganti et al., 2016a, b). Backwater effects can dynamically control the degree of channel migration avulsion, bifurcation, and switching on the delta plain, such as observed in the Mississippi delta (Nittrouer et al., 2012) where the backwater length could be extended up to 600 km upstream, thus resulting in internal controls of channel architecture without external forcing (Blum et al., 2013).

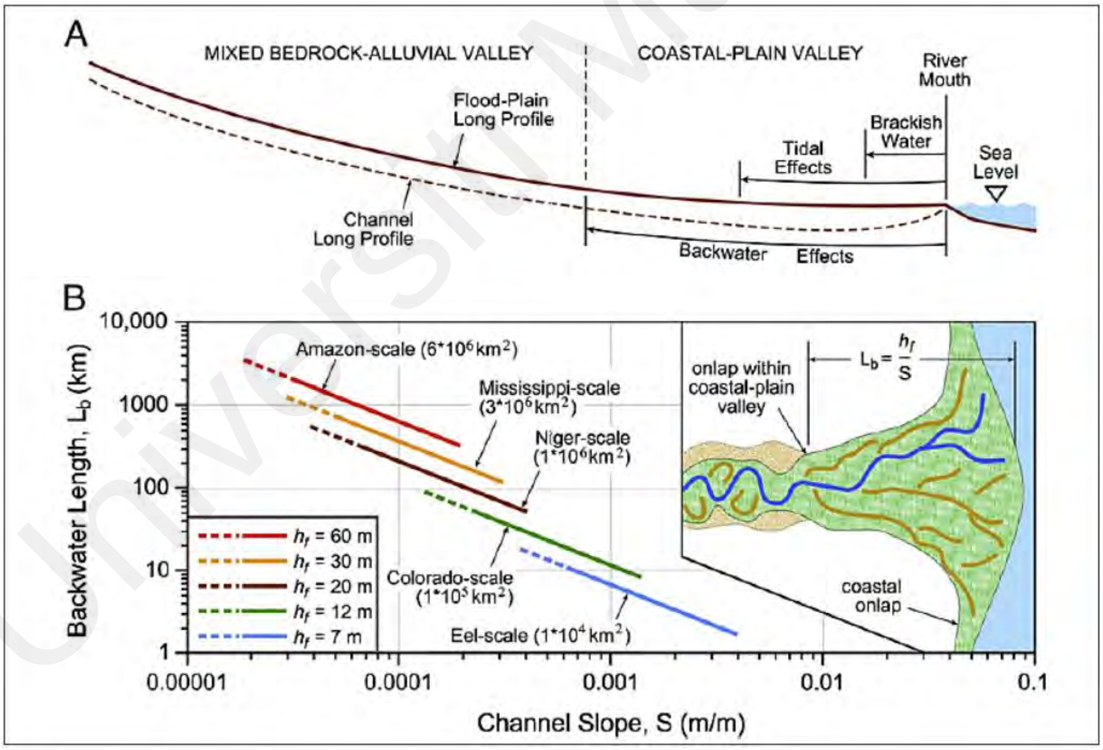

Figure 2.32: A) Backwater length theory controls downstream propagation upstream. B) The plan-view of delta shows the interactions of backwater length with channel and floodplain area. (After Blum et al., 2013).

2.7.1.2 Allogenic

Three major external controls on sedimentation and geomorphology in fluvio-tidal systems include climate change, tectonic events, and sea-level change. Upstream controls comprise tectonism and climate, while downstream control is mainly sea-level change. Climate controls flood and vegetation land shelter and has a significant impact on the supply rate of sediments (Hall & Nichols, 2002). The topography gradient and the source area relief are influenced by tectonism and also play a significant role in the regulation of sediment load volume and rate.

Figure 2.33 illustrates a conceptual scheme by Shanley & McCabe (1994), which explains qualitatively how the transition of fluvial systems from the river mouth to the source is governed by allogenic control. It also shows how buttresses and buffer principles explain longitudinal alterations in fluvial facies and upstream architecture from Holbrook et al. (2006). Buttress refers to the fixed point of ultimate base-level, located down-dip of the river. It forms a barrier that anchors the sediment profile, where rivers cannot significantly incise below it and cannot significantly build above it, which anchors sediment profile. The buffer zone refers to the upstream longitudinal river profile. The river can change due to downstream buttress fluctuations. In this model, upstream controls such as tectonism or climate change that govern the discharge and sediment load of the river mainly influenced downstream channel deposits and geomorphologies. The buffer profiles are converged to the buttress and typically accommodate multi-storey channel belts within valley sizes where they are dense, but only single-storey channel loops are narrow. All profiles must converge towards the position of buttress, and the change in the buttress must be followed by aggradation and erosion.

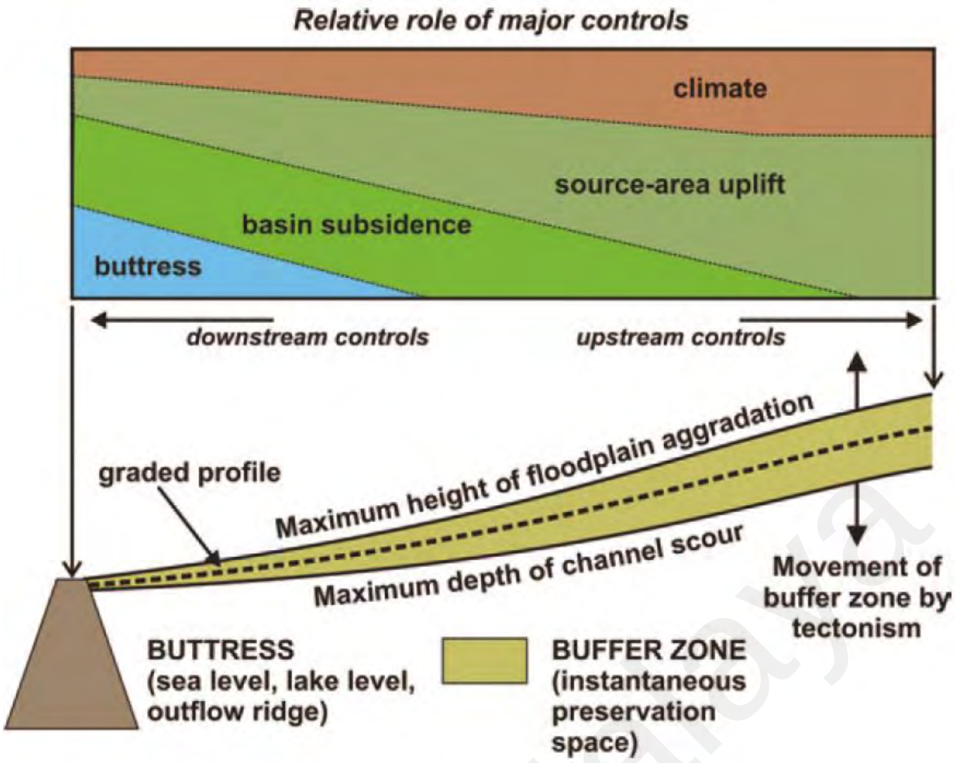

Figure 2.33: Schematic diagram of upstream and downstream controls of river longitudinal profile. Upstream depositional controls are from Shanley & McCabe (1994), and buttress and buffer concepts are from Holbrook et al. (2006).

2.7.2 Hydrodynamic controls on channel dimension

There does not seem to be any apparent link between the depositional area to the geometries of the channel in a tidal channel network (Marani et al., 2002, 2003). The cause for channel geometries resides in several factors that influence tidal channel development, which is driven by hydrodynamic factors and/or physical environmental controls. Hydrodynamic effects on channel development include the combination of tidal and fluvial currents. The tidal currents inside a channel can be either driven by external or local forces such as offshore tides or can be simply a reaction of local morphology. Therefore, their interplay is dynamic and complex (Marani et al., 2002; 2003). As such, the size and shape of the channel are related to the ratio of the tidal prism through the channel. Their dimensions not only rely on the basin scale and tidal range, but local morphology on the floodplain also offers the alternate pathway from the progressing tidal current (Marani et al., 2003).

Additional aspects that affect hydrodynamics are the elevation where the runoff takes place (from very rapid, regional changes in the tide range in connection with a transition in floodplain topography and vegetation), the domination of the accelerations of flood or ebb tidal currents, and the channel curvature which reflects the width-to-depth ratio (Fagherazzi & Mariotti, 2012; Hughes, 2012). Paleogeography, sediment deposition trends and grain size, existence, and the type of vegetation are essential physical factors for the development of the channels. Bed stratification, tides and sediment density, wind waves, and wind-induced currents, and drainage processes are the mechanisms for sediment transport (Eisma, 1998; Le Hir et al., 2000; Friedrichs, 2011).

Lateral mechanisms consist of increasing channel width through bank erosion and headward erosion, which affects variation of sedimentation in channel migration and the intensity of meandering (D'Alpaos et al., 2005), which can lead to channel avulsions and bifurcations (Hughes, 2012). The vertical mechanisms include downstream accretion throughout erosion and sediment compaction due to the rise of base-level (Hughes, 2012).

2.8 Seismic Geomorphology

There have recently been many advances in the sedimentological analysis of subsurface 3D seismic datasets, and a number of regional studies have been published in recent years. The foundation of seismic geomorphology, which is the analysis of landforms and processes of deposition from seismic information, was laid by Posamentier et al. (2007). For this purpose, horizontal seismic datasets (i.e., plan-view) are essential.

Improvements in 3D seismic software and technology for visualisation have also made it possible to clearly image depositional elements at different scales and in various depositional environments. Great progress has been made on this topic in deep-marine (e.g., Posamentier & Kolla, 2003; Hadler-Jacobsen et al., 2007; Omosanya et al., 2019) and coastal plain settings (e.g., Posamentier, 2001; Miall, 2002; Darmadi et al., 2007;

Alqahtani et al., 2015; Heldreich et al., 2017). This provides a new perspective into channel architecture and valuable qualitative and quantitative data from the subsurface reservoirs. Such technologies and data will specifically contribute to a better understanding of fluvial-tidal channel systems and thus have significant implications for the understanding of paralic environments.

A three-dimensional (3D) approach of seismic analysis allows horizontal sections to be rendered by volume of data at any selected interval. Such segments can also be drawn along user-defined stratigraphic surfaces (known as stratal slices), which thus gives an opportunity to take into account the structural dipping, drape, and stratal orientations. These images are potentially much more beneficial than the conventional vertical section to analyse depositional processes. However, the main issue related to the vertical section is seismic resolution, i.e., the ability to resolve thin beds (classically, as 1/4 of the seismic wavelength). Integrating seismic data with borehole data, including wireline logs and core data, where accessible, is vital to better understand and interpret the depositional system. Variability of lithology is strongly supported by wireline logs and core data, in particular where vertical seismic resolution is poor and for other associated calculations provides quantitative data. Zeng & Hentz (2004) have referred to this integrated method study as' seismic sedimentology'.

2.8.1 Applications of 3D Seismic Geomorphology

This section reviews several examples of 3D geomorphological 3D seismic analyses of channel systems. Brown (2011) established an approach to this type of analysis in its seventh edition. Ethridge & Schumm (2007) also listed several pioneer cases of seismic geomorphology interpretation.

Miall (2002) studied a sequence of time slices of Pleistocene fluvial systems in the northern area beneath the Malay Basin to evaluate fluvial types and architecture. Several forms of channels, including meandering, braided channels with low sinuosity, and incised valleys, have been identified (Fig 2.34). Remarkable features are clearly visible in the 196 ms image, including incised valleys and associated tributaries, a meandering system within a valley, and complex channels interplay of the fluvial system within this succession. Figure 2.35 illustrates the evolution of a meandering river based on five successive times slices from the East corner of the Miall (2002) dataset. Many other small channels, mainly of low sinuosity, are noticeable. Typically, several elements are visible in a couple of slices, which is caused by the prominent seismic data 'shadow' effects. He concluded that fluvial style changes are driven by accommodation space creation and destruction brought on by both fluctuations in relative sea-level and subsidence rate.

With sufficient seismic data and well control, the visualisation of incised valleys and other attributes may make a significant contribution in constructing a model of river or valley stratigraphic evolution. Maynard et al. (2010) provided a detailed illustration of the fill architecture of incisions from a Cretaceous heavy-oil field in Alberta. The stratigraphy of this data set was segmented based on known flooding surfaces, which were employed in the seismic-to-well data correlation. Based on core analysis and the well-and seismic evidence, facies were identified and classified, resulting in a detailed paleo-geographic model.

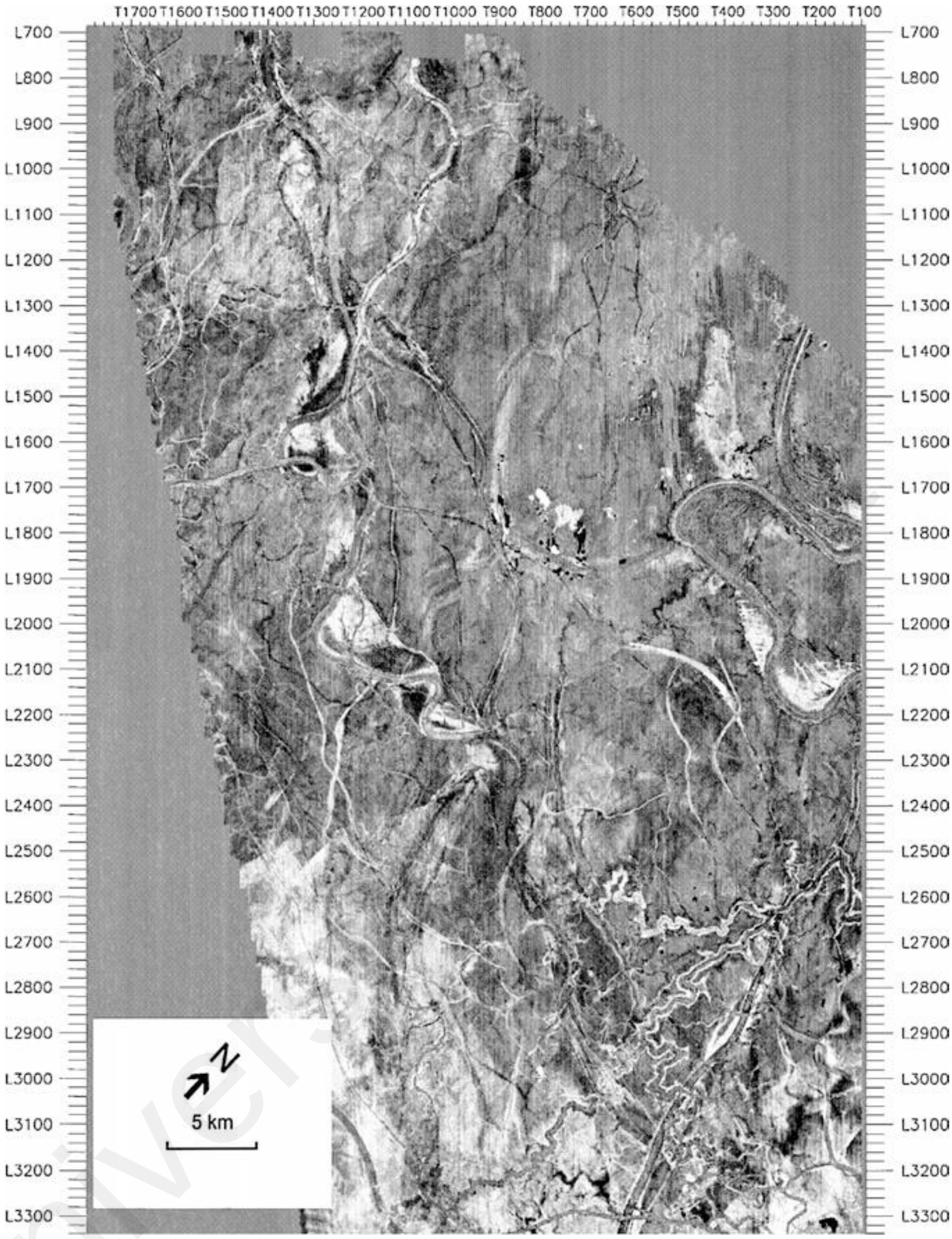

Figure 2.34: 196 ms time slice illustrating a broad range of fluvial systems in the Late Pleistocene of the Malay Basin (from Miall, 2002).

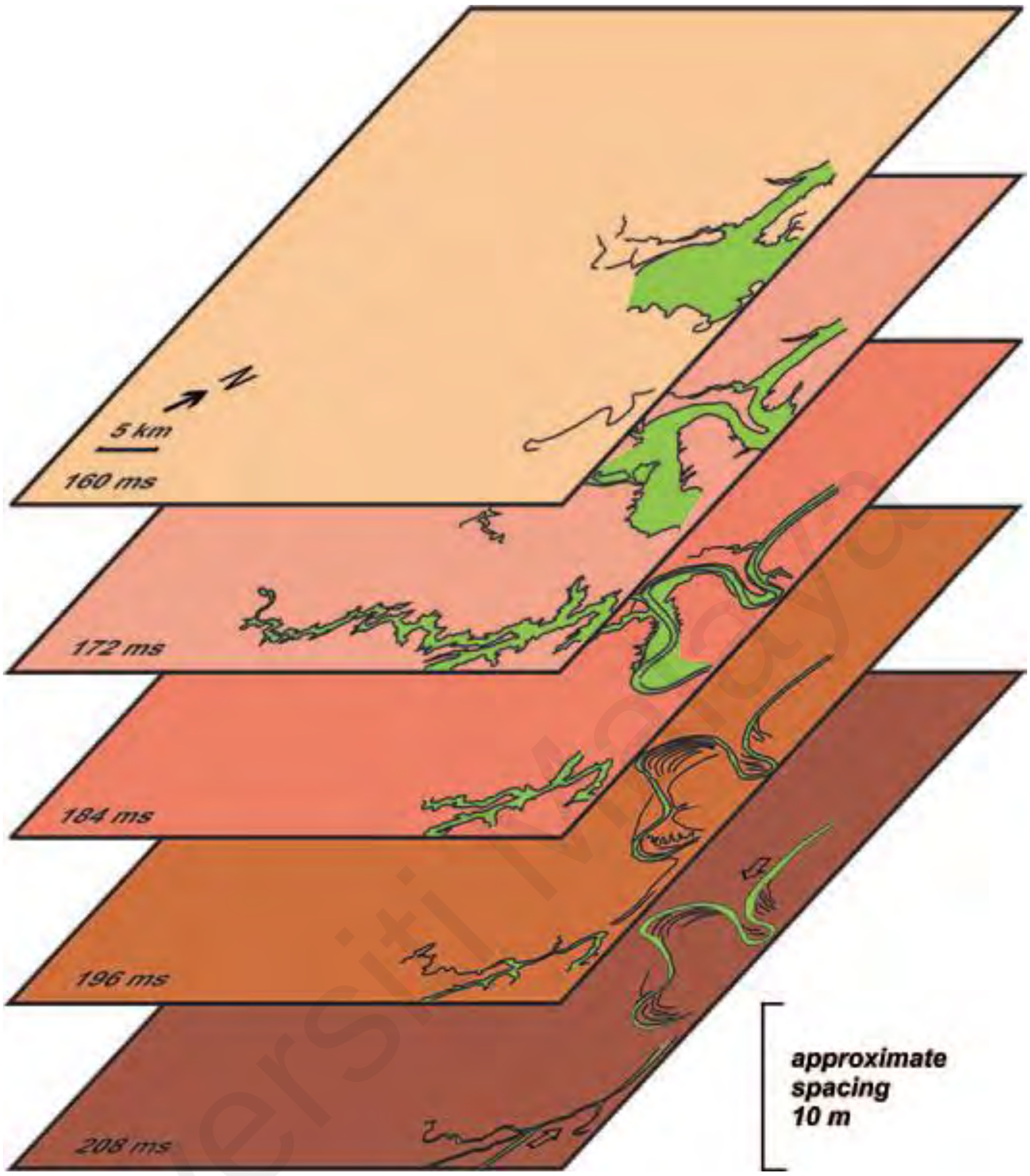

Figure 2.35: An overlay of five slices drawn to highlight the vertical sequence of channel geobody evolution in the Late Pleistocene of the Malay Basin. The main feature is a valley-fill, with a tributary draining into it from the South. Other fluvial architecture elements seem to change their morphology accordingly (From Miall, 2002).

A seismic geomorphological study of Pleistocene channels in the Malay Basin was carried out by Alqahtani et al. (2017). The study demonstrates an improved understanding of the variation in spatial and temporal of fluvial systems that may be assessed with detailed high-resolution 3D seismic data analysis (Fig 2.36). A combination of horizontal time-slices and iso-proportional slices was used to identify and map fluvial channels. Measurements of the geomorphological data were assisted by using a developed semiautomated workflow in ArcGIS software. He concluded that the rivers observed are part of a larger, through-going axial drainage system that connected the hinterland area of northern Thailand with the receiving basin in the South China Sea.

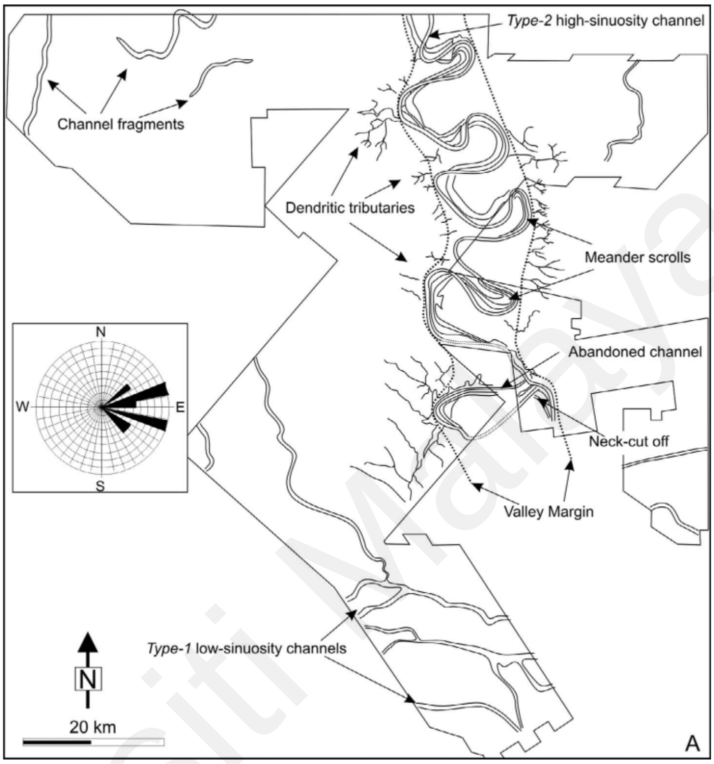

Figure 2.36: Example interpretive plan view map from Alqahtani et al. (2017). Such channels have been derived in Unit 7 from a combination of time and iso-proportional slices.

Heldreich et al. (2017) conducted a thorough analysis of the Triassic Mungaroo Formation in Northwest Shelf, Australia, and discussed the complexity and restriction of assumptions on reservoir architecture and the emergence of paralic depositional environments. This study utilises a dataset of 21 well logs and 10 000 km^2 of 3D seismic data. Twenty 40ms isoslices were analysed using multiple seismic attributes such as root mean square (RMS) energy, and spectral decomposition (Heldreich et al., 2013) to enhance the results of plan-view images. Channels can clearly be seen in the images (Fig 2.37). The study identified three scales of geobodies: 1) large-scale geobodies with >900 m wide channel-belt complexes; 2) medium-scale geobodies ranging from 400 – 900 m in width, which are interpreted as multi-storey channel belts, and 3) small-scale geobodies that are typically < 400 m wide and are likely to be single storey channel belts or distributary channels. A variety of factors was deduced to control the depositional environment's system within Mungaroo Formation. However, the most notable control is sea-level change.

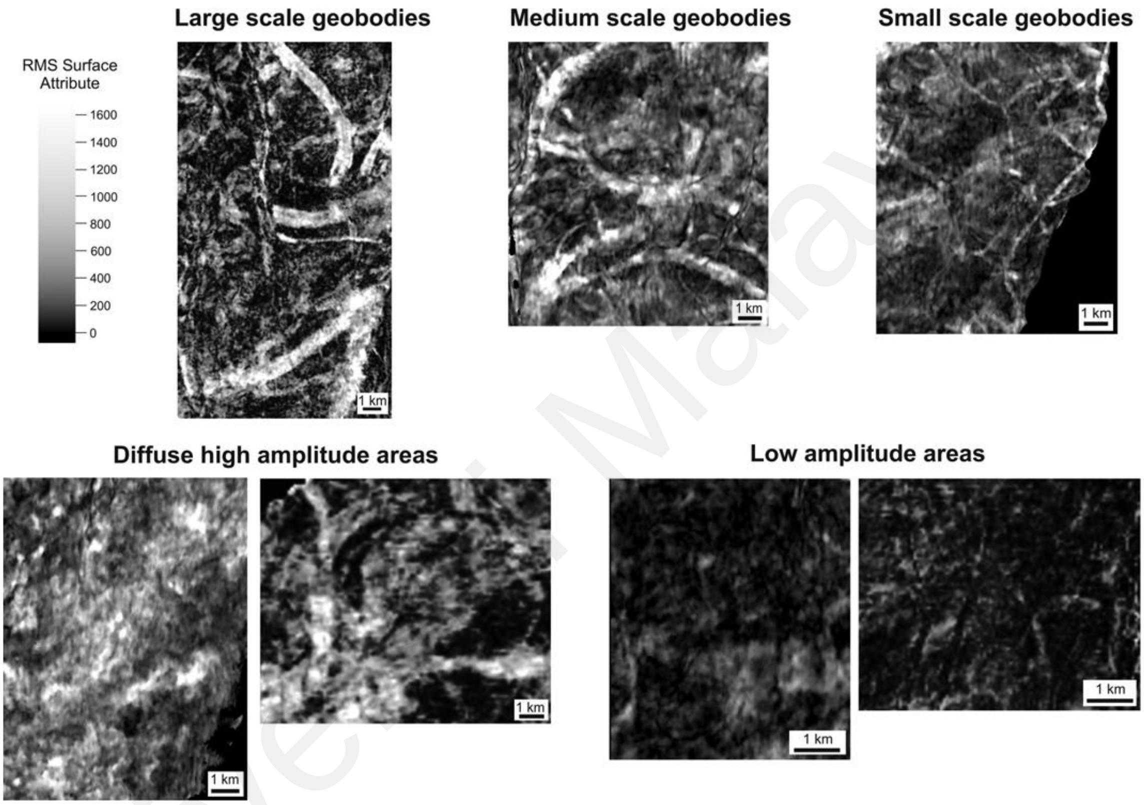

Figure 2.37: Seismic features detected from the study of seismic attributes. Large, medium and small geobodies reflect different scales of fluvial channel belts (Heldreich et al., 2017).

2.9 Hypothesis

I hypothesise that the knowledge of the depositional processes and fluvial developments on the modern day of fluvio-tidal channels can be utilised to explain the ancient channel systems seen in 3D seismic images. Images from the 3D seismic analysis in the deeper sections are the combination of more than 10 meters-thick interval depositional environment. Hence, accessible for a variable interpretation especially for channel geomorphology.

Understanding overall depositional environment in the marginal marine system is the essential facts in this study, because all these knowledges are interrelated for facies and channel geomorphology analysis. Data integration of cores, well logs, and 3D seismic used in this study are expected to resemble the marginal marine of fluvio-tidal depositional environment.

CHAPTER 3: DATASET AND METHODOLOGY

3.1 Dataset

This study uses high-quality 3D seismic data with an improved seismic resolution, integrated with well logs and core data, to analyse the channel geobody geometries of the late Early Miocene to Middle Miocene Group I and Group H of the Malay Basin (Fig 3.1). The study focuses on an area covering approximately 1563 km^2 (Fig 4.1) in the middle part of the Malay Basin, which encompasses the Jambu, Cendor and Laba Barat fields. The stratigraphic interval of study is bounded by two seismic reflection surfaces, i.e., the near bottom Group I to Near Top Group H. The main targets are a complex network of channel geobodies which are imaged on several horizons within this stratigraphic interval.

A seismic subset 3D cube was extracted from a 2015 'mega-merged' re-processed 3D pre-stack data. This re-processed data applied an updated broadband technology to enhance the signal-to-noise ratio and provide a solution for better images, especially in seismic attributes analysis. The seismic was calibrated with well data from Laba-Barat-1 and also integrated with data from 3 other wells (Cendor-2, Cendor-3A and Jambu-3), which include well logs and 83.15 m of conventional core (Table 3.1). The core and well logs were used to identify depositional facies and to understand the spatial and temporal distribution and evolution of geobody units within Group H and Group I of the Malay Basin. Few wells have been drilled within the 3D dataset. Two wells (Laba Barat-1 and Cendor-3A) provide the key controls where seismic, wireline log and core can be calibrated with confidence. However, only Cendor-3A has core data within the 3D seismic dataset. Thus, data integration must be made with caution by incorporating data from nearby reference wells (Jambu-3 and Cendor-2) (Fig 3.1c), obtained from confidential in-house well reports.

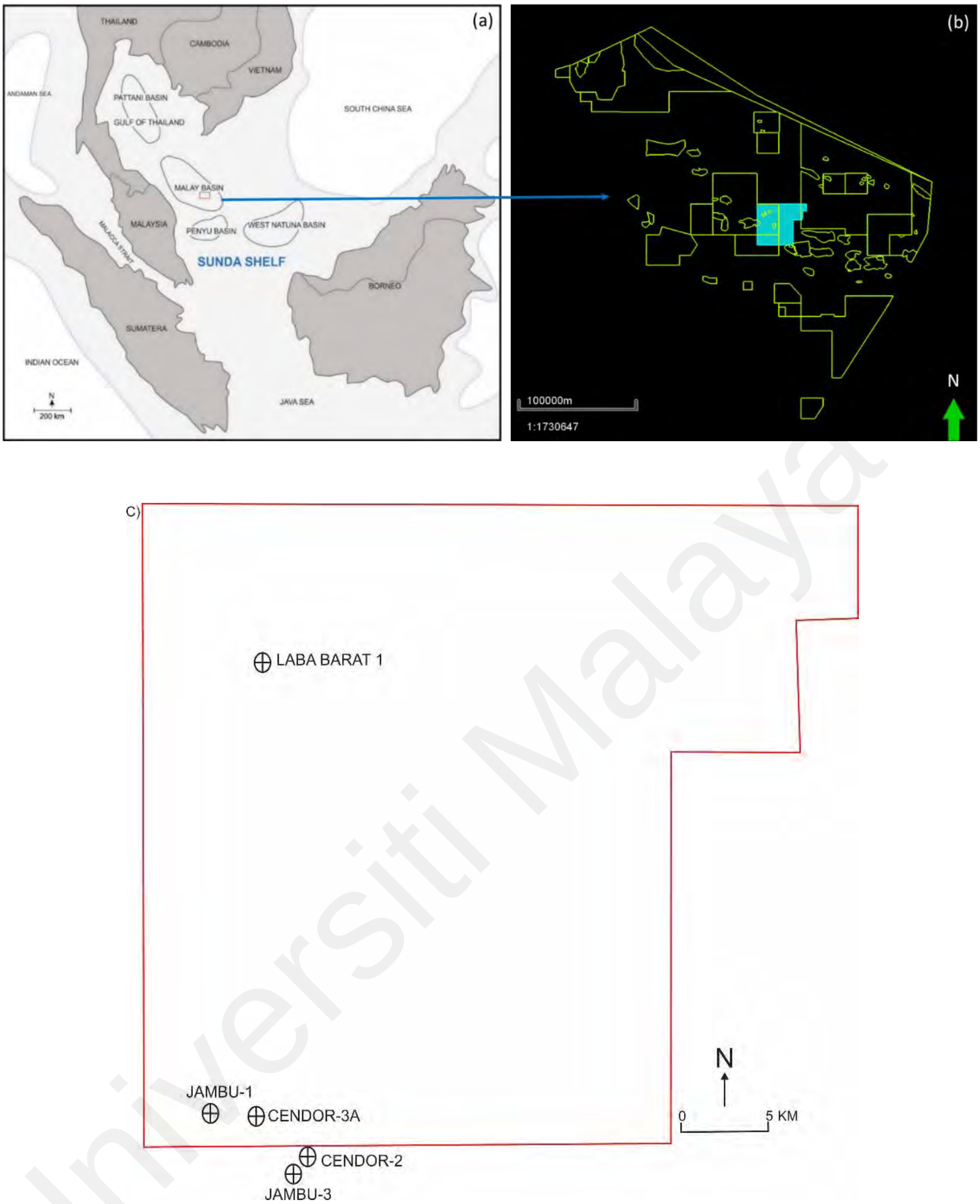

Figure 3.1: (a) Location of the study area within the Malay Basin (modified from Voris, 2000), (b) Blue box represents the study area in the of Malay Basin and green polygons are the oil and gas operating blocks in the Malay Basin, (c)Red-line polygon is an enlarged area from (b), which marks the boundary of the 3D seismic and well information available.

The target interval is located at depths of >1.5 km below the sea bottom. This makes stratigraphic and geomorphological interpretations very challenging due to increasing low seismic resolution at greater depths. Therefore, the study also uses core and well log data to interpret depositional facies and to quantify sandstone reservoir unit thicknesses. Hypothetically, the facies analysis will show that there was significant tidal influence in the Miocene Group I and H of the Malay Basin. The Miocene Group I and H of the Malay Basin most likely represent the deposits of a tide-influenced delta, with the channels being tide-dominated/influenced. Also, it should be possible to identify tidal geomorphological features associated with channel bodies buried in the deep subsurface from high quality 3D seismic.

3.1.1 Core data

Conventional cores from three wells were made available by PETRONAS for this study, which has a total thickness of 83.15 m (Table 3.1). The available core penetrates Miocene Group H, which is the interval of interest in this study. Cores from Cendor-2 and Cendor-3A wells were the best preserved and most continuous, with a total thickness of 75.15 m. Facies analysis of the cores was carried out at the PETRONAS Geo-Sample Centre core store, and detailed sedimentary logs were produced (see Chapter 4). The succession was divided into facies and facies associations based on lithology, texture, sedimentary structures, and degree of bioturbation. The facies analysis results were then used to interpret depositional processes, environments and calibrated with the geomorphological interpretations.

3.1.2 Well Logs

Only gamma-ray logs from Laba Barat-1 and Cendor-3A were available for well correlations from positions within the available 3D seismic cube. The other two wells are beyond the seismic boundary. Gamma-ray logs aid in the determination of the lithological composition of the channels. Before picking the seismic reflections on the 3D seismic data, sonic and density logs are used to create acoustic impedance profiles to model seismograms.

Table 3.1: List of the available dataset for this study. These cores are from the Early to Middle Miocene succession of Group H of the Malay Basin

Well	Composite logs					Core			Within Seismic 3D data
	GR	Neutron	Density	Sonic	Checkshot	Availability	Depth	Total length (m)	
Laba Barat-1	√	√	√	√	√	X	NA	NA	√
Jambu-3	√	√	√	√	√	√	1313 - 1321m	8.00	X
Cendor-2	√	√	√	√	√	√	1250 - 1298m	48.00	X
Cendor-3A	√	X	X	X	√	√	1402 - 1429 m	27.15	√

√	Available	X	Not Available

Conventional methods require transfer of the depth domain dataset into the time-domain before inversion because it would be inappropriate to assume the convolution model on the depth dataset. However, the conversion between time and depth may result in artefacts due to inaccurate velocity or insufficient time-depth conversion algorithm on the 3D data volume, which necessitates the application of inversion and wavelet extraction on the depth domain dataset.

Well log facies were established by correlation and calibration with core descriptions and confidential well reports (etc., biostratigraphy), allowing interpretation of possible sedimentary facies over intervals without core. Figure 3.2 illustrates the well correlation across the study area, grounded by the integration of vertical well log patterns with palynological records by Yakzan et al. (1996), as palynomorph distribution depends on local geographical factors, including depositional environment. Markers within Group I and H represent approximate regional "maximum flooding surfaces" and "flooding surfaces". Morley et al. (2021) termed these markers as "sequence boundaries" of transgressive-regressive series which are considered to signify times of maximum basinward shift of facies. Topmost of Group I is marked by the occurrence of *Globorotalia birnageae* and *Catapsydrax dissimilis,* whereas the bottommost of Group H is marked by the major planktonic zone N8 with the overlap of *P. Glomerosa* with *Globarotalia birnageae, Praeorbulina sinacus, and* nannofossils zone NN4 (Morley et al., 2021). Top of Group H is fingerprinted by the *Praeorbulina* glomerosa, *P. transitoria,* and nannofossil zone NN5). The interval of this study is within the PR9-PR10 palynomorph assemblages.

However, to avoid misunderstanding, markers used in this study are referred to here as representing MFS and FS, which is consistent with the geological marker terminology used in PETRONAS well reports for Laba Barat-1.

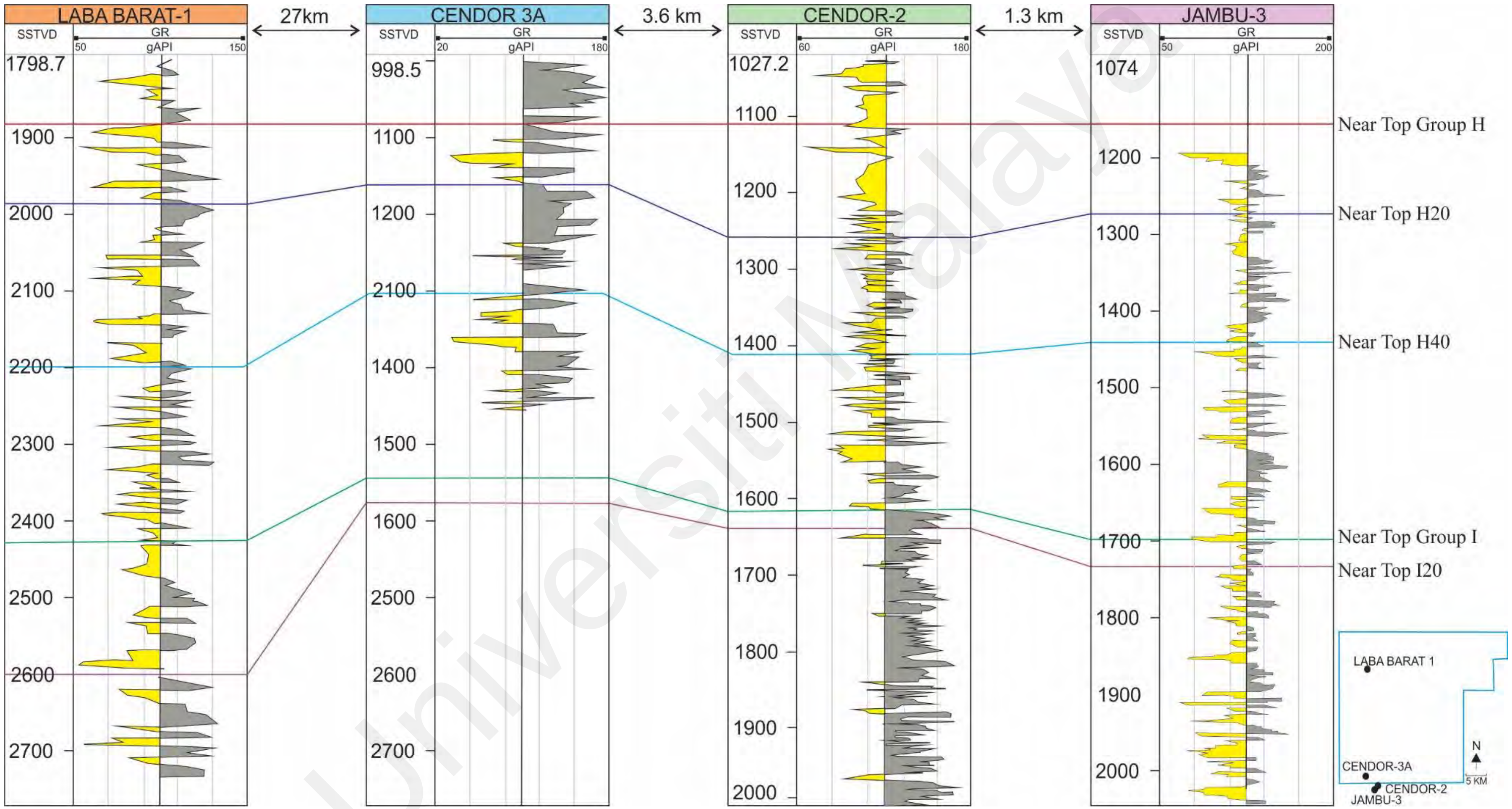

Figure 3.2: Well correlation across the study area. Two wells (Laba Barat-1, and Cendor-3A) are within the 3D seismic area, while the other two wells (Cendor-2 and Jambu-3) are beyond the seismic boundary. Depths are in metres true vertical depth subsea (TVDSS)

3.1.3 Seismis Resolution

The 3D seismic volume used in this study covers an area of approximately 1,563 km^2 (42 km wide by 38 km long). The volume available is a subset extracted from a "mega-merge" of 10 separate volumes which covers an area of 11,500 km^2 of the Malay Basin. The seismic is zero-phase processed and displayed so that a downward increase in acoustic impedance is represented by a positive event (black reflection), and a downward decrease in acoustic impedance is represented by a negative event (white reflection) (Brown, 2004). The spacing interval of both in-lines and cross-lines is 12.5 m, whereas the total two-way time of the vertical extent is 7682 milliseconds (ms TWT). The vertical sampling interval is 2 ms across the whole seismic data. Such seismic is time-migrated data, and data from only one well data (Laba Barat-1) was available for confident calibration of well to seismic to identify the interval of interest of the succession in the seismic window.

Seismic resolution decreases with depth within the interval of interest in Group H and Group I of the Malay Basin. Typically, seismic depth is measured in milliseconds (ms) by two-way journey times (TWT). The sound wave's frequency decreases with increasing depth, whereas the velocity and wavelength increase exponentially. Significantly, seismic data resolution becomes poorer with increasing depth. Theoretically, the measures of depth and thickness can be converted from milliseconds two-way time (ms TWT) to meters (m) by employing the recorded interval velocity within the particular interval of the interest succession, which for this study is derived from checkshot from well Laba Barat-1. Frequency, average interval velocity, and wavelength were derived from the Group H and Group I intervals of the seismic data in order to estimate the vertical and horizontal resolution of the study area (Table 3.2).

The average interval velocity in Group H is 3240 ms^{-1}, and in Group I it is 3320 ms^{-1}, whereas the dominant frequency within these intervals is 20 – 50 Hz. This gives an average range of minimum vertical resolution of approximately 16 m, and the lateral seismic resolution is 32 m (e.g., vertical resolution = λ/4; horizontal resolution = λ/2) (Sheriff & Geldart, 1983; Brown, 2004). These calculations allow assured identification of discrete small channel systems with a fair to high degree of precision.

Table 3.2: Resolution of seismic data within the interval of interest in Group H and Group I of the Malay Basin

Tops Marker	Velocity (ms^{-1})	Frequency (Hz)	Wavelength (λ)	Vertical Resolution (λ/4)	Horizontal Resolution (λ/2)
Group H	3240	20-50	65-162 m	16-41 m	32-81 m
Group I	3320	20-50	66-166 m	17-42 m	33-83 m

3.1.3.1 Seismic tuning thickness

The tuning-bed thickness (vertical resolution) of seismic data is the minimum thickness at which two-bed interfaces can be distinguished from each other and identified on the basis of the frequency value and the related wavelet. Widess (1973) notes that geologic features or beds less than λ/4 wavelength can be detected and proposed λ/8 as the resolution limit. However, 1⁄4 wavelength (λ) is typically used due to the presence of noise and the consequence of the wavelet during transmission (Fig. 3.3) (Chopra & Marfurt, 2016). Tuning wedge amplitude response diagrams highlight these occurrences (for a given frequency and velocity of the data). At the tuning thickness, reflections at the top and base of the beds interfere constructively, creating an amplitude maximum and limiting which true bed thicknesses can be calculated (Sheriff & Geldart, 1983; Brown, 2004). The amplitude is progressively attenuated below λ/4 wavelength until the limit of visibility is reached (i.e., the minimum thickness at which two interfaces can be detected without accurately pinpointing their position or thickness), and the reflection signal becomes obscured by the background noise (Brown, 2004). As such, beds significantly thinner (i.e., λ/20 or λ/30) than the resolvable limit (λ/4) can still produce a significant reflection.

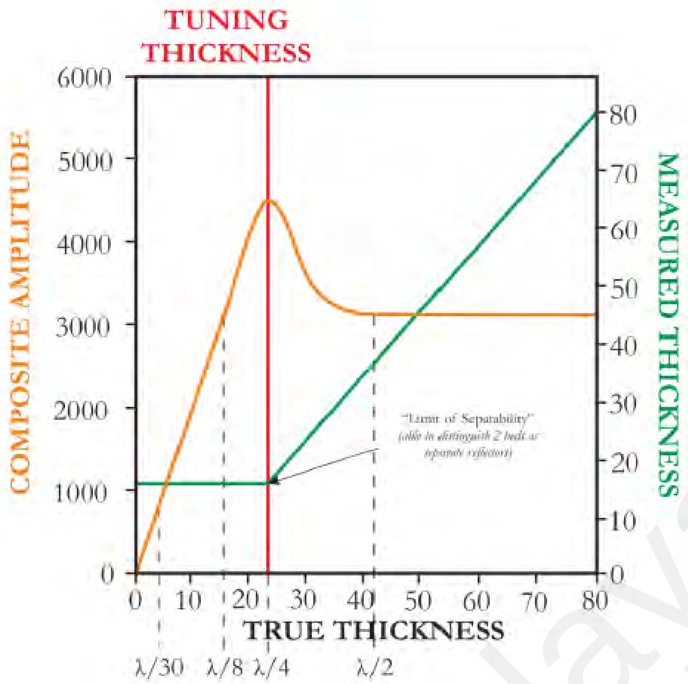

Figure 3.3: Tuning wedge amplitude response curve. Measured thickness is the real thickness above the tuning layer. Tuning thickness = High amplitude due to constructive interference from top and base of the bed between the reflected energy. Detectability of thin beds is down to λ/30 wavelength (Modified from Brown, 2004).

Spectral (frequency) decomposition allows gross reservoir thicknesses to be determined below the tuning thickness of the full bandwidth seismic data (Brown, 2004). Spectral decomposition interrupts the seismic signal into narrow frequency band, which reflects the thin beds that are also indicative of the bed thickness. Consequently, analysis of individual frequency slices can be related to their corresponding tuning frequencies and thickness. This analysis is critical for understanding the range of channel dimensions that can be resolved using 3D seismic and highlights the important issue of the varying scales of observation and levels of resolution between core, wireline log, and seismic data, which have to be carefully measured when using subsurface datasets. This resolution analysis is also important for defining and classifying the range of channels that can be imaged via seismic attribute analysis. The dimensions of individual channels, channel belts, channel belt complexes, and incised valleys differ on several orders of magnitude. Consequently, understanding the size and dimensions of geobodies that can be imaged (within the limits of seismic resolution and detection) becomes vital for understanding how these channels evolve through space and time and to subsequently develop predictive 3D depositional models.

3.1.4 Seismic mapping

Vertical seismic coverage of the Malay Basin extends below the reference well penetration depth in the available dataset (Laba Barat-1 at 2627 m). However, the study was somewhat limited by the fact that well Laba Barat-1 does not reach the base of Group I. Here in this study, I use semiautomatic tools to seismically analyse the 3D seismic dataset (Paleoscan©). Three main processes were required in order to get the best images for geomorphological analysis (Fig 3.4). Firstly, key surfaces were mapped across the seismic dataset using calibrated well tops (interpreted maximum flooding surface/ flooding surfaces) from well Laba Barat-1. Next, a Relative Geological Time (RGT) model was created for each series in which the process is aligned with the main surfaces using the Paleoscan © method in each seismic sequence. Lastly, an advanced stratigraphic method (a module in the Paleoscan) is used to identify important stratigraphic surfaces in time domain.

The algorithm initially tracks every possible horizon within the seismic volume and automatically constructs a relative geological stratigraphy. Relationships between horizons were then edited, and the model was updated in real-time in order to obtain an optimum solution. A geological time volume is computed from the seismic based on the interpreted horizon grid. This process is fully interactive, which enables refinement of the interpretation of every horizon and iteratively increases the level of accuracy of the geological model (Fig 3.4A). The interpretation is therefore made faster and of better quality. For example, a study on Central North Sea using a massive dataset with a 15,000 km^2 area by Beller et al. (2012) only took a short time frame of 8 weeks to interpret. The interpretation was carried out by creating a 3D Relative Geological Time (RGT) model from seismic data to optimize the information in the seismic dataset. The results of this procedure can be used for various applications, including seismic strata slicing and demarcation of geological elements.

Paumard et al. (2018) presented a case study using Paleoscan© to interpret a 3D seismic dataset from the Lower Barrow Group (LBG) of North Australia. They used a threefold approach to interpreting the high-resolution 3D dataset. Firstly, they mapped the key regional seismic unconformities. Secondly, they created an RGT model and identified chronostratigraphic surfaces. The method allowed for the complete 3D mapping of all clinoforms in the LBG. This study was able to reveal the detailed variations in the source and accommodation of sediments in the LBG in time and space and shed new light into the allocation of deep and shallow marine spaces in the basin. Such an approach offers a higher degree of certainty in 3D mapping of every significant continuous seismic sequence. These methods may improve the prediction of fluvio-tidal plays in the study area.

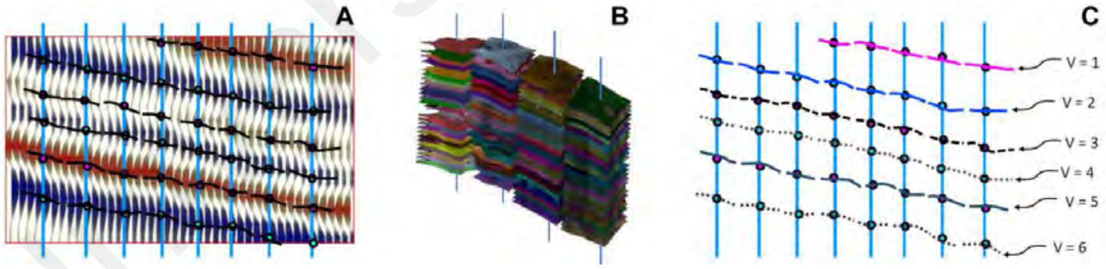

Figure 3.4: Processes for complete semi - automatic horizon tracking in Paleoscan ©. (A) Auto-tracked horizons of the model-grid linking patches. (B) Patches of the model-grid in 3D view. (C) Every horizon has a specific geological time. (from Pauget & Lacaze, 2017).

3.1.4.1 Seismic-to-well tie

Seismic-to-well tie was performed prior to seismic data analysis (Fig 3.5). Seismic well tie is a technique to convert depth to time. Time-depth conversion was done using sonic logs and check-shot surveys from the Laba Barat-1 well. This is in order to utilize well tops of Group H and I markers from confidential in–house well reports made available by PETRONAS. Checkshot data of Laba Barat-1 well is used to calibrate time to depth. The synthetic seismogram can be compared directly to the seismic with the estimated time-depth relationship. The synthetic ties the borehole to seismic with strong amplitude at the same spot, data with similar frequency, and seismic translucent spot aligned in a synthetic seismogram with little reflectivity.

Well markers from well log correlation (Fig 3.2) were used as references in interpreting the key surfaces on laterally continuous seismic reflections across the dataset and to develop a regional stratigraphic framework. Six (6) surfaces (Fig 3.6) were mapped i.e., near Top Group H, near Top H20, near Top H40, near Top Group I, near Top I20, and near Bottom Group I. These surfaces represent flooding surfaces which were highlighted by continuous high amplitude seismic reflector and analogous to the geological markers from the in-house geological reports. Figure 3.7 illustrates Near Top Group H structure time map (twt). Black lines highlight the orientation and nature of the normal faults. The near Top Group H and near Bottom Group I surfaces define the top and base of the interval of interest for analysis of seismic attributes. However, the maximum well control is only down to the near Top I20 surface. The produced isopach map (Fig 3.8) shows that TWT-thickness is dominantly thinner in the Northern and Eastern part of the study area with thickening towards the West.

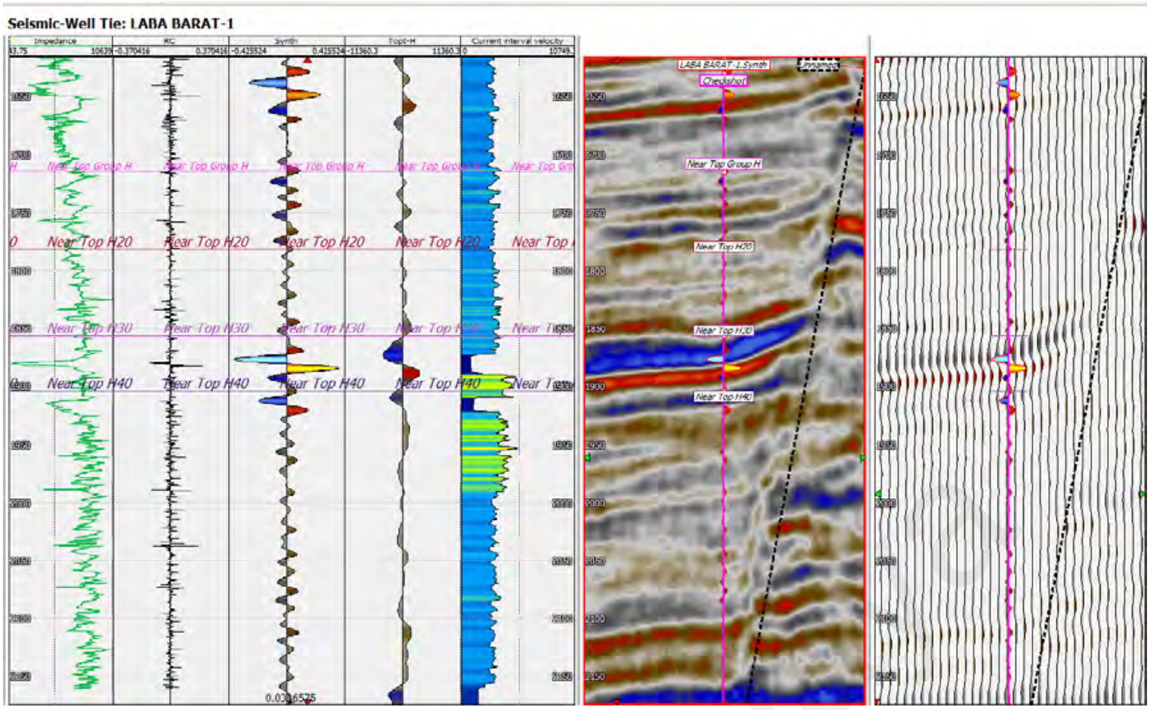

Figure 3.5: Seismic to well tie in Laba Barat-1 well to assist in seismic surface mapping. This calibration process used sonic, density and checkshot data.

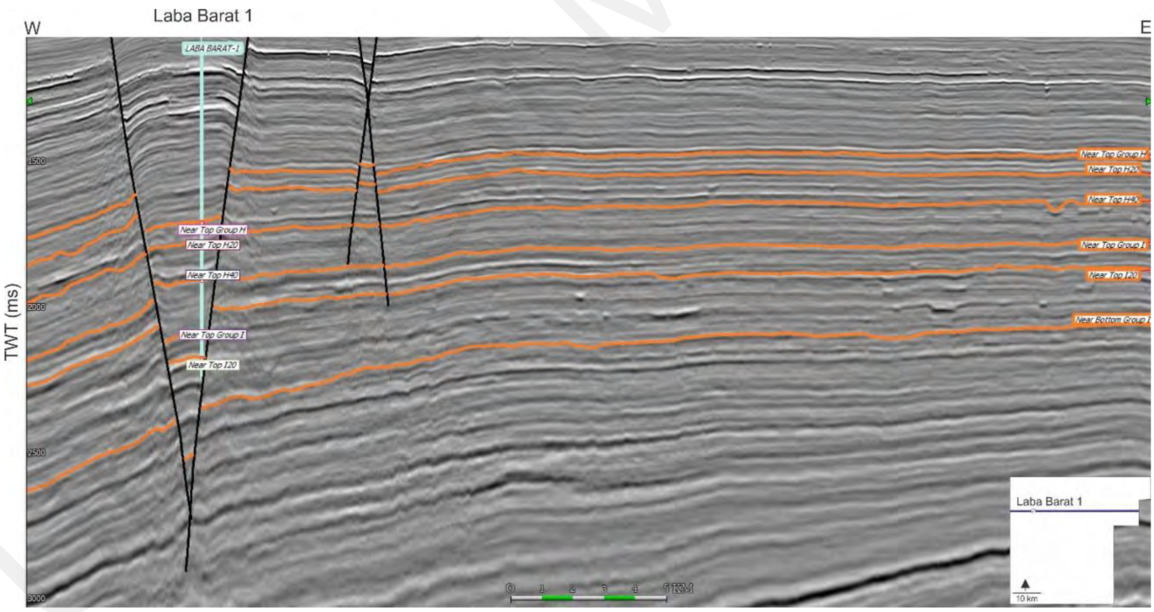

Figure 3.6: Regional seismic segment described using a 3D seismic data set displaying the six (6) main horizons used in this analysis. These horizons were interpreted based on the well tops (Group H and Group I) provided in the confidential in-house report of well Laba Barat 1. These horizons were picked at the most extensive continuous reflectors which also correspond to the top markers of Laba Barat-1 well.

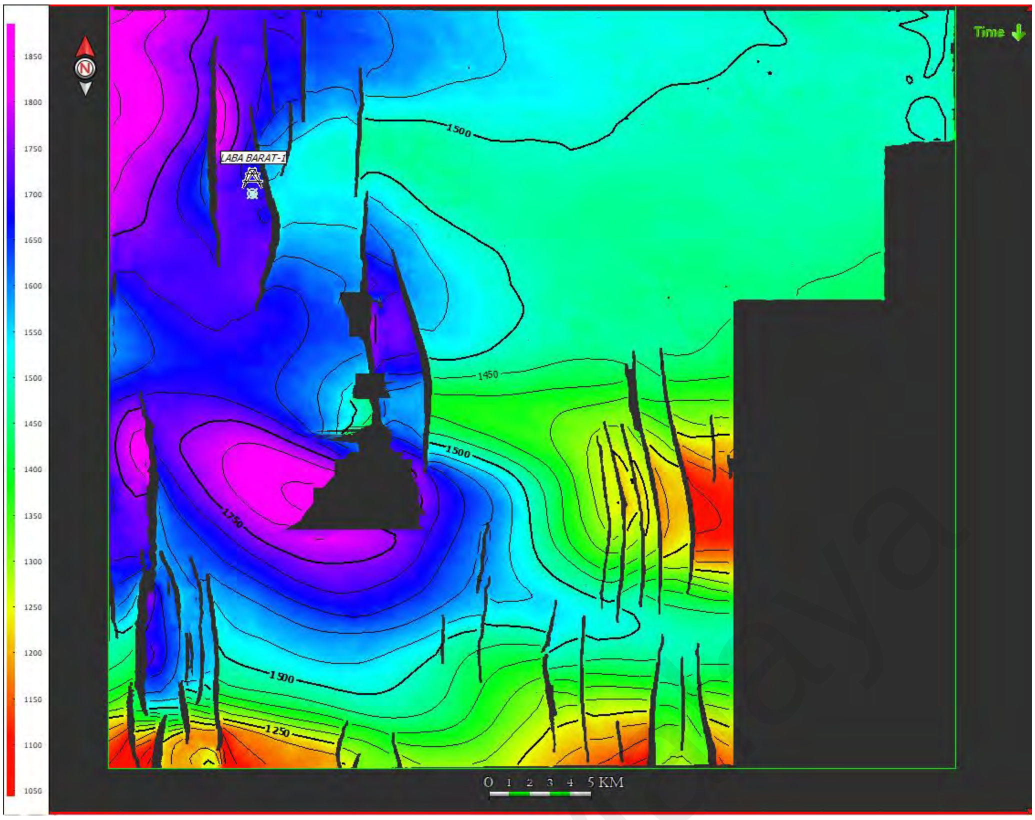

Figure 3.7: Near Top Group H structure time map (twt). Black lines highlight the orientation and nature of the normal faults.

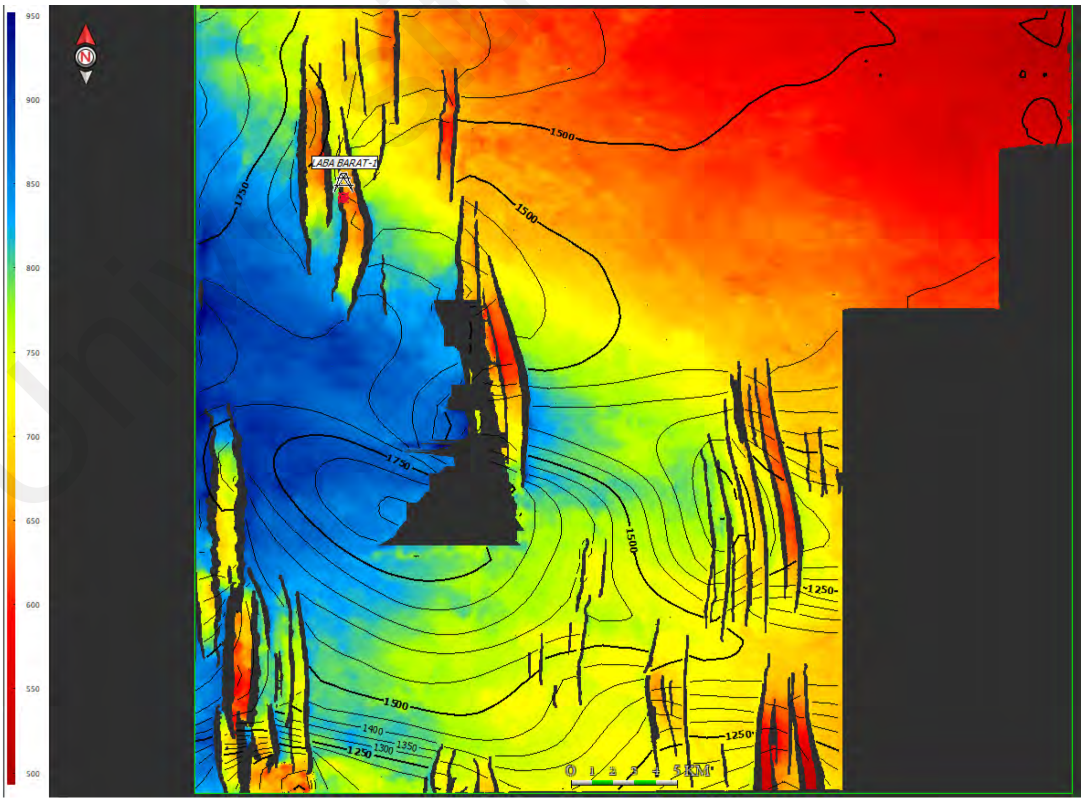

Figure 3.8: TWT-thickness map of the Near Top Group H within the study area. Thickness is dominantly uniform in the Northeastern and Southeastern part of the study area with thickening towards the Western area.

3.1.5 Seismic Attributes Analysis

Several seismic attributes were generated over time at selected iso-proportional slices. Ten (10) iso-proportional slices (iso-slice) (Fig 3.10) were produced with each slice being 15 ms thick (approximately 20 m thick). The isoslices are conformant to the six (6) key surfaces as top and bottom horizons and are parallel to the stratigraphy.

Four attributes were analysed in this study: (1) variance attribute (similar to similarity and coherency attribute), which compares path to trace equivalents in order to enhance geological relief and surface discontinuities (e.g., faults); (2) Root Mean Square (RMS) attribute measures the reflectivity factor by detecting variability in intensity, which can be used to identify channels, lithological changes, and hydrocarbon indicators; (3) envelope attribute is determined by the seismic record independently of its polarity and primarily emphasizes channelised features (for example, fluvial-tidal channels), and variations in amplitude (for example bright spots), and; (4) spectral decomposition attribute (i.e., frequency-based attribute), which splits the seismic signal into different frequencies to better reflect geological features such as channels, and geological properties of seismic resolution such as bedding thickness and lateral discontinuity. The colour-blending (RGB) module is used to combine these attributes. Such analyses help to identify geological features at high-resolution, allowing the distinction within Group H and Group I of the Malay Basin of various network channel morphologies and geometries.

Frequency decomposition generates a series of magnitude slices at discrete frequencies (Fig 3.11a). Colour blending of three magnitude slices (with red, green and blue colours assigned to the specified frequency volumes) (Fig 3.11b) enables channel architectural seismic facies and its boundaries to be imaged more clearly in plan-view (Fig 3.11c), consequently, revealing a variety of geobodies within the succession of interest.

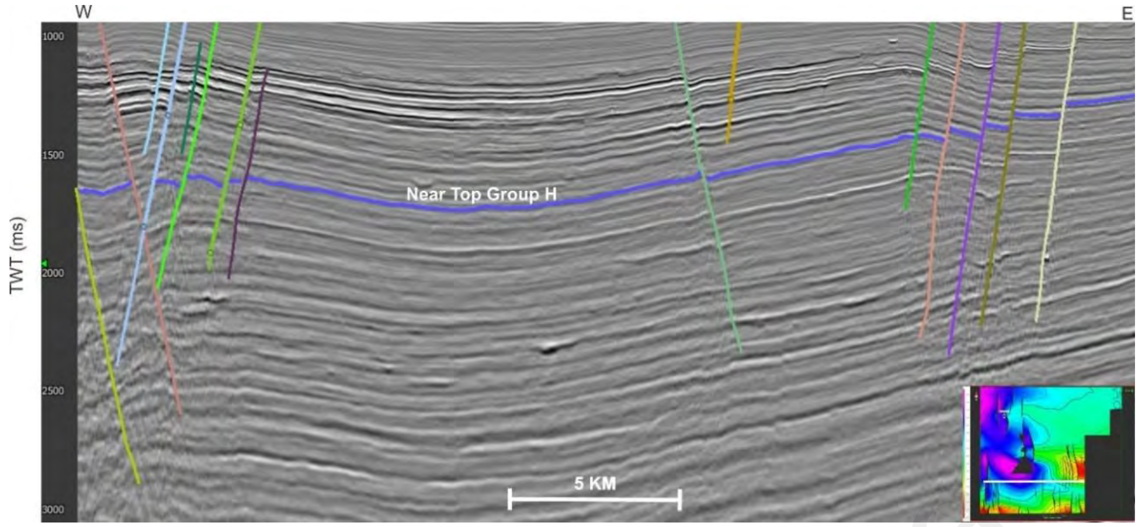

Figure 3.9: Example seismic cross line highlighting the orientation and nature of the normal faults (Blue line traces interpreted Near Top Group H surface).

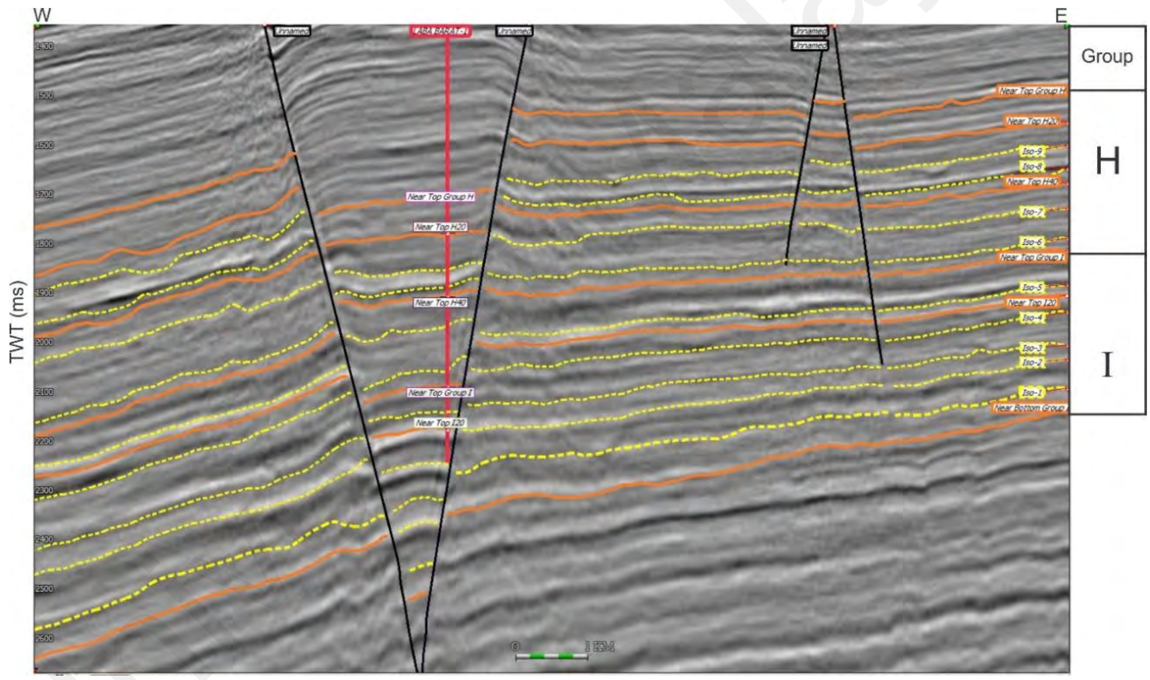

Figure 3.10: Iso-proportional slices (isoslice) are obtained by slicing in between two stratigraphic horizons, conformant to top and base key surfaces.

Nonetheless, descriptive fluvial channel systems at different stratigraphic levels have been determined by the combined analysis of iso-proportional slices and vertical seismic sections.

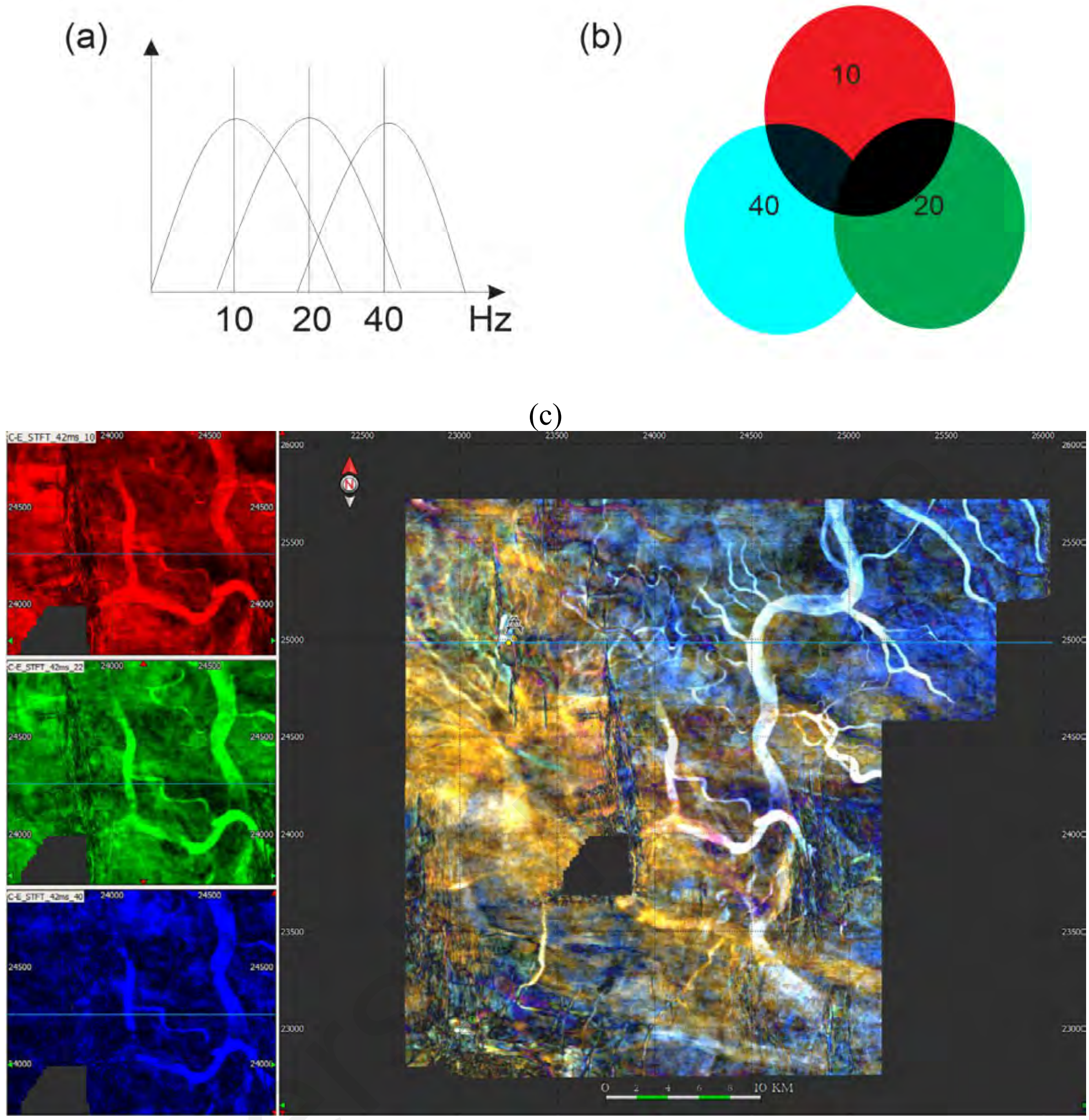

Figure 3.11: (a) Three (3) frequencies selected in the study interval. (b) Frequencies are being assigned to each Red, Green and Blue colours, therefore we have to overlap between the frequencies to show better visualization. (c) Result of colour blending of the overlapping frequencies.

3.1.6 Scale of Observation and Resolution

The identification of discrete seismic facies "geobodies" (Fig 3.12) and subsequent statistical analysis of a series of extracted measurements were performed on each isoslice. The thickness of the geobody, which can be imaged by seismic analysis, is assessed by vertical seismic resolution.

The minimum seismic data wavelength within the interval of interest in Group H and Group I is approximately 65 m and 66 m, respectively, (where wavelength (λ) = V/F).

Hence, if 1⁄4 wavelength of the dominant frequency of the seismic survey is the thinnest resolvable vertical range, the minimum resolvable geobody thickness is about 16 – 17 m. It is very likely that the smallest features represent the "maximum limit of seismic resolution" and not the smallest geobodies within the depositional system.

The resolution issue is crucial in the interpretation of cross-cutting geobody relationships. Over a 15 ms seismic attribute window, cross-cutting geobodies could either be connected or unconnected (Fig. 3.14), depending on their individual thickness. This is currently unresolvable in the dataset and has significant implications for interpretation of the relationship between these geobodies and their potential connectivity (e.g., are apparently intersecting geobodies lateral feeder tributaries into an incised valley or merely randomly cross-cutting unconnected channel belts of different age?) (Fig. 3.14b). Defining the relationship is extremely important when interpreting geobodies in order to accurately describe the subsurface architecture of geobodies. To mitigate this issue, additional data such as pressure data from well control would be required to resolve the uncertainties related to channel connectivity, which is not available for this study.

Note that interpretation of stratigraphic trends defined by vertical changes of the fluvial architecture was a challenge because channel deposits of different sizes and incision depth that are cut down from a variety of horizons may be superimposed within individual seismic slices.

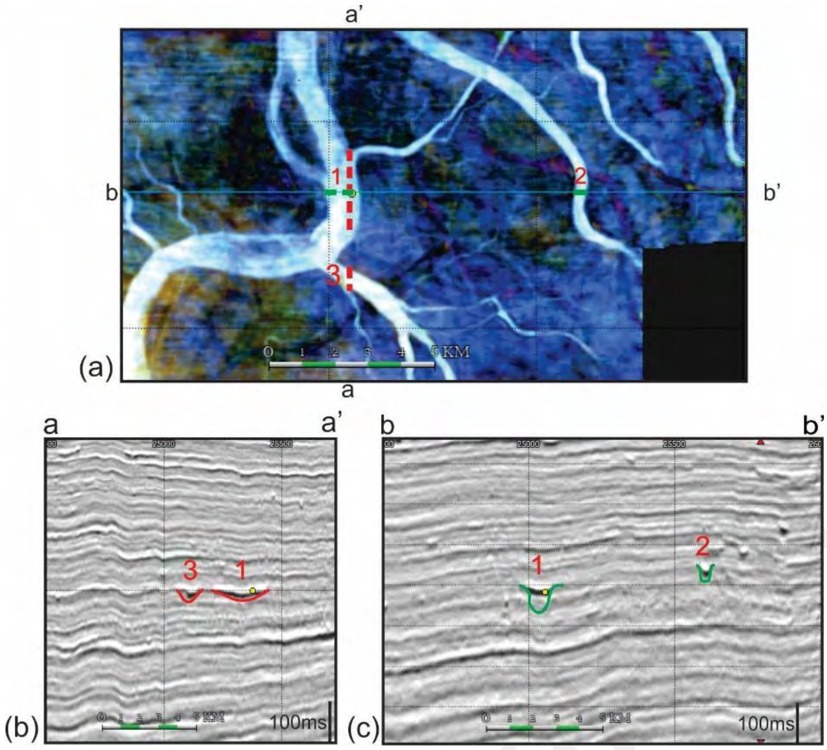

Figure 3.12: Scales of observation and resolution of the horizontal and vertical resolution of the seismic datasets within this research area. a) Planform view of the isoslice show in geobody morphology, b) inline cross-section view, and c) cross-line cross-section view of high amplitude channel geobody, showing slightly concave-upward seismic reflection.

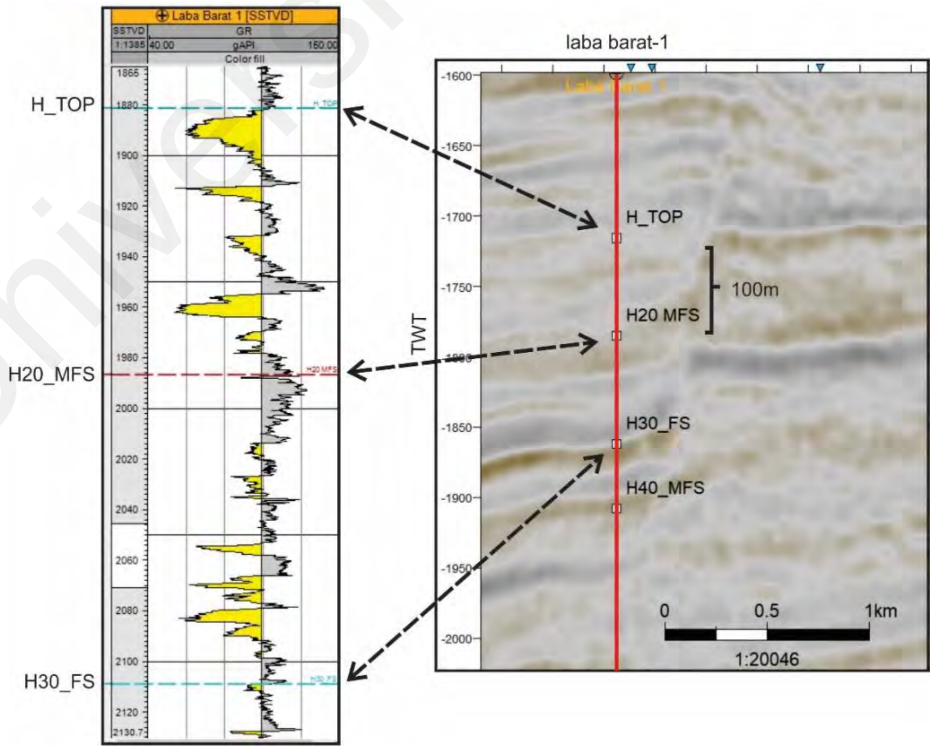

Figure 3.13: Scales of observation and resolution of vertical resolution of the seismic dataset used in this study in the Malay Basin.

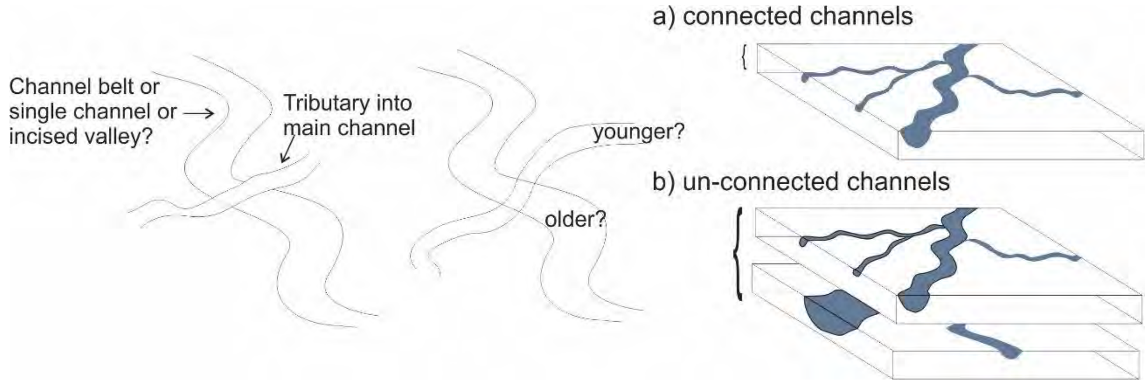

Figure 3.14: Implications of cross-cutting geobodies observed in seismic attribute maps for vertical and lateral connectivity of geobodies (modified from Heldreich et al., 2017)

3.2 Quantitative Analysis Parameters

The parameters of morphometric elements utilised in this seismic analysis study comprise channel thickness (CT), channel width (CW), meander wavelength (ML), meander amplitude (MA), channel length (CL), radius of curvature (RC), sinuosity (SI) and channel orientation (CO) (Fig 3.15). These properties were measured using Paleoscan interpretive maps. Channel thickness can also be measured directly from the seismic volume vertical section, core, and seismic frequency through spectral decomposition analysis. Relationship analysis of these parameters were done using Micosoft Excel. For example, scatter cross-plots of X and Y axis were done to understand relationships between channel width and channel thickness.

The geometry of 120 channels was measured, and the interrelated properties data were used to inaugurate pragmatic relations between these parameters. These parameters were measured according to methods described by Schumm (1977), Ethridge & Schumm (2007), and Wood (2007). The following sections describe these geometric parameters and how they were measured in this study.

3.2.1 Channel Width (CW)

Channel width (CW) is the maximum width from flank edge-to-edge of a confined channel (Fig 3.15). CW is measured from channels in the seismic isoslices in which the channel margins are well-defined.

In this analysis, CW is directly measured from the interpretive surface map and is defined as the horizontal distance between the erosion borders binding the channel. CW is measured on lines perpendicular to the centreline of the channel body every 500 to 1000 m.

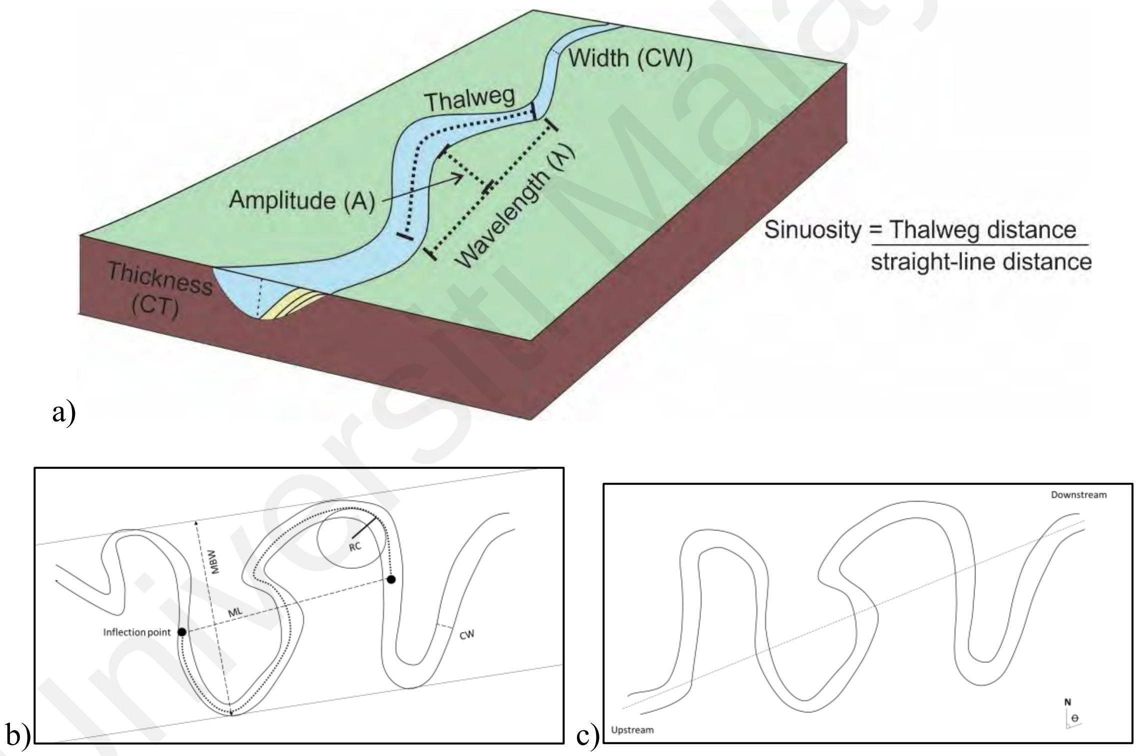

Figure 3.15: Sketch illustrating the approach used to calculate the fluvial system morphometric and channel orientation parameters. (a & b) The morphometric parameters include channel width (CW), meander belt width (MBW), radius of curvature (RC), meander wavelength (ML), and channel length (L). Sinuosity (SI) is calculated as the thalweg distance divided by the meander wavelength (ML). Thickness (CT) data is the only metric taken from spectral decomposition with reference from wireline log and core. (c) The direction of the channel is defined as the azimuth of a line drawn between two (upstream and downstream) locations.

3.2.2 Channel Thickness (CT)

Channel thickness (CT) or channel depth (CD) is the maximum depth of geobody incision. CT measurements are made from seismic vertical sections and are defined as the vertical distance seen between the top and base of the channel-related incision (Fig 3.15). Tentatively, channel thickness can be measured from the seismic frequency in spectral decomposition analysis. Tuning frequency derived from frequency cubes of spectral decomposition is inversely proportional to the thickness of reservoirs, where the higher frequency indicates thinner reservoirs.

Nonetheless, due to post-depositional compaction that decreases channel filling thickness during burial, the thickness measured should be less than the original thickness. Ethridge & Schumm (1978) suggested adding 10% to channel filling density estimates to compensate for compaction after deposition. In general, modern river channel thickness (CT) is defined as the bank depth of the channel where discharges are the most effective in the development of the channel (Dunne & Leopold, 1978).

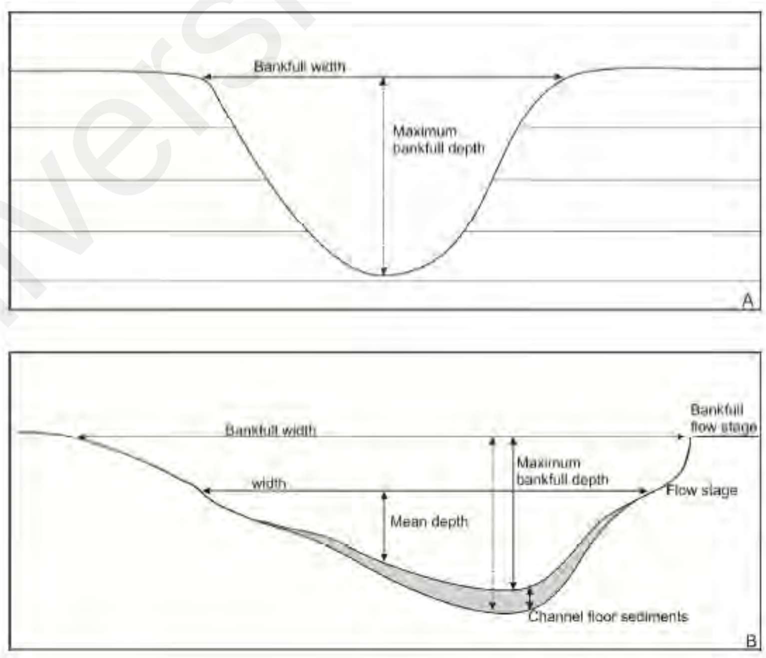

Figure 3.16: The channel thickness measurement (CT) approach from the (A) seismic section and the (B) recent-day river (after Bridge, 2003).

3.2.3 Channel Length (CL)

The channel length (CL) is measured along the centreline between the top and the bottom points along the channel course (thalweg). CL is used with meander wavelength (ML) to measure and calculate channel sinuosity.

3.2.4 Meander Wavelength (ML)

Meander wavelength (ML) is the measured length between the upstream and downstream inflection points of a single complete meander bend (Fig 3.15b). ML is harder to measure from well logs or outcrops alone in ancient rivers. An empirical relationship between ML and CW was developed by Leopold & Wolman (1960) based on high sinuosity of modern-day channels:

$$Lm=10.9Wc^{1.01} \tag{3.1}$$

Where Lm is the wavelength of the meander (ML), and the Wc is the channel width (CW).

3.2.5 Amplitudes/ Meander Belt Width (MBW)

Meander belt width (MBW) is described as the width of a channel geobody that forms in response to lateral migration of numerous individual channel systems (Fig 3.15b). In practice, this value defines the width of the 'container' within which the individual channels migrate. As with CW, it is challenging to determine MBW for ancient rivers using well log and outcrop datasets, although it may be possible to estimate this parameter from CW. For example, Lorenz et al. (1985) developed this empirical relationship between the CW and MBW for modern rivers:

$$Wm=7.44Wc^{1.01} \tag{3.2}$$

Where the Wm is the meander belt width (MBW) and the Wc is the channel width (CW). This relationship was established by mainly using data combined from the previous studies of Leopold & Wolman (1960) and Carlston (1966). MBW can also be estimated from the CD. Based on the quantitative data collated by Carlston (1966), Collinson (1978) established the following empirical relationship relating MBW to CD, and h is the channel thickness (CT):

$$Wm=64.6h^{1.54} \tag{3.3}$$

In addition, Fielding & Crane (1987) compiled published data on CD and MBW to produce the following empirical relationship:

$$Wm=12.1h^{1.85} \tag{3.4}$$

In this study, because it is a seismic amplitude-based parameter, it may only be a measure of a specific lithological contrast within that area. Therefore, when measured from seismic, it is considered the minimum width that the meander belt might be. Therefore, MBW is measured directly from the interpretive iso-slices map as the width between two lines that bound outermost visible meander-loop sets. MBW is measured on a line which is perpendicular to the valley centreline every 500 m to 1000 m along the valley axis.

3.2.6 Sinuosity (SI)

Sinuosity (SI) is determined by dividing the channel length (Thalweg distance) with the meander wavelength (ML) in the channel meander segments. The overall plan view fluvial style (for example, meandering, straight and braided) is defined by sinuosity. SI cannot be calculated from well logs or outcrops alone (see Bridge & Tye, 2000). Schumm (1977) demonstrated a strong empirical relationship between the SI and the grain size of the fluvial system. He showed that fluvial channel systems with 1-1.3 SI are bed-dominated systems; 1.4-2 SI systems are mixed-load systems; and SI->2.0-systems are suspended-load systems. Leopold & Wolman (1957) use a SI value of 1.5 to categorize channels with either low sinuosity (SI less than 1.5) or high sinuosity (SI more than 1.5) for single-channel fluvial systems. When a variety of active channels is detected, the SI value of 1.5 is used for the separation of anastomosing channels (SI < 1.5) from the braided channels (SI > 1.5).

Leeder (1973) established an equation from modern high sinuosity rivers (>1.7) to describe the empirical relationship between depth and width for channels with a sinuosity of >1.7:

$$Wc = 6.8h^{1.54} \tag{3.5}$$

where the Wc is the channel width (CW), and h is the channel thickness (CT). This relationship is invalid for low-sinuosity channels (i.e., <1.7).

3.2.7 Radius of Curvature (RC)

Radius of curvature (RC) in modern and ancient systems is the radius of a best-fit circle located within a meander bend (Fig 3.15b). Similarly, to those parameters described above, RC is difficult to estimate from the well logs and outcrops. An empirical relationship between the RC and ML has been proposed by Brice (1984), which states that the ratio of ML to RC is ca. 1:5.

3.2.8 Channel Orientation (CO)

The overall trend or orientation for each channel is the azimuth of a line that has been drawn between two points in the channel, i.e., one each at the upstream and downstream reaches, at the limits of the dataset (Fig 3.15c). After determining the orientations of all the channels observed on the interpretive maps, the data are plotted on Rose diagrams to assess the vertical changes in channel orientation for Group H and Group I channel systems.

Channel orientation has been constrained by measuring the mean azimuth of the channel from where it enters and exits the seismic survey. In the case where the entire system is not imaged in the survey, the orientation is measured as the mean azimuth for the channel where it is imaged. Prediction of the paleo-flow direction of the channels also took into consideration the following aspects of the geological setting of the study area which show that the paleoshoreline during Group I time was trending NW- SE (Madon, 1999) (Fig 3.17).

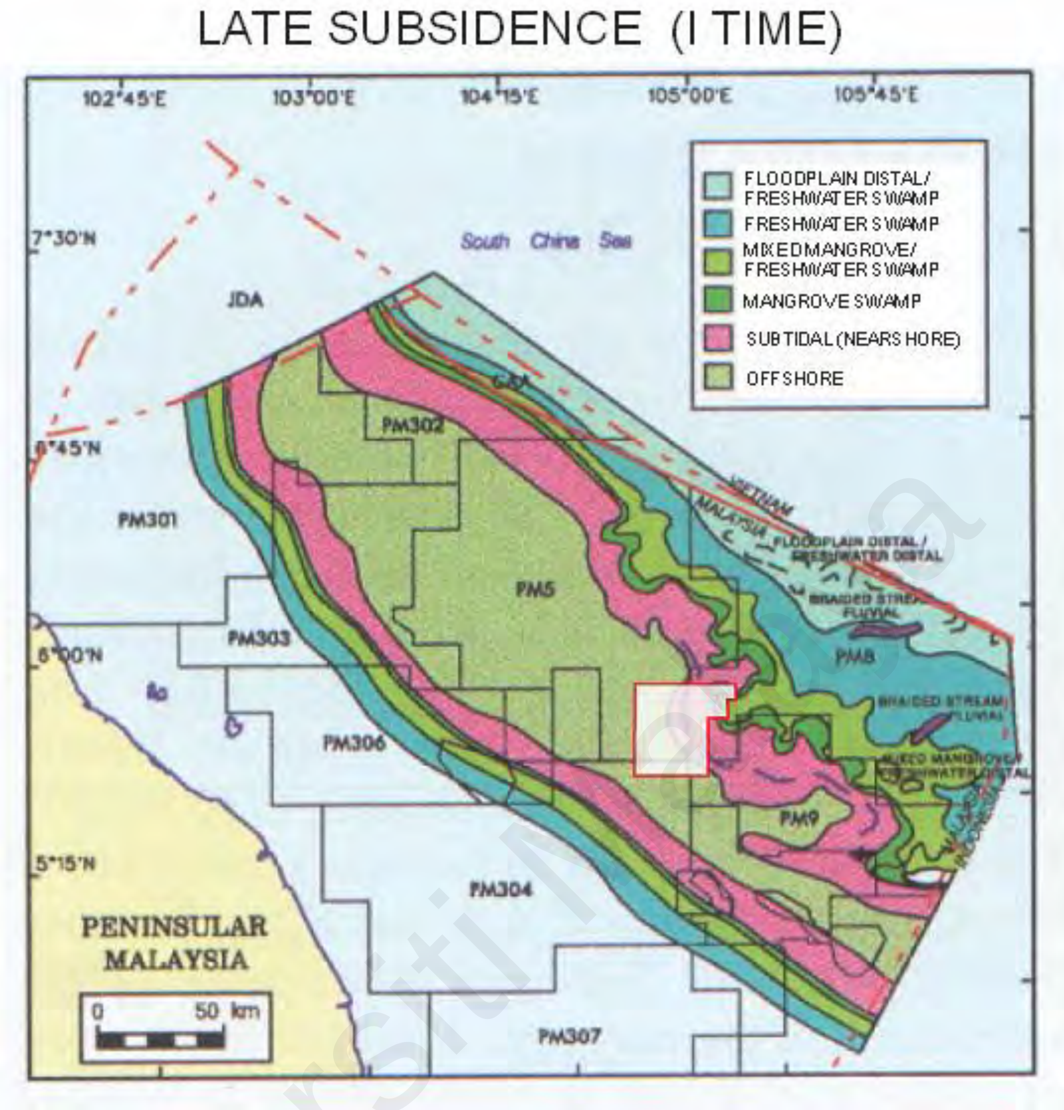

Figure 3.17: Schematic reconstruction of paleogeographic development of the Malay Basin, based on the EPIC (1994) regional study. The transparent white box is the study area bounded with 3D seismic data for this research—this area located adjacent to the center of the Malay Basin.

3.3 Summary

Generally, methodology used in this study will integrate dataset from well logs, core and 3D seismic. These datasets were integrated for two main assessment of facies analysis and seismic geomorphology analysis. Morphometric channel elements extracted from seismic geomorphology analysis is a bonus to further understand channel geomorphology concepts and their depositional environments.

CHAPTER 4: FACIES COMPOSITION AND ARCHITECTURE IN THE GROUP H STRATIGRAPHIC INTERVAL OF JAMBU AND CENDOR FIELDS, MIOCENE MALAY BASIN

4.1 Introduction

Tide-dominated and tide-influenced depositional systems form along both modern-day transgressive and regressive shorelines (Dalrymple & Zaitlin, 1994; Dalrymple et al., 2003; Dalrymple & Choi, 2007; Goodbred & Saito, 2012). Analogous tidally influenced coastal depositional systems have also been interpreted from the rock record and include both transgressive and progradational examples (e.g., Maguregui & Tyler, 1991; Willis, 2005; Martinius et al., 2015; van Cappelle et al., 2016). Such ancient examples have been associated with incised valley fills, tide-influenced/dominated deltas, straits and embayments and have been identified in lowstand, transgressive as well highstand sequence stratigraphic systems tracts.

The complex relationship between fluvial, wave and tidal processes (wherever predominant) is the main control over geobody deposition, composition, structure, dimensions, geometry, distribution, and orientation in coastal settings (Ainsworth et al., 2011). Currently, there is relatively good understanding of general depositional element distributions within tidal depositional systems. However, more recently, there has been more interest towards understanding facies distribution along the course of fluvio-tidal rivers associated with deltas, estuaries and embayments. Tidal processes are very important within the fluvial- to-tidal transition area of coastal and delta plains, where fluvial and tidal currents interact (Plink-Björklund, 2005; van den Berg, 2007; Salahuddin & Lambiase, 2013; Yankovsky et al., 2012).

Grain size distribution, hydrodynamic drive, sand-mud ratio, and facies associations varies along the course of fluvio-tidal rivers. This is caused by the progressively increasing influence of tidal processes basin-ward and its interaction with progressively decreasing fluvial influence (Dalrymple & Choi, 2007).

Gugliotta et al. (2017) describe the area of mixed fluvial current and tidal current energy as the ‘fluvial to marine transition zone’ (FMTZ), where sedimentation is mainly driven by the complex interplay of fluvial and marine processes. Recent studies on the present-day Mekong River delta system in Vietnam have provided some understanding of depositional processes operating in the FMTZ (Nguyen et al., 2000; Gugliotta et al., 2018). Additionally, recent detailed studies on the Mungaroo Formation also highlight the complex relationship of facies architecture and evolution of temporal and spatial stratigraphic, including their depositional processes in a vast fluvio-deltaic system (Stuart et al., 2014; Heldreich et al., 2017).

Heterolithic bedding is common facies observed in Miocene strata of the offshore Malay Basin. Many published studies interpreted these as tidal deposits. As an example, Amir Hassan et al. (2013) describe thick heterolithic strata in Group H of the Cendor Field in the Malay Basin, initially interpreted as tidal deposits associated with channel fills and barforms developed in a marginal marine setting. They identified the presence of three separate, NW-SE trending incised valleys associated with base sea-level-fall. The valleys are filled with progradational tidal heterolithic delta deposits and transgressive embayment deposits.

In this study, I use a more extensive core and well log data set from Group H of the Malay Basin in order provide a more detailed facies analysis of the tidal heterolithic strata. The facies analysis will be used to identify the types of depositional elements present in the studied interval, and to test the hypothesis that these represent components of a fluvial-tidal depositional system. The facies analysis will then be integrated with seismic facies and geomorphological results in Chapter 5 in order to construct a depositional model and stratigraphic history. Group H of the Malay Basin will then be compared to models of modern-day fluvial to tidal transition zones. One (1) well (Cendor-3A) is located within the seismic boundary (available 3D seismic dataset), whereas the other two wells are beyond the seismic boundary (Cendor-2 and Jambu-3) (Fig 4.1b, c). However, these two wells are only less than 2 km from the seismic edge. Core for Cendor-2, Cendor-3A, and Jambu-3 are available up to the upper section of Group H (within Top of Group H to Near Top H20 markers, see Chapter 5).

4.2 Geological Setting

The study area is within Block PM-304, located off the east coast of Peninsular Malaysia within the southeastern flank of the Malay Basin and approximately 140 km from Terengganu, covering an area up to 1563 km^2. The southeast flank of the Malay Basin is steeper and displays strong structural deformation. Wells available for this study are located in the Cendor and Jambu fields and penetrated the Group H reservoir of the post-rift sedimentary succession in the Malay Basin.

The Malay Basin was a narrow, gulf-like basin partly connected to the open ocean at its southeastern end during the Miocene. During the Late Oligocene to Early Miocene, sedimentation in the area was dominated by fan-deltas and deltas flanking the gulf (Nik Ramli, 1988). The Upper Miocene sequence in the Jerneh field was deposited in a southward-flowing alluvial-deltaic system along the axis of the basin based on the paleocurrent analysis from dipmeter data (Madon, 1994).

The post-rift phase began in the late Lower Miocene, which is marked by the termination of extensional faulting. The thermal subsidence of the basin continues to the present day (Madon et al., 2006). This thermal subsidence resulted in the development of a broad sag basin. Thermal subsidence was interrupted by a major inversion phase, which began in the late Early Miocene. The inversion triggered a regional uplift and tilting northwest, which led to the development of a major Upper Miocene erosional unconformity in the southern part of the basin (Madon et al., 2006). This inversion produced large E–W compressional anticlines over the pre-existing grabens and half-grabens, predominantly in the central area of the basin, which led to the formation of the 'Jambu-Liang' structure in the studied fields. The Jambu-Liang structure is an elongated E-W trending, faulted inversion anticline. The structures in the southern part of the basin exhibit complex positive flower structures associated with strike-slip faults, and wrench faults.

Group H sediments were deposited during an overall sea-level rise and are mainly composed of marine to deltaic sediments with fluvial/estuarine channels (Madon et al., 1999a). Average thickness of the Group H sedimentary succession is about 200 m. An unconformity developed due to the major uplift and erosion truncates folded strata of Groups H and older groups, while undeformed sediments of Groups A/B overlie the unconformity. Erosion along the crests of anticlinal structures within the study area has removed up to 1.2 km of sediment overburden, while deposition continued on the flanks during this inversion.

The source of the sediments infilling the Malay Basin during the Miocene was from the West, uphill of the Mae Ping fault region, the Chainat Ridge, and the pre-Tertiary rocks which is now an almost peneplaned area (Morley & Westaway, 2006). Eroded sediments from the Western mountains in the area between Thailand and Myanmar, and the western margin of the Khorat Plateau (O'Leary & Hill, 1989) were also transported into the Malay Basin and nearby basins during this period. Group H sediments record widespread peat swamp development, indicating that the climate was everwet. Temporary acmes of conifer pollen indicate recurrent episodes of cooler climates during periods of low sea-level, with limited evidence of seasonality (Yakzan et al., 1996).

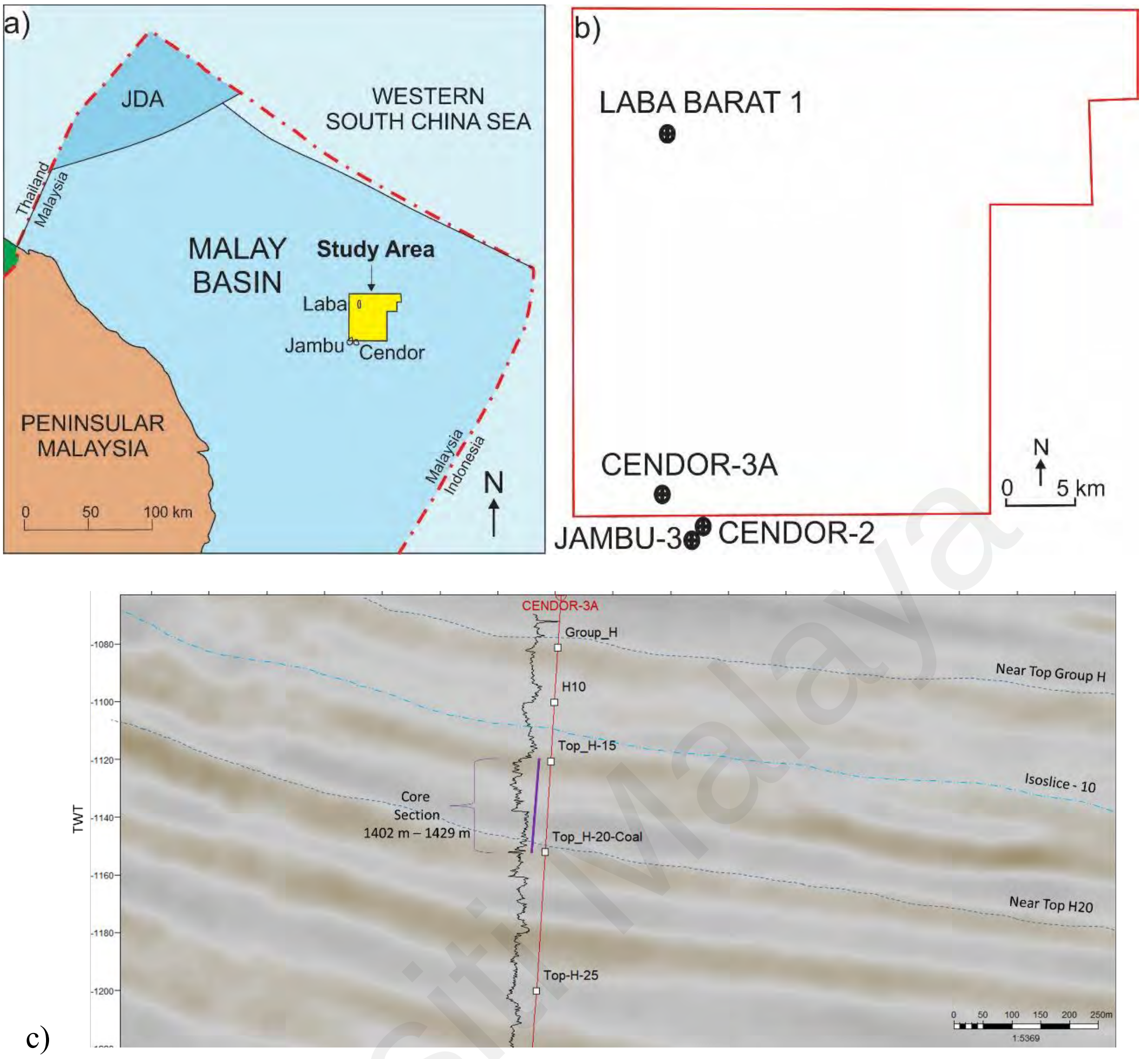

Figure 4.1: a) Location map of the study area in the Malay Basin, marked by yellow box. b) Study area, which is bounded by the available 3D seismic data set (red polygon), and c) shows Cendor-3A well lied onto the seismic data, where the core interval is between the Near Top H20 and Near Top Group H seismic surfaces.

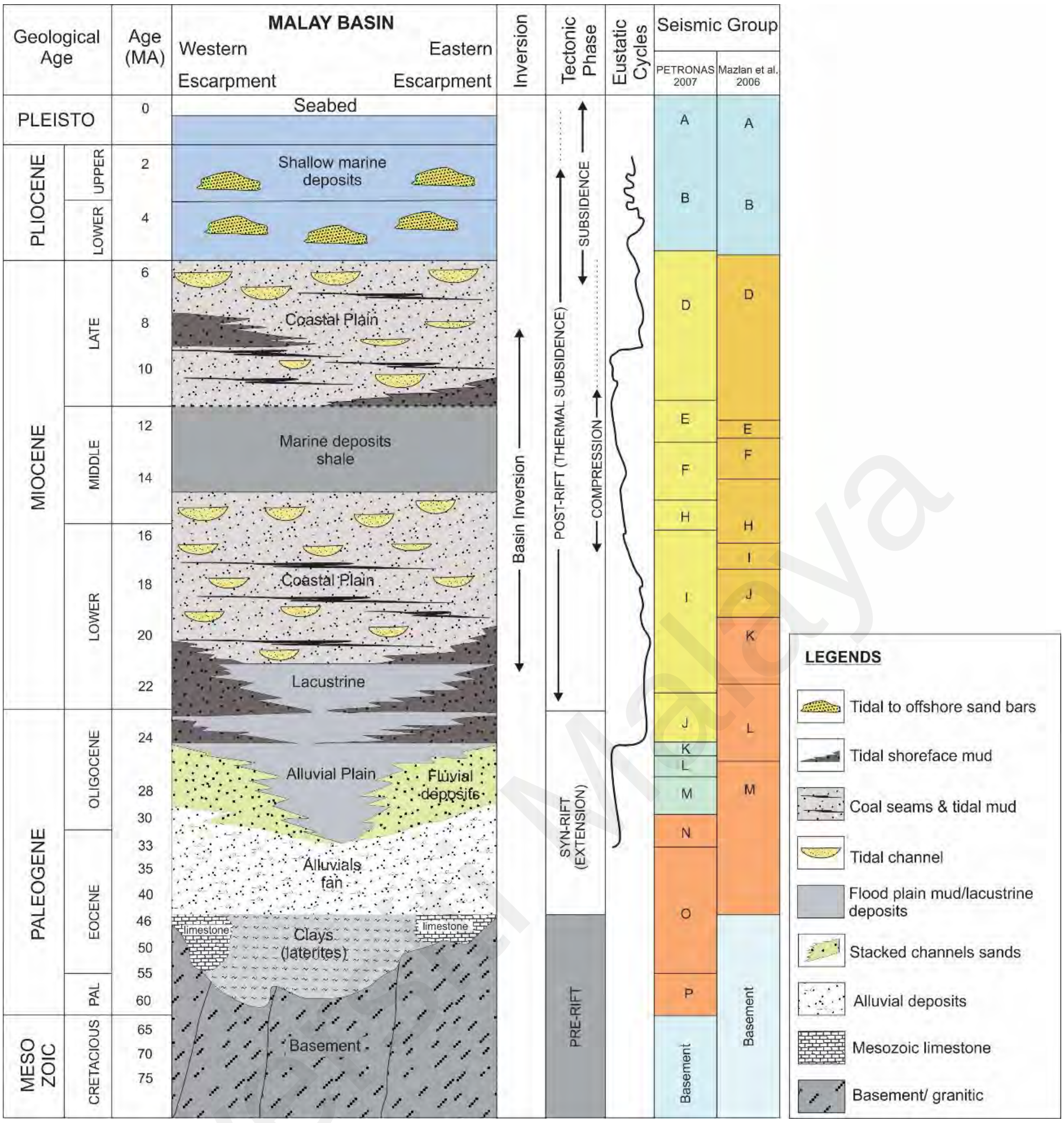

Figure 4.2: Malay Basin chronostratigraphic chart (modified after Madon et al., 1999), representing a range of lithologies, depositional environments, tectonic phases, and seismic groups.

4.3 Dataset and Methodology

Detailed sedimentary logs of 83.15 m of conventional core from three wells in the dataset have been produced, i.e., Cendor-2, Cendor-3A and Jambu-3 (Table 4.1). The cores provide good data for a detailed facies analysis of the Miocene, upper Group H, as they sample different intervals of the stratigraphic unit. However, only well Cendor-3A is within the boundaries of the 3D seismic area of study, while the other wells are beyond the seismic boundary at about 2 km away (Fig 4.1b).

The available cores from Cendor-2, Cendor-3A and Jambu-3 penetrate the interval between the Near Top H20 surface and Near Top H Group surface (see Chapter 5). More specifically, the studied core penetrates the interval between the interpreted top H20 Flooding Surface (H20FS) and the top H15 Flooding Surface (H15FS), as defined by Petrofac Malaysia in-house reports. This cored interval will be referred throughout the report as the 'H15-H20' interval. Only Cendor-2 core shows a complete H15-H20 interval succession. The cores in Cendor-3A cover almost 70% of the H15-H20 interval. Cores from Jambu-3 only penetrate the main reservoir sand in the middle of the H15-H20 interval.

Facies as well as facies associations were identified based on the core descriptions and calibrated with their equivalent gamma-ray log motifs to delineate identifiable well log facies. Interpretation of depositional environments was made based on the facies analysis and ichnology. Well correlations were made across the study area, which provides useful references for spatial and temporal facies trends to be recognised and to provide a better understanding of the temporal evolution of the depositional system.

Table 4.1: List of wells with conventional cores used in this facies analysis study. These cores penetrate Early to Middle Miocene strata of the Malay Basin.

Well	Core depth (m)	Length (m)
Jambu-3	1313 – 1321m	8
Cendor-2	1250-1298m	48
Cendor-3A	1402-1429 m	27.15

4.4 Results and Interpretations

4.4.1 Sedimentary Facies

Eleven facies are recognized in the studied cores, which were defined based on lithology, texture, sedimentary structures, and type and degree of bioturbation. They are summarized in Table 4.2. In general, the studied core intervals are composed of siliciclastic rocks associated with thin coal seams. Heterolithic units of thin, interlayered sandstone and mudstone (heteroliths) are the most common facies (Facies Hm, Hs). Several mudstone facies are recognized, i.e., thick structureless mudstone, thinner bioturbated mudstone, and rooted mudstone. Sandstone in the form of laminated and cross-bedded sandstone can form intervals up to 4 m thick.

4.4.2 Facies Associations

Sedimentary features identified from the core and the organisation of discrete lithofacies and ichnofacies calibrated with equivalent wireline log signatures were used to define six (6) facies associations in the 'H15-H20' interval of the Middle Miocene succession of the Malay Basin (Near Top Group H). This classification of facies associations is interpretative, with names representing the inferred depositional environment (Fig 4.3).

Table 4.2: Lithofacies classification scheme for the interval of interest in the Cendor and Jambu fields of the Malay Basin.

	Facies		Thickness	Lithology	Descriptions	Interpretation
C	C	Coal	up to 0.2 m	Coal	Rootlets	Peat accumulation
Mudstone	Mm	Structureless Mudstone	0.5 -7 m	Mudstone	Structureless, dark grey to light grey, occasional sand streaks, carbonaceous material, common pyrite and siderite concretions/bands, subtle bedding	Low energy deposition of fines from suspension fallout, low energy currents/waves and/or rapid deposition through flocculation (i.e. fluid muds)
	Mr	Rooted Mudstone	0.5-2 m	Mudstone, silty/carbonaceous mudstone	Rootlets, organic debris and laminae, pedogenic slickensides and carbonaceous material.	Vegetated and subaerial exposure of fines deposited from low energy suspension. Early soil development.
	Mb	Bioturbated Mudstone	up to 3 m	Silty mudstone	Dark grey – black coloured, moderate to intense bioturbation, mottled texture	Condensed sections, depositional hiatus, period of quiescence. Pedogenic developments causing uneven dispersal of iron oxides in the sediment resulting in colour mottling. Plant colonisation within quiet, low energy area like overbank floodplain, shallow water, brackish embayment, and swamps/marshes.
	Mno	Nodular/Mottled siltstone and mudstone	0.2-0.5cm	Siltstone and mudstone	Siderite nodules/bands within dark brown to black colored siltstone and mudstone.	Deposition under reducing environments such as overbank floodplain. Associated with undeveloped and saturated paleosols.

Table 4.2, continued.

Facies			Thickness	Lithology	Descriptions	Interpretation
	Stg	Graded Silt Sandstone	0.2- 2 m	Silty mudstone, siltstone, and very fine-grained sandstone	Normal or reverse graded with basal scour with indistinct undulating lamination	Tidal modulation, subtidal storm, waning storm and/or gravity flow deposits
Heterolith	Hm	Mudstone Heteroliths	0.3-4 m	Mudstone interlayered with fine- to medium-grained sandstone lenses and/or laminae (Sand content up to 40%)	Wavy, and lenticular bedding, rhythmic lamination, sand streaks, synaeresis cracks, unidirectional and/or bidirectional current ripples	Periodic, alternating high and low energy deposition (tidal and/or seasonal) Intervals of current or wave flow regularly interspersed with slack water periods. Subtidal - intertidal
Heterolith	Hs	Sandstone Heteroliths	0.3-4 m	Fine- to medium-grained sandstone interlayered with mudstone (Sand content from 60 to 85%)	Wavy and flaser bedding, ripples and mud drapes, mud clasts, unidirectional and/or bidirectional current ripples	Periodic, alternating high and low energy deposition (tidal and/or seasonal) Intervals of current or wave flow regularly interspersed with slack water periods. Subtidal – intertidal

Table 4.2, continued.

	Facies		Thickness	Lithology	Descriptions	Interpretation
	Stg	Graded Silt Sandstone	0.2- 2 m	Silty mudstone, siltstone, and very fine-grained sandstone	Normal or reverse graded with basal scour with indistinct undulating lamination	Tidal modulation, subtidal storm, waning storm and/or gravity flow deposits
Heterolith	Hm	Mudstone Heteroliths	0.3-4 m	Mudstone interlayered with fine- to medium-grained sandstone lenses and/or laminae (Sand content up to 40%)	Wavy, and lenticular bedding, rhythmic lamination, sand streaks, synaeresis cracks, unidirectional and/or bidirectional current ripples	Periodic, alternating high and low energy deposition (tidal and/or seasonal) Intervals of current or wave flow regularly interspersed with slack water periods. Subtidal - intertidal
Heterolith	Hs	Sandstone Heteroliths	0.3-4 m	Fine- to medium-grained sandstone interlayered with mudstone (Sand content from 60 to 85%)	Wavy and flaser bedding, ripples and mud drapes, mud clasts, unidirectional and/or bidirectional current ripples	Periodic, alternating high and low energy deposition (tidal and/or seasonal) Intervals of current or wave flow regularly interspersed with slack water periods. Subtidal – intertidal

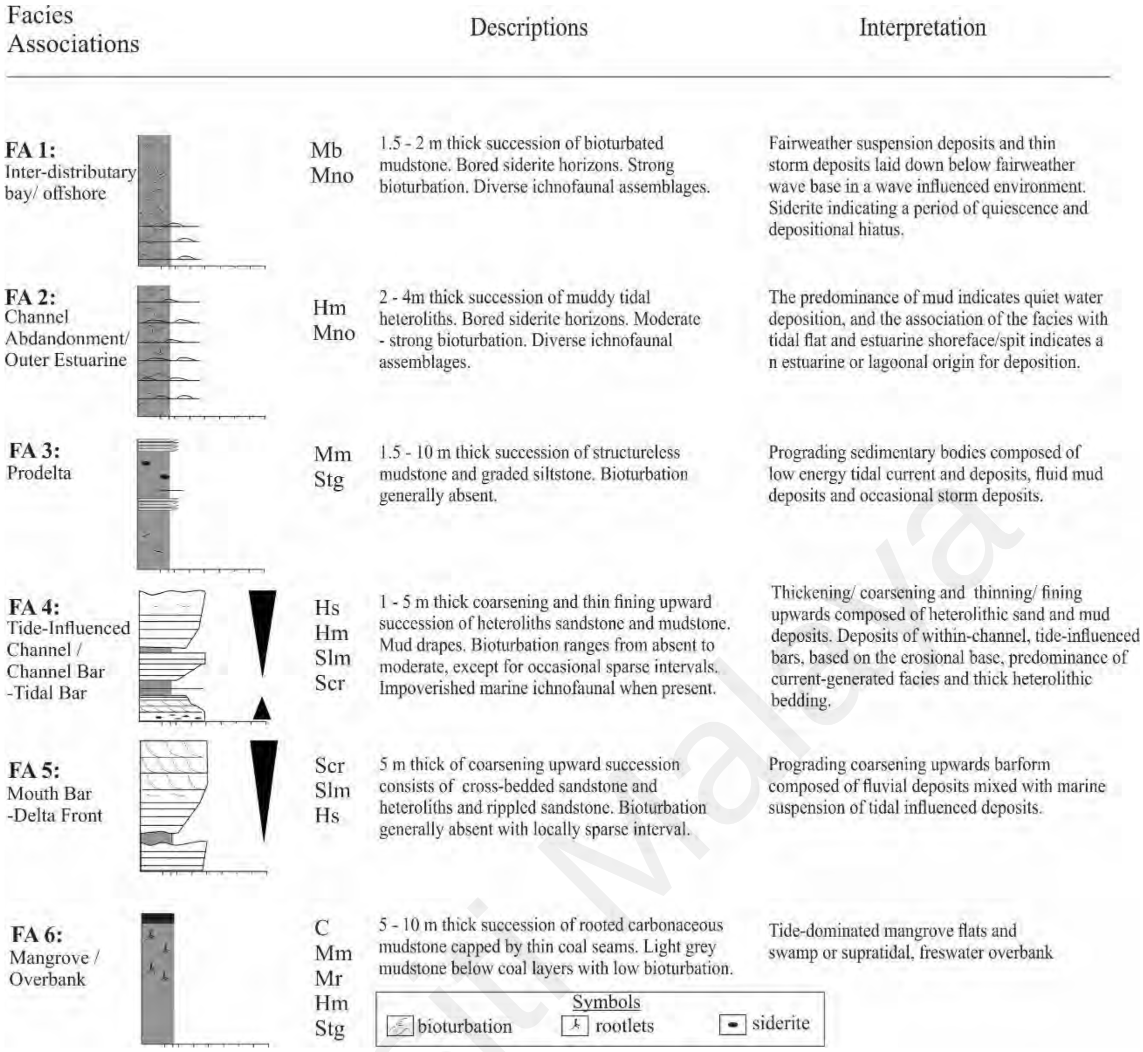

Figure 4.3: Facies Associations recognised within the 'H15-H20' interval in the upper Group H of the Miocene interval of the Cendor and Jambu wells, Malay Basin.

FA 1: Inter-distributary bay/ Offshore

Sedimentology: FA1 typically forms 1-2 m thick successions dominated by laminated bioturbated mudstone and nodular mudstone facies. The mudstone is commonly grey buff-coloured and comprises argillaceous sub-arkose siltstone, with moderate sorting. Brownish siderite concretions are observed at several intervals. A high percentage of carbonaceous matter is found in the mudstone. Sand heterolithic facies in the form of wavy bedding is present as thin intervals intercalated between mudstone and at the base of FA1 with normal grading. FA1 shows a fining upward trend from bioturbated sand heteroliths into mudstone. Millimetre-thick lenses of very fine- to fine-grained sandstones form symmetrical ripples in lenticular-bedded mudstones, displaying bundled up-building of cross-laminae. Figure 4.4 shows the only example of this facies association, which is observed in Jambu-3 well.

Ichnology: FA 1 is strongly bioturbated (Ichnofabric Index 4-5) and mainly characterised by general mottling. The observable trace fossil assemblage is relatively diverse, including ichnotaxa such as *Asterosoma, Planolites, Palaeophycus, Terebellina,* and *Anconichnus*.

Interpretation: Predominance of mudstone facies and a strong degree of bioturbation by an impoverished marine ichnofauna indicates a low energy, possibly restricted, depositional setting. Mudstone facies were probably deposited by a combination of suspension settling and flocculation. Intercalated heterolithic intervals record periodic fluctuations in energy, with currents and/or waves transporting and depositing thin rippled sand layers. Such fluctuations may be due to tides and/or seasonal fluctuations in fluvial energy. The strong degree of bioturbation is also consistent with a low energy subtidal or intertidal setting. The trace fossil assemblage is typical of marine, subtidal, and soft substrates of the *Cruziana* ichnofacies (Gerard & Bromley, 2008). However, the relatively low diversity and predominance of simple traces e.g., *Planolites* and *Palaeophycus* suggest a stressed, possibly brackish water environment (Pemberton & Wightman, 1992; MacEachern & Gingras, 2007; Hovikoski et al., 2007; Carmona et al., 2009). Bored siderite horizons probably represent periods of depositional hiatus, resulting in the formation of a condensed section with a cemented firm ground, and would represent a substantial mixture of freshwater and seawater. The intense and diverse bioturbation may also indicate shallow marine environment below fair-weather wave base, where the deposition was mostly from suspension settling.

There are no significant features of major storm events such as interbedded micro-hummocky cross-stratified sandstone beds (Harms et al., 1975; Dott & Bourgeois, 1982;

Duke, 1985). Even so, millimetre- thick of undulating parallel lamination sandstone and siltstone, and the thicker siltstone beds displaying normal grading suggest storm deposition (Aigner, 1982), with some events transforming into weak gravity flows traveling below the storm wave base (Walker, 1985; Davis et al., 1989). The symmetrical wave ripples suggest wave reworking during waning storm events (Raaf et al., 1977). Mudstone dominated facies with thin interbedded storm beds are consistent with an offshore depositional environment below fair-weather wave base (e.g., Hampson & Storms, 2003). Thus, FA 1 may probably represent depositional elements such as brackish water inter-distributary bays, or a shallow marine offshore setting.

FA 2: Outer Estuarine/ Abandoned Channel Facies Association

Sedimentology: FA2 comprises an approximately 4 m thick succession dominated by mud heteroliths. The mud heteroliths are separated into 10 - 25 cm thick packages. These packages are composed of lenticular bedding displaying alternating layers of thicker mudstone (up to 1 cm thick) and thinner (mm-thick) sandstone. The sandstone layers are very-fine to fine-grained and display ripple profiles. Internally, the sandstones contain ripples cross-laminations well as low angle to wavy laminations and mud-drapes. Small load casts are visible along the ripple bases. Mudstone intervals are usually parallel laminated. Synaeresis cracks are also common. Siderite concretions and bands are often observed in the mudstone heterolith unit. A thin, bored siderite horizon (about 4 cm thick) caps the facies association and separates it from the overlying Prodelta Facies Association (FA 3) (Fig. 4.5B). Another bored siderite horizon is also present in the middle of the succession (Fig 4.5B). FA2 is present in the cored interval of well Cendor-2 (Fig 4.5).

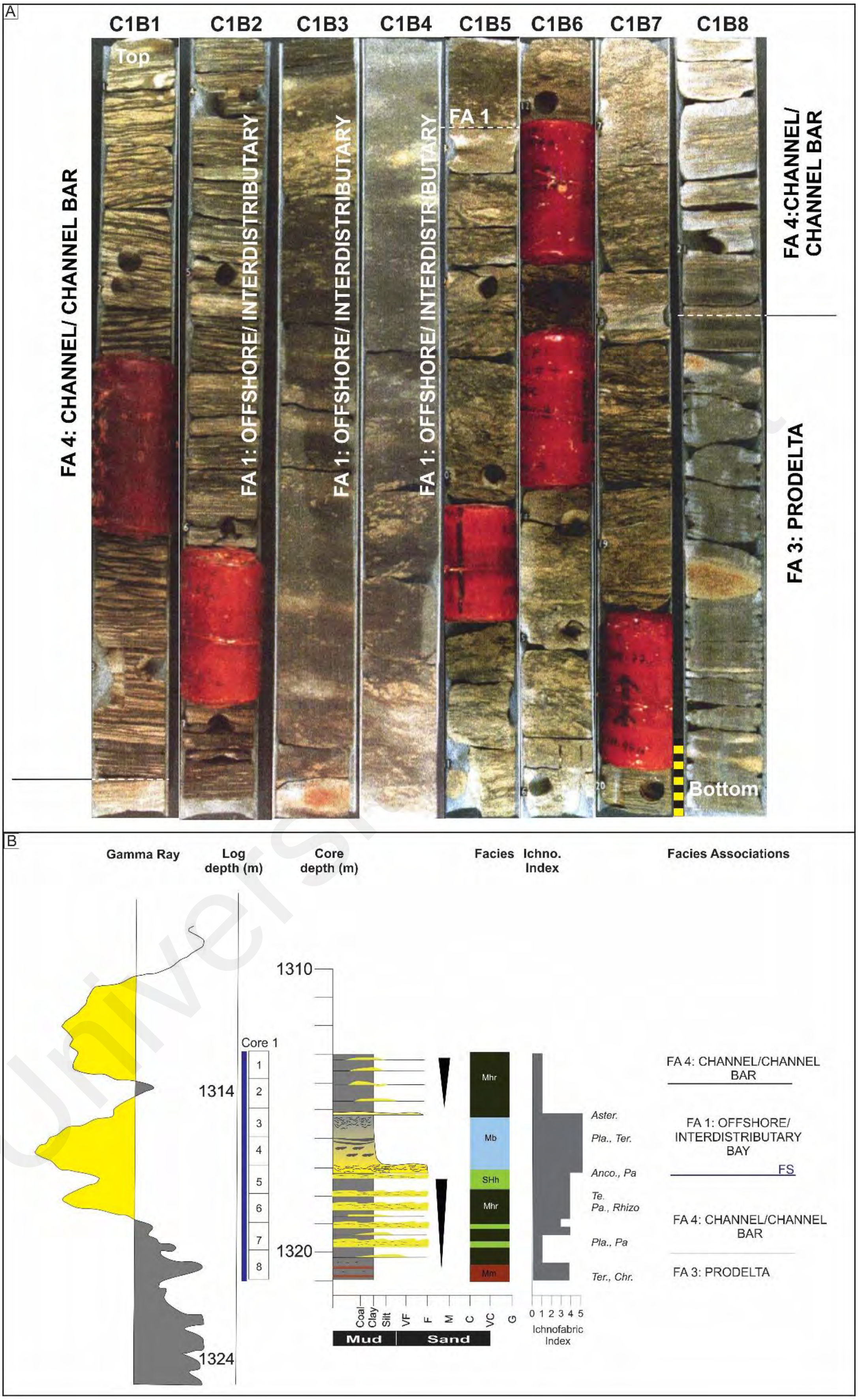

Figure 4.4: Inter-distributary/Offshore facies Association (FA1) overlying Channel Bar Facies Associations (FA4) from well Jambu-3, H15-H20 interval of The Malay Basin.

Ichnology: Bioturbation generally increases upwards in FA 2, from no bioturbation in the lower section (Ichnofabric Index 0-1) to moderate bioturbation in the upper section (Ichnofabric Index 4-5) (Fig 4.5A). Locally dense assemblages of *Chondrites* are observed in the lower section of the sequence. The upper section is dominated by a relatively diverse trace fossil assemblage, composed of *Asterosoma*, *Anconichnus, Chondrites, Planolites, Siphonichnus, Thalassinoides* and *Teichichnus*, which in combination constitute the archetypal *Cruziana* ichnofacies (MacEachern & Bann, 2008). No complex overprinting of trace fossil assemblages is observed. A possible amber fragment associated with the upper siderite horizon appears to have an irregular surface, interpreted as possible *Teredolites*. The upper and lower sections are both capped by a bored early siderite interval. The siderite horizons appear to be bored by a network of *Thalassinoides* (Fig. 4.5B). Local intervals of strong bioturbation underlie the bored siderite horizons and also at other local horizons in the succession.

Interpretation: The high proportion of fine-grained facies, evidence for weak currents, the presence of probable tidal deposits and the upward increase in diversity of marine ichnofauna is consistent with a mixed brackish and marine setting interpretation for FA2 (Reineck & Singh, 1980; Miall, 2010; Bridge, 2006), perhaps within the distal part of abandoned tidal channels or an outer estuarine setting. The high mudstone ratio of the facies association suggests low flow velocities, high concentrations of suspended sediment and insufficient sand supply. Thick mudstone intervals may represent fluid mud deposition from high concentration of suspension-load, which were deposited during decelerating tides or slackwater periods in between ebb and flood tidal currents. Mud drapes may also develop on cross-bed foresets, again due to suspension fallout during slackwater period between current reversals (Dalrymple, 1992).

Mud deposits with faint ripples also indicate a low energy setting, which might have been restricted from the open sea. Other evidence, such as the preservation of ripples, and the absence of rootlets, also suggest deposition in a subtidal environment. Small load casts on ripple bases indicate ripple migration on a soft substrate and high depositional rates (Dzulynski & Kotlarczyk, 1962; Reineck & Singh, 1980). Load casts form where higher density sand has rapidly sunk into the underlying soft mud resulted to downward-facing, bulbous structures. Lenticular bedding is the result of local wave activity (Reineck & Singh, 1980) and can also form by episodic cycle of ebb and flood tidal current flow and prevailing slackwater periods (Reineck & Wunderlich, 1968; Reineck & Singh, 1980).

The near absence of bioturbation at the bottom of the succession suggests a highly stressed environment (MacEachern & Bann, 2008). Further upward in the facies succession, the trace fossil assemblage displays a relatively moderate diversity of ichnotaxa, suggesting an increase in marine influence. This may be due to the transgression in abandoned tidal channels which can often extend marine ichnofauna to potentially more proximal locations (Hubbard et al., 2011). It is expected that these abandoned tidal channels had an open connection with the sea during abandonment, forming estuarine channels (Dalrymple et al., 1992). These facies most closely resembles the abandoned distributary channel fills described from the Sego Sandstone in Utah by van Capelle et al. (2016). Therefore, it is concluded that FA2 records deposition in a tide-influenced depositional setting, which may represent the fill of abandoned channels or the outer estuary.

FA 3: Prodelta Facies Association

Sedimentology: FA3 is composed of 3 to 11 m thick successions dominated by mudstone and subordinate muddy heterolithic intervals in the form of lenticular bedding (Fig 4.6). Structureless mudstone is the main facies observed in this facies association, forming intervals up to 7 m thick. The mudstone is commonly light grey to dark grey in colour and occasionally displays faint bedding. Faint, nearly symmetrical ripples are observed in certain lenticular bedded intervals. Siderite bands and concretion horizons are also present at certain intervals. Graded siltstone facies form coarsening upward packages (up to 2 m thick) of 1-2 cm-thick, reverse graded beds (Fig 4.6C), which are commonly interbedded between structureless mudstone intervals. Reverse grading from clay to silt is marked by a vertical colour changing upward from dark to light grey. Synaeresis cracks are absent within this facies association. Carbonaceous debris is finely dispersed throughout the mudstone.

Ichnology: Bioturbation in FA 3 is generally sparse to absent (Ichnofabric Index 1-2).

Interpretation: The mudstone dominated facies with regular 'starved' current and wave ripples indicate low sand supply, low current and wave velocities, and alternating periods of suspension deposition of mud and the bed-load transport of fine-grained sand (Reineck & Wunderlich, 1968; Raaf et al., 1977). The predominance of fine-grained sediment, absence of any distinct bioturbation and evidence for hyperpycnal flows is used to interpret a distal delta front to prodelta depositional environment for FA3. The predominance of mudstone is indicative of a low energy environment dominated by suspension fallout. The inverse graded siltstone beds record deposition waxing flows and are interpreted here as the deposits of river-induced hyperpycnal flows, which indicate the presence of sustained flows due to river floods (Mulder et al., 2003; Bhattacharya & MacEachern, 2009).

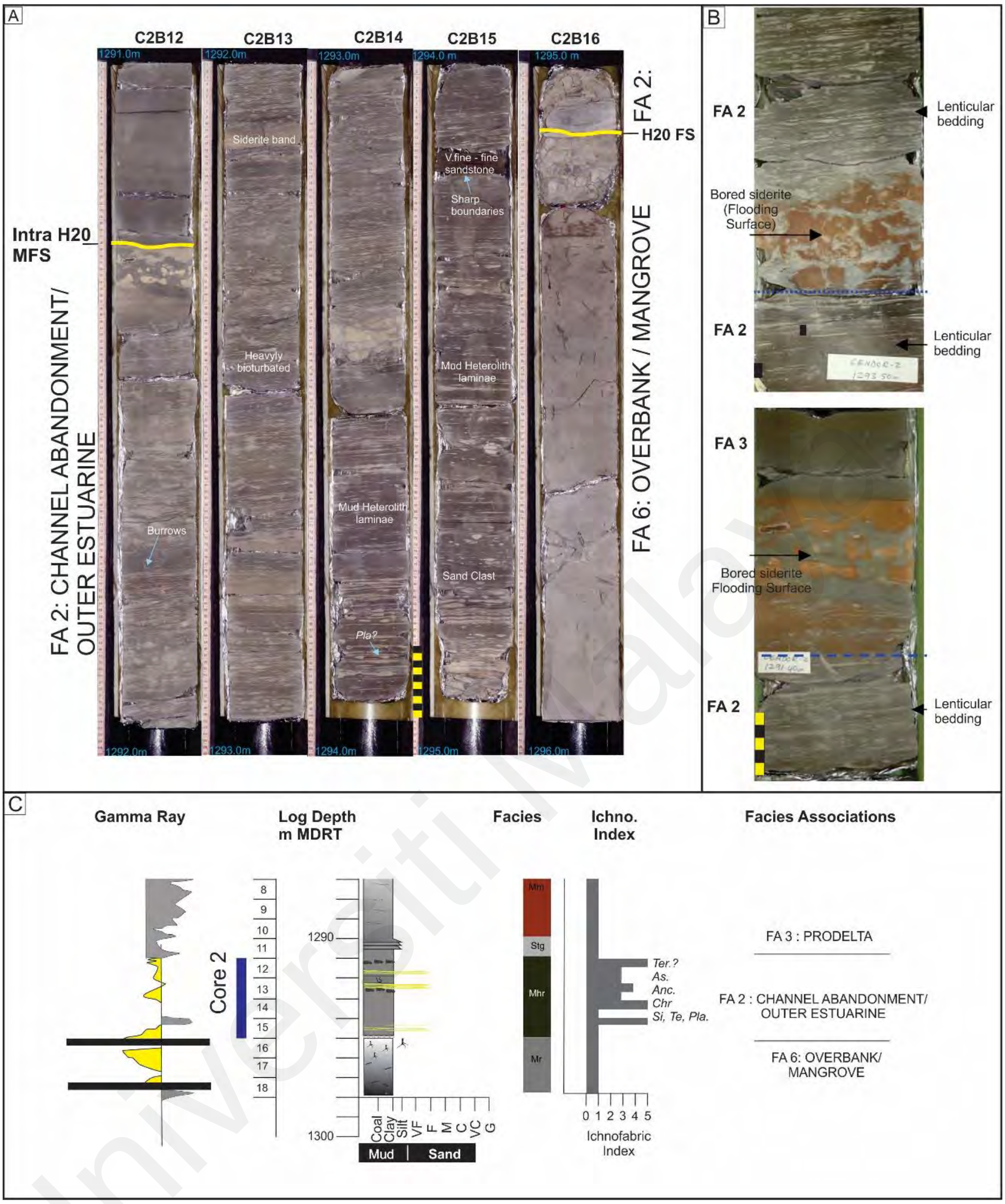

Figure 4.5: (A) Core photos of the Channel Abandonment/Outer Estuarine Facies Association (FA2) within the H15-H20 interval. (B) Bored siderite horizons separating heterolithic packages of FA 2. These siderite horizons are interpreted as flooding surfaces. Scale bars in (A) and (B) at 1 cm intervals. (C) FA2 core log from well Cendor-2 of the H15-H20 interval, Malay Basin.

Lenticular bedding suggests deposition in tidal setting due to alternating of ebb and flood tidal currents, and slackwater periods. Homogenous thick mudstone with low degree of bioturbation is consistent with the deposition of fluid mud. Thick structureless fluid mud deposits can form through rapid deposition of suspended sediment through flocculation, and the development of soup ground conditions. Deposition of fluid muds within a prodelta environment can be faster compared to typical hyperpycnal fluid muds and suspension fallout from hypopycnal plumes (Bhattacharya, 2010). The normally graded beds of millimetre to centimetre-thick sandstone and siltstone are indicative of waning flow events, such as either gravity flows (hyperpycnites) or distal storm-generated deposits (Aigner, 1982; Davis et al., 1989; Walker & Plint, 1992). The inverse graded beds of clay to silt may represent hyperpycnites (Mulder et al., 2003; Bhattacharya & MacEachern, 2009).

Ripples observed may indicate significant wave influence in certain intervals. The extremely low degree of bioturbation and the presence of abundant carbonaceous debris is interpreted as evidence of freshwater input. The continuous freshwater supply with episodes of higher freshwater discharge due to floods, produced a stressful environment for marine organisms (Pemberton & Wightman, 1992; Pemberton et al., 2001). Also, siderite bands and concretion horizons are possibly the result of freshwater infiltration into seawater due to proximity to land (Postma, 1982). Therefore, these features support a prodelta depositional environment that has been influenced by episodic storms and/or river flood events.

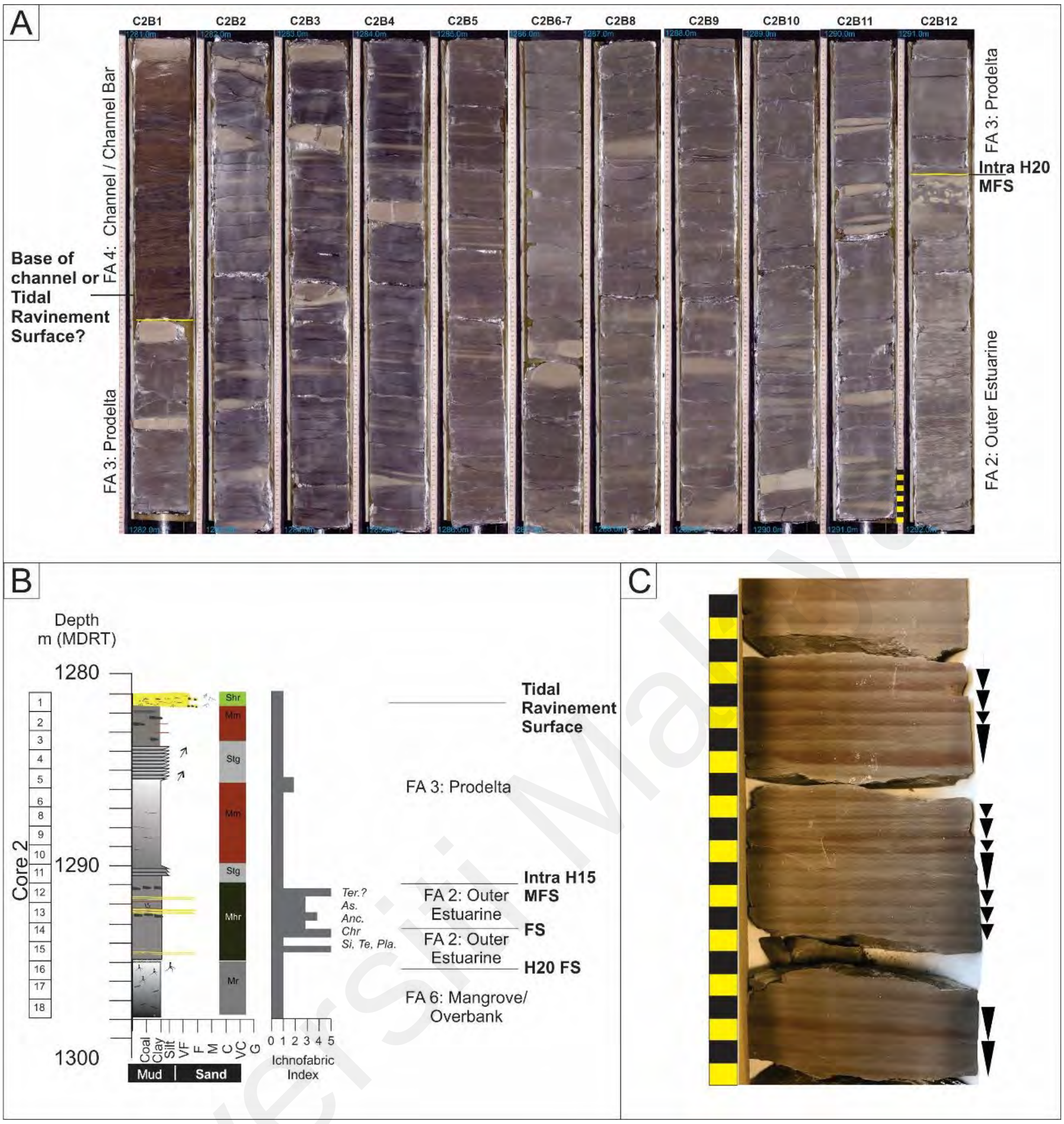

Figure 4.6: Prodelta Facies Association (FA 3), H15-H20 interval, well Cendor-2, Cendor Field, PM-304 Malay Basin. (C) Inverse graded siltstone layers interpreted as hyperpycnites (hyperpycnal flow deposits) Core 2 Box 4.

FA 4: Channel / Channel Bar (Tide influenced) Facies Association

Sedimentology: FA4 is represented by up to 24 m thick successions composed of alternating, meter-thick (up to 5 m thick) thickening/coarsening upward and thinning/fining upward heterolithic packages. Well-developed heterolithic, wavy, flaser, and lenticular bedding are the main facies in FA 4. Individual fining/thinning upward packages are 1-2 m thick and comprise rhythmic interlayering of mm-thick sandstone and mudstone laminae. These units commonly fine upward from erosive based, fine-grained cross-bedded sandstone (30 – 40 cm thick) into heterolithic wavy and/or lenticular bedding (Fig 4.8A). Cross-bed foresets and parallel laminated sandstone are commonly draped by carbonaceous debris. The heterolithic packages more commonly thicken/coarsen upward from lenticular bedded muddy heteroliths at the base, into sandier wavy and flaser bedding at the top. The ripple lenses within the lenticular bedded intervals are fine-grained and millimetres-thick. The ripples have asymmetrical profiles and typically show opposing cross-lamination and lee dip orientations. However, some intervals show an apparent unidirectional ripple orientation. Load casts and synaeresis cracks are frequently found at the base of ripples.

Sand heterolith intervals are composed of rhythmic interlayering of thin sandstone layers and mud drapes. Wavy and flaser bedding is common and display rippled and cross-laminated sand layers which are usually 5-15 mm thick. Similarly, ripples are of a millimetres-thick fine-grained sand and are commonly asymmetrical (Fig 4.7C). Intercalated mud drapes are usually thin (millimetres-thick). The upper part of the FA4 facies association in Cendor-2 (Fig 4.7B) and Cendor-3A are sandier than the upper part of the FA4 in Jambu-3, which is muddier, with wavy and flaser bedding forming a thin layer at the top of the association (Fig 4.4B).

Ichnology: Bioturbation in FA 4 is generally absent (Ichnofabric Index 1), with rare intervals of sparse bioturbation (Ichnofabric Index 1-2) in the form of *Teichnichnus* (Cendor-2). However, some muddier intervals display a stronger degree of bioturbation in Jambu-3, at depth 1318 m (Ichnofabric Index 3-4) (Fig 4.4). Sparse bioturbation is discernible at the upper part of FA 4. Trace fossil assemblage in the muddier intervals of FA4 include *Palaeophycus, Rhizocorallium, Planolites, Terebellina*, and *Chondrites*.

Interpretation: FA 4 is interpreted as the deposits of within-channel, tide-influenced bars, based on the erosional base, predominance of current-generated facies and thick heterolithic bedding. Bars here refer to laterally migrating, within channel barforms including bank-attached point bars and lateral bars as well as bank detached tidal bars. Sharp-based erosional scours at the base of the FA4 interval, which are overlain by cross-bedded sandstone, indicate moderate energy erosion and deposition probably associated fluvial and/or tidal currents within a channel. Thick heterolithic sheets and ripple lamination, with intervals of bidirectional ripple orientations indicate significant tidal influence (Reineck & Wunderlich, 1968). However, there are also unidirectional intervals, which may be explained by channel mutual evasion, which is common in tide-influenced channels, or periodic fluctuations in tidal influence, resulting in more fluvial-dominated, tide-influenced successions (Nio & Yang, 1989, 1991; Reineck & Wunderlich, 1968).

Fining upward heterolithic intervals are common components of tide-influenced channels, where they typically represent the deposits of laterally or vertically accreting barforms, e.g., point bars, lateral bars and/or within-channel tidal bars. Coarsening upward heterolithic packages have commonly been interpreted as the deposits of frontally accreting/prograding bar forms, such as mouth bars or delta fronts. Interestingly, the pattern of alternating coarsening and fining upward heterolithic packages observed in FA4 is also observed in cores from the tide-influenced distributary channels of the modern-day

Fly River Delta of Papua New Guinea (Dalrymple et al., 2003). Here, the coarsening upward patterns were explained by the common deposition of thick fluid muds at the base of distributary channels due to the high suspended sediment concentration, with mud drapes becoming thinner upward. The alternating thickening and coarsening upward pattern probably reflect within channel bar migration, with thicker mud being concentrated in the channel axis.

The general absence of bioturbation throughout most of the thickness of the FA4 succession is consistent with strong fluvial influence and a mainly freshwater setting (Dalrymple & Choi, 2007; MacEachern & Bann, 2008). The presence of an impoverished marine ichnofauna at local intervals is consistent with short periods of marine influence and brackish water incursion. A low degree of bioturbation of the FA4 in Cendor-2 and Cendor-3A suggest a proximal location, while strong bioturbation in the muddier variant of FA 4 in Jambu-3 represents a bar developed in a more distal location, away from main fluvial input.

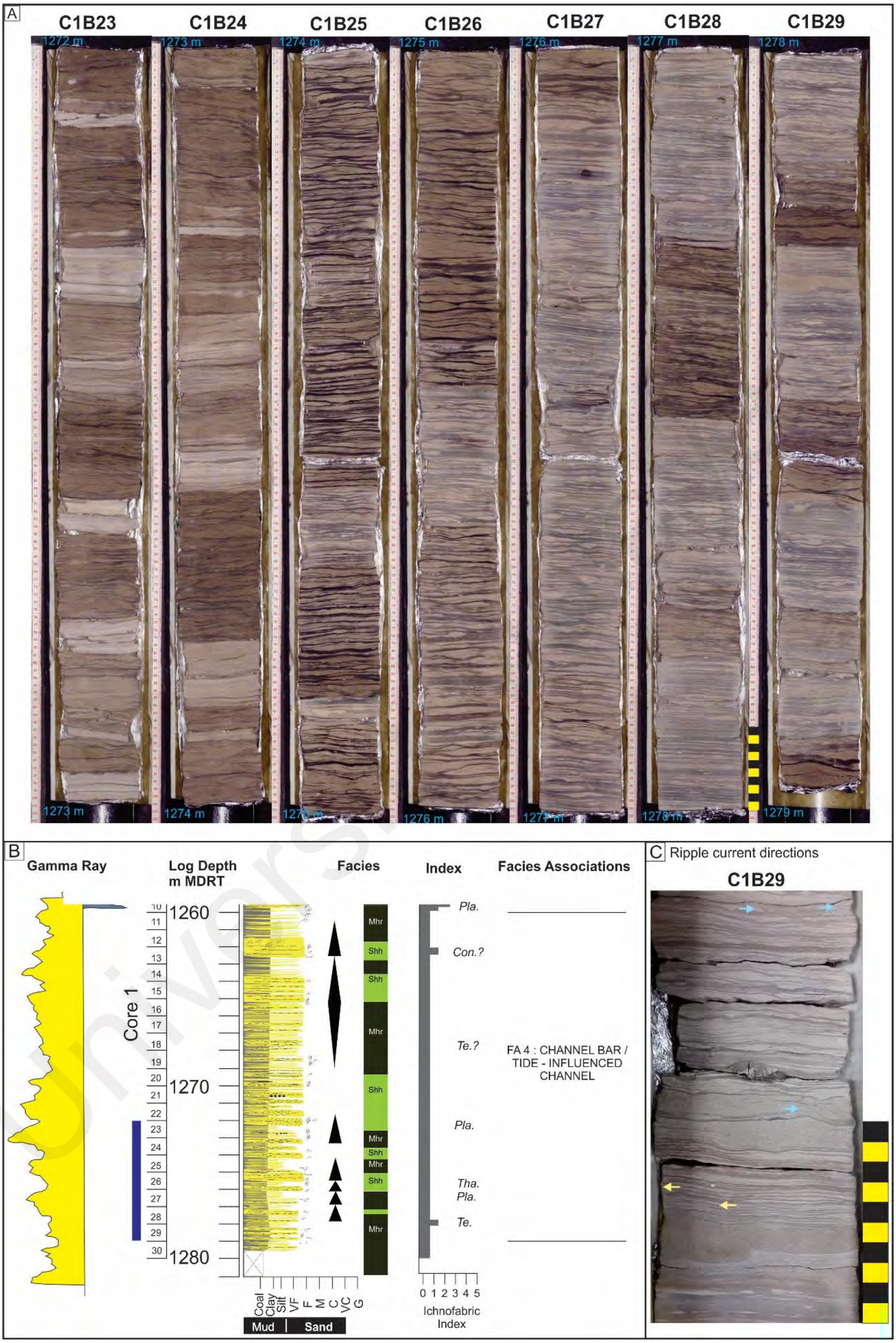

Figure 4.7: Lower section of the Channel/ Channel Bar Facies Association (FA 4), H15-H20 interval, well Cendor-2, Malay Basin.

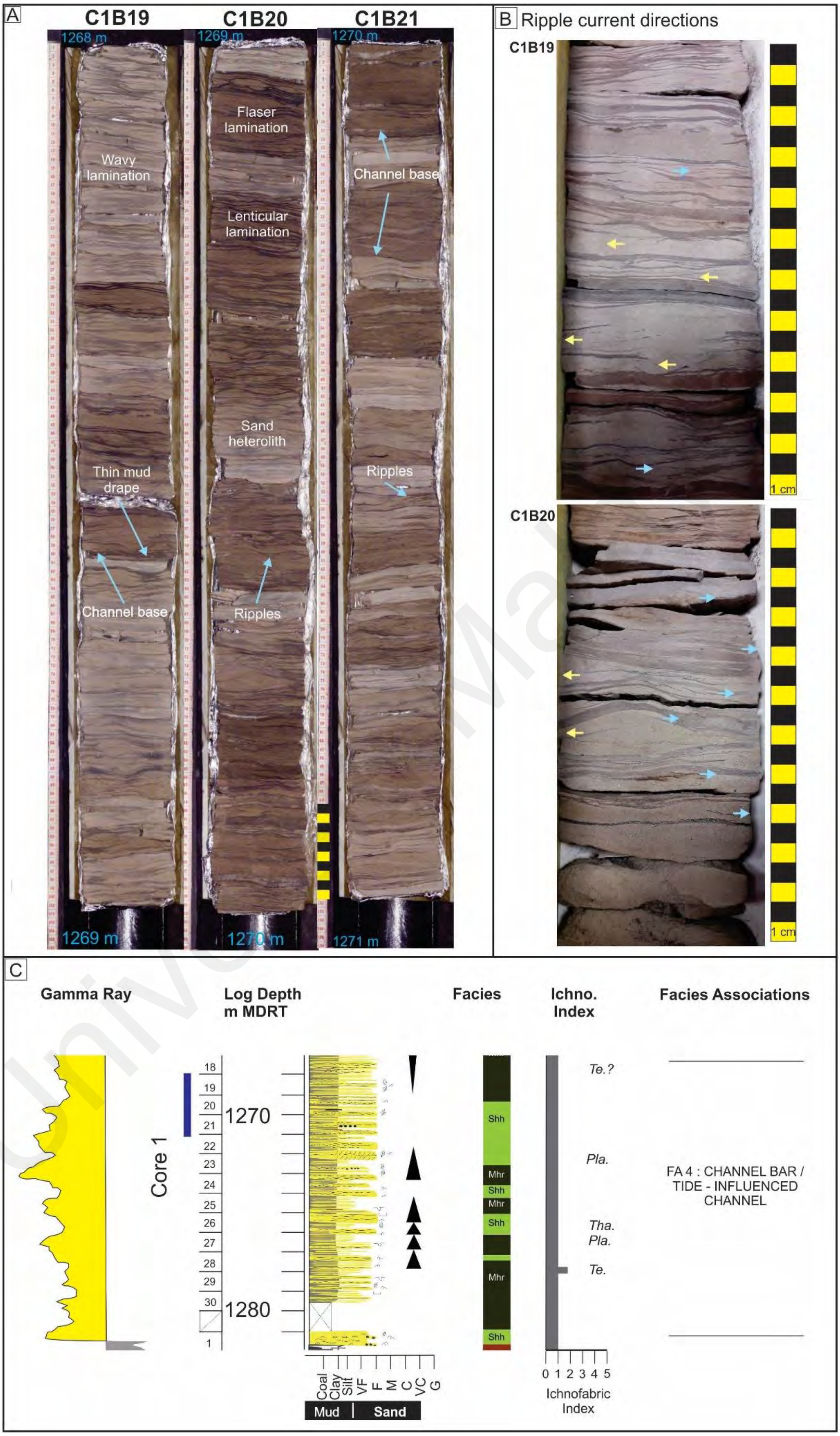

Figure 4.8: Upper section of Channel / Channel Bar Facies Association (FA 4), H15-H20 interval, well Cendor-2, Malay Basin.

FA 5: Mouth Bar Facies Association

Sedimentology: FA 5 is represented by a single example from Cendor-3A well. FA 5 forms a 4 m thick succession which coarsens and thickens upwards from sand heterolith into sandstone (Fig 4.9). Heterolithic intervals contain well-developed wavy and flaser bedding. Sedimentary features (ripples) display apparently bidirectional currents. The sand heterolithic unit coarsens upwards into an approximately 3 m thick package of sandstone displaying low angle planar and trough cross-bedded sandstone. Dewatered and slumped, cross-bed foresets are often mud draped and/or lined by carbonaceous debris.

Ichnology: Bioturbation is sparse to absent (Ichnofabric Index 1-2), and when present, is in the form of sporadic occurrences of *Palaeophycus*. Some of the carbonaceous foreset drapes display a ‘chewed texture’ reflecting ambiguous bioturbation.

Interpretation: FA 5 is interpreted as the deposit of a tide-influenced mouth bar, based on the predominance of current-generated bedforms, mixture of possible fluvial and tide-generated facies, coarsening upward vertical trend and absent to impoverished marine ichnofauna. Heterolithic bedding with sporadic, apparently bidirectional current indicators support tidal influence (similar to FA4). The thick coarsening upward trend from heteroliths into cross-bedded and planar laminated sandstone is interpreted as representing downward accretion or progradation of a tidal barform (e.g., Yang, 1989; Berné et al., 2002). This pattern was also seen in bars in the tide-distributary channels of the modern-day Fly River Delta of Papua New Guinea (Dalrymple et al., 2003) and in the Neoproterozoic Jura Quartzite (Levell et al., 2020). The thick cross-stratified succession is also common in tidal deposits, especially in the shallow marine environment (Colella & D'Alessandro, 1988; Nio & Yang, 1989; Longhitano, 2011). The presence of parallel-laminated or wavy, millimetres- to centimetre-thick mud beds within intervals of ripple cross-laminated sandstone is indicative of low flow velocity periods in the trough of the dunes during tidal-current reversals. The ripples locally show apparent bidirectionality in the form of opposing ripple orientation, suggesting opposing tidal currents. Ripple cross-lamination, cross-bedding and planar lamination are current-generated bedforms which can be deposited by both fluvial and tidal currents. The presence of cross-bedded sandstones indicates sufficient current flow to produce subaqueous dunes (Baas et al., 2015). The general absence of bioturbation, with only sporadic occurrence of marine trace fossils is consistent with a fluvial-dominated, stressed (brackish water?) tide-influenced setting.

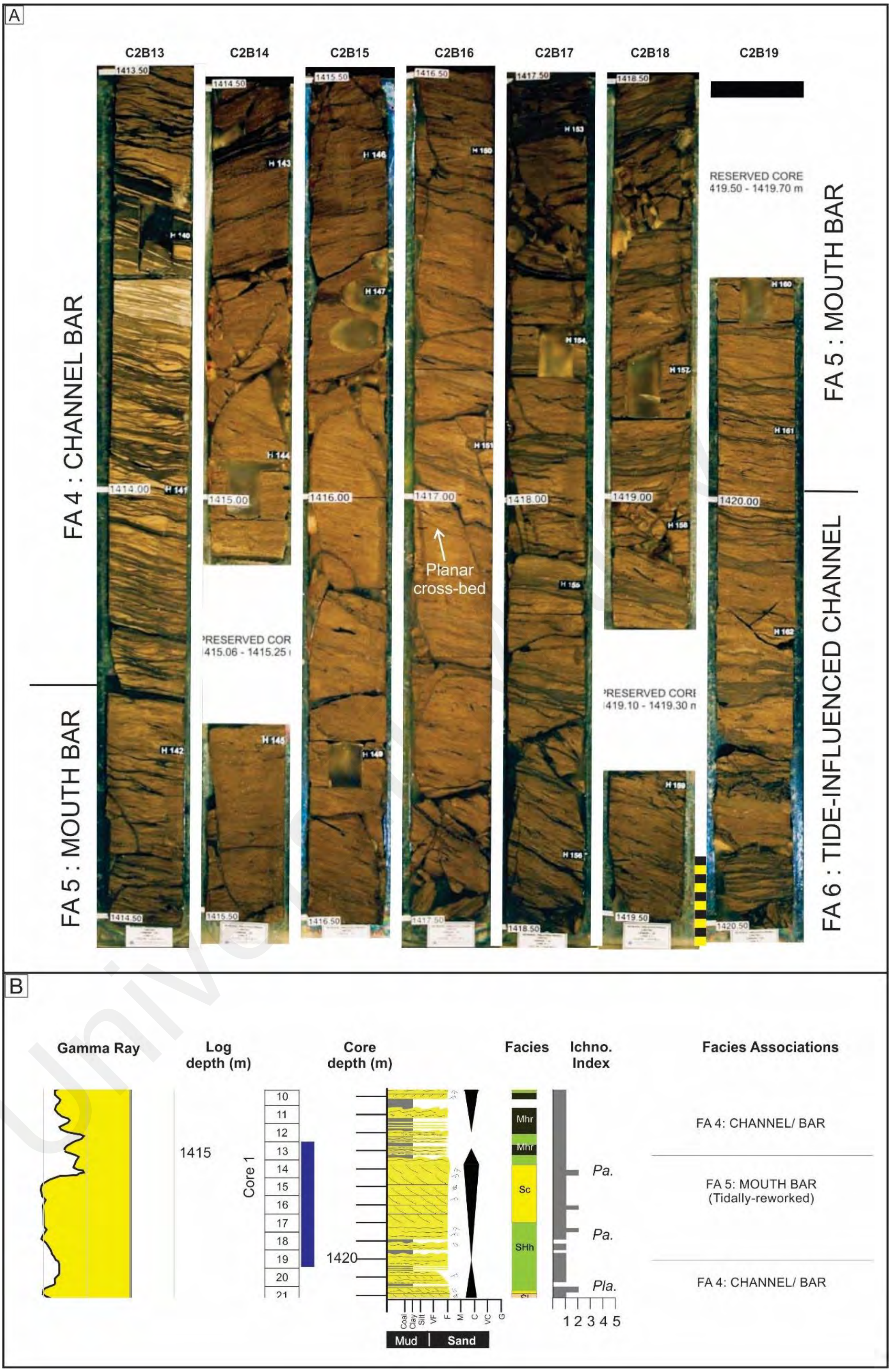

Figure 4.9: Mouth Bar Facies Association (FA 5), H15-H20 interval, well Cendor-3A, Malay Basin.

FA 6: Mangrove/Overbank Facies Association

Sedimentology: FA6 is dominated by light grey-coloured, rooted mudstone with associated small coal clasts. An up to 4 m thick carbonaceous mudstone marks the base of the cored interval of Cendor-2 well (Fig 4.10B) and up to 3 m thick at the upper section of the same well. At one interval, the mudstone is mottled light grey to dark grey. Thick rooted mudstone with rounded coal clasts dominates in the upper section of the facies association. The coal seam intercalated between the rooted mudstone is thin (<1 m thick) and is impure, with mixed carbonaceous mudstone. Subtle lamination is preserved at the base of the facies association, which is increasingly disturbed and destroyed (broken beds) in the upper section by bioturbation. Brownish, possibly iron oxide, concretions are present near the base of the facies association.

Ichnology: Bioturbation ranges from absent (Ichnofabric Index 1) to intense. Intense bioturbation is mainly in the form of general mottling, which has destroyed primary sedimentary structures. Visible trace fossils are mainly represented by rootlets at the top of FA6 and *Planolites* associated with sparsely bioturbated intervals.

Interpretation: The predominance of fine-grained facies indicates a low energy setting, with deposition mainly through suspension fallout and/or low energy currents. Roots indicate vegetation and periodic/prolonged subaerial exposure. Preservation of sand laminae indicates occasional higher energy periods, reflecting regular alternation of high energy tidal currents and low energy slackwater periods within a protected tidal environment. Abundant organic material in the mudstone further suggests proximity to or in a densely vegetated environment. Broken beds within the mudstone could be the effect of mangrove roots. It is likely that FA 6 represents mangrove swamp deposits. This interpretation is consistent with record on depositional of Group H sediments indicate the climate still everwet, and coal occurrences across the Malay Basin indicative of widespread peat mangrove swamps (Yakzan et al., 1996; Morley et al., 2021). A mangrove interpretation is consistent with the close vertical association of FA6 with tide-influenced channel/bar -fill deposits in the upper section of Cendor-2 well, which indicates that some intervals may represent supratidal/intertidal vegetated floodplains.

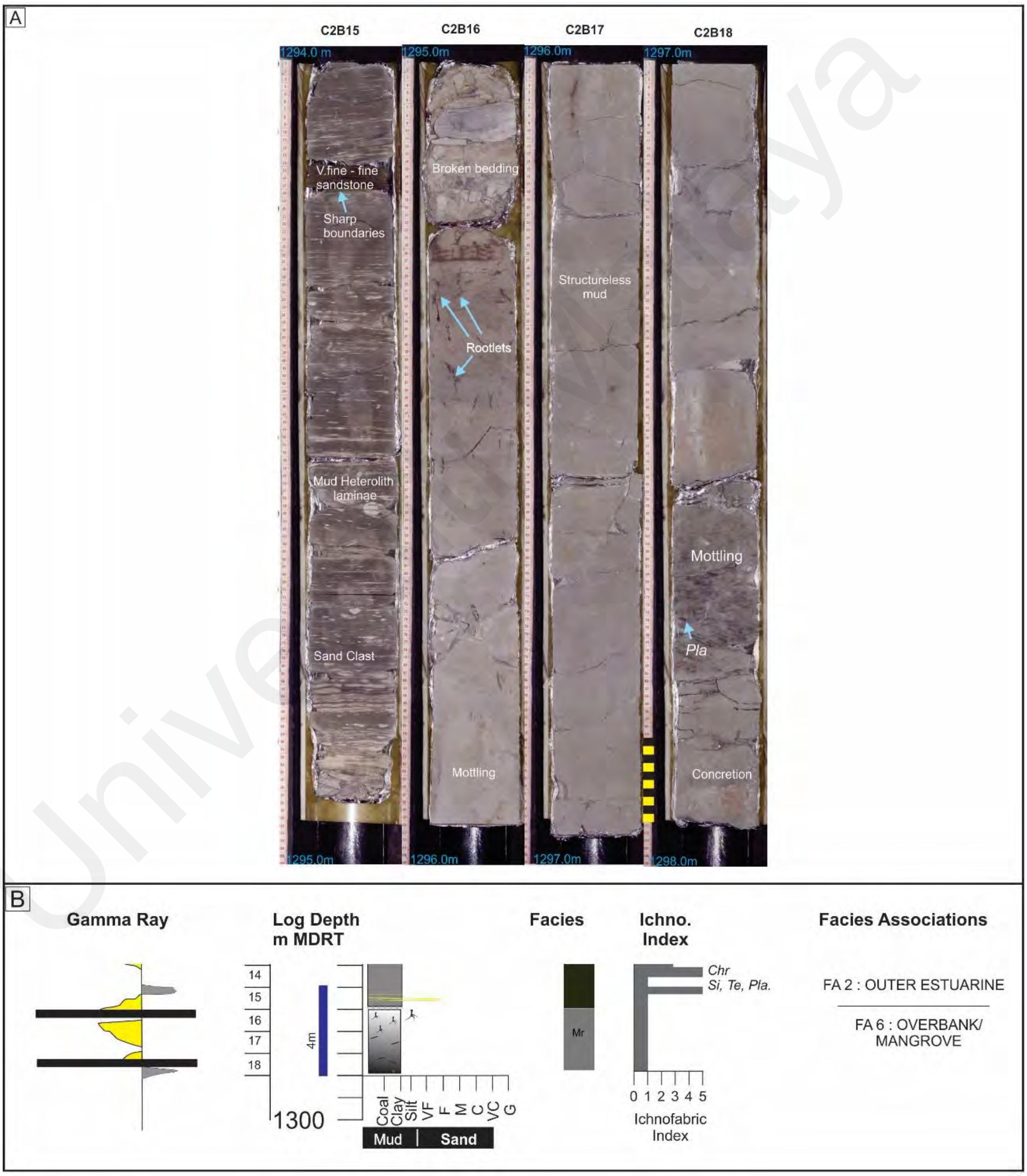

Figure 4.10: Overbank/Mangrove Facies Association (FA6) overlain by FA2 from well Cendor-2, H15-H20 interval of the Malay Basin.

4.5 Discussion

4.5.1 Tidal Signatures

Tidal indicators are formed as the result of interaction between tidal currents and the sediment bed. These include tidal rhythmites which comprise cyclical stacking of mud and sand laminae of varying thickness (Reineck & Singh, 1973; Kvale et al., 1989; Dalrymple et al., 1991), tidal bundles of vertical or cross-stratified beds recording variations in flow velocities in a neap–spring cycle (Visser, 1980), reactivation surfaces which are minor erosional contacts between successive migrating bedforms produced by flow reversals (Klein, 1970). Heterolithic bedding comprises interlayered sand and mud, which are manifested as flaser, wavy and lenticular bedding, subject to the sand and mud ratio within the interval succession, and mud-drapes produced through suspension fallout during slackwater periods in between ebb and flood tidal currents.

There are several tidal sedimentary features which were observed in the studied cores. Preservation of these tidal signatures ranges from moderate to good and includes cross stratification, rhythmites packages of thin fine-grained lamination, heterolithic strata in the form of lenticular, flaser, and wavy bedding, mud-drapes, synaeresis cracks and low diversity, impoverished marine trace-fossil assemblages.

Based on these tidal signatures, the study area and stratigraphic interval are interpreted to have been located within a tide-influenced coastal area. In well Cendor-2, thick heterolithic successions (up to 24 meter- thick), cross-beds with mud drapes, bidirectional paleocurrent indicators in the studied interval suggests significant tidal influence (Reineck & Wunderlich, 1968; Davis & Dalrymple, 2012; de Boer et al., 1989). The upward decrease in mudstones and increasing sand content indicate an upward increase in tidal energy on the delta front, with the development of tide-influence distributary channel bars and distributary mouth bars. The upper part of the succession showing low tidal current energy was dominated by suspension fallout.

The Cendor-3A succession also records similar evidence of overall upward increase in sandstone and decrease in mudstone. The heterolithic packages, representing channel bars and distributary mouth bar facies associations, are up to 20 m thick, and probably reflect deposition in a more axial position of a tide-influenced area with significant fluvial influence. Sedimentary features such as herring-bone cross-lamination, thin mud drapes and ripples with opposing orientations record possible tidal deposition.

A higher degree of bioturbation observed in the FA 1 and FA 3 of the Jambu-3 well succession suggests a more distal position in the depositional system, away from main fluvial input, and may also indicate a position below fair-weather base, i.e., a position further offshore.

The low diversity, but low to highly abundant, impoverished marine trace-fossil assemblages consisting of elements of the *Cruziana*, *Skolithos* and *Glossifungites* ichnofacies, are consistent with a stressed, brackish water, tide-influenced setting (Pemberton & Wightman, 1992). Synaeresis cracks demonstrate varying salinity levels in the water, which means both saline and brackish water co-existed in the system (Burst, 1965; Pemberton & Wightman, 1992).

Nevertheless, the interpretation of tidal influence based on sedimentary features should be made with caution as many similar sedimentary structures can also be produced by river or wave processes. For instance, heterolithic alternating of sand and mud layers may also be linked to seasonal fluctuations in river discharge, alternation between storm and fair-weather conditions as well as basin plain/channel levee thin-bedded turbidite deposition (e.g., Cain & Mountney, 2009; Jablonski & Dalrymple, 2016). Synaeresis cracks may be confused with desiccation cracks, where they are merely the result of alternating wet and dry conditions. These conditions are common in the transition zone of fluvial-tidal channels, which are prone to river processes. However, the combination of rhythmites, thick heterolithic bedding, bidirectional current indicators, rooted horizons, and an impoverished marine trace fossil assemblage provides strong support for a fluvial-dominated, tide-influenced coastal setting.

4.5.2 Stratigraphic Architecture

Figure 4.11 shows a correlation between Cendor-2, Cendor-3A and Jambu-3 for the interval between the top H20 Flooding Surface and top H15 Flooding Surface, referred to here as the H15-H20 interval. The correlation is based on core facies integrated with calibrated gamma-ray logs. The top H20 FS is marked by a thin coal overlying a package of coastal plain rooted mudstone and can be traced in all three wells. The surface is then overlain by a 5-8 m thick, muddy heterolithic interval interpreted as channel abandonment/ outer estuarine (FA2). Channel abandonment / estuarine deposits (FA2) are immediately overlain by a thick (1 -11 m) prodelta mudstone succession (FA3) which can be identified in all three wells. A sharp boundary which is represented by a bored siderite horizon in between FA2 at depth 1293 m in Cendor-2 well. A second bored siderite surface overlies the first one and separates thick prodelta deposits from underlying outer estuarine deposits, which is marked at depth 1291m in Cendor-2 well. This surface can also be correlated with the other two wells, where they are identified based on a sharp deflection of the Gamma Ray log from low to high readings. These horizons show a moderate to high degree of bioturbation (Ichnofabric Index 4-5) between these FA2.

A 3 - 24 m thick multistorey sandstone and heterolithic succession abruptly overlies the prodelta mudstone succession in all three wells. At wells Cendor-3A and Cendor-2, this sharp boundary is marked by an erosional surface (referred to as the Base H15 Reservoir surface in Fig, 4.11). The multistorey succession overlying the Base H15 Reservoir surface at Cendor-3A, and Cendor-2 is composed of stacked, coarsening and fining upward, within-channel, tide-influenced bar deposits (FA4). Coastal plain overbank / mangrove /swamp mudstone and coals cap the H15-20 core interval in the Cendor-3A and Cendor-2 wells. The stratigraphy of well Jambu-3 is slightly different compared to the Cendor wells. Here, the contact between the thick prodelta mudstone and overlying heteroliths is gradational. The overlying heteroliths are also more mud-dominated, with thick bioturbated mudstone intervals. The trace fossil assemblage has a higher diversity and is more marine-influenced. There is also no coal cap in the Jambu-3 heterolithic succession.

Interpretation: The channel abandonment or outer estuarine interval (FA2) directly overlying the top H20 FS is interpreted as transgressive estuarine deposits, based on the sharp landward facies shift from coal-capped coastal plain deposits underlying Top H20 flooding surface into more distal channel abandonment / estuarine deposits which overly the Top H20 flooding surface. The bored siderite horizon separating estuarine deposits is interpreted as a possible flooding surface and condensed section, indicating a period of quiescence and depositional hiatus. The successive bored siderite horizon is interpreted as an Intra H20 Maximum Flooding Surface, which marks facies shift from transgressive to regressive deposits. The overlying prodelta deposits represent the progradational deposition during the regressive phase. The Jambu-3 interval is slightly different, with a more mud-dominated heterolithic succession overlying the prodelta mudstone, and no coal capping the heteroliths.

In Cendor-2 and Cendor-3A the sharp contact between prodelta mudstone and tidal heteroliths can be interpreted in two ways. Firstly, the erosional surface may represent a subaerial unconformity, with the overlying, multistorey, tidally influenced heterolithic succession representing the fill of an incised valley. In this model, the tidal barforms were elements of a tidally influenced estuary depositional system.

Secondly, the surface may represent a tidal ravinement surface (Fig 4.12). In this second model, the stacked bar deposits were the infill of tide-influenced distributary channels associated with a tide-influenced/dominated delta system, with the underlying prodelta succession being genetically related. Deep scouring (up to 30 m) of tidal distributaries have been reported from modern-day tide-influenced paralic systems, e.g., the Mahakam Delta of Indonesia and the Fly River Delta of Papua New Guinea and Brunei Bay (Allen & Chambers, 1998; Razak Damit, 2001; Dalrymple et al., 2003). The gradational contact between prodelta and overlying heteroliths observed at Jambu-3 suggests a location away from the main distributary channels. The higher degree and diversity of bioturbation is also consistent with a more distal, tide-dominated, inter-distributary location.

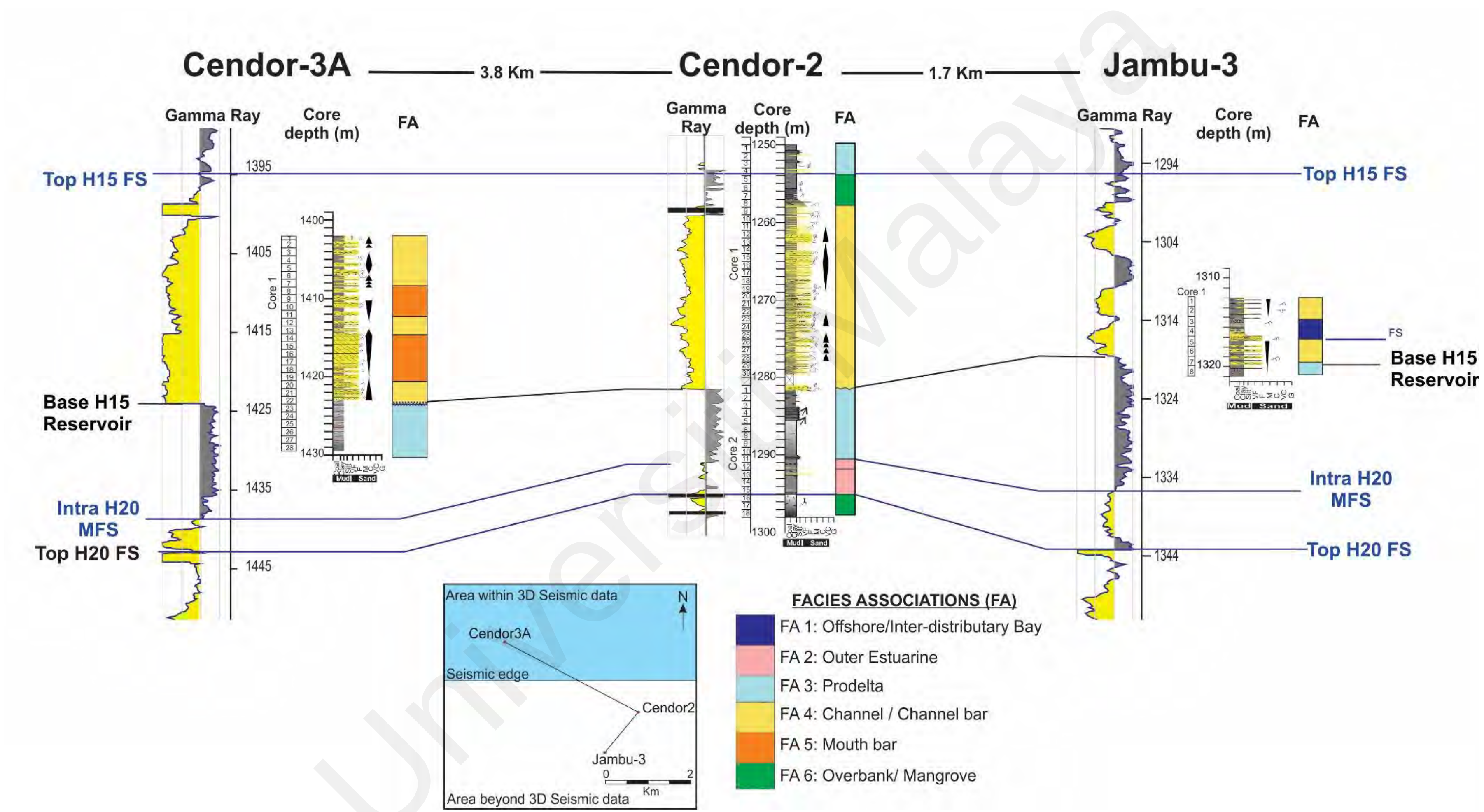

Figure 4.11: Lithostratigraphic correlation scheme for the H15-H20 interval based on three wells integrated core data and gamma ray available in this study. Only Cendor-3A well is within 3D seismic data (blue box), whereas the other wells are near the seismic boundary (white box).

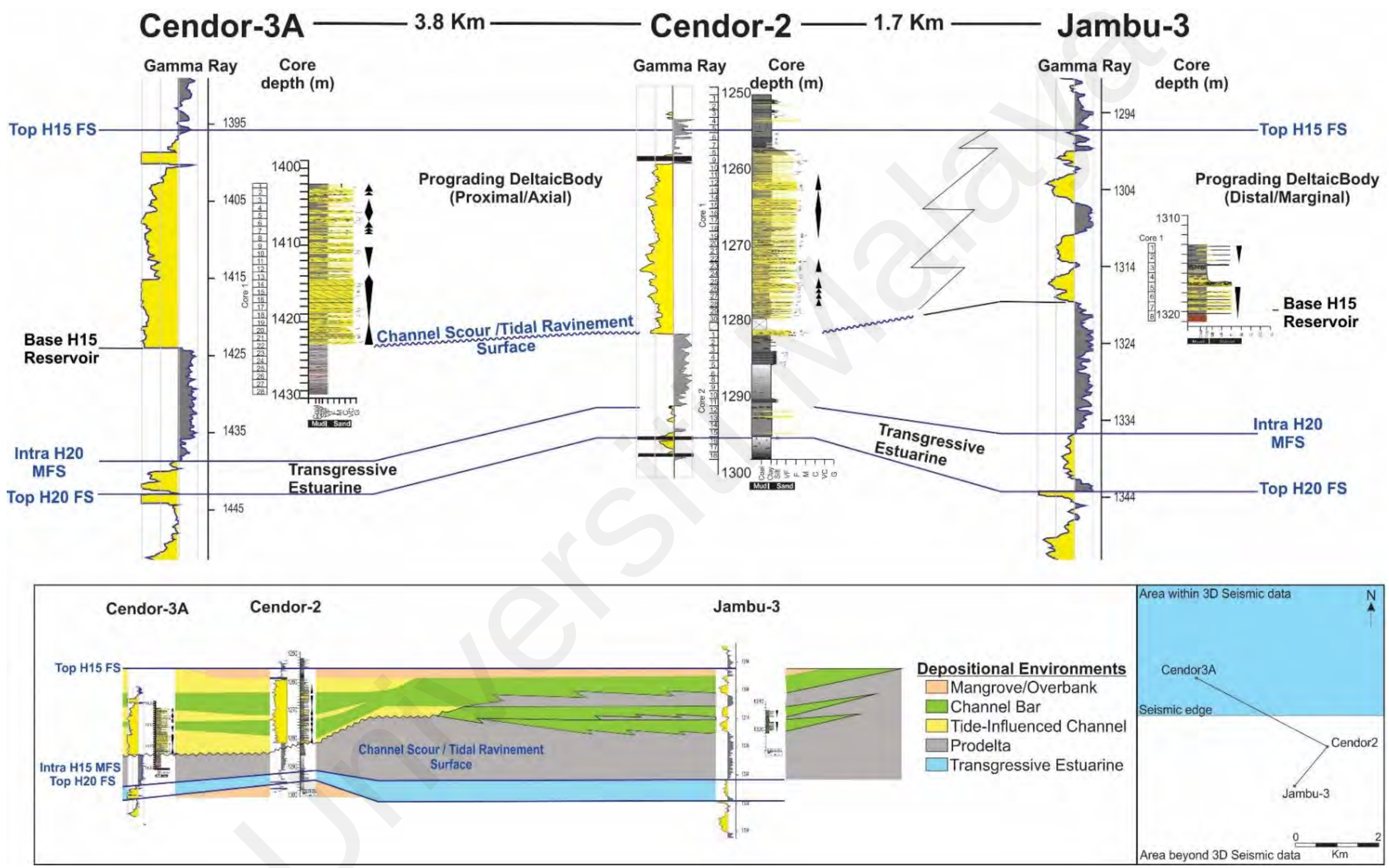

Figure 4.12: Correlation scheme of H15-H20 interval based on three wells integrated core data and gamma-ray available in this study. Only Cendor-3A well is within 3D seismic data (blue box), whereas the other wells are near the seismic boundary (white box). Interpretation as inherently connected facies succession comprises of tide-influenced to tide-dominated delta system. The erosive surface interpreted as a tidal ravinement surface.

4.5.3 Depositional Model

A depositional model for the studied core and well interval (H15-H20 interval) in the Jambu and Cendor fields is constructed here based on the core description, calibrated gamma ray logs and correlations. The model will then be used with the H Group in general and integrated with 3D seismic in order to reconstruct the palaeogeography and understand the geomorphology of the studied area in the Malay Basin.

The constructed model must explain the following sedimentary features: (1) the predominance of mixed fluvial and tidal facies; (2) the presence of paralic depositional elements such as prodelta mudstone, outer estuarine/abandoned channel deposits and within channel, tide-influenced barforms, and (3) the presence of a marine ichnofauna with varying degrees of diversity and bioturbation intensity.

The system was definitely paralic or marginal marine in nature due to the presence of facies deposited by fluvial and marine (tidal) processes. The range in degree of bioturbation from none to sparse and moderate and the impoverished nature of the marine ichnofauna are also consistent with a marginal marine environment, with different locations experiencing different levels of salinity and fluvial influence. The mixture of fluvial and tidal facies associations may be representative of a fluvial-dominated and tide-influenced, or tide-dominated and fluvial-influenced setting (Ff to Tf on plots in the classification scheme of Ainsworth et al., 2011 and Vakarelov & Ainsworth, 2013). The vertical trend from prodelta mudstone into overlying fluvial-tidal sandstone and heteroliths is consistent with a progradational delta succession, with the coarser heterolithic facies representing parts of the delta plain and delta front. Observations of modern-day tide-influenced and tide-dominated deltas also show that tidal heterolithic facies tend to be restricted to proximal settings on the delta and are typically absent from the deeper prodelta (e.g., Dalrymple et al., 2003; Lambiase et al., 2003). Metre-thick, coarsening and also fining upward tidal heterolithic successions are interpreted as tidal barforms developed within distributary channels. Channel bars usually form elongate, narrow sand forms that are oriented parallel to the prominent tidal flow direction (e.g., Willis, 2005). The bars may either be attached to the channel banks and form lateral bars or point bars, depending on the channel sinuosity, but can also form isolated “islands” in the middle of channels, i.e., elongate tidal bars. Continued lateral migration of channels and bars, combined with deep tidal scouring and subsidence, will produce a thick multistorey, heterolithic succession. Similar alternating fining and coarsening upward heterolithic successions are also observed in the distributary channels of the modern-day Fly River Delta (Dalrymple et al., 2003), where thick fluid mud can be concentrated at the base of channels. Sandier, coarsening upward packages are interpreted as distributary mouth bar deposits, and developed at the mouths of active tide-influenced distributary channels (e.g., Allen & Chambers, 1998).

The mangrove/coastal-plain facies association represents low energy areas on the delta plain away from the main distributary channels. Tidal heterolith packages overlying the erosion surface are interpreted to have been deposited in laterally migrating tide-influenced distributary channels. These tidal heterolith deposits indicate amalgamation of the tide-influenced channel fill deposits. Mud heterolith dominated successions represent the infill of abandoned distributary channels, less active, relatively low energy distributary channels, and/ or laterally migrating channels that drain lower delta plain / outer estuarine section. Alternating sand heteroliths may be the result of high fluvial discharge, and strong tidal currents eroded the delta front sand.

Tidal heteroliths and underlying prodelta mudstone at the base of Cendor-2 and Cendor-3 form a genetically connected facies succession, which represent laterally adjacent sub-settings within a larger scale depositional environment (Fig. 3.12). The vertical change upward from prodelta mud into the channel with tide-influenced bar, mouth bar, and tide-influenced channel deposits capped by mud overbank and coals is interpreted as representing a gradual shallowing characteristic of a prograding shoreline, i.e., a delta.

It is challenging to interpret the abrupt facies shift from prodelta mudstone into tide-influenced channel and bar deposits observed in Cendor-2 and Cendor-3A wells, which is marked by an erosional surface (Fig 4.13b). Ideally, prograding delta successions gradually coarsen upward from muddier sediments. However, in this scenario, the sharp boundary may indicate either autocyclic channel base scouring related to distributary abandonment and tidal ravinement, and/or sediment bypass during erosion at the base of mobile, lateral migrating of distributary channels. Strong tidal currents would have transported finer muds seaward of the proximal delta front (Dalrymple & Choi, 2007).

A ravinement surface is produced because of channels migrating across and cutting into underlying inner-estuary tidal flats during delta abandonment. Distributary abandonment will produce a transgressive succession due in decreasing fluvial input but increasing tidal influence (Dalrymple & Choi, 2007). The erosion surface in Cendor-2 and Cendor-3A was probably associated with an abandoned distributary channel, which, similar to tidal scour (up to 30 m deep) has been described from an abandoned distributary channel of the tide-dominated Fly River Delta in Papua New Guinea (Dalrymple et al., 2003) as well as in Brunei Bay (Razak Damit, 2001).

The stratigraphic succession of the H15-H20 interval in Jambu-3 well is slightly different compared to the Cendor wells. The Top H20 FS coal marker and overlying exhibits a typical gradual coarsening upward pattern from prodelta into tidal heterolith deposits. This thin package is laterally correlated to the thick multi-story tidal deposits in Cendor-2 and Cendor-3A wells. The absence of an erosion surface and thinness of the heterolithic package in Jambu-3 may due to the location of the well, which was probably located in a more distal location away from distributary channels, e.g., inter-distributary bays or delta front margin.

The thick layers of mudstone observed in the studied successions may represent fluid mud deposits. Fluid mud deposits are typically more than 10 mm thick and homogeneous. This minimum thickness is rather subjective but has been used to differentiate these mass-flow deposits from slowly accumulating suspension deposits (Ichaso & Dalrymple, 2009). The interpretation of mud lamination styles in these successions is very difficult because of the complex interplay of high density of fine-grained sediments of sand and mud, sediment transport, erosion and depositional processes. For instance, sand and mud may be subdivided into laminae after deposition, as a result of particle interaction with the flocculation (Manning et al., 2010). This could change the conventional understanding of lamination as reflecting single tides, neap-spring cycles, seasonal effects, and riverine inputs. The layers of mud in the transition zone are due to individual grains settled from high-concentration suspensions over several tides. While grading is sometimes absent, they may be related to high-density suspension (MacKay & Dalrymple, 2011). Close-up analysis of each layer of mud shows additional fine grain size grading and colour shade because of darker organic material (Cendor-3A and Cendor-2).

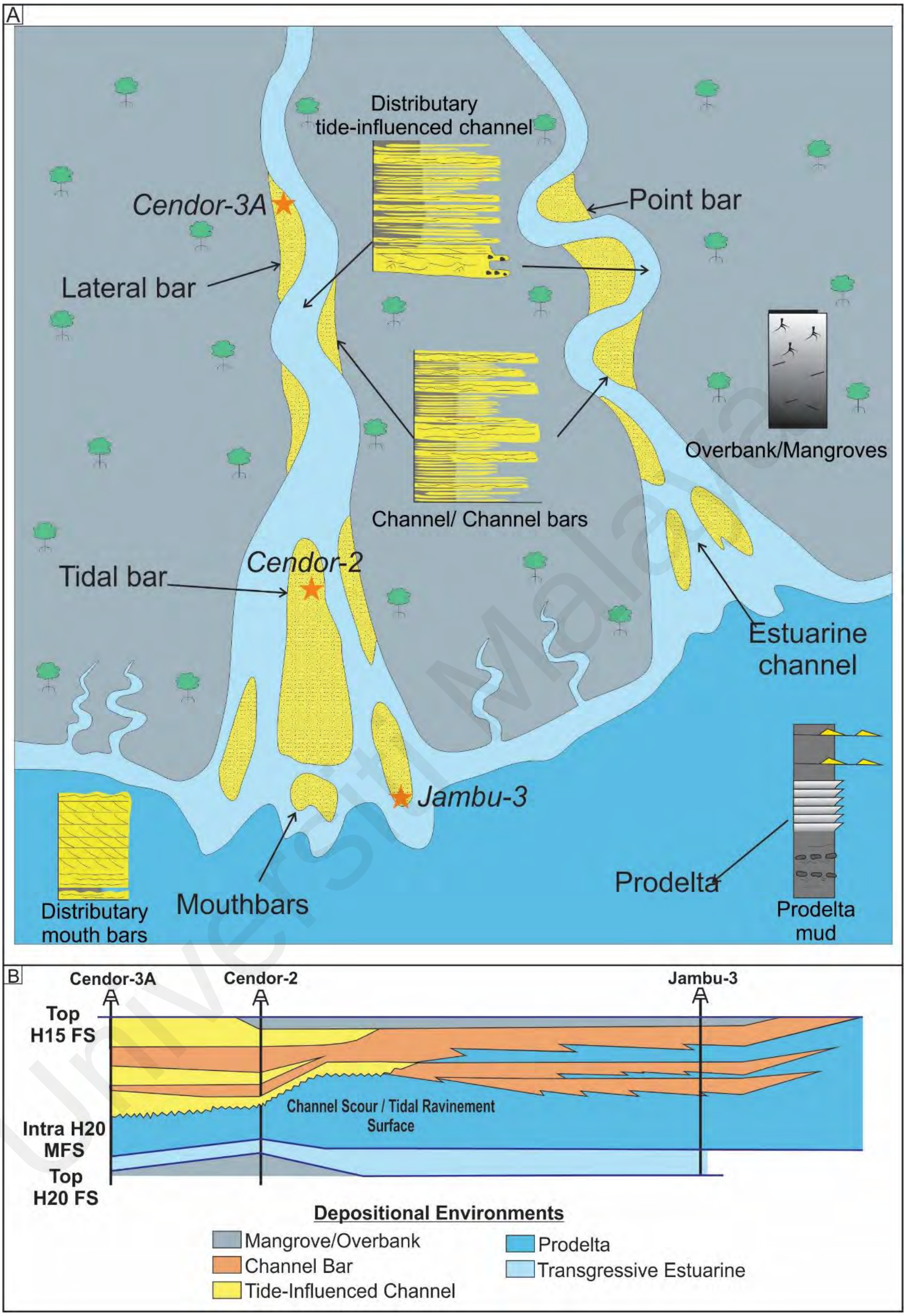

Figure 4.13: Interpretation of the H15-H20 interval in the study area as a tide-influenced/ tide-dominated delta system with deeply erosive tidal ravinement surfaces. Positioned of Cendor-2, Cendor-3A and Jambu-3 wells are likely located at the positions marked in orange color stars.

CHAPTER 5: ANALYSIS OF PARALIC GEOBODY GEOMETRIES AND ARCHITECTURAL ELEMENTS IN THE EARLY TO MIDDLE MIOCENE GROUPS I AND H OF THE MALAY BASIN

5.1 Introduction

Fluvial-tidal channels and tidal channels are important elements in both modern and ancient paralic depositional systems (de Boer et al., 1988; Dalrymple, 1992). Tidal channels often consist of a large tidal inlet channel, with smaller branching channels, which finally give way to tidal gullies and tidal creeks, usually in intertidal environments. The intricate branching patterns of tidal channel systems resemble fractal patterns, comparable to the fractal patterns of river networks (Stark, 1991).

The modelling of ancient tidal channel geobodies and prediction of their distribution, connectivity, and scale in the subsurface is very challenging, and is mainly based on outcrop analogue databases. There are few studies on the ancient tidal channel systems using seismic and well data. This study describes and analyses numerous subsurface seismic geomorphological features identified as fluvial-tidal channels, which were observed in a small sub-seismic area, at a depth of >1.5 km below the seafloor, in the Malay Basin. A range of dimensions for fluvial-tidal channel facies and geobodies have been identified. The spatial and temporal evolution of the depositional system has also been assessed, in particular, focusing on changes in channel geomorphology and dimensions, which are crucial for understanding channel stacking patterns and potential reservoir connectivity in order to build accurate, predictive 3D reservoir models.

This research integrates core (see Chapter 4), wireline (Gamma Ray) and seismic data. A statistical analysis of over 1000 measurements were made from over 120 measured channels. The interval of interest extends from near the base of Group I to near the top of Group H stratigraphic succession of the Malay Basin, which is a current focus of exploration and development activity.

Seismic attribute and frequency decomposition analysis of the 3D seismic volume was employed to identify a variety of seismic geobodies. The geobodies have been classified based on their width distributions and interpreted as fluvial-tidal distributary channels, tributary channels, tidal channels, and potential channel belts. To reconstruct the depositional history of the studied interval and area, an analysis of the spatial and temporal variation of these channel geobodies along with core and well log interpretations was used. Very-large-scale (VLC) channel geobodies >3000 m wide dominate in the bottommost interval of interest in Group I. Further up-section, the size of channels populated in each strata varies from large channel (LC), medium channel (MC), to small channel (SC). An overall decrease in the frequency of small- and medium-scale geobodies vertically through the succession has also been observed. The stratal stacking and architecture of channel geobodies in the Group H and Group I of the Malay Basin are likely to have been mainly controlled by autocyclic processes and transgressive-regressive cycles. Transgressive-regressive cycles in the Malay Basin are strongly influenced by the interaction between tectonic and sea-level fluctuation (Madon, 2011; Jirin et al., 2013).

5.2 Geological Background

The Malay Basin is one of the largest Tertiary basins on the northern Sunda Shelf of Southeast Asia, with an area of approximately 83,000 km^2 (500 km long by 250 km wide) (Fig 5.1). It is situated north of the Penyu and West Natuna basins and south of the Pattani Basin (Hutchison, 1989; Madon et al., 1999; Morley & Westaway, 2006; Pubellier & Morley, 2014) (Fig 5.1a). The basin has an elongate shape, with a NW-SE axial trend. The basin fill comprises a >14 km thick succession of Oligocene to Recent sediments. The Oligocene sediments are generally continental deposits with minor marine influence, while the Miocene to Recent sediments is mainly composed of coastal plain to shallow marine deposits (Madon et al., 1999). The vertical sedimentary succession is divided into seismic stratigraphic units, denoted as "Groups" which have been labelled alphabetically (Group A to M, from youngest to oldest) (Fig 5.2). This study focused on the sedimentary succession within the late Early Miocene to Middle Miocene stratigraphic units of Group I and Group H.

The Malay Basin has undergone three major Cenozoic tectonic events: 1) Late Eocene to Oligocene crustal extension with left-lateral shear and significant subsidence; 2) Middle to Late Miocene, north-to-south compression with inverse or right-lateral shear, folding, and inversion; 3) Pliocene to Recent regional thermal subsidence and minor extension (Hutchison, 1996; Ng, 1987; Ngah et al., 1996).

Miocene stratigraphic development of the Malay Basin was directly related to its structural evolution and thermal subsidence (Madon, 1999; Madon et al., 2006), which happened in three stages: (1) Pre-Miocene (Oligocene or early Miocene) extensional or syn-rift phase; (2) Early-Middle Miocene thermal/tectonic subsidence, followed by inversion of the basin, and (3) Late Miocene to Quaternary subsidence and tectonic quiescence.

Tidal range within the Early Miocene Gulf of Thailand as well as the West Natuna Basin was microtidal and capable of moving sand within the shallow north - west to south - east trending Malay Basin. Tides within the Early Miocene GOT were regulated by frictional damping rather than amplification (Collins et al., 2018). Based on the tide coverage area, rivers flowed seawards in a SE direction from the land region in the NW area.

There was a reduction in the tidal range during the Middle Miocene, from macrotidal to mesotidal along accessible coastlines in the western South China Sea (SCS), which is correlated to a decrease in shelf width from about > 250 to 200 km. Consequently, the trend of the river flow was likely from the hinterland in the NE to SE (seaward) direction.

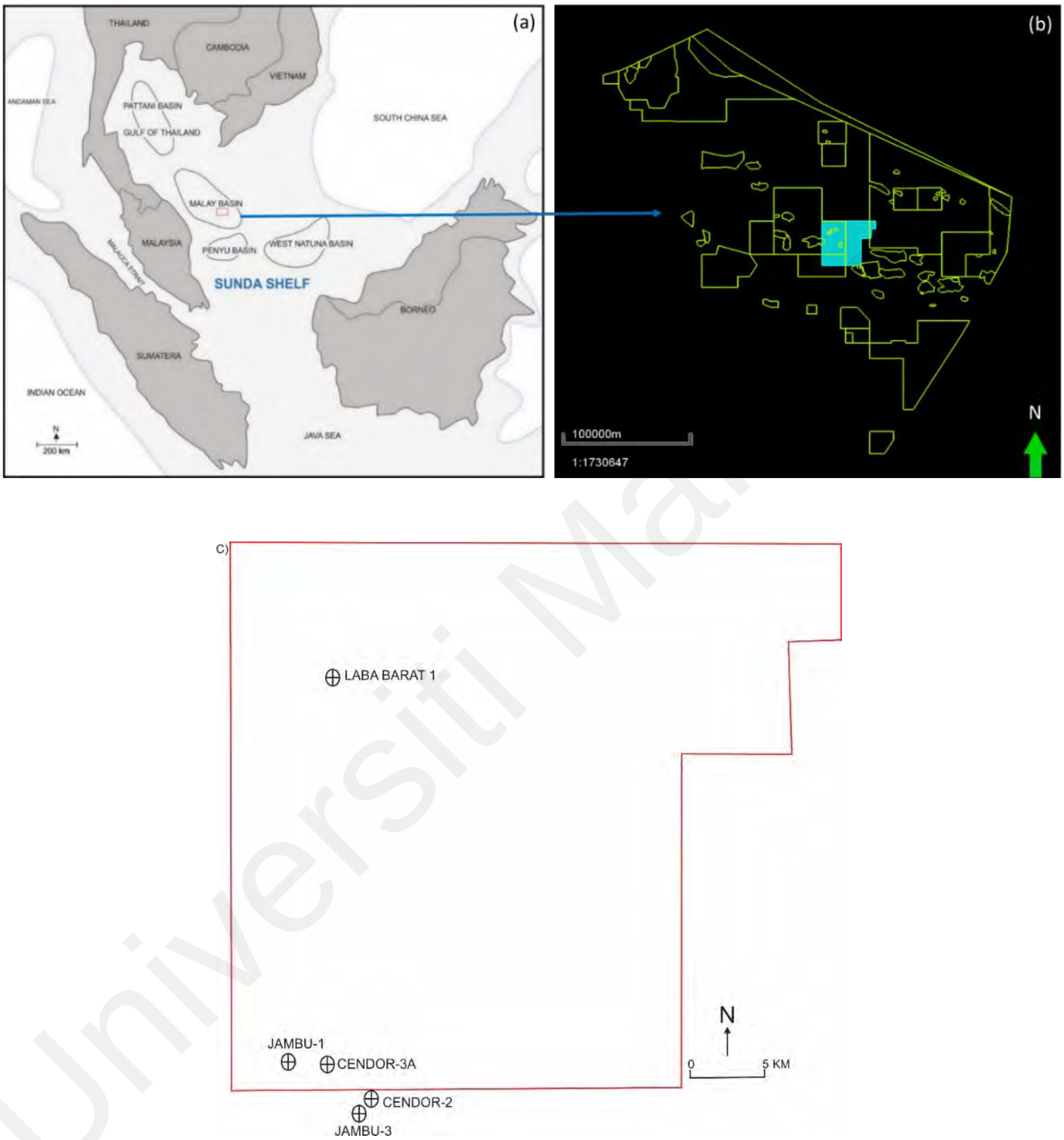

Figure 5.1: (a) Study area located in the Malay Basin on the Sunda Shelf, Southeast Asia (modified from Alqahtani et al., 2017), (b) Blue box marks the study area on the of Malay Basin and green polygons are the oil and gas operating blocks in the Malay Basin, (c) The red line polygon is an enlargement of the area marked in blue in (b), which bounds the 3D seismic and well data used in this study.

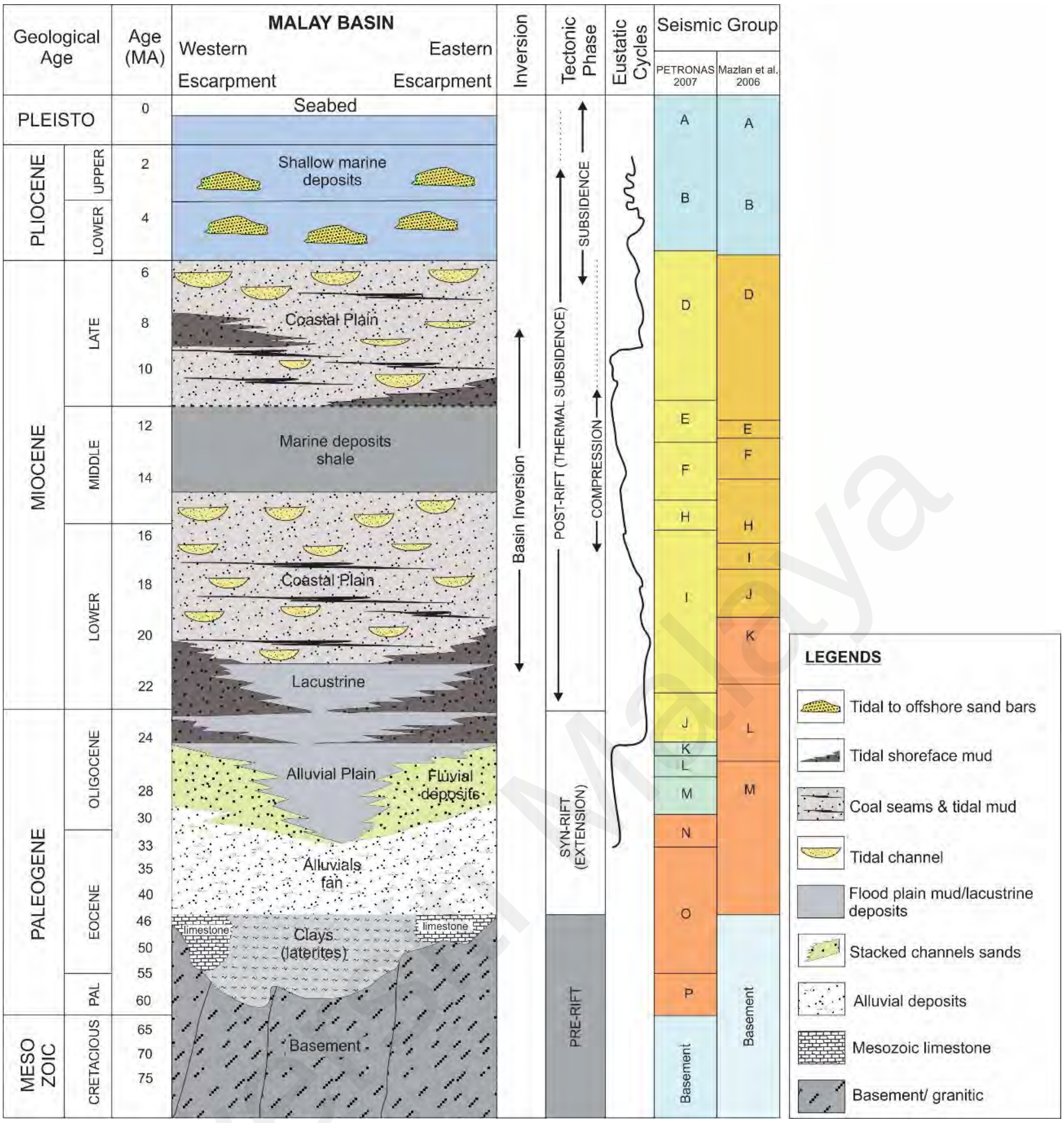

Figure 5.2: Chrono-stratigraphic framework of the Malay Basin (modified from Madon, 1999: Mansor et al., 2014), displaying Geological Age Range, Depositional Environment and Lithology, inversion events, local Tectonic Phases, Eustatic cycles (from EPMI, 1999) and Seismic groups, schematically represented on seismic sections.

5.3 Dataset and Methodology

Petroliam Malaysia Berhad (PETRONAS) provided permission and access to data used in this study. The dataset comprises a high-quality 3D seismic dataset (1563 km^2) (Fig 5.1c) located in the middle of the Malay Basin. The seismic dataset is used together with the core and well log dataset described in Chapter 4. The interval studied in this work is within Groups H and I (see Chapter 4 for detailed facies analysis of Group H). The 3D seismic dataset, incorporated with well log and core data, were used to analyse the channel geobody geometries of the Group I and Group H of the Malay Basin (Fig 5.2).

The 3D seismic volume is a merged dataset of three surveys shot within the Malay Basin. The seismic data used were pre-stack migrated volumes. The data has been zero-phase converted during processing, and its output polarity convention is SEG standard polarity, which reflects an acoustic impedance downwards by a positive (peak) event (black seismic reflection on seismic segments). A negative (trough) occurrence (white seismic effect on seismic areas) is a downward decrease in acoustic impedance (Brown, 2004). The spacing of inline and cross-line in these surveys is 9.38 m and 12.5 m, respectively. The vertical period of sampling for all the samples is 2 ms. The prevailing seismic frequency contrasts from 50-70 Hz. Unfortunately, well data for this study is limited for calibration of well to seismic data, hence tying the depth to time.

Accordingly, measurements of depth and thickness were translated from the milliseconds two-way time (ms TWT) to metres (m) by applying velocity information (i.e., check-shot data) from a single reference well (Laba Barat-1) which contains this data. The average interval velocity in the Group H is 3240 ms^{-1}, and in the Group I is 3320 ms^{-1}, whereas the dominant frequency within these intervals is of 20 – 50 Hz (Table 5.1). This gives an average range of minimum vertical resolution is approximately 16 m, and the lateral seismic resolution is 32 m (e.g., vertical resolution = λ/4; horizontal resolution = λ/2) (Sheriff & Geldart, 1983; Brown, 2004). These measurements enabled a reliable identification and measurement with a high level of precision of comparatively small channel systems.

Table 5.1: Seismic resolution within an interval of interest in Group H and Group I of the Malay Basin

Tops Marker	Velocity (ms^{-1})	Frequency (Hz)	Wavelength (λ)	Vertical Resolution (λ/4)	Horizontal Resolution (λ/2)
Group H	3240	20-50	65-162 m	16-41 m	32-81 m
Group I	3320	20-50	66-166 m	17-42 m	33-83 m

Vertical seismic coverage of Malay Basin extends below the reference well (Laba Barat-1 at 2627m) penetration in the available dataset. However, the focus in this study was limited to slightly below the maximum depth of well penetration (Laba Barat-1) covering over the Group H and I succession. In this thesis, I use an application (Paleoscan ©) for semi-auto seismic interpretation in 3D to understand the seismic dataset.

This analysis is critical for understanding the range of channel dimensions that can be resolved using 3D seismic and highlights the critical issue of the varying scales of observation and levels of resolution between core, wireline log, and seismic data, which have to be carefully measured when using subsurface datasets. Besides, this resolution analysis is essential when defining and classifying the range of channels that can be imaged via seismic attribute analysis. The dimensions of individual channels, channel belts, channel belt complexes, and incised valley differ on several orders of magnitude.

These paralic fluvial-tidal channel targets in the Malay Basin have complex geobody architectures. Interpretations are often difficult because they are situated within syn- and post-rift basinal settings (deeper than 1.5 km), which are of low seismic resolution. Thus, the analysis and interpretation must be assisted by core and wireline-log data, which provide information on lithofacies to interpret depositional environments and measurement of sandstone and mudstone thickness. Width: thickness (W: T) ratios are often based on analogue data for different channel architectural elements.

Seismic-to-well tie was performed, where 3D seismic subset was tied to Laba Barat-1 borehole, which is time-depth, converted using check-shot surveys in order to utilise well tops of Group H and I markers from confidential in–house well reports. Markers within Group I and H in this study represent approximate regional "maximum flooding surfaces" (MFS) and "flooding surfaces" (FS). In addition, recently, Morley et al. (2021) termed theses markers as "sequence boundaries" of a series of transgressive-regressive cycles which considered to signify times of maximum basinward shift of facies based on the biostratigraphy studies in the Malaysian Basins. However, to avoid misunderstanding, these markers use in this study are best to represent MFS and FS according to the well logs of Laba Barat-1 and PETRONAS well reports.

These markers were used as references in interpreting the key surfaces on laterally continuous seismic reflection across the dataset and develop a localised stratigraphic framework in this study. Six (6) surfaces (Fig 5.8b) were mapped including near Top Group H, near Top H20, near Top H40, near Top Group I, near Top I20, and near Bottom Group I. The near Top Group H and near Bottom Group I surfaces define the top and base of the interval of interest for subsequent seismic attribute analysis. However, the maximum well control is only penetrated down to near Top I20 surface.

5.3.1 Seismic Attributes Analysis

For the seismic geomorphology analysis performed in this study, ten (10) iso-proportional slices (isoslice) (Fig 5.8c) were produced over a time frame of ~15 ms (approximately 15-20 m thick) conformant to six (6) primary key surfaces (Fig 5.8b). Each key surface serves as the top, and bottom horizons and these isoslices are parallel to stratigraphy. Four types of seismic attributes were analysed in this study i.e.: (1) Variance attribute which is similar to resemblance and coherence attribute contrasting trace-to-trace comparisons to maximize geological relief and surface discontinuity (e.g., faults); (2) Root Mean Square (RMS) attribute which denotes acoustic impedance assessment by enabling amplitude discrepancies to be observed, highlights channels, shifts in lithology, and bright spots; (3) The envelope attribute (similar to the instantaneous amplitude attribute), which is determined independently of its polarity from the record of seismic data, shows more channel features (e.g., fluvial and tidal channels) and amplitude variations (e.g., bright spots), and; (4) Spectral decomposition attribute (i.e. seismic trace-based attribute), which dissolves the seismic image into different frequencies signal that can be chosen and blended in a colour blending interface (RGB) to properly illuminate geological characteristics (e.g., channels, faults) and geological sub-seismic resolution (e.g., lateral distortion, variations in sediment thickness).

These attributes help to identify high - resolution shallow-marine characteristics (i.e., fluvial and tidal) that relate to the presence of different types of channel network systems and other geobodies within the Group H and Group I of the studied area in the Malay Basin.

The resolution issue is crucial in the interpretation of cross-cutting geobody relationships. Over a ~15 ms seismic attribute window, cross-cutting geobodies could either be connected or unconnected, depending on their individual thickness. This is currently unresolvable in the dataset and has significant implications for interpretation of the relationship between these geobodies and their potential connectivity (e.g., are intersecting geobodies lateral feeder tributaries into an incised valley or merely randomly cross-cutting unconnected channel belts (younger over older?). Defining the relationship is extremely important when interpreting geobodies to identify the accurate subsurface architecture of geobodies. Therefore, to mitigate this issue, additional data such as pressure data from well control would be required to resolve the uncertainties related to channel connectivity, which is not available for this study.

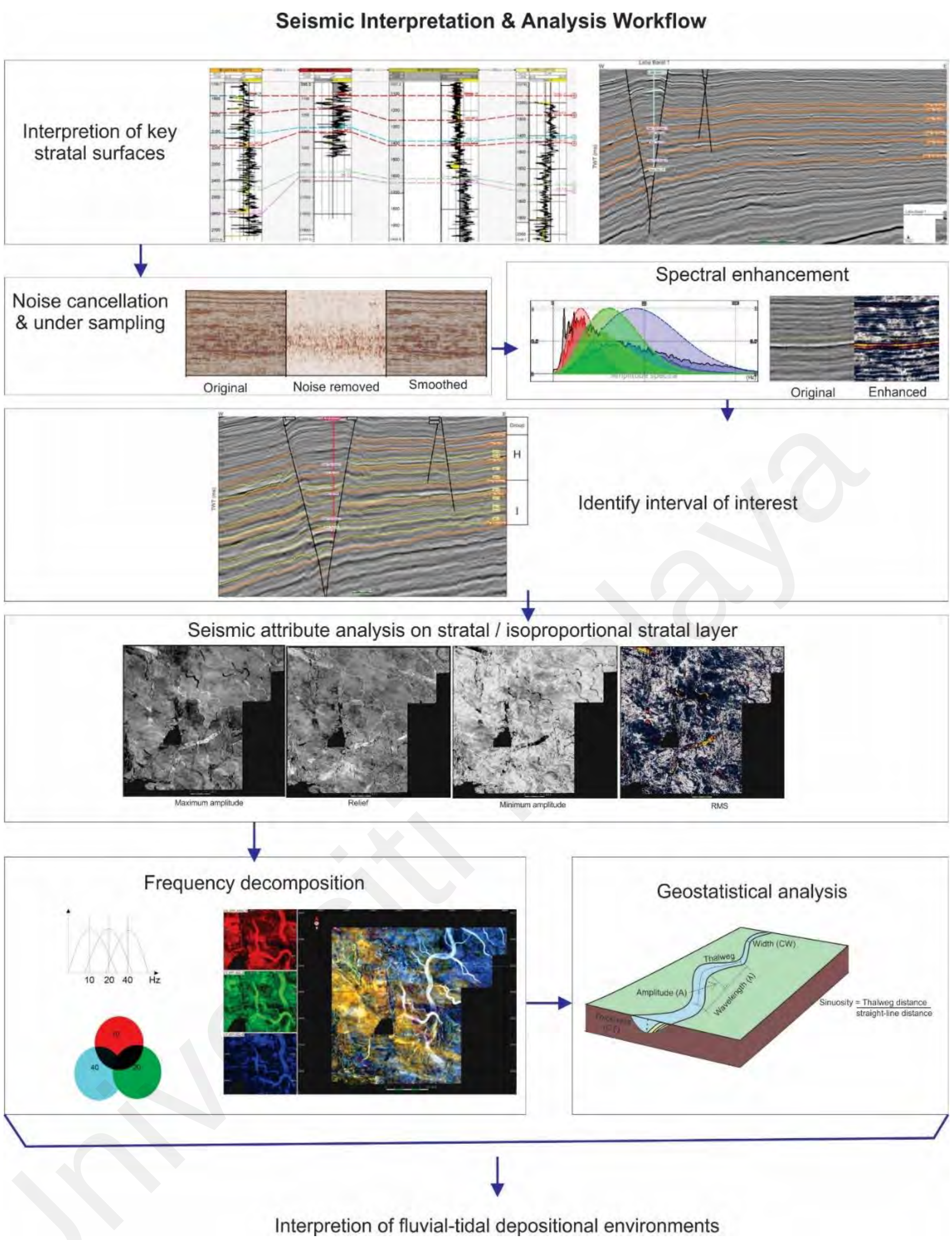

Figure 5.3: Workflow used in this study, beginning with interpretation of stratal surfaces on seismic data, followed by seismic-well tie, seismic attribute analysis and spectral decomposition analysis.

It must be noted that interpretation of stratigraphic trends defined by vertical changes of the fluvial architecture was a challenge because channel deposits of different sizes and incision depth that are cut down from a variety of horizons might be superimposed within individual seismic slices. Frequency decomposition generates a series of magnitude slices at discrete frequencies. The colour blending of three magnitude slices (with red, green and blue colours assigned to the specified frequency volumes) (Fig 5.3) enabled channel architectural seismic facies and its boundaries to be imaged more clearly in plan-view, consequently, revealing a variety of geobodies within the interval of interest. Nonetheless, descriptive fluvial channel systems at different stratigraphic levels have been determined by the combined analysis of iso-proportional slices and vertical seismic sections.

In this analysis, the morphometric parameters derived include channel width (CW), channel depth (CD), meander-belt width (MBW), meander wavelength (ML), channel length (CL), sinuosity (SI), and curvature radius (RC). Channel thickness was measured directly from vertical slices through the seismic volume and also by using frequency decomposition. Barnes et al. (2004) used Gabor and Morlet wavelets in spectral decomposition analysis, noting that both decomposed spectrum effects have qualitative analysis and valuation of channel thickness. Using spectral decomposition attributes to generate 3D geological channel simulation is also practical (Wallet, 2016). Recent research uses colour-blended multiple frequencies (RGB) to measure thin bed thickness and their fine-grained elements (Zeng, 2017).

5.3.2 Horizon slicing

Visualization of fluvial channel depositional characteristics can be accomplished by using timeslices, horizon slices and iso-stratal slices. Time-slice views of undeformed depositional surfaces provide an opportunity to study the preserved but buried geomorphology in map view (*sensu* Zeng et al., 1998; Brown, 2004; Posamentier et al., 2007; Miall, 2002; Posamentier, 2005; Ethridge & Schumm, 2007; Reijenstein et al., 2011). The image quality generated however decreases with depth.

The differences between slices, time slices, and iso-stratal slices is illustrated in Figure 5.4. The resolution is decreased in the deeper sections of the dataset (> 1500 ms TWT). Therefore, the depositional features were not clearly imaged here. In this analysis, amplitude attributes for iso-proportional slices were derived over a seismic window interval of 15 - 20 ms to properly visualize the channel morphology and geometry. Figure 5.5 displays a high-resolution seismic of a shallow time slice of <500 ms TWT. The level of detail of the deposits is discernible enough by using time slices. Figure 5.6 shows images that were taken at a greater depth in the seismic section >1000ms TWT by employing iso-stratal slicing with the spectral decomposition method to enhance the poor seismic resolution in the deeper section.

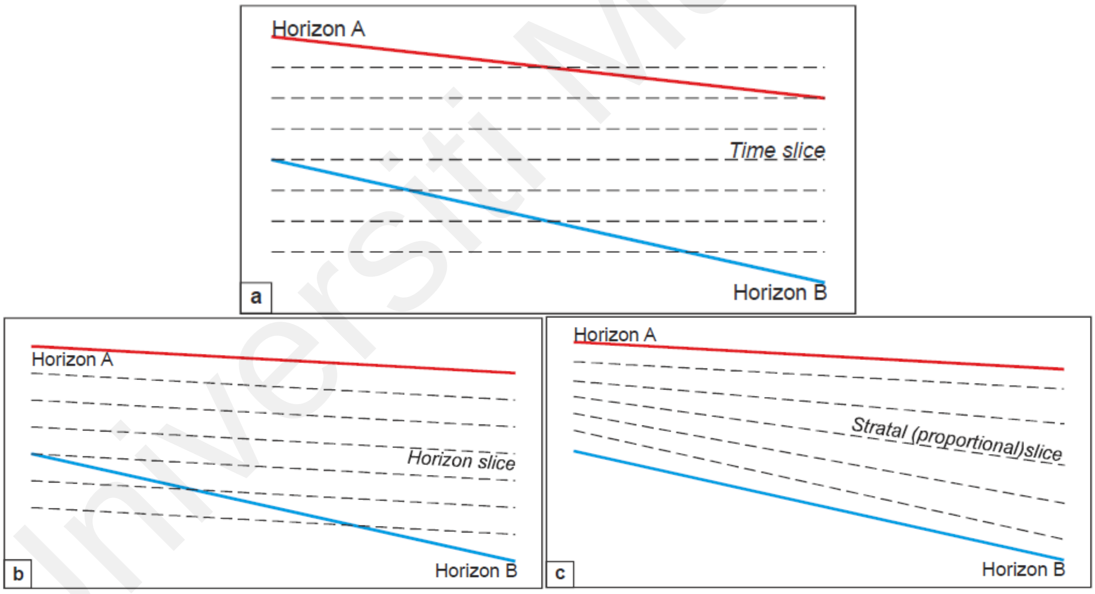

Figure 5.4: Slicing techniques of surface imaging for seismic geomorphology in time, horizon and iso-stratal. Solid lines (red and blue) denote reference seismic horizons. Dashed black lines are horizontal slices. (a) Time slice shows that horizon slices can cut cross-reference time horizons which do not capture individual depositional and stratigraphic surfaces. (b) Horizon slices associated with horizon A are consistent with stratigraphy when using horizon A as reference, but as the lower horizon B dips at a higher angle, they are not stratally matched to the lower horizon. This is normal when strata package thickness varies laterally. If the two horizons are similar or identical, horizon slices would be compatible across the represented set. (c) Iso-stratal slices are aligned with both horizons and best suited by dipping strata following lateral and parallel thickness changes.

Group H and Group I strata are cut by post-depositional faults, which implies that the channel deposits cannot be imaged using standard time slices. Seismic data in this study are all conformant and parallel to the key surfaces (i.e., a layer cake arrangement). Therefore, the best method for observing channel deposits is by horizon slice and iso-stratal slicing (iso-proportional slices /isoslice) technique. Horizon slice is employed to understand the *in-situ* depositional architecture and settings, whereas isoslice may enhance images of the subtle channels, and its ability to handle common and significant lateral thickness variations in this 3D seismic cube.

To apply this technique, sequences of sub-volumes were generated, and flattened on specific seismic surfaces. Horizon slices from each flattened sub-volume reveal deposits that are associated stratally with the flattened horizon (Hardage, 1994). Horizon slices are significant when strata are parallel and align with the seismic horizon (Zeng et al., 2001). Where flattened horizon slices did not clearly image deposits, iso-proportional slices were used to extract amplitudes between defined seismic window intervals to catch a subtle function, thus enhancing geobody edges. Iso-stratal slices extracted are conformable to top and bottom reference seismic horizons (Zeng et al., 1998).

Figure 5.7 illustrates the differences between the amplitude map of a time slice, horizon slice, and iso-proportional slice with RGB blended spectral decomposing from the Group I of the area of study. The isoslices were extracted with RMS amplitude attribute where the values extracted over a 15-20 ms window. Subtle features of geobodies are discernible in both horizon and iso-stratal slices but is clearer in iso-stratal slice (Fig 5.7C). The use of this methodology ensures that subtle characteristics that would otherwise have been undetected could be imaged.

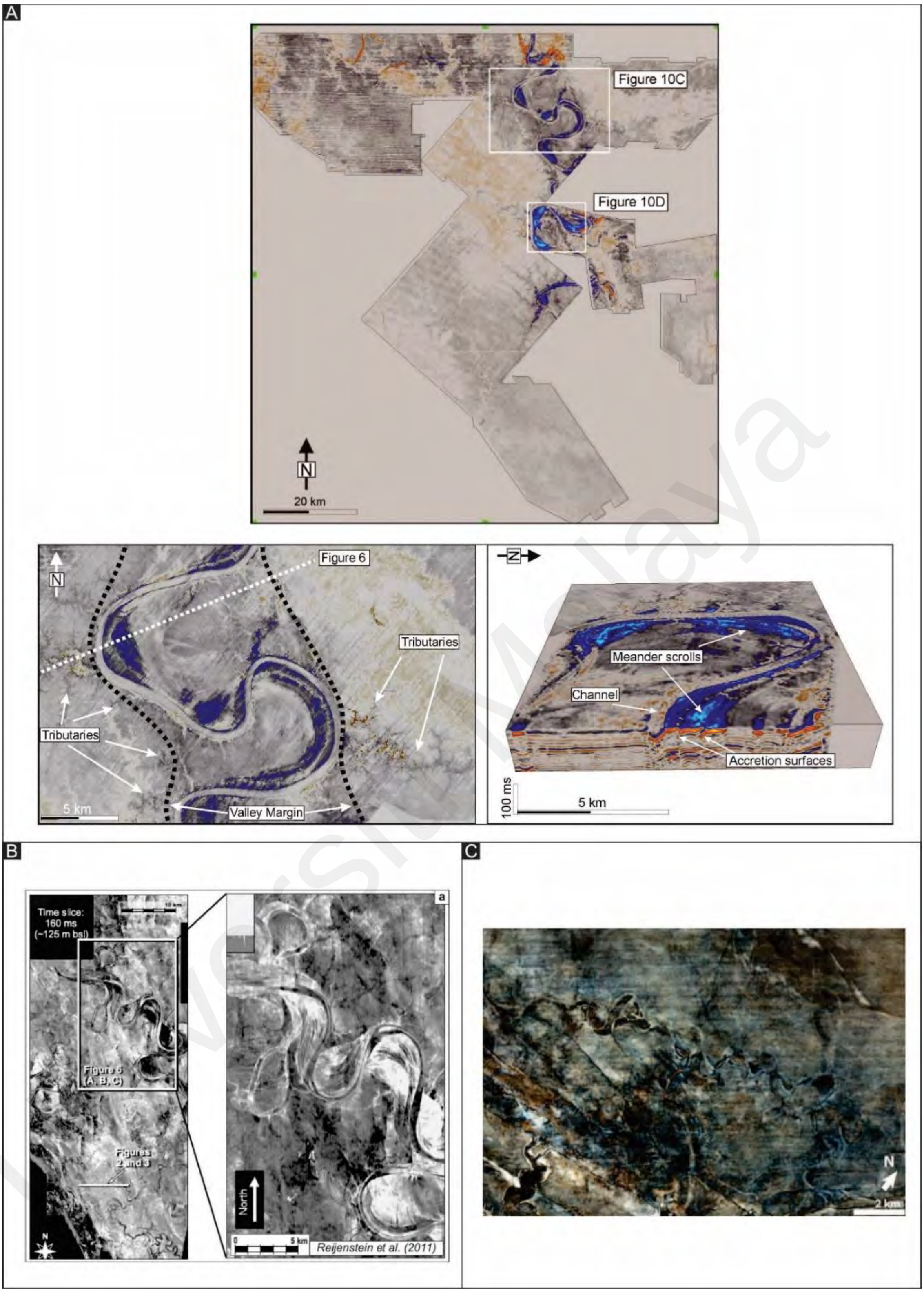

Figure 5.5: Examples of seismic imaging in shallow, high-resolution subsurface datasets. A range of fluvial architectural elements can be observed from meander scroll bars, channel belts and incised valleys by employing time slice technique. (Taken from (A) Alqahtani et al., 2015; B) Reijenstein et al., 2011; C) RGB-blended spectral-decomposition volume in the shallow sub-surface; Klausen et al., 2014)

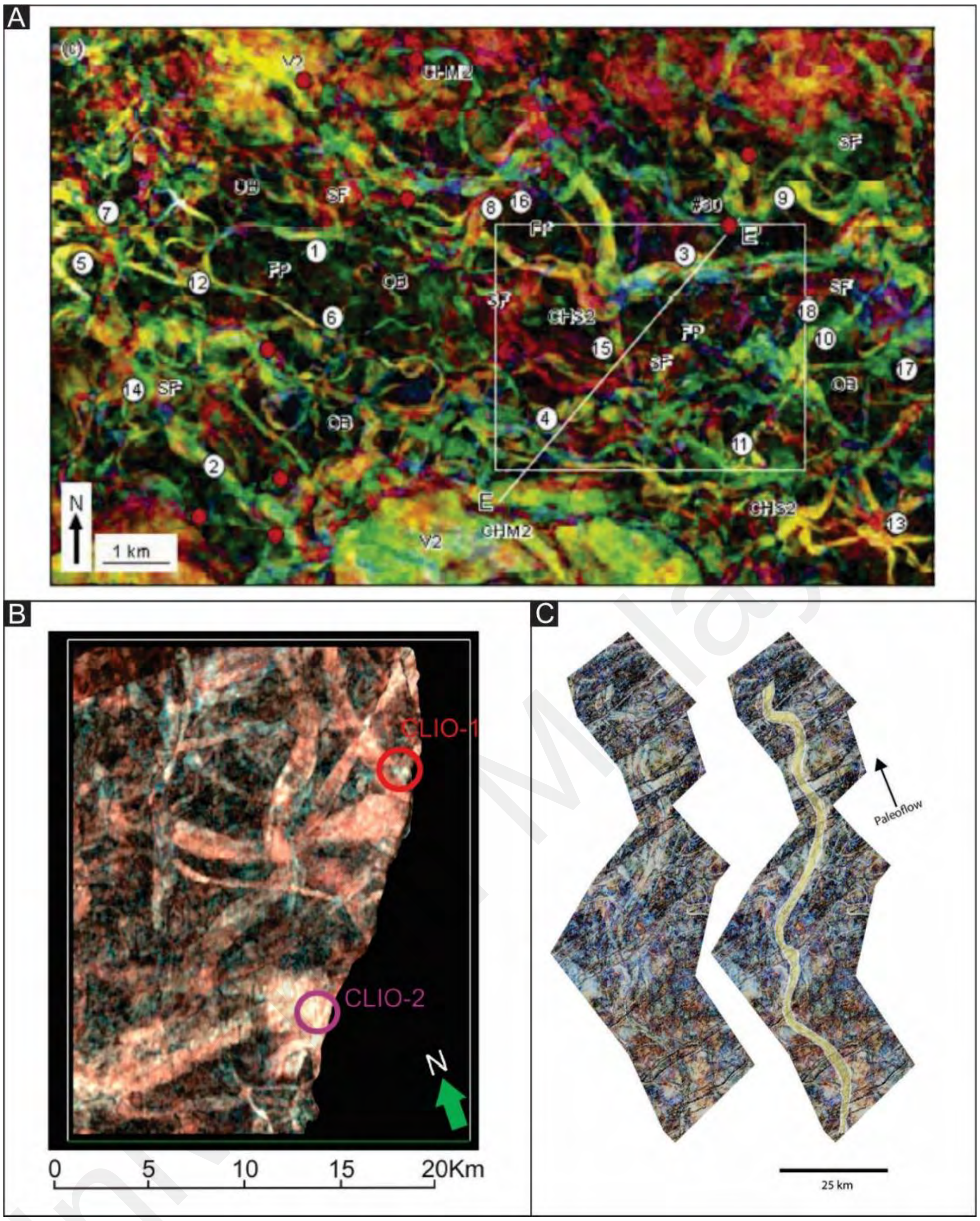

Figure 5.6: Examples of seismic imaging in deeper subsurface datasets. These images were extracted by employing iso-stratal slice technique with RGB-blended spectral decomposition. (Taken from (A) Zeng et al., 2020; B) Heldreich et al., 2013; C) Martin et al., 2018).

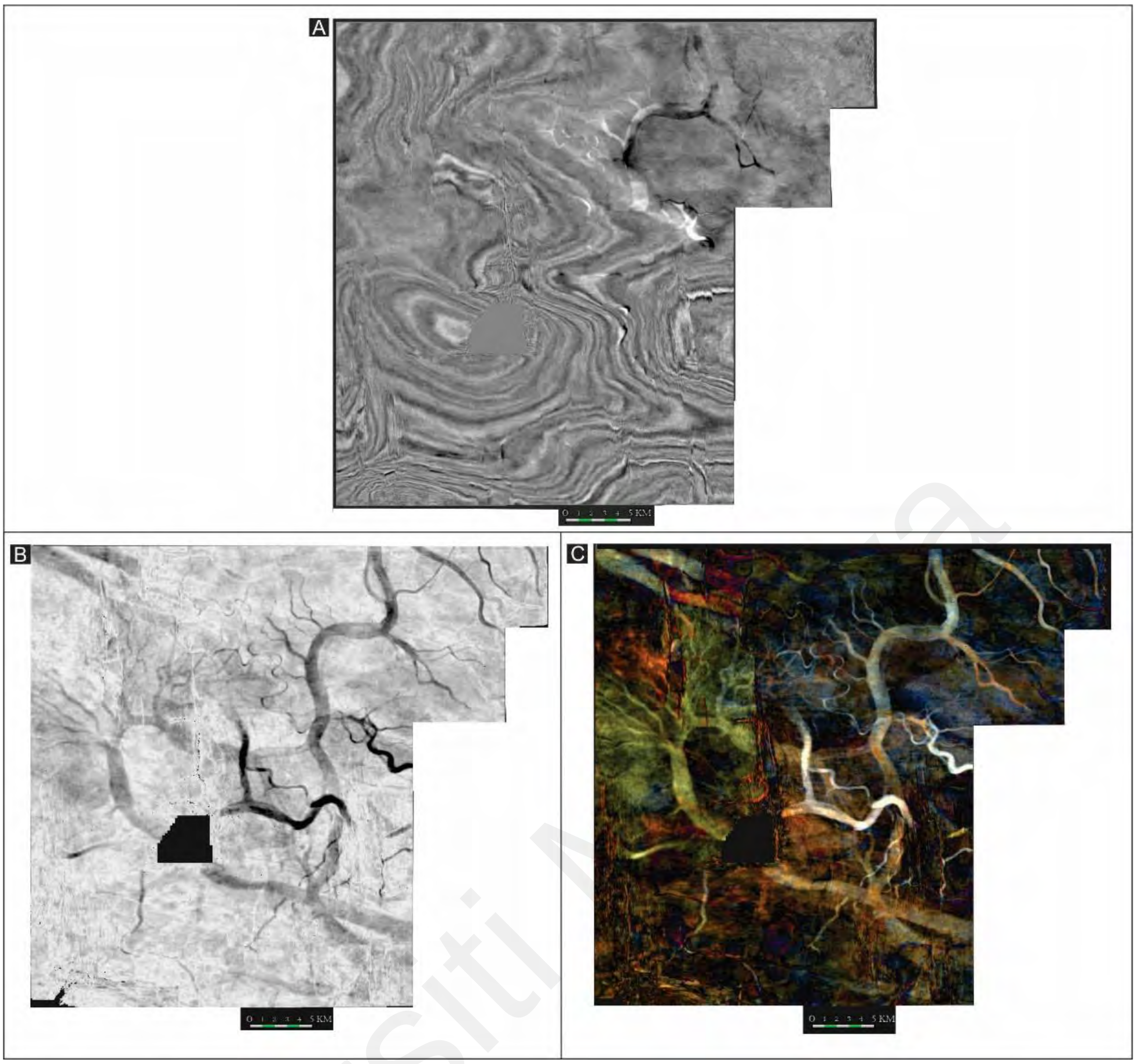

Figure 5.7: Comparison of seismic imaging in deeper subsurface of this study. These images were extracted by employing; (A) time slice at 2000 ms B) horizon slice with RMS attribute; C) iso-stratal slice technique with RMS attribute and RGB-blended spectral decomposition.

5.4 Results and Interpretation

5.4.1 Seismic Stratigraphic Analysis

Based on seismic facies study and consistency of seismic reflection, six (6) seismic horizon surfaces were mapped across the study area (from Near Top H Group to Near Bottom I Group) (Fig 5.8 b). The interval of interest within Group H and Group I succession was divided into five (5) seismic sequence stratigraphic units (i.e., Unit I, II, III, IV, and V) (Fig 5.8c). Ten (10) iso-proportional slices (isoslices) with 15 ms TWT seismic windows (approximately 20 m thick) were produced, based on well tops from Laba Barat-1, which lie approximate to the flooding surfaces. Figure 5.8c is a schematic stratigraphic cross-section, which demonstrates the stratigraphic and nomenclature structure used in this study.

5.4.2 Seismic Interpretation and Data Analysis

Sequence stratigraphic surfaces selected and identified based on well tops from Laba Barat-1 were used to subdivide the seismic volume into five stratigraphic units and generated a total of ten isoslices within these units (Fig. 5.8c). A range of attribute maps were generated for each isoslice, with minimum amplitude, maximum amplitude, envelope, RMS amplitude and spectral decomposition attribute maps providing the optimal imaging. In planform section, four major seismic channel geobodies and architectural elements are identified and imaged within the Group H and Group I succession, constrained by the minimum vertical seismic resolution of approximately 15 ms (TWT). High amplitude linear geobodies with a clearly defined edge (interpreted here as channels) are divided into four seismic channel geobodies groups (very-large, large, medium, and small). These channel geobodies are interpreted to represent a range of estuarine, fluvial, fluvial-tidal and tidal channel types (including single channel, channel belt, amalgamated channels, distributaries, and tributaries).

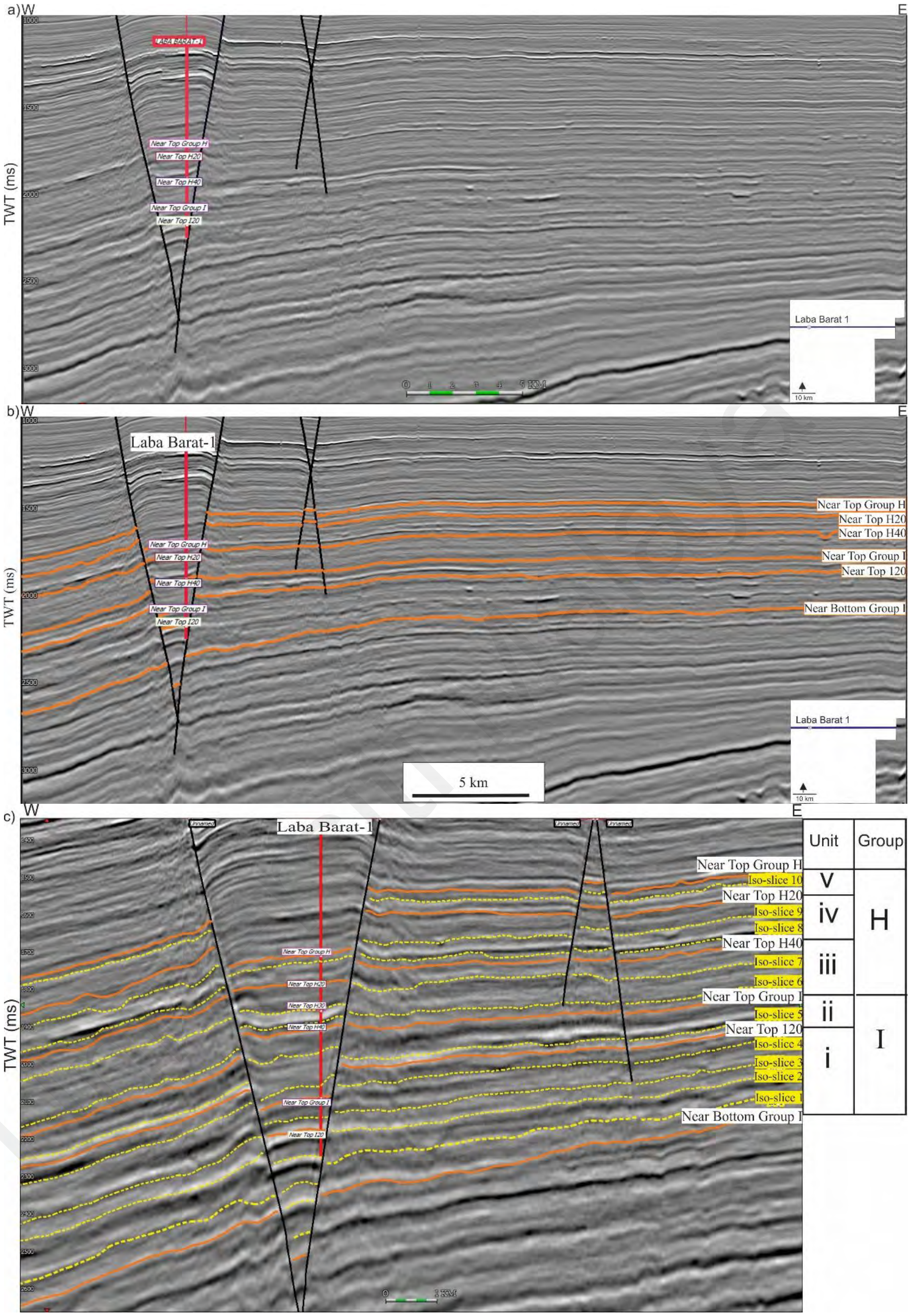

Figure 5.8: (a) Un-interpreted, (b) interpreted inline seismic section across the 3D seismic dataset demonstrating the six (6) key surfaces used in this study, and c) Five (5) units bounded by seismic sequence boundaries and ten (10) isoslices were produced for seismic geomorphological analysis.

Diffuse high amplitude facies observed in the seismic could either represent seismic noise or depositional features such as crevasse splays or levees. Diffuse low amplitude areas forming the "background seismic signal" may represent overbank and/or other coastal plain deposits.

Statistical data was extracted from the full range of channel architectural elements imaged within the seismic volume, providing a dense, statistically significant, channel geobody database. The significant geostatistical values extracted include morphometric elements such as meander-belt width (amplitude), meander belt wavelength, channel thickness, orientation, and sinuosity. Such parameters have been used to classify such channel geobodies and to enable comparisons between their measurements and channel geobodies in the published literature.

5.4.3 Channel Geobody Geometry Analysis

Channel geobodies are identified in the seismic volume as high amplitude packages of reflectors, commonly with moderate frequency, surrounded by distinctly different amplitudes. The variation in continuity of high seismic amplitude may reflect the relative proportions of sand or mud which fill these features, but this needs to be verified with core and wireline log data. In this study, only one well with core (i.e., Cendor-3A) penetrates the interval of interest near the top of Group H. Image resolution within the penetration area shows broad diffused high amplitude. Therefore, the integration of this core to the 3D seismic attribute study is not suitable, especially as a direct constraint for measurement of channel thickness. However, core analysis results in Chapter 4 from Cendor-3A and nearby wells are used as reference and constraint in the study area, despite two of them being outside of the seismic boundary. This is justified as they are very close to the seismic area boundaries.

Figure 5.9 illustrates the presence of reflector terminations and basal incisions within the seismic volume, which allow geobodies to be identified in cross-section. These channel types are grouped together into seismic groups primarily based on their channel width for further quantitative channel geometry analysis in Chapter 6.

5.4.3.1 Channel Type Geomorphologies

Channel types in this study are classified based on variations in planform channel geometries, features and dimensions, and differences in seismic amplitude signals in a cross section. By incorporating both cross-section and plan-view of these channels, ten (10) types of channels have been identified (Table 5.2, Fig 5.9).

Type-1: Very large channels (width between 3500 and 5000 m) characterised by a broad U-shaped channel morphology and shallow channel depth (37 – 42 ms TWT or 42 – 55 m thick). Internally composed of variable amplitude, laterally continuous seismic reflections, revealing the variable frequency. Medium-scale channels of *Type-4* (<600 m wide) are observed attached to this channel type, and some small-scale channels of *Type-8* (<450 m wide) are located within these very large channels. *Type-1* channels exhibit low to moderate sinuosity (~1.5), with the channel width widening eastward.

Type-2: Large channels (width between 1000 and 1800 m) characterised by asymmetric channels (i.e., the cross-section shape of concave-up channel is skewed towards the outside of a bank either right or left channel bank), some areas display a complex shape, laterally continuous seismic reflections, consistently high amplitude, channel thicknesses of 35 –52ms TWT (40 - 70 m) and moderate to high sinuosities (1.8 – 2.0). Type 2 channels are frequently associated with small channels (< 350 m wide, branching almost perpendicularly ~90^0), and exhibit a meander bends with a cuspate morphology.

Type-3: Large channels (1000 to 1800 m wide) with a wide U-shaped cross-section, infilled with laterally continuous, high amplitudes, high regular sinuosity (1.5 – 2.0). Type

3 channels exhibit a stable meandering pattern. Small associated channels are rare to absent. The channel thickness is approximately 31 – 42 ms TWT (35 – 54 m) thick.

Type-4: Medium channels (500 to 950 wide) with an asymmetric channel shape in cross-section, and internally exhibiting moderate to high amplitudes. Channel thickness is about 30 – 50 ms TWT (35 - 65 m). Channel Type 4 display low sinuosities or are straight (1.1 – 1.2), is rarely associated with small channels and exhibits bifurcation.

Type-5: Medium channels (450-800 m wide) characterised by an asymmetric and complex shape channel morphology in cross-section, thickness of 20 – 33 ms TWT (15 – 35 m), internally composed of bright high amplitudes. Type 5 channels display moderate to high sinuosities (1.4 – 1.5). They tend to branch and taper to form 'blind end' features.

Type-6; Small channels (100 to 200 m wide) characterised by asymmetric channel morphology in cross-section, channel thickness of about 15 – 30 ms TWT (10 - 35 m) thick, laterally continuous seismic reflection, consistently exhibit bright amplitudes. Type channels are typically single dendritic with low sinuosity and tends to bifurcate.

Type-7; Small (150-450 m wide) asymmetric channels, internally composed of laterally continuous seismic reflections, consistently showing bright amplitudes. Type 7 channels are typically expressed as several parallel channels with highly irregular sinuosities (1.2 – 2.0). Channel thickness is about 25 - 30 ms TWT (10 – 35 m). Meander scrolls are visible in some examples. The channels commonly bifurcate and exhibit cuspate meander bends.

Type-8; Small channels (150-250 m wide) with an asymmetric channel morphology, internally composed of laterally discontinuous high amplitudes. The channels appear to be short in visible length and are 25 - 35 ms TWT (37.5 – 52.0 m) thick. Channel Type 8 tends to narrow and become blind-ended. They display moderate to high sinuosities (>1.5) (tortuous) and are dendritic.

Type-9; Small channels (100 to 200 m wide) with an asymmetric channel morphology and characterised by low amplitude, laterally continuous seismic reflections. Channel thickness is about 10 - 15 ms TWT (10 – 20 m). Type 9 channels tend to exhibit linear dendritic patterns.

Type-10; Small channels (50 to 150 m wide) defined by low to moderate seismic amplitudes, laterally discontinuous seismic amplitude, narrow, exhibit blind-ended, small dendritic creeks of low order are visible, channel thickness is about 10 - 22 ms TWT (10 - 20 m) thick, moderate to high sinuosities, and display meandering dendritic features.

5.4.3.2 Seismic Group Analysis –Planform View

Seismic geobodies identified within the studied seismic volume can be classified into five (5) seismic geobody groups. These groups are: (1) Very-large scale channels; (2) Large-scale channels; (3) Medium-scale channels; (4) Small-scale channels, and (5) Additional seismic geobodies. The channel types described in Section 5.4.3.1 form elements of the four (4) seismic channels geobody groups. The classification of seismic groups is based on seismic amplitude reflection of geobodies, width distributions and geometries in the planform-view of surface isoslices (Fig 5.10).

A) Very large-scale channels (VLC)

Description: This channel group comprises features which are >3000 m wide, with a maximum width of approximately 6 km. The channels are characterised by frequently continuous high amplitudes and infilled with variable amplitudes, laterally continuous seismic reflections, revealing variable frequency. The channels exhibit low sinuosity (~0.7). The VLC group is composed of only *Type-1* channels. They typically have a broad U-shaped channel morphology and are 37 - 42 ms TWT (14 - 55 m) thick. The channels predominantly trend E-W.

Table 5.2: Channel morphology types observed in Group H and Group I in the study area within the Malay Basin. The classification and morphometric parameters are defined, with their channel width (CD), channel width (CT) and sinuosity.

Channel type	Seismic group	Seismic facies description	Remarks	Morphometric parameters					Reference to isoslice
				Channel width CW (m)	Thickness (CT) ms	Thickness (CT) m	Sinuosity (SI)	CW/CT	
1	Very large channel	U-shaped, wide channel, medium and small channels are attached and infills in the channel area, laterally continuous seismic reflection, variable frequency and amplitude, funnel-shape/broadening feature.		3500 - 6000	37-42	42-55	1.3	79.1 - 310.7	Isoslice 1
2	Large channel	Assymmetric, high amplitude seismic reflection, moderate to high sinuosity, meandering, small channel infills, frequently associated with small channels brancing perpendicular-90 deg, visible cuspate feature.	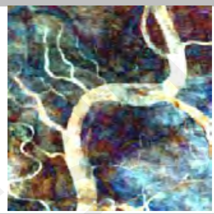	1000 - 1800	35-52	40 - 70	1.8 - 2.0	25.9 - 46.7	Isoslice 2
3	Large channel	U-shaped, variable seismic frequency, laterally continuous, low to moderate regular sinuosity, meandering, small channels are rarely attached	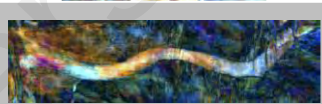	1000 - 1800	31-42	35 - 54	1.5 - 2.0	25.9 - 46.7	Isoslice 2,3,7
4	Medium channel	Assymmetric,low to moderate sinuosity, rarely associated with small channels, moderate to high seismic amplitude, low sinuosity, laterally continuous channels.	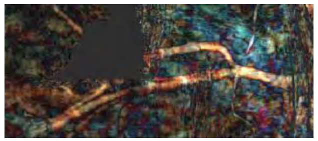	500 - 950	30-50	35 - 65	1.1 - 1.2	14.5 - 48.3	Isoslice 1,7
5	Medium channel	Assymmetric, high amplitude, significant narrowing/broadening, 'blind/dead end' tributaries, moderate to high sinuosity	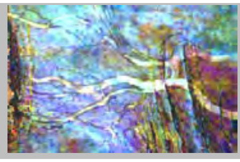	450 - 800	20-33	15 - 35	1.4 - 1.5	3.0 - 10.0	Isoslice 6,8

Table 5.2, Continued.

Channel type	Seismic group	Seismic facies description	Remarks	Morphometric parameters					Reference to isoslice
				Channel width CW (m)	Thickness (CT)		Sinuosity (SI)	CW/CT	
					ms	m			
6	Small channel	Assymmetric, laterally continuous seismic reflection, consistantly showing high amplitude, single dendritic, low sinuosity		100 - 200	15-30	10 - 35	1.1 - 1.5	8.6 - 30.0	Isoslice 1,4,7
7	Small channel	Assymmetric, laterally continuous, high irregular sinuosity,cuspate feature, bright amplitude, few channels visible trending the same direction, meander scrolls, bifurcation.	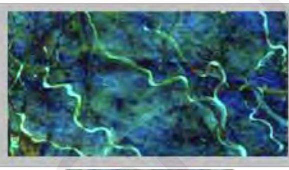	150 - 450	25-30	10 - 35	1.5 - 2.5	2.9 - 10.0	Isoslice 2,3,5,9
8	Small channel	Assymmetric, laterally discontinuous, narrow, 'blind/dead end' feature, short channel length, dendritic, moderate - high sinuosity (tortuous)		150 -250	25-35	10 - 35	1.5 - 2	5.7 - 20.0	Isoslice 1,2,3,6,7,8
9	Small channel	Assymmetric, low to moderate amplitude, laterally continuous seismic reflection,low sinuosity, linear dendritic.		100-200	10-15	10 - 20	1.1 - 1.3	7.5 - 15.0	Isoslice 4,7
10	Small channel	Low to moderate amplitude, laterally discontinuous, narrow, 'blind/dead end' feature, moderate to high sinuosity, meandering dendritic.	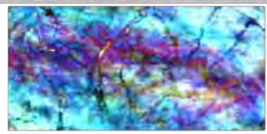	50 - 150	10-22	10 - 20	1.1 - 1.3	5.0 - 10.0	Isoslice 8

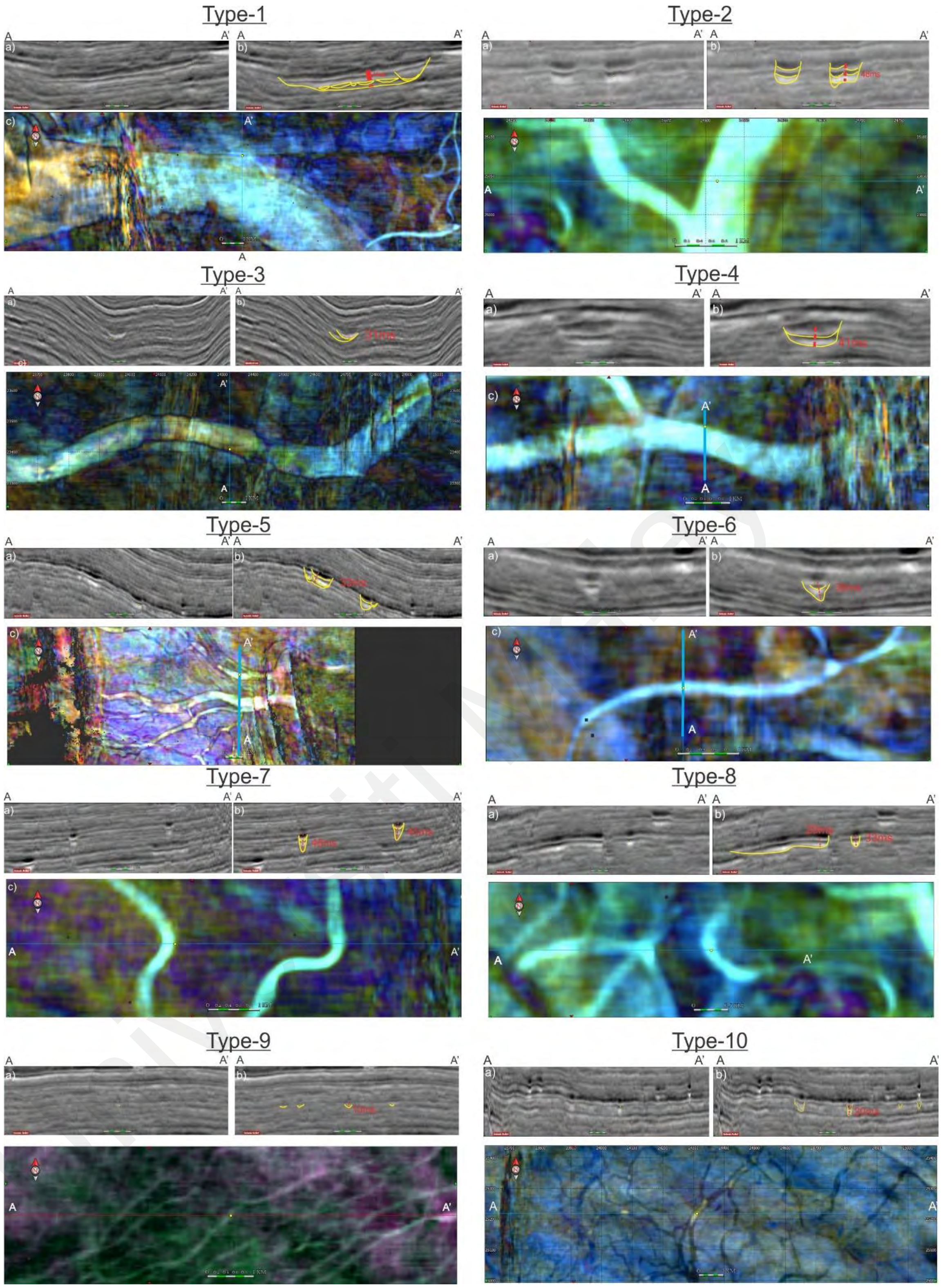

Figure 5.9: Vertical section and the planform view of each type of channel (*Type 1-Type 10*) observed in the study area.

B) Large scale-channels (LC)

Description: This channel group comprises >1000 m wide channels. In plan-view, they are expressed as bright seismic amplitudes and laterally continuous seismic reflections. The channels have a funnel-shaped plan-view geomorphology. The LC group is composed of *Type-2* and *Type-3* channels. These individual channels are dominantly 1 - 1.8 km wide. *Type-2* channels are thicker (40 - 70 m) than the *Type-3* channels (35 – 54 m). *Type-2* channels are frequently associated with smaller channels (<300 m wide with high amplitude) with observable infill, whereas this morphology is rarely associated with *Type-3* channels. Both these channel types exhibit a meandering morphology with clearly defined edges. *Type-2* channels display a higher sinuosity compared to *Type-3* channels. Additionally, *Type-2* channels have a distinct cuspate morphology at meander bends. Such features are not visible in the *Type-3* channels. The channel orientations range from N-S through to E-W.

C) Medium-scale channels (MC)

Description: In plan-view, these medium-scale channel geobodies range in width between 500 and 950 m, with often clearly defined margins and exhibit very low sinuosities. The seismic character is typically bright with high amplitude, discontinuous reflectors, which are one or two seismic reflector loops thick. The channels are mostly 500-750 m wide and predominantly trend NE-SW. *Type-4* and *Type-5* channels are categorised in this group, with channel thicknesses approximately 15 – 65 m. *Type-4* channels exhibit low sinuosities, while *Type*-5 channels have moderate to high sinuosities. Small channels (< 300m wide) with high amplitude are observed to be in close association with *Type-4* channels. *Type-5* channels commonly bifurcate and narrow into small channels.

D) Small-scale channels (SC)

Description: These small-scale channel geobodies have widths ranging from the limits of horizontal seismic resolution (typically >50 m wide) up to 450 m. However, the channels are predominantly 200 – 350 m wide and are approximately 10 – 35 m thick. They are visible as high amplitude features, with frequently continuous seismic reflections and variable sinuosities. Some of the small channels display low amplitude features and discontinuous seismic reflections. In comparison to the large and medium-scale geobodies, their seismic amplitudes are typically subdued due to seismic resolution. Channel group SC often displays much higher sinuosities than the large- and medium-scale geobodies, and they predominantly trend NNW-SSE or E-W. The small-scale channel group includes *Type-6*, *Type-7*, *Type-8*, *Type-9*, and *Type-10* channels. These small-scale channels are the most dominant channels throughout the entire interval of interest within Group H and Group I of the Malay Basin.

In plan-view, *Type-6* channels are laterally continuous with consistently bright amplitudes. The channels have low sinuosity, are single dendritic and commonly bifurcate. Channel width ranges between 100 and 200 m. These channels form the deepest channels observed in the interval of interest. *Type-7* channels are very similar to *Type-6* channels, but they differ in displaying highly irregular sinuosities (1.2 – 2.0) with a more extensive channel width range (150 – 450 m), visible cuspate morphology, and fewer parallel channels. In the specified interval, smaller channels of <100 m wide are commonly associated with the *Type-7* channels.

Type-8 channels are dendritic small channels which show bright amplitudes and discontinuous seismic reflections. The channels commonly have tortuous high sinuosities and are blind-ended. They are often adjoined at almost right angle (90^0) to medium and large channels (Type-2 and *Type-4* channel morphologies). *Type-9* and *Type-10* channels are both characterised by low to moderate amplitude seismic reflections. Their widths are typically narrower than other types of small channels (<200 m wide). In plan-view, *Type-9* channels show laterally continuous low amplitudes with a low sinuosity or linear dendritic morphology. Their orientation is predominantly NNE-SSW. *Type-10* channels often display discontinuous seismic reflections with low amplitude and moderate to high sinuosities. The dendritic channels often narrow and blind-ended.

E) Additional Seismic Geobodies

Extensive patches with diffuse high amplitudes and low amplitude areas represent the background seismic signature, which correspond to architectures which are below seismic resolution. Two subtly different seismic facies can be described; however, it should be noted that their interpretation is based only on seismic attribute imaging in this study. The two additional seismic geobodies are:

a) Diffuse high amplitudes:

These units contain diffuse brighter amplitudes and patches of lower amplitudes (Fig. 5.10e). Sinuous features of *Type-8* small channels are observed within these diffuse areas and are typically <100 – 150 m wide and regularly display varying degrees of amplitude response.

b) Low amplitude areas:

In the vertical seismic section, this facies forms packages >5 ms thick which comprise low to variable amplitude reflectors displaying distinct, discontinuous, and low amplitude reflectors (Fig 5.10f). In plan-view, this area is composed of dominantly homogeneous, low amplitudes where ≤100 m wide sinuous geobodies of *Type-8* channel morphologies are visible.

Seismically Resolved Architectural Elements

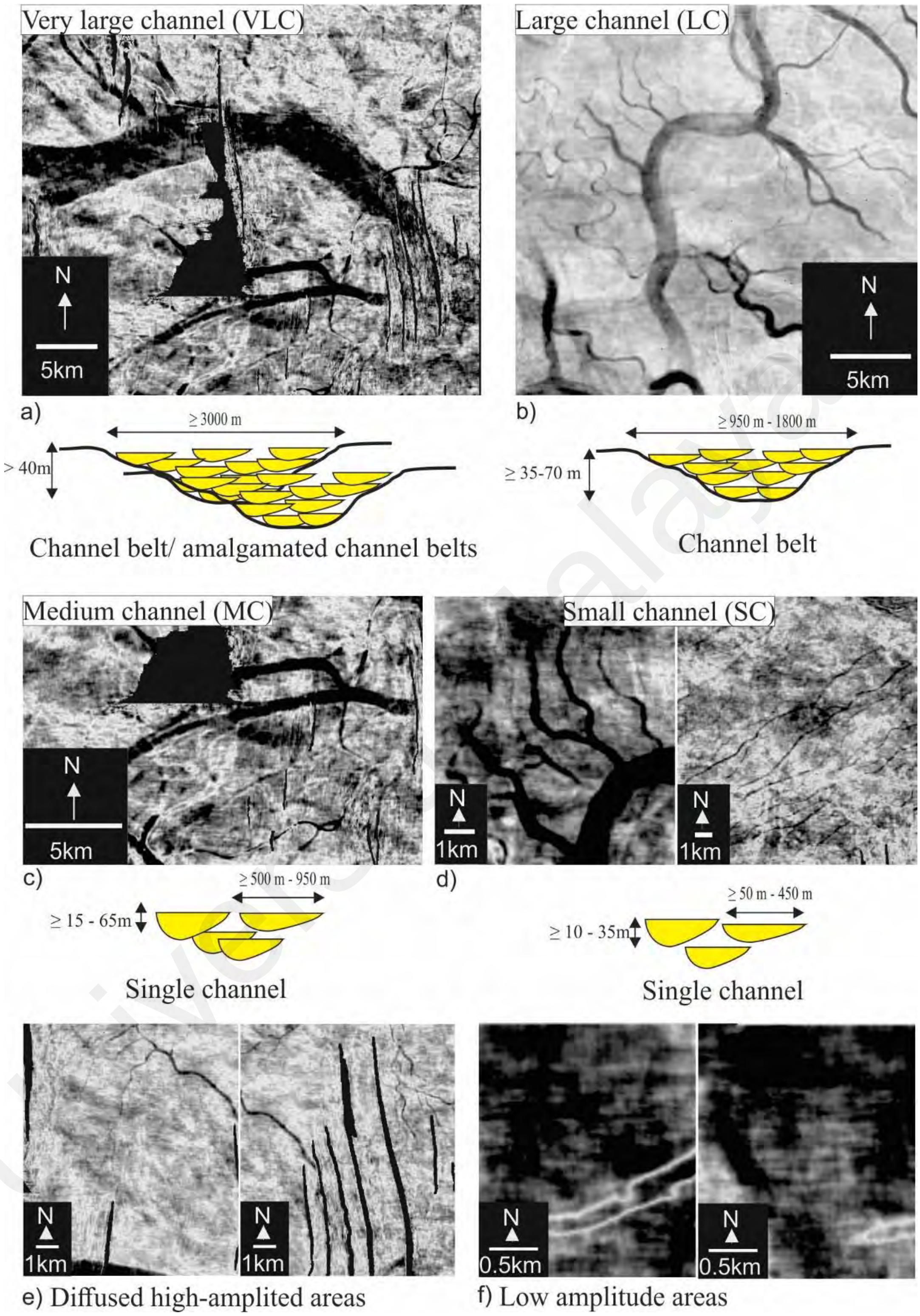

Figure 5.10: Seismically resolved architectural elements identified within the interval of interest. (a-d) These represent seismic geobodies on a range of scales based on their width distributions (large, medium and small). (e-f) Diffused high-amplitude and low-amplitude seismic area might represent seismic background.

5.4.4 Stratigraphic Evaluation of the Interval of Interest

The interval of interest within the studied seismic volume has been divided into five (5) stratigraphic units (Fig 5.8c). Two units (Unit-I and II) are within Group I, and another three units (Unit-III, IV, and V) are within Group H. Unit I is bounded by the Near Bottom Group I flooding surface and the younger Near Top I20 flooding surface. Unit II is bounded by the Near Top I20 flooding surface and the younger Near Top Group I flooding surface. Unit III is bounded by the Near Top Group I flooding surface and the younger Near Top H40 flooding surface. Unit IV is bounded by the Near Top H40 flooding surface and the younger Near Top H20 flooding surface. Lastly, Unit V is bounded by the Near Top H20 flooding surface and the younger Near Top Group H flooding surface.

In the following sections, the vertical and lateral distribution of channel types discussed above are defined and explained within terms of the key controls for channel development outlined in Chapter 2. Fluvial systems were imaged using the spectral decomposition method constrained within 15 ms TWT seismic interval (approximately 15 - 20 m thick) for each isoslice.

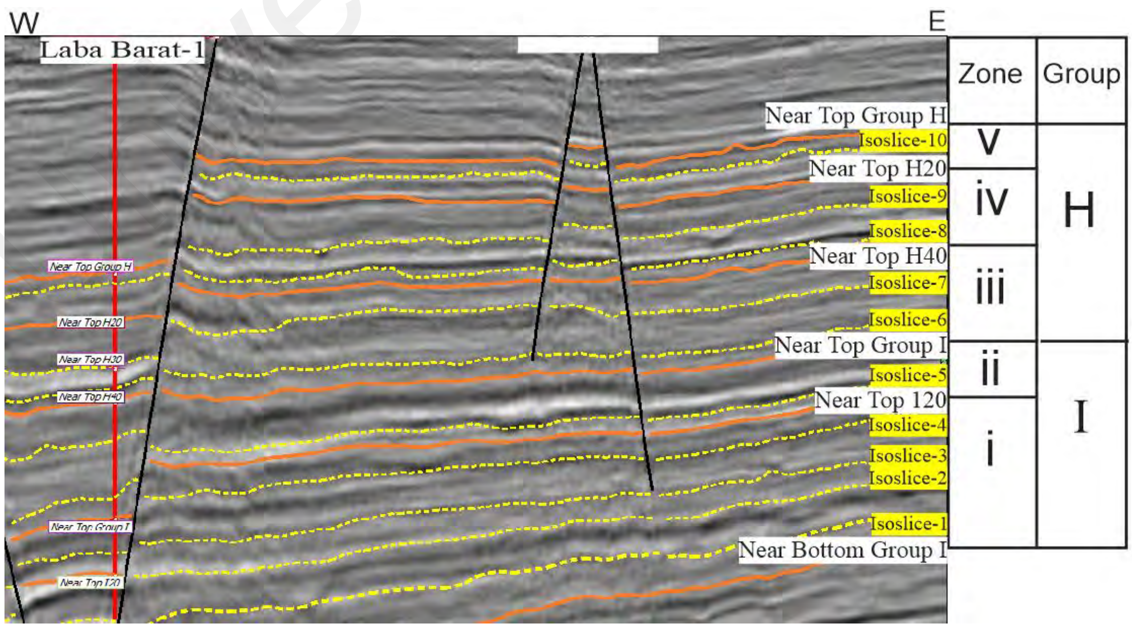

Figure 5.11: Five (5) units bounded by flooding surfaces and ten (10) isoslices were produced for seismic geomorphological analysis.

5.4.4.1 Unit I

Unit I is bounded by the Near Bottom Group I flooding surface and the younger Near Top I20 flooding surface. This unit is the bottommost stratigraphic unit in the interval of interest. The unit is approximately 280 m thick. Four isoslices (isoslice-1 to 4) were created within this unit.

a) Isoslice-1 (Fig 5.12c)

Description: Isoslice-1 is located near the bottom of Unit-I, Group I. In general, channel geobodies observed within isoslice-1 exhibit variable seismic amplitudes and frequency, inconstant widths and sinuosities, and laterally continuous and discontinuous seismic reflections (Fig 5.12b). A single, very large-scale, E-W trending, Type-1 channel dominates and crosses the middle part of the area of Isoslice-1. The very large-scale channel has a funnel-shaped morphology, meanders and also widens towards the eastern part of the study area. The average width of this channel is 3 km but reaches 6 km in the eastern end.

The maximum channel thickness is about 42 ms TWT (~ 55 m thick). Small- to medium-scale channels are observed to be attached to the very large-scale channel. Some small-scale channels of *Type-8* are located within the *Type-1* channel. However, it must be noted that the edges of these small-scale channels are not clearly defined, and the channels are expressed as frequently discontinuous amplitude reflections. Medium-scale *Type-4* channel morphologies are present south of the very large *Type-1* channel, and they also trend E-W. Small *Type-6* channels with clearly defined edges are observed cross-cutting the very large *Type-1* channel. These *Type-6* channels are long, of low sinuosity and cross the whole isoslice area in a SSW-NNE orientation. Small-scale channels of *Type-8* are dominant in the northern part of the study area. Some of the channel edges are not clearly defined, with discontinuous seismic amplitude reflections.

Interpretation: The wide range and variation of seismic channel geobodies in isoslice-1 indicates that the bottommost Unit I most likely represent part of the late lowstand to transgressive systems tract of a depositional sequence, with the geobodies recording widespread fluvial incision (Posamentier & Allen 1999; Posamentier 2001). Based on the cross-cutting relationships, the very large *Type-1* channel observed in Isoslice-1 is the basal-most incision channel and can be interpreted as either: (1) a possible bypass channel which developed when relative sea-level fell slowly and the shelf was not broadly exposed, or (2) an estuary funnel based on the visible eastward flaring geomorphology. A flaring, funnel-shaped geomorphology is typical of tide-influenced and tide-dominated channel mouths, including estuaries, and is caused by the seaward increase in the tidal prism (Dalrymple et al., 2012). However, it must be noted that there is some uncertainty in this interpretation, given that the observed flaring is very near to the edge of the seismic slice. Likewise, bypass channels may widen due to higher river discharge and erosion (Posamentier & Allen, 1999; Posamentier, 2001). The flaring feature suggests that the very large *Type-1* channel flowed eastward.

The medium-scale channels are interpreted as fluvial-tidal distributaries, while the small-scale channels are interpreted as tributaries draining into the medium-scale channels. Most of the small-scale *Type-8* channel morphologies may represent tidal channels, including through-flowing interconnecting channels and dead-end channels which diminish into lakes or marshes/mangrove. Interestingly, *Type-6* channel morphologies would probably represent single fluvial or fluvial-tidal channels, where they are bifurcating into distributaries at the northern part of the study area.

The large variation in channel dimensions suggests rapid switching and migrating within this isoslice, which may be explained by tidal processes, variations in river discharge, and changes in accommodation space (Dalrymple et al., 2015). Fluctuations in relative sea-level and the subsequent period of floodplain aggradation may instigate channel incision in this system. There is also clear deflection of the path of the small-scale channels (e.g., *Type-6*) by the clearly defined edge of the large-scale channel (Posamentier, 2001).

b) Isoslice-2 (Fig 5.13c)

Description: Isoslice-2 is located approximately 70 m above Isoslice-1 (Fig 5.13). This isoslice is also within Unit-I and is characterised by laterally continuous and discontinuous (chaotic) seismic facies. Large-scale Type-2 channels are dominant in isoslice-2, forming incisions which are 35-52 ms TWT (40 - 70 m) thick and 1.0 km - 1.8 km wide. *Type-3, Type-4, Type-5, Type-7*, and *Type-8* channels are closely associated with the large *Type-2* channels (Fig 5.12a). Channels in the lower tiers of the isoslice are concentrated in the northern area and dominated by *Type-2* and *Type-8* channels, and channels in the upper tier are present all across Isoslice-2. Large-scale *Type-2* and *Type-3* channels observed in the southeastern part of the isoslice appear to cross-cut each other. Both of these channel types exhibit funnel shaped morphologies which flare towards S-SE. The *Type-2* channels clearly show a N-S orientation, and often have small-scale *Type-8* (less than 250 m wide) channels attached to them. The *Type-8* channels are commonly connected to the large *Type-2* channels at right angles (90^0). The *Type-8* channels mostly trend NW-SE with decreasing channel thickness toward the South. The large-scale *Type-2* channels show clear cuspate morphologies at meander bends (Fig. 5.12b). Large *Type-3* channels mainly trend NW-SE and seldom have smaller connected channels. Several *Type-5* medium-scale channels that interconnect with *Type-8* channels are also observed.

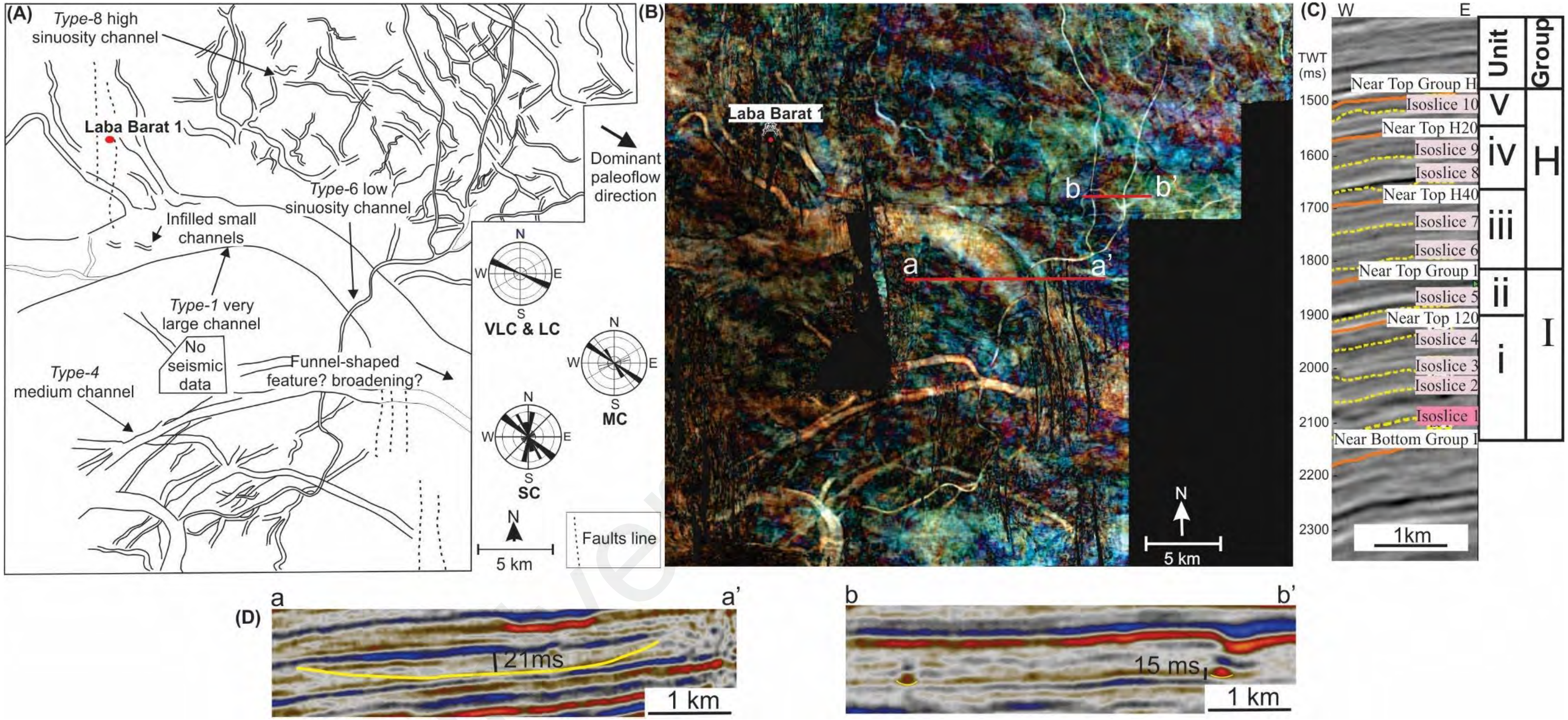

Figure 5.12: Channel systems of Isoslice-1, , Unit I, Group I, (A) Interpreted plan-view map; (B) Un-interpreted plan-view map; (C) Isoslice-1 is near the bottom of the interval of interest in Group I; (D) Example of the horizontal and vertical relationships of the channel in the fluvial system of isoslice-1.

Type-5 channels tend to narrow from medium-scale channels into small-scale channels and are blind-ended. A large number of *Type-8* channels are discontinuous, short and blind-ended. Their orientations vary, but the dominant trend is NW-SE. Some of discontinuous small-scale channels in the western area of the isoslice display dendritic patterns and low to moderate sinuosities, but their edges are not clearly imaged in this isoslice.

Interpretation: The basal-most tiers of Isoslice-2 are dominated by large-scale channel *Type-2* and *Type-3* channels. The greater abundance of small-scale channels in this isoslice relative to Isoslice-1 are interpreted to be more prevalent in transgressive and highstand systems tracts. Abundant cuspate morphologies associated with channel meander bends and probable funnel-shaped, flaring (broadening channel width) of channels in a S to SE direction suggest that these channels are fluvial channels with tidal influence. Such features are characteristic of tidal channels including estuary funnels, tidal creeks, and fluvial-tidal distributary channels (e.g., Dalrymple et al*.,* 2012; Hughes, 2012). The southward decreasing sinuosity of *Type-2* channels combined with the southward flaring of channels in the same direction is consistent with paleoflow towards the south. Tide-influenced and tide-dominated distributary channels tend to straighten seaward (Dalrymple & Choi, 2007).

The tidal limit of these channels may be located beyond the study area's seismic coverage. Small-scale *Type-8* channels tend to form a tributary system connected to the large *Type-2* channels. Typically, tributaries always drain into the larger channels (Kvale & Archer, 2007; Dalrymple et al., 2012). Large-scale *Type-3* channels in the NW region of the isoslice may also represent distributary channels which have been truncated by faults. Small-scale channels of *Type-8* in the NW also connect to these large-scale channels which flowed towards the SE.

The predominance of high sinuosity small-scale channels was probably due to local variations in tidal current energy, bedrock strength and/or low flow discharge. Small-scale channels in the western area of the isoslice are interpreted as possible crevasse splay channels on a floodplain. The fluvial system in Isoslice-2 has inherited the same fluvial patterns from the older fluvial system in Isoslice-1. Based on the vertical and lateral variability within Unit I, variation in channel geometry may be related to autogenic processes in the downstream region, e.g., rapid channel migration and channel switching due to low accommodation space and low discharge. Tidal processes were also a strong control on the channel morphologies observed in Isoslice-2.

c) Isoslice-3 (Fig 5.14c)

Description: Isoslice-3 is also within Unit 1 and is located approximately 45 m above Isoslice-2. The basal-most tier of Isoslice-3 is characterised by prominent *Type-3* channel incisions which are more than 1 km wide and 31-50 ms TWT (35 – 65 m) thick. *Type-4, Type-7,* and *Type-8* channel morphologies are associated with the large-scale *Type-3* channels (Fig 5.14). The lower tiers show large-scale channels of *Type-3* morphologies with straight to low sinuosity and NW-SE and NE-SW orientations. Smaller channels are rarely associated with the *Type-3* channels. Faults truncate this channel type in the middle part of the study area. These channels are overlain by high sinuosity small channels of *Type-7* and *Type-8*, which are dominant in the northern part of the study area. *Type-7* channels have highly irregular sinuosities (SI 1.5 – 2.5), exhibit skewed (goose-neck) and cuspate morphologies at meander bends, and predominantly trend NW-SE. They tend to form parallel series of more than one channel. *Type-8* channels discontinuous and are not clearly defined. However, they are visible in between *Type-7* channels. The relationship between both of these small-scale channel types is not clear.

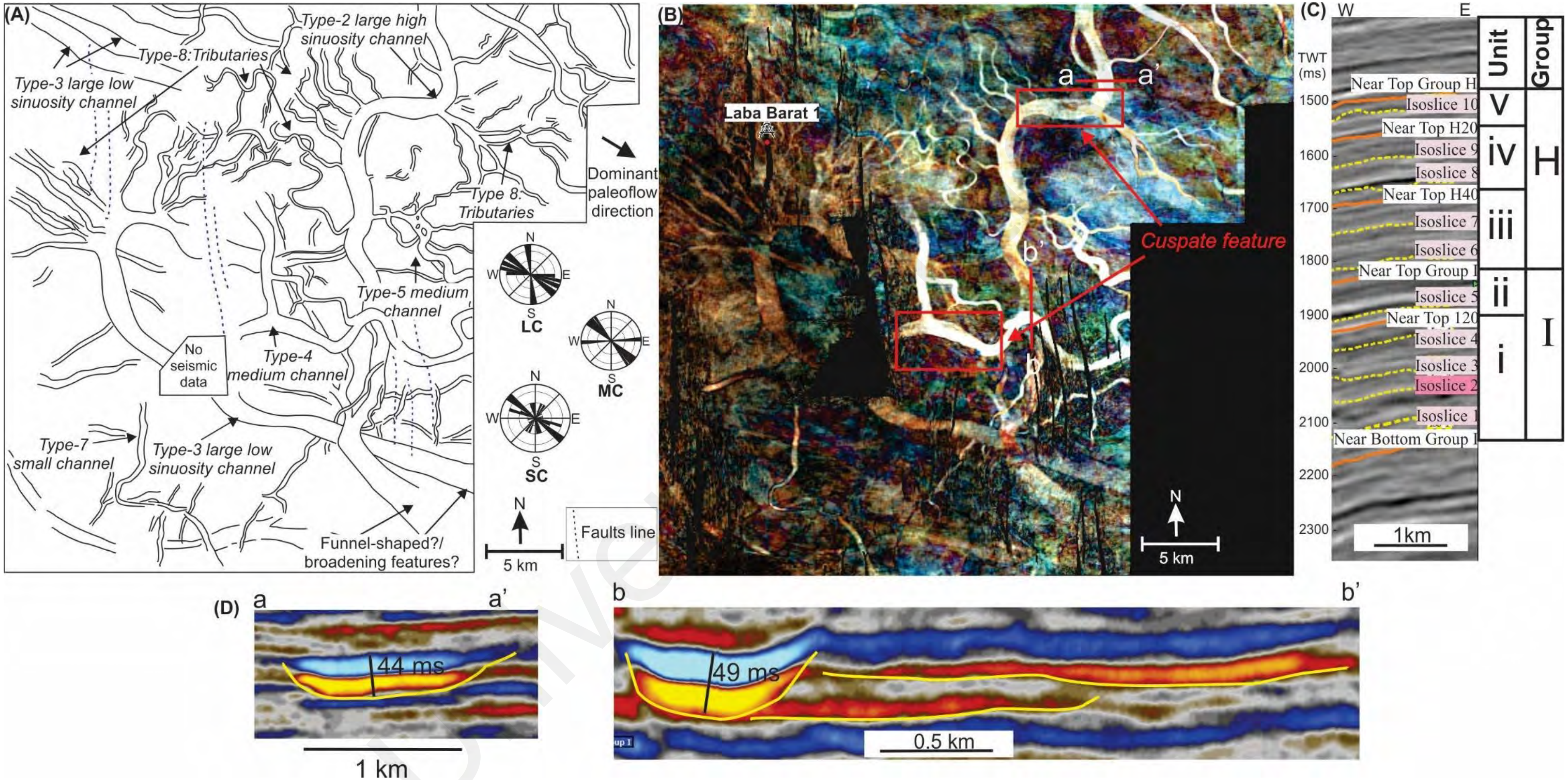

Figure 5.13: Channel systems of Isoslice-2, Unit I, Group I. (A) Interpreted plan-view map; (B) Un-interpreted plan-view map; (C) Isoslice-2 overlie isoslice-1 in Unit I; (D) Example on the horizontal and vertical relationships of the channel in the fluvial system of isoslice-2.

Interpretation: Large channels of *Type-3* morphologies with low sinuosities suggest high stability and are thus interpreted as fluvial or distributary channels. High sinuosity *Type-7* channel are meandering and trend NE-SW. The meanders are skewed. The skewed meanders (goose-neck) in the small channels suggest energy variations in opposing ebb and flood currents (Fagherazzi et al., 2004; Seminara, 2006; Hughes, 2012). The presence of cuspate meanders is diagnostic of tidal influence in these channels because their formation requires erosion on opposite sides of a meander beds, which indicates the presence of strong opposing currents (Hughes, 2012). The fluvial system in Isoslice-3 may represent the landward section of a lower delta plain, located seaward of the tidal limit (Summerfield, 1985; Posamentier et al., 1992; Holbrook et al., 2006).

d) Isoslice-4 (Fig 5.15c)

Description: This is the top-most isoslice studied within Unit I and is located approximately 85 m above isoslice-3. *Type-1, Type-3, Type-4, Type-6, Type-8* and *Type-9* channel morphologies are visible within isoslice-4 (Fig 5.15a, b). There is less variation in channel geometries and orientations in isoslice 4 compared to the previous older isoslices. The basal-most channel tier in isoslice-4 comprises *Type-8* and *Type-9* small-scale channels. *Type-9* channels are small and display an elongate dendritic channel pattern. They are located near Type 3 channels and display low amplitudes, are narrow and blind-ended. These small-scale channels are dominantly 100 - 200 m wide and 10 - 20 m thick. The channels trend NE-SW. A very large-scale, NW-SE trending *Type-1* channel is observed in the SW area of the isoslice but is not clearly image and appears discontinuous. *Type-8* (150 - 250m wide) channel morphologies are visible and display varied orientations. However, they are also not clearly imaged within this isoslice. Small *Type-6* channels are also observed at the Northern part of the isoslice.

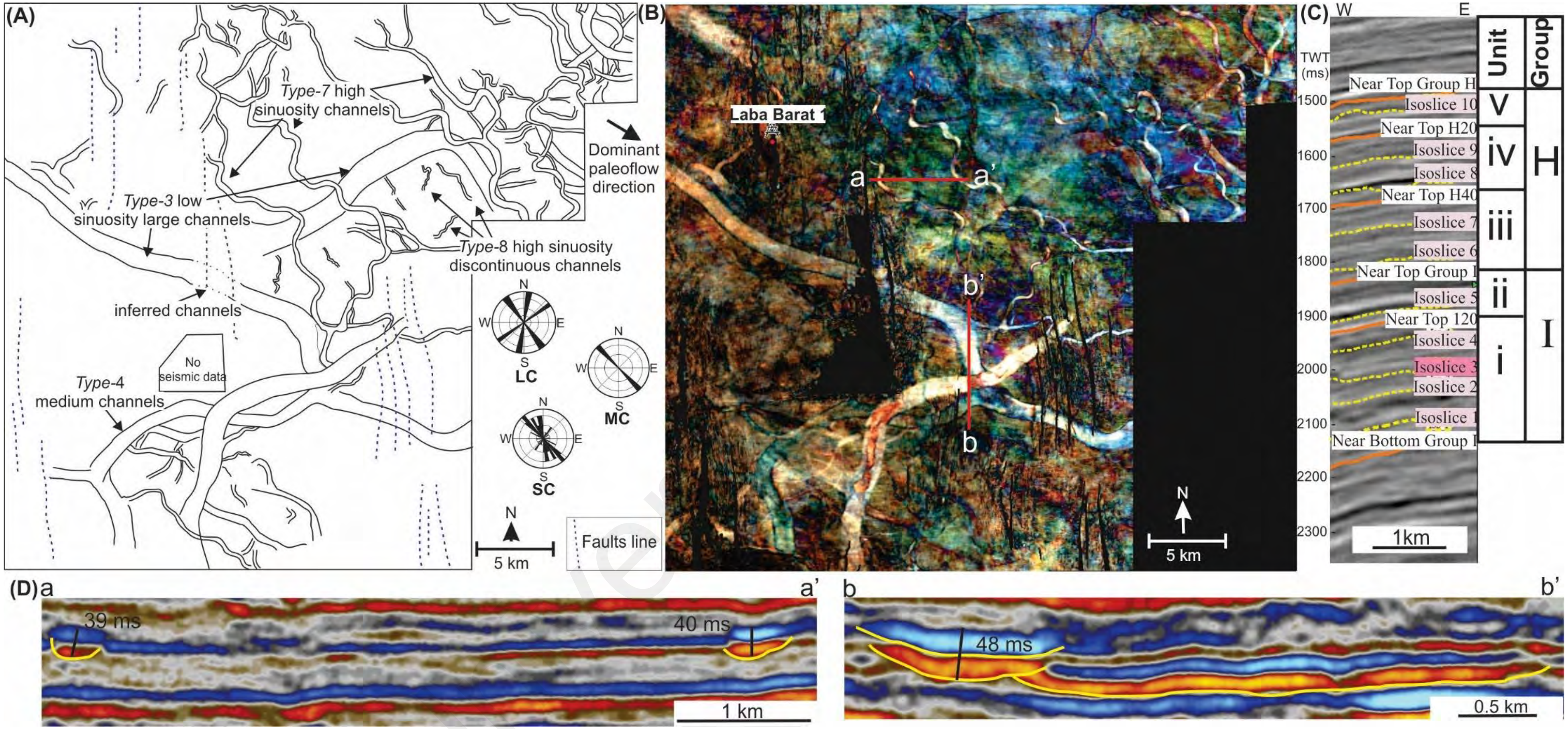

Figure 5.14: Channel systems of Isoslice-3, Unit I, Group I. (A) Interpreted plan-view map; (B) Un-interpreted plan-view map; (C) Isoslice-3 overlain isoslice-2 in Unit I; (D) Example of the horizontal and vertical relationships of the channel in the fluvial system of isoslice-3.

They form laterally continuous, high amplitude features which are 100-200 m wide and 10 - 35 m thick. The Type-6 channels have low sinuosity and trend NW-SE. These dendritic channel networks are then overlain by a younger, large-scale *Type-3* channel which has low sinuosity and trends NW-SE. Several small channels (less than 200 m wide) are observed to infill this *Type-3* channel. *Type-4* medium-scale channel (500 – 900 m wide) also display low sinuosities and trend NE-SW.

Interpretation: The variation in channel morphologies in Isoslice 4 is a product of moderate fluvial discharge and downstream controls, including tidal influence. The presence of dendritic channel networks composed of long, small-scale channels of *Type-9* morphologies suggest significant tidal influence. Dendritic channel networks are typically found on tidal flats and salt marshes, and usually have shallow channel depths (Hughes, 2012). However, the *Type-9* channel morphologies in isoslice-3 have thicknesses of up to 20 m. Deep tidal channels (up to 30 m) are observed to incise tidal flats in the modern-day lower delta plains of Brunei Bay and Mahakam Delta of tropical Southeast Asia (Razak Damit, 2001; Roberts & Sydow, 2003). These deep tidal channels may be abandoned distributary channels which have been deeply scoured by tidal currents. The large-scale *Type-3* channel overlying the older Type 9 small channels is interpreted as a large, tide-influenced distributary channel, based on the low sinuosity and the presence of cuspate meanders. The small, low sinuosity single channels of *Type-6* probably represent mixed load channels flowing SE. Low to moderate sinuosities in these channels may occur due to low discharge on a low gradient coastal plain.

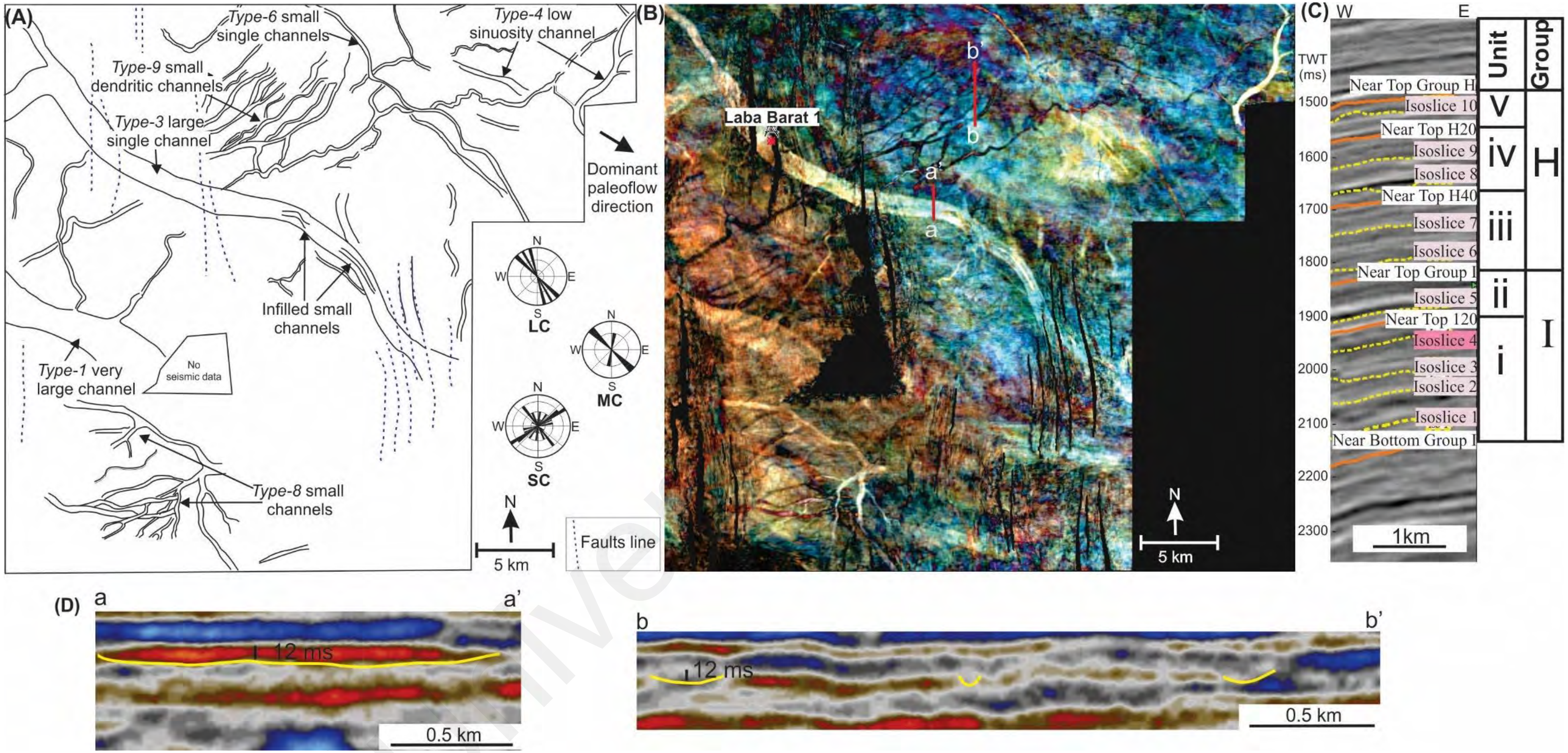

Figure 5.15: Channel systems of Isoslice-4, Unit I, Group I (A) Interpreted plan-view map; (B) Un-interpreted plan-view map; (C) Isoslice-4 being the top-most in Unit I; (D) Example on the horizontal and vertical relationships of the channel in the fluvial system of isoslice-4.

5.4.4.2 Unit II

Unit II overlies Unit I and is also part of Group I. Unit II is bounded by the Near Top I20 flooding surface and the younger Near Top Group I flooding surface. Thickness of this unit is approximately 150 m. Only one isoslice (isoslice-5) was produced within this unit.

a) Isoslice-5 (Fig 5.16c)

Description: Isoslice-5 is located approximately 75 m above isoslice-4. Isoslice-5 is dominated by large-scale channels of *Type-1*, *Type-3*, and medium-scale channels of *Type-4* morphologies (Fig 5.16a, b). A very large-scale *Type-1* channel is present in the middle of the isoslice. It displays bright amplitude, but the channel edges are not clearly delineated. The channel is more than 3 km wide and less than 10 m thick, and trends E-W. Medium-scale and small-scale channels with clearly-defined edges are seen to infill this very large-scale channel. Large channels are present and trend NNW-SSE. These channels have low to moderate sinuosities (1.2 – 1.5), and exhibit a clear funnel-shaped geomorphology, with flaring towards the south. *Type-4* medium-scale channels with low sinuosities are observed attached to *Type-3* channels, and trend NW-SE. Small-scale channels are rarely visible within this isoslice. Only *Type-7* small-scale channel morphologies are observed, which also trend NW-SE. The northern area of the isoslice is mostly dominated by diffused high amplitudes while the southern area is dominated by diffused low amplitudes.

Interpretation: The moderate sinuosities of distributary channels within isoslice-5 suggest that the fluvial system developed on a low gradient, such as on a coastal or delta plain. The very-large-scale *Type-1* channel probably represents an unconfined channel belt, based on the poorly-defined channel boundaries and the shallow relief. The small and medium-scale channels infilling this very large-scale channel probably represent laterally shifting channels due to variations in fluvial discharge and low accommodation space. The large-scale channels are interpreted as fluvial or distributary channels. The funnel-shaped geomorphology indicates strong tidal influence and a paralic, river mouth position. The channels show southeast ward increase in width and decrease in thickness, which indicate that the sea was roughly located south-southeast of the study area. However, it must be cautioned that due to the limited area of the isoslice, it is also possible that the funnel-shaped geomorphology may only be because of channel widening due to frequent flood and local controls such as overbank lateral accretion and erosion (Piégay et al., 2005; Krapesch et al., 2011; Buraas et al., 2014; Nardi & Rinaldi, 2015; Comiti et al., 2016; Surian et al., 2016).

5.4.4.3 Unit III

Unit III is bounded by bottom surface of Near Top Group I to top surface of Near Top H40. This unit overlies Unit II in the interval of interest succession. Thickness of this unit is approximately 270 m. Two isoslices (isoslice-6 and 7) were produced within this unit.

a) Isoslice-6 (Fig 5.17c)

Description: Isoslice-6 is in the lower part of Unit III and is located approximately 95 m above isoslice-5. There is high variability in channel morphology within isoslice-6. Isoslice-6 contains channel geometries of *Type-3*, *Type-4*, *Type-5,* and *Type-8* (Fig 5.17a, b). A large-scale *Type-3* channel is observed in the southwestern area of the isoslice. It exhibits high seismic frequency and low seismic amplitude reflection. The channel is >1 km wide and 10 – 15 m thick, but the channel edges are not well-defined. Medium-scale channels of *Type-4* (<1km wide) are clearly defined, have low sinuosity to straight morphologies and trend E-W. These channels cross the length of the isoslice and have low amplitudes and chaotic seismic reflections (Fig 5.17d).

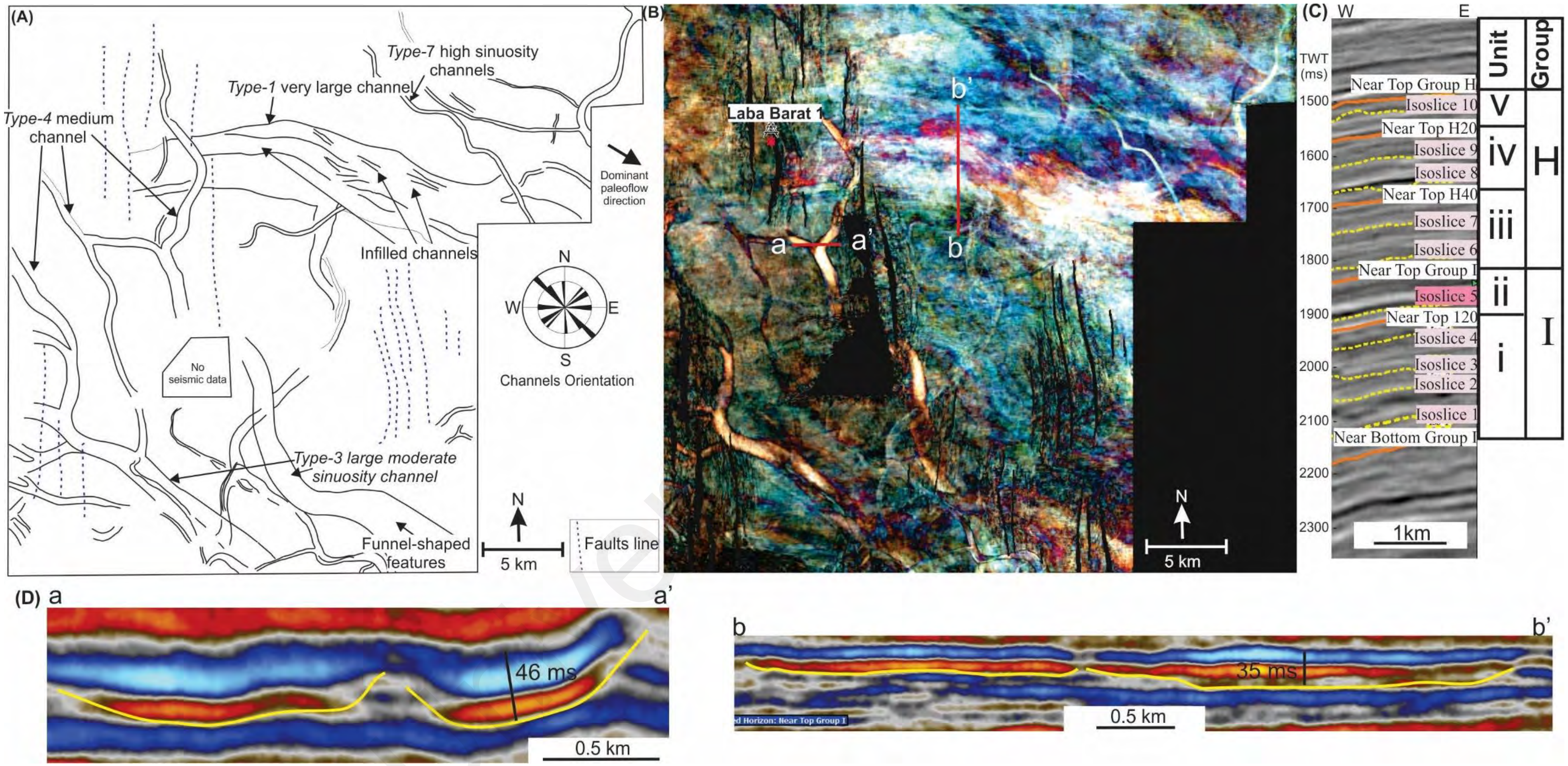

Figure 5.16: Channel systems of Isoslice-5, Unit II, Group I (A) Interpreted plan-view map; (B) Un-interpreted plan-view map; (C) Isoslice-5 of Unit II; (D) Example on the horizontal and vertical relationships of the channel in the fluvial system of isoslice-5.

Medium-scale channels of *Type-5* are also visible and trend NW-SE. The Type 5 channels tend to narrow into small channels and are blind-ended. Small *Type-8* channels are discontinuous, have variable orientations and are found throughout the isoslice. Some of the small-scale channels act as through-flowing channels connecting between larger channels, with channels disappearing into marshes or lakes.

Interpretation: Type-3, Type-4, and Type-5 channels in the basal-most incision tier in isoslice-6 are interpreted as fluvial or distributary channels. High energy and cohesive factors maybe from clay minerals or chemical weathering increase the shear stress to entrained sediments, thereby increase the bank stability, and led to the straight channel morphology. The low amplitude character of the channels suggests that channel-fill lithology is very similar to the adjacent floodplain deposits during transgression, i.e., fine-grained.

b) Isoslice-7 (Fig 5.18c)

Description: Isoslice-7 is located near the top of Unit III, and approximately 75 m above isoslice-6. The channels within isoslice-7 include *Type-3, Type-4, Type-6, Type-8* and *Type-9* morphologies (Fig 5.18a, b). A large E-W trending *Type-3* channel (1 – 1.8km wide) of moderate sinuosity (1.5-2.0) is present in the basal tier of the isoslice. This large channel is clearly defined with bright amplitude and laterally continuous seismic reflection. The channel is meandering and rarely has any attached small channels. *Type-4* medium-scale channels trend NW-SE. Smaller *Type-8* channels are commonly attached to *Type-4* channels at right angles (around 90°, i.e., trending NE-SW). Small *Type-9* channels (100 - 200m wide) form dendritic networks of parallel channels trending NE-SW. These small channels are clearly defined with low to moderate seismic amplitude and laterally continuous seismic reflection. These small-scale channels are also interconnected to each other and separated by island-like features.

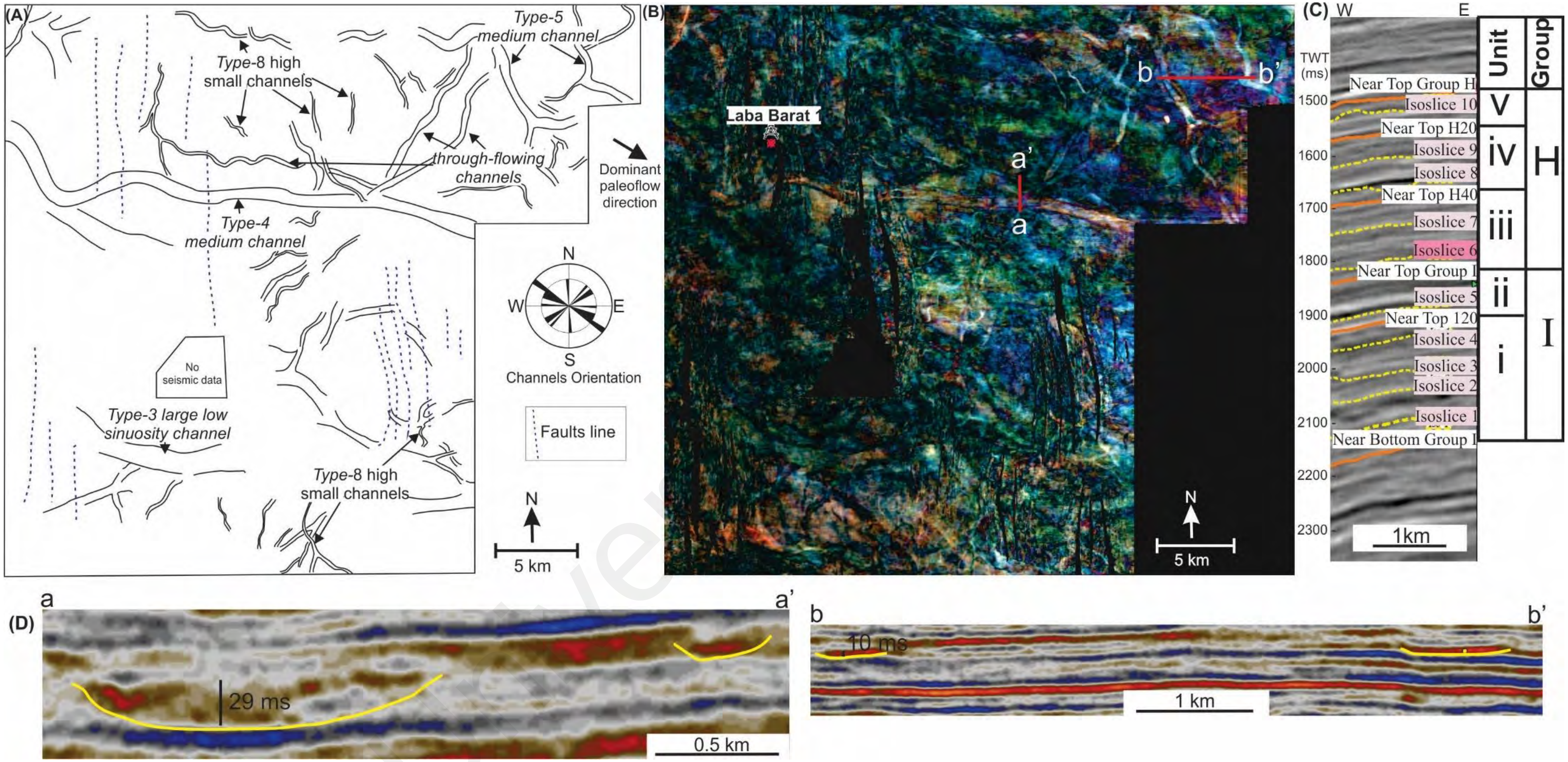

Figure 5.17: Channel systems of Isoslice-6, Unit III, Group H (A) Interpreted plan-view map; (B) Un-interpreted plan-view map; (C) Isoslice-6 is at the bottom section of Unit III; (D) Example of the horizontal and vertical relationships of the channel in the fluvial system of Isoslice-6.

Interpretation: The channel system in Isoslice-7 suggests that the upper part of Unit III is a tidally influenced channel system associated with a transgressive systems tract. This interpretation is supported by the clear presence of dendritic *Type-9* channel networks, which are typical of tidal channel networks. The tidal channels drain into NW-SE trending, medium channel streams. A dendritic network with elongate, parallel trending tidal channels often develops in regions with longitudinally elongated landforms such as outcropping resistant rock bands or vegetated islands (Hughes, 2012). Along the land slope, tributary streams continue to branch out in a parallel manner. These dendritic parallel and shallow channels suggest an immature drainage pattern which often occur on flats that are repeatedly impacted by storms (Hughes, 2012). Periodic storm events will either moderately or completely 'reset' these channels. Thus, these parallel channels morphologies are regularly straight, ephemeral, some perennial, and possibly being removed and recreated with every storm. The *Type-3* channels are interpreted as meandering fluvial bypass channels. This meandering shape of the channel also suggests that it carried mixed-load sediments with low discharge.

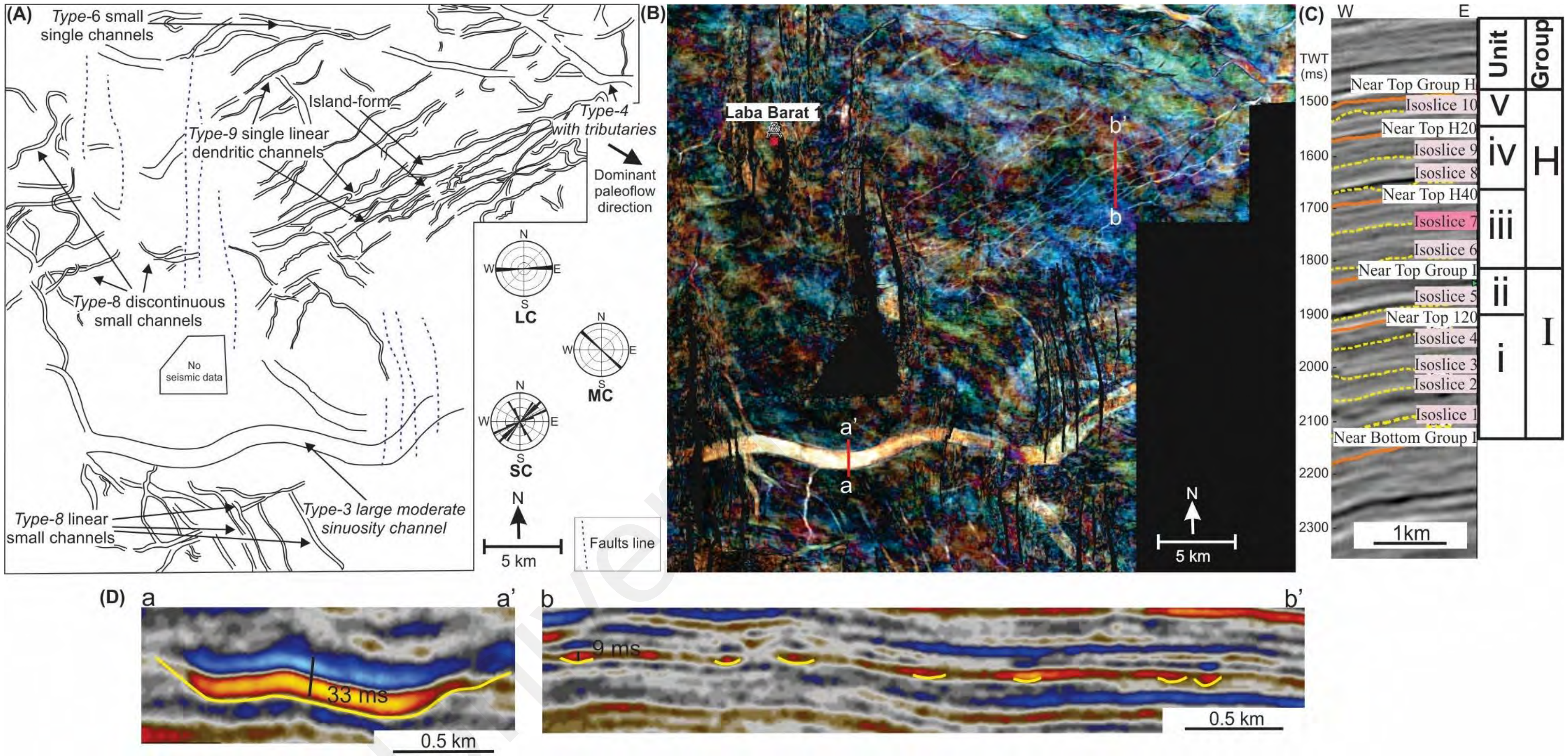

Figure 5.18: Channels systems of Isoslice-7, Unit III, Group H (A) Interpreted plan-view map; (B) Un-interpreted plan-view map; (C) Isoslice-7 is at the upper section of Unit III; (D) Example on the horizontal and vertical relationships of the channel in the fluvial system of isoslice-7.

5.4.4.4 Unit IV

Unit IV is bounded by the Near Top H40 surface and the overlying Near Top H20 surface. This unit overlies Unit III in the interval of interest. Thickness of this unit is approximately 190 m. There are two isoslices (isoslice-8 and 9) produced within this unit.

a) Isoslice-8 (Fig 5.19c)

Description: Isoslice-8 represents fluvial systems at the lower part of Unit IV and is located approximately 80 m above Isoslice-7. Isoslice-8 contains *Type-3*, *Type-4, Type-5*, and *Type-8* channels (Fig 5.19a, b). Small-scale channels of *Type-8* (100 – 200 m wide) are abundant in the northern part of the isoslice. They have a high sinuosity and trend SW-NE. The medium-scale channel of *Type-4* in the north is seen to overlie small dendritic channels. This low sinuosity medium-scale channel trends in a NE-SW direction. *Type-5* medium-scale channels show anastomosing-like patterns and tend to broaden from small channels into larger channels or *vice-versa*. The channels trend W-E and are blind-ended. The southern part of Isoslice-8 is dominated by diffuse low seismic amplitudes. This area shows indistinguishable margin of *Type-3* large-scale channel morphologies, and *Type-8* small-scale channels.

Interpretation: According to the sequence framework developed by Hentz & Zeng (2003), the prevalence of small-scale channels in this isoslice suggests that they are part of a highstand systems tract. *Type*-5 channels are interpreted to flow in an eastward direction, based on the eastward widening of the channels. The small channels closely associated with the Type-5 channels may represent tributary channels, based on their right-angle relationship. These small channels are not well-defined and appear to be blind-ended. It is possible that they are tidal channels originating within marshes or tidal swamps. Numerous tributary channels feeding them would contribute to a higher volume of flow discharge; therefore, eroding channel banks, hence broadening the channel. Other than that, the tidal flood currents may also contribute to channel widening. Low accommodation space contributes to channel switching. Anastomosing-like channel patterns observed in this isoslice might be due to image superimposition of channels at different tiers within a 20 m vertical thick succession. Based on the subtle low diffuse amplitude at the southern part area, the large-channel may be an abandoned distributary channel, where their channel fills being similar to the overbank fills, i.e., fine grained (Wood, 2007; Hubbard, 2011). Over time, overbank deposition will interact with abandoned channels as they fill (Rowland et al., 2005; Citterio & Piégay, 2009). Their unclear channel edges may be due to limit of seismic resolution. Another reason for the unclear channels imaged maybe due to no prevalent changes in lithology such as coal seams occurring immediately above the channel bed (Carter, 2003), thus dampening the variation in seismic frequency in isoslice-8.

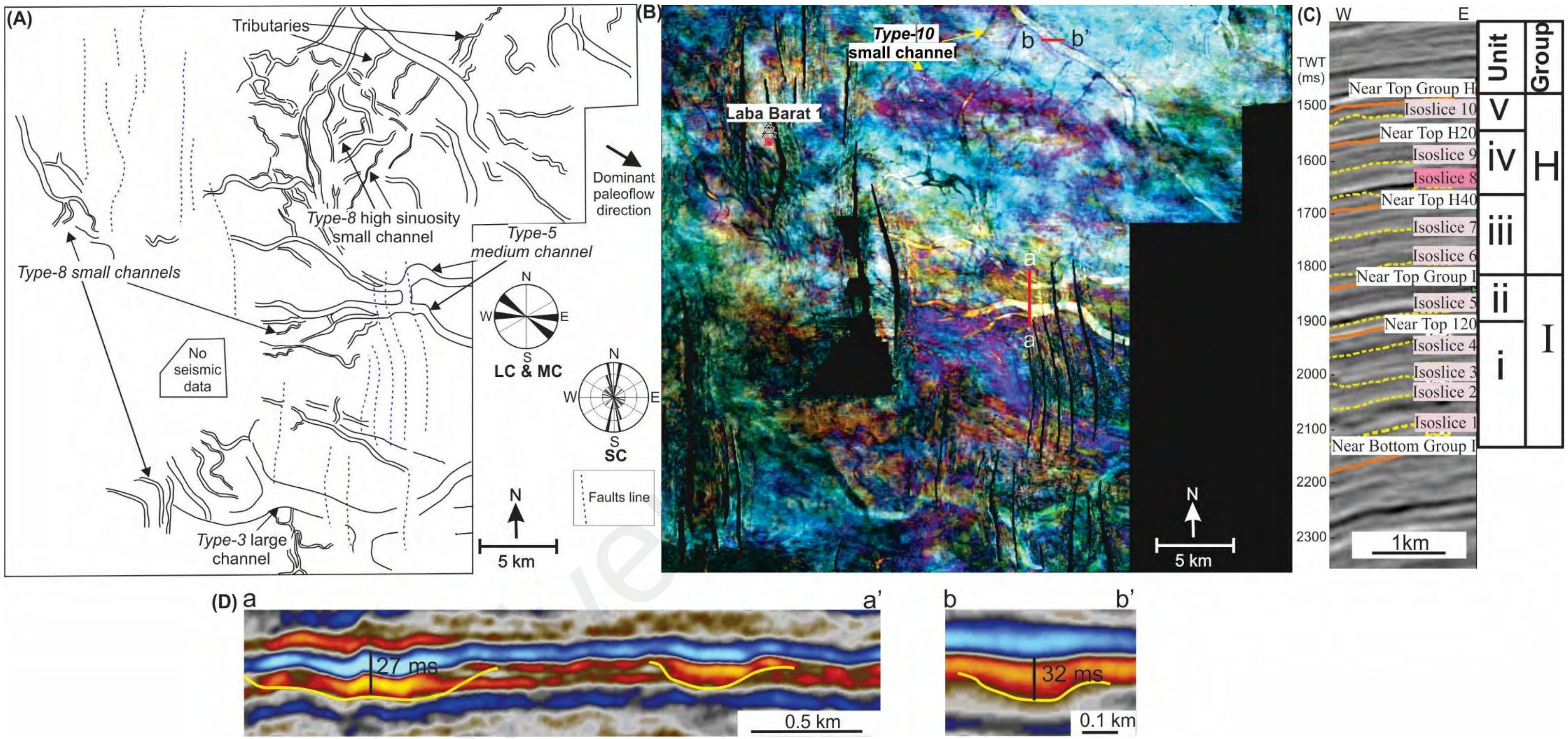

Figure 5.19: Channel systems of Isoslice-8, Unit IV, Group H (A) Interpreted plan-view map; (B) Un-interpreted plan-view map; (C) Isoslice-8 is at the bottom section of Unit IV; (D) Example of the horizontal and vertical relationships of the channels in the fluvial system of isoslice-8.

b) Isoslice-9 (Fig 5.20c)

Description: Isoslice-9 is in the upper part of Unit IV and located approximately 60 m above Isoslice-8. The isoslice contains *Type-1, Type-3, Type-4, Type 7,* and *Type-8* channels (Fig 5.20a, b). The basal-most tier of isoslice-9 is characterised by small-scale channels of *Type 7* (150 – 450 m wide) and *Type-8* (<150 m wide). They are abundant at the northern part of the isoslice area. *Type-8* channels are adjoined to *Type-7* channels at almost 90^0, and trend NE-SW. They are only visible at one side of the *Type-7* channel margin at the north-eastern part, however none visible at the opposite margin. *Type-7* channels are highly sinuous, exhibit meander scrolls, trend SE-NW and are thicker (up to 35 m) compared to the *Type-8* channels. Larger channels of *Type-1* and *Type-3* are present in the southern part of the study area and appear to be younger. The southwest area of the isoslice is dominated by diffused low seismic amplitudes.

Interpretation: The small-scale channels of *Type-7* in this isoslice may be interpreted as possible incised valleys due to the presence of dendritic tributary channels along their north-eastern margins (*Type-8* small channels morphologies) (Posamentier, 2001). However, this interpretation is not concrete enough as the presence of dendritic tributary channel is only one-sided. Active tectonic compression and inversion activities during the Miocene period of the Malay Basin may have resulted in the local tectonic uplift on one-side of the channel margin. Evidence of meander scroll bars is consistent with lateral migration over time of meandering channels (Allen, 1965; Ielpi & Ghinassi, 2014). Scroll bars developed as a result of primary flow that erodes the outer bank and at the same time deposit sediment in the inner bank (Van de Lageweg et al., 2014). The sharp meander bends of *Type-7* channel channels indicate higher migration rates from confluence channels of *Type-8* from the NW direction. Therefore, the *Type-7* channels are more likely to be fluvial channels.

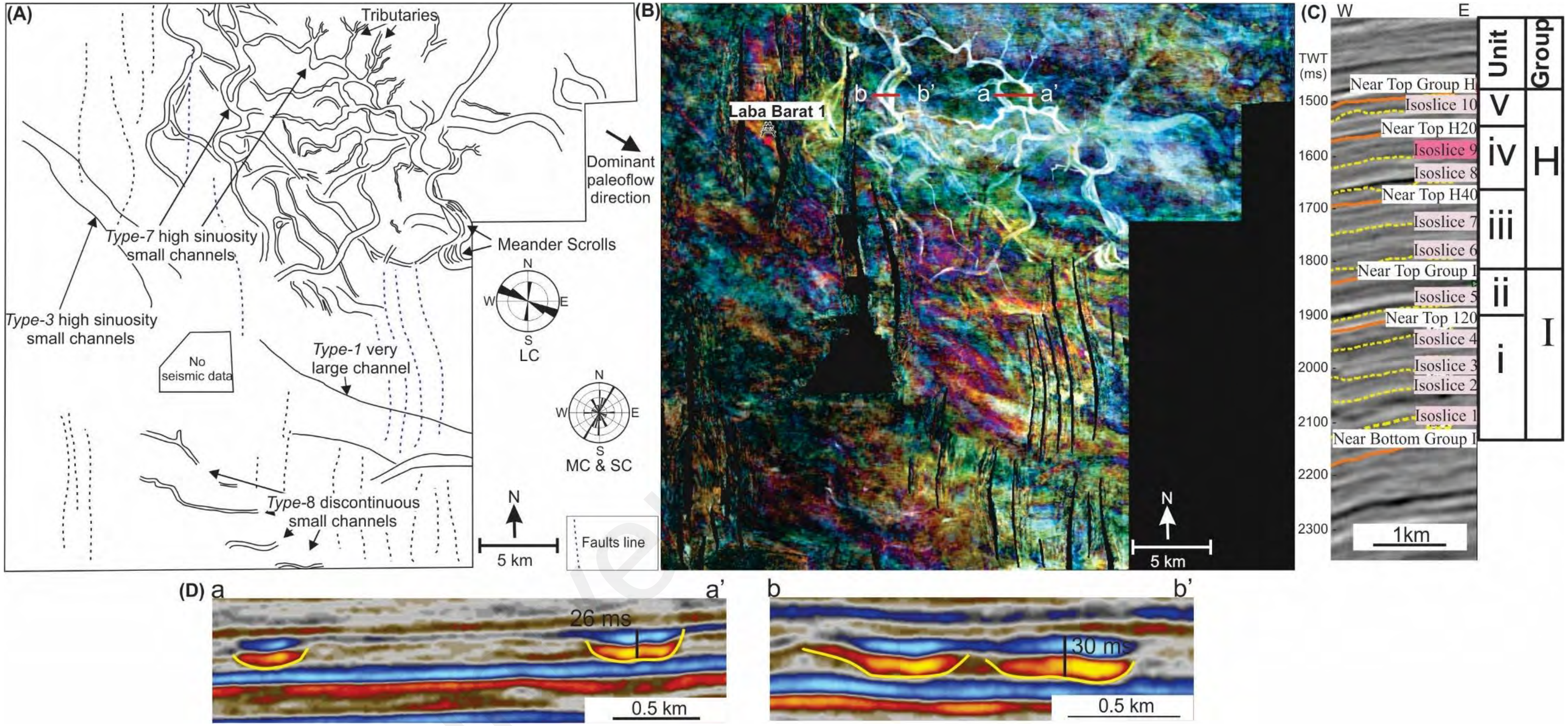

Figure 5.20: Channel systems of Isoslice-9, Unit IV, Group H (A) Interpreted plan-view map; (B) Un-interpreted plan-view map; (C) Isoslice-9 is at the upper section of Unit IV; (D) Example of the horizontal and vertical relationships of the channel in the fluvial system of isoslice-9.

5.4.4.5 Unit V

Unit V is bounded by the Near Top H20 flooding surface and the younger Near Top Group H flooding surface. This unit overlies Unit IV in the interval of interest. Thickness of this unit is approximately 100 m thick. There is only one isoslice (isoslice-10) produced within this unit.

a) Isoslice-10 (Fig 5.21c)

Description: Isoslice-10 is the shallowest, and the youngest imaged isoslice from Unit V. It is located approximately 100 m above isoslice-9. This isoslice contains *Type-3*, and *Type-6* channels (Fig 5.21a). Isoslice-10 is dominated by overall diffused low amplitude geobodies. It comprises large-scale channels of *Type 3* which are >1 km wide and trend W-E. The *Type-3* channels exhibit low amplitude with high-frequency seismic reflection. All the channel margins are not clear enough due to low seismic amplitude. In cross-section, this channel type is expressed as low amplitude concave-up features. Small-scale channel morphologies of *Type-6* are rarely visible but also trend W-E.

Interpretation: The lower number of channels within this isoslice may suggest that most channels have switched to another adjacent location due to progressive superposition of distributary channels and prograding of the coastline. Channels in isoslice-10 are interpreted as representing a late highstand fluvial system in the H Group of the Malay Basin. Additionally, this interval is within the Middle Miocene age of the Malay Basin, which is within the duration of compressional uplift which has continued since early Miocene times and thus the rate of reduction of accommodation space has progressively increased with associated relative sea-level fall. The low amplitude seismic suggests that the channel fill lithology is most likely similar to the adjacent overbank and that the channels may represent abandoned distributary channels. The channels were abandoned due to autogenic controls such as channel switching and avulsion.

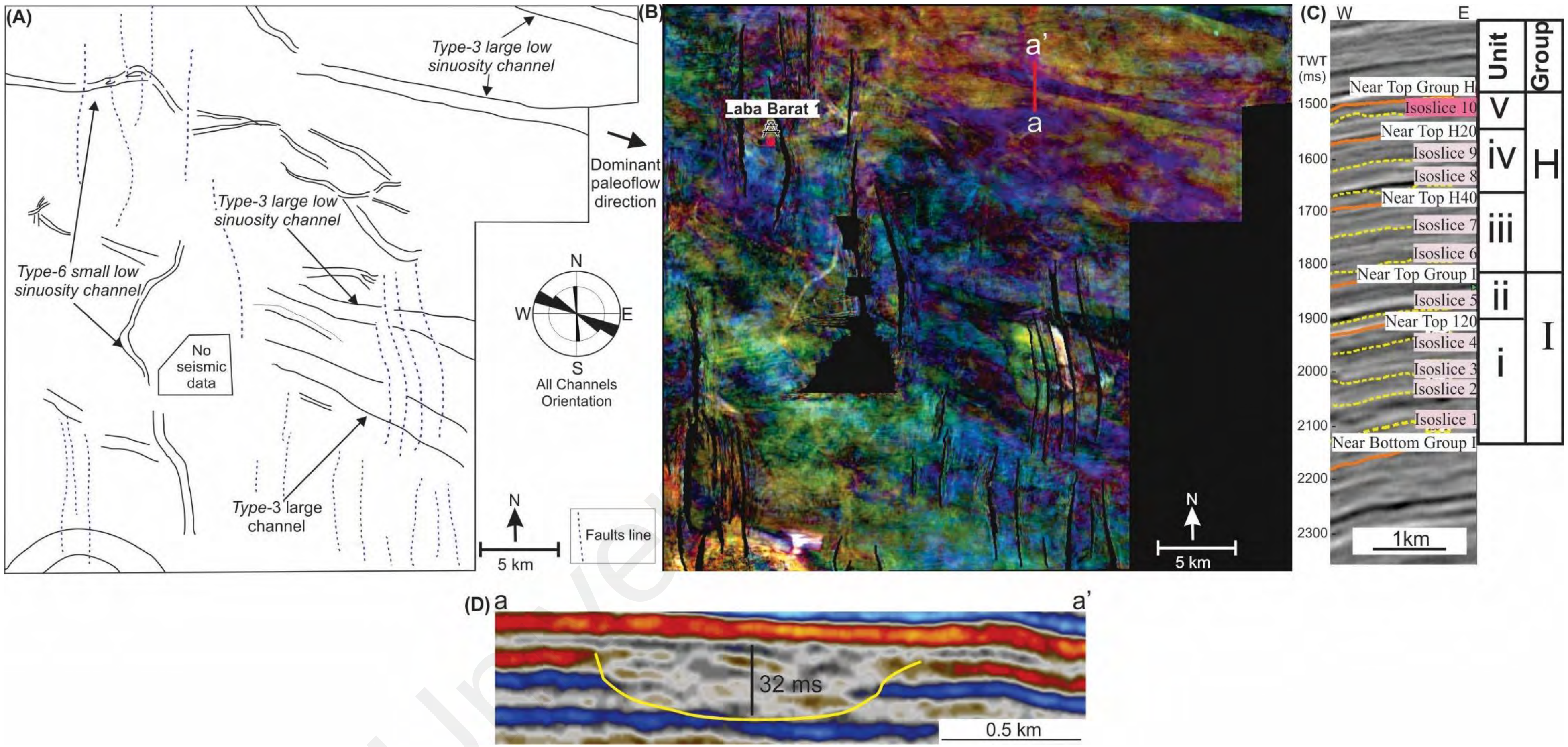

Figure 5.21: Channel systems of Isoslice-10, Unit V, Group H (A) Interpreted plan-view map; (B) Un-interpreted plan-view map; (C) Isoslice-10 of Unit V, marked the uppermost fluvial systems in this study; (D) Example of the horizontal and vertical relation of the channel in the fluvial system of isoslice-10.

5.4.5 Evidence for Significant Tidal Influence from Planform Geometry

Several planform seismic geomorphological features observed in the studied isoslices provide strong evidence for significant tidal influence within the Group H and I fluvial systems of the Malay Basin (Fig 5.22 and Fig 5.23). Tidal channel systems commonly form dendritic networks of low order, usually three- to four- orders of branching channels, with lower order blind-ended tidal creeks connected to higher order tidal channels (Fig 5.22) (e.g., van Veen, 1950; Eisma, 1998; Hibma et al., 2004). This fractal hierarchy of channels is imaged in almost all the isoslices in this study. The lowest order is the smallest creeks at the edge of the network, which meet to form a channel of the next order, which is often more extensive. The channel branch lengths decrease from low to high order channels, and their widths usually increase from low to high order channels. Once channels begin to form, cross-grading (the tangential slope to the primary channel gradient) and micropiracy (flow capture by a slightly deeper channel) will result in channel combination which produces through-flow channels and dendritic network formation (Leopold et al., 1964; Hughes, 2012). These narrow, through-flowing or dead-end channels are usually called tributary or affluent waterways (van Veen, 1950; Hibma et al., 2004a; Hughes, 2012). Some of the dead-end channels observed in this study are assumed to have drained into lakes or bays, and they might also have dried up when they entered marshes or perish on an alluvial or flood plain.

The interpreted distributary channels in the studied isoslices form a branching network of channels that radiate from a single channel (Fig 5.22E). The distributary channels exhibit low to high sinuosities, depending on their hydrodynamic energy and autogenic processes. Bifurcations usually occur in the channels at sharp bends resulting in intense thalweg scouring (Ottevanger et al., 2012; Blanckaert et al., 2013). The modern-day river systems of Rajang Delta, Sarawak and Klang-Langat, Selangor share a similar characteristic of the branching network to this study.

Cuspate meanders differ from typical meanders in being composed of two concave inner bends flanking a pointed tip (Fig 5.23). The outer bend is rounded, as in typical meanders. Cuspate meanders are only found associated with channels experiencing significant tidal influence (Dalrymple et al., 2012; Hughes, 2012). Opposing, mutually evasive ebb and flood tidal currents in a channel result in the erosion of the point bar and reworking into a cuspate morphology. Within a tidal cycle period, the division of flood and ebb flow paths, intensified by fluvial mechanisms, produces a pronounced meander cuspate bend. Stationary cuspate meanders tend to revert to the sinuous form in the fluvio-tidal zone due to the coinciding energy of fluvial and tidal currents. Many modern-day tidal and fluvial-tidal channels exhibit cuspate meanders. Examples from Malaysia include the tidal channels of the tide-dominated Klang Langat Delta, The river mouth of the Perak and Ayer Tawar Rivers, the tidal channels of Kuala Sepetang of Kuala Gula tidal channel complex in Perak, and the distributary channels of the tide-dominated Rajang Delta and Lupar Estuary in Sarawak (Fig 5.24).

Based on relative strength of the flood and ebb tides, the meandering within the affected tidal channel can be distorted (Figure 5.21E). The distortion of the meanders is called ' goose-necking ' (see Fagherazzi et al., 2004; Seminara, 2006). Skewed goose-neck meander bends indicate that sediment movement was towards the skewedness (Seminara, 2006). Clear funnel-shaped channel morphologies, where channel width widens in a certain direction, are observed within the isoslices in this study (Fig 5.22d). They most likely represent downstream channel broadening at the distributary mouth of fluvial-tidal channels. Channel broadening is caused by the seaward increase in the tidal prism at tide-influenced and tide-dominated channel mouths. A funnel-shaped feature at the distributary channel mouth (modern-day) is due to tidal amplification associated with tidal resonance (Dalrymple & Choi, 2007; Dalrymple et al., 2012).

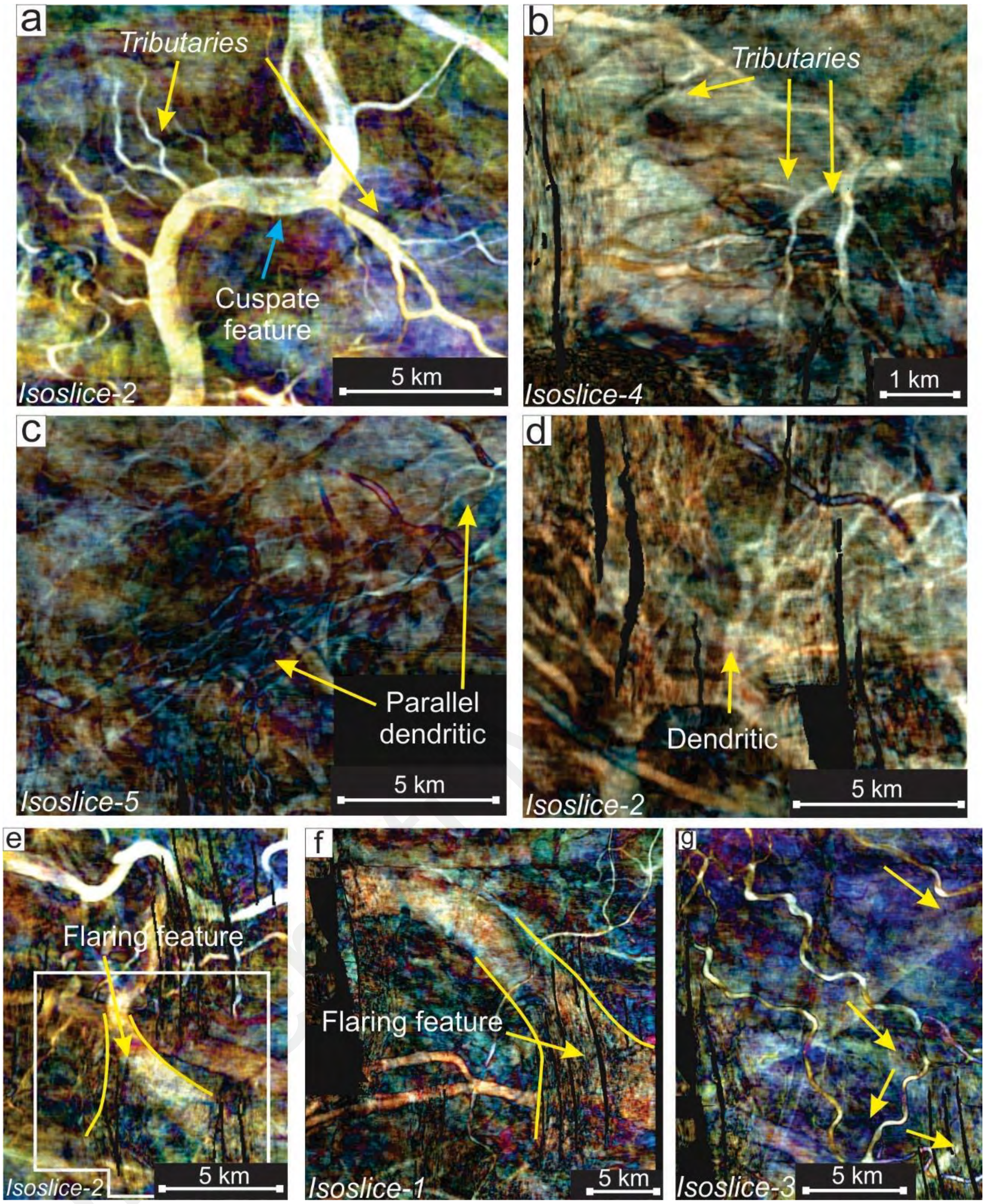

Figure 5.22: Geomorphological characteristics indicative of tidal influence observed in the isoslices from Miocene Group H and I of the Malay Basin. (A) Cuspate meanders and flaring feature; (B)Tributaries; (C) Elongated parallel dendritic channel networks; (D) Dendritic channel networks; (E&F) Flaring features; (G) Gooseneck features indicative of sediment movement towards the skewedness, the yellow arrows show channels flow direction.

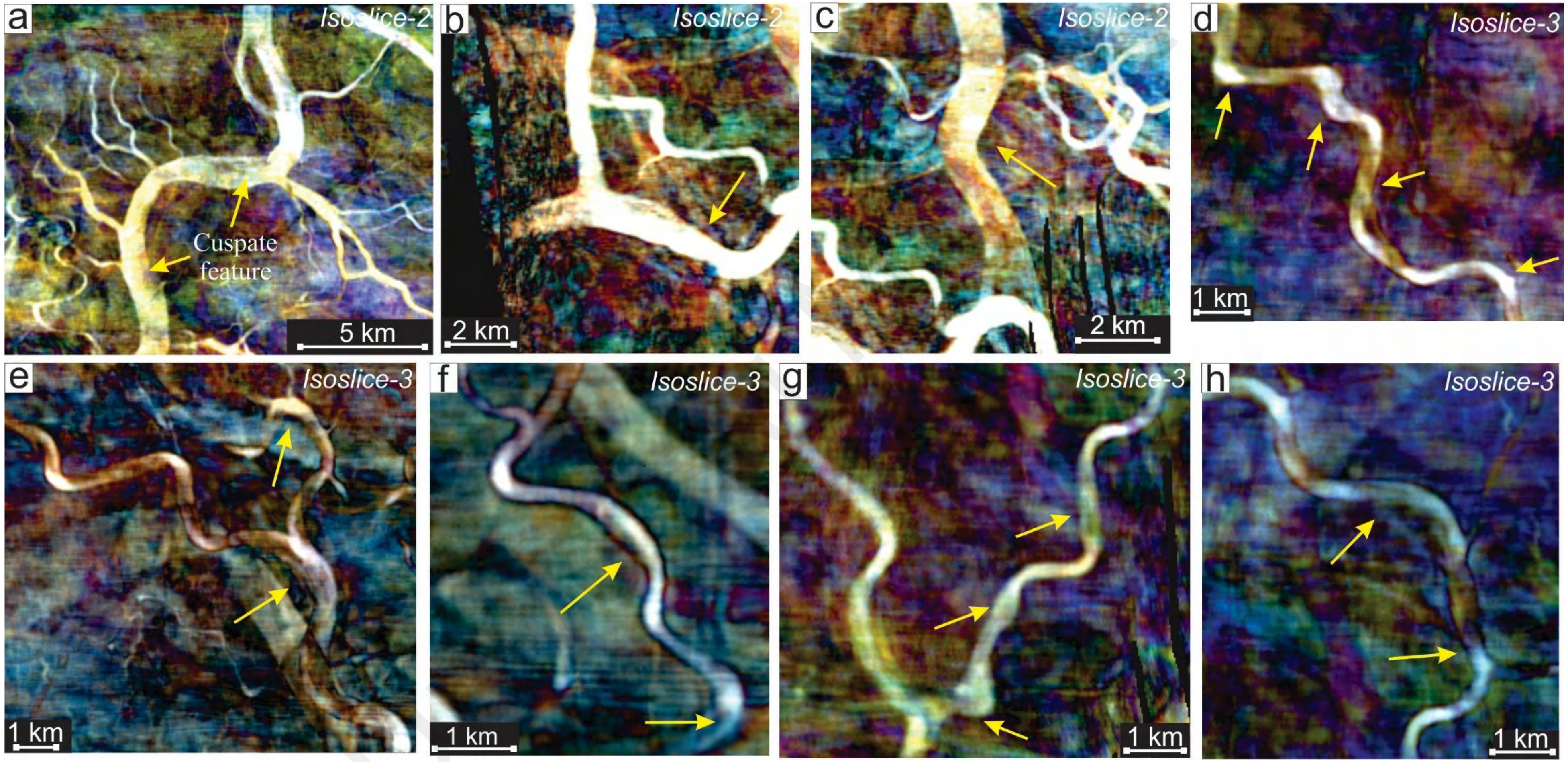

Figure 5.23: Geomorphological characteristics of cuspate meanders indicative of tidal influence observed in the isoslices from Miocene Group H and I of the Malay Basin. Arrows indicate the meander bend associated with 'pinch and swell' of cuspate/box-like meander feature.

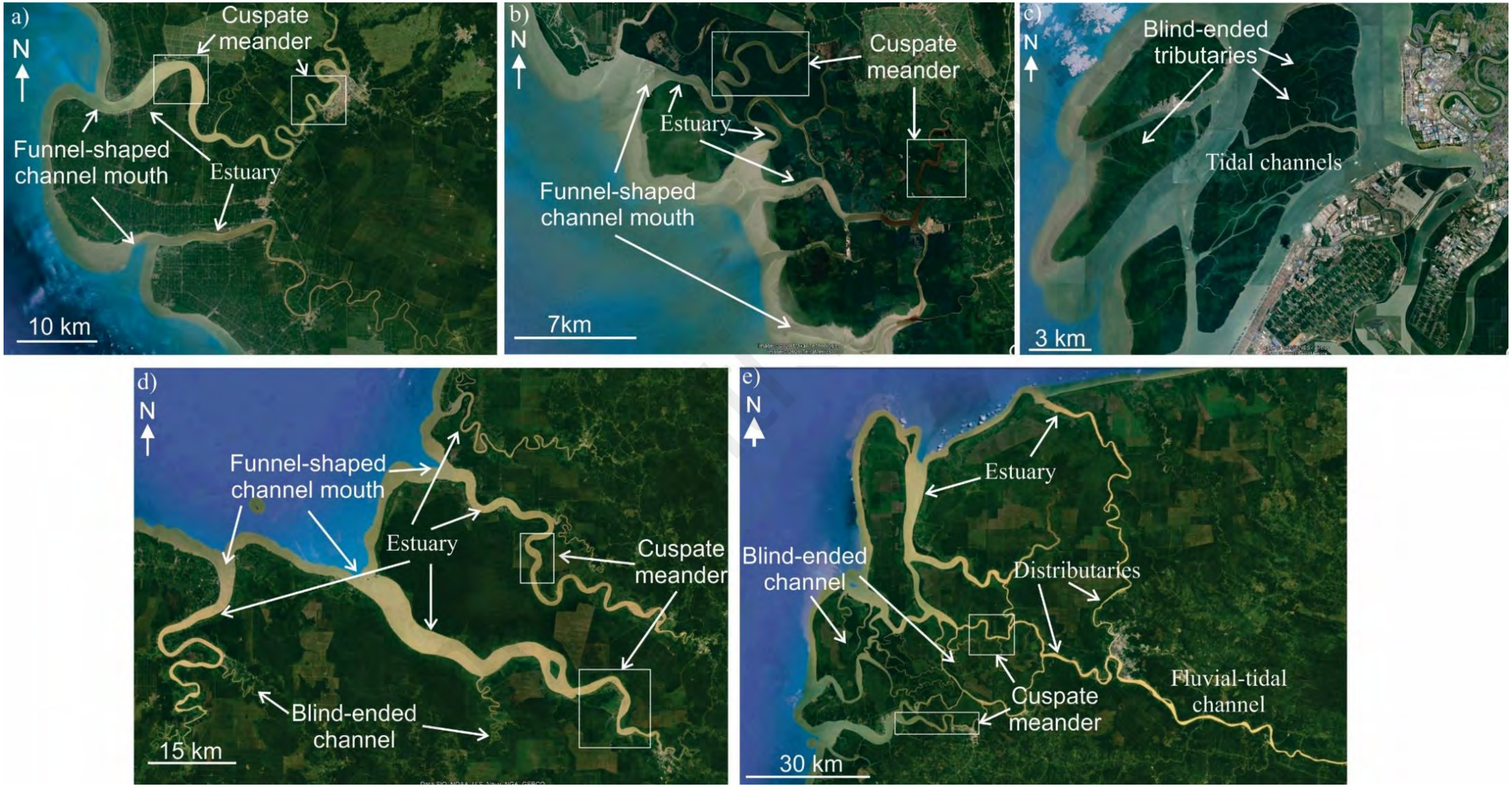

Figure 5.24: Examples of modern-days tide-influenced to tide-dominated river systems. A) Perak and Air Tawar Rivers; b) Tidal channel complex in Kuala Gula, Perak; c) Klang-Langat Delta, Selangor; d) Lupar Estuary, Sarawak; and e) Tide-dominated Rajang Delta, Sarawak. White outlined boxes in images show cuspate or box-like meanders, typical of tide-influenced and tide-dominated channels.

5.4.6 Channel Geobody Evolution

Channel geobody geomorphologies were imaged on selected isoslices within the studied seismic volume using RMS amplitude analysis, combined with spectral decomposition analysis. The spatial and temporal mapping of channel geobody distributions within these isoslices provides a relatively good record of channel stratigraphy of Group H and I in the selected study area. Figures 5.25 to 5.26 illustrate the evolution of the channel network through time.

Isoslice-1 to 4 (Unit I) and isoslice-5 (Unit II) are part of Group I. The largest channel geobody observed in the seismic data is in Unit I, in Isoslice-1 near the bottom of the interval of interest. It is more than 3-6 km wide, trends E-W with low sinuosity (Fig. 5.11). Another large - scale channel geobody is also observed in isoslice-5, where it is 5 - 6 km wide and trends W – E. However, its channel edges are not clearly defined compared to the one in isoslice-1.

Channel sizes are highly variable in all the isoslices of Unit I and Unit II, ranging between very large-scale and small-scale channel geobodies. Channel geobodies are more abundant in Unit I become in Unit II. Variable channel geomorphologies dominate in Isoslice-1 to 4 (Unit I), with abundant NW-SE trending small-scale channel morphologies. In contrast, Isoslice-5 (Unit II) which is in a shallower position in Group I, contains fewer channel geobodies, which trend NW-SE. Large-scale channels in the deeper tiers of Isoslice-5 are clearly defined with low to high sinuosities, and are associated with clearly observed small-scale channels which have variable orientations. Medium-scale channels may or may not be associated with small-scale channels.

Interestingly, small channels within Isoslice-1 to 4 reveal a variety of morphologies, but all dominantly trend NW-SE. Isoslice-1 and Isoslice-2 display plentiful small-scale channels regardless of their association with larger channels. The small-scale channels of Isoslice-3 and Isoslice-4 reveal much more diverse morphologies, where they exhibit different channel arrays with higher sinuosities and laterally continuous seismic reflections.

The younger Group H includes Isoslice-6 and Isoslice-7 (Unit III), Isoslice-8 and Isoslice-9 (Unit IV), and Isoslice-10 (Unit V). The channel evolution within Group H is almost similar to that observed in Group I. Abundant channels are visible at the lower section of Group H in Unit III, and progressively decrease in number through time.

The shallowest isoslices typically have a higher seismic resolution than deeper isoslices. Therefore, it is expected that channel geobodies are better imaged especially smaller scale channels in shallower isoslices, giving rise to an increased dominance/ frequency of small-scale geobodies in the uppermost part of the stratigraphy. Nevertheless, despite the improved resolution in shallower parts of the succession, the trends observed vertically are concluded here as representing real changes in sedimentary style and geobody architecture through time.

In general, the largest (widest) channel geobodies and the largest number of small-scale channels geobodies are present in the older stratigraphy in Group I and consistently continue almost similar patterns in Group H through time. However, there are no very large-scale channels observed within Group H. Small- and medium-scale geobodies are dominant in the older isoslices. They become less common in the younger isoslices, which may reflect the overall back-stepping and/or lateral shift in facies belts through time as the fluvial-tidal system underwent transgression. It is also observed that channel geobodies of all scales display a NW-SE orientation consistently through time with only slight variations.

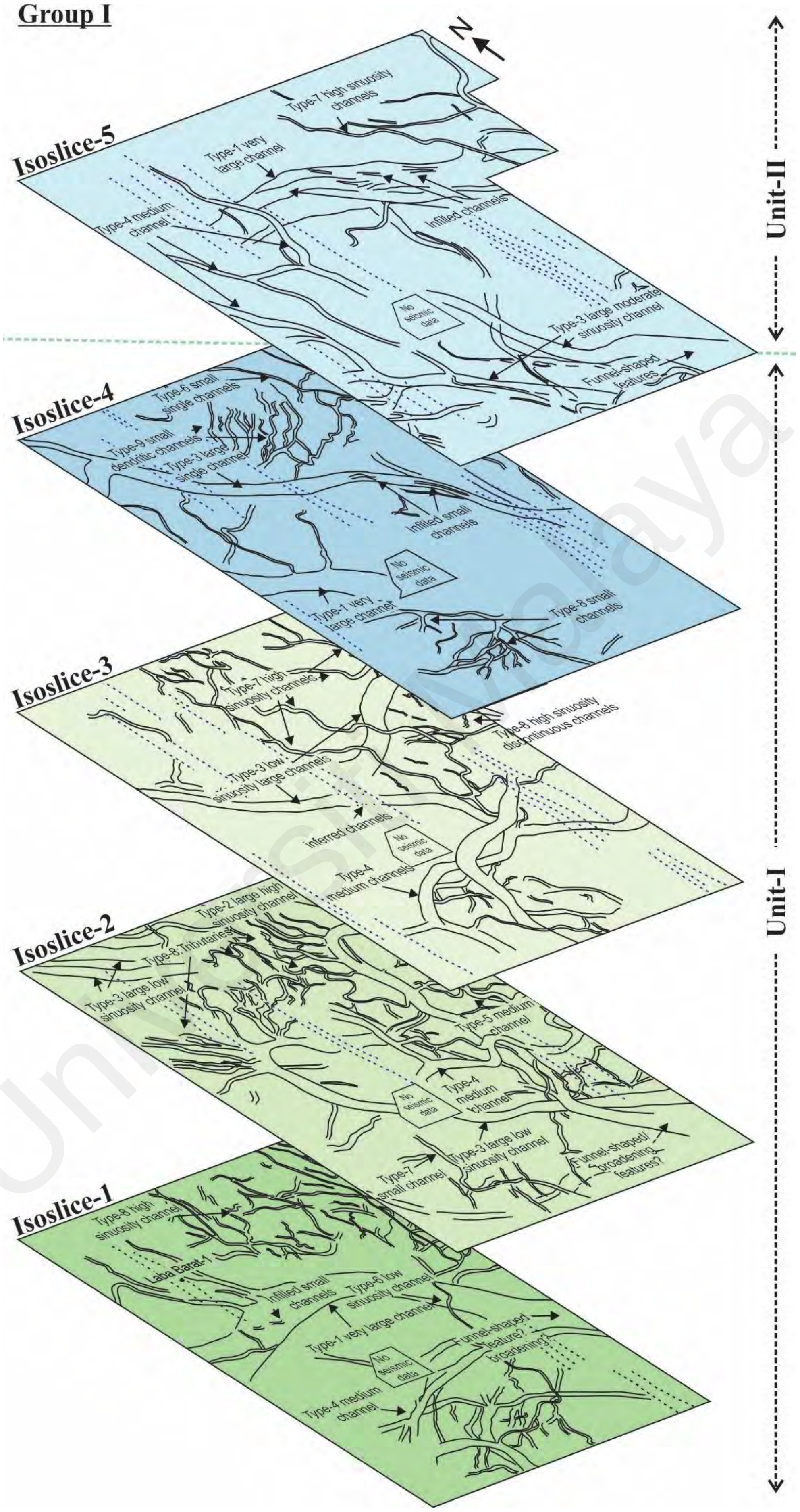

Figure 5.25: Evolution of fluvial system from bottom to upper section of Group I.

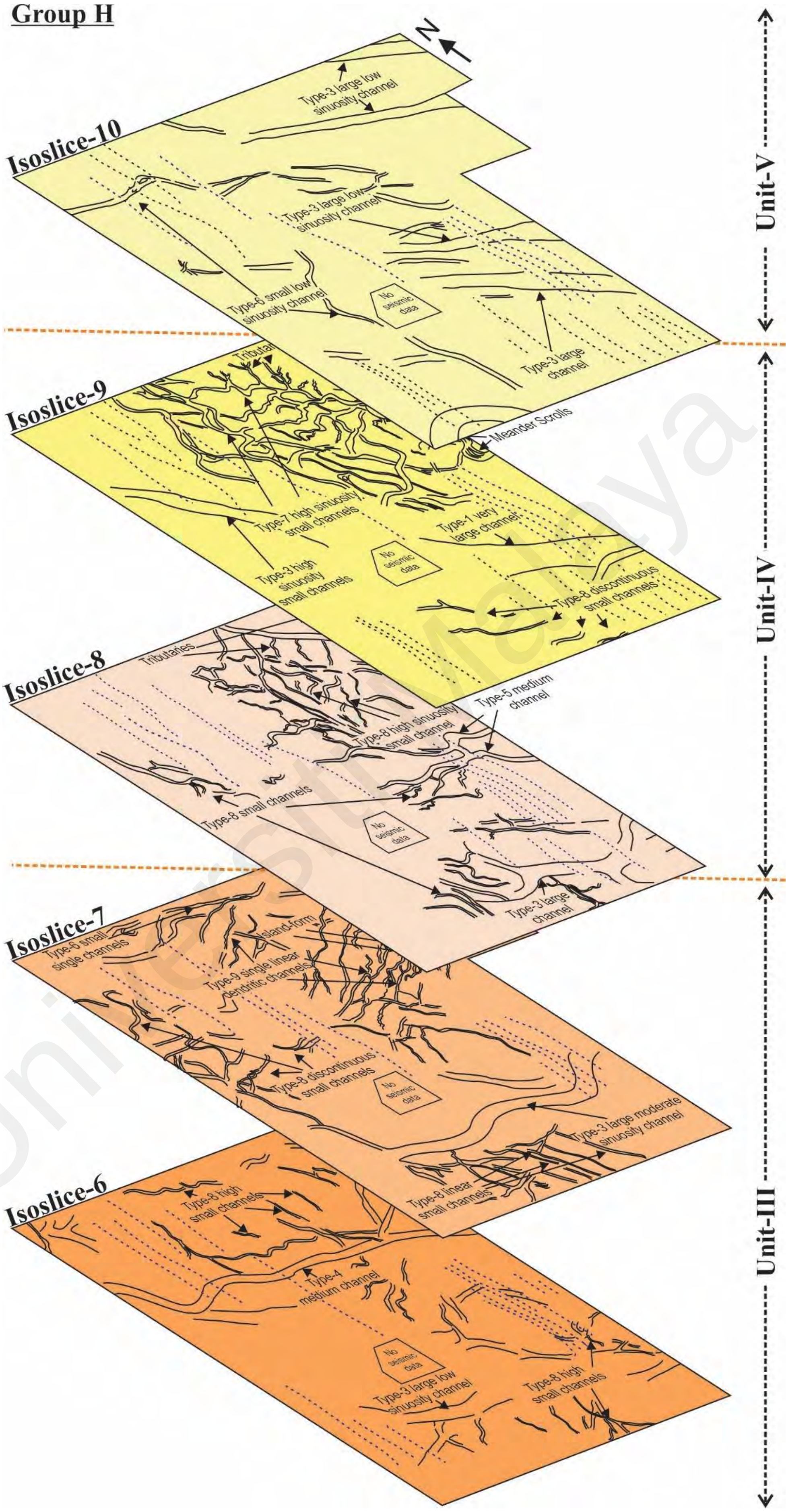

Figure 5.26: Evolution of fluvial system from bottom to upper section of Group H.

5.5 Discussion

5.5.1 Channel Bounding Surfaces and Architectural Elements

The characteristics of the surfaces bounding geobody units which may provide useful information including the relationship between the surfaces and the underlying strata (erosional or gradational), their shape (flat, circular, concave), the areal magnitude and the form of the associated facies (Miall, 1996). Basal bounding surfaces in this study make up to fifth-order, relatively up to group 7 deposits of the hierarchy of the architectural elements (see Miall, 1996). In cross-section, channel bases in the study area are often flat to slightly concave-upward, and in planform view, they are broad (Miall, 1991b; Miall, 1996). This is consistent with the fluvial system in this study area experiencing long-term geomorphic processes such as channel avulsion.

Chapter four of this study elaborates more on the lithology in the study area. Figure 5.27 and 5.28 illustrates the range of architectural elements that can be imaged within the 3D seismic data in this study. The range of width and thickness is comparable to the published literature (e.g., Gibling, 2006). Large-scale channels more than 1 km in width are usually classified as estuaries or amalgamated channel-belt complexes. Medium-scale channels (500 m to 1 km wide) are interpreted as bypass channels which are probably single or distributary channels. The small-scale channels are interpreted as single fluvial-tidal or tidal channels. Channel thickness depends on the channel stacking patterns, where some channels are of single stacked or multi-storey.

Fluvial architecture includes the geometry and internal arrangement of channel and overbank deposits within a fluvial sequence (Miall, 1996). A generic classification scheme based on previous studies throughout the world (Miall, 1985, 1988, 1996) is always somewhat subjective. Therefore, it is difficult to demonstrate explicitly the bounding surfaces and architectural elements that suited channel morphologies analysis in this study. Additionally, data constraints, with regards to the study area make channel classification difficult.

A cut-off width-to-thickness ratio of 15 was suggested to distinguish between sheets (more than 15) and ribbons (less than 15) by Friend et al. (1979) and Friend (1983) (Fig 5.27). The description applies to the internal architecture of the channel by considering whether it is made up of one stacked sequence (ribbon) or whether it is complex (sheets), including several or many individual sequences or 'storeys'.

The width-thickness ratio of the large-scale and medium-scale channels in this study is more than 15, thus they are classified as sheets (Fig 5.28). Some of the medium-scale channels and small-scale channels have a width-to-thickness ratio of less than 15 and are classified as ribbons. The channel mobile-belt concept was proposed by Friend (1983) for the external geometry of the ribbon and sheet body (Fig 5.27). The ribbon bodies represent fixed channels, while the lateral movement of the channel implied the lateral amalgamation of the channel-filling units. Through steady lateral migration or channel shifting, mobile channel belts may be developed.

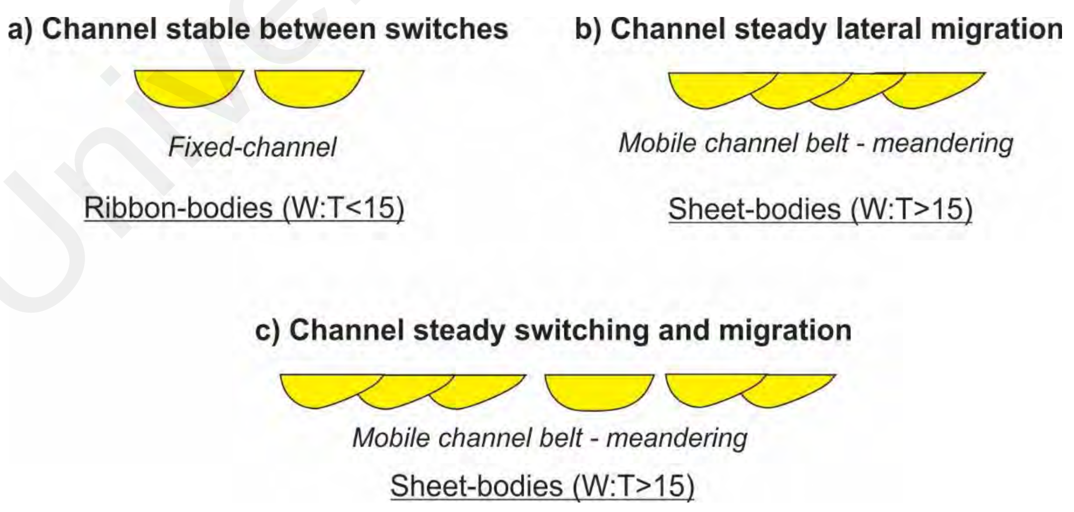

Figure 5.27: Classification of channel behaviour from Friend, 1983. a) Width and thickness ratio (W:T) less than 15 is described as ribbon-body of fixed-channel. b) W:T more than 15 is described as sheet-bodies of meandering mobile channel-belt. c) amalgamation of both fixed-channel and mobile channel belts also described as sheet bodies.

High amplitude channel geobodies of varying scales and morphologies have been identified in this study by using seismic attribute analysis. Core and wireline log analysis enables the identification of fluvial, fluvial-tidal, and tidal channel deposits, while calibration with seismic allows the areal planform geometries of geobodies to be mapped. All channel architectural elements observed in planform-view of the seismic data were analysed carefully as the image produced is the result of superimposed 20 m thick vertical intervals.

Identifying the differences between estuary/channel belts and incised valleys is very critical for interpreting the depositional environment and understanding the evolution and architecture of channel geobodies. Thus, this research provided some insight into whether estuary/channel belts and incised valleys can be identified from subsurface datasets greater than 1.5 km wide.

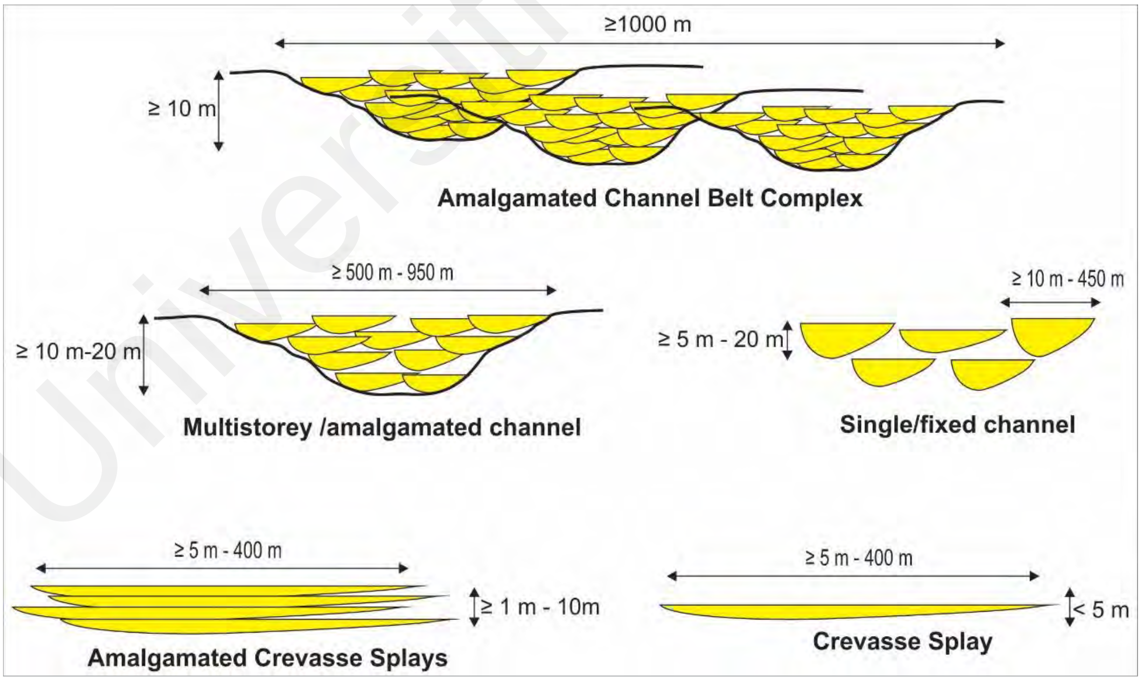

Figure 5.28: Channel width – thickness ranges observed within Group H and Group I of the Malay Basin.

5.5.1.1 Channel Geobody Stacking Patterns

Seismic attribute analysis has identified high amplitude sinuous channel geobodies, with complex internal characters that are likely to represent single channels or multi-storey channel-belts of varying scales and morphologies. I have observed in Group I and H in the studied seismic that channel patterns would differ distinctly in space and time in various styles and morphologies of a single channel and/or channel belt. Channel stacking patterns depend on such factors as variations in sediment load, basin subsidence rate, channel migration and switching rate, the effects of particularly severe floods, bed cut-offs, and accommodation space (Bridge, 2003; Miall, 1996, 2014).

There are several general vertical trends which are observed in both the studied Group I and H intervals. In each stratigraphic Group, there is a gradual and systematic vertical change in the size and pattern of the channels. Prominently, the channel geobodies generally decrease in width and become less common upwards in both Group I and Group H. Channel geomorphologies vary immensely within the stratigraphy of each Group. Channels generally exhibit higher sinuosity in deeper isoslices compared to the shallower isoslices of each seismic group. Based on the seismic analysis, it is interpreted that channels inherently flow in a NW to SE direction, and these channels are within an unconfined-distributive setting.

Identifying channel style based on the analysis of core and wireline log data alone is difficult. It is hard to distinguish between lateral and downstream accretion from such one-dimensional data (Bridge & Tye, 2000). Internal complexities of seismic characters and detail of channel and bar morphologies within channel belts can be interpreted from core data if available. These features are commonly beyond seismic resolution. Differentiating between single and superimposed channel bars, channels, and channel belts are very challenging in this analysis. The distinction between these three scales is difficult even in the core because the defining characteristics of the deposits are not exclusively known.

5.5.1.2 Channel Identification

A recent regional study by Rapi et al. (2019) of the Group I succession, covering an approximately 40,000 km^2 (170 km x 240 km) study area which includes the southern part of the Malay Basin, recorded a total of seven hundred channels. They divided channels in Group I into two sub-groups of Lower and Upper Group I. Ten (10) high amplitude and seven (7) low amplitude long channels trending NW-SE were observed in the Lower Group I, and seven (7) main long channels, trending NW-SE in the Upper Group I. Channels in the Lower Group I are concentrated at flanks whilst in the Upper Group I, many low sinuosity channels are concentrated in the central part of the basin and the meandering channels are concentrated in the southeast of the basin.

Channels observed in their study were classified based on channel's sinuosity regardless of channel geometries and length. Eighty percent of the channels are low sinuosity, trend in southeast direction including the channels in the central basin. Most of the low sinuosity channels in the central basin are mainly shale-filled but are sand-filled in the southern area. Other twenty percent are high sinuosity channels trending towards the basin centre, and some channels trending in a south direction along strike of the basin margin.

In contrast, the 120 channels described, measured, and classified in my study (including both channels in Group I and Group H) are restricted to a much smaller area (1563km^2) in the centre of the Malay Basin. However, I have presented a more detailed morphometric element analysis of channel geometries and dimension, primarily channel width and sinuosity. Channel width in this study ranges from very large- scale channels (CW> 3000m), large-scale channels (CW>1000m), medium-scale channels (CW>500m-

950m), to small-scale channels (CW> 50m up to 450m). Relationship of these morphometric elements including channel meander belt width (MBW), meander wavelength (ML), channel thickness (CT), and radius of curvature (RC) are discussed further in next chapter of this dissertation (Chapter 6).

Therefore, based on the quantitative seismic facies analysis and sedimentological facies analysis (see Chapter 4) in this study, the channel geobodies are interpreted as fluvial, fluvial-tidal and tidal channels which developed in a fluvial to tide-influenced, middle to lower delta plain setting. Quantitative seismic facies analysis on 3D seismic data suggests that the low to high sinuosity large-scale channels most likely represent estuary or bypass channel systems. Medium-scale channels most likely represent fluvial-dominated, tide-influenced channels and small-scale channels represents small fluvial-dominated, tide-dominated channels or tide-dominated (i.e., tidal) channels. Respectively, small-scale channel geobodies of *Type-6 – Type-10* channel morphologies represent small tidal creeks and channels feeding larger tidal channels/fluvial-tidal channels.

5.5.1.3 Seismic Geomorphology of Channels

Recent seismic geomorphological studies based on 3D seismic data can provide essential insights into and allow for the imaging and analysis in the subsurface of a variety of fluvial structural elements and internal complexities (Posamentier, 2001; Miall, 2002; Carter, 2003; Ethridge & Schumm, 2007; Nordfjord et al., 2006; Wood, 2007; Burton & Wood, 2010; Hubbard et al., 2011; Reijenstein et al., 2011; Klausen et al., 2014; Alqahtani et al., 2015; Heldreich et al., 2017). Geomorphic features imaged in published studies include meandering channels, channel belts, estuaries, interfluves, oxbow lakes, neck and chute cut-offs and point-bar meander scrolls. However, the vast majority of these studies are based upon relatively shallow successions where seismic resolution is great and ranges between <5 and 10 m thick.

In contrast, the interval of interest in this study is much deeper at approximately >1.5 km below the seafloor. It is a well-known observation that seismic resolution becomes poorer at greater depths in the subsurface. Therefore, typically only larger scale fluvial architectures, such as channel belts, can be imaged, whereas smaller channels are usually not clearly defined as they are often below seismic resolution.

One of the most important observations made in this study are the abundance of tidal geomorphic features associated with the Group I and H channels in the Malay Basin, including a funnel-shaped morphology, cuspate or box meanders, goose-necking of meanders and the presence of channel networks with characteristics such as through-flowing channels, blind-ended channels, and dendritic networks of small meandering channels with low order branching. Throughout images within the isoslices, we can see channels tend to narrow in one direction, and often flaring or widening in the opposite direction. Such funnel-shaped morphologies are typical of tide-dominated channel mouths, including tidal channels/creeks, tide-dominated delta distributary channels and tide-dominated estuary mouths. However, it must be noted that there is some uncertainty in this interpretation, most of the funnel-shaped geometries were observed very near to the boundary of the isoslice area due to the seismic data boundary limit. It is possible that the flaring may simply represent channel broadening downstream as the channel is possibly continuous beyond the seismic boundary, and channel broadening may be due to a series of flooding events that eroded the banks. According to the Schumm model (Schumm, 2005), as the channels are flowing downstream, channel width increases with increasing discharge.

However, the abundance of other tidal geomorphological features as well as evidence for tidal as well as marginal marine influence from core facies analysis are consistent with a tide-influenced channel interpretation.

5.5.1.4 Channel Dimensions

Based on dimensional data from published work on ancient and modern channel systems (e.g., Gibling, 2006; Wood, 2007; Abreu et al., 2010; Heldreich et al., 2017), the thickest and widest geobodies in Group H and Group I of the Malay Basin fall within the mobile channel belt category, whereas medium-scale channels are categorised as multi-storey channels and small channels are single channels. Most of the small channel dimensions fall within the range of tidal channel dimensions (e.g., Hughes, 2012; Perillo, 2019). However, some channels in the shallower section of Group H (Isoslice-9) display some characteristics of incised valleys (Table 5.3). The key query considered here is whether the incisions are incised valleys with sequence boundaries at their bases or deeply incised distributary channels that are in genetic relationship with the adjacent deposits.

Channel characteristics of this study have been compared to the typical incised valley dimensions documented by Posamentier et al. (2002) and Maynard et al. (2010). However, without significant high-resolution subsurface data, it is difficult to qualify the erosive, incisional bases of fluvial bodies to be confidently interpreted as a sequence boundary.

5.5.1.5 Very Large- and Large-Scale Channel Geobodies in Group I and H: Estuaries, Bypass Channels, or Incised Valleys?

Very large- and large-scale channel geobodies described in this study can represent either estuary/bypass channels or incised valleys. It is not likely that these large channels represent incised valleys, given the seismic coverage (1563 km^2) presented in this study is relatively smaller than other studies which have identified incised valleys in their fluvial system (e.g., Alqahtani et al., 2015 (11,500 km^2); Heldreich et al., 2013, 2017 (17,500 km^2)). Furthermore, the poorer seismic resolution at the deeper vertical seismic section (> 1.5 km deep), planform image of isoslices do not clearly image the channel margins and often most of small channels (which may or may not be connected to larger channels) are not resolvable at this depth. Thus, interpretation as incised valleys are highly dubious. The architectural elements observed and recorded most likely represent estuary/bypass channels.

Numerous criteria have been proposed for the identification of incised valleys. Van Wagoner et al. (1990, 1995) stated that incised valleys are created by fluvial systems that expand their basin channels and erode into underlying strata in reaction to relatively low sea-level. Later, Zaitlin et al. (1994) and Boyd et al. (2006) proposed a broader definition of incised valley and therefore added several main criteria for their recognition. They define an incised valley as a "fluvially eroded, elongate topographic low that is typically larger than a single channel form and characterised by an abrupt basin-ward shift in facies at its base" (Zaitlin et al., 1994; Boyd et al., 2006). This definition also notes that valleys should be larger and wider than channels. Large channels are not necessarily incised valleys.

Payenberg & Lang (2003) used criteria such as the presence of a significantly thick multistorey succession of amalgamated fluvial channels to identify incised valley fills. The succession typically exceeds 30 m in thickness and comprises numerous internal scour surfaces. Fielding & Gibling (2005) and Gibling (2006) propose three criteria for incised valley identification: (1) a basal erosion and correlative surfaces in extra-channel deposits that can be mapped; (2) fluvial body dimensions of greater magnitude than the others fluvial bodies in the network, and (3) Erosional relief of the basal surface is greater than the depth of the scours apparent from its constituent channels.

Posamentier (2001) stated that all incised valleys must have frequent, clearly detectable, small tributaries that drain the interfluve and feed into a larger channel system, which similar to what is observed in the shallower section of Group H. Here, some of the smaller channels (< 450 m wide, > 30m deep) recorded in the shallower section of Group H (isoslice-9) have small dendritic tributaries feeding a larger channel. However, this criterion alone does not justify that the channels represent incised valleys.

Previous regional seismic geomorphology studies on shallow Pleistocene to Recent successions in the offshore Malay Basin by Miall (2002), Posamentier (2001) and Alqahtani et al. (2015, 2017) identified incised valleys (up to 18 km wide and 80 m deep) based on the following criteria: (1) regional extent of the basal channel erosion surface, which is lined with pebbles and cobbles; (2) presence of small incised dendritic tributaries that drain the valley margin, with basal erosion surfaces cutting into adjacent interfluves; (3) the absence of stratigraphic sequences preserved beneath and adjacent to the interfluves in the main erosional conduit; (4) observable multi-storey stratigraphic fill, and; (5) valley features which are significantly larger than single channels.

In contrast, the widest and largest channels observed in my study in Group I and H of the Malay Basin are only up to 6 km wide and up to 70 m thick. Their basal erosion surfaces might be traced extensively beyond seismic data. However, these channels are rarely associated with small tributary channels, and even so, some of infilled small channels are detectable within these large channels. Therefore, with lack of the criteria set for incised valley based on published literatures, the channels in the I and H Group of the studied seismic volume are most probably estuaries, channel belts and/or bypass channels rather than of incised valleys.

Classic models for incised valley development require full subaerial exposure of the shelf for the formation of long-distance incised valleys related to sea-level fall and headward migration of the knickpoint (Posamentier & Vail, 1988; van Wagoner et al., 1990, 1995). Later, Posamentier (2001) and Reijenstein et al. (2011) introduced the concept of unincised lowstand alluvial systems (i.e., bypass channels) which develop on a very low gradient shelves, where minor fluctuations in relative sea-level results in only partial exposure of the inner and mid-shelf (as sea-level retreats but does not fall beyond the shelf edge during lowstand).

Lowstand bypass alluvial systems are the common response to relative sea-level lowering rather than incised valley systems. During regressive periods and subsequent lowstand conditions, river down cuts its floodplain significantly. During the flood period, water flow could not overtop the riverbank resulted in the abandonment of previous active floodplains and became interfluves (Blum & Törnqvist, 2000; Posamentier, 2001). This type of system also displays abundant channels without tributaries observed on the interfluves on either bank.

The stratigraphy of the Malay Basin is a generally arranged in a simple "layer cake" fashion at the seismic scale, with some compressional inversion structures. Its location in the centre of the Sunda Shelf, topographically low-gradient (<0.1º) (Madon et al., 1999; Hall & Morley, 2004), on a very wide lowland area of alluvial-fluvial-shoreface indicate a long distance progradation south-eastward of the Malay Basin (Shoup et al., 2012). These channels are imaged on a few successive slices in this study, which suggest they are significantly deeper than documented bypass channels. Hence, the very large- and large-scale channels are interpreted as amalgamated channel belt deposits/ bypass channels. Their characters are consistent with the criteria established by these previous workers for identifying unincised valleys.

Table 5.3: Checklist of criteria for identification of incised valley systems in the rock record compared to what is observed in the shallower succession of the Malay Basin by Alqahtani et al. (2015, 2017) as well as in this study. These criteria are from van Wagoner et al. (1990), Zaitlin et al. (1994), Posamentier (2001), Boyd et al. (2006) and Maynard (2010).

	Criterias of Incised Valley	Datasets				
		Seismic (This Study)		Alqahtani et al. (2014, 2017)		Modern analogues
		Cross section	Plan-view	Cross section	Plan-view	
1	Sequence boundary at the base of incised valley	X	X	Yes	X	Yes
2	Negative erosional relief- truncation of underlying strata	X (typically show bright amplitude)	X (If the region of seismic data is wider, extend of the incision would be visible)	Yes	X	Yes
3	Small dentritic tributaries fed incised valley system	X	Yes (e.g small channels in Isoslice-9, but only one-sided)	X	Yes	Yes
4	Widespread to regional extent with deep incision	X	X (limitation of study area)	Yes	Yes	Yes
5	Basin-ward shift in facies	X	Possible (based on extensive geomorphology)	Yes	Yes	Yes
6	Interfluves contain well develop paleosols	X	X	X	X	Yes
7	Infill of incised valley onlap the valley base and walls	X (typically observed as bright amplitudes due to seismic resolution)	X	Yes	Yes	Yes
8	Several sequence stratigraphic surfaces at the base, transgressive surface and maximum flooding surface	X	X	Yes	X	Yes
9	Smaller-scales channels within the incised valley	X	Possible (however most of them are not clearly defined and discontinuos)	Yes	Yes	Yes
10	Estuarine/tidal influenced facies and deposits (at seaward extent)	X	Possible (Based on channel geomorphic tidal features)	X	X	Yes
11	Combination of sedimentary facies from terrestrial to marine	X	X	X	X	Yes
12	Multistorey and lateral character of infill- upward increasing accomodation during valley filling	X (not in this resolution)	X	Yes	Yes	Yes

5.5.2 Process Variations and Controls on Channel Geometries

Based on the observed channel geomorphologies, it is evident that the channel systems of the study area in the Miocene succession of the Malay Basin developed in a fluvial - tidally influenced setting. Collins et al. (2018) showed that tidal currents significantly influenced sediment transport and deposition along the western part of the South China Sea during the Miocene and affected both lowstand and highstand coastlines. Tides along lowstand coastlines show an overall temporal decrease in tidal range compared to highstand coastlines. Convergence effects of tides increased within the East Natuna and Sarawak (ENS) embayment along with the size reduction of the Gulf of Thailand. Given the location of the Malay Basin in between them, it is therefore expected to experience the same increase in convergence effects of tides. Therefore, the tidal range is expected to be higher during deposition of Group I and Group H. Interestingly, Collins et al. (2017) presented numerical tidal models which show that the tidal range was microtidal during the Aquitanian (Early Miocene) and Langian (Mid-Miocene) in the Malay Basin. No models were shown for Group I and H times (i.e., Burdigalian). However, the tidal currents were calculated to be strong enough to transport coarse sand and gravel.

Furthermore, the Late Oligocene–Early Miocene and late Middle Miocene of the Malay Basin strata comprise paralic mudstones, laterally extensive coals and abundant swamps and freshwater flora pollen (Shamsudin & Morley, 2006; Morley et al., 2011). Likewise, the adjacent Early–Middle Miocene of the West Natuna Basin strata also contain similar paralic mudstones and coals with common mangrove pollen (Morley et al., 2003). Thus, this supports the idea of tidal influence with mangrove colonization of coastal plains of Group I and H of the Malay Basin.

Regarding the spatial and temporal evolution, fluvial system geometries within Group I and H may represent two main depositional successions separated by maximum flooding /transgressive surfaces. Group I consist of progradational to aggradational fluvial to tidally-dominated estuarine sands, and Group H is dominantly marine to deltaic sediments with fluvial/estuarine channels (Madon et al., 1999). Facies analysis from the upper section of Group H in this study (see Chapter 4) indicate the predominance of thick heterolithic strata deposited in marginal marine and deltaic settings.

Most of the channels within the dataset broaden towards the east or southeast, most probably reflecting downstream flow and flaring of tidal river mouths in these directions. The upward decrease in geobody dimensions identified in the interval of interest likely reflects the increased frequency of distributary channels in a relatively distal location on the lowland river plain. The bifurcation and avulsion of numerous distributary channels and tidal channels greatly reduce fluvial currents and processes.

In fluvial-tidal channels, transport capacity is typically distributed unevenly, and channel systems often switch and reconfigure their routes autogenically (Dalrymple et al., 2015, Gugliotta et al., 2019). Along distributary channel systems, for example, water and sediments are funnelled through an isolated channel network. This ultimately leads to shifting of the fluvial-tidal channel to another position on the lower delta plain (Mohrig et al., 2000; Törnqvist & Bridge, 2002; Slingerland & Smith, 2004; Miall, 2014). The cycle begins again when a new channel is created. Channel avulsion is an example of a natural, autogenic mechanism in a sediment transportation network. Note that dynamic conditions in upstream parts of source-to-sink networks can also impact the lower floodplain/ delta (Hajek et al., 2017). In this sense, the variable sediment supply forced by the upstream sediment system could be considered an allogenic influence on the channel systems. These more complex allogenic controls illustrate why the scope of the system of concern should be defined clearly and how external factors can influence its dynamic is carefully considered.

It is also important to consider whether the spatial trends in geobody morphology and size reflect fluvial deposition from a series of distributaries caused by successive channel bifurcation (see distributive fluvial systems of Nichols & Fisher, 2007; Hartley et al., 2010; Weissmann et al., 2010; and Fielding et al., 2012) or a set of radiating channels anchored to a proximal nodal avulsion point situated beyond the study area in the west.

Bifurcations typically occur in four natural environments: alluvial fans, braided-rivers, lowlands, and flood plains (Kleinhans et al., 2013). However, distributive bifurcations of individual channels/ channel belts are rarely observed in planform view from this study. Each isoslice through the seismic data is approximately 20 m thick and although a subset of candidate flooding surfaces were correlated in the 3D seismic volume, the seismic data lack the vertical resolution to outline higher order stratigraphic discontinuities/ unconformities to classify different geomorphic units imaged in plan-view. The generated isoslices superimpose several depositional events (tiers of channels) into a single planform view map (2D map). Therefore, it is challenging to distinguish between closely spaced or cross-cutting channels/ channel belts which lie within different stratigraphic sequences or are connected vertically. Thus, whether the fluvial-tidal channel systems were controlled by distributive bifurcation or radial avulsion secured to a nodal point cannot be resolved using the available dataset.

Geomorphic tidal features such as funnel-shaped, cuspate, goose-neck, dead-end channels and abundance of small single channels displaying dendritic and parallel patterns (tributaries) provide strong evidence for tidal influence within the fluvial-tidal systems of Group I and Group H. Besides, variation in the fluvio-tidal environments of Group I and Group H can be the primary characteristic of the channel systems. Evolution of tidal channel morphologies may due to environmental constraints and/or hydrodynamic factors. Hydrodynamic influences encompass the equilibrium of channel exposure to fluvial and tidal currents, tidal prism, tidal range, and other spatial impacts on the underlying stratigraphy transition.

The presence of stacked and amalgamated fluvial-tidal channel deposits within Group I and Group H suggests deposition of high sediment load in a low accommodation setting. Given the low shelf gradient of deposition, it is likely that dynamic controls of channel relocation, shifting, and switching play major roles depending on local processes, leading to the stacking patterns and fluvial architecture of the fluvial systems within Group I and Group H. Backwater lengths probably reached far enough inland to have a significant effect on channels/ channel belts (Van Wagoner et al., 1990; Gibling et al., 2011; Holbrook & Bhattacharya, 2012; Blum et al., 2013).

The spatial and temporal differences in geobody channel distribution may also be explained by minor external factors such as the concept of buffers and buttresses *sensu* Holbrook et al. (2006). The concepts of buffers and buttresses accounted for longitudinal variations in architecture and fluvial facies upstream from the shoreline (Fig 5.29). In this model, upstream controls such as tectonism or climate change, that govern the discharge and sediment load of the river, mainly influenced downstream channel deposits and geomorphologies. The buffer profiles are converged to the buttress and typically accommodate multi-storey channel belts within valley sizes where they are dense, but only single-storey channel loops are narrow. All profiles must converge towards the position of the buttress, and the change in buttress must be followed by aggradation and erosion.

During the Early to Middle Miocene, the Malay Basin underwent thermal subsidence and continued with compression and uplifting until the Late Miocene. Tectonic uplift in the north-western basin may increase the sediment load, causing the river to aggrade towards its upper buffer limit. Buttress positions drop as a result of relative sea-level fall may also result in multiple incisions of the fluvial system. Thus, river system will aggrade and erode towards a new equilibrium profile that balances out the sediment flux, discharge, and the rate of change in accommodation.

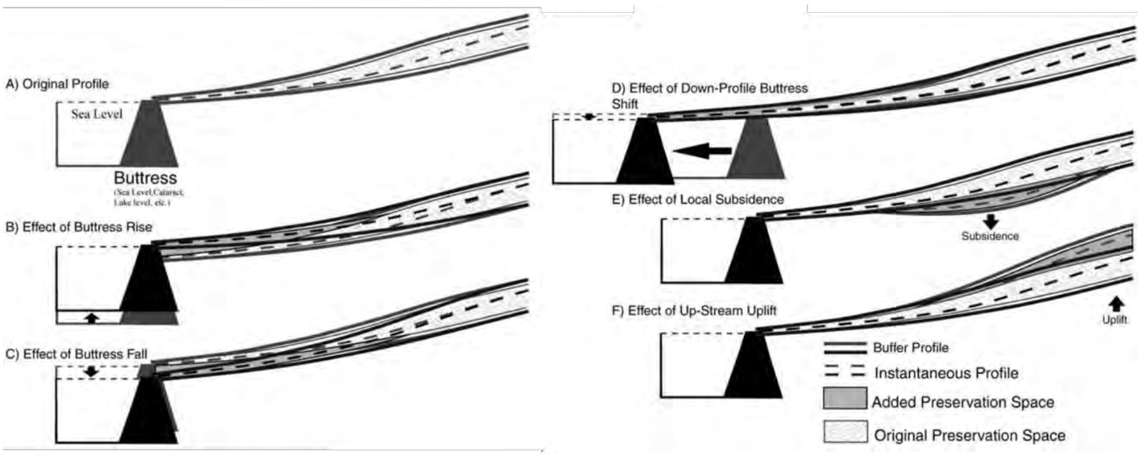

Figure 5.29: (A) Initial buffer profiles; (B, C) Simple buttress rise and fall increase accommodation space;(D) Buttress point shifts forward from the original longitudinal profile and lengthens accommodation space; (E) Subsidence lowers sediments deposited beneath active erosion; (F) Upstream uplift may leave previous deposits as terraces and highly likely to be eroded before burial (from Holbrook et al., 2006).

The isoslices (Isoslice 3, 4, 5) where large channels are dominant possibly represent intervals within deltaic progradational successions. A regressive event may result in increased fluvial incision and low accommodation. Higher rate of sediment supplies relative to sea-level rise during progradation resulted in multistorey amalgamation of fluvial deposits. A sequence boundary marking relative sea-level fall and/ or 'regional composite scour' (RCS) surface is developed at the base of the amalgamated channel stacks (Fig 5.30). Another factor such as flooding events may have contributed to fluvial incision and deposition and developed the RCS that bound the scour surface of amalgamated channel belts (Fig 5.30D). Series of flooding events increase water discharge and sediment supply which affected floodplain stability, vegetation, thus contribute to fluvial incisions and develop amalgamation of channel belts (Blum et al., 2013; Holbrook & Bhattacharya, 2012).

Therefore, in relation to this study, stacked and amalgamated channel belt deposits documented may be underlain by a 'regional composite scour' (RCS) surface at their bases. The RCS is a diachronous composite of numerous channel scours which developed due to long-term channel erosion and migration (Fig 5.30D). In this case, sediment bypass seems to be the exception instead of the norm (Holbrook & Bhattacharya, 2012; Blum et al., 2013).

Nonetheless, the vertical decrease in width of channel geobodies and an overall increase in mud-rich delta plain deposits in my study, reflects a fluvio-tidal system under net-transgression. Backstepping and transgression of the estuaries/deltaic system occurred in response to a rise in relative sea-level/ base-level during transgression and highstand. Even slight fluctuations in relative base-level would cause channel facies belts to shift laterally over large distances across the very low angle stratigraphy. These vertical facies change resulting from a relative rise in base-level may have also driven frequent avulsions of channel bodies under higher accommodation conditions, resulting in a heterolithic succession in Group I and Group H.

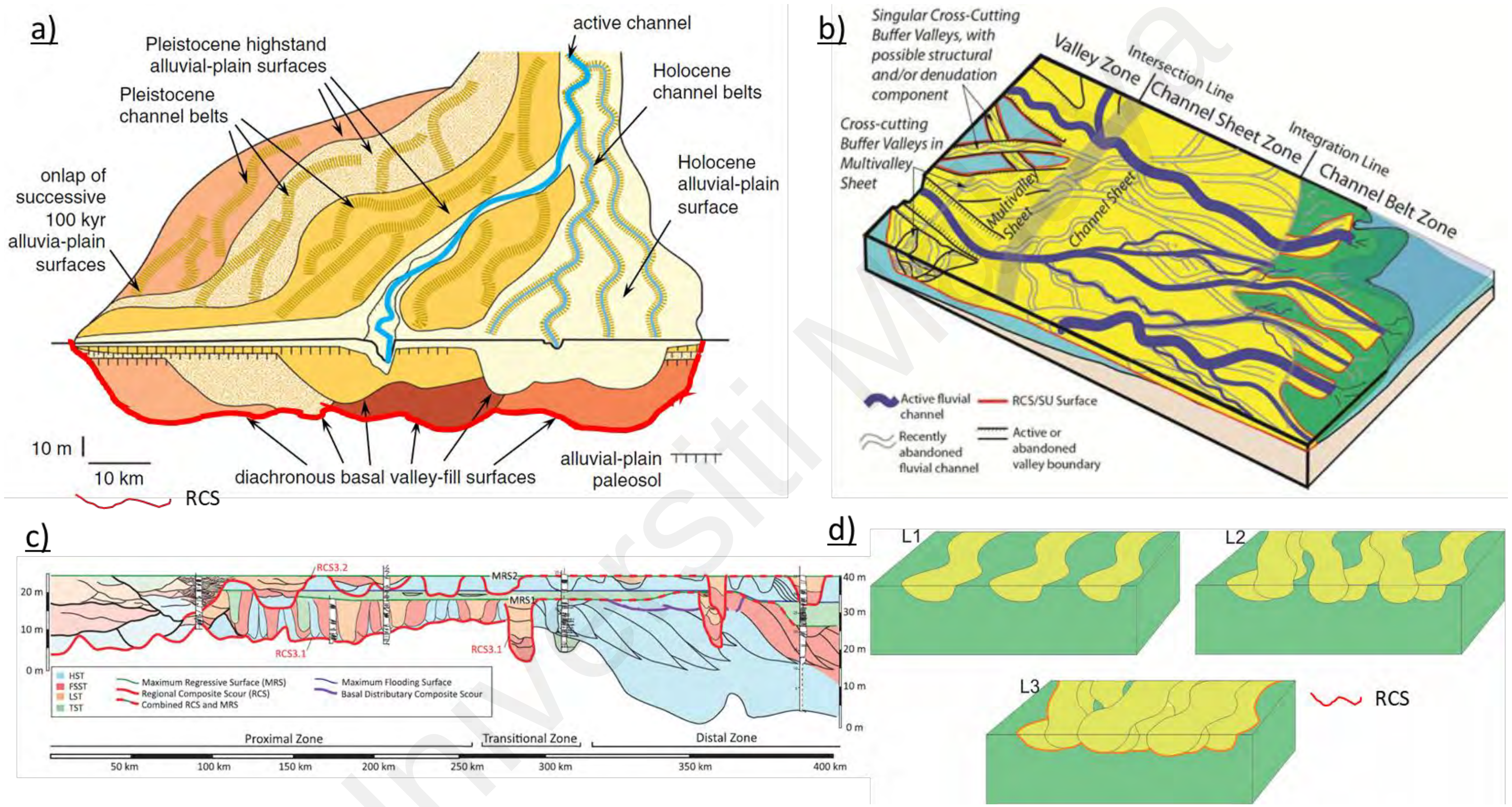

Figure 5.30: Examples of regional composite scour (RCS) surfaces from published studies of amalgamated fluvial channels; a) Bases of cross-cutting paleovalleys in Blum et al. (2013) may develop as a RCS surface; b) An RCS surface is developed beneath multiple generations of buffer valleys (Holbrook & Bhattacharya, 2012); c) Cross-cutting of younger channels into older fluvial-marine transition channel systems, marked their bases as the RCS combined with maximum regressive surface (MRS) (van Yperen et al., 2020); d) A model to highlight multiple phases of cross cutting geobodies of individual channels forming a channel belt and channel belts forming an amalgamated channel belt complex, and their bases form a RCS surface.

5.5.3 Sea-Level Fluctuations and Transgressive-Regressive Cycles

The depositional setting of the Malay Basin during the late Early Miocene to Middle Miocene (represented by stratigraphic intervals of Group I and H) has been interpreted as brackish, marginal marine including lower coastal plain. This is supported by an abundance of mangrove palynomorphs in the Group H, which is consistent with a marginal marine, lower coastal plain setting, however some marine foraminiferal indicate that some part of Group H is marine (Yakzan et al., 1996). Furthermore, tidal influence was also observed in the same stratigraphic intervals of Group I and H further inland in the northern part of the Malay Basin, within the Malaysia-Thailand Joint Development Area (MTJDA) (Carney et al., 2008). In addition, based on the regional channels recorded in Rapi et al., 2019, channel development in the Group I were interpreted to be governed by palaeoslope and sea-level fluctuations. Basin centre was repeatedly drowned and exposed due to fluctuations in relative sea-level (Madon, 2011; Jirin et al., 2013; Rapi et al., 2019).

Consequently, low sinuosity channels observed in this study may be associated with lowstand period of relative sea-level fall when the basin was exposed, and these channels drained southward. Moderate to high sinuosity channels probably developed during relative sea-level rise. Where the main channels were drowned, tidal incursion upstream developed many tidal features which can be observed in this study. The large axial rivers changed into fluvio-tidal channels. During highstand, meandering tidal channels and fluvio-tidal channels drained into the drowned basin centre (axial Malay Basin). However, confirmation of these interpretations requires a larger basin-scale dataset despite most of larger channels are widening downstream south-southeastward, their thicknesses do not record any trend.

Understanding transgressive-regressive cycles during late Lower Miocene to Middle Miocene is crucial as they play important roles in channels morphology and architectural elements both spatially and temporally (Madon, 2011; Morley et al., 2021). Evidence acquired from biostratigraphy analyses (Yakzan et al., 1996) and seismic studies indicates marine transgressions have occurred since the Late Oligocene (Group L). However, the Malay Basin did not become completely marine until the Pliocene (Yakzan et al., 1996; Madon, 2011; Jirin et al., 2013; Morley et al., 2021). Partially marine conditions were well established since the middle Lower Miocene of Group J (Fig 5.31). Consequently, based on the idea that there was a constant relation to the open sea to allow the tides to impact sedimentation, Group I and H were then interpreted as tidal or tidally influenced. Several marine transgression events were documented within the study interval of Group I and Group H (Jirin et al., 2013; Morley et al., 2021) (Fig 5.28). These events definitely played important roles in defining temporal variation of channel morphologies and architectural elements in the study area.

The transgressive-regressive cycles in the Miocene are not correlatable to the frequently cited global eustatic curve of Haq et al. (1987). They are strongly influenced by the interaction between tectonics and sea-level fluctuation (Madon, 2011; Morley et al., 2021). In addition, a considerable number of published studies have established the tectonic processes and effects, e.g., lithospheric flexure and thermal subsidence have a significant impact on the development of the stratigraphy (e.g., McKenzie, 1978; Watts et al., 1982; Klitgord et al., 1988).

Many reports have shown evidence of tectonic deformation and its impact on the Malay Basin (e.g., Ngah et al., 1996; Tjia & Liew, 1996). The presence of major structures in the semi-regional basement high at the southeastern end of the basin is the most significant result of the main inversion event (Madon, 1997). Thus, tectonic uplift may have produced the one-sided tributaries associated with small meandering channels in the isoslice-9 (Fig 5.20).

A basement high, or sill, separates the Malay Basin from the adjacent West Natuna and the ancestral South China Sea. The sill would have played a significant role in influencing relative sea-level changes in the Malay Basin. The basin experienced prolonged compressional uplift of increasing intensity since the Middle Miocene (Group H). The long-term uplift of the basement in the south would have been plastered upon by the series of fluctuations in relative sea-level. At times, the rate of relative sea-level rise surpassed the rate of uplift resulting in marine flooding into the basin (Fig. 5.32).

Figure 5.32b illustrates a model of the basement uplift in the south acts as a "door" that opens and shuts in response to sea-level cycles. During high sea-level, restricted marine conditions will be formed, while during low sea-level, the basin serves like an internally drained lake basin that may be subject to changes in the base-level controlled by climate. Changes in sedimentation patterns associated with these two environments may also be recognised. This model explained the variation of channel morphologies and architecture observed in this study temporally. During low sea-level, the basin is assumed to be a restricted basin, thus channels would be fluvial-dominated, with less occurrence of small channels. During high sea-level, marine flooding into the basin thus allowed tidal currents to influence sediment transport and deposition as well as channel morphology. This event resulted in development of many tidal channels in the system.

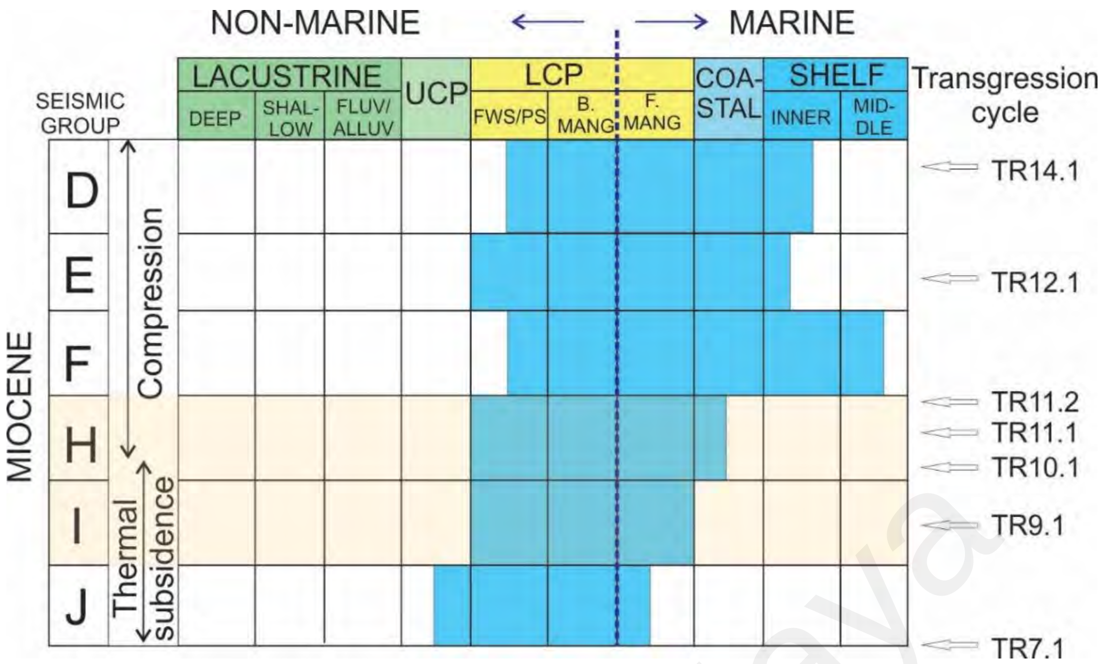

Figure 5.31: General trend in depositional environments in the Malay Basin (Note: UCP= upper coastal plain, LCP=lower coastal plain, FWS/PS= freshwater/peat swamp). Series of marine transgression occurred within the study interval of Group I and H (modified from Madon, 2011).

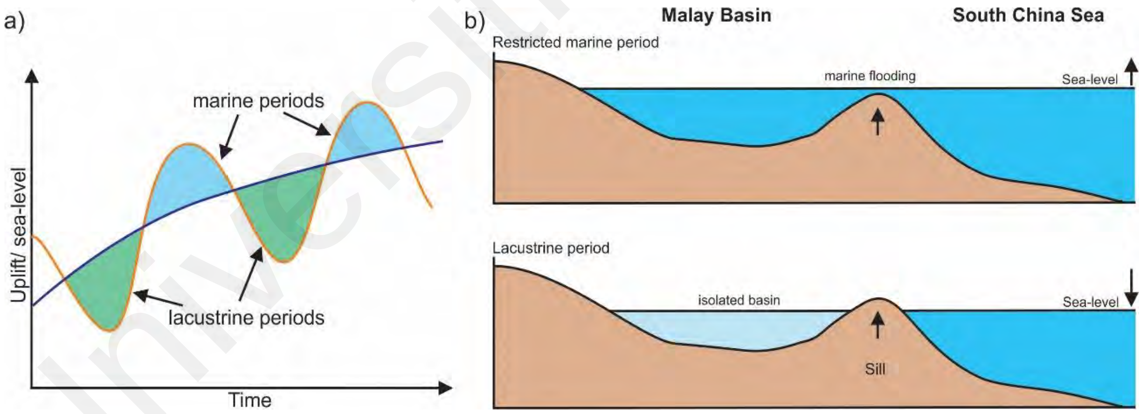

Figure 5.32: Schematic diagram showing the a) interaction of uplift and relative sea-level fluctuation in creating cycle of transgression in a semi-restricted basin; b) Model of Malay Basin as semi-restricted basin with a structural high (sill) controlling the marine flooding events when the rate of sea-level rise exceeds that of the sill's crest (modified from Madon, 2011).

5.5.4 Reservoir Implications

Key reservoir elements (along with subordinate mouth-bar sands) within Group I and Group H successions are interpreted as fluvial-tidal distributary channels. However, they have been frequently being mistaken for purely fluvial channels. Factors influencing their scale and geometry include the size of the paleo-delta system and the grain-size range of the sediment supplied. In typical mixed-load delta systems, sand and mud will be expected within the distributary channels as described above. If the succession is too coarse-grained, however, the lack of stable banks results in the dominance of more mobile, shallower, braid-delta distributary channels. If the delta coastline was influenced by moderate to intense wave energy, then the distributary channels will be confined behind a barrier or strand plain. If tide energy is important, then the distributary channels will have evidence of brackish marine ichnofauna and paralic microfossils/palynomorphs. This will be particularly obvious in the upper abandoned parts of distributary channels, where bioturbation will churn up the silty, carbonaceous channel-fill. Channel evolution in this study shows evidence of distributary channel switching and abandonment, thus distributary channels will commonly be mud-plugged even in a sand-prone system. This has important implications for reservoir heterogeneity within Group I and Group H fluvial-deltaic successions and, in some cases, will lead to stratigraphic traps.

5.6 Conclusions

Ten channel geomorphology types are identified based on variations in planform channel geometries, features and dimensions, and variations in seismic amplitude signals in a cross-section. These channel types are then grouped into four main channel geobody groups based on geobody width distributions and geometries in the planform-view of surface isoslices.

1. Very large-scale features comprising *Type-1* channel morphologies, being ≥ 3 km wide, low sinuosity, high amplitude geobodies with clearly defined margins. Smaller, 100–600 m wide, higher sinuosity features are observed within these channels.

2. Large-scale features comprising *Type-2* and *Type-3* channel morphologies, which are ≥1 km wide, low sinuosity, high amplitude geobodies with clearly defined margins; Smaller (80–400 m wide), higher sinuosity features have been observed within these channels. The large-scale geobodies are commonly observed in two or more isoslices. A population of 100–200 m wide geobodies can also be observed trending 90° to and apparently intersecting the larger geobodies.

3. Medium-scale geobodies comprise *Type-4* and *Type-5* channel morphologies, commonly 300– 800 m wide, with high amplitudes, low sinuosities and clearly defined margins. Associated with them are 100–200 m wide, sinuous, high amplitude features.

4. Small-scale sinuous geobodies comprise *Type-6* to *Type-10* channel morphologies which typically range from 80– 450 m wide with variable sinuosities and display more subdued seismic amplitudes.

Additional geobodies observed are diffuse high amplitude areas containing remnant sinuous geobodies ≤100–200 m wide of varying degrees of amplitude along with patches of lower amplitude areas. Broad low amplitude areas commonly contain residual ≤150 m wide sinuous geobodies.

Channels in this study dominantly trend NW-SE, with evidence of flow towards the SE. In summary, channel architecture in the fluvial-tidal settings of the Miocene Group I and Group H in the Malay Basin can be divided into three classes on the basis of their morphometric elements. Class-1 are aggradational bypass channels or estuaries showing low to high sinuosity, wide meander belts, and larger meander arc angles. These systems are large systems where the meander belts nearly overwhelm the study area and often start and end beyond the bounds of the study area. These most likely represent amalgamated channel belt complexes in the distal area of the delta plain. Class-2 are amalgamated channel-belts which are several kilometres wide; with low sinuosity, well-defined meander belts, low meander arc angles and moderate incisions. Type-3 are single-thread channels include fluvial-tidal channels, tidal channels and creeks with high sinuosity, narrow widths, small meander-arc angle, discontinuous and shallow incision.

The primary factors controlling channel geometries and morphologies was governed by transgressive-regressive cycles which were recorded during the Miocene of the Malay Basin. Transgressive-regressive cycles were influenced by the interaction between tectonics and sea-level fluctuation. Downstream autogenic processes do play important roles in the channel morphology by responding to local changes in internal conduit path, sediment load, erodibility of channel walls, and turbulence of the hydrodynamic bidirectional flows, can intensely influence channel geomorphologies. Even so, autogenic processes in the upstream channels may act as an external force to the downstream such as alternation in sediment discharge rate and velocity.

CHAPTER 6: QUANTITATIVE ANALYSIS OF CHANNEL GEOMETRIES WITHIN A PARALIC DEPOSITIONAL SYSTEM: THE MIOCENE GROUPS I AND H, MALAY BASIN

6.1 Introduction

Determining the geometry and dimensions of ancient paralic sand bodies is important for oil and gas exploration and development. Most of the existing methods have drawbacks due to the limitation of field data and outdated technology. Recent technology such as improved 3D seismic reprocessing and 3D imaging techniques have enhanced the cognitive 3D data analysis. Enhanced 3D seismic surface attribute analysis enables more definite measurements of geostatistical data. A range of quantitative geometric channel body measurements can be made. Better imaging results in easier and more accurate identification of architectural elements as well as better determination of geobody dimensions, orientations, spatial distributions, and connectivity. These parameters are vital for reservoir assessment (Bryant & Flint, 1993; Reynolds, 1999). Numerous hierarchical classification schemes for fluvial architectural elements have been proposed (e.g., Miall, 1985; Gibling, 2006; Abreu et al., 2010; Ford & Pyles, 2014, Ainsworth et al., 2011; Vakarelov & Ainsworth, 2013). However, according to published datasets by previous workers on channel geometries and dimensions (e.g., Gibling, 2006; Klausen et al., 2014; Alqahtani et al., 2015), the range in dimension of each channel class are large, thus contributing to high uncertainty in classifying channels in the deeper subsurface. Therefore, assigning accurate channel geometry into the existing classification is difficult and should be done with caution. Previous studies of ancient and modern fluvial systems were primarily concerned with identification of channel architectural elements and their spatial organization, with focus on channel body heterogeneities (Miall, 1988, 1996; Jordan & Pryor, 1992; Lunt et al., 2004; Gibling, 2006). Many studies have also dealt broadly with the external geometries and dimensions of fluvial channel deposits (e.g., Potter, 1967; Friend ,1983; Fielding & Crane, 1987; Reynolds, 1999, Gibling, 2006; Leuven et al., 2018). However, there are not many studies on fluvial-tidal channel geometries and dimensions. Hughes (2012) provided a thorough review of the characteristics of tidal channels developed on present-day coasts. My study provides a database for geomorphic elements present within fluvial – tidal channel networks of Group H and I of the Malay Basin. Interpretation of these channels are refined and compared to potential present-day analogues. In order to better constrain my interpretations of the observed seismic channel geomorphologies, I compared the imaged isoslices in Chapter 5 with potentially analogous modern-day river systems. Geostatistical data of geometries and dimensions of channels extracted from the 3D seismic surfaces (Chapter 5) were compiled into a quantitative database of Miocene fluvial-tidal systems within a selected area of the Malay Basin. In order to use the wealth of geometric data most effectively, an understanding of the relationship between these dynamic dimensional aspects of channel geobodies is needed to clarify the control mechanisms on channel architectural elements and geometry. This geostatistical data will be beneficial to modellers to reduce uncertainties related to analogous depositional systems.

6.2 Geological Framework

The Malay Basin has an area of approximately 83,000 km^2 (500 km long by 250 km wide). It has an elongate, NW-SE trending shape and is one of the largest Tertiary basins on the Northern Sunda Shelf of Southeast Asia (Fig. 1). The basin is located north of the Penyu and West Natuna basins and is south of the Pattani Basin (Hutchison, 1989; Madon et al., 1999; Morley & Westaway, 2006; Pubellier & Morley, 2014; Fig. 6.1). Overall, the basin is filled with a more than 14 km thick succession of Oligocene to Recent deposits in the central regions. The Oligocene strata are commonly terrestrial deposits with insignificant marine influence, while the Miocene to Recent sediments is mainly coastal plain to shallow marine deposits (Madon et al., 1999).

The southwestern margin of the Malay Basin is bounded by the Western Hinge Fault Zone (Liew, 1994, 1996), and north-eastern margin is more gently sloping and ramp-like. Extensional half-grabens exist on both the southwest and northeast flanks, which developed during the initiation phase of the Malay Basin in the Oligocene. The central basin extensional structures have been reactivated and developed major sub-vertical wrench faults, which are the most targeted structures for hydrocarbon traps.

Structural analyses suggest that the Malay Basin was originated during the early Tertiary with crustal extension in response to strike-slip movement along a major NW-trending shear zone (Madon, 1997). Crustal extension is marked by the half-graben structures and normal faults in the pre-Tertiary basement, high heat flows and geothermal gradients (85-125 mW/m2, 45-60º C/km) (Madon, 1997, 1999; Madon et al., 2006).

The stratigraphic succession of the Malay Basin is divided into seismic stratigraphic units, referred to as "Groups" which have been labelled alphabetically as group A to M downwards, and comprises lacustrine to shallow marine deposits. This study focused on strata within the late Lower Miocene to Middle Miocene Group I and Group H.

The main syn-rift strata are represented by Group M which was deposited during basin initiation in the Late Eocene (Ngah et al., 1996; Tjia &Liew, 1996) and extension in the Middle to Late Oligocene and are composed of lacustrine deposits. Late Oligocene to early Miocene strata has been interpreted as part of the syn-rift package in earlier works (e.g., Madon, 1997) but are now believed to represent the earliest post-rift (sag-phase) sedimentation, including transgressive shale units of the Group L and K.

Post-rift strata are represented by Early Miocene Group J and younger packages. These groups are composed of lower coastal plain and shallow marine sediments. During the Early to Middle Miocene, the basin endured an inversion phase, due to the reversal of shear along the axial shear zone, from sinistral to dextral. This event resulted in the development of large wrench-faults.

Most of the Miocene stratigraphic units have been interpreted as brackish or tidal influenced coastal plain deposits, with the absence of a fully marine ichnofauna assemblage indicating a restricted marine depositional setting (Madon, 2011). The main inversion event was during the Middle-Late Miocene period (Madon, 1997) which was more intense in the southeastern end of the Malay Basin. A semi-regional basement high in that area borders the adjacent West Natuna Basin and separates them from the ancestral South China Sea. The diachronous nature of the Late Miocene unconformity indicates a prolonged compressional uplift since the Early Miocene (Group H) to Late Miocene-Pliocene.

6.3 Methodology

Two wells (Laba Barat-1 and Cendor-3A) which penetrated the interval interest zone of Group H and Group I of the Malay Basin were made available for this study. However, core data is only available for Cendor-3A. Two other wells with available core (Cendor-2 and Jambu-3) were used but located around 2 km beyond the 3D seismic boundary. It should also be noted that none of these wells penetrated the whole section of the interval of interest succession of Group H and Group I. Therefore, channel geobody thickness data here were extracted from spectral decomposition analysis from the 3D seismic cube, which covers the entire study area.

Six main seismic surfaces were mapped across the 3D seismic cube. These surfaces tie and correspond to the flooding surfaces defined from well log correlations (see Chapter 3, section 3.1.2, Fig 3.2). The Near Top Group H surface is the topmost and the Near Bottom Group I is the bottommost surface of the interval of interest, respectively.

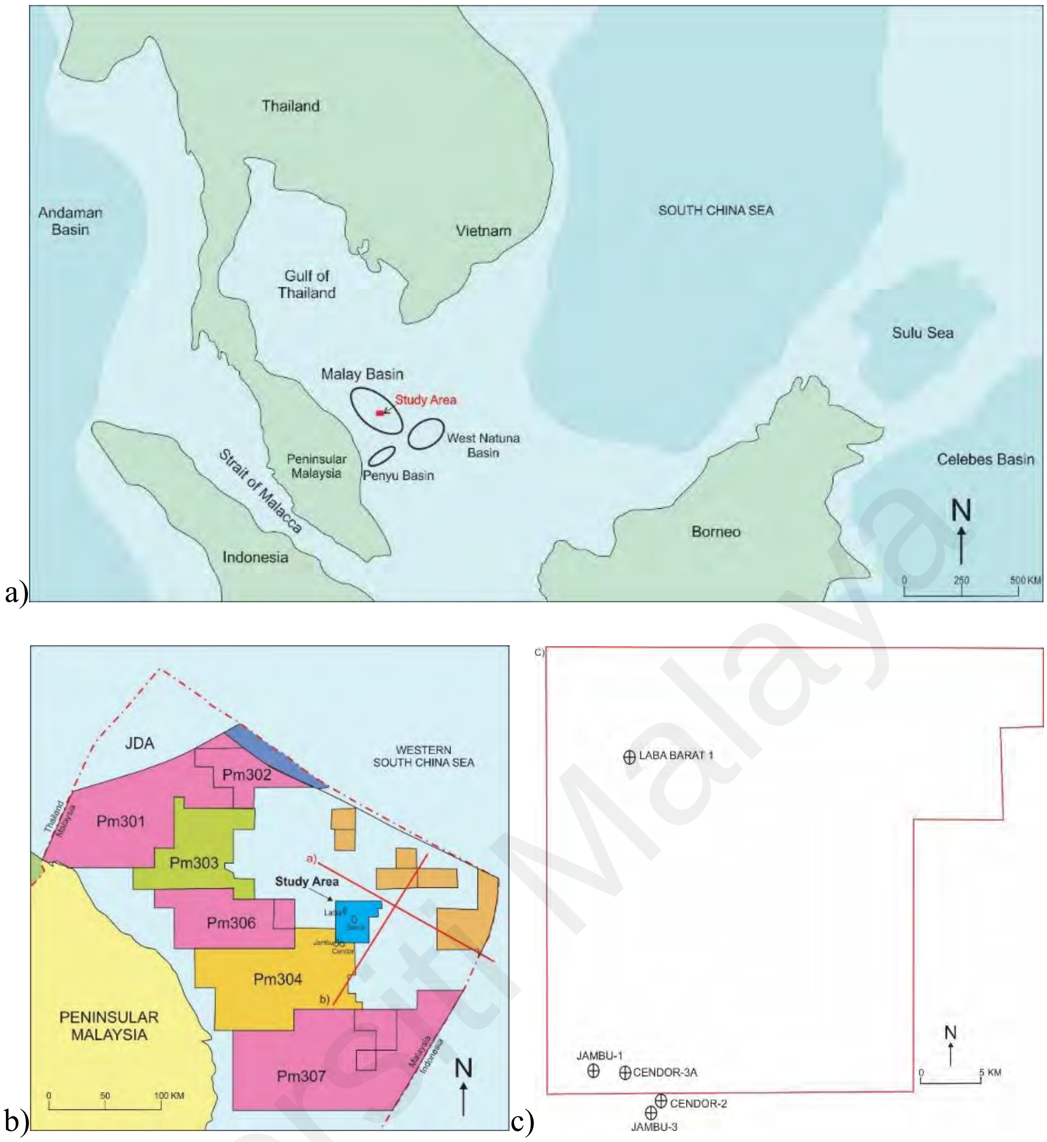

Figure 6.1: a) Map of the Sunda Shelf with sedimentary basins mentioned in the text. The study area is located in the middle part of the Malay Basin, highlighted in red. b and c) The study focused on a 5,632 km^2 area, and used data in the form of a 3D seismic cube, wireline logs, and core data from 3 wells (Cendor-3A, Cendor-2, and Jambu-3). Wireline data from well Laba Barat-1 was used to calibrate and tie the seismic to wells. Data was provided by PETRONAS.

Ten (10) iso-proportional slices (isoslices) with 15 ms TWT thick (approximately 20 m thick) were produced conformant to the key surfaces as top and bottom horizons for subsequent seismic attribute analysis. Several seismic attributes were extracted from the seismic data such as minimum and maximum attributes, dominant frequency, and root mean square (RMS amplitude).

This study utilizes RMS attributes and frequency decomposition techniques to optimize the visualization of seismic surfaces from planform view. The planform views show a wide range of seismic facies and their architectural elements. Channel geometries and dimensions can be extracted and measured. The quantitative geostatistical analysis within the selected seismic volume of Group H and Group I of the Malay Basin includes extracting meaningful statistical data from the range of channel geometries, orientations, and dimensions. A total of 120 channels with over 1000 of data points have been measured and extracted from this study. Geostatistical data extracted from this study include the morphometric elements of planform views such as channel width, wavelength, amplitude, sinuosity, radius of curvature and sinuosity, and thickness data from seismic spectral decomposition analysis (Fig 6.2).

6.4 Quantitative Analysis; Results and Relationship

Channel width (CW), channel depth (CD), meander wavelength (ML), meander belt width (MBW-amplitude), channel length (Lc), sinuosity (SI), and radius of curvature (RC) are the vital morphometric elements extracted and evaluated in this study (refer Chapter 3). All of these parameters have been acquired and measured by using interpretative maps imaged in Paleoscan and Petrel. This study documents the geometries and dimensions of 120 channels within Group H and Group I of the Malay Basin. These morphometric parameters have been cross-plotted to establish relationships between these variables in this study.

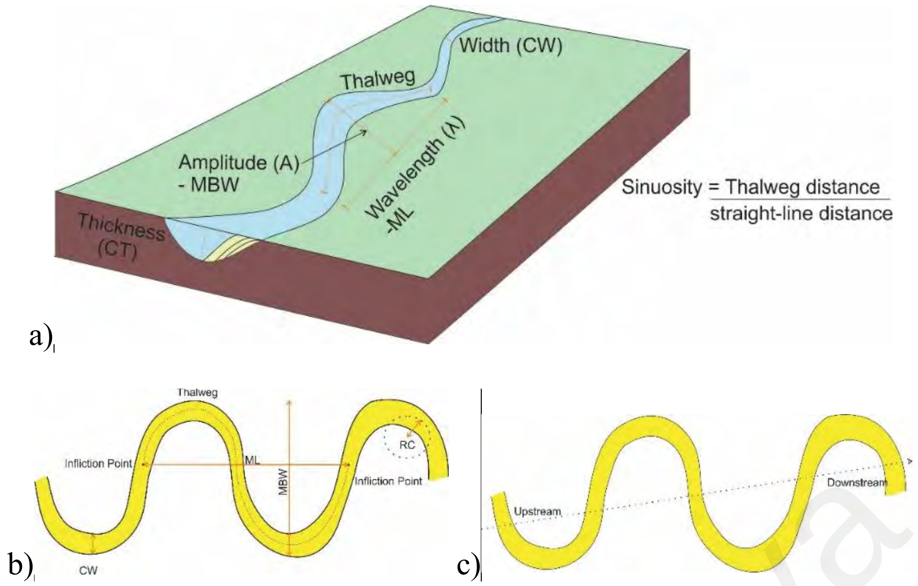

Figure 6.2: Schematic drawing showing the methodology adopted to measure the morphometric parameters of the fluvial systems and the channel orientation. (A, B) The morphometric parameters include channel width (CW), meander belt width (MBW), radius of curvature (RC), meander wavelength (ML), and channel length (L). Sinuosity (SI) is calculated as the thalweg distance divided by the meander wavelength (ML). Thickness (CT) data is the only metric taken from spectral decomposition with reference from wireline log and core. (c) The channel orientation is determined by defining the azimuth of a line that has been drawn between two points of the upstream and downstream reaches.

6.4.1 Channel Classification

Channel width (CW) is measured from side edge-to-edge of a confined channel. Channel sinuosity is measured by dividing the distance between points along a thalweg centreline by the straight-line distance between these points. These two elements are the primary parameters used to classify the channel types. In addition, the planform morphology of the channels is used for channel classification in this study. Planform morphologies identified within the dataset include cuspate meanders, dendritic channel networks, through-flowing and dead-end channels. Channels in this study have been categorized into three main classes.

1. Class-1: Large-scale bypass channel systems comprising fluvial channel belts and/or estuary channels which make up to 8% of the total channel types observed in this study area. This group of channel systems have very low sinuosity (SI 1 –

1.3) and have the highest W/D ratio (>70). These channel systems do not display any tributaries. Class 1 is the largest fluvial system type observed within the Miocene Malay Basin, being more than 1000 - 6000 m wide and with an average thickness of between 14 and 55 m. These channels are characterised by Type-1 channel morphologies.

2. Class-2: Fluvial channel/ channel belt/ distributary channels with tidal influence. Claas-2 makes up to 50% of the total channels. These channels have low to high sinuosity (SI 1.1-2.0) and W/D ratios ranging from 14 – 47. These channels display an extensive range of CT and CW, ranging from 500 – 1000 m wide and 15 – 54 m thick. Class-2 can be further divided into two sub-classes:
   a) Sub-class 2.1 are characterised by Type-2 and Type-4 channel morphologies which are 500 - 1800 m wide, and 15 – 54 thick. These channels typically have connected smaller tributary channels. These are large fluvial channel systems and dominate up to 15 % of the channels observed in the study area. These channels are meandering, with a sinuosity index ranging from 1.8- 2.0.
   b) Sub-class-2.2 is characterised by Type-3 and Type-5 channel morphologies which are 450 – 1800 m wide and 15-54 m thick. This sub-class includes the majority of the channel systems, which account for 35% of the total channels observed in this study area. They display low amplitudes, and their sinuosity varies from low to high (SI 1.1-2.0) with W/T ratios of 10-47.
3. Class-3 is characterised by small channels of Type 7, 8, 9 and 10 are interpreted as small fluvial-tidal channels, tidal channels, or tributaries. This channel class makes up to 42 % of the total channels recorded in the study area. These channels have a high variance of CW, range from 50-450 m wide and with channel thickness ranging from 10 – 35 m, with W/T ratio of <30. Their sinuosities vary from low to high (SI 1.1 – 2.5). Class-3 channels is divided into three sub-classes:

a) Sub-class 3.1 represents low sinuosity fluvial-tidal channels with high amplitudes and extend beyond the study area.
b) Sub-class 3.2 represents through-flowing channels of moderate to high sinuosity (SI 1.1-2.5). These usually form a connected through-flowing network separated by areas of low amplitude seismic reflection, which are interpreted as possible vegetated islands/ bars.
c) Sub-class 3.3 represents the dead-end channels/ tidal creeks with short and narrowing channel morphologies (Type-10). They are 50-200 m wide and 10-35 m thick. These channels generally end within subtle areas of low amplitude seismic reflection, which probably represent tidal flat environments, marshes/ vegetated area/lakes.

6.4.2 Channel Orientation

Channel orientation has been determined by measuring the mean azimuth of the channel from where it enters and exits the seismic survey. In the case where the entire system is not imaged in the survey, the orientation is measured as the mean azimuth for the channel where it is imaged. The orientation of 120 channels was measured in the study area and plotted on rose diagrams for each major seismic facies, i.e., Large Channel (LC), Medium Channel (MC), and Small Channel (SC). Estuary and alluvial bypass channel systems of Class-1 and Class 2 have a dominantly NW-SE and N-S orientation, i.e., possibly from the north-western basin margin towards the axial zone of the Malay Basin. This is based on the evidence shown by funnelling features in isoslice-1 and isoslice-2 (see Chapter 5, Fig 5.11, and Fig 5.12). During deposition of Groups I and H the Malay Basin was a low land which extended until the northern area and was flooded with marine water from the South China Sea in the southeast part of the basin due to sea-level rise during the Miocene thermal maximum. Highlands were present in the north-western and southwestern area of the Malay Basin (Shoup et al., 2012). Tidal channels (Class-3 channels) oriented in variable directions. Many of these most likely fed into the fluvio-tidal channels and form dendritic through-flowing networks with variable orientations. This scenario is significant to the nature of tidal channels (Subclass-3.1 and Subclass-3.2) that experienced bimodal tidal currents. All of these channels apparently flowed into the ancestral South China Sea. My observations are consistent with previous work which show that the paleo-shoreline during I Group time trended NW- SE (EPIC, 1994), and the regional trend of the Miocene Malay Basin fluvial systems was to the southeast (Rapi et al., 2019).

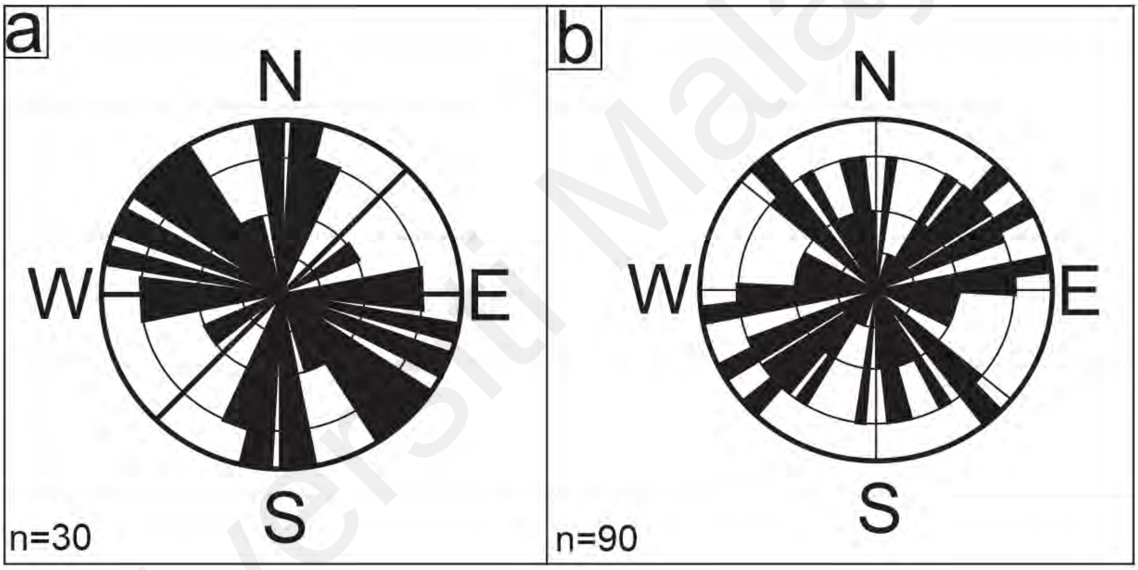

Figure 6.3: Rose diagrams show the orientation of the channel systems in Group H and Group I of the Malay Basin. a) Class-1 (n=10) and Class-2 (n=20) channel systems dominant flow orientation in NW-SE direction. b) Class-3 (n=90) channels system oriented in variable direction from northeast, southeast, northwest and southwest direction.

6.5 Geomorphic Relationships

All the geostatistical parameters extracted from the 120 channels have been cross-plotted against each other to establish their relationship. Generally, channels in this study have been divided into three major seismic facies groups solely based on channel width (CW) i.e.: small-scale (CW= <500m), medium-scale (500 – 1000 m), and large-scale channels (>1000m) (Fig 6.4). Spatially, the study area is dominated by small-scale channels, where some of them are associated with medium- and large-scale channels. Thus, any geostatistical relationships with CW would be elaborated according to these three major seismic facies groups.

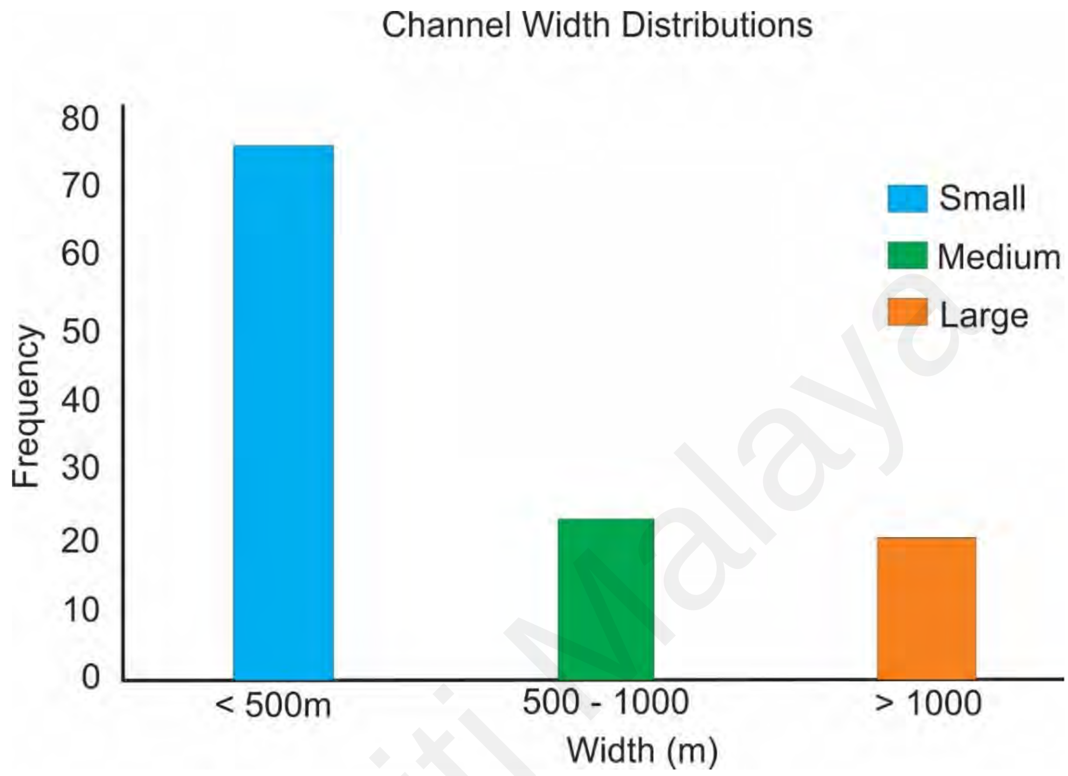

Figure 6.4: Channel width distribution within Group H and Group I of the Malay Basin. Three major seismic facies are recognised i.e. large-scale channel (LC), medium-scale channel (MC), and small-scale channel (SC).

6.5.1 Channel Width (CW) vs Channel Thickness (CT)

Figure 6.5 shows the relationship between mean values of channel width and channel thickness, with R^2= 0.21. Data extracted for CW range from 50 – 6000 m wide, and CT range from 10 – 70 m thick. The plot shows that small-scale channels are on average thinner (10 – 35 m) than the other channel types. Interestingly, the thickness of medium- and large-scale channels are also in the same range with those of the small-scale channels. However, some of larger channels do have greater thickness (35 – 55 m). CW to CT ratio from this plot is CW: CT= >20:1. Results from this plot are consistent with the channel width and channel thickness ranges as compiled in Gibling (2006) (see Table 3, pg.7), where medium- and large-scale channels are typically less than 50 m thick. This table describes fluvial-channel bodies and fluvial-valley fills according to size and form based on the published study.

The deepest and widest channel systems are the estuary, alluvial bypass system, and distributary channels (Class-1 and Class-2 channel types). Even so, some of the observed small-scale channels also have deep incisions. Shallower and narrower channels are predominantly Class-3 channel types, which are interpreted as tidal channels/tributaries.

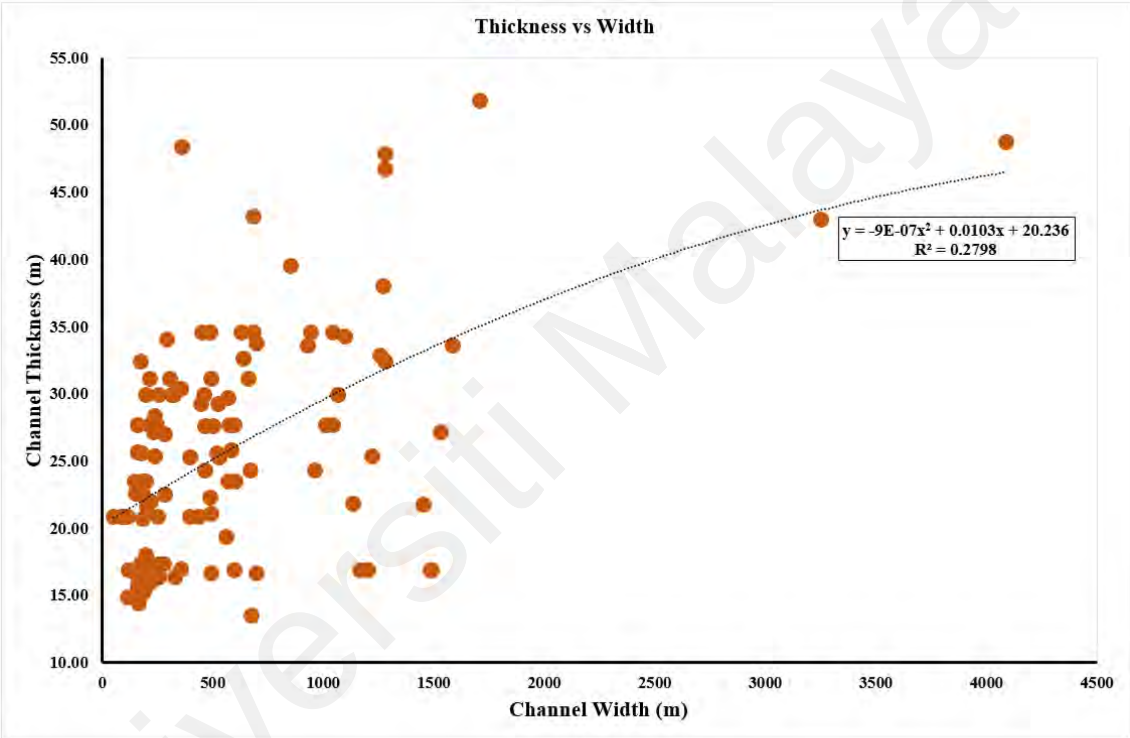

Figure 6.5: Cross-plot of CT against CW of channels observed in within Group H and Group I of the studied seismic volume from the Malay Basin.

6.5.2 Sinuosity (SI) versus all parameters

Figure 6.6 shows data plots of SI against all measured parameters (CW, CT, MWB, ML, and RC) extracted for this study. Figure 6.6a shows the relationship between SI and CW. Most of the high-sinuosity channels (SI =>1.5) are small-scale channels, but some of the larger channels are also highly sinuous. Medium- and large-scale channels generally have low sinuosity (SI= <1.5). The plot shows that SI does not increase exponentially with CW. Nevertheless, according to the relationship between the mode of the sediment transport and planform and cross-sectional geometry by Schumm (1977), sinuosity against channel's width distribution show that small- and medium-scale channels indicate that these channels are mixed-load to suspended-load transport dominated, and larger channels are of bed-load and mixed-load transport type.

Figure 6.6b shows that there is a very poor relationship between SI and CT. Figure 6.6c also shows that there is a poor linear relationship between SI and MBW. The plot indicates that narrower meander belts typically have low sinuosity, whereas wider MBW have higher sinuosity. However, this relationship is dependent on the ML value. If the ML is shorter, and MBW is wider, the channel will display moderate to high sinuosity.

Figure 6.6d shows that there is a moderate relationship between SI and ML. This plot indicates that shorter ML influences channel sinuosity from moderate to high, and sinuosity increases as the ML increase. Similarly, this relationship needs to include MBW, as narrower MBW with long ML decrease the sinuosity. Lastly, Figure 6.6e shows a good exponential relationship between SI and RC. Smaller value of RC suggests low sinuosity, and SI increases as the RC increases.

6.5.3 Channel Width (CW) vs Meander Belt Width (MBW)

Figure 6.7 illustrates that there is a linear relationship between channel width and channel meander belt width (amplitude). The trend is observed in all channel groups, with R^2=0.7. Data extracted varies extensively for both channel width (50 – 6000 m), and meander belt width (500 – 5000 m). Channel meander belt width increases exponentially with channel width. The ratio of MBW: CW in the study area ranges from 1:3 (MBW=3CW) to 1:5 (MBW=5CW). Larger-scale channels appear to have smaller ratio values (1:3), while small- and medium-scale channels have much higher ratio values (1:5). This shows that small- and medium-scale channels are strongly sinuous, while larger-scale channel sinuosity is much lower than that of small- and medium-scale channels.

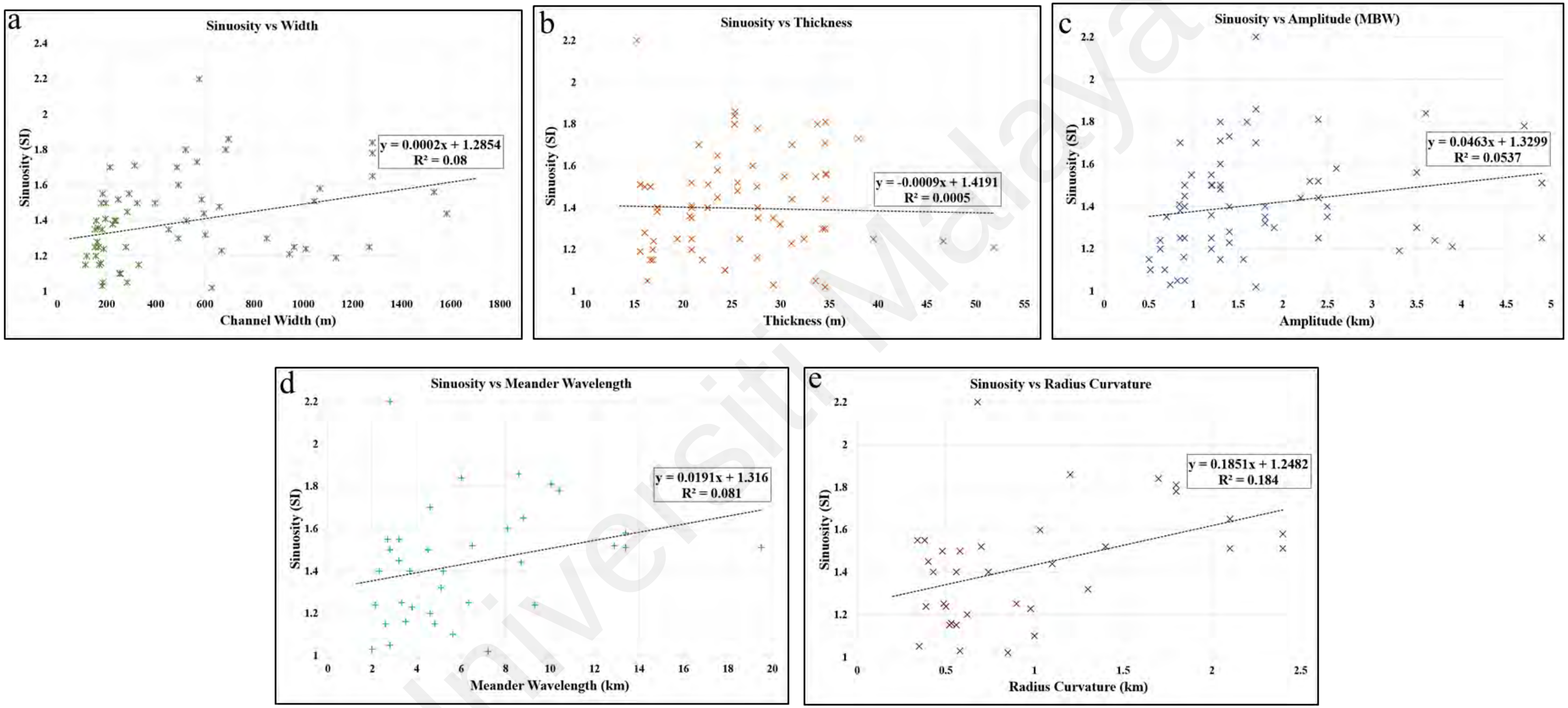

Figure 6.6: Cross-plot of sinuosity (SI) versus a) channel width (CW), b) channel thickness (CT), c) channel meander belt wavelength (amplitude), d) meander wavelength (ML), and e) radius of curvature (RC).

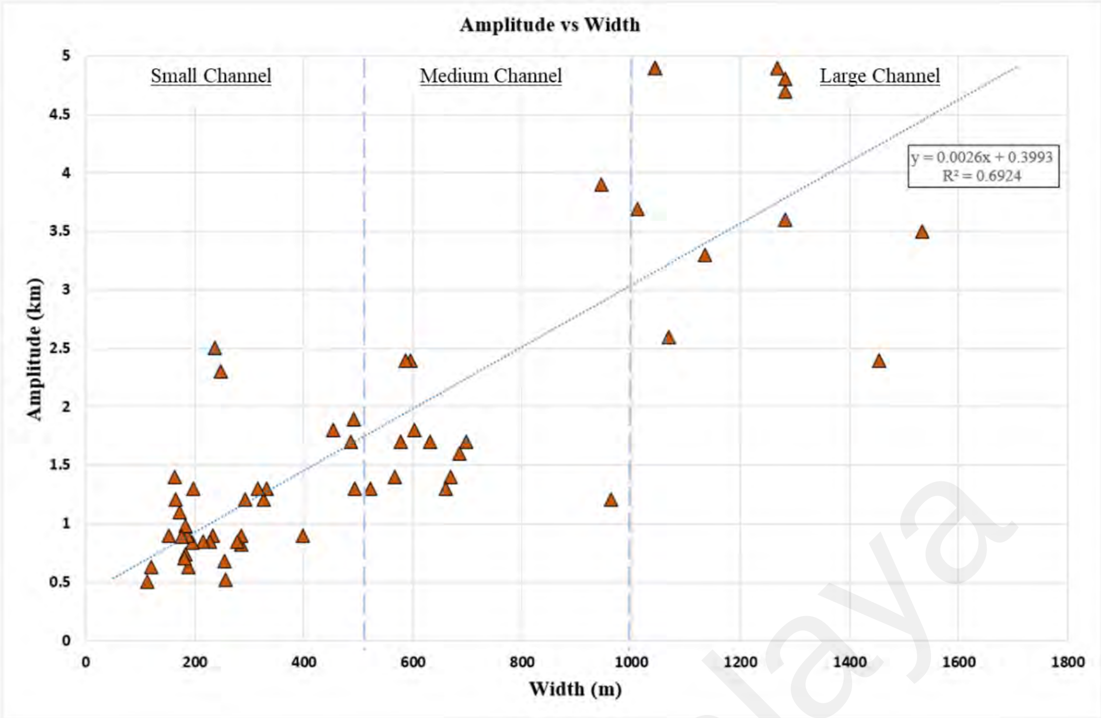

Figure 6.7: Cross-plot of channel meander belt width (MBW-amplitude) versus channel width (CW) for all major group channels (small, medium and large channels). These plots show a direct exponential relationship between these two parameters, for moderate to high sinuosity channel.

6.5.4 Channel Width (CW) vs Meander Wavelength (ML)

Figure 6.8 shows that there is a linear relationship between channel meander wavelength versus channel width (average linear blue line with R^2=0.327). Generally, for moderate to high sinuosity (SI >1.5), wider channels tend to have longer channel meander wavelengths. Based on this plot, the ratio of ML: CW is 1:10, which is consistent with ratios previously reported by Leopold & Wolman, 1960, Zeller, (1967), and Brice (1984).

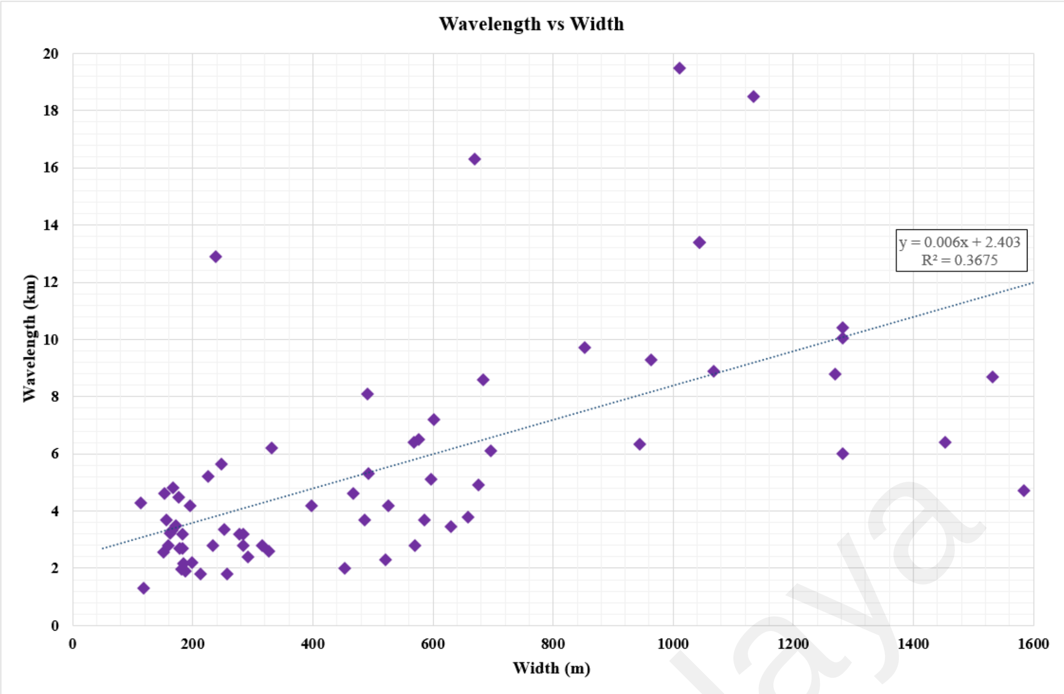

Figure 6.8: Cross-plot of channel wavelength (ML) versus channel width (CW) for all major group channels (small, medium and large channels). These plots show a direct exponential relationship between these two parameters, for moderate to high sinuosity channel.

6.5.5 Amplitude (Meander Belt Width-MBW) vs Meander Wavelength (ML)

The relationship between channel amplitude and meander wavelength is illustrated in Figure 6.9. It shows that each group of channels (SC, MC, and LC) demonstrate a linear relationship between channel amplitude and meander wavelength, which is related to channel sinuosity.

Generally, small-scale channels have lower amplitudes and wavelengths, whereas medium- and large-scale channels have a wide distribution of wavelengths. Some of the highly-sinuous large channels show wider channel amplitudes with smaller wavelength. Wider channel wavelengths with low amplitude resulted in low sinuosity channels.

Interestingly, based on the geostatistical analysis in this study, channel amplitudes are frequently half the size of the channel meander wavelength. Channels tend to be highly sinuous when the amplitude exceeds more than half of the channel meander wavelength. When channel amplitude is lower than half of the channel wavelength, the channel tends to be straight or has a low sinuosity.

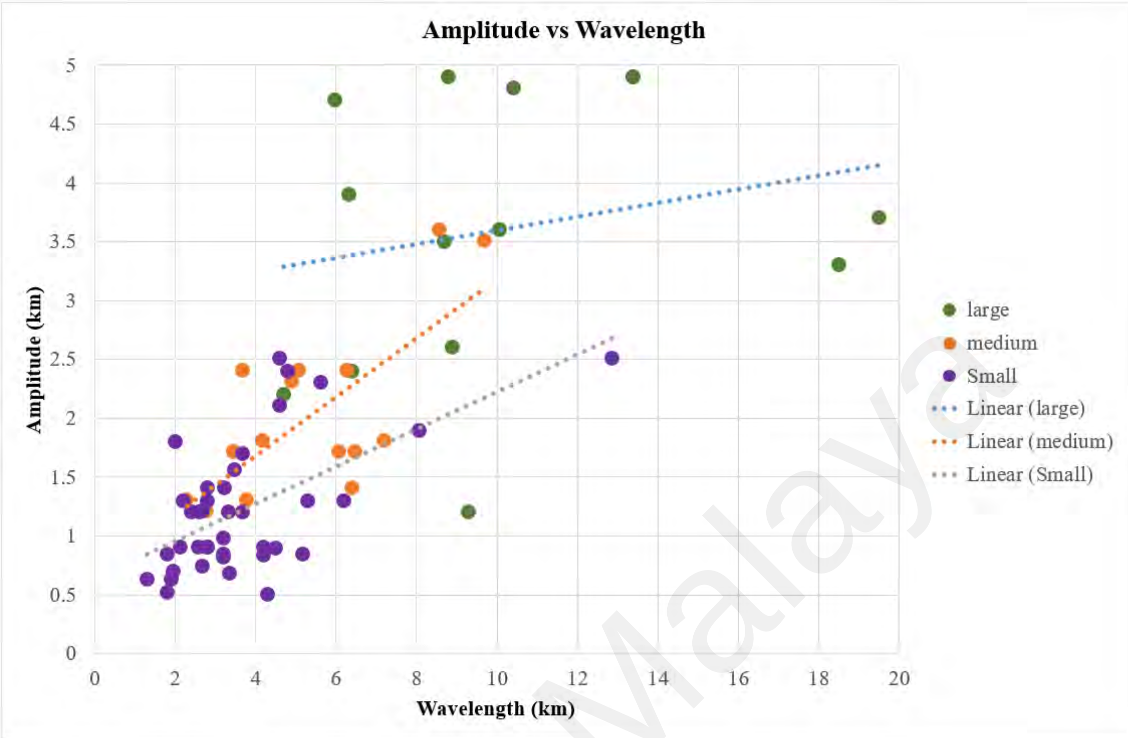

Figure 6.9: Cross-plot of channel amplitude (MBW) versus channel meander wavelength for all major group channels (small, medium and large channels). These plots show a direct exponential relationship between these two parameters. Channel amplitude increases as channel wavelength increases.

6.5.6 Meander Wavelength vs Radius of Curvature

Generally, channel meander wavelength shows a direct exponential relationship with the radius of curvature. Figure 6.10 shows that the relationship between these two parameters is great (R^2= 0.56). According to Brice (1984), ratio of ML:RC for channels is typically ca. 1:5. The ratio of ML:RC in this study is 1:6, which is slightly higher. Channel meander wavelength and radius of curvature of meanders are generally highly variable because of the local tidal hydrodynamic in the tide-dominated regions. When flood and ebb tidal flows began to dominate the depositional system, channel meander geometries became highly meandered and skewed (Fagherazzi et al., 2004), and meander bend tend to have a cuspate-shape (Hughes, 2012).

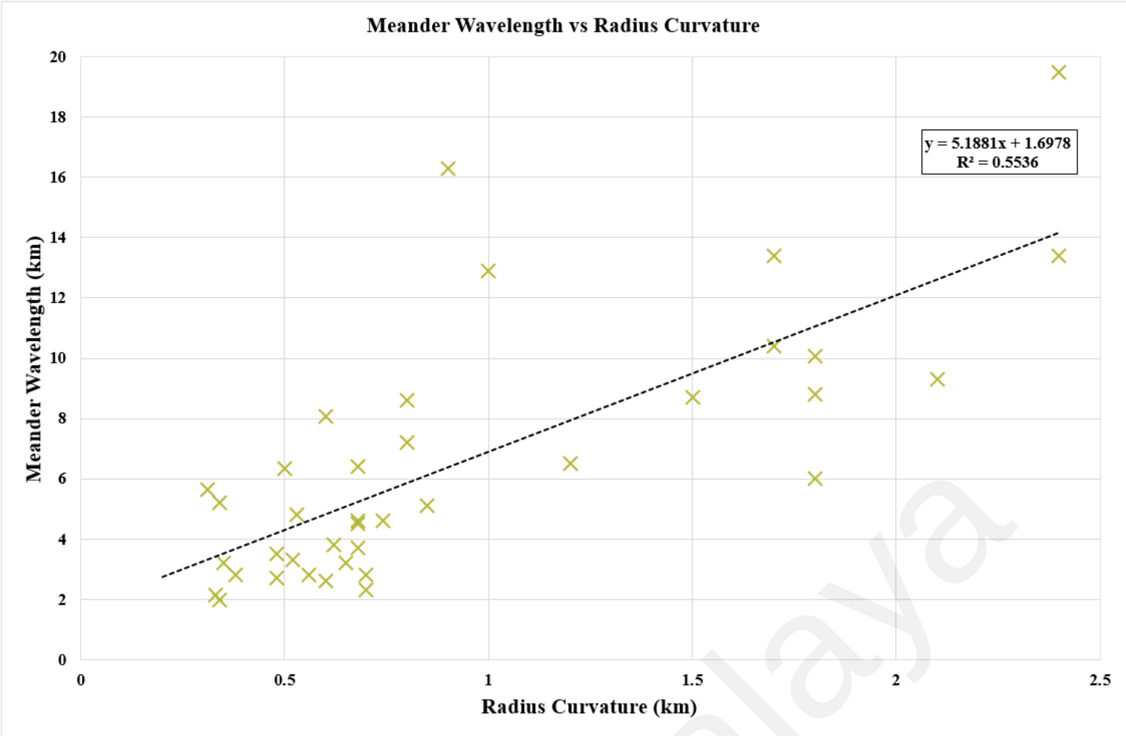

Figure 6.10: Cross-plot of meander wavelength versus radius curvature for all channels (small, medium and large channels). This plot shows a direct exponential relationship between these two parameters and resulted in 1ML=6RC.

6.6 Limitations and Uncertainties of the Geostatistical Analysis

This study measured the geomorphic parameters of fluvial channels within the Group I and H interval of a 3D seismic cube acquired from the Malay Basin. Time-slices and iso-proportional slices were created where channels can be observed. This approach has also been used previously on other deeper ancient fluvial systems (e.g., Wood, 2007; Heldreich et al., 2013). Some of these studies integrated the geomorphic data using ArcGis software (e.g., Kiel, 2009; Alqahtani et al., 2015).

Extraction of geomorphic elements from a 3D seismic cube is associated with several uncertainties. Primarily the main issues are with the horizontal and vertical resolution of the 3D seismic data resolution. Horizontally, uncertainties are related to the lateral measurements such as CW, MBW, and ML. The uncertainties are estimated to be ±50 m of lateral measurement, because the spacing interval of both in-lines and cross-lines is 12.5 m. Therefore, channels of less than 50 m wide are not imaged on the seismic surface slices. Additionally, some channel fills and overbank deposits may be of low amplitude reflection, which effects channels visibility in the seismic.

Vertical uncertainty is primarily associated with the measurement of CT. CT should ideally be extracted from the integration of seismic with well data. However, due to limited well data available in the study area, CT was extracted from spectral decomposition analysis, which means that average seismic interval velocity and seismic frequency will influence the results. The vertical sampling interval of the 3D seismic survey is 2 ms (TWT), which indicate that vertical error could be up to 5m thick. Another factor that contributes to this uncertainty is the fact that the study is in a much deeper section of seismic interval (>1000 ms TWT), thus influencing the average interval velocity and seismic frequency. These uncertainties have a significant impact on the detection of the full range of channel sizes present in the study area. This will complicate the understanding of channel connectivity.

Another issue is related to the internal heterogeneity within the large-scale channels/channel belts. This matter is not addressed in this study as the small channels within the large channels are not seismically resolved and are beyond the seismic resolution attained by the methods used on this dataset. It is assumed that many smaller channels of less than < 5 0m width exist in the systems.

Mis-interpretation of channel types may happen due to the limitation of the study area. The channel length of the large- and medium-scale channels is known to extend beyond the seismic data boundary (Rapi et al., 2019). Therefore, their overall channel morphologies may be different from what has been described in this study. For example, it is possible that the Class-1 channels may be incised valleys. However, the dataset available for this study does not support that interpretation.

6.7 Discussion

6.7.1 Geomorphological Relationships

Many published 3D seismic geomorphological analysis studies on ancient channel systems have been done using time, horizon, and iso-proportional slices (Alqahtani et al., 2015; El-mowafy et al., 2016; Heldreich et al., 2017). These data can be used to understand the evolution of ancient fluvial systems through time, and most importantly can be used for quantifying the characteristics of fluvial sandstone reservoirs.

Channel thickness dataset are important for sandstone reservoirs, which need a large dataset of closely–spaced wells in order to get true thickness of the channel beds, and to map the channel bodies. However, such datasets are rare, given the complexity of channel styles and the uncertainty inherent in datasets for ancient subsurface channels. If the channel bed thickness is known, other geomorphic channel elements such as channel width and sinuosity may be estimated using recorded equations based on modern river studies (e.g., Leeder, 1973; Gibling, 2006). However, especially in this study, even when the thickness is known, the use of the equation to estimate channel planform dimensions is not reliable because these studies focused on fluvial rather than fluvial-tidal systems. Thus, seismic surface attribute analysis is an important method to evaluate and measure the planform channel dimensions spatially.

Geomorphological analysis in this study indicates that there is no pure relationship between channel thickness and channel width. The relative thickness of the amalgamated channels may due to variations in accommodation. Under low accommodation, channel reoccupation within a channel belt will result in a high degree of amalgamation of channel deposits vertically and laterally, thus widening the channel and thickening overall channel fill. In contrast, under high accommodation, channels tend to show narrower channel width and shallower channel thickness. Given the small-scale study area is located within a fluvial-tidal deltaic system, channel distributions and geomorphology likely were controlled by interplay of climate variation and fluctuation of relative sea-level. Hence, the flooding events due to climate change may intensify fluvial incision, and therefore increase channel geobody width and thickness. Whereas the accommodation space available to deposit channels are controlled by relative sea-level.

In addition to the channel width and thickness relationship, even the result is very vague, as thicker channels do not result in wider channels. It can be otherwise, especially in a tidal system, estuary mouth areas are typically shallow, while at further upstream area of the channel, it is narrower and deeper.

Gugliotta & Saito (2019) studied the longitudinal profiles of fluvial-marine transition zones (FMTZ) (85 – 250km channel length). They observed that in the upstream area of FMTZ, fluvio-tidal channels frequently show a constant width and a relatively high sinuosity, with the depth increasing seaward. Further downstream, channel sinuosity is relatively low, channel width increases seaward, while channel depth decreases seaward. Fluvial dynamic is dominantly controlling the upstream section, where tidal influence is less significant. Whereas tidal dynamic is controlling the downstream section, where fluvial influence is subordinate and dampens the tides (Sassi et al., 2012; Nienhuis et al., 2018).

In the upstream section, the channel is wider, deeper, and less sinuous because of the large river discharge (e.g., Yangtze River) (Gugliotta & Saito, 2019), whereas smaller river discharge will result in narrower, low, and sinuous channel morphology (e.g., Fly River Delta). In the strongly tide-dominated downstream section, channel morphologies are wider and shallower at the river mouths (Leonardi et al., 2013; Fagherazzi et al., 2015) (e.g., Lupar Estuary and Rajang Delta). Hence, in the study area, the region of changes in channel morphologies is related to the landward limits of tidal discharge, bidirectional tidal currents, and hydrodynamic energy.

Most of the previous research focused on the alluvial plain and upper coastal plain area, which reveals much information of geomorphic elements of the fluvial channels. Geomorphic element studies of modern rivers also mostly focus on fluvial channels. Their findings are in contrast with the channels observed in this study. It is evident that a variety of factors significantly contribute to the development of the fluvial-tidal channel geomorphologies. For example, autogenic factors such as ebb and flood currents strength, and back- water effects influence much of the channel's morphologies, whereas other factors such as sea-level variations, climate and tectonic would be the secondary factors controlling the channel morphologies.

The methodology used for measurement of geomorphic elements of the channels is directly from seismic surface data. As mentioned in the uncertainties, there would be errors in lateral and vertical measurements due to the seismic spacing interval. These errors most likely arise from the difficulty in obtaining accurate points of measurement on the seismic surface, thus influencing the measurements for channel width, channel meander belt width and channel wavelength. Poor vertical seismic resolution at >1000ms (TWT) in the deep subsurface, with 2ms (TWT) time interval, also affects measurement of channel thickness. Therefore, in this study, channel thickness is taken from spectral decomposition analysis. Hence, all the measurements for channel thickness were given an average instead of absolute values.

6.7.2 Comparison with Ancient and Modern-Day Analogues

Geomorphometric data from Group H and I of the Malay Basin (CW, CT, MBW, ML and SI) have been compared with morphometric data for various channel elements from ancient successions in the published literature. Table 6.1 displays published quantitative morphometric data from throughout the world records, compared with channels from this study. It is noted that published quantitative morphometric data were deposited under a different climatic and tectonic regime. Thus, the comparison was made merely based on channel morphometric elements and dimensions. Some of the Group I and H morphometric elements such as CW, CT and SI fall in the range of some of the global examples, however some of the elements are different.

The widest channels (>10,000 m wide) were observed in Gibling (2006), Klausen et al. (2014) and Alqahtani et al. (2015), and the smallest channels recorded from Gibling (2006) are less than 10 m wide. In comparison, the widest channel observed in this study is up to 6000 m wide, and the smallest channel is 50 m wide. Note that there may be smaller channels in this study, however, they could not be imaged on the surface slices due to poor seismic resolution. Klausen et al. (2014) and Heldreich et al. (2017) record the highest sinuosity channels in their study. Most of the high sinuosity channels are in the proximal area of fluvial channels. In comparison, this study records up to 2.5 SI, and the highest sinuosity was recorded from small-scaled channels of 150 – 450 m width.

Nevertheless, given the small area focused on this study, this study is more consistent with Darmadi et al. (2007) and the distal part in Heldreich et al. (2017). However, Darmadi et al. (2007) channel analysis was from shallower seismic. They did not execute a morphometric analysis on the channels observed in the slices produced, whilst focused on relating stratigraphic variations defined by vertical variations in channel size associated with plan-view changes in the distribution and pattern of observed channel bodies and evaluate potential factors that may have caused these changes. Heldreich et al. (2017) recorded all the morphometric elements and classified their channel types based on the channel width and width/thickness ratio.

Table 6.2 presents a database of channel classifications based on the widths and thicknesses of fluvial–paralic channels. There are differences in terminology that cause considerable confusion when individual depositional components are compared between various literary studies and when they are interpreted in terms of their proportions and geometries.

Gibling (2006) proposed a classification based on the dimensions of fluvial external architectural elements, in which the width-to-thickness ratios are used to determine the style of a fluvial system (straight, braided, meandering, or distributive). This classification is widely applied to planform images of channel geometries to understand the type of fluvial system and its environment. Gibling (2006) separated channel bodies based on their geomorphic setting, geometry, and internal structure, whilst acknowledging the considerable instability of the results. He also reviewed fluvial channel geometries and compiled dimensions from the published literature (e.g., Reynold, 1999). From Reynold (1999), it is recorded that fluvial channel width ranges from 57 - 1400 m. In contrast, the width of the channels in this study are generally from 50 – 1800 m, and some exceed 3000 m wide. Furthermore, Gibling (2006) also proposed a revised channel classification according to their width and thickness, which range from very narrow ribbons less than 10 m to very wide sheets greater than 10,000 m (Table 6.2A).

An extensive range of morphometric data from Gibling (2006) proposed that detailed interpretation of both subsurface and outcrop depositional settings require suitable outcrop analogues given that many other depositional models are qualitative, thus making interpretation challenging. Outcrops are seldom broad enough to ensure that channel geometries and measurements are defined confidently (Bridge & Tye, 2000), and they may not be representative of the overall fluvial-paralic system. Figure 6.11 shows width versus thickness (CW vs CT) results from this study, overlaid with the Gibling (2006) database. Results from this study fall into all the fluvial types recorded from Gibling's (2006). However, given the evidence of facies analysis and planform shape of the channels in the study area do not support the idea of CT versus CW plots determining channel types.

Based on these comparisons, a realistic interpretation of the vast number of studies indicates that there is currently no efficient way to properly evaluate the width-to-thickness ratio of channel bodies from seismic and well data alone, with some degree of confidence. Thickness and width of the channels are not relatable to each other in order to properly evaluate the channel types, as there is considerable overlap of width values between different channel types is, thus, making it challenging to use these data to practically constrain channel geometries and dimensions (Fig 6.11).

Gibling (2006) and Heldreich et al. (2017) noted that this issue most likely arises due to the inability to precisely classify channel types, especially for the ancient channel systems. Furthermore, there are various methodologies and channel terminologies being used by different workers in their study, therefore further complicating the understanding and interpretation of channel types in this study (Fig 6.12).

The morphometric variations tabulated in the Table 6.1 and 6.2a may be attributed to three main factors; 1) data type used for the study (e.g., 3D seismic only, core, or outcrops), 2) measuring technique (e.g., measuring CW on the 3D seismic surface slice may include part of overbank area), and 3) geological background (riverbank and floodplain lithology and vegetation, load and supply and channel gradient).

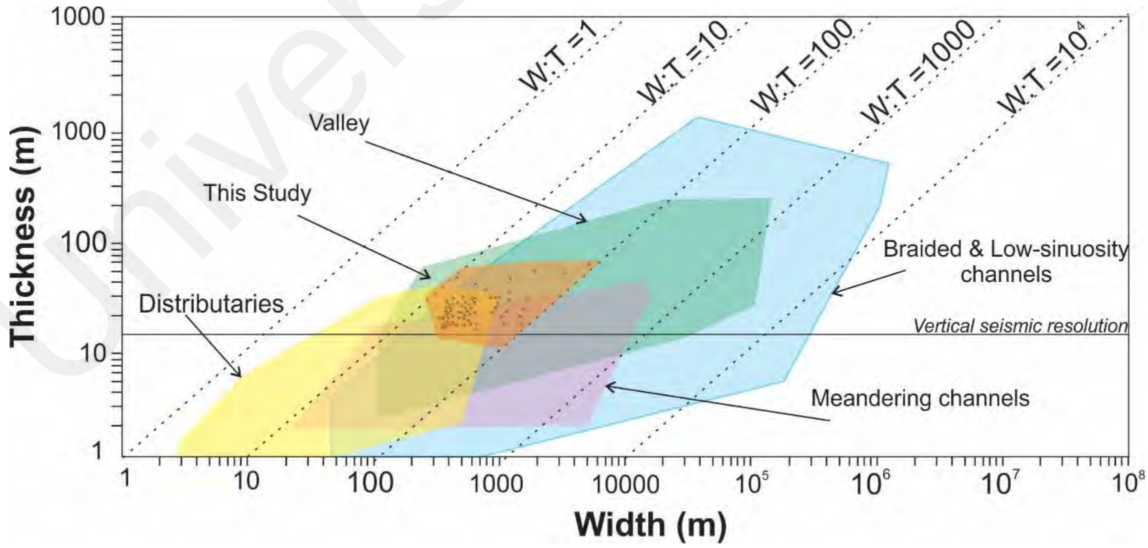

Figure 6.11: Comparison of width: thickness plots of data from this study to the ancient analogues (comparison with Gibling's (2006) fluvial geobody database).

Table 6.1: Examples of published quantitative morphometric data of fluvial systems throughout the world compared with those of Group I and H in the Malay Basin.

Reference	Area	Dataset	Channel Thickness (m)	Channel Width (m)	Meander Belt Width (km)	Meander Wavelength (km)	Sinuosity (SI)	Depositional Environments	Tectonic	Paleoclimate
This Study	Miocene Malay Basin	3D Seismic	10-70	50 - 3500	0.5-5.0	1.5-20	1.1-2.5	Fluvial-tidal delta/ estuary	Early post-rift, Thermal subsidence and inversion event	Tropical-Everwet
Heldreich et al. (2017)	Munggaroo Fm, Autralia	3D Seismic	5->30	200-1000	-	-	1.1-3.0	Fluvial-deltaic	intracratonic sag basin	Temperate to warm, humid & monsoonal climate
Elmowafy and Marfurt, 2016	Frio Formation, south Texas	3D Seismic	-	80–571	-	-	1.05–1.87	Fluvial system	passive margin	Dry, semi-arid
Nuse et al. (2015)	Cedar Mountain Formation, Utah	Outcrops	-	-	0.08	-	1.2	Alluvial system	foreland basin-uplift	-
Klausen et al., 2014	Snadd Fm, Offshore Norway	3D Seismic, wireline logs,and cores	40-58	Up to 20km	-	-	1.1-3.9	Alluvial-Deltaic	Epicontinental basin, syn- to post-depositional salt mobilization	Continental - temperate
Alqahtani et al. (2014)	Pleistocene, Malay Basin	3D Seismic	6-78	75-13000	-	-	1.1-3.5	Coastal plain	Late post-rift, inversion and thermal subsidence	Tropical-Everwet
Kukulski et al. (2013)	Late Jurassic–Early Cretaceous, Monteith Formation, Alberta, Canada	Wireline logs and cores	-	126–320	0.83–2.85	-	-	Fluvial fan/ distributive fluvial system	Retro-arc foreland basin	-
Labrecque, et al (2011)	L. Cretaceous McMurray, Alberta, Canada	3D Seismic and wireline logs	-	500–584	-	-	2.4	Tidally-influenced fluvial or estuaries	-	-
Hubbard et al., (2011)	L. Cretaceous McMurray, Alberta, Canada	3D Seismic	-	390–640	-	-	-	Fluvial with tide influence	-	-
Darmadi et al. (2007)	Sunda Shelf, Indonesia	3D Seismic	~ 20-40	-	-	-	-	Fluvial-deltaic	Post inversion, slow regional subsidence, inversion, deformed	Tropical-Everwet
Wood, 2007	Late Miocene–Pliocene, northern Gulf of Mexico, United States	3D Seismic	-	200–1800	3.0–16.0	5.0–18.0	1.0–2.35	Fluvial-deltaic	Large displacement, dominantly down-to-the-basin, listric growth faults	-
Gibling (2006)	Geological record on fluvial channel bodies and chanel fills	3D Seismic, wireline logs, cores, and outcrops	-	<10 to >10,000	-	-	-	World record	Variable	Variable
Carter (2003)	Widuri Field, Java Sea, Indonesia	3D Seismic	-	50–150	-	0.6–2.5	-	Fluvial system	Post inversion, slow regional subsidence, inversion, deformed	Tropical-Everwet

Table 6.2: a) Comparison of Group I and H channel classification in the Malay Basin, with published quantitative morphometric data from **the ancient rock record. b) Comparison of the Group I and H Malay Basin channel classification with modern-day Rajang Delta.**

a) Channel Classification	This study		Heldreich (2017)		Alqahtani (2014)		Gibling (2006)		Reynolds (1999)	
	Width (m)	Thickness (m)	Width (m)	Thickness (m)	Width (m)	Thickness (m)	Width (m)	Thickness (m)	Width (m)	Thickness (m)
Incised Valley	-	-	>900	≥30	>6000	35-78	100-105000	2-210	500-63000	2-152
Channel Belt	>1000	>35	>900	≥30	-	-	-	-	-	-
Bypass channel/ Fluvial-Tidal Channel	<1000	>30	-	-	450-3000	10-48	-	-	57-1400	2.5-2.4
Multistorey Channel Belt	-	-	400-900	20-30	-	-	-	-	-	-
Single Storey Channel Belt	-	-	≤400	10-20	-	-	-	-	-	-
Braided-Low Sinuosity River	-	-	-	-	-	-	50-13000	1-1200	-	-
Meandering River	-	-	-	-	50-600	8-25	30-15000	1-38	-	-
Distributary Channel	>450-1800	>25	≤400	5-10	-	-	3-1000	1-38	20-5900	1-40
Eustary	>1000	10-35	-	-	-	-	-	-	-	-
Tributary Channel	>50-450	10-35	-	-	-	-	-	-	-	-

b) Channel Classification	This study		Rajang Delta	
	Width (m)	Thickness (m)	Width (m)	Thickness (m)
Bypass Channel/ Fluvial -Tidal Channel	>500-1000	>14-54	>500	5-20
Eustary	>1000	>14-54	>1500	<10
Tidal Channel	200 - 500	10-35	<450	5-20
Tributary/ Tidal Creeks	50 - 200	10-35	10-200	<10

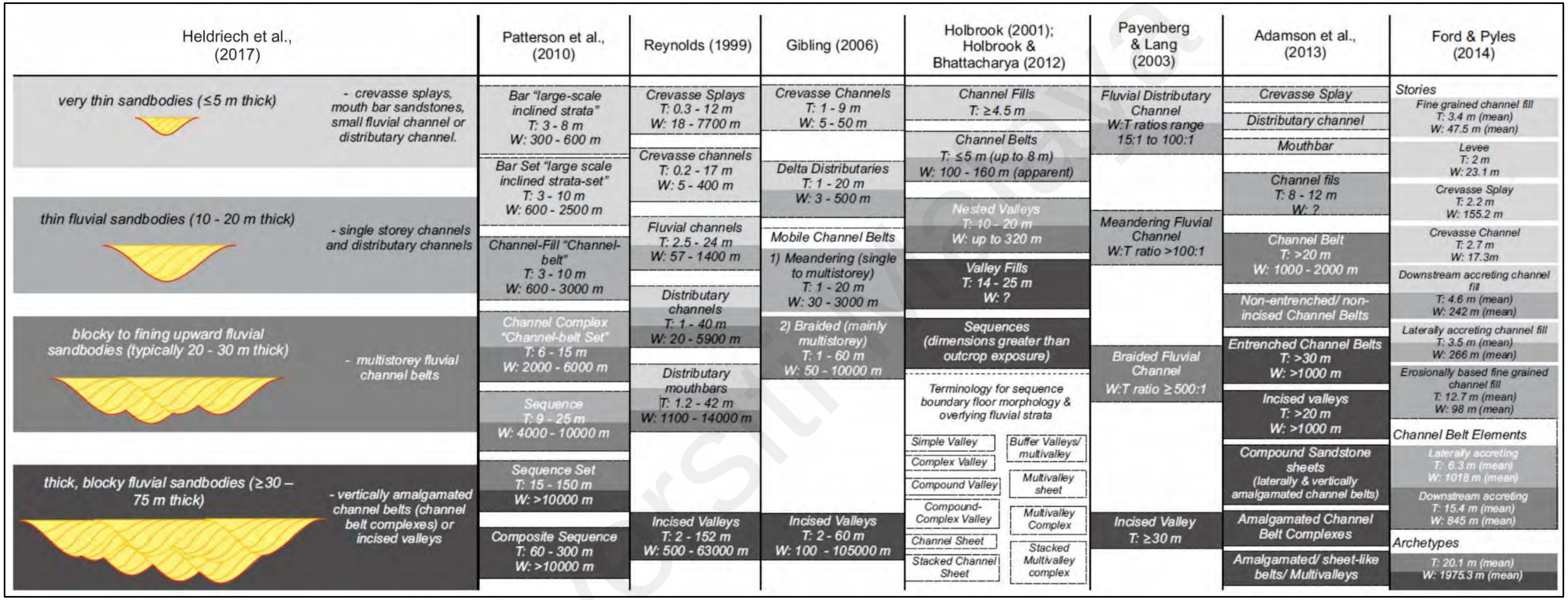

Figure 6.12: Variety of the terminology and nomenclature used from different authors in the published literature. Width and thickness were listed in this chart shows that channel type is irrelevant to their geometries (from Heldreich et al., 2017). This may due to different depositional environments, and the nature of the study area.

6.7.3 Spatial and Temporal Channel Depositional Patterns

Geomorphic data extracted such as the distribution of channel width and images of iso-proportional surface slices has revealed spatial variability within the depositional systems of Group I and H in the Malay Basin. The data has demonstrated that channels often dominate in the centre and upper part of the study area. Channel systems with larger channels in close association with small, high-sinuosity channels displaying high amplitudes are imaged in multiple slices (e.g., isoslice-2) and may reflect a distributive fluvial-tidal system on a delta plain. Diffuse amplitude variance in between channel bodies is broadly lobate, and may record lithological variations across adjacent channel bars, mouth bars or inter-distributary bay deposits.

Large- and medium-scale channels tend to widen towards the south-east, and small channels are mostly concentrated in the southeast part within the overlying slices. Medium- and small-scale channels also tend to have higher sinuosity in the eastern area. This pattern is consistent with south-eastward increasing tidal influence within a distal lower delta plain depositional environment (Bhattacharya, 2010), i.e., the northwest area is interpreted to be located in the proximal area of delta plain, while the southeast area is towards distal area of lower delta plain.

Several stratigraphic models of fluvial evolution show a systematic vertical pattern (e.g., Wright & Marriott, 1993; Shanley & McCabe, 1994). The evolution of fluvial elements and architecture is governed by several factors, including fluctuation of sea-level, tectonics and climate. Figure 6.13 shows two stratigraphic models of a fluvial depositional sequence influenced by base-level fluctuations, i.e., an incised valley (Fig 6.13a) and bypass channel system (Fig 6.13b).

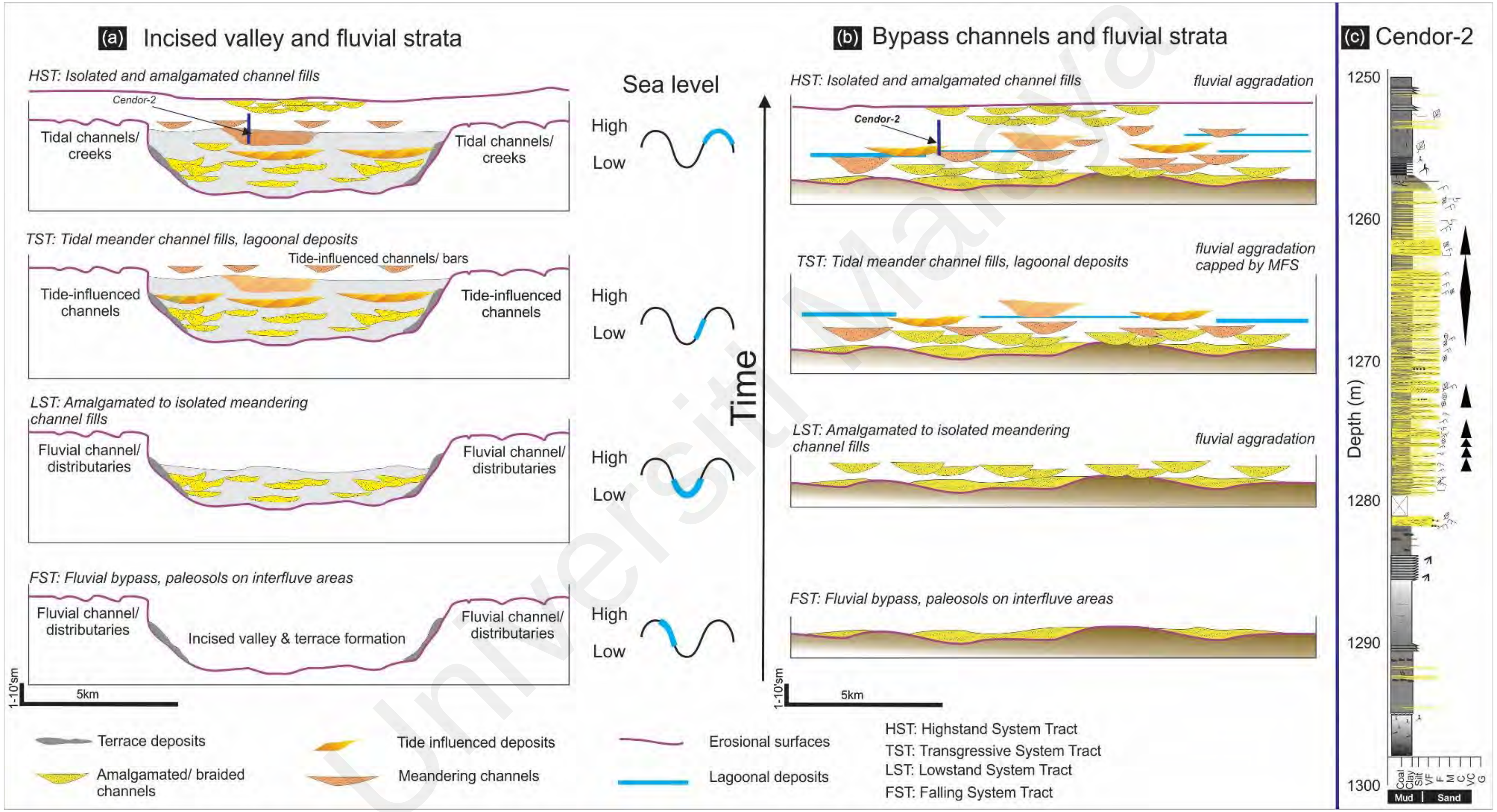

Figure 6.13: Illustration of stratigraphic architecture of a fluvial depositional sequence influenced by base-level fluctuations (a) for an incised valley, and (b) bypass channels. (c) Cendor2 well represents tide-influenced facies association recorded in this study. Modified from Shanley & McCabe (1994).

In this study, vertical variation in channel morphologies and dimensions appears much more relevant with the bypass channel system interpretation. However, it should be noted that the existence of incised valley within the entire I and H Groups channel systems is no conclusive. Even though the channel descriptions within the study area do not support their presence, they might be visible beyond the study area.

Channel types in this study are divided into three classes. Class 1 channels have large and very large channel widths and are interpreted as lowstand fluvial bypass channels (channel belt) or estuaries. Class 2 channels of medium and large channel scale are interpreted as smaller fluvial bypass or distributary channels, and Class 3 channels of smaller size are interpreted as smaller fluvial-tidal and tidal channels.

Class 1 channels incised into older strata when relative sea-level fell slowly and the shelf was not broadly exposed. Class 1 channels have a considerable width and thickness (> 3 km wide and > 14 – 55 m thick). The Sunda Shelf is noted to have had a very subtle gradient profile since the Pleistocene until present-day (Alqahtani et al., 2015), which suggests that even a slight relative sea-level fall may possibly expose some of the shelf area that led to the formation of wide and deep channel systems (Alqahtani et al., 2015). Internal architecture of these Class 1 channels indicate that these incisions are filled by individual channels. During lowstand stage these channels reveal significant sediments basin ward, then as base-level starts to rise, they show sediments trapped within the large channel system (Schumm, 1993; Ethridge et al., 2005). Some of Class 1 channels incise into older late highstand distributary channels that trending to the southeast. Similar channel types have also been observed by Miall (2002) and Alqahtani et al. (2015) in the Pleistocene of the Malay Basin, Darmadi et al. (2007) in Miocene of West Natuna Basin, and Wood (2007) in the Gulf of Mexico.

Geomorphic elements of Class 2 channel systems may represent lowstand systems tracts, transgressive systems tracts, and early highstand system tracts. The transgressive systems tract consists of a series of backstepping parasequences, and abundant tidal facies (Miall, 2010). Throughout transgression, channels tend to rapidly modify their styles and scales, frequently increasing in sinuosity, with well-developed laterally accreting point bars. Class 2 channels are 500 – 1000 m wide and 15 – 54 m thick. Based on their planform geometries, they are interpreted to be fluvial or distributary channels with tidal influence. Some of these low amplitude channels are interpreted to be mud-filled (Wood, 2007) and were likely part of a highstand coastal/deltaic system (Zeng & Hentz, 2004). Interestingly, the geomorphology of channels described here and the remarkable similarities among the offshore Miocene deposits on the Sunda Shelf (Carter, 2003; Darmadi et al., 2007) strongly suggest that the Class 2 channels interpreted here are tide-influenced and associated with the transgression of a broad channel (Posamentier, 2002). With each transgressive landward step of strata/parasequences, a new cluster of tidal channels and bars are formed in a tide-influenced setting.

Based upon the geomorphological elements, Class 3 channels are more prevalent in transgressive and highstand systems tracts. Class 3 systems represent fluvial- tidal channels and creeks with high sinuosity and narrow widths. Some of the channels are through-flowing and others appear to be blind-ended channels with shallow incision. When base-level starts to fall during the late highstand, channels again react by changing their sinuosity and size, typically becoming wider and being characterised by low to highly-sinuous channels (Schumm, 1993; Ethridge et al., 2005).

Channel systems in this study record different channel dimensions and styles compared to the Pleistocene to Recent fluvial system of the Malay Basin. The Pleistocene of the Malay Basin have two main channel types, i.e., incised valleys and alluvial bypass channels. However, there is no direct evidence of incised valley occurrence in this fluvial system of the deeper section studied in this project.

6.7.4 Controls on Channel Geometries in Fluvio-Tidal Depositional Systems

6.7.4.1 Tectonics

Uniform isopach maps and minimal faulting (Fig 6.14) supports a post-rift basin tectonostratigraphic setting for the deposition of Group I and H in the Malay Basin and are consistent with deposition on a low gradient shelf. The late Early to Middle Miocene post-rift period was characterized by thermal subsidence associated with intermittent compressional deformation. These events contributed to the inversion of localised syn-rift half-grabens, reactivation of their bounding faults and development of semi-regional basement highs, mainly concentrated within the southeastern area of the Malay Basin (Madon, 1999), which is near to the study area.

Basement uplift and inversion resulted in the development of basement highs in the southeastern region of the Malay Basin, which are clearly observed in seismic data around the Belumut-Peta area (Madon, 1997, 1999; Ngah, 2000). The Malay Basin was separated from the West Natuna and the ancestral South China Sea by basement highs, or sills. This structure must have a strong influence on relative sea-level in the Malay Basin. Frequent fluctuations in sea-level during the Miocene masked the long-term uplift of the basement high in the southern Malay Basin (Liew, 1996; Madon, 2011). Basement uplift acted as a gate which needed to be breached in order for marine flooding into the basin. This would happen when the rate of sea-level rise was higher than the rate of basement uplift. This would allow tidal hydrodynamics to influence channel geometries in the study area. During low sea-level, the basement high would form a barrier which disconnected the Malay Basin from the sea. The basin may turn into a restricted lake basin. During this period, channel geometries are most likely driven by fluvial processes, and climate may have played a major role in discharge rate. Therefore, tectonics does play an important role in the depositional processes, channel geometries, stacking patterns of the lithostratigraphy of Group I and H in the Malay Basin.

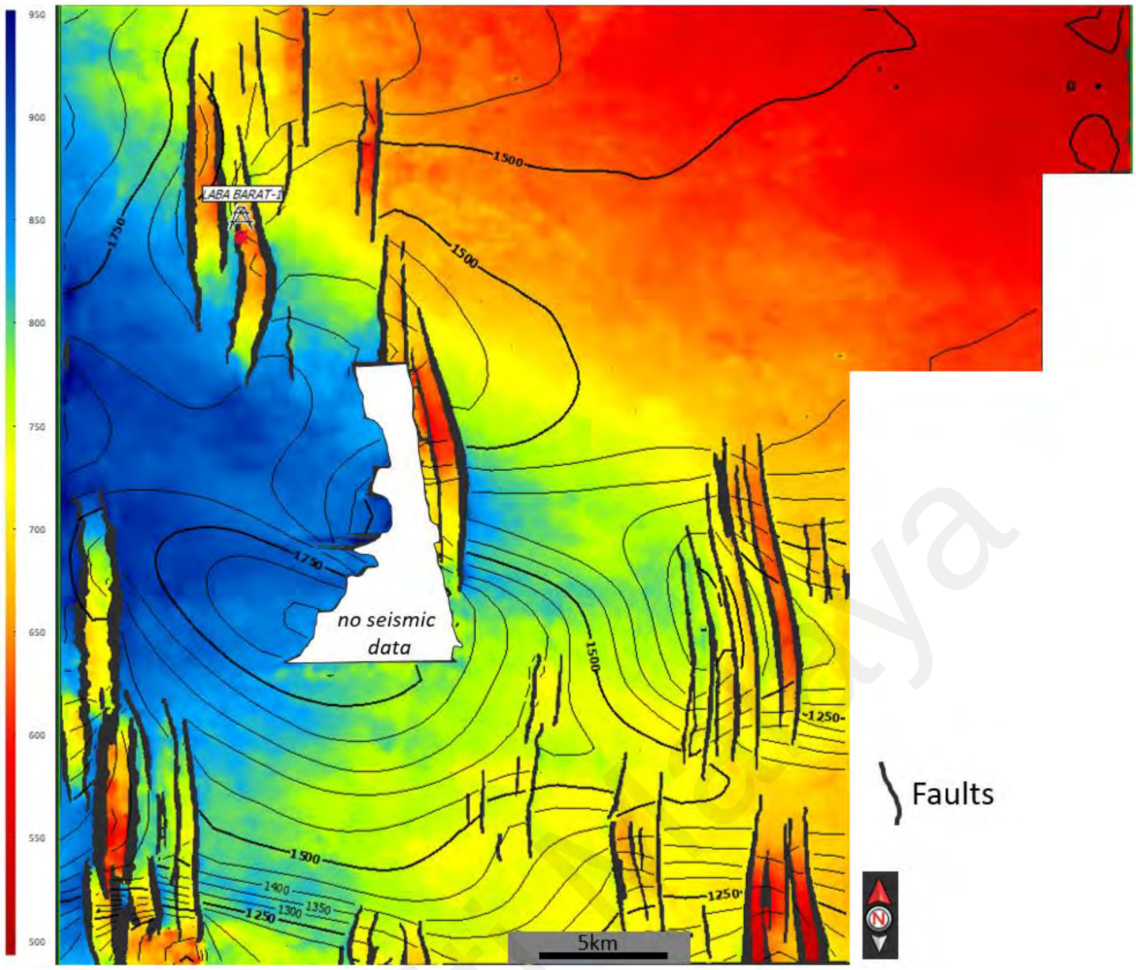

Figure 6.14: TWT-thickness map of the Near Top Group H within the study area. Thickness is dominantly lesser in the Northern and Eastern part of the study area with thickening towards the West. Black lines highlight the orientation and nature of the normal faults.

6.7.4.2 Climate

It is widely understood that climate variations may significantly influence rainfall and vegetation, resulting in fluctuations in rate of sediment supply, rate of erosion and their processes, and flow discharge, from upstream through the longitudinal fluvial profile until the sedimentary basin (Shanley & McCabe, 1994). During the Early to Middle Miocene, the basins located at the southern area of the Gulf of Thailand, including the Malay Basin, received a large supply of sediment attributed from the rising mountain belts in the north-western region in the Thailand and Myanmar border, Mae Ping fault zone in the western highlands, the Chainat Ridge (Hutchison, 1989; Morley & Westaway, 2006), and the western margin of the Khorat Plateau (Upton,1999; Watcharanantakul & Morley, 2000;

Rigo de Rhigi et al., 2003), as well as from local highs adjacent to the basins (O'Leary & Hill, 1989). Those sediments were transported by a paleo–Mekong River which flowed through the Malay Basin into the South China Sea.

The occurrence of herbaceous swamp elements in the northern area of the Malay Basin suggests a seasonal swamp setting (Morley, 2012). Spores associated with strata of Group I in the northern Malay Basin suggest that the swamps were largely dominated by terrestrial marsh ferns (Morley, 2012). The coals indicate an everwet climate, even in the lowstand deposits (Morley & Shamsuddin, 2006; Wong et al., 2006; Morley, 2012). The Early Miocene is interpreted as the period of the wettest climates and the most extensive rainforest development in the region. In the period of thermal maximum in the Middle Miocene (Group H time of deposition), widespread of peat swamps are recorded, indicating the climate was still everwet (Yakzan et al., 1996). Temporary acmes of conifer pollen indicate recurrent episodes of cooler climate during low sea-level, whereby evidence for seasonality is limited. Coals record widespread peat swamps across the Malay Basin during late Middle Miocene.

During the Miocene, the Malay Basin went through rapid-subsidence, which was not associated with displacement of major normal or strike-slip faults (Hall & Morley, 2004; Morley & Westaway, 2006). Thus, the Middle Miocene of the basin was set at a low gradient topography from northwest to the southeast of the basin. However, note that the diachronous nature of the late Miocene unconformity reflects a prolonged compressional uplift since Early Miocene (Group H) to Late Miocene times, with increasing intensity from north to south (Madon, 1997), where the most significant structure is the basement uplift in the southern end of the Malay Basin. There were times, during sea-level low, when basement uplift will disconnect Malay Basin from the South China Sea. Hence during this period, apart from downstream autogenic controls, climate may contribute to changes in channel geometries.

Given the study area is very localised (1563km^2) and the structural high was in the southern Malay Basin during the Miocene, spatial and temporal variation of channel geometries and dimension observed in this study, at times when southern basement uplift is higher than sea-level, the channel geometries and deposition may have been governed by variations in discharge due to the everwet climate.

6.7.4.3 Autocyclic Controls on Channel Geometries and Deposition

Fluvial-tidal deltaic stratigraphy is typically interpreted as being the product of allogenic (external) influences, including eustatic adjustments, tectonic influences and/or climate effects (Jervey, 1988; Perlmutter et al., 1998; Ross et al., 1995). However, recent research has acknowledged that autogenic influence, which are characterised by internal dynamics inherent to the sediment transport and dispersal system, also drive significant changes in sediment deposition and channel geometry (Hajek & Straub, 2017), predominantly over relatively short periods (i.e., 100 - 103 years; Kim et al., 2006; Jerolmack & Paola, 2010; Wang et al., 2011).

Facies depositional analysis and channel geobody geomorphology study (see Chapter 4 and 5) indicate that channel sedimentation geometries are also strongly influenced by autocyclic (or autogenic) factors such as channel switching, tidal flat progradation, lateral channel migration, bar accretion and reworking of floodplain deposits.

The spatial and temporal variation in patterns of channel geometry identified in Group I and H of the Malay Basin (see Fig 5.25 & 5.26) was also influenced by tidal interaction with the coastline which is termed as ‘backwater flow’ (Lane, 1957; Nittrouer et al., 2012; Chatanantavet et al., 2012; Wu & Nittrouer et al., 2020). Backwater effect is a non-uniform hydrodynamic flow condition developed near the river mouth. It can extend 10’s to 100’s of kilometres upstream along the low-gradient channel profiles (Lane, 1957; Nittrouer et al., 2012). The upstream limit of the backwater zone is where the channel bed falls below sea-level. When the river enters the backwater zone in deltaic settings, avulsions occur more frequently. Other dynamic processes of distributary channel and bed-load transport and deposition drop in this area (Chatanantavet et al., 2012).

Channel width: depth ratios, wavelength, and radius of curvature of meanders in the tide-dominated regions are generally highly variable because of the local tidal hydrodynamics, with a seaward exponential increase in channel width (Marani, 2002). As the flood and ebb tidal flows begin to dominate the depositional system, channel meander geometries became skewed (Fagherazzi et al., 2004), and meander bends tend to have a cuspate-shape (Hughes, 2012). Increasing tidal flow energy may result in tighter meanders to the convergence of seaward fluvial current and opposing tidal flood currents (Dalrymple, 2012).

Spatial and temporal trends observed in the Cendor-2, Cendor-3A and Jambu-3 wells such as increased stacking of channels in a relatively proximal location (towards Cendor-2) and downdip (Jambu-3) decrease in geobody thickness and N: G within each stratigraphic interval, may have been controlled by backwater extent of less than 10 kilometres upstream. It is difficult to determine whether backwater processes or climate or a combination of both controlled the flow discharge and sediment supply, especially with limited available data used in this study. Regardless of the significance of backwater hydrodynamic processes in influencing channel geomorphology and sediment spreading patterns, their process does complicate the already complex nature of fluvial–tidal deltaic systems.

The stronger currents of spring tides are likely to increase the fine and sandy sediments in the water column, as the degree of tidal currents typically will increase due to decrease of river flood and neap spring tides transition. Spring tides would be able to transport sediment further landward. The basal sandy deposits are homogeneous in grain size with frequent amalgamated bed. In spite of the prevalence of fine silt in suspension, the base of sand within the cores are remarkably homogeneous in grain size and much lamination is amalgamated.

6.8 Conclusions

The Group I and H stratigraphic units within the studied area of the Malay Basin, comprises an approximately 1000 m thick succession which can be subdivided into 5 stratigraphic units. Each stratigraphic unit in this study presents a range of channel sizes, styles, and dimensions. According to their geomorphometric elements (especially channel width), they have been classified into three main classes. They are estuaries/bypass channel systems, fluvial distributary channels with tidal influence and tidal channels. The main factors governing channel geomorphology in the studies area and interval of the Malay Basin are transgressive-regressive events where prolonged uplift basement in the southern Malay Basin had strongly influence relative sea-level in the basin. Autogenic processes such as channel avulsion and backwater flow of tidal processes also influenced the characteristics of channel morphologies.

Geomorphometric elements of channels from Group I and H such as channel width, channel thickness, meander belt width, meander length and sinuosity have been catalogued and compiled as a database for the Miocene age channels of the Malay Basin. Relationships of these sinuosity and channel width distribution in this study show that most of small- and medium-scale channels are highly meandering, and transport mixed and suspended-load, whereas larger-scale channels transport bed to mixed-load. The resultant channel morphologies are due to the interaction of rivers and tides in a fluvial-tidal depositional system.

CHAPTER 7: CONCLUSIONS AND FUTURE WORK

7.1 Introduction

This project aimed to document the geometries, dimensions, orientations, and distribution of sub-surface geobodies present within the Miocene Group I and Group H of the Malay Basin. This study applied core, well logs and 3D seismic geomorphological analysis for better understanding of channel architecture and their depositional environments, while considering the main controls on development of channel geomorphologies. This study also catalogued geostatistical parameters from channel geobodies and has found statistically significant relationships between them (see Fig 6.5-6.10). These databases are very important better understanding of fluvio-tidal depositional systems and to constrain geological models for Group I and H of the Malay Basin. The findings of this studies, described in the previous chapters, are outlined, analysed, and structured into four majors 'concluding statements' to answer the objectives of this study. Following these final conclusions, recommendations are made for future work.

7.2 Sedimentary Facies of the H Group of the Malay Basin

Depositional facies analysis of the upper section of the H Group of the Malay Basin has been discussed in Chapter 4 of this dissertation through detailed sedimentological analysis on core logging calibrated with gamma-ray logs. Detailed analysis of available cores from three wells of Cendor-2, Cendor-3A, and Jambu-3 of approximately 83.15 m thick and wireline log data allows identification of a suite of facies within the H15-H20 interval of H Group.

Core analysis recorded eleven (11) lithofacies (refer Chapter 4, Table 4.2), and these lithofacies with ichnofacies calibrated with equivalent wireline log signatures were used to define six (6) facies associations of FA1 (Inter-distributary bay/ Offshore), FA2 (Outer

Estuarine/ Abandoned Channel), FA3 (Prodelta), FA4 (Channel/ Channel Bar), FA5 (Mouth Bar), and FA6 (Mangrove/Overbank). This analysis records deposition within lower delta plain channel, overbank, mangrove to lower delta plain distributary channels, restricted embayment, and delta front to prodelta settings.

Common tidal signatures observed in this study strongly indicates that the depositional setting of Group H of the Malay Basin encompassed the fluvial – tidal transition zone (FTTZ) within a deltaic system. The apparent tidal heterolithic facies association suggests a more proximal delta front and delta plain environment. Group H delta system can be assigned to the Ft to Tf plots, indicative of setting where fluvial processes are dominant with a moderate tidal influence to tide-dominated with fluvial-influenced throughout the stratigraphy.

The fluvial–tidal deltaic facies in Group H were deposited in a more seaward position within the FTTZ, i.e., within the zone of higher suspended sediment concentration. The predominance of thick tidally-influenced heterolithic facies that make up the Group H is consistent with a position within the FTTZ.

7.3 Geostatistical Analysis of Channel Morphometric Elements

This study provides a geostatistical database of channel geobodies from the Miocene Group I and H succession located more than 1.5 km subsurface of the Malay Basin. Key morphometric elements of channel width, wavelength, amplitude, thickness, and sinuosity were extracted for over 120 channels observed within the study area and stratigraphic interval. Generally, all the channel geobodies are flowing toward east to southeast into the Miocene South China Sea.

Channel geobodies groups observed in this study have been classified into three main channel classes according to their geostatistical data extracted from the planform seismic surfaces. Class-1 consists of large-scale bypass channel systems comprising fluvial channel belts and/or estuary channels, Class-2 comprises fluvial channel/ channel belt/ distributary channels with tidal influence, and Class-3 is characterised by small channels of Type 7, 8, 9 and 10, which are interpreted as small fluvial-tidal channels, tidal channels, or tributaries.

Despite the lack of published materials for a similar depositional environment as that observed in my project, I managed to classify the channels in this study by characterising them according to their geometries and dimensions, supported with geomorphological elements and core analysis. Subsequently, geomorphometric elements from Group I and H channels such as channel width, channel thickness, meander belt width, meander length and sinuosity have been catalogued and compiled into a database for part of the Miocene succession the central area of the Malay Basin. Databases from this study would be a great reference for future detailed regional study of the Miocene Malay Basin and similar depositional systems in other parts of the world.

7.4 Geomorphological Analysis of Channel Geobodies

Geomorphological study of identification of channels geobodies by using deeper section of 3D seismic data is one of the primary objectives of this dissertation which is discussed in Chapter 5. Ten channel types have been described by integrating both cross-section and plan-view of these channels. Subsequently, four mains seismic geobodies groups have been identified from this study listed as very-large-, large-, medium-, and small-scale channels. They were classified mainly based on their width distributions which were extracted from planform view of seismic surface attributes.

Planform view of the seismic surfaces provide strong evidence of geomorphological features such as meandering channels with cuspate meanders, flaring funnel-shapes, dendritic networks of abundant tributaries, and through-flowing and dead-end small channels. These geomorphological features within the Group H and I fluvial systems of the Malay Basin strongly indicate tidal influence in the basin.

7.5 Possible Controls on Sedimentation and Geobody Architecture

Chapter 4 of this dissertation highlights temporal and spatial variations in depositional facies which were identified from core and well logs, particularly in the upper section of Group H. 3D geomorphology analysis in Chapter 5 describes temporal and spatial variation of channel geometries, in the fluvio-tidal depositional system which can be imaged in planform view.

Lower to Middle Miocene strata of Groups I and H of the Malay Basin are interpreted as representing on the low gradient depositional system. Section 5.5.2, 5.53 and 6.7.4 discussed potential controls on the spatial and temporal variation of sedimentation and channel geomorphologies within the strata. Geobody architectural elements and stacking patterns are controlled by a complex interplay of transgressive-regressive cycles, climate variation which governed sediment supply and water discharge, and downstream autocyclic processes.

The Malay Basin during the Miocene is interpreted as a restricted marginal marine setting, due to the controls of basement high in the southeastern basin during inversion and uplifting tectonic period. This event had a strong influence on the relative sea-level. When rate of sea-level rise exceeded the basement high, marine waters intruded into the basin, and when rate of uplift is higher than sea-level, this structure will block marine influence into the basin. Thus, this event contributes to the transgressive-regressive cycles in the basin, which were observed from biostratigraphy (Yakzan et al., 1996; Morley et al., 2021).

7.6 Recommendations for Future Work

The findings outlined above, and the research carried out as part of this study could be continued and extended in several ways.

7.6.1 Three-dimensional modelling of the Group H and Group I of the Malay Basin

The geobody database compiled in this study can be used to create static three-dimensional models (3D model) of reservoir sandstones for Group H and Group I fields in the Malay Basin. 3D modelling was beyond the scope of this study but could form the basis for future work. The seismic attributes map, in particular, could be scaled up in order to populate reservoir models, following the methods outlined by Massey et al. (2013). Production data, specifically pressure, porosity, and permeability data, can also be incorporated to test geobody continuity in the depositional model.

7.6.2 Seismic stratigraphy and sedimentology

Seismic responds to sedimentary bodies differently at low and high-resolutions, or equally at seismically thick and thin beds. They also respond differently to different lithologies (Zeng, 2017). Although this study has focused on both qualitative interpretation techniques and quantitative seismic geomorphology study, a quantitative interpretation (QI) study of the seismic and well data would further facilitate quantitative assessment of the seismic response to different lithofacies, such as seismic sedimentology analysis with the heavy use of well data and outcrop analogues. Seismic lithological analysis has become one of the basic elements of reservoir geophysics by applying QI techniques from simple 900 phasing of seismic data guided by an acoustic impedance (AI) to attribute analysis, amplitude variation with offset (AVO, and multivariate seismic. This would allow greater constraint of the lithofacies present at each of the studied intervals, potentially removing some ambiguity.

7.6.3 Fluvial hierarchy and architectural scheme for ancient fluvial systems

There are so many confusing terminologies used by different authors in describing and classifying fluvial channel systems. A systematic and identical classification scheme for fluvial architecture elements especially for ancient fluvial systems is essential for future works. Results from this study may be beneficial to improve the existing hierarchy schemes.

7.6.4 Regional study

This study is very localized within a small subset of 3D seismic data. The degree to which these local aspects of stratigraphic architecture and elements can be related to regional patterns is still not clear. Hence, results from this study may assist future work regionally in the Miocene of the Malay Basin. An analysis on more regionally extensive data may give better understanding of proximal and distal areas of the channel systems. Larger-scale images from seismic data will contribute to better interpretation of depositional environments and the controls on the fluvial systems.

7.6.5 Comparison with modern and ancient analogues

Assessment of the findings from this study with other ancient tidally influenced, fluvially dominated delta settings would further extend the dataset and improve the quality of subsurface interpretations. Collective study of modern and ancient analogues could help to clarify the interplay of different controlling factors, including the extent to which local and regional architecture is controlled by autogenic and/or allogenic processes. This work would contribute to the developing of fluvial architecture knowledge catalogue (e.g., the FAKTS database by Colombera et al., 2013).

REFERENCES

Abad, M., Ruiz, F., Pendón, J. G., Tosquella, J., & González-Regalado, M. L. (2006). Escape and equilibrium trace fossils in association with *Conichnus conicus* as indicators of variable sedimentation rates in Tortonian littoral environments of SW Spain. *Geobios, 39*, 1–11.

Abreu, V., Neal, J.E, Bohacs, K.M & Kalbas, J.L. (2010). S*equence stratigraphy of siliciclastic systems – The Exxon Mobil methodology, atlas of exercises: Concepts in sedimentology and palaeontology, 9* (2nd ed.). Tulsa, Okla: SEPM, Society for Sedimentary Geology.

Ager, D.V. (1981). *The nature of the stratigraphical record* (2nd ed.). London: Macmillan.

Ainsworth, R., Flint, S., & Howell, J. (2008). Predicting coastal depositional style: influence of basin morphology and accommodation to sediment supply ratio within a sequence stratigraphic framework. In G.J. Hampson, R.J. Steel, P.M. Burgess & R.W. Dalrymple, (Eds.), R*ecent advances in models of siliciclastic shallow-marine stratigraphy: SEPM Special Publication, 90.* (pp. 237-263). Tulsa, Okla: SEPM, Society for Sedimentary Geology.

Ainsworth, R.B., Vakarelov, B.K. & Nanson, R.A. (2011). Dynamic spatial and temporal prediction of changes in depositional processes on clastic shorelines: toward improved subsurface uncertainty reduction and management. *American Association of Petroleum Geologists Bulletin, 95*, 267–297.

Aigner, T. (1982). Calcareous tempestites: storm-dominated stratification in Upper Muschelkalk limestones, Middle Trias, SW-Germany. In G. Einsel & A. Seilacher (Eds.), *Cyclic and event stratification* (pp 180-198). Berlin: Springer.

Alexander, C.R., Davis, R.A., Henry, V.J. (1998). *Tidalites: Processes and products: SEPM Special Publication, 61*. University of California: Tulsa, Okla: SEPM, Society for Sedimentary Geology.

Allen G. P., & Chambers L. C. C. (1998). *Sedimentation in the modern and Miocene Mahakam delta*. Jakarta, Indonesia: Indonesian Petroleum Association, Field Trip Guidebook.

Allen, G. P., & Posamentier, H. W. (1993). Sequence stratigraphy and facies model of an incised valley fill; the Gironde Estuary, France. *Journal of Sedimentary Research*, *63*(3), 378–391.

Allen, G.P., Salmon, J.C., Bassoulet, P., Du Penhoat, Y. & De Grandprb, C., (1980). Effects of tides on mixing and suspended sediment transport in macrotidal estuaries. *Sedimentary Geology, 26,* 69-90.

Allen, J.R.L. (1964). Studies in fluviatile sedimentation: six cyclothems from the Lower Old Red Sandstone, Anglo-Welsh Basin. *Sedimentology, 3,* 163.

Allen, J.R.L. (1965). A review of the origin and character of recent alluvial sediments. *Sedimentology, 5,* 89–191.

Allen J.R.L. (1965). Coastal geomorphology of eastern Nigeria: Beach ridge barrier islands and vegetated tidal flats. *Geologie en Mijnbouw, 44, 1*–21.

Allen, J.R.L. (1970). Sediments of the modern Niger Delta: a summary and review. In J.P. Morgan & R.H Shaver (Eds.), *Deltaic sedimentation, modern and ancient: SEPM Special Publication, 15* (pp. 138- 151). Tulsa, Okla: SEPM, Society for Sedimentary Geology.

Allen, J. R. L. (1981). Lower Cretaceous tides revealed by crossbedding with mud drapes. *Nature*, *289*, 579 – 581.

Allen J.R.L. (1983). Studies in fluviatile sedimentation: bars, bar complexes and sandstone sheets (low-sinuosity braided streams) in the Brownstones (L. Devonian), Welsh Borders. *Sedimentary Geology, 33*, 237–293.

Allen J.R.L. (1984). *Sedimentary structures: their character and physical basis: Developments in sedimentology, 30*. Amsterdam: Elsevier.

Allison, M. A., Khan, S. R., Goodbred, S. L., & Kuehl, S. A. (2003). Stratigraphic evolution of the late Holocene Ganges–Brahmaputra lower delta plain. *Sedimentary Geology*, *155*(3), 317–342.

Alqahtani, F. A., Johnson, H. D., Jackson, C. A.-L., & Som, M. R. B. (2015). Nature, origin and evolution of a Late Pleistocene incised valley-fill, Sunda Shelf, Southeast Asia. *Sedimentology*, *62*(4), 1198–1232.

Alqahtani, F. A., Jackson, C. A.-L., Johnson, H. D. & Som, M. R. B. (2017). Controls on the geometry and evolution of humid tropical fluvial systems: Insights from 3D seismic geomorphological analysis of the Malay Basin, Sunda Shelf, Southeast Asia. *Journal of Sedimentary Research*, *87*(1), 17–40.

Amir Hassan, M.H., Johnson, H.D., Allison, P.A. & Abdullah, W.H. (2013). Sedimentology and stratigraphic development of the upper Nyalau Formation (Early Miocene), Sarawak, Malaysia: a mixed wave- and tide-influenced coastal system. *Journal of Asian Earth Sciences, 76,* 301–311.

Amir Hassan, M.H., Johnson, H.D., Allison, P.A. & Abdullah, W.H. (2017). Sedimentology and stratigraphic architecture of a Miocene retrogradational, tide-dominated delta system: Balingian Province, offshore Sarawak, Malaysia. In G.J. Hampson, A.D. Reynolds, B. Kostic & M.R. Wells (Eds.), *Sedimentology of paralic reservoirs: Special Publications, 444* (pp 215 – 250). Geological Society of London.

Amir Hassan, M.H., Tahir, R., & Ali, A.K. (2013). *Facies architecture of a complex, heterolith-filled incised valley system, Miocene Malay Basin, Malaysia.* Poster Presented at Petroleum Geoscience Conference and Exhibition 2013, Kuala Lumpur, pp.309-312.

Amos, C.L., (1995). Siliclastic tidal flats. In G.M.E. Perillo (Eds.), *Geomorphology and sedimentology of estuaries* (pp. 273–306). Amsterdam: Elsevier.

Archer, A.W., (1991). Modelling of tidal rhythmites using modern tidal periodicities and implications for short term sedimentation rates. In E.K. Franseen, W.L. Kendall & W.

Ross (Eds.), *Sedimentary modelling: Computer simulations and methods for improved parameter definition: Kansas Geological Survey Bulletin, 223* (pp. 185–194). Kansas: Kansa Geological Survey.

Archer, A.W. (1996). Panthalassa: paleotidal resonance and a global paleocean-seiche. *Palaeoceanography 11*, 625–632.

Archer, A.W. (1998). Hierarchy of controls on cyclic rhythmites deposition, Carboniferous basins of eastern and midcontinental USA. In C.R. Alexander, R.A. Davis & V.J. Henry (Eds.), *Tidalites: Processes and products: SEPM Special Publication, 61* (pp. 59-68). Tulsa, Okla: SEPM, Society for Sedimentary Geology.

Archer, A.W., & Greb, S.F. (1995). An Amazon-scale drainage system in the Early Pennsylvanian of central North America. *The Journal of Geology, 103*, 611–627.

Armitage, J.H. & Viotti, C. (1977). Stratigraphic nomenclature – southern end Malay Basin. *Proceedings of the Indonesian Petroleum Association 6th Annual Convention, Jakarta, Indonesia* (pp. 69–94). Jakarta: Indonesian Petroleum Association.

Arshad, A.R.M., D. Mohd and H.D. Tjia. (1995). A deep seismic section across the Malay basin: Processing of data and tectonic interpretation. *Proceeding of the Abstracts of Geological Society of Malaysia Petroleum Geology Conference: Warta Geologi, 21*, 412.

Ashley, G.M., & Zeff, M.L. (1988). Tidal channel classification for a low mesotidal salt marsh. *Marine Geology, 82* (1–2), 17–32

Ashley, G.M, Boothroyd, J. C., Bridge, J. S., Clifton, H. E., Dalrymple, R., Elliott, T., & Twitchell, D. C. (1990). Classification of large-scale subaqueous bedforms: a new look at an old problem. *Journal of Sedimentary Petrology*, *60*, 160–172.

Ashmore, P. E. (1993). Anabranch confluence kinetics and sedimentation processes in gravel-braided streams. In J.L. Best & C.S. Bristow (Eds.), *Braided rivers* (pp. 129-146). Geological Society of London, Special Publication, 75.

Ashmore, P. (2013). Morphology and dynamics of braided rivers. *Treatise on Geomorphology*, *9*, 289–312.

Baas, J. H., McCaffrey, W. D., & Knipe, R. J. (2005). The deep-water architecture knowledge base: Towards an objective comparison of deep-marine sedimentary systems. *Petroleum Geoscience, 11*, 309-320.

Baas, J.H., Best, J.L. & Peakall, J. (2015). Predicting bed- forms and primary current stratification in cohesive mixtures of mud and sand. *Journal of the Geological Society of London, 173,* 12–45.

Barnes, A. E., Fink, L., & Laughlin, K. (2004). Improving frequency domain thin bed analysis. In *SEG Technical Program Expanded Abstracts*. *SEG Technical Program Expanded Abstracts 2004*,1929–1932.

Barwis, J.H. (1978). Sedimentology of some South Carolina tidal-creek point bars, and a comparison with their fluvial counterparts. In A.D. Miall (Eds.), *Fluvial* *sedimentology: Canadian Society of Petroleum Geologists, 5* (pp. 129-160). Calgary: Canadian Society of Petroleum Geologists.

Bates, C.C. (1953). Rational theory of delta formation. *American Association of Petroleum Geologists Bulletin, 37*, 2119–2162.

Beller, M., Lacaze, S., Pauget, F., & Mangue, M. (2012, June). *Fast leveraging of seismic information over large areas - A Central North Sea case study*. Paper presented at EAGE Conference and Exhibition incorporating EUROPEC, Copenhagen, Denmark.

Belknap, D. F., & Kraft, J. C. (1985). Influence of antecedent geology on the stratigraphic preservation potential and evolution of Delaware's barrier system. *Marine Geology, 63,* 235-262.

Berg, Jan H. (2006). Bedform migration and bed-load transport in some rivers and tidal environments. *Sedimentology, 34,* 681 - 698.

Berné, S., Vagner, P., Guighard, F., Lericolais, G., Liu, Z., Trentesaux, A., Yin, P., & Yi, H.I. (2002). Pleistocene forced regressions and tidal sand ridges in the East China Sea. *Marine Geology, 188*, 293–315.

Bhattacharya, J. (2010). Deltas. In N.P James & R.W. Dalrymple (Eds.), *Facies models 4* (pp. 233 – 264). St. John's, Newfoundland: Geological Association of Canada.

Bhattacharya. J & MacEachern, J. (2009). Hyperpycnal rivers and prodeltaic shelves in the Cretaceous Seaway of North America. *Journal of Sedimentary Research, 79*. 184-209.

Bhattacharya, J., & Walker, R.G. (1992). Deltas. In R.G. Walker & N.P. James (Eds.), *Facies models: Response to sea level change* (pp. 157–177). St. John's, Newfoundland: Geological Association of Canada.

Bhattacharya, J.P., Payenberg, T., Lang, S. & Bourke, M. (2012). *Martian deltas and origin of life*. University of Houston and American Association of Petroleum Geologists.

Billeaud, I., Tessier, B., Lesueur, P., & Caline, B. (2007). Preservation potential of highstand coastal sedimentary bodies in a macrotidal basin: Example from the Bay of Mont-Saint-Michel, NW France. *Sedimentary Geology*, *202*(4), 754–775.

Bishop, M. G. (2002). *Petroleum systems of the Malay Basin province, Malaysia*. Retrieved from https://pubs.er.usgs.gov/publication/ofr9950T. Reston, VA: U.S. Geological Survey.

Blanckaert, K., Kleinhans, M. G., McLelland, S. J., Uijttewaal, W. S. J., Murphy, B. J., van de Kruijs, A., & Chen, Q. (2013). Flow separation at the inner (convex) and outer (concave) banks of constant-width and widening open-channel bends. *Earth Surface Processes and Landforms*, *38*(7), 696–716.

Blum, M. & Törnqvist, T. (2000). Fluvial responses to climate and sea-level change: a review and look forward. *Sedimentology, 47,* 2-48.

Blum, M., Martin, J., Milliken, K., & Garvin, M. (2013). Paleovalley systems: Insights from Quaternary analogs and experiments. *Earth-Science Reviews*, *116*, 128–169.

Boaga, J., Ghinassi, M., D'Alpaos, A., Deidda, G. P., Rodriguez, G., & Cassiani, G. (2018). Geophysical investigations unravel the vestiges of ancient meandering channels and their dynamics in tidal landscapes. *Scientific Reports*, *8*(1), Article#1708.

Boersma, J.R. (1969). Internal structure of some tidal mega-ripples on a shoal in the Westerschelde Estuary, the Netherlands, report of a preliminary investigation. *Netherlands Journal of Geosciences, 48* (4), 409-414.

Boersma, J.R. & Terwindt, J.H.J. (1981). Neap-spring tide sequences of intertidal shoal deposits in a mesotidal estuary. *Sedimentology, 28,* 151–170.

Boyce, B., Wong, R., Krebs, W., Mansor, Y.Z., Barber, P., Morley, R.J., Shamsuddin, J., Jaizan, H. B. Jais, M., Hoesni, J.B., Kirk, R., & Meldrum, G., (2006, Nov). Chronostratigraphic chart of the sedimentary basins of Malaysia. *Conference Proceedings, Petroleum Geoscience Conferences & Exhibition, Kuala Lumpur* (pp. 82-84). European Association of Geoscientists & Engineers.

Boyd, R., Dalrymple, R., & Zaitlin, B.A. (1992). Classification of clastic coastal depositional environments. *Sedimentary Geology, 80,* 139-150.

Boyd, R., Dalrymple, R.W., & Zaitlin, B.A. (2006). Estuary and incised valley facies models. In H.W. Posamentier & R.G. Walker (Eds.), *Facies models revisited: SEPM Special Publication, 84* (pp. 171-234). Tulsa, Okla: SEPM Society for Sedimentary Geology.

Bransden, P. J. E. & Matthews, S. J. (1992). A stratigraphic and structural evolution of the East Java Sea, Indonesia. *Proceedings of the Indonesian Petroleum Association 21st Annual Convention*, *Jakarta, Indonesia* (pp. 418 –53). Jakarta: Indonesian Petroleum Association.

Brettle, M., Mcilroy, D., Elliott, T., Davies, S., & Waters, C. (2002). Identifying cryptic tidal influences within deltaic successions: An example from the Marsdenian (Namurian) interval of the Pennine Basin, UK. *Journal of The Geological Society, 159,* 379–391.

Brice, J. C. (1982). *Stream channel stability assessment*. Report no. FHWA/RD-82/021. Washington, DC: Federal Highway Administration.

Brice, J.C. (1984). Planform properties of meandering rivers. In C.M. Elliott (Ed.), *River meandering*: *Proceedings of the Conference, River, 983,* (pp 1–15). New Orleans, Louisiana: American Society of Civil Engineers.

Bridge, J.S. (2003). *Rivers and floodplains: Forms, processes, and sedimentary record*. Oxford, UK: Blackwell.

Bridge, J. S. (2006). Fluvial facies models: Recent developments. In H.W. Posamentier & R.G. Walker (Eds.), *Facies models revisited: SEPM Special Publication, 84* (pp. 88-170). Tulsa, Okla: SEPM Society for Sedimentary Geology.

Bridge J.S & Leeder M.R. (1979). A simulation model of alluvial stratigraphy. *Sedimentology, 26,* 617–644

Bridge, J.S. & Tye, Bo. (2000). Interpreting the dimensions of ancient fluvial channel bars, channels, and channel belts from wireline-logs and cores. *American Association of Petroleum Geologists Bulletin, 84*(8)*,* 1205-1228.

Brink G., Hernandez, J., Bencomo, J., Jiang, L., Koronful, N., Basu, D., Ishak, A.Z., Ali, M.F., & Skulsanjutr, J. (2019). *Oligocene and Miocene sequence stratigraphy of The North Malay Basin, Malaysia & Thailand*. Poster presented at the Asia Petroleum Geoscience & Exhibition, Kuala Lumpur, Malaysia.

Bromley, R.G. (1996). *Trace fossils: Biology, taphonomy and applications* (2nd ed). London, UK: Chapman and Hall.

Brown, A. R. (2004). *Interpretation of three-dimensional seismic data* (6th ed.). Tulsa, Okla: American Association of Petroleum Geologists, 42 & Society of Exploration Geophysicists, 9.

Brown, A.R. (2011). *Interpretation of three-dimensional seismic data* (7th ed.). Tulsa, Okla: American Association of Petroleum Geologists, 42 & Society of Exploration Geophysicists, 9.

Brown, M.K., Archer, A.W., & Kvale, E.P., (1990). Neap-spring tidal cyclicity in laminated carbonate channel-fill deposits and its implication: Salem Limestone (Mississippian), south-central Indiana, U.S.A. *Journal of Sedimentary Petrology, 60,* 152–159.

Bryant, I.D. & Flint, S.S. (1993). Quantitative clastic reservoir geological modelling: Problems and perspectives. In I. Bryant & S. Flint (Eds.), *The geological modelling of hydrocarbon reservoirs and outcrop analogs* (pp. 205-212). Chichester: Wiley-Blackwell.

Buatois, L. A., Gingras, M. K., MacEachern, J., Mángano, M. G., Zonneveld, J.-P., Pemberton, S. G., Netto, R.G., & Martin, A. (2005). Colonization of brackish-water systems through time: Evidence from the trace-fossil record. *Palaios*, *20*(4), 321–347.

Buatois, L., Saccavino, L. L., & Zavala, C. (2011). Ichnologic signatures of hyperpycnal flow deposits in Cretaceous river-dominated deltas, Austral Basin, southern Argentina. *American Association of Petroleum Geologists Studies in Geology*, *61*, 153–170.

Buraas, E. M., Renshaw, C. E., Magilligan, F. J., & Dade, W. B. (2014). Impact of reach geometry on stream channel sensitivity to extreme floods. *Earth Surface Processes and Landforms, 39*(13), 1778–1789.

Burnett, A. W., & Schumm, S. A. (1983), Alluvial-river response to neo-tectonic deformation in Louisiana and Mississippi. *Science, 222,* 49-50.

Burningham H. (2008). Contrasting geomorphic response to structural control: The Loughros Estuaries, northwest Ireland. *Geomorphology, 97*, 300–320.

Burst, J. F. (1965). Subaqueously formed shrinkage cracks in clay. *Journal of Sedimentary Research*, *35*(2), 348–353.

Burton, D & Wood, L. (2010). Seismic geomorphology and tectonostratigraphic fill of half grabens, West Natuna Basin, Indonesia. *American Association of Petroleum Geologists Bulletin, 94,* 1695-1712.

Cain, S.A. & Mountney, N.P. (2009). Spatial and temporal evolution of a terminal fluvial fan system: The Permian Organ Rock Formation, Southeast Utah, USA. *Sedimentology, 56,* 1774–1800.

Carlston, C. W. (1966). The effect of climate on drainage density and streamflow. *International Association of Scientific Hydrology Bulletin, 11*(3), 62–69.

Carney, S., Barr, D. C., Chai, S. N., Leal, L. A., & Abu Bakar, M. F. (2008, Oct). *Reservoir characterisation of the Mid Miocene Reservoirs of the North Malay Basin, Joint Malaysian Thailand Development Area (MTJDA).* Paper presented at the SPE Asia Pacific Oil and Gas Conference and Exhibition, Perth, Australia.

Carmona, N. B., Buatois, L. A., Ponce, J. J., & Mángano, M. G. (2009). Ichnology and sedimentology of a tide-influenced delta, Lower Miocene Chenque Formation, Patagonia, Argentina: Trace-fossil distribution and response to environmental stresses. *Palaeogeography, Palaeoclimatology, Palaeoecology*, *273*(1), 75–86.

Carter, D.C. (2003). 3-D seismic geomorphology: Insights into fluvial reservoir deposition and performance, Widuri field, Java Sea. *American Association of Petroleum Geologists Bulletin, 87*, 909-934.

Carson, M. A. (1984). The meandering-braided river threshold: A reappraisal. *Journal of Hydrology*, *73*(3), 315–334.

Catuneanu. O. (2006). *Principles of sequence stratigraphy*. Amsterdam: Elsevier.

Chatanantavet, P., Lamb, M. P., & Nittrouer, J. A. (2012). Backwater controls of avulsion location on deltas. *Geophysical Research Letters, 39*(1).

Chen, F., Chen, L., Zhang, W., Han, J., & Wang, J. (2019). Responses of channel morphology to flow-sediment variations after dam construction: a case study of the Shashi Reach, middle Yangtze River. *Hydrology Research, 50*(5), 1359–1375.

Chen, J., Blume, H.-P., & Beyer, L. (2000). Weathering of rocks induced by lichen colonization — a review. *Catena*, *39*(2), 121–146.

Chen, S., Steel, R.J., Dixon, J.F. & Osman, A. (2014). Facies and architecture of a tide-dominated segment of the Late Pliocene Orinoco Delta (Morne L'Enfer Formation) SW Trinidad. *Marine and Petroleum Geology, 57*, 208–232.

Choi, K. (2010). Rhythmic climbing-ripple cross-lamination in inclined heterolithic stratification (IHS) of a macrotidal estuarine channel, Gomso Bay, west coast of Korea. *Journal of Sedimentary Research, 80*(6), 550-561.

Choi, K.S., & Dalrymple, R.W. (2004). Recurring tide-dominated sedimentation in Kyonggi Bay (west coast of Korea); similarity of tidal deposits in late Pleistocene and Holocene sequences. *Marine Geology, 212*(1-4), 81-96.

Choi, K.S., Dalrymple, R.W., Chun, S.S., & Kim, S.P. (2004). Sedimentology of modern, inclined heterolithic stratification (IHS) in the macrotidal Han River delta, Korea. *Journal of Sedimentary Research, 74,* 677–689.

Choi, K.S., Hong, C.M., Kim, M.H., Oh, C.R., & Jung, J.H. (2013). Morphologic evolution of macrotidal estuarine channel in Gomso Bay, west coast of Korea: implication for the architectural development of inclined heterolithic stratification. *Marine Geology, 346,* 343–354.

Choi, K.S., & Park, Y.A. (2000). Late Pleistocene silty tidal rhythmites in the macrotidal flat between Youngjong and Yongyou Islands, west coast of Korea. *Marine Geology 167*(3-5)*,* 231–241.

Chopra, S., & Marfurt, K. J. (2016). Spectral decomposition and spectral balancing of seismic data. *The Leading Edge, 35*(2), 176–179.

Citterio, A. & Piégay, H. (2009). Overbank sedimentation rates in former channel lakes: characterization and control factors. *Sedimentology, 56*(2), 461–482.

Cleveringa J, & Oost A.P. (1999). The fractal geometry of tidal channel systems in the Dutch Wadden sea. *Geologi en Mijnbouw, 78*, 21–30.

Clifton, H.E. (1983). Discrimination between subtidal and intertidal facies in Pleistocene deposits, Willapa Bay, Washington. *Journal of Sedimentary Petrology, 53* (2), 353-369.

Colella, A., & D'Alessandro, A. (1988). Sand waves, Echinocardium traces and their bathyal depositional setting (Monte Torre Palaeostrait, Plio-Pleistocene, southern Italy). *Sedimentology*, *35*(2), 219–237.

Collins, D. S., Avdis, A., Allison, P. A., Johnson, H. D., Hill, J., & Piggott, M. D. (2018). Controls on tidal sedimentation and preservation: Insights from numerical tidal modelling in the Late Oligocene–Miocene South China Sea, Southeast Asia. *Sedimentology*, *65*(7), 2468–2505.

Collins, D.S., Avdis, A., Allison, P.A., Johnson, H.D., Hill, J., Piggott, M.D., Amir Hassan, M. & Damit A.R. (2017). Tidal dynamics and mangrove carbon sequestration during the Oligo Miocene in the South China Sea. *Nature Communications, 8*(1), Article#15698.

Collinson, J.D. (1970). Bedforms of the Tana River, Norway. *Geografisca Annaler, 52A*, 31-56.

Collinson, J.D. (1978). Vertical sequence and sand body shape in alluvial sequences. In A.D. Miall (Eds.), *Fluvial sedimentology: Canadian Society of Petroleum Geologists, 5 (*pp 577-586). Calgary: Canadian Society of Petroleum Geologists.

Collinson, J.D., Mountney, N., & Thompson, D. (2006). *Sedimentary structures*. Hertfordshire: Terra Publishing.

Colombera, L., Mountney, N.P. & McCaffrey, W.D. (2013) A quantitative approach to fluvial facies models: Methods and example results. *Sedimentology, 60*(6), 1526–1558.

Colombera, L., Mountney, N. P., Hodgson, D. M., & McCaffrey, W. D. (2016). The shallow-marine architecture knowledge store: A database for the characterization of shallow-marine and paralic depositional systems. *Marine and Petroleum Geology*, *75*, 83–99.

Comiti, F., Righini, M., Nardi, L., Lucía, A., Amponsah, W., Cavalli, M., & Surian, N. (2016). Channel widening during extreme floods: how to integrate it within river corridor planning? *Proceedings 13th Congress Interpraevent, Lucerne, Switzerland* (pp. 477–486). Istituto di Ricerca per la Protezione Idrogeologica.

Coughenour, C.L., Archer, A.W., & Lacovara, K.J., (2009). Tides, tidalites, and secular changes in the Earth–Moon system. *Earth-Science Reviews, 97*, 59–79.

Cowan, E. J. (1991). The large-scale architecture of the fluvial Westwater Canyon Member, Morrison Formation (Upper Jurassic), San Juan Basin, New Mexico. In A. D. Miall & N. Tyler (Eds.), *The three-dimensional facies architecture of terrigenous clastic sediments and its implications for hydrocarbon discovery and recovery: Concepts in Sedimentology and Palaeontology, 3* (pp 80-93). Tulsa, Okla: SEPM Society for Sedimentary Geology.

Cummings, D., Dalrymple, R., Choi, K., & Jin, J. (2015). *The tide-dominated Han River delta, Korea*: *Geomorphology, sedimentology, and stratigraphic architecture.* Amsterdam: Elsevier Science & Technology Books.

Curran, H.A., & Frey, R.W. (1977). Pleistocene trace fossils from North Carolina (U.S.A.), and their Holocene analogues. In T.P. Crimes & J.C. Harper (Eds.), *Trace fossils 2*. *Geological Journal Special, 9,* 138–162.

D'Alpaos, A., Lanzoni, S., Marani, M., Fagherazzi, S., & Rinaldo, A. (2005). Tidal network ontogeny: Channel initiation and early development. *Journal of Geophysical Research: Earth Surface*, *110*(2).

Dalrymple, R.W. (1992). Tidal depositional systems. In R.G. Walker & N.P. James (Eds.), *Facies models: Response to sea level change* (pp 195–218). St. John's, Newfoundland: Geological Association of Canada.

Dalrymple, R.W. (1984). Morphology and internal structure of sandwaves in the Bay of Fundy. *Sedimentology, 31*, 365-382.

Dalrymple, R.W. (1999). Tide-dominated deltas: do they exist or are they all estuaries? *American Association of Petroleum Geologists Annual Meeting, Official Program, San Antonio* (pp. A29–A30).

Dalrymple, R.W. (2006). Incised valleys in time and space: introduction to the volume and an examination of the controls on valley formation and filling. In R.W. Dalrymple, D.A. Leckie & R. Tillman (Eds.), *Incised valleys in time and space: SEPM Special Publication, 85* (pp. 5–12). Tulsa, Okla: SEPM Society for Sedimentary Geology.

Dalrymple, R.W. (2010). Tidal depositional systems. In N.P James & R.W. Dalrymple (Eds.), *Facies models 4* (pp. 201 – 231). St. John's, Newfoundland: Geological Association of Canada.

Dalrymple, R.W., & Choi, K.S. (2003). Sediment transport by tidal currents. In Middleton, G.V. (Ed.), *Encyclopedia of sediments and sedimentary rocks* (pp. 606-609). Dordrecht: Kluwer Academic Publishers.

Dalrymple, R. W., & Choi, K.S. (2007). Morphologic and facies trends through the fluvial–marine transition in tide-dominated depositional systems: A schematic framework for environmental and sequence-stratigraphic interpretation. *Earth-Science Reviews*, *81*(3), 135–174.

Dalrymple, R.W., & Rhodes, R.N. (1995). Estuarine dunes and bars. In: Perillo, G.M.E. (Eds.), *Geomorphology and sedimentology of estuaries* (pp. 359–422). Amsterdam: Elsevier.

Dalrymple, R.W., & Zaitlin, B.A. (1994). High-resolution sequence stratigraphy of a complex, incised valley succession, the Cobequid Bay–Salmon River estuary, Bay of Fundy, Canada. *Sedimentology, 41,* 1069–1091.

Dalrymple, R.W., Baker, E.K., Harris, P.T., Hughes, M. (2003). Sedimentology and stratigraphy of a tide-dominated, foreland–basin delta (Fly River, Papua New Guinea). In F.H. Sidi, D. Nummedal, P. Imbert, H. Darman & H.W. Posamentier (Eds.), *Tropical deltas of southeast asia- sedimentology, stratigraphy and petroleum geology: SEPM Special Publication, 76* (pp. 147–173). Tulsa, Okla: SEPM Society for Sedimentary Geology.

Dalrymple, R.W., Knight, R.J., Zaitlin, B.A., & Middleton, G.V. (1990). Dynamics and facies model of a macrotidal sand bar complex. *Sedimentology, 37*, 577–612.

Dalrymple, R.W., Kurcinka, C.E., Jablonski, B.V.J., Ichaso, A.A. & MacKay, D.A. (2015). Deciphering the relative importance of fluvial and tidal processes in the fluvial-marine transition. In P.J. Ashworth, J.L. Best & D.R. Parsons (Eds.), *Fluvial-tidal sedimentology: development in sedimentology, 68* (pp. 3–40). Amsterdam: Elsevier.

Dalrymple, R.W., Makino, Y., & Zaitlin, B.A. (1991). Temporal and spatial patterns of rhythmite deposition on mud flats in the macrotidal, Cobequid Bay–Salmon River estuary, Bay of Fundy, Canada. In D.G. Smith, G.E. Reinson, B.A. Zaitlin, & R.A. Rahmani (Eds.), *Clastic tidal sedimentology: Canadian Society of Petroleum Geologists, 16* (pp. 137–160). Calgary: Canadian Society of Petroleum Geologists.

Dalrymple, R., Mackay, D., Ichaso, A., Choi, and, & Choi, K. (2012). Processes, morphodynamics, and facies of tide-dominated estuaries. In R.A. Davis & R.W. Dalrymple (Eds.), *Principles of tidal sedimentology* (pp. 79–107). Germany: Springer Verlag.

Dalrymple, R.W., Zaitlin, B.A., & Boyd, R., (1992). Estuarine facies models: conceptual basis and stratigraphic implications. *Journal of Sedimentary Petrology, 62,* 1130–

1146.

Dana, J.D. (1850b). On the degradation of the rocks of New South Wales and formation of valleys. *American Journal of Science, 9,* 289-294.

Darmadi, Y., Willis, B., & Dorobek, S. (2007). Three-dimensional seismic architecture of fluvial sequences on the low-gradient Sunda shelf, Offshore Indonesia. *Journal of Sedimentary Research*, *77*, 225–238.

Dashtgard, S. E., & La Croix, A. D. (2015). Chapter 3 - Sedimentological trends across the tidal–fluvial transition, Fraser River, Canada: A review and some broader implications. In P.J. Ashworth, J.L. Best & D.R. Parsons (Eds.), *Fluvial-Tidal Sedimentology: Development in Sedimentology, 68* (pp. 111–126). Amsterdam: Elsevier.

Dashtgard, S.E., MacEachern, J.A., Frey, S.E., & Gingras, M.K., (2012). Tidal effects on the shoreface: towards a conceptual framework. *Sedimentary Geology, 279*, 42–61.

Dashtgard, S.E., Gingras, M.K., & MacEachern, J.A., (2009). Tidally modulated shorefaces. *Journal of Sedimentary Research, 79*, 793–807.

Davies, R. J., Posamentier, H. W., Wood, L. J., & Cartwright, J. A. (2007). *Seismic geomorphology: applications to hydrocarbon exploration and production: The Geological Society of London Special publication, 277*. Bath, UK: Geological Society of London.

Davis, R. A. Jr., (2012). Tidal signatures and their preservation potential in stratigraphic sequences. In R.A. Davis & R.W. Dalrymple (Eds.), *Principles of tidal sedimentology* (pp 35-55). Germany: Springer Verlag.

Davis, R. A. Jr., & Dalrymple, R.W. (2012). *Principles of tidal sedimentology*. Germany: Springer Verlag.

Davis, W. M. (1898). The grading of mountain slopes. *Science, 7,* Article #1449.

Davis, W. M. (1899). The geographical cycle. *The Geographical Journal, 14*(5), 481-504.

Davis, H.R., Byers, C.W., & Pratt, L.M. (1989). Depositional mechanisms and organic matter in Mowry Shale (Cretaceous), Wyoming. *American Association of Petroleum Geologists Bulletin, 73,* 1103–1116.

De Boer, P.L., Van Gelder, A. & Nio, S. (1988). *Tide-influenced sedimentary environments and facies*. Dordrecht, Holland: D. Reidel Publishing Company.

De Boer, P.L., Oost, A.P., & Visser, M.J. (1989). The diurnal inequality of the tides as a parameter for recognizing tidal influences. *Journal of Sedimentary Petrology, 59*, 912-921.

Desjardins, P., Buatois, L., & Mangano, M. (2012). Tidal flats and subtidal sand bodies. In *Developments in Sedimentology*, *64*, 529–561.

Dickinson, W.R., 1974b, Plate tectonics and sedimentation. In W. R. Dickinson (Eds.), *Tectonics and sedimentation: SEPM Special Publication, 22* (pp. 1-27). Tulsa, Okla: SEPM Society of Sedimentary Geology.

Dixon, J. L., Heimsath, A. M., & Amundson, R. (2009). The critical role of climate and saprolite weathering in landscape evolution. *Earth Surface Processes and Landforms*, *34*(11), 1507–1521.

Donovan, D. T., & Jones, E. J. W. (1979). Causes of world-wide changes in sea level. *Journal of the Geological Society*, *136*(2), 187 – 192.

Donselaar, M. E., & Overeem, I. (2008). Connectivity of fluvial point-bar deposits: An example from the Miocene Huesca fluvial fan, Ebro Basin, Spain. *American Association of Petroleum Geologists Bulletin*, *92*(9), 1109–1129.

Dott, R.H., & Bourgeois, J. (1982). Hummocky stratification; significance of its variable bedding sequences. *Geological Society of America Bulletin, 93*, 663–680.

Dronkers, J. J. (1975). Tidal theory and computations. In V.T. Chow (Eds.), *Advance in hydroscience, 10* (pp. 145-230). Elsevier.

Duke, W.L. (1985). Hummocky cross-stratification, tropical hurricanes, and intense winter storms. *Sedimentology, 32*, 167–194.

Dunne, T. R., & L. Leopold. (1978). *Water in environmental planning*. New York, NY: Freeman.

Dzulynski, S., & Kotlarczyk, J. (1962). On load-casted ripples. *Annales de la Societe Geologique de Pologne, 32*, 147–159.

Eaton, B., Millar, R., & Davidson, S. (2010). Channel patterns: braided, anabranching, and single-threaded. *Geomorphology, 120*, 353–364.

Eisma, D. (1998). *Intertidal deposits: river mouths tidal flats & coastal lagoons*. Boca Raton: CRC Press.

El-Mowafy, H. Z., & Marfurt, K. J. (2016). Quantitative seismic geomorphology of the middle Frio fluvial systems, south Texas, United States. *American Association of Petroleum Geologists Bulletin*, *100*(4), 537–564.

Elliott, T. (1986a). Deltas. In H.G Reading (Eds.), *Sedimentary environments and facies* (pp. 113-154). Oxford, UK: Blackwell Scientific Publications.

EPIC, (1994). *Regional study of the Malay Basin-Final Portfolios*. Esso-Petronas Integrated Collaborative Study, Unpublished report, Esso Production Malaysia Inc.

Ethridge, F.G. & Schumm, S.A. (1978). Reconstructing palaeochannel morphologic and flow characteristics: methodology, limitations and assessment. In A.D. Miall (Eds.), *Fluvial sedimentology: Canadian Society of Petroleum Geologists, 5* (pp 703-721). Calgary: Canadian Society of Petroleum Geologists.

Ethridge, F.G. & Schumm, S.A. (2007). Fluvial seismic geomorphology: a view from the surface. In R.J. Davies, H.W. Posamentier, L.J. Wood, & J.A. Cartwright (Eds.), *Seismic geomorphology: applications to hydrocarbon exploration and production: The Geological Society of London Special publication, 277* (pp. 205–222). Bath, UK: Geological Society of London.

Ethridge, F. G., Germanoski, D., Schumm, S. A., & Wood, L. (2005). The morphological and stratigraphical effects of base-level change: a review of experimental studies. In M.D. Blum, S.B. Marriott & S.F. Leclair (Eds.), *Fluvial Sedimentology VII: IAS Special Publication, 35* (pp. 213–241). Malden, MA: Wiley-Blackwell.

Fagherazzi, S., & Furbish, D. (2001). On the shape and widening of salt marsh creeks. *Journal of Geophysical Research, 106*, 991–1004.

Fagherazzi, S., Bortoluzzi, A., Dietrich, W. E., Adami, A., Lanzoni, S., Marani, M., & Rinaldo, A. (1999). Tidal networks: 1. Automatic network extraction and preliminary scaling features from digital terrain maps. *Water Resources Research*, *35*(12), 3891–3904.

Fagherazzi, S., Carniello, L., D'Alpaos, L., & Defina, A. (2006). Critical bifurcation of shallow microtidal landforms in tidal flats and salt marshes. *Proceedings of the National Academy of Sciences*, *103*(22), 8337– 8341.

Fagherazzi, S., Edmonds, D. A., Nardin, W., Leonardi, N., Canestrelli, A., Falcini, F., Jerolmack, D. J., Mariotti, G., Rowland, J. C., & Slingerland, R. L. (2015). Dynamics of river mouth deposits. *Reviews of Geophysics*, *53*, 642– 672,

Fagherazzi, S., Gabet, E. J., & Furbish, D. J. (2004). The effect of bidirectional flow on tidal channel planforms. *Earth Surface Processes and Landforms*, *29*(3), 295–309.

Fagherazzi, S., & Mariotti, G. (2012). Mudflat runnels: Evidence and importance of very shallow flows in intertidal morphodynamics. *Geophysical Research Letters*, *39*(14).

Feng, W.-J., Zhang, C.-M., Yin, T.-J., Yin, Y.-S., Liu, J.-L., Zhu, R., Xu, Q.-H., & Chen, Z. (2019). Sedimentary characteristics and internal architecture of a river-dominated delta controlled by autogenic process: implications from a flume tank experiment. *Petroleum Science*, *16*(6), 1237–1254.

Fenies, H., & Tastet, J. (1998). Facies and architecture of an estuarine tidal bar (the Trompeloup bar, Gironde Estuary, SW France). *Marine Geology, 150* (1–4), 149-169.

Fielding C.R. (1993b). A review of recent research in fluvial sedimentology. *Sedimentary Geology, 185,* 3-14.

Fielding, C.R. & Crane, R.C., (1987). An application of statistical modelling to the prediction of hydrocarbon recovery factors in fluvial reservoir sequences. In F.G. Ethridge, R.M. Flores & M.D Harvey (Eds.), *Recent developments in fluvial sedimentology: SEPM, Special publication, 39,* (pp. 321–327). Tulsa, Okla: SEPM Society for Sedimentary Geology.

Fielding, C.R. & Gibling, M.R, (2005). *Distinguishing between channel and valley fills: definitions, diagnostic criteria, and dimensional data*. Presented abstract at 8th International Conference on Fluvial Sedimentology, Delft, Netherlands.

Fielding, C.R., Ashworth, P.J., Best, J.L., Prokocki, E.W., & Smith, G.H.S. (2012). Tributary, distributary and other fluvial patterns: What really represents the norm in the continental rock record? *Sedimentary Geology, 261–262*, 15–32.

Fisk, H.N. (1944). *Geological investigation of the alluvial valley of the lower Mississippi River*. Vicksburg: U.S. Army Corps of Engineers, Mississippi River Commission.

Flemming, B.W, & Bartholomä, A. (1995). *Tidal signatures in modern and ancient sediments: International Association of Sedimentologists Special Publication, 24*. Oxford: Blackwell Scientific Publications.

Ford, G. L., & Pyles, D. R. (2014). A hierarchical approach for evaluating fluvial systems: Architectural analysis and sequential evolution of the high net-sand content, middle Wasatch Formation, Uinta Basin, Utah. *American Association of Petroleum Geologists Bulletin*, *98*(7), 1273–1304.

Friedman, G. M., & Chakraborty, C. (2006). Interpretation of tidal bundles: Two reasons for a paradigm shift. *Carbonates and Evaporites, 21*(2), 170–175.

Friedman, G.M., Sanders, J.E. & Kopaska-Merkel, D.C. (1992). *Principles of sedimentary deposits; stratigraphy and sedimentology*. New York, NY: Macmillan Publication Co.

Friedrichs, C. (2011). Tidal flat morphodynamics: A synthesis. In: J.D. Hansom & B. W, Flemming (Eds.), *Treatise on estuarine and coastal science: Sedimentology and geomorphology* (pp. 137–170). Elsevier.

Friend, P. F. (1983). Towards the field classification of alluvial architecture or sequence. In J. D. Collinson & J. Lewin (Eds.), *Modern and ancient fluvial systems: International Association of Sedimentologists Special Publication, 6* (pp. 345–354). Oxford: Blackwell scientific.

Friend, P. F., Slater, M. J. & Williams, R. C. (1979). Vertical and Lateral building of river channels, Ebro Basin, Spain. *Journal of the Geological Society of London, 136*, 39-46.

Freitas, P. T., Silveira, O. F., & Asp, N. E. (2012). Tide distortion and attenuation in an Amazonian tidal river. *Brazilian Journal of Oceanography, 60*(4), 429–446.

Fustic, M., Hubbard, S., Spencer, R., Smith, D., Leckie, D., Bennett, B., & Larter, S. R. (2012). Recognition of down-valley translation in tidally influenced meandering fluvial deposits, Athabasca Oil Sands (Cretaceous), Alberta, Canada. *Marine and Petroleum Geology*, *29*, 219–232.

Gabet, E.J. (1998). Lateral migration and bank erosion in a salt marsh tidal channel in San Francisco Bay, California. *Journal of the Coastal and Estuarine Research Federation, 21*, 745–753.

Galloway, W.E. (1975). Process framework for describing the morphologic and stratigraphic evolution of deltaic depositional system. In M.L Broussard (Eds.), *Deltas: Models for exploration* (pp 87–98). Houston: Houston Geological Society.

Galloway, W. E. (1981). Depositional architecture of Cenozoic gulf coastal plain fluvial systems. In F.G. Ethridge & R.M. Flores (Eds.), *Recent and ancient nonmarine depositional environments: Models for exploration: SEPM Special Publication,31* (pp. 127-155). Tulsa, Okla: SEPM Society for Sedimentary Geology.

Galloway, W.E, & Hobday, D. (1996). *Terrigenous clastic depositional systems* (2nd ed.). New York, NY: Springer.

Ganti, V., Chadwick, A. J., Hassenruck-Gudipati, H. J., Fuller, B. M., & Lamb, M. P. (2016a). Experimental river delta size set by multiple floods and backwater hydrodynamics. *Science Advances, 2*(5), Article#e1501768.

Ganti, V., Chadwick, A. J., Hassenruck-Gudipati, H. J., & Lamb, M. P. (2016b). Avulsion cycles and their stratigraphic signature on an experimental back- water-controlled delta. *Journal of Geophysical Research: Earth Surface, 121*(9), 1651–1675.

Ganti, V., Chu, Z., Lamb, M. P., Nittrouer, J. A., & Parker, G. (2014). Testing morphodynamic controls on the location and frequency of river avulsions on fans versus deltas: Huanghe (Yellow River), China. *Geophysical Research Letters, 41*, 7882–7890.

Garofalo, D., (1980). The influence of wetland vegetation on tidal stream channel migration and morphology. *Estuaries 3,* 258-270.

Gastaldo, R.A., Allen, G.P. & Huc, A.Y. (1995). The tidal character of fluvial sediments of the modern Mahakam River delta, Kalimantan, Indonesia. In: B.W. Flemming & A. Bartholoma (Eds.), *Tidal Signatures in Modern and Ancient Sediments: International Association of Sedimentologists Special Publication, 24* (pp 171–182). Oxford: Blackwell Scientific Publications.

Gérard, J., & Bromley, R. G. (2008). *Ichnofabrics in clastic sediments: applications to sedimentological core studies: a practical guide*. Paris: Association des S dimentologistes Fran ais.

Gibling, M. (2006). Width and thickness of fluvial channel bodies and valley fills in the geological record: a literature compilation and classification. *Journal of Sedimentary Research*, *76*, 731–770.

Gibling, M.R., Fielding, C.R. & Sinha, R. (2011). Alluvial valleys and alluvial sequences: Towards a geomorphic assessment. In S.K. Davidson, S. Leleu & C.P. North (Eds.), *From river to rock record: The preservation of fluvial sediments and their subsequent interpretation: SEPM Special Publication, 97* (pp. 423–447). Tulsa, Okla: SEPM Society for Sedimentary Geology.

Gingras, M., & MacEachern, J. (2012). Tidal ichnology of shallow-water clastic settings. In R.A. Davis & R.W. Dalrymple (Eds.), *Principles of tidal sedimentology* (pp. 57–77). Germany: Springer Verlag.

Gingras, M.K., MacEachern, J.A. & Dashtgard, S.E. (2012). Chapter 16: Estuaries. In D. Knaust & R.G. Bromley (Eds.), *Trace fossils as indicators of sedimentary environments: Developments in Sedimentology, 64* (pp 471–514). Amsterdam: Elsevier.

Gingras, M.K., Pemberton, S.G., & Saunders, T. (1999). The ichnology of modern and Pleistocene brackish-water deposits at Willapa Bay, Washington: variability in estuarine setting. *Palaios, 14,* 352–374.

Gingras, M.K., Rasamen, M., & Ranzi, A. (2002). The significance of bioturbated inclined heterolithic stratification in the southern part of the Miocene Solimoes Formation, Rio Acre, Amazonia, Brazil. *Palaios, 17,* 591–601.

Ginsberg, S.S., & Perillo, G.M.E. (2004). Characteristics of tidal channels in a mesotidal Estuary of Argentina. *Journal of Coastal Research, 20*, 489–497.

Giusti, E. V, & Schneider, W. J. (1965). *The distribution of branches in river networks.* Washington: U.S. Govt. Print. Office.

Godin, G. (1999). The propagation of tides up rivers with special considerations on the upper Saint Lawrence River. *Estuarine, Coastal and Shelf Science*, *48*(3), 307–324.

Goodbred, S. L., & Kuehl, S. A. (2000). The significance of large sediment supply, active tectonism, and eustasy on margin sequence development: Late Quaternary stratigraphy and evolution of the Ganges–Brahmaputra delta. *Sedimentary Geology*, *133*(3), 227–248.

Goodbred, S.L., & Saito, Y. (2012). Tide-dominated deltas. In R.A. Davis & R.W. Dalrymple (Eds.), *Principles of Tidal Sedimentology* (pp. 129–149). Germany: Springer Verlag.

Greb, S. F., & Archer, A. W. (1995). Rhythmic sedimentation in a mixed tide and wave deposit, Hazel Patch Sandstone (Pennsylvanian), eastern Kentucky coal field. *Journal of Sedimentary Research*, *65*(1b), 96–106.

Greb, S.F., & Archer, A.W. (2007). Soft-sediment deformation produced by tides in a meizoseismic area, Turnagain Arm, Alaska. *Geology, 35*, 425–438.

Griffith, W.M. (1927). A theory of silt and scour. *Institute of Civil Engineers Proceedings, Tulsa, Okla,* (pp 223-314).

Gugliotta, M., Flint, S.S., Hodgson, D.M. & Veiga, G.D. (2016). Recognition criteria, characteristics and implications of the fluvial to marine transition zone in ancient deltaic deposits (Lajas Formation, Argentina). *Sedimentology, 63,* 1971-2001.

Gugliotta, M., Saito, Y., Nguyen, V.L., Ta, T.K.O., Nakashima, R., Tamura, T., Uehara, K., Katsuki, K., & Yamamoto, S. (2017). Process regime, salinity, morphological, and sedimentary trends along the fluvial to marine transition zone of the mixed-energy Mekong River Delta, Vietnam. *Continental Shelf Research*, *147*, 7–26.

Gugliotta, M., Saito, Y., Nguyen, V.L., Ta, T.K.O., & Tamura, T. (2019). Sediment distribution and depositional processes along the fluvial to marine transition zone of the Mekong River Delta, Vietnam. *Sedimentology, 66* (1), 146–164.

Gugliotta, M., Saito, Y., Nguyen, V. L., Ta, T. K. O., Tamura, T., & Fukuda, S. (2018). Tide- and river-generated mud pebbles from the fluvial to marine transition zone of the Mekong River Delta, Vietnam. *Journal of Sedimentary Research*, *88*(9), 981–990.

Gugliotta, M., & Saito, Y. (2019). Matching trends in channel width, sinuosity, and depth along the fluvial to marine transition zone of tide-dominated river deltas: The need for a revision of depositional and hydraulic models. *Earth-Science Reviews*, *191*, 93–113.

Gulliford, A., Flint, S.S., & Hodgson, D.M. (2014). Testing applicability of models of distributive fluvial systems or trunk rivers in ephemeral systems: reconstructing 3-d fluvial architecture in the Beaufort Group, South Africa. *Journal of Sedimentary Research, 84,* 1147-1169.

Hall, R. (1998). The plate tectonics of Cenozoic SE Asia and the distribution of land and sea. In R. Hall & J. Holloway (Eds.), *Biogeography and geological evolution in SE Asia* (pp. 99–131). Amsterdam: Bukhuys Publishers.

Hall, R. & Morley, C.K. (2004). Sundaland basins. In P. Clift, P. Wang, W. Kuhnt & E.E. Hayes (Eds.), *Continent-ocean interactions within the East Asian Marginal Seas, AGU Geophysical Monograph, 149* (pp. 55-85). Washington, DC: American Geophysical Union.

Hall, R., & Nichols, G., (2002). Cenozoic sedimentation and tectonics in Borneo: climatic influences on orogenesis. In: S.J Jones, & L. Frostick (Eds.), *Sediment flux to basins; causes, controls and consequences: Geological Society of London Special Publications, 191.* (pp 5-22). Bath, UK: Geological Society of London.

Hadler-Jacobsen, F., Gardner, M.H., & Borer, J.M. (2007). Seismic stratigraphic and geomorphic analysis of deep-marine deposition along the West African continental margin. In R.J. Davies, H.W. Posamentier, L.J. Wood & J.A. Cartwright (Eds.), *Seismic geomorphology: applications to hydrocarbon exploration and production: The Geological Society of London Special publication, 277* (pp. 47-84). Bath, UK: Geological Society of London.

Hajek, E. A., & Straub, K. M. (2017). Autogenic sedimentation in clastic stratigraphy. *Annual Review of Earth and Planetary Sciences, 45*(1), 681–709.

Hamilton, P.B., Strom, K. & Hoyal, D.C.J.D. (2013). Autogenic incision-backfilling cycles and lobe formation during the growth of alluvial fans with supercritical distributaries. *Sedimentology, 60*, 1498–1525.

Hampson, G.J. & Storms, J.E. (2003). Geomorphological and sequence stratigraphic variability in wave- dominated, shoreface-shelf parasequences. *Sedimentology, 50*, 667–701.

Hampson, G.J., Gani, M.R., Sahoo, H., Rittersbacher, A., Irfan, N., Ranson, A., Jewell, T.O., Gani, N.D.S., Howell, J.A., & Buckley, S.J. (2012), Controls on large-scale patterns of fluvial sandbody distribution in alluvial to coastal plain strata: Upper Cretaceous Blackhawk Formation, Wasatch Plateau, Central Utah, USA: *Sedimentology, 59*, 2226–2258.

Hampson, G. J., Reynolds, A. D., Kostic, B., & Wells, M. R. (2017). Introduction to the sedimentology of paralic reservoirs: recent advances. In G.J. Hampson, A.D. Reynolds, B. Kostic & M.R. Wells (Eds.), *Sedimentology of paralic reservoirs: special publications, 444* (pp. 1– 6). Geological Society of London.

Hanebuth, T. J. J., & Stattegger, K. (2003). The stratigraphic evolution of the sunda shelf during the past fifty thousand years. In F. H. Sidi, D. Nummedal, P. Imbert, H. Darman, & H. W. Posamentier (Eds.), *Tropical deltas of Southeast Asia- Sedimentology, stratigraphy, and petroleum geology: SEPM Special Publication, 76* (pp. 189–200). Tulsa, Okla: SEPM Society for Sedimentary Geology.

Haq, B.U., Hardenbol, J., & Vail, P.R. (1987). Chronology of fluctuating sea levels since the Triassic. *Science, 235*, 1156–1167.

Hardage, B. A., Levey, R. A., Pendleton, V., Simmons J. & Edson, R. (1994). A 3d seismic case history evaluating fluvially deposited thin-bed reservoirs in a gas-producing property. *Geophysics, 59,* 1650-1665.

Harms, J.C. & Fahnestock, R.R. (1965). Stratification, bedforms and flow phenomena (with an example from the Rio Grande). In G.V. Middleton (Eds.), *Primary sedimentary structures and their hydrodynamic interpretation: SEPM Special Publication, 12* (pp. 84-115). Tulsa, Okla: SEPM Society of Sedimentary Geology.

Harms, J.C., Southard, J.B., Spearing, D.R., & Walker, R.G. (1975). *Depositional environments as interpreted from primary sedimentary structures and stratification sequences; Short Course, 2*. Tulsa, Okla: SEPM Society of Sedimentary Geology.

Harris, P.T. (1988). Large scale bedforms as indicators of mutually evasive sand transport and the sequential infilling of wide-mouthed estuaries. *Sedimentary Geology, 57*, 273–298.

Harris, P. T., & Whiteway, T. (2011). Global distribution of large submarine canyons: Geomorphic differences between active and passive continental margins. *Marine Geology, 285*, 69-86.

Harris, P.T., Baker, E.K., Cole, A.R., & Short, S.A., (1993). A preliminary study of sedimentation in the tidally dominated Fly River delta, Gulf of Papua. *Continental Shelf Research, 13*(4), 441–472.

Harris, P.T., Heap, A.D., Bryce, S.M., Porter-Smith, R., Ryan, D.A., & Heggie, D.T. (2002). Classification of Australian clastic coastal depositional environments based upon a quantitative analysis of wave, tidal, and river power. *Journal of Sedimentary Research, 72,* 858–870.

Harris, P. T., Hughes, M. G., Baker, E. K., Dalrymple, R. W., & Keene, J. B. (2004). Sediment transport in distributary channels and its export to the pro-deltaic environment in a tidally dominated delta: Fly River, Papua New Guinea. *Continental Shelf Research*, *24*(19), 2431–2454.

Harris, P.T., Pattiaratchi, C.B., Cole, A.R., & Keene, J.B. (1992). Evolution of subtidal sandbanks in Moreton Bay, eastern Australia. *Marine Geology, 103* (1–3), 225-247.

Hartley, A.J., Weissmann, G.S., Nichols, G.J., & Warwick, G.L. (2010). Large distributive fluvial systems: characteristics, distribution, and controls on development. *Journal of Sedimentary Research, 80,* 167–183.

Hassaan, M., Bhattacharya, S., Mathew, M., & Siddiqui, N. (2015). Understanding basin evolution through sediment accumulation modeling: a case study from Malay Basin. *Research Journal of Applied Sciences, Engineering and Technology*, *11*, 388–395.

Hayes, M., & FitzGerald, D. (2013). Origin, evolution, and classification of tidal inlets. *Journal of Coastal Research*, *69*, 14–33.

Hentz, T. F., & Zeng, H. (2003). High-frequency Miocene sequence stratigraphy, offshore Louisiana: Cycle framework and influence on production distribution in a mature shelf province. *American Association of Petroleum Geologists Bulletin*, *87*(2), 197–230.

Heldreich, G., Redfern, J., Legler, B., Gerdes, K., Taylor, S., Hodgetts, D. & Williams, B. P. J. (2013). Analysis of geobody geometries within the Fluvio-Deltaic Mungaroo Formation, NW Australia. In M. Keep & S.J. Moss (Eds.), *The Sedimentary Basins of Western Australia 4: Proceedings of Petroleum Exploration Society of Australia Symposium, Perth, 18 August 2013* (pp 18–21). Perth, WA: Petroleum Exploration Society of Australia.

Heldreich, G., Redfern, J., Legler, B., Gerdes, K., & Williams, B. (2017). Challenges in characterizing subsurface paralic reservoir geometries: a detailed case study of the Mungaroo Formation, Northwest Shelf, Australia. In G.J. Hampson, A.D. Reynolds, B. Kostic & M.R. Wells (Eds.), *Sedimentology of paralic reservoirs: Special Publications, 444* (pp 59 – 108). Geological Society of London.

Hibma, A., de Vriend, H. J., & Stive, M. J. F. (2003). Numerical modelling of shoal pattern formation in well-mixed elongated estuaries. *Estuarine, Coastal and Shelf Science*, *57*(5), 981–991.

Hibma, A., Schuttelaars, H. M., & de Vriend, H. J. (2004). Initial formation and long-term evolution of channel–shoal patterns. *Continental Shelf Research*, *24*(15), 1637–1650.

Hibma, A., Stive, M. J. F., & Wang, Z. B. (2004). Estuarine morphodynamics. *Coastal Engineering*, *51*(8), 765–778.

Hoitink, A. J. F., & Jay, D. A. (2016). Tidal river dynamics: Implications for deltas. *Reviews of Geophysics, 54*(1), 240–272.

Holbrook, J. (2001). Origin, genetic interrelationships, and stratigraphy over the continuum of fluvial channel-form bounding surfaces: an illustration from middle Cretaceous strata, southeastern Colorado. *Sedimentary Geology*, *144*(3), 179–222.

Holbrook, J., & Bhattacharya, J. (2012). *What happened to my marine reservoir? Implications of falling stage and lowstand fluvial sediment storage during ''sequence-boundary'' scour for sand starvation of coastal marine reservoirs*. Presented abstract at the American Association of Petroleum Geologists, Annual Meeting, unpaginated.

Holbrook, J., Scott, R., & Oboh-Ikuenobe, F. (2006). Base-level buffers and buttresses: a model for upstream versus downstream control on fluvial geometry and architecture within sequences. *Journal of Sedimentary Research, 76*, 162–174.

Hori, K., Saito, Y., Zhao, Q., Cheng, X., Wang, P., Sato, Y.& Li, C. (2001). Sedimentary facies and Holocene progradation rates of the Changjiang (Yangtze) delta, China. *Geomorphology, 41*, 233–248.

Hori, K., Saito, Y., Zhao, Q., & Wang, P. (2002). Architecture and evolution of the tide-dominated Changjiang (Yangtze) River delta, China. *Sedimentary Geology*, *146*(3), 249–264.

Horton, R. E. (1945). Erosional development of stream and their drainage basin, hydrological approach to quantitative morphology. *Geological Society of America Bulletin*, *56*(3), 275–370.

Hornung, J., & Aigner, T. (1999). Reservoir and aquifer characterization of fluvial architectural elements: Stubens and stein, Upper Triassic, southwest Germany. *Sedimentary Geology, 129,* 215–280.

Houbolt, J.H.C. (1968). Recent sediment in the Southern Bight of the North Sea. *Geologie en Mijnbouw, 47*, 245–273.

Hovikoski, J., Gingras, M., R s nen, M., Rebata, L. A., Guerrero, J., Ranzi, A., Melo, J., Romero, L., Nunez Del Prado, H., Jaimes, F., & Lopez, S. (2007). The nature of Miocene Amazonian epicontinental embayment: High-frequency shifts of the low-gradient coastline. *Geological Society of America Bulletin*, *119*(11–12), 1506–1520.

Hubbard, S.M., Smith, D.G., Nielsen, H., Leckie, D.A., Fustic, M., Spencer, R.J. & Bloom, L. (2011). Seismic geomorphology and sedimentology of a tidally influenced river deposit, Lower Cretaceous Athabasca oil sands, Alberta, Canada. *American Society of Petroleum Geologists Bulletin, 95,* 1123–1145.

Hughes, Z.J. (2012). Tidal channels on tidal flats and marshes. In R.A. Davis & R.W. Dalrymple (Eds.), *Principles of tidal sedimentology* (pp. 269–300). Germany: Springer Verlag.

Husein, S., & Lambiase, J. (2013). Sediment dynamics and depositional systems of the Mahakam delta, Indonesia: Ongoing delta abandonment on a tide-dominated coast. *Journal of Sedimentary Research*, *83*, 503–521.

Hutchison, C. S. (1996). *Geological evolution of South-East Asia*. Kuala Lumpur: Geological Society of Malaysia Publication.

Hutchison, C. S. (1989). *Geological evolution of South-East Asia*. Oxford, UK: Oxford University Press.

Hutchison, C.S. (2007). *Geological evolution of South-East Asia* (2nd ed.). Kuala Lumpur: Geological Society of Malaysia Publication.

Hutchison, C.S. (2009a). Tectonic evolution. In C.S Hutchison & D.N.K Tan (Eds.), *Geology of Peninsular Malaysia* (pp 309-330). Kuala Lumpur: Geological Society of Malaysia Publication & Universiti Malaya.

Hutchison, C.S. (2009b). Metamorphism. In C.S Hutchison & D.N.K Tan (Eds.), *Geology of Peninsular Malaysia* (pp 233-245). Kuala Lumpur: Geological Society of Malaysia Publication & Universiti Malaya.

Ichaso, A.A., & Dalrymple, R.W. (2006). *On the geometry of tidal channels*. American Association of Petroleum Geologists annual meeting, Houston. Search and Discovery Article #90052.

Ichaso, A. A., & Dalrymple, R. W. (2009). Tide- and wave-generated fluid mud deposits in the Tilje Formation (Jurassic), offshore Norway. *Geology*, *37*(6), 539–542.

Ielpi, A., & Ghinassi, M. (2014). Planform architecture, stratigraphic signature and morphodynamics of an exhumed Jurassic meander plain (Scalby Formation, Yorkshire, UK). *Sedimentology*, *61*(7), 1923–1960.

IHS Energy. (2004). *Basin monitor Malay Basin – Malaysia, Vietnam, Thailand, Indonesia, Cambodia, Malaysia/Thailand JDA*, August 2004.

Ingersoll, R. (1988). Tectonics of sedimentary basins. *Geological Society of America Bulletin, 100,* 1704–1719.

Ismail, M. T., Abdullah, S. A., & Rudolph, K. W. (1994). Structural and sedimentary evolution of the Malay Basin. *Abstracts of Petroleum and Geoscience Conference & Exhibition, Kuala Lumpur, Malaysia: American Association of Petroleum Geologists Bulletin, 78*, 1148.

Jablonski, B. V. J., & Dalrymple, R. W. (2016). Recognition of strong seasonality and climatic cyclicity in an ancient, fluvially dominated, tidally influenced point bar: Middle McMurray Formation, Lower Steepbank River, north-eastern Alberta, Canada. *Sedimentology*, *63*(3), 552–585.

Jackson, R.G. II. (1975). Hierarchical attributes and a unifying model of bed forms composed of cohesionless material and produced by shearing flow. *Geological Society of American Bulletin, 86,* 1523-1533

Jerolmack, D. J., & Paola, C. (2010). Shredding of environmental signals by sediment transport. *Geophysical Research Letters, 37*(19).

Jerolmack, D. J., & Swenson, J. B. (2007). Scaling relationships and evolution of distributary networks on wave-influenced deltas. *Geophysical Research Letters*, *34*(23).

Jervey, M. T. (1988). quantitative geological modeling of siliciclastic rock sequences and their seismic expression. In C.K. Wilgus, B.S. Hastings, H. Posamentier, J. Van Wagoner, C.A. Ross, & C.G. S.C. Kendall (Eds.), *Sea-level changes: An integrated approach: SEPM Special Publication, 42* (pp 47-69). Tulsa, Okla: SEPM, Society for Sedimentary Geology.

Jirin, S., Mohamed, M., & Hasan, S. S. (2013). *Transgressive-regressive cycles in the Malay Basin.* New Insights. International Petroleum Technology Conference. doi:10.2523/IPTC-16838-Abstract.

Johnson, D. W. (1932a). Rock fans of arid regions. *American Journal of Science*, *S5-23*(137), 389– 416.

Johnson, D., (1932b). Rock planes of arid regions. *Geographical Review, 22*(4), 656-665.

Johnson, D., (1932c). Miniature rock fans and pediments. *Science, 75*, 546.

Jones, C. M., & McCabe, P. J. (1980). Erosion surfaces within giant fluvial cross-beds of the Carboniferous in northern England. *Journal of Sedimentary Research*, *50*(2), 613–620.

Jordan, D.W. & Pryor, W. A. (1992). Hierarchical levels of heterogeneity in a Mississippi river meander belt and applications to reservoir systems. *American Association of Petroleum Geologists Bulletin, 76,* 1601–1624.

Kästner, K., Hoitink, A. J. F., Vermeulen, B., Geertsema, T. J., & Ningsih, N. S. (2017). Distributary channels in the fluvial to tidal transition zone. *Journal of Geophysical Research: Earth Surface*, *122*(3), 696–710.

Kiel, B. (2009). *Three-dimensionality, seismic attributes, and long profile setting of valleys in recent sequences of the Sunda Shelf, Indonesia.* (Unpublished doctoral dissertation). University of Texas at Austin. United States.

Kim, W., Paola, C., Swenson, J. B., & Voller, V. R. (2006). Shoreline response to autogenic processes of sediment storage and release in the fluvial system. *Journal of Geophysical Research: Earth Surface, 111*(F4).

Kingston, D.R., Dishroon, C.P. & Williams, P.A. (1983). Global basin classification system. *American Association of Petroleum Geologists Bulletin, 67*, 2175–2193.

Klausen, T., Ryseth, A., Helland-Hansen, W., Gawthorpe, R., & Laursen, I. (2014). Spatial and temporal changes in geometries of fluvial channel bodies from the Triassic Snadd formation of offshore Norway. *Journal of Sedimentary Research*, *84*, 567–585.

Klein, G. D. (1970). Depositional and dispersal dynamics of intertidal sand bars. *Journal of Sedimentary Research*, *40*(4), 1095–1127.

Klein, G. D. (1971). A sedimentary model for determining paleotidal range. *Bulletin of the Geological Society of America, 82,* 2585-2592.

Klein, G.D., (1998). Clastic tidalites — a partial retrospective view. In C.R. Alexander, R.A. Davis & V.J. Henry (Eds.), *Tidalites: Processes and products: SEPM Special Publication, 61 (*pp. 5-14). Tulsa, Okla: SEPM, Society for Sedimentary Geology.

Kleinhans, M. G., Ferguson, R. I., Lane, S. N., & Hardy, R. J. (2013). Splitting rivers at their seams: bifurcations and avulsion. *Earth Surface Processes and Landforms*, *38*(1), 47–61.

Klitgord, K. D., Hutchinson, D. R., & Schouten, H. (1988). U.S. Atlantic continental margin: Structural and tectonic framework. In R. E. Sheridan & J. A. Grow (Eds.), *The geology of North America, I-2, the Atlantic Continental Margin, US* (pp. 19–55). Boulder, CO: Geological Society of America.

Klitgord, K., & Schouten, H. (1986). Plate kinematics of the central Atlantic. In P. R. Vogt & B. E. Tucholke (Eds.), *The geology of North America, Vol. M, the western North Atlantic region* (pp. 351–378). Boulder, CO: Geological Society of America.

Knighton, A.D. (1984). *Fluvial forms and process*. London: Edward Arnold.

Knighton, A. D., Woodroffe, C. D., & Mills, K. (1992). The evolution of tidal creek networks, Mary river, northern Australia. *Earth Surface Processes and Landforms*, *17*(2), 167–190.

Krapesch, G., Hauer, C., & Habersack, H. (2011). Scale orientated analysis of river width changes due to extreme flood hazards. *Natural Hazards and Earth System Sciences, 11*(8), 2137–2147.

Kuecher, G.M., Woodland, B.G., & Broadhurst, F.M., (1990). Evidence of deposition from individual tides and of tidal cycles from the Francis Creek Shale (host rock to the MazonCreek Biota), Westphalian (Pennsylvanian), northeastern Illinois. *Sedimentary Geology, 68*(21), 1–221.

Kuehl, S.A., Allison, M.A., Goodbred, S.L. & Kudrass, H.R. (2005). The Ganges-Brahmaputa delta. In L. Giosan & J.P Bhattacharya (Eds.), *River deltas – Concepts, models, and examples: SEPM Special Publication, 83* (pp. 413–434). Tulsa, Okla: SEPM Society of Sedimentary Geology.

Kukulski, R., Hubbard, S., Moslow, T., & Raines, M. (2013). Basin-scale stratigraphic architecture of upstream fluvial deposits: Jurassic-Cretaceous Foredeep, Alberta Basin, Canada. *Journal of Sedimentary Research*, *83*, 704–722.

Kvale, E.P., & Archer, A.W. (1991). Characteristics of two, Pennsylvanian-age, semidiurnal tidal deposits in the Illinois Basin, U.S.A. In G.G, Smith, G.E. Reinson, B.A. Zaitlin, & R.A. Rahmani (Eds.), *Clastic tidal sedimentology: Canadian Society of Petroleum Geologists, 16* (pp 179–188). Calgary: Canadian Society of Petroleum Geologists.

Kvale, E.P., & Archer, A.W. (2007). Paleovalley fills trunk vs. tributary. *American Association of Petroleum Geologists Bulletin, 91*(6), 809–821.

Kvale, E.P., Archer, A.W., & Johnson, H.R. (1989). Daily, monthly, and yearly tidal cycles within laminated siltstone of the Mansfield Formation (Pennsylvanian) of Indiana. *Geology, 17,* 365–368.

Kvale, E.P., Archer, A.W., Mastalerz, M., Feldman, H.R., & Hester, N.C., (1997). *Guidebook to: Tidal rhythmites and their applications*. Canadian Society of Petroleum Geologists-Society of Economic Palaeontologists and Mineralogists Joint Convention.

Kvale, E. P., Cutright, J., BIlodeau, D., Archer, A., Johnson, H. R., & Pickett, B. (1995). Analysis of modern tides and implications for ancient tidalites. *Continental Shelf Research, 15*(15), 1921–1943.

Kvale, E.P., Fraser, G.S., Archer, A.W., Zawistoski, A., Kemp, N., & McGough, P. (1994). Evidence of seasonal precipitation in Pennsylvanian sediments of the Illinois Basin. *Geology, 22*(4), 331–334.

Kvale, E. P., Johnson, H. W., Sonett, C. P., Archer, A. W., & Zawistoski, A. (1999). Calculating lunar retreat rates using tidal rhythmites. *Journal of Sedimentary Research*, *69*. 1154–1168.

Labourdette, R. (2010). Quantitative seismic geomorphology applied to heterogeneous sediment distribution in a point-bar setting, example from the fluvio-estuarine McMurray Formation, Northeast Alberta, Canada. In L. J. Wood, T. T. Simo, & N. C. Rosen (Eds.), *Seismic Imaging of Depositional and Geomorphic Systems: 30th Annual GCSSEPM Foundation Bob F. Perkins Research Conference, Houston, Texas* (pp. 330-375). SEPM Society for Sedimentary Geology.

Lamb, M. P., Nittrouer, J. A., Mohrig, D., & Shaw, J. (2012). Backwater and river plume controls on scour upstream of river mouths: Implications for fluvio-deltaic morphodynamics. *Journal of Geophysical Research: Earth Surface*, *117*(F1).

Lambiase, J., Damit, A., Simmons, M., Abdoerrias, R., & Hussin, A. (2003). A depositional model and the stratigraphic development of modern and ancient tide-dominated deltas in NW Borneo. In F.H. Sidi, D. Nummedal, P. Imbert, H. Darman, & H.W. Posamentier, (Eds.), *Tropical deltas of Southeast Asia- Sedimentology, stratigraphy and petroleum Geology: SEPM Special Publication, 76* (pp. 109–124). Tulsa, Okla: SEPM Society for Sedimentary Geology.

Lane, E.W. (1957). *A study of the shape of channels formed by natural streams flowing in erodible material*. Omaha: U.S. Army Corps of Engineers, Missouri River Division.

Langford, R., & Bracken, B. (1987). Medano Creek, Colorado, a model for upper-flow-regime fluvial deposition. *Journal of Sedimentary Research*, *57*(5), 863–870.

Lasemi, Y., Jahani, D., Amin-Rasouli, H., & Lasemi, Z. (2012). Ancient carbonate tidalites. In R.A. Davis & R.W. Dalrymple (Eds.), *Principles of tidal sedimentology* (pp. 567–607). Germany: Springer Verlag.

Lazarus, E. D., Harley, M. D., Blenkinsopp, C. E., & Turner, I. L. (2019). Environmental signal shredding on sandy coastlines. *Earth Surface Dynamics*, *7*(1), 77–86.

Le Hir, P., Roberts, W., Cazaillet, O., Christie, M., Bassoullet, P., & Bacher, C. (2000). Characterization of intertidal flat hydrodynamics. *Continental Shelf Research*, *20*(12), 1433–1459.

Leeder, M.R. (1973). Fluviatile fining-upwards cycles and the magnitude of paleochannels. *Geological Magazine, 110*, 265-276.

Leeder, M. R. (1993). Tectonic controls upon drainage basin development, river channel migration and alluvial architecture: implications for hydrocarbon reservoir development and characterization. In C.P. North & D.J. Prosser (Eds.), *Characterization of fluvial and aeolian reservoirs*, *Geological Society of London, Special Publication, 73* (pp. 7-22). London, UK: Geological Society of London.

Legler, B., Johnson, H.D., Hampson, G.J., Massart, B.Y.G., Jackson, C.A.-L. & Jackson, M.D. (2013). Facies model of a fine-grained, tide-dominated delta: Lower Dir Abu Lifa Member (Eocene), Western Desert, Egypt. *Sedimentology, 60*, 1313–1356.

Legler, B., Hampson, G. J., Jackson, C. A.-L., Johnson, H. D., Massart, B. Y. G., Sarginson, M., & Ravnås, R. (2014). Facies relationships and stratigraphic architecture of distal, mixed tide- and wave-influenced deltaic deposits: Lower Sego Sandstone, Western Colorado, U.S.A. *Journal of Sedimentary Research*, *84*(8), 605–625.

Lentsch, N., Finotello, A., & Paola, C. (2018). Reduction of deltaic channel mobility by tidal action under rising relative sea level. *Geology*, *46*(7), 599–602.

Leo, C. T. A. M. (1997). Exploration in the Gulf of Thailand in deltaic reservoirs, related to the Bongkot Field. In A.J. Fraser, S.J Matthews & R.W. Murphy (Eds.), *Petroleum geology of Southeast Asia: Geological Society of London, Special Publications*, *126* (pp. 77 – 87). Bath, UK: Geological Society of London.

Leonardi, N., Canestrelli, A., Sun, T., & Fagherazzi, S. (2013). Effect of tides on mouth bar morphology and hydrodynamics. *Journal of Geophysical Research: Oceans*, *118*(9), 4169–4183.

Leopold, L.B., & Wolman, M.G. (1957). *River channel patterns: Braided, meandering, and straight*. Washington: Geological Survey Professional Paper 282-B. (original from the University of California)

Leopold, L.B., & Wolman, M.G. (1960). River meanders. *Geological Society of America Bulletin, 71*, 769-794.

Leopold, L. B., Wolman, M. G., & Miller, J. P. (1964). *Fluvial processes in geomorphology.* San Francisco: W. H. Freeman & Company.

Leuven, J. R. F. W., van Maanen, B., Lexmond, B. R., van der Hoek, B. V, Spruijt, M. J., & Kleinhans, M. G. (2018). Dimensions of fluvial-tidal meanders: Are they disproportionally large? *Geology*, *46*(10), 923–926.

Levell, B. K., Johnson, H. D., Collins, D. S., & van Cappelle, M. (2020). Deposition and preservation of fluvio-tidal shallow-marine sandstones: A re-evaluation of the Neoproterozoic Jura Quartzite (western Scotland). *Sedimentology*, *67*(1), 173–206.

Liew, K.K. (1994). Structural development at the west-central margin of the Malay Basin. *Geological Society of Malaysia Bulletin, 36*, 67–80.

Liew, K.K. (1996). Structural history of Hinge fault system of the Malay Basin. *Geological Society of Malaysia Bulletin, 39*, 33–50.

Liew, K.K. (1997). Structural analysis of the Malay Basin. *Geological Society of Malaysia Bulletin, 40,* 157–176.

Liew, W.L, Hashim.H, Tahir, R, Mokhtar. Z, Kusyairi, A., Pawanteh, N., & Hassan, M. (2011). An integrated geoscience and engineering efforts leading to increased development planning confidence. *Proceeding of the Abstracts of Geological Society of Malaysia Petroleum Geology Conference, Warta Geologi, 37*, 27.

Longhitano, S. (2011). The record of tidal cycles in mixed silicibioclastic deposits: examples from small Plio-Pleistocene peripheral basins of the microtidal central Mediterranean Sea. *Sedimentology, 58*(3), 691–719.

Longhitano, S., Mellere, D., Steel, R., & Ainsworth, R. B. (2012). Tidal depositional systems in the rock record: A review and new insights. *Sedimentary Geology*, *279*, 2–22.

Longhitano, S., Sabato, L., Tropeano, M., & Gallicchio, S., (2010). A mixed bioclastic–siliciclastic flood-tidal delta in a microtidal setting depositional architectures and hierarchical internal organization (Pliocene, southern Apennine, Italy). *Journal of Sedimentary Research, 80,* 36–53.

López-Gómez, J., Arche, A., Vargas, H., & Marzo, M. (2010). Fluvial architecture as a response to two-layer lithospheric subsidence during the Permian and Triassic in the Iberian Basin, eastern Spain. *Sedimentary Geology*, *223*(3), 320–333.

Lorenz, J.C., Heinze, J.M., Clark, J.A. & Searls, C.A. (1985). Determination of widths of meander-belt sandstone reservoirs from vertical downhole data, Mesaverde Group, Piceance Creek Basin, Colorado. *American Association of Petroleum Geologists Bulletin, 69*, 710–721.

Lunt I.A, Bridge J.S, & Tye R.S. (2004). A quantitative, three-dimensional depositional model of gravelly braided rivers. *Sedimentology, 51*, 377–414.

MacEachern, J.A., Bann, K.L., Bhattacharya, J.P., Howell, C.D. (2005a). Ichnology of deltas: Organism responses to the dynamic interplay of rivers, waves, storms and tides. In L. Giosan & J.P Bhattacharya (Eds.), *River deltas – Concepts, models, and examples: SEPM Special Publications, 83* (pp. 49–85). Tulsa, Okla: SEPM Society of Sedimentary Geology.

MacEachern, J.A., Bann, K.L., Pemberton, S.G., Gingras, M.K. (2005b). The ichnofacies paradigm: high-resolution paleoenvironmental interpretation of the rock record. In J.A. MacEachern, K.L. Bann, M.K. Gingras, & S.G. Pemberton (Eds.), *Applied Ichnology: SEPM Short Course Notes, 52* (pp. 27–64). Tulsa, Okla: SEPM, Society for Sedimentary Geology.

MacEachern, J.A. & Bann, K.L. (2008). The role of ichnology in refining shallow marine facies models. In G.J. Hampson, R.J. Steel, P.M. Burgess & R.W. Dalrymple (Eds), *Recent Advances in Models of Siliciclastic Shallow-Marine Stratigraphy: SEPM Special Publication, 90.* (pp. 73-116). Tulsa, Okla: SEPM, Society for Sedimentary Geology.

MacEachern, J.A, & Gingras, M. (2007). Recognition of brackish-water trace-fossil suites in the Cretaceous interior seaway of Alberta, Canada. In R.G. Bromley, L.A. Buatois, G. Mangano, J.F. Genise & R.N. Melchor (Eds.), *Sediment-Organism Interactions: A Multifaceted Ichnology*: *SEPM Special Publication, 89* (pp. 149–193). Tulsa, Okla: SEPM, Society for Sedimentary Geology.

MacEachern, J.A., Pemberton, S.G., Bann, K.L., Gingras, M.K. (2005c). Departures from the archetypal ichnofacies: Effective recognition of physico-chemical stresses in the rock record. In J.A. MacEachern, K.L. Bann, M.K. Gingras, & S.G. Pemberton (Eds.), *Applied Ichnology: SEPM Short Course Notes, 52* (pp. 65–93). Tulsa, Okla: SEPM, Society for Sedimentary Geology.

MacKay, D. A., & Dalrymple, R. W. (2011). Dynamic mud deposition in a tidal environment: The record of fluid-mud deposition in the Cretaceous Blue-sky formation, Alberta, Canada. *Journal of Sedimentary Research*, *81*(12), 901–920.

Madon, M. (1994). Depositional and diagenetic histories of reservoir sandstones in the Jerneh Field, central Malay Basin. *Bulletin of the Geological Society of Malaysia, 36*, 31-35.

Madon, M. (1997). The kinematics of extension and inversion in the Malay Basin, offshore Peninsular Malaysia. *Bulletin of the Geological Society of Malaysia, 41*, 127-138.

Madon, M. (1999). Basin types, tectono- stratigraphic provinces, structural styles. In PETRONAS (Eds.), *The Petroleum Geology and Resources of Malaysia* (pp 77-111). Kuala Lumpur, KL: Petronas.

Madon, M. (2011). *Transgressive-regressive cycles in the Malay Basin: the interplay of tectonics and sea level changes in a silled basin*. Petroleum Geology Conference and Exhibition, Kuala Lumpur.

Madon, M. & Watts, A.B. (1998). Gravity anomalies, subsidence history, and the tectonic evolution of the Malay and Penyu basins. *Basin Research, 10*, 375-392.

Madon, M., Abolins, P., Hoesni, J., & Ahmad, M. (1999a). Malay basin. In: PETRONAS (Eds.), *The Petroleum Geology and Resources of Malaysia,* (pp 171–217). Kuala Lumpur, KL: Petronas.

Madon, M., Jiu-Shan Yang, Abolins, P., Redzuan Abu Hassan, Azmi M. Yakzan & Saiful Bahari Zainal, (2006). Petroleum systems of the Northern Malay Basin. *Bulletin of the Geological Society of Malaysia, 49,* 125-134.

Maguregui, J., & Tyler, N. (1991). Evolution of middle Eocene tide-dominated deltaic sandstones, Launillas Field, Maracaibo Bain, western Venezuela. In A.D. Miall & N. Tyler (Eds.), *The Three-Dimensional Facies Architecture of Terrigenous Clastic Sediments and Its Implications for Hydrocarbon Discovery and Recovery: SEPM Concepts in Sedimentology and Paleontology, 3* (pp. 233–244). Tulsa, Okla: SEPM, Society for Sedimentary Geology.

Manning, A. J., Langston, W. J., & Jonas, P. J. C. (2010). A review of sediment dynamics in the Severn Estuary: Influence of flocculation. *Marine Pollution Bulletin*, *61*(1), 37–51.

Mansor, M. Y., Rahman, A. H. A., Menier, D., & Pubellier, M. (2014). Structural evolution of Malay Basin, its link to Sunda Block tectonics. *Marine and Petroleum Geology*, *58*, 736–748.

Marani, M., Belluco, E., D'Alpaos, A., Defina, A., Lanzoni, S., & Rinaldo, A. (2003). On the drainage density of tidal networks. *Water Resources Research*, *39*(2), 1–11.

Marani, M., Lanzoni, S., Zandolin, D., Seminara, G., & Rinaldo, A. (2002). Tidal meanders. *Water Resources Research, 38*, 1225.

Marani, M., Lanzoni, S., Silvestri, S., & Rinaldo, A. (2004). Tidal landforms, patterns of halophytic vegetation and the fate of the lagoon of Venice. *Journal of Marine Systems*, *51*(1), 191–210.

Martin, J., Fernandes, A.M., Pickering, J., Howes, N., Mann, S., & McNeil, K. (2018). The stratigraphically preserved signature of persistent backwater dynamics in a large paleodelta system: the Mungaroo formation, North West Shelf, Australia. *Journal of Sedimentary Research, 88*(7), 850–872.

Martinius, A. W., Jablonski, B. V. J., Fustic, M., Strobl, R., & Van den Berg, J. H. (2015). Chapter 12 - Fluvial to tidal transition zone facies in the McMurray Formation (Christina River, Alberta, Canada), with emphasis on the reflection of flow intensity in bottomset architecture. In P.J. Ashworth, J.L. Best, & D.R. Parsons (Eds.), *Fluvial-tidal sedimentology: Development in sedimentology, 68* (pp. 445–480). Amsterdam: Elsevier.

Martinius, A.W., Kaas, I., Naess, A., Helgesen, G., Kjaeref jord, J.M., Keith, D.A., (2001). Sedimentology of the heterolithic and tide-dominated Tilje Formation (Early Jurassic, Halten Terrace, offshore mid-Norway). In O.J. Martinsen & T. Dreyer (Eds.), *Sedimentary Environments Offshore Norway — Palaeozoic to Recent: Norwegian Petroleum Foundation Special Publication, 10* (pp. 103-144). Amsterdam: Elsevier.

Maselli, V., & Trincardi, F. (2013). Large-scale single incised valley from a small catchment basin on the western Adriatic margin (central Mediterranean Sea). *Global and Planetary Change*, *100*, 245–262.

Maselli, V., Trincardi, F., Alessandra, A., Ceregato, A., Rizzetto, F., & Taviani, M. (2014). Delta growth and river valleys: The influence of climate and sea level changes on the South Adriatic shelf (Mediterranean Sea). *Quaternary Science Reviews*, *99*, 146–163.

Masselink, G., & Hegge, B., (1995). Morphodynamics of meso- and macrotidal beaches: examples from central Queensland, Australia. *Marine Geology, 129*, 1–23.

Masselink, G., & Short, A.D., (1993). The effect of tide range on beach morphodynamics and morphology: a conceptual beach model. *Journal of Coastal Research, 9*, 785–800.

Masselink, G., & Hughes, M. (2003). *An introduction to coastal processes and geomorphology* (1st ed.). London, UK: Hodder Arnold.

Masselink, G., Hughes, M., & Knight, J. (2011). *An introduction to coastal processes and geomorphology* (2nd ed.). London, UK: Hodder Arnold.

Masselink, G., Cointre, L., Williams, J., Gehrels, R., & Blake, W. (2009), Tide-driven dune migration and sediment transport on an intertidal shoal in a shallow estuary in Devon, UK: *Marine Geology, 262*(1–4), 82-95.

Massey, T., Fernie, A., Ainsworth, R. B., Nanson, R., & Vakarelov, B. (2013). Detailed mapping, three-dimensional modelling and upscaling of a mixed-influence delta system, Mitchell River delta, Gulf of Carpentaria, Australia. In A.W. Martinius, J.A. Howell & T.R. Good (Eds.), *Sediment-Body Geometry and Heterogeneity: Analogue Studies for Modelling the Subsurface: Geological Society of London, Special Publications*, *387* (pp. 135–151). Bath, UK: Geological Society of London.

Mata, S., Corsetti, C., Corsetti, F., Stanley, A., & Bottjer, D. (2012). Lower Cambrian anemone burrows from the upper member of the wood canyon formation, death valley region, United States: Paleoecological and paleoenvironmental significance. *Palaios*, *27*, 595–607.

Maynard, J. R. (2006). Fluvial response to active extension: evidence from 3D seismic data from the Frio Formation (Oligo-Miocene) of the Texas Gulf of Mexico Coast, USA. *Sedimentology*, *53*(3), 515–536.

Maynard, J., Feldman, H., & Alway, R. (2010). From bars to valleys: the sedimentology and seismic geomorphology of fluvial to estuarine incised-valley fills of the Grand Rapids Formation (Lower Cretaceous), Iron River Field, Alberta, Canada. *Journal of Sedimentary Research*, *80*, 611–638.

McKenzie, D. (1978). Some remarks on the development of sedimentary basins. *Earth and Planetary Science Letters*, *40*(1), 25–32.

Melton, F. (1936). An empirical classification of flood-plain streams. *Geographical Review, 26*(4), 593-609.

Miall, A. D. (1977). A review of the braided-river depositional environment. *Earth-Science Reviews*, *13*(1), 1–62.

Miall, A.D. (1978b). Fluvial sedimentology: an historical review. In A.D. Miall (Ed.), *Fluvial sedimentology: Canadian Society of Petroleum Geologists, 5* (pp. 1-47). Calgary: Canadian Society of Petroleum Geologists.

Miall, A.D. (1978c). Lithofacies types and vertical profile models in braided river deposits: A summary. In A.D. Miall (Eds.), *Fluvial sedimentology: Canadian Society of Petroleum Geologists, 5* (pp 597-604). Calgary: Canadian Society of Petroleum Geologists.

Miall, A.D. (1985). Architectural element analysis: a new method of facies analysis applied to fluvial deposits*: Earth-Science Reviews*, *22,* 261–308.

Miall, A. D. (1991b). Sedimentology of a sequence boundary within the nonmarine Torrivio Member, Gallup Sandstone (Cretaceous), San Juan Basin, New Mexico. In A.D. Miall & N. Tyler (Eds.), *The three-dimensional facies architecture of terrigenous clastic sediments and its implications for hydrocarbon discovery and recovery: SEPM Concepts in Sedimentology and Paleontology, 3* (pp. 224–232). Tulsa, Okla: SEPM, Society for Sedimentary Geology.

Miall, A.D. (1996). *The geology of fluvial deposits*: New York, Springer-Verlag, 582.

Miall, A. D. (1988). Reservoir heterogeneities in fluvial sandstones: lessons from outcrop studies. *American Association of Petroleum Geologists Bulletin*, *72*, 682-697.

Miall, A.D. (1991a). Hierarchies of architectural units in clastic rocks, and their relationship to sedimentation rate. In A.D. Miall & N. Tyler (Eds.), *The three-dimensional facies architecture of terrigenous clastic sediments and its implications for hydrocarbon discovery and recovery: SEPM Concepts in Sedimentology and Paleontology, 3* (pp. 6–12). Tulsa, Okla: SEPM, Society for Sedimentary Geology.

Miall, A. D. (1991b). Stratigraphic sequences and their chronostratigraphic correlation. *Journal of Sedimentary Research*, *61*(4), 497–505.

Miall, A.D. (2002). Architecture and sequence stratigraphy of Pleistocene fluvial systems in the Malay Basin, based on seismic time-slice analysis. *American Association of Petroleum Geologists Bulletin*, *86*, 1201–1216.

Miall, A.D. (2006). Reconstructing the architecture and sequence stratigraphy of the preserved fluvial record as a tool for reservoir development: A reality check. *Bulletin of American Association of Petroleum Geologists*, *90*, 989–1002.

Miall, A. (2010), Alluvial deposits. In N.P James & R.W. Dalrymple (Eds.), *Facies models 4* (pp. 105 – 137). St. John's, Newfoundland: Geological Association of Canada.

Miall, A. (2014). *Fluvial depositional systems*. Switzerland: Springer.

Middleton, G.V. (1977). Introduction - progress in hydraulic interpretation of sedimentary structures. In G.V. Middleton (Eds.), *Sedimentary process: hydraulic interpretation of primary sedimentary structures: SEPM Special Publication, 12* (pp. 1-15). Tulsa, Okla: SEPM Society for Sedimentary Geology.

Miller, D. J., & Eriksson, K. (1997). Late Mississippian prodeltaic rhythmites in the Appalachian Basin: A hierarchical record of tidal and climatic periodicities. *Journal of Sedimentary Research*, *67*, 653–660.

Milli, S., D'Ambrogi, C., Bellotti, P., Calderoni, G., Maria, G., Carboni, G., & Ricci, V. (2013). The transition from wave-dominated estuary to wave-dominated delta: The Late Quaternary stratigraphic architecture of Tiber River deltaic succession (Italy). *Sedimentary Geology*, *284–285*, 159–180.

Mohd Tahir, I., Shahrul Amar, A., & Rudolph, K.W. (1994). Structural and sedimentary evolution of the Malay Basin. *Abstracts American Association of Petroleum Geologists International Conference & Exhibition, Kuala Lumpur, American Association of Petroleum Geologists Bulletin, 78*, 1148.

Mohrig, D., Heller, P.L., Paola, C., & Lyons, W.J. (2000). Interpreting avulsion process from ancient alluvial sequences: Guadalope-Matarranya system (northern Spain) and Wasatch Formation (western Colorado). *Geological Society of America Bulletin 112*, 1787-1803.

Morley, C.K., (2016). Major unconformities/termination of extension events and associated surfaces in the South China Seas: Review and implications for tectonic development. *Journal of Asian Earth Sciences, 120*, 62-86.

Morley, R.J. (1998). Palynological evidence for Tertiary plant dispersals in the Southeast Asian region in relation to plate tectonics and climate. In R. Hall & J.D. Holloway (Eds.), *Biogeography and geological evolution of SE Asia* (pp 211-234). Netherlands: Backhuys.

Morley, R. J. (2000). *Origin and evolution of tropical rainforests*. London: Wiley & Sons.

Morley, R. J. (2012). A review of the Cenozoic palaeoclimate history of Southeast Asia. Biotic evolution and environmental change in Southeast Asia. *Systematics Association Special Volume*, *82,* 79-114.

Morley, R. J, Christopher & Westaway, Rob. (2006). Subsidence in the super-deep Pattani and Malay basins of Southeast Asia: A coupled model incorporating lower-crustal flow in response to post-rift sediment loading. *Basin Research, 18*, 51 - 84.

Morley, R. J., Hasan, S. S., Morley, H. P., Jais, J. H. M., Mansor, A., Aripin, M. R., & Rohaizar, M. H. (2021). Sequence biostratigraphic framework for the Oligocene to Pliocene of Malaysia: High-frequency depositional cycles driven by polar glaciation. *Palaeogeography, Palaeoclimatology, Palaeoecology*, *561*, 110058.

Morley, R. J., Morley, H.P., & Restrepo-Pace, P. (2003). Unravelling the tectonically controlled stratigraphy of the West Natuna Basin by means of palaeo-derived mid Tertiary climate changes. *Indonesian Petroleum Association, 29th Annual Convention Proceedings, 1*, 561–584. Jakarta: Indonesian Petroleum Association.

Morley, R. J., Salvador, P., Challis, M. L., Morris, W. R., & Adyaksawan, I. R. (2007). Sequence biostratigraphic evaluation of the North Belut Field, West Natuna Basin. *Proceedings of the Indonesian Petroleum Association 31st annual convention, Jakarta*, *Indonesia* (pp. IPA-07-G-120). Jakarta: Indonesian Petroleum Association.

Morley, R. J & Shamsudin, J. (2006*).* Integrating biostratigraphy with seismic for sequence stratigraphic interpretation in the Malay Basin. *Petroleum Geology Conference and Exhibition Proceedings*, Kuala Lumpur (pp. 1-24).

Morley, R. J., Swiecicki, T. & Pham, D.T.T. (2011). A sequence stratigraphic framework for the Sunda region, based on integration of biostratigraphic, lithological and seismic data from Nam Con Son basin, Vietnam. *Proceedings of the Indonesian Petroleum Association 35th Annual Convention*, *Jakarta*, *Indonesia* (pp IPA11-G-002). Jakarta: Indonesian Petroleum Association.

Morley, R.J., Swiecicki, T., Restrepo Pace, P., (2015). Correlation across the South China Sea using VIM transgressive-regressive cycles. In: Search and Discovery Article #51109.

Mulder, T., Syvitski, J. P. M., Migeon, S., Faugères, J.-C., & Savoye, B. (2003). Marine hyperpycnal flows: initiation, behavior and related deposits. A review. *Marine and Petroleum Geology*, *20*(6), 861–882.

Muller, J. (1968). Palynology of the Pedawan and Plateau Sandstone Formations (Cretaceous-Eocene) in Sarawak, Malaysia. *Micropaleontology, 14* (l), pp. 1-37.

Mutti, E., Rosell, J., Allen, G.P., Fonnesu, F., Sgavetti, M. (1985). The Eocene Baronia tide dominated delta-shelf system in the Ager Basin. In M.D. Mila & J. Rosell (Eds.), *Excursion Guidebook, 6th European Regional Meeting* (pp. 579–600). Lleida, Spain: Institut d'Estudis Ilerdencs.

Myrick, R. M., & Leopold, L. B. (1963). *Hydraulic geometry of a small tidal estuary, Professional Paper,422(B)*. Washington, D.C: United States Government Printing Office.

Nardi, L., & Rinaldi, M. (2015). Spatio-temporal patterns of channel changes in response to a major flood event: The case of the Magra River (central-northern Italy). *Earth Surface Processes and Landforms, 40*(3), 326–339.

Ng, T.S. (1987). Trap styles of the Tenggol Arch and the southern part of the Malay Basin. *Geological Society of Malaysia Bulletin, 21*, 177–193.

Ngah, K., Madon, M., & Tjia, H. (1996). Role of pre-Tertiary fractures in formation and development of the Malay and Penyu basins. In: Hall, R. & Blundell, D.J., (Eds.), *Tectonic evolution of Southeast Asia. Geological Society of London Special Publication, 106*, (pp. 281-289). Bath, UK: Geological Society of London.

Ngah, K. (2000). Structural framework of Southeastern Malay Basin. AAPG Journal Online. Search and Discovery, Article #10009. Retrieved from http://www.searchanddiscovery.com/documents/khalid02/

Nguyen, V.L., Ta, T.K.O, & Tateishi, M. (2000). Late Holocene depositional environments and coastal evolution of the Mekong River Delta, Southern Vietnam. *Journal of Asian Earth Science, 18*, 427–439.

Nichols, G. (2009). *Sedimentology and stratigraphy*. London, UK: Blackwell Science Ltd.

Nichols, G.J., & Fisher, J.A. (2007), Processes, facies and architecture of fluvial distributary system deposits: *Sedimentary Geology*, v. 195, p. 75–90.

Nienhuis, J., Hoitink, A. J. F., & Törnqvist, T. (2018). Future change to tide-influenced deltas. *Geophysical Research Letters*, *45*, 3499–3507.

Nik Ramli. (1986). Depositional model of a Miocene barred wave-and storm-dominated shoreface and shelf, southeastern Malay Basin, offshore West Malaysia. *American Association of Petroleum Geologists Bulletin, 70*, 34-47.

Nio, S.D., & Yang, C.S. (1991). Diagnostic attributes of clastic tidal deposits: a review. In D.G. Smith, G.E. Reinson, B.A. Zaitlin, & R.A. Rahmani (Eds.), *Clastic Tidal Sedimentology: Canadian Society of Petroleum Geologists, 16* (pp. 3–28). Calgary: Canadian Society of Petroleum Geologists.

Nio, S.D., & Yang, C.S. (1989). *Recognition of tidally-influenced facies and environments*. International Geoservices.

Nittrouer, J.A. (2013). Backwater hydrodynamics and sediment transport in the lowermost Mississippi river delta: implications for the development of fluvial-deltaic landforms in a large lowland river. In G.J. Young, G.M.E. Perillo, H. Aksoy, J. Bogen, A. Gelfan, G. Mahé, P. Marsh & H.H.G Savenije (Eds.), *Deltas: landforms, ecosystems, and human activities (pp. 48–61).* Gothenburg, Sweden: International Association of Hydrological Sciences Publication.

Nittrouer, J. A., Shaw, J., Lamb, M. P., & Mohrig, D. (2012). Spatial and temporal trends for water-flow velocity and bed-material sediment transport in the lower Mississippi River. *Geological Soceity American Bulletin*, *124*(3–4), 400–414.

Nordfjord, S., Goff, J. A., Austin Jr., J. A., & Gulick, S. P. S. (2006). Seismic Facies of Incised-Valley Fills, New Jersey Continental Shelf: Implications for Erosion and Preservation Processes Acting During Latest Pleistocene–Holocene Transgression. *Journal of Sedimentary Research*, *76*(12), 1284–1303.

Novakowski, K. I., Torres, R., Gardner, L. R., & Voulgaris, G. (2004). Geomorphic analysis of tidal creek networks. *Water Resources Research*, *40*(5). W05401.

O'Leary, H. & Hill, G.S. (1989). Tertiary basin development in the Southern Central Plains, Thailand. *International Symposium on Intermontane Basins, Geology and Resources* (pp 254–264). Chiang Mai, Thailand: Chiang Mai University.

Octavian, C., & Zecchin, M. (2012). High-resolution sequence stratigraphy of clastic systems: Autocyclic and allocyclic controls, and implications to the concept of sequence. *Rendiconti Online Della Società Geologica Italiana*, *21*, 891–892.

Omosanya, K., & Harishidayat, D. (2019). Seismic geomorphology of Cenozoic slope deposits and deltaic clinoforms in the Great South Basin (GSB) offshore New Zealand. *Geo-Marine Letters*, *39*. 77–99.

Oomkens, E. (1974). Lithofacies relations in the Late Quartenary Niger Delta complex. *Sedimentology,21*, 195-222.

Oomkens, E., & Terwindt, J.H.J. (1960). Inshore estuarine sediments in the Haringvliet (Netherlands). *Geologie en Mijnbouw. 39*, 701-710.

Ottevanger, W. & Blanckaert, K. & Uijttewaal, W. (2012). Processes governing the flow redistribution in sharp river bends. *Geomorphology*, *163-164,* 45-55.

Paola, C., & Mohrig, D. (1996). Palaeohydraulics revisited: palaeoslope estimation in coarse-grained braided rivers. *Basin Research*, *8*(3), 243–254.

Parker, G., Diplas, P., & Akiyama, J. (1983). Meander Bends of High Amplitude. *Journal of Hydraulic Engineering, 109,* 1323-1337.

Pauget, F., & Lacaze, S. (2017). *Method to generate a watertight geological model directly from a seismic volume*. 79th EAGE Conference and Exhibition 2017, Paris, France.

Paumard, V., Bourget, J., Payenberg, T., Ainsworth, R. B., George, A. D., Lang, S., & Peyrot, D. (2018). Controls on shelf-margin architecture and sediment partitioning during a syn-rift to post-rift transition: Insights from the Barrow Group (Northern Carnarvon Basin, North West Shelf, Australia). *Earth-Science Reviews*, *177*, 643–677.

Payenberg, T.H.D., Willis, B.J., Bracken, B., Posamentier, H.W., Pyrcz, M.J., Pusca, V., & Sullivan, M.D. (2011). Revisiting the subsurface classification of fluvial sandbodies. *American Association of Petroleum Geologists, Annual Convention and Exhibition, Houston, Texas.* Search and Discovery Article #90124.

Payenberg, T.H.D., & Lang, S.C. (2003). Reservoir geometry of fluvial distributary channels—implications for Northwest Shelf, Australia, Deltaic Successions. *The APPEA Journal*, *43*(1), 325.

Pemberton, S.G., & Wightman, D.M. (1992). Ichnological characteristics of brackish water deposits. In S. G. Pemberton (Ed.), *Applications of ichnology to petroleum exploration: a core workshop: SEPM Special Publication, 17*(pp 141-167). Tulsa, Okla: SEPM Society for Sedimentary Geology.

Pemberton, S.G., MacEachern, J.A. & Frey, R.W. (1992a). Trace fossil facies models: environmental and allostratigraphic significance. In R.G. Walker & N.P. James (Eds.), *Facies models: response to sea level change* (pp. 47–72). St. John's, Newfoundland: Geological Association of Canada.

Pemberton, G., Spila, M., Pulham, A. J., Saunders, T., MacEachern, J., Robbins, D., & Sinclair, I. (2001). Ichnology and sedimentology of shallow to marginal marine systems: Ben Nevis & Avalon Reservoirs, Jeanne d'Arc Basin. *Geological Association of Canada, Short Course Notes*, *15*, 343–349.

Pemberton, S.G., Van Wagoner, J.C. & Wach, G.D. (1992b). Ichnofacies of a wave-dominated shoreline. In S.G. Pemberton (Eds.), *Applications of ichnology to petroleum exploration: a core workshop: SEPM Special Publication, 17* (pp 339-382). Tulsa, Okla: SEPM Society for Sedimentary Geology.

Perillo, G. M. E. (2019). Chapter 6 - Geomorphology of tidal courses and depressions. In G. M. E. Perillo, E. Wolanski, D. R. Cahoon, & C. S. Hopkinson (2nd ed.), *Coastal wetlands: An integrated ecosystem approach* (pp. 221-261). Elsevier.

Parker, G., Diplas, P., & Akiyama, J. (1984). Meander bends of high amplitude. *Journal of Hydraulic Engineering*, *109*(10), 1323–1337.

Perlmutter, M. A., Radovich, B. J., Matthews, M. D., & Kendall, C. G. S. C. (1998). The impact of high-frequency sedimentation cycles on stratigraphic interpretation. In F. M. Gradstein, K. O. Sandvik, & N. J. Milton (Eds.), *Sequence stratigraphy–Concepts and applications: Special publication, 8* (pp 141–170). Norway: Norwegian Petroleum Society.

Perron, J. (2017). Climate and the pace of erosional landscape evolution. *Annual Review of Earth and Planetary Sciences*, *45*, 561-591.

Pestrong, R. (1965). The development of drainage patterns in tidal marshes. *Stanford University Publications in Earth Science, 10*, 1-87.

Peterson, C., Scheidegger, K., Komar, P., & Niem, W. (1984). Sediment composition and hydrography in six high-gradient estuaries of the northwestern United States. *Journal of Sedimentary Research*, *54*(1), 86–97.

PETRONAS. (2007). *Chronostratigraphic chart of the Cenozoic and Mesozoic Basins of Malaysia*. Kuala Lumpur: Petronas.

PETRONAS, (1999). *The Petroleum Geology and Resources of Malaysia. Petronas, Kuala Lumpur, Malaysia*. Kuala Lumpur: Petronas.

Phillips, T. L., Noble, R. A., & Sinartio, F. F. (1991). Origin of hydrocarbons, Kangean Block, Northern Platform, Offshore N.E. Java Sea. *Proceedings of the Indonesia*

Petroleum Association 20th Annual Convention, *Jakarta*, *Indonesia* (pp 637-661). Jakarta: Indonesian Petroleum Association.

Piégay, H & Schumm, S.A. (2003). System approaches in fluvial geomorphology. In G.M. Kondolf & H. Piégay (Eds.), *Tools in fluvial geomorphology (2nd ed)* (pp 79-102). Wiley-Blackwell.

Piégay, H., Darby, S. E., Mosselman, E., & Surian, N. (2005). A review of techniques available for delimiting the erodible river corridor: A sustainable approach to managing bank erosion. *River Research and Applications, 21*(7), 773–789.

Picard M. D. & High L. R. (1973). *Sedimentary structures of ephemeral streams*: *developments in sedimentology, 17.* Amsterdam: Elsevier Scientific Publishing Company.

Plink-Bjorklund, P. (2005). Stacked fluvial and tide-dominated estuarine deposits in high-frequency (fourth-order) sequences of the Eocene Central Basin, Spitsbergen. *Sedimentology*, *52*, 391–428.

Plink-Björklund, P. (2012). Effects of tides on deltaic deposition: Causes and responses. *Sedimentary Geology*, *279*, 107–133.

Plink-Bjorklund, Piret & Steel, Ronald. (2006). Deltas on falling-stage and lowstand shelf margins, Eocene Central Basin of Spitsbergen. In L. Giosan & J.P Bhattacharya (Eds.), *River deltas – Concepts, models, and examples: SEPM Special Publications, 83* (pp. 179–206). Tulsa, Okla: SEPM Society of Sedimentary Geology.

Posamentier, H. W. (2001). Lowstand alluvial bypass systems: incised vs. unincised. *American Association of Petroleum Geologists Bulletin*, *85*(10), 1771–1793.

Posamentier, H. W. (2002). Ancient shelf ridges—a potentially significant component of the transgressive systems tract: case study from offshore Northwest Java. *American Association of Petroleum Geologists Bulletin*, *86*(1), 75–106.

Posamentier, H. W. (2004). Seismic geomorphology: imaging elements of depositional systems from shelf to deep basin using 3d seismic data: implications for exploration and development. *Geological Society of London, 29*(1), 11– 24.

Posamentier, H. W. (2005). Application of 3D seismic visualization techniques for seismic stratigraphy, seismic geomorphology and depositional systems analysis: Examples from fluvial to deep-marine depositional environments. In A.G. Doré & B.A. Vining (Eds.), *Petroleum geology: North-West Europe and global perspectives. Proceedings of the 6th Petroleum Geology Conference*, *London* (pp. 1565–1576). Geological Society of London.

Posamentier, H. W. (2010). Integrated seismic stratigraphy and seismic geomorphology: workflows and techniques. In L. J. Wood, T. T. Simo, & N. C. Rosen (Eds.), *Seismic imaging of depositional and geomorphic systems*, 30.

Posamentier, H.W. & Allen, G.P. (1999*). Siliciclastic sequence stratigraphy—concepts and applications: Concepts in Sedimentology and Paleontology, Special Publication, 7*. Tulsa, Okla: SEPM Society of Sedimentary Geology.

Posamentier, H.W., & Kolla, V. (2003). Seismic geomorphology and stratigraphy of depositional elements in deep-water settings. *Journal of Sedimentary Research, 73*(3), 367-388.

Posamentier, H.W., & Vail, P.R. (1988). Eustatic controls on clastic deposition II– sequence and systems tracts models. In C.K. Wilgus, B.S. Hastings, H.W. Posamentier, J.C. Van Wagoner, C.A. Ross & C.G.St.C Kendall (Eds.), *Sea-level research: an integrated approach: SEPM Special Publication, 42* (pp. 125–154). Tulsa, Okla: SEPM Society of Sedimentary Geology.

Posamentier, H.W., Allen, G., James, D.P., & Tesson, M. (1992). Forced regressions in a sequence stratigraphic framework: concepts, examples, and exploration significance. *American Association of Petroleum Geologists Bulletin*, *76*, 1687-1709.

Posamentier, H.W, Davies, R., Cartwright, J., & Wood, L. (2007). Seismic geomorphology - An overview. In R.J. Davies, H.W. Posamentier, L.J. Wood, & J.A. Cartwright (Eds.), *Seismic geomorphology: applications to hydrocarbon exploration and production: The Geological Society of London Special publication, 277* (pp. 1–14). Bath, UK: Geological Society of London.

Posamentier, H. W., Jervey, M. T., & Vail, P. R. (1988). Eustatic controls on clastic deposition: conceptual framework. In C.K. Wilgus, B.S. Hastings, H.W. Posamentier, J.C. Van Wagoner, C.A. Ross & C.G.St.C Kendall (Eds.), *Sea-level research: an integrated approach: SEPM Special Publication, 42* (pp. 109–124). Tulsa, Okla: SEPM Society of Sedimentary Geology.

Postma, H. (1982). Hydrography of the Wadden Sea: movements and properties of water and particulate matter, final report on 'Hydrography' of the Wadden Sea Working Group. In W.J. Wolff (Eds.), *Ecology of the Wadden Sea* (pp. 2/1-2/75). Rotterdam: Balkema-CRC Press.

Potter, P. E. (1967). Sand bodies and sedimentary environments: a review. *American Association of Petroleum Geology,51*, 337–365.

Powell, J.W. (1875). *Exploration of the Colorado River of the West and its tributaries*. Washington, D.C: Government Printing Office.

Pratt, B. R. (1998). Syneresis cracks: subaqueous shrinkage in argillaceous sediments caused by earthquake-induced dewatering. *Sedimentary Geology*, *117*(1), 1–10.

Pritchard, D. W. (1960). *Lectures on estuarine oceanography*. In B. Kinsman (Eds.), Kinsman notes (unpublished). Baltimore: John Hopkins University.

Pritchard, D. W. (1989). Estuarine classification — A Help or a Hindrance. In B.J. Neilson, A. Kuo & J. Brubaker (Eds.), *Estuarine circulation.* Contemporary Issues in Science and Society. Humana Press.

Pubellier, M., & Morley, C. K. (2014). The basins of Sundaland (SE Asia): Evolution and boundary conditions. *Marine and Petroleum Geology*, *58*(B), 555–578.

Pye, K., & French, P. (1993). *Erosion and accretion processes on British Salt Marshes. Volume 1: Introduction: saltmarsh processes and morphology*. Cambridge:

Cambridge Environmental Research Consultants.

Qui, Y., Xue, P. & Xiao, J. (1987). Fluvial sandstone bodies as hydrocarbon reservoirs in lake basins. In F. G. Ethridge, R. M. Flores, & M. D. Harvey (Eds.), *Recent Developments in fluvial sedimentology: SEPM, Special publication, 39,* (pp. 329–342). Tulsa, Okla: SEPM Society for Sedimentary Geology.

Raaf, J.F.M. de, Boersma, J.R. & Van Gelder, A. (1977). Wave-generated structures and sequences from a shallow marine succession, Lower Carboniferous, County Cork, Ireland. *Sedimentology, 24*, 451–483.

Rapi, M., Nor, A. & Ghosh, D. (2019). Fluvial channel characterization. In D. Ghosh (Eds.), *Geophysical applications in Malaysian Basins* (pp. 69-90). Kuala Lumpur: Petroleum Nasional Berhad and European Association of Geoscientists and Engineers.

Razak, D., (2001). *Brunei Bay, Northwest Borneo: depositional system*. (Unpublished doctoral dissertation). University of Aberdeen. United Kingdom.

Reading, H.G. & Collinson, J.D., (1996), Clastic coasts. In H.G. Reading (Eds.), *Sedimentary environments. - Processes, facies and stratigraphy* (pp 154-231). Cornwall: Wiley-Blackwell.

Rees, A. J., Lucas, P. M., McCants, C. Y., & Rae, S. F. (2008, Dec). *An integrated sedimentological approach to the characterisation of an incised valley system: example from the Miocene of the Malay Basin.* Paper presented at the International Petroleum Technology Conference, Kuala Lumpur, Malaysia.

Reijenstein, H.M., Posamentier, H.W., & Bhattacharya, J.P. (2011). Seismic geomorphology and high-resolution seismic stratigraphy of inner-shelf fluvial, estuarine, deltaic, and marine sequences, Gulf of Thailand. *American Association of Petroleum Geologists Bulletin, 95*, 1959–1990.

Reineck, H. E. (1967). Layered sediments of tidal flats, beaches and shelf bottom of the North Sea. In G.H. Lauff (Eds.), *Estuaries, American Association for the advancement of science publication: American Association for the Advancement of Science, 83* (pp. 191-206). Washington, D.C: American Association for the Advancement of Science.

Reineck, H. E. & Singh, I.B. (1973). *Depositional sedimentary environments; with reference to terrigenous clastics*. Berlin: Springer-Verlag.

Reineck, H. E. & Singh, I.B. (1980). *Depositional sedimentary environments; with reference to terrigenous clastics* (2nd ed). Berlin: Springer-Verlag.

Reineck, H. E. & Wunderlich, F. (1968). Classification and origin of flaser and lenticular bedding. *Sedimentology, 11*(1-2), 99–104.

Reynolds, A.D. (1999). Dimensions of paralic sandstone bodies. *American Association of Petroleum Geologists Bulletin, 83*(2), 211–229.

Reynolds, A.D. (2016). Paralic reservoirs. In G.J. Hampson, A.D. Reynolds, B. Kostic & M.R. Wells (Eds.), *Sedimentology of paralic reservoirs: recent Advances: Special Publications, 444* (pp 7-34). Geological Society of London.

Rigo de Rhigi, L., Baranowski, J., Chaikiturajai, C., Nelson, G., Wechsler, D. & Mattingly, G. (2003). Block B8/32, Gulf of Thailand petroleum system and implementation of technology in field development. *Southeast Asia Petroleum Exploration Society Bimonthly Newsletter, 6*, 46-55. Seapex Press.

Rinaldi, M., Gurnell, A., González del Tánago, M., Bussettini, M., & Hendriks, D. (2015). Classification of river morphology and hydrology to support management and restoration. *Aquatic Sciences*, *78*. 17–33.

Rinaldo, A., Belluco, E., D'Alpaos, A., Feola, A., Lanzoni, S., & Marani, M. (2004). Tidal networks: form and function. In S. Fagherazzi, M. Marani & L.K. Blum (Eds.), *The ecogeomorphology of tidal marshes*, (pp 75–91). Washington, D.C: American Geophysicist Union.

Robinson, A.H.W. (1960). Ebb-flood channel systems in sandy bays and estuaries. *Geography, 45*, 183–199.

Roberts, H. H., & Sydow, J. (2003). Late Quaternary stratigraphy and sedimentology of the offshore Mahakam Delta, East Kalimantan (Indonesia). In F.H. Sidi, D. Nummedal, P. Imbert, H. Darman & H.W. Posamentier (Eds.), *Tropical deltas of Southeast Asia- Sedimentology, stratigraphy and petroleum geology: SEPM Special Publication, 76* (pp. 125–145). Tulsa, Okla: SEPM Society for Sedimentary Geology.

Ross, W. C., Watts, D. E., & May, J. A. (1995). Insights from strati- graphic modeling: Mud-limited versus sand-limited depositional systems. *American Association of Petroleum Geologists Bulletin, 79*(2), 231–258.

Rowland, J. C., Lepper, K., Dietrich, W. E., Wilson, C. J., & Sheldon, R. (2005). Tie channel sedimentation rates, oxbow formation age and channel migration rate from optically stimulated luminescence (OSL) analysis of floodplain deposits. *Earth Surface Processes and Landforms*, *30*(9), 1161–1179.

Salahuddin, H. & Lambiase, J. J. (2013). Sediment dynamics and depositional systems of the Mahakam Delta, Indonesia: Ongoing delta abandonment on a tide-dominated coast. *Journal of Sedimentary Research, 83*(7), 503–521.

Sassi, M. G., Hoitink, A. J. F., de Brye, B., & Deleersnijder, E. (2012). Downstream hydraulic geometry of a tidally influenced river delta. *Journal of Geophysical Research: Earth Surface*, *117*(F4).

Savenije, H. H. G. (2012). *Salinity and tides in alluvial estuaries* (2nd Eds.).

Schumm, S.A. (1960). The effect of sediment type on the shape and stratification of some modern fluvial deposits. *American Journal of Science, 258*(3)*,* 177–184.

Schumm, S.A. (1963). Sinuosity of alluvial rivers on the great plains. *Geological Society of America Bulletin, 74*(9)*,* 1089–1100.

Schumm, S.A. (1969). River metamorphosis. *Journal of the Hydraulics Division, 95,* 255-274.

Schumm, S.A., & Khan, H.R. (1972). Experimental study of channel patterns. *Geological*

Society of American, Bulletin, 83(6)*,* 1755–1770.

Schumm, S.A. (1977), *The Fluvial System*. New York: Wiley.

Schumm, S.A. (1981). *Experimental fluvial geomorphology*. New York, Wiley & Sons.

Schumm, S.A (1993). River response to base-level change. implications for sequence stratigraphy. *The Journal of Geology, 101*(2), 279-294.

Schumm, S. A. (2005). *River variability and complexity*. Cambridge: Cambridge University Press.

Schumm, S.A. & Brackenridge, S.A. (1987). River response. In W.F. Ruddiman & H.E. Wright, Jr (Eds.), *North America and Adjacent Oceans during the last deglaciation* (pp. 221-240*).* Boulder: Geological Society of America.

Schumm, S.A. & Ethridge, F.G. (1994). Origin, evolution, and morphology of fluvial valleys. In R.W. Dalrymple, R. Boyd & B.A. Zaitlin (Eds.), *Incised-valley systems: Origin and sedimentary sequences: SEPM Special Publication, 51* (pp. 10-27). Tulsa, Okla: SEPM Society for Sedimentary Geology.

Schumm, S.A., Harvey, M.D. & Watson, C.C. (1984). *Incised channels: morphology, dynamics and control*. Chelsea: Water Resources Publication.

Seely, M., Henderson, J., Heyns P, Jacobson, P., Nakale, T., Nantanga, K., & Schachtschneider, K. (2003). Ephemeral and endoreic river systems: relevance and management challenges. In A. Truton, P. Ashton & E. Cloete (Eds.), *Transboundary rivers, sovereignty and development*: *hydropolitical drivers in the Okavango River basin* (pp. 187–212). African Water Issues Research Unit and Green Cross International, Pretoria and Geneva

Seminara, G. (2006). Meanders. *Journal of Fluid Mechanics*, *554*, 271–297.

Shanley, K. W., & McCabe, P. J. (1994). Perspectives on the sequence stratigraphy of continental stratal. *American Association of Petroleum Geologists Bulletin*, *78*(4), 544–568.

Shamsudin, J. & Morley, R.J. (2006). Integrating Biostratigraphy with Seismic for Sequence Stratigraphic Interpretation in The Malay Basin. *Petroleum Geoscience Conferences and Exhibition 2006, 101-102*. European Association of Geoscientists an Engineers.

Sheriff, R.E., & Geldart, L.P. (1983). *Exploration seismology: History, theory and data acquisition*. New York, NY: Cambridge University Press.

Shoup, R., Morley, R., Swiecicki, T., & Clark, S. (2012). *Tectono-stratigraphic framework and tertiary paleogeography of Southeast Asia: Gulf of Thailand to South Vietnam Shelf**. Presented at AAPG International Conference and Exhibition, Singapore, Article #30246.

Simons, D. B., & Richardson, E. V. (1961). Forms of bed roughness in alluvial channels. *Journal of the Hydraulics Division, New York, 87* (3), 87-105.

Slingerland, R.L. & Smith, N.D. (2004). River avulsions and their deposits. *Annual Reviews of Earth and Planetary Science, 32*, 257–285.

Smith, D.G., Hubbard, S.M., Leckie, D.A., & Fustic, M., (2009). Counter point bar deposits: lithofacies and reservoir significance in the meandering modern Peace River and ancient McMurray Formation, Alberta, Canada. *Sedimentology, 56*, 1655–1669.

Smith, D.G., Hubbard, S.M., Lavigne, J.R., Leckie, D.A., & Fustic, M. (2011). Stratigraphy of counter point bars and eddy accretion deposits in low energy meander belts of the Peace-Athabasca Delta, northeast Alberta, Canada. In S.K. Davidson, S. Leleu & C.P. North (Eds.), *From river to rock record: the preservation of fluvial sediments and their subsequent interpretation: SEPM Special Publication, 97* (pp. 143–152). Tulsa, Okla: SEPM Society for Sedimentary Geology.

Smith, D.G., Reinson, G.F., Zaitlin, B.A., & Rahmani, R.A. (1991). *Clastic tidal sedimentology: Canadian Society of Petroleum Geologists, 16*. Calgary: Canadian Society of Petroleum Geologists.

Solari, L., Seminara, G., Lanzoni, S., Marani, M., Rinaldo, A. (2002). Sand bars in tidal channels: Part 2. Tidal meanders. *Journal of Fluid Mechanics 451,* 203-238.

Sprague, A.R., Patterson, P.E., Hill, R.E., Jones, C.R., Campion, K.M., Van Wagoner, J.C., Sullivan, M.D., Larue, D.K., Feldman, H.R., Demko, T.M., Wellner, R.W., & Geslin, J.K. (2002). *The physical stratigraphy of fluvial strata: A hierarchical approach to the analysis of genetically related stratigraphic elements for improved reservoir prediction*. Presented abstracts at the American Association of Petroleum Geologists Annual Meeting (Article #90007). Houston.

Stark, C.P. (1991). An invasion percolation model of drainage network evolution. *Nature, 352,* 423–425.

Steel, R.J., Plink-Bjorklund, P., & Aschoff, J., (2012). Tidal deposits of the Campanian Western Interior Seaway, Wyoming, Utah and Colorado, USA. In R.A. Davis & R.W. Dalrymple (Eds.), *Principles of Tidal Sedimentology* (pp 437-472). Germany: Springer Verlag.

Steers, J.A. (1969). *The coastline of England and Wales* (2nd ed.). Cambridge: Cambridge University Press.

Straub, K., Duller, R., Foreman, B., & Hajek, E. (2020). Buffered, incomplete, and shredded: the challenges of reading an imperfect stratigraphic record. *Journal of Geophysical Research: Earth Surface*, *125*(3), article# e2019JF005079.

Stuart, J.Y., Mountney, N.P., McCaffrey, W.D., Lang, S.C., & Collinson, J.D. (2014). Prediction of channel connectivity and fluvial style in the flood-basin successions of the Upper Permian Rangal Coal Measures (Queensland). *American Association of Petroleum Geologists Bulletin. 98,* 191–212.

Sulaiman, Z.A., Viparelli, E., Torres, R., Yankovsky, A., & Grego, J. (2021). The influence of tides on coastal plain channel geomorphology: Altamaha River, Georgia, USA. *Journal of Geophysical Research: Earth Surface, 126*(7), e2020JF005839.

Summerfield, M.A. (1985). Plate tectonics and landscape development on the African continent. In M. Morisawa & J. Hack (Eds.), *Tectonic geomorphology* (pp 27–51). Boston: Allen and Unwin.

Sun, X., Li, X., Luo, Y., & Chen, X. (2000). The vegetation and climate at the last glaciation on the emerged continental shelf of the South China Sea. *Palaeogeography, Palaeoclimatology, Palaeoecology*, *160*(3), 301–316.

Surian, N., Righini, M., Lucía, A., Nardi, L., Amponsah, W., Benvenuti, M., Borga, M., Cavalli, M., Comiti, F., Marchi, L., Rinaldi, M., & Viero, A. (2016). Channel response to extreme floods: Insights on controlling factors from six mountain rivers in northern Apennines, Italy. *Geomorphology, 272,* 78–91.

Swan, A., Hartley, A.J, Owen, A., & Howell, J. (2018). Reconstruction of a sandy point-bar deposit: implications for fluvial facies analysis. In M. Ghinassi, L. Colombera, N.P. Mountney, A.J.H. Reesink & M. Bateman (Eds.), *Fluvial meanders and their sedimentary products in the rock record* (pp 445-474). Oxford, UK: Wiley & Sons.

Ta, T. K. O., Nguyen, V. L., Tateishi, M., Kobayashi, I., Tanabe, S., & Saito, Y. (2002). Holocene delta evolution and sediment discharge of the Mekong River, southern Vietnam. *Quaternary Science Reviews*, *21*(16), 1807–1819.

Talling, P.J. (1998). How and where do incised valleys form if sea level remains above the shelf edge?. *Geology, 26,* 87–90.

Tan, D.N.K. (2009). Malay and Penyu basins. In C.S Hutchison & D.N.K Tan (Eds.), *Geology of Peninsular Malaysia* (pp 175-196). Kuala Lumpur: Geological Society of Malaysia Publication & Universiti Malaya.

Tanabe, S., Ta, T.K.O., Nguyen, V.L., Tateishi, M., Kobayashi, I. & Saito, Y. (2003). Delta evolution model inferred from the Holocene Mekong Delta, southern Vietnam. In F.H. Sidi, D. Nummedal, P. Imbert, H. Darman & H.W. Posamentier (Eds.), *Tropical deltas of Southeast Asia- Sedimentology, stratigraphy and petroleum geology: SEPM Special Publication, 76* (pp 175–188). Tulsa, Okla: SEPM Society for Sedimentary Geology.

Tapponnier, P., Peltzer, G., Le Dain, A. Y., Armijo, R., & Cobbold, P. (1982). Propagating extrusion tectonics in Asia: New insights from simple experiments with plasticine. *Geology*, *10*(12), 611–616.

Tessier, B. (2012). Stratigraphy of tide-dominated estuaries. In In R.A. Davis & R.W. Dalrymple (Eds.), *Principles of tidal sedimentology* (pp. 109–128). Germany: Springer Verlag.

Tessier, B., (1998). Tidal cycles, annual versus semi-lunar records. In C.R. Alexander, R.A. Davis & V.J. Henry (Eds.), *Tidalites: Processes and products: SEPM Special Publication, 61 (*pp 69-74). Tulsa, Okla: SEPM, Society for Sedimentary Geology.

Thomas, R. G., Smith, D. G., Wood, J. M., Visser, J., Calverley-Range, E. A., & Koster, E. H. (1987). Inclined heterolithic stratification—Terminology, description, interpretation and significance. *Sedimentary Geology*, *53*(1), 123–179.

Tjia, H.D. (1994). Inversion tectonics in the Malay Basin: evidence and timing of events.

Bulletin of the Geological Society of Malaysia, 36, 119-126.

Tjia, H.D. (1999). Pre-Tertiary hydrocarbon potential. In PETRONAS (Eds.), *The Petroleum Geology and Resources of Malaysia,* (pp 605–635). Kuala Lumpur, KL: Petroleum Nasional Berhad.

Tjia, H.D. & Mohd Idrus Ismail. (1994). Tectonic implications of well-bore breakouts in Malaysian basins. *Bulletin of the Geological Society of Malaysia, 36*, 175-186

Tjia, H.D. & Liew, K.K. (1996). Changes in tectonic stress field in northern Sunda Shelf basins. In: Hall, R. & Blundell, D.J., (Eds.), *Tectonic Evolution of Southeast Asia. Geological Society of London Special Publication, 106* (pp. 291-306). Bath, UK: Geological Society of London.

Tjia, H.D. (1998). Origin and tectonic development of the Malay, Penyu, and West Natuna basins. *Geological Society of Malaysia Bulletin, 42*, 147–160.

Tjia, H.D. (1999b). Geological setting of Peninsular Malaysia. In PETRONAS (Eds.), *The petroleum geology and resources of Malaysia,* (pp 139–169). Kuala Lumpur, KL: Petroleum Nasional Berhad.

Törnqvist, T. E. & Bridge, J. S. (2002). Spatial variation of overbank aggradation rate and its influence on avulsion frequency. *Sedimentology, 49,* 891–905.

Torres, R. (2017). Channel geomorphology along the fluvial-tidal transition, Santee River, USA. *Geological Society of America Bulletin, 129*(11–12), 1681–1691.

Trendell, A.M., Atchley, S.C., & Nordt, L.C. (2013a). Facies analysis of probable large-fluvial-fan depositional system. The Upper Triassic Chinle Formation at Petrified Forest National Park, Arizona, U.S.A. *Journal of Sedimentary Research, 83*, 873–895,

Upton, D.R. (1999). *A regional appetite fission track study of Thailand: implications for thermal history and denudation*. (Unpublished doctoral dissertation), University College, University of London. United Kingdom.

Vakarelov, B., & Ainsworth, R. B. (2013). A hierarchical approach to architectural classification in marginal-marine systems: Bridging the gap between sedimentology and sequence stratigraphy. *American Association of Petroleum Geologists Bulletin, 97*, 1121–1161.

van Cappelle, M., Stukins, S., Hampson, G., & Johnson, H. (2016). Fluvial to tidal transition in proximal, mixed tide-influenced and wave-influenced deltaic deposits: Cretaceous lower Sego Sandstone, Utah, USA. *Sedimentology*, *63*(3), 1333-1361.

van der Wegen, M., Wang, Z. B., Savenije, H. H. G., & Roelvink, J. A. (2008). Long-term morphodynamic evolution and energy dissipation in a coastal plain, tidal embayment. *Journal of Geophysical Research: Earth Surface*, *113*(F3).

van den Berg, J. H., Boersma, J. R., & Gelder, A. (2007). Diagnostic sedimentary structures of the fluvial-tidal transition zone - Evidence from deposits of the Rhine and Meuse. *Geologie en Mijnbouw*, *86*, 253–272.

van de Lageweg, W. I., van Dijk, W. M., Baar, A. W., Rutten, J., & Kleinhans, M. G. (2014). Bank pull or bar push: What drives scroll-bar formation in meandering rivers?, *Geology*, *42*(4), 319–322.

van Straaten, L.M.J.U. (1954). Composition and structure of recent marine sediments in the Netherlands. *Leidse Geologische Mededelingen, 19,* 1–108.

van Veen, J., van der Spek A. J. F., M. J. F. Stive, & T. Zitman. (2005). Ebb and flood channel systems in the Netherlands tidal waters. (J. van Veen). *Journal of Coastal Research, 21*(6), 1107-1120. (Original work published 1950).

van Wagoner, J. C. (1995). Sequence stratigraphy and marine to nonmarine facies architecture of foreland basin strata, Book Cliffs, Utah, U.S.A. In J.C. Van Wagoner & G. T. Bertram (Eds.). S*equence stratigraphy of foreland basin deposits: outcrop and subsurface examples from the Cretaceous of North America: American Association of Petroleum Geologists, 64* (pp 137-223). Tulsa, Okla: American Association of Petroleum Geologists.

van Wagoner, J.C., Mitchum, R.M., Campion, K.M., & Rahmanian, V.D. (1990). *Siliciclastic sequence stratigraphy in well logs, cores, and outcrops*: *concepts for high-resolution correlation of time and facies*: *AAPG Methods in Exploration Series, 7*. Tulsa, Okla: American Association of Petroleum Geologists.

van Yperen, A. E., Holbrook, J. M., Poyatos-Moré, M., & Midtkandal, I. (2019). Coalesced delta-front sheet-like sandstone bodies from highly avulsive distributary channels: the low-accommodation Mesa Rica Sandstone, Dakota Group, New Mexico, U.S.A. *Journal of Sedimentary Research*, *89*(7), 654–678.

van Yperen, A. E., Holbrook, J. M., Poyatos-Moré, M., Myers, C., & Midtkandal, I. (2020). Low-accommodation and backwater effects on sequence stratigraphic surfaces and depositional architecture of fluvio-deltaic settings (Cretaceous Mesa Rica Sandstone, Dakota Group, USA). *Basin Research, 33,* 513–543.

Visser, M.J. (1980). Neap-spring cycles reflected in Holocene subtidal large-scale bedform deposits: a preliminary note. *Geology 8,* 543–546.

Voris, H.K. (2000). Maps of Pleistocene sea levels in Southeast Asia: shorelines, river systems and time durations. *Journal of Biogeography, 27*(5), 1153–1167.

Walker, R.G. (1985). Geological evidence for storm transportation and deposition on ancient shelves. In R.W. Tillman, D.J.P. Swift & R.G. Walker (Eds.), *Shelf sands and sandstone reservoirs: SEPM, Short Course Notes, 13* (pp 243-302). Tulsa, Okla: SEPM Society for Sedimentary Geology.

Walker, R.G. (1992). Facies, facies models and modern stratigraphic concepts. In R.G. Walker & N.P. James (Eds.), *Facies models: Response to sea level change* (pp. 1–14). St. John's, Newfoundland: Geological Association of Canada.

Walker, R.G., James, N.P. (1992). *Facies models: Response to sea level change.* St. John's, Newfoundland: Geological Association of Canada.

Walker, R.G., Plint, A.G. (1992). Wave-and storm-dominated shallow marine system. In R.G. Walker & N.P. James (Eds.), *Facies models: Response to sea level change* (pp. 219–238). St. John's, Newfoundland: Geological Association of Canada.

Wallet, B. (2016). Is spectral decomposition suitable for 3D modeling of channels? In *SEG Technical Program Expanded Abstracts*. *SEG Technical Program Expanded Abstracts 2016* (pp. 2007–2011). Society of Exploration Geophysicists.

Wang, L., Sarnthein, M., Erlenkeuser, H., Grimalt, J., Grootes, P., Heilig, S., Ivanova, E., Kienast, M., Pelejero, C., & Pflaumann, U. (1999). East Asian monsoon climate during the Late Pleistocene: high-resolution sediment records from the South China Sea. *Marine Geology*, *156*(1), 245–284.

Wang, Y., Straub, K. M., & Hajek, E. A. (2011). Scale-dependent compensational stacking: An estimate of autogenic time scales in channelized sedimentary deposits. *Geology, 39*(9)*,* 811–814.

Waples, D.W., Mahadir, R. & Leslie, W. (1995). Implications of vitrinite-reflectance suppression for the tectonic and thermal history of the Malay Basin. *Geological Society of Malaysia Bulletin, 37*, 269–284.

Watcharanantakul, R., & Morley, C. K. (2000). Syn-rift and post-rift modelling of the Pattani Basin, Thailand: evidence for a ramp-flat detachment. *Marine and Petroleum Geology*, *17*(8), 937–958.

Watts, A., Karner, G., & Steckler, M. (1982). Lithospheric flexure and the evolution of sedimentary basins. *Philosophical Transactions of The Royal Society A: Mathematical, Physical and Engineering Sciences*, *305*(1489), 249–281.

Weissmann, G.S., Hartley, A.J., Nichols, G.J., Scuderi, L.A., Olson, M., Buehler, H., & Banteah, R. (2010). Fluvial form in modern continental sedimentary basins: Distributive fluvial systems. *Geology, 38*(1)*,* 39–42.

Wetzel, A., Feldens, A., Unverricht, D., Stattegger, K., & Tjallingii, R. (2021). Late Pleistocene sea-level changes and the formation and fill of bent valleys incised into the shelf of the western South China Sea. *Journal of Asian Earth Sciences*, *206*, Article#104626.

Wetzel, A., Szczygielski, A., Unverricht, D. & Stattegger, K., (2017). Sedimentological and ichnological implications of rapid Holocene flooding of a gently sloping mud-dominated incised valley – an example from the Red River, Gulf of Tonkin. *Sedimentology, 64*(5)*,* 1173–1202.

White, J.M., Jr. & Wing, R.S. (1978). Structural development of the South China Sea with particular reference to Indonesia. *Proceedings of the Indonesia Petroleum Association 7th Annual Convention, Jakarta*, Indonesia (pp. 159–177). Jakarta: Indonesian Petroleum Association.

Widess, M. B. (1973). How thin is a thin bed? *Geophysics, 38*, 1176–1180.

Williams, G.E. (2004). Earth's Precambrian rotation and the evolving lunar orbit: implications of tidal rhythmite data for palaeogeophysics. In P.G. Eriksson, W.

Altermann, D.R. Nelson, W.U. Mueller & O. Catuneanu (Eds.), *The Precambrian Earth: Tempos and events: Developments in Precambrian Geology, 12* (pp. 473–482). Elsevier.

Willis, B.J. (1993). Ancient river systems in the Himalayan foredeep, Chinji Village area, northern Pakistan. *Sedimentary Geology, 88,* 1–76.

Willis, B.J. (2005). Deposits of tide-influenced river deltas. In L. Giosan & J.P Bhattacharya (Eds.), *River deltas – Concepts, models, and examples: SEPM Special Publications, 83* (pp. 87–129). Tulsa, Okla: SEPM Society of Sedimentary Geology.

Willis, B.J. & Fitris, F. (2012). Sequence stratigraphy of Miocene tide-influenced sandstone in the Minas Field, Sumatra, Indonesia. *Journal of Sedimentary Research, 82*(6)*,* 400–421.

Wilson, A., Flint, S., Payenberg, T., Tohver, E., & Lanci, L. (2014). Architectural Styles and Sedimentology of the Fluvial Lower Beaufort Group, Karoo Basin, South Africa. *Journal of Sedimentary Research. 84*(4), 326-348.

Wong, R., Ahmad, M., Boyce, B., Jirin, S., Hoesni, J., Kirk, R., Barber, P., & Morley, R.J. (2006, Nov). *Sequence stratigraphy and chronostratigraphy of the Malay Basin unravels new exploration plays*. Presented abstract in the AAPG International Conference and Exhibition, Perth, West Australia (Article #90061). Retrieved from http://www.searchanddiscovery.com/abstracts/pdf/2006/intl_perth/abstracts/ndx_wong.pdf

Wood, L. J. (2007). Quantitative seismic geomorphology of Pliocene and Miocene fluvial systems in the Northern Gulf of Mexico, U.S.A. *Journal of Sedimentary Research*, *77*(9), 713–730.

Wood, L.J., Ethridge, F.G. & Schumm, S.A. (1993). The effects of base-level fluctuation on coastal-plain, shelf and slope depositional systems: an experimental approach. In H.W. Posamentier, C.P. Summerhayes, B.U. Haq & G.P. Allen (Eds.), *Sequence stratigraphy and facies associations: The International Association of Sedimentologists, 18* (pp. 43-54). Blackwell scientific.

Wright, L., Coleman, J., & Thom, B. (1973). Processes of channel development in a high-tide-range environment: Cambridge Gulf-Ord River Delta, Western Australia. *The Journal of Geology, 81*(1), 15-41.

Wright, V.P. & Marriott, S. B. (1993). The sequence stratigraphy of fluvial depositional systems: the role of floodplain sediment storage. *Sedimentary Geology*, *86*(3), 203–210.

Wu, C. & Nittrouer, J. A. (2020). Impacts of backwater hydrodynamics on fluvial–deltaic stratigraphy. *Basin Research*, *32*(3), 567–584.

Yakzan, A. M., Awalludin, H., Bahari, M.N., & Morley, R.J. (1996). Integrated biostratigraphic zonation for the Malay Basin. *Geological Society of Malaysia, 39*, 157 –184.

Yang, C.-S. (1989). Active, moribund and buried tidal sand ridges in the East China Sea and the Southern Yellow Sea. *Marine Geology*, *88*(1), 97–116.

Yang, Z., & Yang, W. (1984). Tidal deposits of carbonate facies and their microfacies types in the Qiziqiao Formation of Middle Devonian, South China. *Geochemistry*, *3*(4), 364–376.

Yankovsky, A., Torres, R., Legña, M., & Jeon, K. (2012). Interaction of tidal and fluvial processes in the transition zone of the Santee River, SC, USA. *Estuaries and coasts*, *35*, 1500–1509.

Yu, S.M. & Yap, K. T. (2019). Malay and Penyu basins: seismic stratigraphy and structural styles. In D. Ghosh (Eds.), *Geophysical applications in Malaysian Basins.* (pp. 51-68). Kuala Lumpur: Petroleum Nasional Berhad and European Association of Geoscientists and Engineers.

Zand-Moghadam, H., Moussavi-Harami, R., Mahboubi, A., & Bavi, H. (2013). Comparison of tidalites in siliciclastic, carbonate, and mixed siliciclastic-carbonate systems: examples from Cambrian and Devonian Deposits of East-Central Iran. *International Scholarly Research Notice: Geology*, *2013*, Article #534761.

Zachos, J. C., MO, P., Sloan, L. C., Thomas, E., & Billups, K. (2001). Trends, rhythms, and aberrations in global climate 65 Ma to Present. *Science*, *292*(5517), 686–693. Retrieved from https://science.sciencemag.org/content/292/5517/686.

Zaitlin, B. A., Dalrymple, R. W., & Boyd, R. (1994). The stratigraphic organization of incised-valley systems associated with relative sea-level change. In R.W. Dalrymple, R. Boyd & B.A. Zaitlin (Eds.), *Incised-valley Systems: Origin and sedimentary sequences: SEPM Special Publication, 51* (pp. 45-60). Tulsa, Okla: SEPM Society for Sedimentary Geology.

Zavala, C., & Pan, S. (2018). Hyperpycnal flows and hyperpycnites : Origin and distinctive characteristics. *Lithologic Reservoirs*, *30*, 1–27.

Zeff, M. L. (1988). Sedimentation in a salt marsh-tidal channel system, southern New Jersey. *Marine Geology*, *82*(1), 33–48.

Zeller, J. (1967). Meandering channels in Switzerland. *Symposium on river morphology*, International Association of Scientific Hydrology, General Assembly of Bern.

Zeng, H. (2007). Seismic imaging for seismic geomorphology beyond the seabed: potentials and challenges. In R.J. Davies, H.W. Posamentier, L.J. Wood, & J.A. Cartwright (Eds.), *Seismic geomorphology: applications to hydrocarbon exploration and production: The Geological Society of London Special publication, 277* (pp. 15–28). Bath, UK: Geological Society of London.

Zeng, H. (2017). What is seismic sedimentology? A tutorial. *Interpretation*, *6*(2), SD1–SD12.

Zeng, H., Ambrose, W. A., & Villalta, E. (2001). Seismic sedimentology and regional depositional systems in Mioceno Norte, Lake Maracaibo, Venezuela. *The Leading Edge*, *20*(11), 1260–1269.

Zeng, H., & Hentz, T. F. (2004). High-frequency sequence stratigraphy from seismic sedimentology: Applied to Miocene, Vermilion Block 50, Tiger Shoal area, offshore Louisiana. *American Association of Petroleum Geologists Bulletin*, *88*(2), 153–174.

Zeng, H., Backus, M. M., Barrow, K. T., & Tyler, N. (1998). Stratal slicing, Part I: Realistic 3-D seismic model. *Geophysics*, *63*(2), 502–513.

Zeng, H., Zhu, X., Liu, Q., Zhu, H., & Xu, C. (2020). An alternative, seismic-assisted method of fluvial architectural-element analysis in the subsurface: Neogene, Shaleitian area, Bohai Bay Basin, China. *Marine and Petroleum Geology*, *118*, 104435.